

ADVANCES IN
QUANTUM CHEMISTRY

VOLUME 47

EDITORIAL BOARD

Jiri Cizek (Waterloo, Canada).
David P. Craig (Canberra, Australia).
Raymond Daudel (Paris, France).
Ernest R. Davidson (Bloomington, Indiana).
George G. Hall (Nottingham, England).
Jan Linderberg (Aarhus, Denmark).
Fredrick A. Matsen (Austin, Texas).
Roy McWeeny (Pisa, Italy).
William H. Miller (Berkley, California).
Keiji Morokuma (Atlanta, Georgia).
Josef Paldus (Waterloo, Canada).
Ruben Pauncz (Haifa, Israel).
Siegrid Peyerimhoff (Bonn, West Germany).
John A. Pople (Evanston, Illinois).
Alberte Pullman (Paris, France).
Pekka Pyykkö (Helsinki, Finland).
Leo Radom (Canberra, Australia).
Klaus Ruedenberg (Ames, Iowa).
Henry F. Schaefer III (Athens, Georgia).
Isaiah Shavitt (Columbus, Ohio).
Per Siegbahn (Stockholm, Sweden).
Au-Chin Tang (Changchun, People's Republic of China).
Rudolf Zahradnik (Prague, Czech Republic).

ADVISORY EDITORIAL BOARD

David M. Bishop (Ottawa, Canada).
Giuseppe Del Re (Naples, Italy).
Fritz Grein (Fredericton, Canada).
Mu-Sik Jhon (Seoul, Korea).
Mel Levy (New Orleans, Louisiana).
Jens Oddershede (Odense, Denmark).
Mark Ratner (Evanston, Illinois).
Dennis Salahub (Quebec, Canada).
Harel Weinstein (New York, New York).
Robert E. Wyatt (Austin, Texas).
Tokio Yamabe (Kyoto, Japan).

ADVANCES IN QUANTUM CHEMISTRY

**A TRIBUTE VOLUME IN HONOUR OF PROFESSOR
OSVALDO GOSCINSKI**

EDITORS

JOHN R. SABIN

QUANTUM THEORY PROJECT
UNIVERSITY OF FLORIDA
GAINESVILLE, FLORIDA

ERKKI BRÄNDAS

DEPARTMENT OF QUANTUM CHEMISTRY
UPPSALA UNIVERSITY
UPPSALA, SWEDEN

FOUNDING EDITOR

PER-OLOV LÖWDIN

1916–2000

GUEST EDITORS

ERKKI BRÄNDAS

DEPARTMENT OF QUANTUM CHEMISTRY
UPPSALA UNIVERSITY
UPPSALA, SWEDEN

EUGENE KRYACHKO

DIVISION OF QUANTUM CHEMISTRY
UNIVERSITY OF LIEGE
BELGIUM

VOLUME 47



ELSEVIER
ACADEMIC
PRESS

Amsterdam · Boston · Heidelberg · London · New York · Oxford
Paris · San Diego · San Francisco · Singapore · Sydney · Tokyo

ELSEVIER B.V.
Sara Burgerhartstraat 25
P.O. Box 211, 1000 AE Amsterdam
The Netherlands

ELSEVIER Ltd
The Boulevard, Langford Lane
Kidlington, Oxford OX5 1GB
UK

ELSEVIER Inc.
525 B Street, Suite 1900
San Diego, CA 92101-4495
USA

ELSEVIER Ltd
84 Theobalds Road
London WC1X 8RR
UK

© 2004 Elsevier Inc. All rights reserved.

This work is protected under copyright by Elsevier Inc., and the following terms and conditions apply to its use:

Photocopying

Single photocopies of single chapters may be made for personal use as allowed by national copyright laws. Permission of the Publisher and payment of a fee is required for all other photocopying, including multiple or systematic copying, copying for advertising or promotional purposes, resale, and all forms of document delivery. Special rates are available for educational institutions that wish to make photocopies for non-profit educational classroom use.

Permissions may be sought directly from Elsevier's Rights Department in Oxford, UK: phone (+44) 1865 843830, fax (+44) 1865 853333, e-mail: permissions@elsevier.com. Requests may also be completed on-line via the Elsevier homepage (<http://www.elsevier.com/locate/permissions>).

In the USA, users may clear permissions and make payments through the Copyright Clearance Center, Inc., 222 Rosewood Drive, Danvers, MA 01923, USA; phone: (+1) (978) 7508400, fax: (+1) (978) 7504744, and in the UK through the Copyright Licensing Agency Rapid Clearance Service (CLARCS), 90 Tottenham Court Road, London W1P 0LP, UK; phone: (+44) 20 7631 5555; fax: (+44) 20 7631 5500. Other countries may have a local reprographic rights agency for payments.

Derivative Works

Tables of contents may be reproduced for internal circulation, but permission of the Publisher is required for external resale or distribution of such material. Permission of the Publisher is required for all other derivative works, including compilations and translations.

Electronic Storage or Usage

Permission of the Publisher is required to store or use electronically any material contained in this work, including any chapter or part of a chapter.

Except as outlined above, no part of this work may be reproduced, stored in a retrieval system or transmitted in any form or by any means, electronic, mechanical, photocopying, recording or otherwise, without prior written permission of the Publisher.

Address permissions requests to: Elsevier's Rights Department, at the fax and e-mail addresses noted above.

Notice

No responsibility is assumed by the Publisher for any injury and/or damage to persons or property as a matter of products liability, negligence or otherwise, or from any use or operation of any methods, products, instructions or ideas contained in the material herein. Because of rapid advances in the medical sciences, in particular, independent verification of diagnoses and drug dosages should be made.

First edition 2004

ISBN: 0-12-034847-0

ISSN: 0065-3276

© The paper used in this publication meets the requirements of ANSI/NISO Z39.48-1992 (Permanence of Paper). Printed and bound in Great Britain.

Working together to grow
libraries in developing countries

www.elsevier.com | www.bookaid.org | www.sabre.org

ELSEVIER

BOOK AID
International

Sabre Foundation

Contents

<i>Contributors</i>	xiii
<i>Osvaldo Goscinski: Preface</i>	xvii
<i>To My Colleagues by Osvaldo Goscinski</i>	xix
<i>Announcement: Quantum Chemistry – Theory, Models, and Computations</i>	xxi
<i>List of Publications of Prof. Osvaldo Goscinski</i>	xxiii

Development of Chiral Catalysts for Stereoselective Synthesis by Deprotonations – Experimentation in Interplay with Computational Chemistry

1

Sten O. Nilsson Lill, Peter Dinér, Daniel Pettersen,
Mohamed Amedjkouh and Per Ahlberg

1. Preamble	1
2. Introduction	3
3. Chiral lithium amides	5
4. Activated complexes in the epoxide deprotonations	7
5. Computational and experimental stereoselectivity	9
6. Origin of stereoselectivity	13
7. Search for more stereoselective chiral lithium amides	14
8. Catalytic stereoselective deprotonations	16
Acknowledgements	21
References	21

Proton Insertion in Polycrystalline WO₃ Studied with Electron Spectroscopy and Semi-empirical Calculations

23

A. Henningsson, A. Stashans, A. Sandell, H. Rensmo, S. Södergren,
H. Lindström, L. Vayssieres, A. Hagfeldt, S. Lunell and H. Siegbahn

1. Introduction	24
2. Experimental methods	25
3. Theoretical methods	26
4. Results	27
5. Discussion	32
6. Conclusions	35

Acknowledgements	35
References	35
On the Effects of Spin–Orbit Coupling on Molecular Properties: Dipole Moment and Polarizability of PbO and Spectroscopic Constants for the Ground and Excited States	37
Björn O. Roos and Per-Åke Malmqvist	
1. Introduction	38
2. Details of the calculations	40
3. Results	41
4. Conclusions	48
Acknowledgements	48
References	49
Is There a Favorite Isomer for Hydrogen-Bonded Methanol in Water?	51
Eudes E. Fileti, Kaline Coutinho and Sylvio Canuto	
1. Introduction	51
2. Methods	53
3. Results	57
4. Final remarks and conclusions	61
Acknowledgements	61
References	62
Validation of the Applicability of Force Fields to Reproduce <i>Ab Initio</i> Noncovalent Interactions Involving Aromatic Groups	65
Guilin Duan, Vedene H. Smith, Jr. and Donald F. Weaver	
1. Introduction	66
2. CHARMM force field	67
3. Validation strategies	69
4. Results and discussion	75
5. Conclusion	91
Acknowledgements	91
References	91
Are Jordan Blocks Necessary for the Interpretation of Dynamical Processes in Nature?	93
Erkki J. Brändas	
1. Introduction	93
2. Hamiltonian level	95
3. Liouvillian level	98
4. Conclusions	102
Acknowledgements	103
Appendix A. Properties of reduced density matrices	103
References	106

Antisymmetrized Geminal Power Coherent States	107
Brian Weiner	
1. Introduction	107
2. Lie algebras	111
3. One-particle groups	112
4. Coherent states	115
5. Summary and discussion	124
Appendix A. AGP states	125
References	126
Current Methods for Coulomb Few-Body Problems	129
Frank E. Harris	
1. Introduction	130
2. Basis wavefunctions	131
3. Kinetic energy	134
4. Matrix elements	138
5. Four-body exponentially correlated wavefunctions	143
6. Three-body exponentially correlated wavefunctions	145
7. Correlated Gaussian wavefunctions	146
8. Hylleraas methods	146
9. Other methods	148
Acknowledgements	149
Appendix A. Angular momentum identities	149
Appendix B. Differential properties of the $\mathcal{Y}_{LM}^{ll'}$	150
References	153
Atomic Densities, Polarizabilities, and Natural Orbitals Derived from Generalized Sturmian Calculations	157
John Avery, James Avery, Vincenzo Aquilanti and Andrea Caligiana	
1. Introduction	157
2. Generalized Sturmians	160
3. Potential-weighted orthonormality relations	161
4. The generalized Sturmian secular equations	162
5. Atomic calculations	162
6. The generalized Slater–Condon rules	166
7. The first-order density matrix	168
8. Natural orbitals	169
9. Atoms in strong external fields; polarizabilities	171
10. Concluding remarks	174
References	174
Electric Field Gradient Effects on Magnetic Susceptibility	177
Paolo Lazzeretti	
1. Introduction	177
2. The expectation value of the electronic moments in a molecule	179

3. Response tensors by continuous transformation of the origin of the current density	182
4. Polarizabilities of susceptibility in different coordinate systems	183
Acknowledgements	189
References	189

Singularity Structure of Møller–Plesset Perturbation Theory 193

David Z. Goodson and Alexey V. Sergeev

1. Introduction	194
2. Functional analysis of the energy	195
3. Extracting singularity structure from perturbation series	199
4. Examples	201
5. Discussion	205
References	206

Approximate Inclusion of the T_3 and R_3 Operators in the Equation-of-motion Coupled-cluster Method 209

Monika Musiał, Stanisław A. Kucharski and Rodney J. Bartlett

1. Introduction	209
2. Theory	210
3. Approximate variants	212
4. Results and discussion	216
5. Conclusions	221
Acknowledgements	221
References	221

Operator Algebra: From Franck–Condon to Floquet Theory 223

Alejandro Palma

1. Introduction	223
2. Franck–Condon factors and ladder operators	224
3. The Lie algebraic approach to the Franck–Condon integral	226
4. The Lie algebraic approach to the Morse oscillator	227
5. The Franck–Condon overlap and squeezed states	230
6. Operator algebra and Floquet states	232
7. The Lie algebraic approach to Floquet quasi-energies	235
8. Discussion	237
Acknowledgements	237
References	237

On the Alleged Nonlocal and Topological Nature of the Molecular Aharonov–Bohm Effect 239

Erik Sjöqvist

1. Introduction	239
2. Locality and topology	241
3. Preferred gauge	243

4. Aharonov–Casher analogue	249
5. Conclusions	250
Acknowledgements	251
References	251

Calculation of Cross Sections in Electron-Nuclear Dynamics 253

R. Cabrera-Trujillo, John R. Sabin, E. Deumens and Y. Öhrn

1. Introduction	254
2. Minimal electron-nuclear dynamics	255
3. END trajectories	257
4. Overview of results	261
5. Conclusions	272
References	273

Generalized Electronic Diabatic Ansatz: A Post-Born–Oppenheimer Approach to Electronuclear Dynamics in External Fields 275

O. Tapia and Gustavo A. Arteca

1. Introduction	276
2. GED ansatz	276
3. Post-BO scheme: process description	279
4. Discussion	287
Acknowledgements	290
References	291

The Quantum–Classical Density Operator for Electronically Excited Molecular Systems 293

David A. Micha and Brian Thorndyke

1. Introduction	294
2. The coupled quantum–classical description	295
3. Approximations for short wavelengths	297
4. Numerical propagation method	300
5. Model calculations	303
6. Reduced density matrices for dissipative dynamics	309
7. Conclusion	312
Acknowledgements	313
References	313

The Generator Coordinate Method for Atomic and Molecular Systems: Revision and Further Developments 315

Milan Trsic, Wagner F. D. Angelotti and Fábio A. Molfetta

Preface: memories	315
1. Introduction	316
2. The generator coordinate method [3]	317

3. An example of analytical solution for the hydrogen atom [8]	318
4. Further developments for simple systems	319
5. Discretization techniques [12]	323
6. The generator coordinate Hartree–Fock method [10]	323
7. A connection between GCM and DFT	326
8. Conclusions	328
Acknowledgements	328
References	329

Hybrid Quantum/Classical Dynamics Using Bohmian Trajectories 331

E. Gindensperger, C. Meier and J. A. Beswick

1. Introduction	332
2. De Broglie–Bohm formulation of quantum mechanics	333
3. From the de Broglie–Bohm formulation to the MQCB method	334
4. Structure of the MQCB equations: initial conditions, reversibility and observables	339
5. An illustrative example: molecule–surface scattering	340
6. Conclusions	345
Acknowledgements	346
References	346

The Hückel Model of Polyacetylene Revisited: Asymptotic Analysis of Peierls Instability 347

Gian Luigi Bendazzoli and Stefano Evangelisti

1. Introduction	348
2. The Hückel model for alternating one-dimensional polyenes	348
3. Perturbation expansion	355
4. Discussion and conclusions	360
Acknowledgements	361
Appendix A. The elliptic integral of second kind	361
Appendix B. The roots of equation (25)	362
Appendix C. Asymptotic behaviour of the sums	364
Appendix D. Derivation of equations (48) and (49)	366
Appendix E. Analysis of the first-order perturbation energy	367
References	368

Conjugated Polymers in External DC Fields 369

Michael Springborg and Yi Dong

1. Introduction	369
2. General considerations and a simple Hückel-like model	372
3. A first-principles method for polymers	383
4. Conclusions	391
Acknowledgements	391
References	392

Atoms, Molecules, Crystals and Nanotubes in Laser Fields: From Dynamical Symmetry to Selective High-Order Harmonic Generation of Soft X-Rays	393
Ofir E. Alon, Vitali Averbukh and Nimrod Moiseyev	
1. Introduction	394
2. On quantum rings and symmetric molecules in circularly polarized laser fields	394
3. Thin crystals in circularly polarized laser fields	397
4. Nanotubes in circularly polarized laser fields	401
5. Selection rules for the high-order harmonic generation spectra	404
6. High-order harmonic generation of soft X-rays by carbon nanotubes	409
7. Summary and conclusions	419
Acknowledgements	420
References	420
Small Gold Clusters $\text{Au}_{5 \leq n \leq 8}$ and Their Cationic and Anionic Cousins	423
F. Remacle and E. S. Kryachko	
1. A short excursion to gold and alchemy	423
2. 2D–3D transition in small neutral, cationic and anionic gold clusters: early views	426
3. Computational framework	428
4. Five atoms of gold	429
5. Six atoms of gold	437
6. Seven gold atoms	441
7. Eight gold atoms	449
8. The low-energy section of the PES of Au_9	456
9. Summary and outlook	458
Acknowledgements	460
References and notes	460
Positron–Electron Annihilation in Hydrogen–Antihydrogen Collisions	465
P. Froelich, S. Jonsell, A. Saenz, S. Eriksson, B. Zygelman and A. Dalgarno	
1. Introduction	465
2. Leptonic annihilation in the hydrogen–antihydrogen system	467
3. Numerical results	474
4. Conclusions	477
Acknowledgements	479
References	479
<i>Subject Index</i>	481

This page intentionally left blank

Contributors

Numbers in parentheses indicate the pages where the authors' contributions can be found.

Per Ahlberg (1), Department of Chemistry, Göteborg University, SE-412 96 Göteborg, Sweden

Ofir E. Alon (393), Department of Chemistry and Minerva Center for Non-Linear Physics of Complex Systems, Technion–Israel Institute of Technology, Haifa 32000, Israel

Mohamed Amedjkouh (1), Department of Chemistry, Göteborg University, SE-412 96 Göteborg, Sweden

Wagner F. D. Angelotti (315), Instituto de Química de São Carlos, Universidade de São Paulo, CP 780, 13560-970, São Carlos, SP, Brazil

Vincenzo Aquilanti (157), Department of Chemistry, University of Perugia, Perugia, Italy

Gustavo A. Arteca (275), Département de Chimie et Biochimie, Laurentian University, Ramsey Lake Road, Sudbury, Ont., Canada P3E 2C6

Vitali Averbukh (393), Department of Chemistry and Minerva Center for Non-Linear Physics of Complex Systems, Technion–Israel Institute of Technology, Haifa 32000, Israel

John Avery (157), Departments of Chemistry and Computer Science, University of Copenhagen, Copenhagen, Denmark

James Avery (157), Departments of Chemistry and Computer Science, University of Copenhagen, Copenhagen, Denmark

Rodney J. Bartlett (209), Quantum Theory Project, Department of Chemistry and Physics, University of Florida, Gainesville, FL 32611, USA

Gian Luigi Bendazzoli (347), Dipartimento di Chimica Fisica e Inorganica, Università di Bologna, Viale Risorgimento 4, I-40136 Bologna, Italy

J. A. Beswick (331), LCAR-IRSAMC, Université Paul Sabatier, Toulouse, France

Erkki J. Brändas (93), Department of Quantum Chemistry, Uppsala University, Box 518, S-751 20 Uppsala, Sweden

R. Cabrera-Trujillo (253), Quantum Theory Project, University of Florida, P.O. Box 118435, Gainesville, FL 32611-8435, USA

Andrea Caligiana (157), Department of Chemistry, University of Perugia, Perugia, Italy

Sylvio Canuto (51), Instituto de Física, Universidade de São Paulo, CP 66318, 05315-970 São Paulo, SP, Brazil

Kaline Coutinho (51), Universidade de Mogi das Cruzes/CIIB, CP 411, 08701-970 Mogi das Cruzes, SP, Brazil

- A. Dalgarno** (465), Harvard-Smithsonian Center for Astrophysics, 60 Garden Street, Cambridge, MA 02138, USA
- E. Deumens** (253), Quantum Theory Project, University of Florida, P.O. Box 118435, Gainesville, FL 32611-8435, USA
- Peter Dinér** (1), Department of Chemistry, Göteborg University, SE-412 96 Göteborg, Sweden
- Yi Dong** (369), Physical Chemistry, University of Saarland, 66123 Saarbrücken, Germany
- Guilin Duan** (65), Department of Chemistry, Queen's University, Kingston, Ont., Canada K7L 3N6
- S. Eriksson** (465), Department of Quantum Chemistry, Uppsala University, Box 518, 75120 Uppsala, Sweden
- Stefano Evangelisti** (347), Laboratoire de Physique Quantique, UMR 5626, Université Paul Sabatier, 118, Route de Narbonne, 31062 Toulouse Cedex, France
- Eudes E. Fileti** (51), Instituto de Física, Universidade de São Paulo, CP 66318, 05315-970 São Paulo, SP, Brazil
- P. Froelich** (465), Department of Quantum Chemistry, Uppsala University, Box 518, 75120 Uppsala, Sweden
- E. Gindensperger** (331), LCAR-IRSAMC, Université Paul Sabatier, Toulouse, France
- David Z. Goodson** (193), Department of Chemistry and Biochemistry, University of Massachusetts Dartmouth, North Dartmouth, MA 02747, USA
- A. Hagfeldt** (23), Department of Physical Chemistry, Uppsala University, P.O. Box 579, S-751 23 Uppsala, Sweden
- Frank E. Harris** (129), Department of Physics, University of Utah, Salt Lake City, UT 84112, USA; Quantum Theory Project, P.O. Box 118435, University of Florida, Gainesville, FL 32611, USA
- A. Henningsson** (23), Department of Physics, Uppsala University, P.O. Box 530, S-751 21 Uppsala, Sweden
- S. Jonsell** (465), Theoretical Physics, Umeå University, SE-90187 Umeå, Sweden
- E. S. Kryachko** (423), Department of Chemistry. Bat. B6c, University of Liege, Sart-Tilman, B-4000 Liege 1, Belgium; Bogoliubov Institute for Theoretical Physics, Kiev 03143, Ukraine
- Stanisław A. Kucharski** (209), University of Silesia, Institute of Chemistry, Szkolna 9, Katowice, Poland
- Paolo Lazeretti** (177), Dipartimento di Chimica, Università degli Studi di Modena e Reggio Emilia, via G. Campi 183, 41100 Modena, Italy
- H. Lindström** (23), Department of Physical Chemistry, Uppsala University, P.O. Box 579, S-751 23 Uppsala, Sweden
- S. Lunell** (23), Department of Quantum Chemistry, Uppsala University, P.O. Box 518, S-751 20 Uppsala, Sweden
- Per-Åke Malmqvist** (37), Department of Theoretical Chemistry, Chemical Center, P.O. Box 124, S-221 00 Lund, Sweden
- C. Meier** (331), LCAR-IRSAMC, Université Paul Sabatier, Toulouse, France

- David A. Micha** (293), Quantum Theory Project, University of Florida, Gainesville, FL 32611-8435, USA
- Nimrod Moiseyev** (393), Department of Chemistry and Minerva Center for Non-Linear Physics of Complex Systems, Technion–Israel Institute of Technology, Haifa 32000, Israel
- Fábio A. Molfetta** (315), Instituto de Química de São Carlos, Universidade de São Paulo, CP 780, 13560-970, São Carlos, SP, Brazil
- Monika Musiał** (209), Quantum Theory Project, Department of Chemistry and Physics, University of Florida, Gainesville, FL 32611, USA
- Sten O. Nilsson Lill** (1), Department of Chemistry, Göteborg University, SE-412 96 Göteborg, Sweden
- Y. Öhrn** (253), Quantum Theory Project, University of Florida, P.O. Box 118435, Gainesville, FL 32611-8435, USA
- Alejandro Palma** (223), Instituto de Física (BUAP), Apartado Postal J-48, Puebla, Pue. 72570, México and Instituto Nacional de Astrofísica, Óptica y Electrónica (INADE), México
- Daniel Pettersen** (1), Department of Chemistry, Göteborg University, SE-412 96 Göteborg, Sweden
- F. Remacle** (423), Department of Chemistry, Bat. B6c, University of Liege, Sart-Tilman, B-4000 Liege 1, Belgium
- H. Rensmo** (23), Department of Physics, Uppsala University, P.O. Box 530, S-751 21 Uppsala, Sweden
- Björn O. Roos** (37), Department of Theoretical Chemistry, Chemical Center, P.O. Box 124, S-221 00 Lund, Sweden
- John R. Sabin** (253), Quantum Theory Project, University of Florida, P.O. Box 118435, Gainesville, FL 32611-8435, USA
- A. Saenz** (465), AG Moderne Optik, Institut für Physik, Humboldt-Universität zu Berlin, Haus-vogteiplatz 5-7, D-10117 Berlin, Germany
- A. Sandell** (23), Department of Physics, Uppsala University, P.O. Box 530, S-751 21 Uppsala, Sweden
- Alexey V. Sergeev** (193), Department of Chemistry and Biochemistry, University of Massachusetts Dartmouth, North Dartmouth, MA 02747, USA
- H. Siegbahn** (23), Department of Physics, Uppsala University, P.O. Box 530, S-751 21 Uppsala, Sweden
- Erik Sjöqvist** (239), Department of Quantum Chemistry, Uppsala University, Box 518, Se-751 20 Uppsala, Sweden
- Vedene H. Smith, Jr.** (65), Department of Chemistry, Queen's University, Kingston, Ont., Canada K7L 3N6
- S. Södergren** (23), Gammadata Scientia AB, P.O. Box 15120, S-750 15 Uppsala, Sweden
- Michael Springborg** (369), Physical Chemistry, University of Saarland, 66123 Saarbrücken, Germany
- A. Stashans** (23), Department of Quantum Chemistry, Uppsala University, P.O. Box 518, S-751 20 Uppsala, Sweden

- O. Tapia** (275), Department of Physical Chemistry, Uppsala University, Box 579, S-751 23 Uppsala, Sweden
- Brian Thorndyke** (293), Quantum Theory Project, University of Florida, Gainesville, FL 32611-8435, USA
- Milan Trsic** (315), Instituto de Química de São Carlos, Universidade de São Paulo, CP 780, 13560-970, São Carlos, SP, Brazil
- L. Vayssieres** (23), Department of Physical Chemistry, Uppsala University, P.O. Box 579, S-751 23 Uppsala, Sweden
- Donald F. Weaver** (65), Departments of Medicine (Neurology) and Chemistry, School of Biomedical Engineering, Dalhousie University, Halifax, NS, Canada B3H 4J3
- Brian Weiner** (107), Department of Physics, Pennsylvania State University, DuBois, PA 15801, USA
- B. Zygelman** (465), Department of Physics, University of Nevada, Las Vegas, NV 89154, USA

Preface

Osvaldo Goscinski



A tribute to honour Osvaldo Goscinski was enthusiastically suggested by his colleagues and friends and was planned to appear in time for his retirement from the “Löwdin Chair” at Uppsala University during the period 2003-5. The mini-symposium and the Birthday Celebration had already taken place on 23-24 October 2003, nevertheless the plans to fulfil our undertaking remained.

The appointment of Per-Olov Löwdin to the first Quantum Chemistry Chair in Sweden on 13 May 1960 led to a remarkable development in the powerful field of Quantum Chemistry. The Changing of the Guards took place in 1982/83 with the inauguration of Osvaldo Goscinski as Per-Olov Löwdin’s successor. During the first decade of his time as Head of the Department and the Program of Quantum Chemistry, Osvaldo Goscinski dedicated profound efforts to the development of natural sciences on a national level through his commitment to the running and development of the Physics Committee of the Swedish Natural Sciences Research Council (NFR). The last two decades of the millennium have witnessed dynamic

structural changes at the NFR leading up to the creation of the present-day Swedish Research Council (VR). We pay particular attention to the display of objectivity, selflessness and independence in the way he satisfied the goals of NFR which, combined with impartiality and lack of prejudice, paved the way for progress. In addition to developing and strengthening the scientific networks in Quantum Chemistry and Chemical Physics he also found time to contribute significantly to the Faculty of Science and Technology as Dean with particular responsibility for graduate education.

It is not possible to cover the accomplishments of Osvaldo Goscinski in such a short tribute as the present one. Nevertheless, we hope that the love and devotion that always characterised his relations with his students, colleagues and friends will be reflected by the contributions in this volume. With these words we wish Osvaldo Goscinski all the best of luck and satisfaction in his new life as a “free man” to read and write what he likes the best!

Erkki J. Brändas
Uppsala University
Uppsala, Sweden

Eugene S. Kryachko
Bogoliubov Institute for Theoretical
Physics, Kiev, Ukraine and
University of Liege, Liege, Belgium

To My Colleagues

Of course, it is a tremendous honour and pleasure to have such a Festschrift volume of *Advances in Quantum Chemistry* produced on one's behalf, and I first extend my thanks and deepest gratitude to all those responsible. Needless to say, the activity undertaken on my behalf by Eugene Kryachko and Erkki Brändas has been of major significance for this project. It is also wonderful to express my indebtedness to all individuals with whom I had the honour and pleasure to collaborate. It is quite clear that the sum of the individual contributions is far more valuable than the ingredients!

I am indebted to the participants of the Löwdin-Lectures 2003 as well as all those who participated and contributed to the Symposium in my honour.

The Editors of *Advances in Quantum Chemistry* have been generous and allowed a scanned version of my list of publications to be included in the present Volume.

My colleagues at the Quantum Chemistry Group and elsewhere, who organised and arranged a Banquet, with many surprise participants including students as well as old friends and family left an everlasting memory in me. The collected books, records and solvents add also to my spiritual education.

Oswaldo Gosinski
Uppsala University

This page intentionally left blank

Quantum Chemistry – Theory, Models, and Computations

October 24, 2003.

Lecture Hall 2005, The Ångström Laboratory.

The Symposium Quantum Chemistry – Theory, Models, and Computations is organized to celebrate Professor Osvaldo Goscinski's 65th birthday. Professor Osvaldo Goscinski will be 65 years on October 29 and retires from his chair as Professor of Quantum Chemistry on November 29

Program

Session I (Chairman: S. Lunell)

9.30-9.35: Sten Lunell (Uppsala University), Opening

9.35-10.20: William H. Miller (University of California at Berkeley).
The Quantum Instanton Model for Thermal Rates of Chemical Reactions

10.20-10.40: Cleanthes Nicolaides (NTU, Athens).
The frontier of attosecond spectroscopy and electron correlations

10.40-11.00: Coffee break

Session II (Chairman: P. Froelich)

11.00-11.20: Sylvio Canuto (University of Sao Paolo, Brazil).
Hydrogen Bonds in Explicit Aqueous Environment

11.20-11.40: Gunnar Nyman (Göteborg University).
Ultrafast dynamics in liquid water and ice

11.40-12.00: Jorge Llano (Uppsala University).
First Principles Thermochemistry of Electron, Proton, and Proton-Coupled
Electron Transfer Reactions in Solution

12.00-13.30: Lunch break

Session III (Chairman: E. Brändas)

13.30-13.50: Karl-Fredrik Berggren (Linköping University).
Quantum Billiards and Electric Network Analogues

13.50-14.10: Frank Harris (University of Utah).
Fully correlated exponential wavefunctions for four-body systems

14.10-14.30: Manuel Berrondo (Brigham Young University).
Distorted Oscillators

14.30-15.00: Coffee break

Session IV (Chairman: H. Karlsson)

15.00-15.20: Olle Eriksson (Uppsala University).
Electronic structures and material properties from first principles
calculations

15.20-15.40: Sven Larsson (Chalmers University of Technology, Göteborg).
Misconceptions in theories of high T_c superconductivity

15.40-16.00: Vladimiro Mujica (Central University of Venezuela).
Electronic Correlation Effects on Transport at Electrode-Molecule Interfaces

16.00-16.20: Björn Hessmo (KTH, Stockholm).
The adiabatic approximation and optical modulators

16.20-16.30: Hans Karlsson (Uppsala University), Closing

List of Publications of Osvaldo Goscinski

- [1] W. J. Meath, K. M. Sando, O. Goscinski and J. O. Hirschfelder: "Truncated Reaction Operators" *J. Chem. Phys.* 39, 2429 (1963).
- [2] O. Goscinski and J. L. Calais: "Some Comments on the AMO Method for the Ground State of the Hydrogen Molecule" *Arkiv Fysik* 29, 135 (1965).
- [3] O. Goscinski: "Upper and Lower Bounds to Eigenvalues by Partitioning Technique" University of Florida, Quantum Theory Project, Technical Report 82 (April 1966).
- [4] O. Goscinski and J. L. Calais: "Kompendium over Gruppteori baserad på föreläsningar av prof. A. J. Coleman" (T XII, 1965).
- [5] O. Goscinski: "Continued Fractions and Upper and Lower Bounds in the Brillouin-Wigner Perturbation Scheme" *Int. J. Quantum Chem.* 1, 769 (1967).
- [6] E. Bosatta and O. Goscinski: "Asymptotic Exchange Coupling and the AMO Method" (Preprint No. 191, May 1, 1967).
- [7] O. Goscinski and O. Sinanoglu: "Upper and Lower Bounds and the Generalized Variation-Perturbation Approach to Many Electron Theory" *Int. J. Quantum Chem.* 2, 397 (1968).
- [8] O. Goscinski and E. Brändas: "Dispersion Forces, Second and Third Order Energies" *Chem. Phys. Lett.* 2, 299 (1968).
- [9] O. Goscinski: "Upper and Lower Bounds to Polarizabilities and Van der Waals Forces" *Int. J. Quantum Chem.* 2, 761 (1968).
- [10] O. Goscinski and Y. Öhrn: "Coupling of Equivalent Particles in a Field of Given Symmetry" *Int. J. Quantum Chem.* 2, 845 (1968).
- [11] O. Goscinski and E. Brändas: "Geometric Approximation in Perturbation Theory" *Phys. Rev.* 182, 43 (1969).
- [12] E. Brändas and O. Goscinski: "Is Second Order Perturbation Theory Sufficient to Treat Second Order Properties?" *Int. J. Quantum Chem.* 3S, 383 (1969).
- [13] E. Brändas and O. Goscinski: "Symmetry-Adapted Second Order Energy. Some Comments and Results for" *J. Chem. Phys.* 51, 975 (1969).
- [14] O. Goscinski and P. Lindner: "Asymptotic Properties of Atomic Form Factors and Incoherent Scattering Functions" *J. Chem. Phys.* 52, 2539 (1970); Erratum: 54, 826 (1971).
- [15] O. Goscinski and P. Lindner: "Natural Spin Orbitals and Generalized Overlap Amplitudes" *J. Math. Phys.* 11, 1313 (1970).
- [16] O. Goscinski: "Bounds to the Overlap" *Int. J. Quantum Chem.* 3, 1064 (1969).
- [17] M. Berrondo and O. Goscinski: "Local Exchange Approximations and the Virial Theorem" *Phys. Rev.* 184, 10 (1969).
- [18] O. Goscinski and E. Brändas: "Padé Approximants via Inner Projections". In "Theory of Electronic Shells of Atoms and Molecules" (A. P. Jucys Ed., Publishing House "Mintis", Vilnius 1970).
- [19] E. Brändas and O. Goscinski: "Variation Perturbation Expansions and Padé Approximants to the Energy" *Phys. Rev.* 1A, 552 (1970).
- [20] P.-O. Löwdin and O. Goscinski: "The Exchange Phenomenon, the Symmetric Group and the Spin Degeneracy Problem" *Int. J. Quantum Chem.* 3S, 533 (1969).

- [21] O. Goscinski and N. Stepanov: "Successive Partitioning and Feenberg Perturbation Theory" *Int. J. Quantum Chem.* 1, 545 (1970).
- [22] G. L. Bendazzoli, O. Goscinski and G. Orlandi: "Padé Approximants and Inner Projections in the Brillouin-Wigner Scheme for He-Like Ions" *Phys. Rev. A* 2, 2 (1970).
- [23] E. Brändas and O. Goscinski: "Critical Point, Singularities and Extrapolations in the Helium Isoelectronic Sequence" *Int. J. Quantum Chem.* 4, 571 (1970).
- [24] P. Lindner and O. Goscinski: "Generalized Polarizabilities and Energy Expressions" *Int. J. Quantum Chem.* 4S, 251 (1971).
- [25] O. Goscinski and E. Brändas: "Padé Approximants to Physical Properties via Inner Projections" *Int. J. Quantum Chem.* 5, 131 (1971); Erratum: 7, 133 (1973).
- [26] O. Goscinski: "Physical Properties of Many-Electron Systems. A Study of Approximation Methods with Emphasis on Perturbation Theory" Inaugural Dissertation; *Acta Univ. Upsal.* 162. (1970).
- [27] O. Goscinski and B. Lukman: "Moment-Conserving Decoupling of Green Functions via Padé Approximants" *Chem. Phys. Lett.* 7, 573 (1970).
- [28] O. Goscinski: "Density of States in Narrow Energy Bands" *Chem. Phys. Lett.* 9, 293 (1971).
- [29] P.-O. Löwdin and O. Goscinski: "Treatment of Constant of Motion, Degeneracies and Symmetry Properties by Means of Multi-Dimensional Partitioning" *Int. J. Quantum Chem.* 5, 685 (1971).
- [30] E. Brändas and O. Goscinski: "Darboux Functions and Power Series Expansions with Examples from Isoelectronic Sequences" *Int. J. Quantum Chem.* 6, 59 (1972).
- [31] O. Goscinski and O. Tapia: "Predissociation by Rotation and Long-Range Interactions" *Mol. Phys.* 24, 647 (1972).
- [32] O. Goscinski: "Outer Vibrational Turning Points Near Dissociation in the State B of and " *Mol. Phys.* 2A, 655 (1972).
- [33] B. T. Pickup and O. Goscinski: "Direct Calculation of Ionization Energies" *Mol. Phys.* 26, 1013 (1973).
- [34] O. Goscinski, B. T. Pickup and G. Purvis: "Direct Calculation of Ionization Energies. II. Transition Operator for the Method" *Chem. Phys. Lett.* 22, 167 (1973).
- [35] R. Ahlberg and O. Goscinski: "Atomic Polarizabilities and Shielding Factors with a Local Linear Response Method" *J. Phys. B* 6, 2254 (1973).
- [36] P. G. Ellis and O. Goscinski: "Transition State Calculations of Oscillator Strengths in the Local Exchange Approximation" *Physica Scripta* 9, 104 (1974).
- [37] R. Ahlberg and O. Goscinski: "Van der Waals Constants" *J. Phys. B* 7, 1194 (1974).
- [38] J. A. Fornes and O. Goscinski: "Long Wavelength Electromagnetic Fluctuating Interactions between Macroscopic Bodies" *J. Chem. Phys.* 61, 2660 (1974).
- [39] O. Goscinski, G. Howat and T. Åberg: "On Transition Energies and Probabilities by a Transition Operator Method" *J. Phys.* B8, 11 (1975).
- [40] G. Howat, O. Goscinski and T. Åberg: "K X-ray and Auger Electron Energies for Ne by a Transition Operator Method" *Physica Fennica* 9, SI, 241 (1974).
- [41] O. Tapia and O. Goscinski: "Self-Consistent Reaction Field Theory of Solvent Effects" *Mol. Phys.* 29, 1653 (1975).
- [42] G. Howat and O. Goscinski: "Relaxation Effects on ESCA Chemical Shifts by a Transition Potential Model" *Chem. Phys. Lett.* 30, 87 (1975).
- [43] R. Ahlberg and O. Goscinski: "On the Optimization of Local Linear Response Calculations of Atomic Properties" *J. Phys. B* 8, 2149 (1975).
- [44] H. Niemeyer, O. Goscinski and P. Ahlberg: "Bifunctional and Monofunctional Catalyses in the CNDO/2 Approximation: Formamidine Acid-base and Base Catalyzed 1,3-Proton Transfers in Propene" *Tetrahedron* 31, 1699 (1975).
- [45] O. Goscinski, M. Hehenberger, B. Roos and P. Siegbahn: "Transition Operators for Molecular Calculations: Ionization in Water and Furan" *Chem. Phys. Lett.* 33, 427 (1975).

- [46] O. Goscinski and B. T. Pickup: "Generalized Overlap Amplitudes and Transition Spin Orbitals" *Chem. Phys. Lett.* 33, 265 (1975).
- [47] O. Goscinski: "On Transition Operators for Describing Ionization and Excitation" *Int. J. Quantum Chem.* S9, 221 (1975).
- [48] M. Berrondo and O. Goscinski: "The Energy as a Functional of the Density Matrix" *Int. J. Quantum Chem.* S9, 67 (1975).
- [49] H. Siegbahn, R. Medeiros and O. Goscinski: "Direct Calculation of Core Electron Ionization and Relaxation Energies Using Transition Potentials Applications to Boron Compounds" *J. Electron Spectroscopy* Q8, 149 (1976).
- [50] H. Siegbahn and O. Goscinski: "Transition Potentials for Auger Electron Spectroscopy" (*Physica Scripta* 13, 225 (1976).
- [51] O. Goscinski: "Bonding Character of Inner-Shell Orbitals in Diatomic Molecules" (*Quantum Science – Methods and Structure*, Eds. J.-L. Calais et al., Plenum Press 1976, p. 427).
- [52] G. Howat, M. Trsic and O. Goscinski: "Geometric Approximation for Molecular Polarizabilities" *Int. J. Quantum Chem.* 11, 283 (1977).
- [53] G. Howat, T. Åberg and O. Goscinski: "Orbital Non-orthogonality and the Wentzel Ansatz" (*Abstr. 2nd Int. Conf. In Shell Ioniz. Phenomena*, Freiburg 1976, p. 126).
- [54] O. Goscinski and A. Palma: "Relaxation' Effects Accompanying Core Ionization in Diatomic Molecules" *Chem. Phys. Letters* 47, 322 (1977).
- [55] G. Howat, T. Åberg and O. Goscinski: "Effects of Relaxation and Continuum Interaction on the Ne KLL Auger Spectrum" (*Extended Abstracts, NBS X-Ray Spectra*, Gaithersburg 1976, p. 35).
- [56] L. Asplund, P. Kelfve, H. Siegbahn, O. Goscinski, H. Fellner-Feldegg, K. Hamrin, B. Blomster and K. Siegbahn: "Chemical Shift of Auger-Electron lines and Electron Binding Energies in Free Molecules. Sulphur Compounds. I" *Chem. Phys. Letters* 40, 353 (1976).
- [57] G. Howat, T. Åberg, O. Goscinski, C. S. Soong, C. P. Bhalla and M. Ahmed: "Effects of Interchannel Interaction on the Ne KLL Auger Electron Spectrum" *Phys. Letters* 60A, 404 (1977).
- [58] G. Howat, T. Åberg and O. Goscinski: "Relaxation and Final State Channel Mixing in the Auger Effect" *J. Phys. B* 11, 1575 (1978).
- [59] A. Calles and O. Goscinski: "The Use of Green Functions for the Calculation of the Dynamic Jahn-Teller Effect in Electron Spin Resonance Spectra" *Rev. Mexicana de Fisica* 26, 23 (1979).
- [60] O. Goscinski and H. Siegbahn: "Equivalent-Cores and Transition Potentials for ESCA and Auger Electron Spectra" *Chem. Phys. Letters* 48, 568 (1977).
- [61] A. Palma, E. Poulain, U. Wahlgren and O. Goscinski: "Vibrational Structure in Inner-Shell Ionization of CO Calculated with the Sudden Approximation" *Chem. Phys. Letters* 62, 368 (1979).
- [62] R. L. Lozes, O. Goscinski and U. Wahlgren: "Core Hole Localization in" *Chem. Phys. Letters* 63, 77 (1979).
- [63] A. Palma and O. Goscinski: "ESCA Peak Intensities in Water in the Sudden Approximation" *Chem. Phys. Letters* 63, 72 (1979).
- [64] O. Goscinski and A. Palma: "Electron and Nuclear Density Matrices and the Separation or Electronic and Nuclear Motion" *Int. J. Quantum Chem.* 15, 197 (1979).
- [65] S. Canuto and O. Goscinski: "Stationarity of Resonant Pole Trajectories in Complex Scaling" *Int. J. Quantum Chem.* 14, 383 (1978).
- [66] G. Howat, M. Trsic and O. Goscinski: "Differential Scaling of Orbitals and the Geometric Approximation for Molecular Polarizabilities" *Int. J. Quantum Chem.* 12, 963 (1977).
- [67] O. Goscinski: "Conjugate Eigenvalue Problems and the Theory of Upper and Lower Bounds" (Preprint No. 217, June 17, 1968).

- [68] B. Weiner and O. Goscinski: "The Fundamentals of Propagator Approximations and the GNS Construction" *Int. J. Quantum Chem.* 12 (Suppl. 1), 299 (1977).
- [69] O. Goscinski, J. Müller, E. Poulain and H. Siegbahn: "Fluorine Core ESCA Line-widths in and" *Chem. Phys. Letters* 55, 407 (1978).
- [70] E. Sanhueza, O. Goscinski and P. Ahlberg: "Concerted Transfer of Two Protons in the Formic Acid Dimer" (Preprint 1978).
- [71] S. Canuto and O. Goscinski: "On the Continuum Contribution to Atomic Polarizabilities" *Int. J. Quantum Chem.* 16, 985 (1979).
- [72] B. Weiner and O. Goscinski: "Theory of Propagator Approximations (I)" (Preprint 1979).
- [73] M. Berrondo and O. Goscinski: "Local Exchange Potential for Atomic Systems" *Chem. Phys. Letters* 62, 31 (1979).
- [74] M. Berrondo, J. P. Daudey and O. Goscinski: "Effective One-Body Hamiltonian for Electrons in Atoms" *Chem. Phys. Letters* 62, 34 (1979).
- [75] J. Müller, E. Poulain, O. Goscinski and L. Karlsson: "Role of Symmetry Restrictions on Valence Electron Binding Energies of and" *Chem. Phys.* 72, 2587 (1980).
- [76] J. Müller, H. Ågren and O. Goscinski: "Role of Localization in The Prediction of Core ESCA Line Shapes of, and NO" *Chem. Phys.* 38, 349 (1979).
- [77] P. Kelfve, B. Blomster, H. Siegbahn, K. Siegbahn, E. Sanhueza and O. Goscinski: "Chemical Shifts of Auger Electron Lines and Electron Binding Energies in Free Molecules. Silicon Compounds" *Physica Scripta* 21, 75 (1980).
- [78] O. Goscinski and B. Weiner: "The Role of Algebraic formulations of Approximate Green's Functions for Systems with a Finite Number of Electrons" *Physica Scripta* 21, 385 (1980).
- [79] B. Weiner and O. Goscinski: "The Self-Consistent Approximation to the Polarization Propagator" *Int. J. Quantum Chem.* 18, 1109 (1980).
- [80] S. Canuto, O. Goscinski and M. Zerner: "Broken Orbital Symmetry of Low-Lying Excited and Core-ionized States of Pyrazine" *Chem. Phys. Letters* 68, 232 (1979).
- [81] B. Weiner and O. Goscinski: "Calculation of Optimal Generalized Antisymmetric Geminal Power Functions (projected-BCS) and their Associated Excitation Spectrum" *Phys. Rev.* 22, 2374 (1980).
- [82] O. Goscinski: "Some Recent Advances in the Use of Propagator Methods in Quantum Chemistry. From MO to AGP" (in "Horizons of Quantum Chemistry" K. Fukui, B. Pullman, Eds., D. Reidel, Dordrecht 1980, p. 17).
- [83] S. Canuto, J.-L. Calais and O. Goscinski: "Alternating Polarity and Friedel Oscillations" *J. Phys.* B14, 1409 (1981).
- [84] A. Palma, E. Gonzalez and O. Goscinski: "ESCA Peak Intensities for Small Molecules in the Sudden Approximation" (*Proc. III ICQC. Int. J. Quantum Chem.* 18, 237 (1980)).
- [85] M. Berrondo and O. Goscinski: "The Coulomb Hole and the Correlation Energy for the Electron Gas at Intermediate Densities" *Chem. Phys. Letters* 81, 75 (1981).
- [86] S. Canuto and O. Goscinski: "Comments on Localized and Delocalized States in the Valence Region of Pyrazine" (Preprint 1981).
- [87] E. Sangfelft, O. Goscinski and J.-L. Calais: "Electronegativities and Transition Densities in the Theory of Metal-Semiconductor Interfaces" *Physica Scripta* 24, 461 (1981).
- [88] B. Weiner and O. Goscinski: "Superoperator Approach to Propagator Approximations" *Int. J. Quantum Chem.* 21, 369 (1982).
- [89] O. Goscinski and F. A. Matsen: "The Pair Ansatz" (Preprint 1982).
- [90] T. Åberg and O. Goscinski: "Information Theoretical Interpretation of Level Populations and Charge Distribution in Beam Foil Spectroscopy" *Phys. Rev. A*, 24, 801 (1981).
- [91] O. Goscinski: "Some Properties of Density Matrices, Correlated and Uncorrelated, for Pure and Mixed States" *Int. J. Quantum Chem.* 21, 269 (1982).

- [92] E. Sangfelt, O. Goscinski, N. Elander and H. A. Kurtz: "An Analysis of AGP and the Projected AGP Wavefunction" Int. J. Quantum Chem. Symp. 15, 133 (1981).
- [93] H. A. Kurtz, N. Elander, O. Goscinski and E. Sangfelt: "On the Energy Optimization of the AGP Wavefunction. The Ground State of the Be Atom" Int. J. Quantum Chem. Symp. 15, 143 (1981).
- [94] B. Weiner and O. Goscinski: "Excitation Operators Associated with Antisymmetrized Geminal Power (AGP) States" Phys. Rev. 27, 57 (1982).
- [95] O. Goscinski and B. Weiner: "The Excitation Spectrum Associated with a Generalized Antisymmetrized Geminal Power Ground State" Phys Rev. A25, 650 (1982).
- [96] O. Goscinski, B. Weiner and N. Elander: "Oscillator Strength Anomalies as Described by the AGP Model" J. Chem. Phys. 77, 2445 (1982).
- [97] B. Blomster, H. Siegbahn, J. E. Sanhueza, and O. Goscinski: "Chemical Shifts of Auger Electron Lines and Electron Binding Energies in Free Molecules. Phosphorus, Sulfur and Chlorine Compounds" (Preprint 1982).
- [98] J.-L. Calais, O. Goscinski, and E. Poulain: "Angular Distribution of Photo Electrons from Surfaces" (Preprint 1982).
- [99] O. Goscinski and O. Sinanoglu: "Lower Bounds to the Pair Correlations of Atoms and Molecules" (Preprint 1982).
- [100] O. Goscinski: "Antisymmetrized-Geminal Power (AGP) Wave functions and Correlation in Finite and Extended Systems" Int. J. Quantum Chem. Symp. 16, 591 (1982).
- [101] O. Goscinski, T. Åberg and M. Peltonen: "Stochastic Analysis of Charge Distributions in Heavy Ion-Atom Collisions" Phys. Letters 90A, 464 (1982).
- [102] O. Goscinski: "Vad är kvantkemi" Upsala Nya Tidning (7 oktober 1978).
- [103] P. Ahlberg och O. Goscinski: "Varför sker kemiska reaction?" Elementa 64, 168 (1981); (Upsala Nya Tidning 20 oktober, 1981).
- [104] M. B. Huang, O. Goscinski, G. Jonsäll and P. Ahlberg: "Studies of; Potential Energy Surface Studied by MINDO/3 and *ab initio* SCF (STO-3G) Calculations" J. Chem. Soc. Perkin Trans. II, 305 (1983).
- [105] T. Åberg and O. Goscinski: "Information Theoretical Description of Heavy -Ion Atom Collisions" (X-82 Conference, AIP Conference Proceedings Series, vol. 1, p. 570 (1982).
- [106] M. Mishra, O. Goscinski and Y. Öhrn: "Numerical Study of the Bivariational SCF Method as a Zeroth Order Dilated Electron Propagator" J. Chem. Phys. 79, 5494 (1983).
- [107] M. Mishra, O. Goscinski and Y. Öhrn: "Application of the Second Order Dilated Electron Propagator to the Treatment of Auger and Shape Resonances of Be" J. Chem. Phys. 79, 5505 (1985).
- [108] M. Mishra, H. A. Kurtz, O. Goscinski and Y. Öhrn: "Treatment of Resonances with the Dilated Electron Propagator: The 2P Shape Resonance in e-Mg Scattering" J. Chem. Phys. 79, 1896 (1983).
- [109] N. Elander, E. Sangfelt, H. A. Kurtz and O. Goscinski: "Applications of AGP Wavefunctions to the Ground State of and" Int. J. Quantum Chem. 23, 1047 (1983).
- [110] P. Froelich, O. Goscinski, U. Gelius and K. Helenelund: "Photon Induced Post Collisional Auger Decay. A Two Potential Complex Coordinate Formalism" J. Phys. B, 17, 979 (1984).
- [111] T. Åberg, A. Blomberg and O. Goscinski: "Stochastic Analysis of Ion-Atom Collision Processes; Electronic and Atomic Collisions" (J. Eichler et al. Eds. Elsevier Science Publ. B. V., p. 215, North Holland, Amsterdam 1984).
- [112] M. Bao Huang, O. Goscinski, G. Jonsäll and P. Ahlberg: "The Potential Energy Surface Studied by MINDO/3 MINDO and *ab initio*-SCF (STO-3G) Calculations" J. Chem. Soc. Perkin Trans. II, 1327 (1984).

- [113] E. Sangfelt, H. A. Kurtz, N. Elander and O. Goscinski: "Excited States via the AGP Polarization Propagator I. Application to" J. Chem. Phys. 81, 3976 (1984).
- [114] E. Sangfelt and O. Goscinski: "A Generalization of the AGP Model Propagator to a Reference State Including Different Geminals" J. Chem. Phys. 82, 4187 (1985).
- [115] V. Mujica, O. Goscinski and E. Sangfelt: "Electron Correlation in Doubly Excited States of Helium and Extensions to Beryllium and Magnesium." Chem. Phys. 87, 473 (1984).
- [116] T. Åberg, A. Blomberg, J. Tulkki and O. Goscinski: "Maximum Entropy Theory of Recoil-Charge Distributions in Electron Capture Collisions" Phys. Rev. Letters 52, 1207 (1984).
- [117] V. Mujica, N. Correia and O. Goscinski: "Fermion Propagator Calculations of Excitations in Polyenes Using a Heisenberg (XYZ) Hamiltonian I. Formalism and Parametrization" Phys. Rev. B 32, 4178 (1985).
- [118] V. Mujica, N. Correia and O. Goscinski: "Fermion-Propagator Calculations of Excitations in Polyenes Using a Heisenberg (XYZ) Hamiltonian II. Applications to Large Systems" Phys. Rev. B 32, 4186 (1985).
- [119] N. Correia and O. Goscinski: "Excitations Energies of Rectangular Cyclobutadiene via the GAGP/Propagator method" (Preprint 1985).
- [120] P. Froelich, O. Goscinski, U. Gelius and K. Helenelund: "Electron Impact Induced Post-Collisional Auger Decay Two Potential Complex Coordinate Treatment II" J. Phys. B19, 387 (1986).
- [121] K. Helenelund, U. Gelius, P. Froelich, O. Goscinski: "Photon Induced Post-Collisional Auger Decay: A Modified 'Shake-Down' Model" J. Phys. B19, 379 (1986).
- [122] K. Helenelund, S. Hedman, L. Asplund, U. Gelius, K. Siegbahn, P. Froelich and O. Goscinski: "Post-Collision Interaction in the Photo-Excited Electron Spectrum of Selenium" (Preprint 1986).
- [123] N. Moiseyev and O. Goscinski: "Effective Potentials and the Gel'fand- Levitan Equation" Chem. Phys. Letters 120, 520 (1985).
- [124] P. Froelich, O. Goscinski and N. Moiseyev: "Resonances from the Complex Dilated Hamiltonians in Dilation-Adapted Basis Set with a New Stabilization Parameter" J. Chem. Phys. 84, 3931 (1985).
- [125] N. Moiseyev, R. Schatzberger, P. Froelich and O. Goscinski: "Study of Mode Specificity by the Natural Expansion Analysis" J. Chem. Phys. 83, 3924 (1985).
- [126] O. Goscinski: "Are Localized Broken Symmetry Solutions Acceptable in Molecular Calculations?" Int. J. Quantum Chem., Symp. Vol. 19, 51 (1986).
- [127] O. Goscinski: "Kvantkemiska Tunnlar och Genombrott" (NFR Årsbok 1985).
- [128] O. Goscinski and V. Mujica: "Adiabatic Coordinate Separation and Large N-Dimensional Limit in Two-Electron Ions" Int. J. Quantum Chem., 29, 897 (1986).
- [129] A. Blomberg, T. Åberg and O. Goscinski: "Stochastic Theory of Equilibrium Charge-state Distributions of Heavy Ions in Gases" J. Phys. B 19, 1063 (1986).
- [130] O. Goscinski and V. Mujica: "Adiabatic Separation, Broken Symmetries and Geometry Optimization" R. M. Erdahl and V. H. Smith Eds., "Density Matrices and Density Functionals" D. Reidel, 597 (1987).
- [131] V. Mujica, Li Yin and O. Goscinski: "Dynamic Coordinate Separation and State-Dependent Potentials. An Analysis of Localization in Helium" Chem. Phys. 112, 159 (1987).
- [132] M. A. Natiello, A. R. Engelmann and O. Goscinski: "A New Treatment of Coupled Channel Resonances Applied to the Study of He-like Ions" (Preprint 1989).
- [133] B. T. Pickup and O. Goscinski: "Ionization and Excitation Phenomena Using a Valence Bond Reference Function" Preprint (1989).
- [134] O. Goscinski and J. Delhalle: "Hyperpolarizability Approximations" Int. J. Quantum Chem. 35, 761 (1989).

- [135] Li Yin and O. Goscinski: "Non Adiabaticity in Terms of Dynamic Potentials. An Analysis in Terms of Linear $E \times e$ Vibronic States" *Chem. Phys.* 137, 67 (1989).
- [136] Li Yin and O. Goscinski: "Differentiability of Degenerate Electronic Wavefunctions with Respect to Parametric Variables" *Int. J. Quantum Chem.* 37, 249 (1990).
- [137] Li Yin and O. Goscinski: "Separation of Slow Motion in $E \times e$ Vibronic States" *Chem. Phys.* 140, 363 (1990).
- [138] M. Springborg, J.-L. Calais, O. Goscinski and L. Eriksson: "A Density-Functional Study of Undoped and Doped Trans-Polyacetylene" *Synthetic Metals* 41, 3309 (1991).
- [139] M. Springborg, Jean-Louis Calais, O. Goscinski and L. A. Eriksson: "LMTO Method for Helical Polymers: A Detailed Study of Trans-Polyacetylene" *Phys. Rev.* 44, 12 713 (1991).
- [140] L. Eriksson and O. Goscinski: "Charge-Transfer Processes in Bipyrazine and Bi-(N-Methylpyridine): A Semiempirical MO Study" *Mol. Engineering* 2, 1 (1992).
- [141] H. O. Karlsson and O. Goscinski: "Perturbed Hydrogenic Manifolds Studied by the Recursive Residue Generation Method" *J. Phys. B* 25, 106 (1992).
- [142] H. O. Karlsson and O. Goscinski: "A Direct Recursive Residue Generation Method. Application to the Photoionization of Hydrogen in Static Electric Fields" *J. Phys. B* 27, 1061 (1994).
- [143] Yngve Öhrn and O. Goscinski: "Analysis of the Thouless Coherent State Using the $1/K$ Expansion" *Phys. Rev. A* 48, 1093 (1993).
- [144] D. R. Herschbach, J. Avery and O. Goscinski, Eds.: "Dimensional Scaling in Chemical Physics" Kluwer Academic Pub (1993).
- [145] L. Hägg and O. Goscinski in *Dimensional Scaling in Chemical Physics: "Dimensional Scaling and Spectral Properties"* D. R. Herschbach, J. Avery and O. Goscinski, Eds. Kluwer Academic Pub. p. 313 (1993).
- [146] O. Goscinski and L. Hägg: "Dimensional Scaling of Local Pseudopotentials" *J. Mol. Struct.* 287, 17 (1993).
- [147] L. Hägg and O. Goscinski: "Maximum Entropy and Equilibrium Charge State Distributions" *J. Phys. B* 26, 2345 (1993).
- [148] L. Hägg and O. Goscinski: "Gaussian Approximations to Equilibrium Charge-State Distributions with the Maximum Entropy Method" *J. Phys. B* 27, 81 (1994).
- [149] E. Sjöqvist and O. Goscinski: "The Molecular Aharonov-Bohm effect in Bound States Beyond the Adiabatic Approximation" *Chem. Phys.* 186, 17 (1994).
- [150] L. Eriksson, N. Salhi-Benachou and O. Goscinski: "Symmetry Breaking in Charge-Transfer Compounds. The Effects of Electric Fields and Substituents on the Properties of Bipyrazine Cations" *Mol. Eng.* 4, 339 (1995).
- [151] H. O. Karlsson and O. Goscinski: "Autocorrelation Functions in the Photoionization of Hydrogen in Electric and Magnetic Fields" *Phys. Rev. A* 51, 1154 (1995).
- [152] O. Goscinski and L. Hägg: "The Maximum Entropy Method and Relaxation in Collision Processes" *Int. J. Quantum Chem.* 58, 689 (1996).
- [153] H. O. Karlsson, G. L. Bendazzoli, O. Goscinski and S. Evangelisti: "Density-of-States of Alternant Cyclic Polyenes (CH) $_N$ in the PPP Approximation by a Direct Lanczos Method" *Int. J. Quantum Chem.* 63, 725 (1997).
- [154] O. Goscinski, Mikael Jondal, Claes Sandgren and Per-Johan Svenningsson: "Costa Rica: Science and Technology Program" Inter-American Development Bank PPR-7/97 October 1997.
- [155] O. Goscinski, Mikael Jondal, Claes Sandgren and Per-Johan Svenningsson: "Uruguay: Science and Technology Program" Inter-American Development Bank PPR-8/97 October 1997.
- [156] O. Goscinski, Mikael Jondal, Claes Sandgren and Per-Johan Svenningsson: "Chile: Science and Technology Program" Inter-American Development Bank PPR-9/97 October 1997.

- [157] O. Goscinski, Mikael Jondal, Claes Sandgren and Per-Johan Svenningsson: "Evaluation of IDB's Science and Technology Programs in Chile, Costa Rica and Uruguay Final Report" Inter-American Development Bank WP-6/98 March 1998.
- [158] M. Ericsson, E. Sjöqvist and O. Goscinski: "Degree of Electron-Nuclear Entanglement in the $E \otimes \epsilon$ Jahn-Teller System" Proceedings of Symposium Electron-Phonon Dynamics and Jahn-Teller-Effect, Eds, Bevilacqua et al. p. 20 World Scientific (1999).
- [159] H. Carlsen and O. Goscinski: "Dynamics of Particles for Circular Rydberg States" Phys. Rev. A 59, 1063 (1999).
- [160] L. M. Andersson, H. O. Karlsson, O. Goscinski, L.-E. Berg, M. Beutter and T. Hansson: "Vibrational Wave Packet Dynamics in NaK: The A State" Chem. Phys. 241 43 (1999).
- [161] H. Carlsen, E. Sjöqvist and O. Goscinski: "Quantal Trajectories for Adiabatic and Nonadiabatic Regimes of Vibronic Systems" Int. J. Quantum Chem. 75, 409 (1999).
- [162] O. Goscinski: "Calculation of dispersion energy shifts in molecular electronic spectra using sum rules" Int. J. Quantum Chem. 81, 202 (2001).
- [163] H. O. Karlsson and O. Goscinski "Correlation Functions and Thermal Rate Constants" J. Phys. Chem. 105, 2599 (2001).
- [164] M. Andersson, F. Burmeister, H. O. Karlsson, and O. Goscinski: "Nonadiabatic effects in the photoelectron spectra of HCl and DCL. II. Theory" Phys. Rev. 65, 12705 (2002).
- [165] M. Mujica, M. A. Ratner and O. Goscinski: "Partitioning technique and transport across molecular interfaces: Many-body effects" Int. J. Quantum Chem. 90, 14 (2002).
- [166] L. M. Andersson, J. Åberg, H. O. Karlsson and O. Goscinski "Properties of a discretized coherent state representation and the relation to Gabor analysis" J. Phys. A Math. Gen. 35, 7787 (2002).
- [167] F. Burmeister, L. M. Andersson, G. Örwall, T. Richter, P. Zimmerman, K. Godehusen, M. Martins, H. O. Karlsson, S. L. Sorensen, O. Björneholm, R. Feifel, K. Wiesner, O. Goscinski, L. Karlsson, S. Svensson and A. J. Yencha: "A Study of the Inner Valence Ionization Region in HCl and DCL" J. Phys. B (2004).
- [168] O. Goscinski: "Conjugate Eigenvalue Problems and Generalized Sturmians" Adv. Quantum Chem. 41, 51 (2002).
- [169] John Avery, James Avery and Osvaldo Goscinski "Natural Orbitals from Generalized Sturmian Calculations" Adv. Quantum Chem. 43, 207 (2003).

Development of Chiral Catalysts for Stereoselective Synthesis by Deprotonations – Experimentation in Interplay with Computational Chemistry

Sten O. Nilsson Lill, Peter Dinér, Daniel Pettersen,
Mohamed Amedjkouh and Per Ahlberg

Department of Chemistry, Göteborg University, SE-412 96 Göteborg, Sweden

A tribute to Osvaldo Goscinski on the occasion of his 65th birthday

Abstract

Results are presented advancing the application of quantum chemistry in the field of organic synthesis. Computational chemistry in interplay with experimental chemistry has been given a key role in the development of stereoselective synthesis. Novel molecular systems are being created for catalytic stereoselective deprotonations, a reaction type useful for synthesizing many new compounds, e.g., some having important biological activities. Problems met in this approach to design catalysts and their solutions are presented.

Contents

1. Preamble	1
2. Introduction	3
3. Chiral lithium amides	5
4. Activated complexes in the epoxide deprotonations	7
5. Computational and experimental stereoselectivity	9
6. Origin of stereoselectivity	13
7. Search for more stereoselective chiral lithium amides	14
8. Catalytic stereoselective deprotonations	16
Acknowledgements	21
References	21

1. PREAMBLE

A light rain was falling when we left the glaciology station in the Tarfala valley one early August morning in the 1960s for an ascent of

Kaskasapakte. Later on the ridge we had difficulties finding our route. At midnight we reached the summit in super-cooled rain. The rock was icy and Osvaldo, our leader Per-Olov Löwdin and the rest of us returned hungry to the station in the crisp morning, when Kebnekaise just started to become enlightened as the sun was rising. It all happened after a few tough days with group theory at the summer school on quantum chemistry held in Abisko. Experiences like these result in special friendships and prepare you for coping with future challenges in life.

‘Kvantkem’ in Uppsala, for a young student like myself (P.A.), was a rich and exciting international academic environment. A major contributor was the broadminded young docent Osvaldo Goscinski with his brilliant intellect and warm personality. During the coffee breaks at Ofvandahl’s, most aspects of life, including those outside quantum chemistry and university politics, were discussed in the circle of the ‘old’ quantum chemists; Jean-Louis Calais, Karl-Fredrik Berggren (inventor of ‘toppolja’¹ and not so old at that time), Jan Linderberg and Yngve Öhrn among others.

In the mid-1960s, Löwdin extensively used projection operators in his method development and this was also the theme of most of his elegant lectures. Accurate predictive tools were not yet available but useful qualitative models for structure and reactivity were emerging. In the 1970s, significant progress had been made when Osvaldo and I cooperated on attempts to predict computationally concerted *vs.* stepwise two-proton transfers and the structure and rearrangement mechanisms of the elusive (CH)₉⁺ barbaralyl cation, which rapidly exchanges all its CH-groups at –160 °C [1–3].

The development during the last decades has been breathtaking and today physical organic chemists like my co-authors and myself have access to useful quantitative computational chemistry tools for prediction of structures and reactivity on our desktops.

In this our tribute to Osvaldo we wish to indicate our appreciation of the results of the research that have emerged from the efforts of the quantum chemists. We have taken advantage of the dramatic development of computational chemistry to advance organic synthesis. Novel catalysts for deprotonations are created making use of an interplay of experimental and computational chemistry.

Dear Osvaldo, our best wishes and hopes that you now will get ample time for further developing your experimental creativity also – in the kitchen together with Gunilla. Ulli and I are most grateful for all the lovely memories that we are sharing with both of you.

¹ Per-Olov Löwdin, to treat his stomach during the mountain climbing expeditions, occasionally had an intake of liquid from a bottle. K.-F. B. and myself were curious about the content and got a taste. It was a terrible experience! Pelle revealed that the bottle contained a mixture of 10% gin (Gordon’s) and 90% vegetable oil. Upon returning to the camp Kalle got the privilege to renew the content. Next day our climb of Kaskasatjåkko went much more smoothly. Kalle’s mixture in Pelle’s bottle now contained 90% gin and 10% vegetable oil. Not only our stomachs showed ‘topp’ performance. Someone gave this student creation the name ‘toppolja’ (summit oil).

2. INTRODUCTION

Many of the compounds associated with living organisms are chiral, for example DNA, RNA, antibodies and hormones. Also enzymes are chiral, as are other receptors that play an important part in cell machinery. This means that they prefer to interact with one of the enantiomers (mirror images) of chiral compounds. In other words, the receptors are extremely selective; only one of the enantiomers fits the receptor's site like a hand in a glove. Since the two enantiomers of a chiral molecule often have totally different effects on cells, it is important to be able to produce each of the two forms in pure form.

Most drugs consist of chiral molecules and since a drug must match the receptors it should bind to itself in the cells, it is often only one of the enantiomers that is of interest. In certain cases the other form may even be harmful. This was the case, for example, with the drug Thalidomide (Neurosedyn), which in the 1960s was prescribed to pregnant women. One of the enantiomers of thalidomide helped against nausea, while the other one could cause foetal damage.

There are other less dramatic examples of how differently two enantiomers can affect our cells. *Limonene*, for example, is chiral but the two enantiomers can be difficult to distinguish at first glance (Fig. 1). The receptors in our nose are more sensitive. One form of limonene certainly smells of lemons but the other of oranges.

It is very important for industry and for our environment to be able to produce products as pure as possible. It is also important to be able to manufacture large quantities of a product. For this the use of catalysts is very important since a catalyst increases the rate of the reactions without being consumed itself.

During the past few decades there has been intensive research into developing methods for producing – synthesizing – one of the enantiomers rather than the other, i.e., stereoselective synthesis. In synthesis, starting molecules (substrate molecules) are used to build new molecules (products) by means of various chemical reactions. In this development, progress in

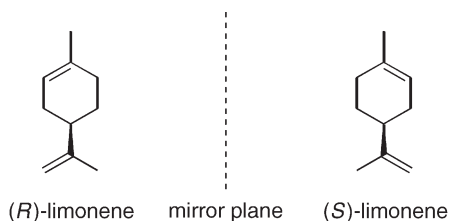
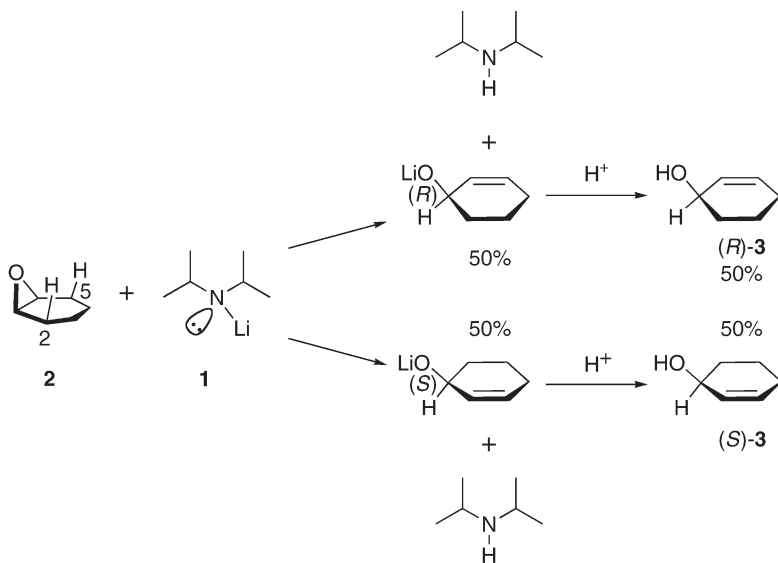


Fig. 1. (*R*)-limonene smells of oranges while its enantiomer (*S*)-limonene smells of lemons.

quantum chemistry as expressed in computational chemistry is playing an increasingly important role.

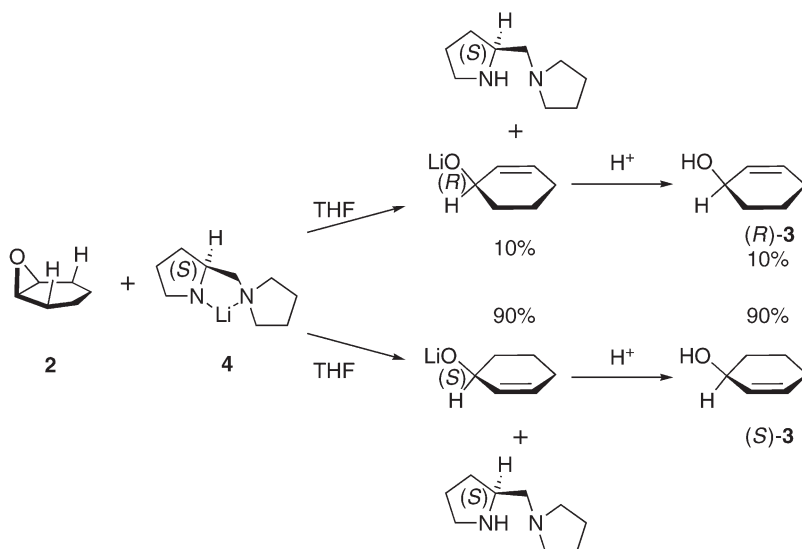
There is a need for highly reactive and highly stereoselective catalysts for deprotonations to be realized since many useful chiral compounds may be reached with such reactions. In this contribution some progress in the field is presented.

Lithium amides derived from secondary amines like lithium diisopropylamide (**1**) appear to be strong enough bases to deprotonate epoxides, ketones, etc. However, when **1**, which is a non-chiral base, deprotonates the non-chiral epoxide cyclohexene oxide (**2**), equal amounts of the two enantiomeric products (*S*)- and (*R*)-cyclohex-2-enol (**3**) are formed in the abstraction of a proton from carbon 2 and 5, respectively, with accompanying opening of the epoxide ring (Scheme 1). Thus, none of the two enantiomeric products is formed in enantiomeric excess (ee), i.e., the reaction shows no stereoselectivity (Scheme 1).



Scheme 1.

During the last decades, a number of chiral lithium amides have been developed for stereoselective deprotonation of, e.g., epoxides. For example, the lithium amide lithium (*S*)-2-(pyrrolidin-1-yl-methyl)pyrrolide (**4**) was for a long time the most stereoselective base used in epoxide deprotonations. It gives 90% of the (*S*)-enantiomer and 10% of the (*R*)-enantiomer upon deprotonation of cyclohexene oxide **2** in THF solution (Scheme 2) [4–6].

**Scheme 2.**

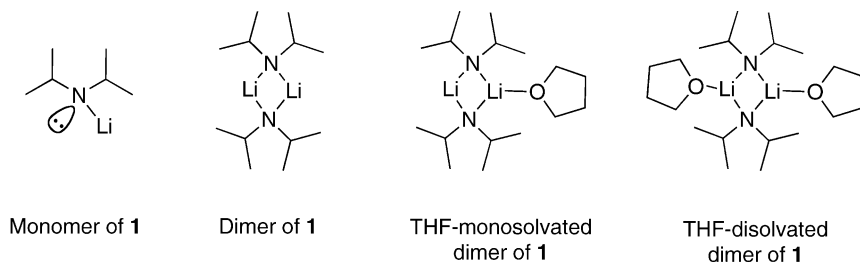
Until recently, progress in the field of stereoselective deprotonations had been achieved by trial and error since detailed knowledge about the nature of reagents and activated complexes was lacking. The structure of the chiral lithium amide was modified in the hope of achieving improved stereoselectivity and occasionally an increased stereoselectivity was obtained [7–13]. The development has been governed by the need for reactive lithium amides yielding stereoselectivities of close to 100%.

Our approach to this goal is rather rational in the sense that our design of chiral lithium amides is based upon a detailed understanding of the nature of the activated complexes involved. Such knowledge is obtained in the interplay of experimental and computational chemistry [6,14–25]. Experiments have been used to obtain both the compositions of the reactant chiral lithium amide and the activated complexes in solution and computational chemistry has been applied to obtain structures and energies. This has put us in a position to modify systematically the chiral lithium amide and to predict the stereoselectivity computationally. Selected lithium amides have been synthesized and investigated with respect to reactivity and stereoselectivity. Improved catalysts have been achieved.

3. CHIRAL LITHIUM AMIDES

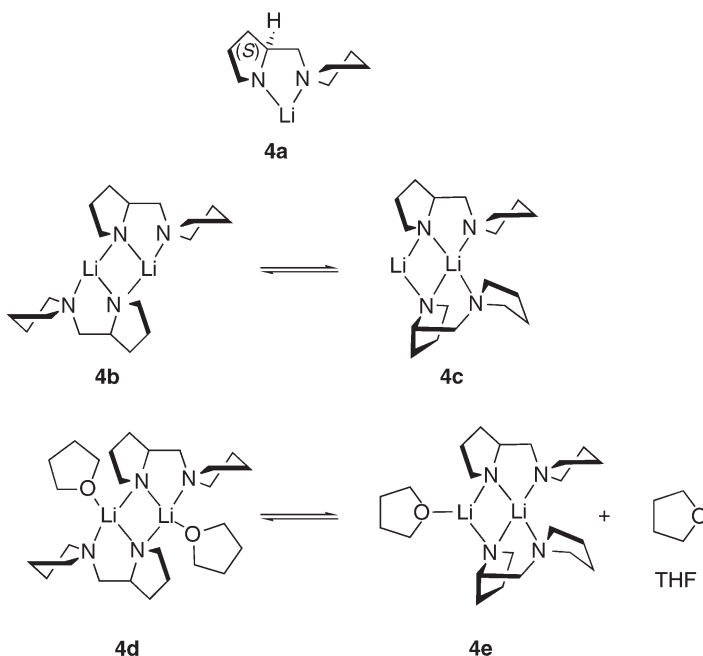
Lithium amides are strong dipoles since the bond between the nitrogen anion and the lithium cation is mainly ionic. Therefore, they are rarely

present as monomers in solution. Rather, they tend to aggregate to yield dimers or larger aggregates. This is true even in ethereal solvents like tetrahydrofuran (THF) or diethyl ether (DEE), which show coordination to lithium. For example, lithium amide **1** is a dimer in THF and is specifically solvated by THF molecules (Scheme 3) [26–28].



Scheme 3.

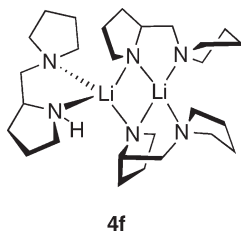
The chiral lithium amide **4** is also aggregated and results indicate that more than one type of aggregates of monomers (**4a**) is present in THF in dynamic equilibrium (cf. **4a–4e** in Scheme 4) [16,29]. A computational



Scheme 4.

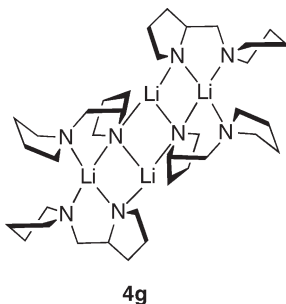
study at the B3LYP/6-31 + G(d)//B3LYP/SVP level of theory indicates that unsolvated (**4b** and **4c**) and THF-solvated dimers (**4d** and **4e**) are close in free energy [30].

In diethyl ether (DEE), compound **4** is found to be insoluble but dissolves upon addition of the diamine corresponding to **4**. NMR investigations have shown that diamine solvated dimer **4f** is formed (Scheme 5) [16].



Scheme 5.

Lithium amide **4** has been crystallized from toluene and X-ray crystallography has shown that the crystals are made up of tetramers of ladder type (**4g**) (Scheme 6) [31].



Scheme 6.

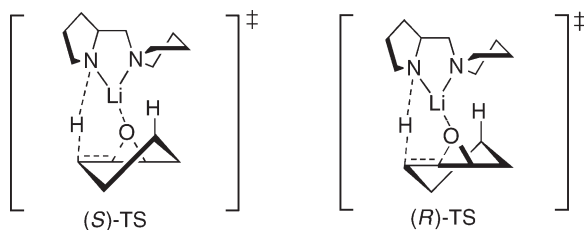
Altogether, these examples reveal the great complexity and diversity of the field of lithium amides making the combination of experimentation and computational chemistry extremely important.

4. ACTIVATED COMPLEXES IN THE EPOXIDE DEPROTONATIONS

Kinetics is capable of giving information about activated complexes (transition states (TSs)). In particular, reaction orders with respect to

the reagents involved inform us about the molecular composition of the activated complexes. However, a prerequisite for obtaining reaction orders is knowledge of the molecular composition of the reagents.

Thus, the determined composition of lithium amide **4** in the initial state in presence of excess of the corresponding diamine has been used in combination with kinetics to determine the composition of the activated complexes in cyclohexene oxide deprotonation. It appears that an activated complex is built from one lithium amide monomer and one epoxide molecule [18]. These results suggest that we are dealing with the TS structures (*S*)-TS and (*R*)-TS shown in Scheme 7 leading to the (*S*)- and (*R*)-enantiomer of the allylic alcohol **3**, respectively.



Scheme 7.

In the activated complexes shown, an electron lone pair on the amide nitrogen of the lithium amide is abstracting a β -proton from the epoxide, while the lithium is coordinating the other lone pair on the amide nitrogen and the pyrrolidine nitrogen besides the epoxide oxygen. Such TSs have previously been proposed by Asami [4,32].

The activated complexes are not enantiomers but rather diastereoisomers and therefore differ in free energy. It is this energy difference between activated complexes that yields the stereoselectivity of the deprotonation reaction. In Fig. 2, we illustrate how the free energy difference (ΔG) between the activated complexes affect the product composition, as given by percent (*S*)-product (%(*S*)-**3**).

A detailed computational study of possible activated complexes involved in the cyclohexene oxide deprotonations has been carried out [17,29,33]. Geometry optimizations of both specifically solvated and unsolvated activated complexes at various levels of theory ranging from PM3 to mPW1K/6-31 + G(d) have been carried out. In Figs 3 and 4 the optimized structures of the activated complexes with the latter theory are shown.

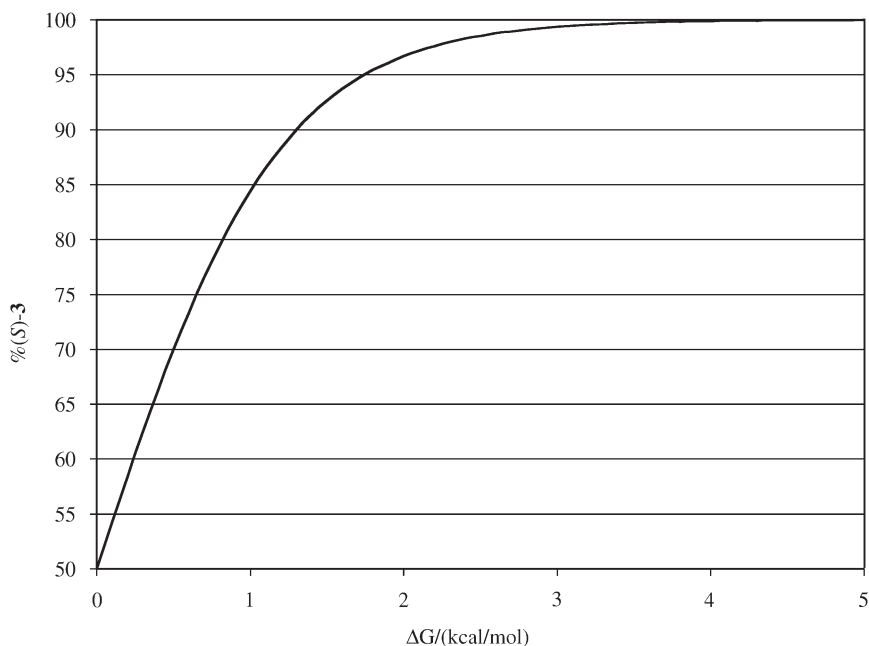


Fig. 2. Percent (*S*)-product (%(*S*)-**3**) as a function of the free energy difference (ΔG) at 298 K.

5. COMPUTATIONAL AND EXPERIMENTAL STEREOSELECTIVITY

From the experimentally obtained product composition in THF: 90% of (*S*)-**3** and 10% of (*R*)-**3**, a free energy difference (ΔG) between the two rate-limiting diastereoisomeric activated complexes of $1.33 \text{ kcal mol}^{-1}$ is calculated. In Table 1, energy differences and product compositions obtained by computational chemistry at various levels of theory are presented for activated complexes built from one molecule of epoxide **2**, monomeric or dimeric lithium amide **4** and no or one specifically solvating THF or DEE molecule.

It is interesting to note that all levels of theory predict the (*S*)-isomer as the major enantiomer product as found experimentally except with PM3//PM3. On this level of theory the unsolvated activated complex (*R*)-TS is favoured (entry 16). Also, at the B3LYP/6-31 + G(d)//PM3 level of theory the THF-solvated activated complex built from a dimer of lithium amide **4** yielding the (*R*)-isomer is favoured (entry 8). At most levels of theory the calculated ΔG values for the THF-solvated activated complexes are in closer agreement



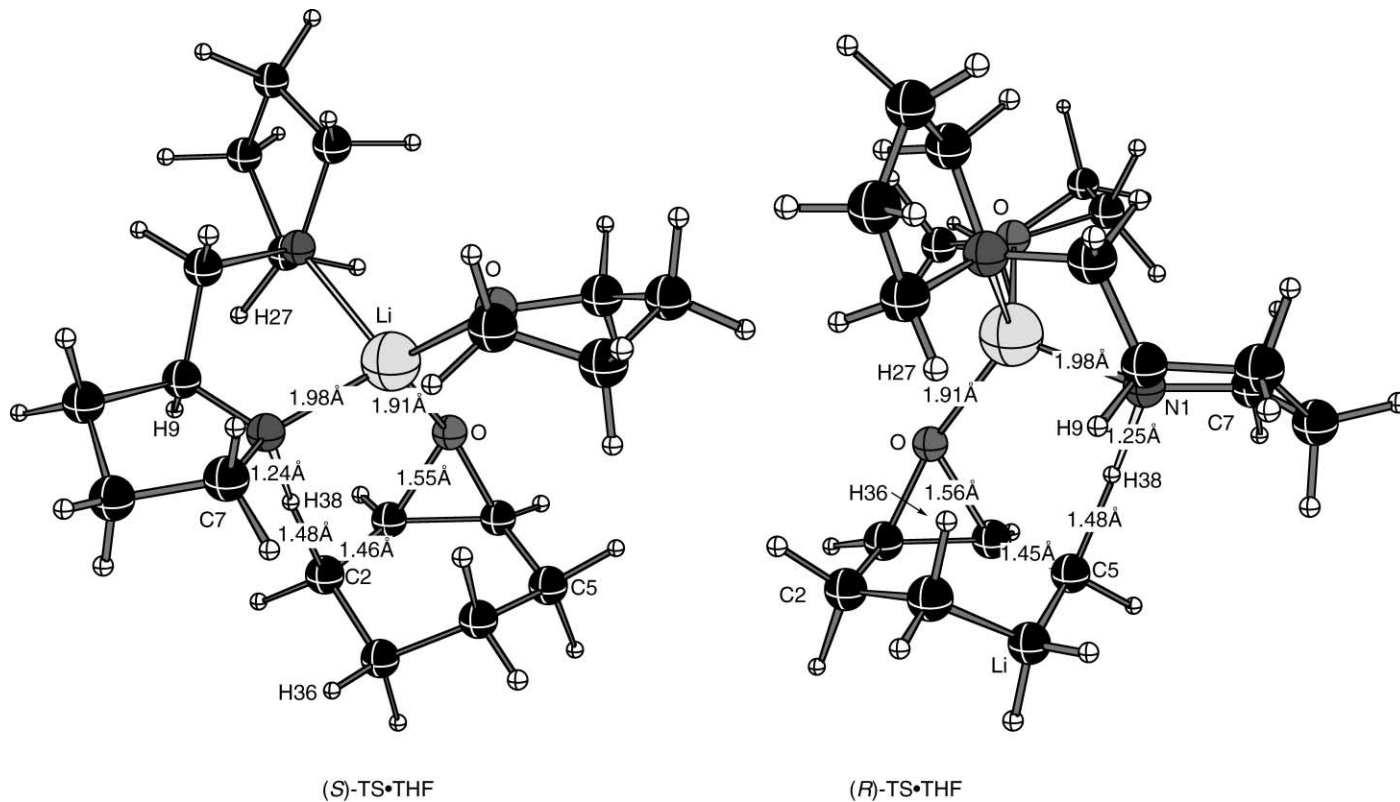


Fig. 4. mPW1K/6-31 + G(d) optimized THF-solvated diastereoisomeric TSs for deprotonation of **2** with lithium amide **4**.

Table 1. Calculated energy differences in kcal mol⁻¹ between diastereoisomeric activated complexes with the composition (4a)_x(2)₁(Solvent)₁, and percent (S)-3 in the mixture of enantiomeric products, together with experimental values

Entry	Computational method	<i>x</i>	Solvent ^{a,b}	Energy differences	%(<i>S</i>) _{Calc.} / <i>%</i> (<i>S</i>) _{Exp.} ^d
			Calc./Exp.	$\Delta G_{\text{Calc.}}^c / \Delta G_{\text{Exp.}}^d$	
1	mPW1K/6-31+G(d)//mPW1K/6-31+G(d)	1	THF/THF	1.43/1.33	92/90
2		1	None/Toluene	0.82/0.43	80/67.5
3	B3LYP/6-31+G(d)//B3LYP/6-31+G(d)	1	THF/THF	0.26/1.33	61/90
4		1	None/Toluene	0.60/0.43	73.5/67.5
5	B3LYP/6-31+G(d)//HF/3-21G	1	THF/THF	1.98/1.33	96.5/90
6		1	None/Toluene	0.83/0.43	80/67.5
				$\Delta E_{\text{Calc.}}^e / \Delta G_{\text{Exp.}}^d$	
7	B3LYP/6-31+G(d)//PM3 ^c	1	THF/THF	1.67/1.33	94.5/90
8		2	THF/THF	0.32/1.33	27/90
9		1	DEE/DEE	0.95/1.01	83.5/86.5
10		2	DEE/DEE	0.77/1.01	78.5/86.5
11		1	None/Toluene	0.73/0.43	77.5/67.5
12		2	None/Toluene	0.42/0.43	67/67.5
13	HF/3-21G//HF/3-21G	1	THF/THF	1.96/1.33	96.5/90
14		1	None/Toluene	0.81/0.43	79.5/67.5
				$\Delta H_{\text{Calc.}}^f / \Delta G_{\text{Exp.}}^d$	
15	PM3//PM3 ^f	1	THF/THF	0.27/1.33	61/90
16		1	None/Toluene	0.55/0.43	28.5/67.5

^a In DEE, it has experimentally been determined that *x* = 1 for lithium amide 4.

^b Activated complexes involved in lithium amide deprotonation of 2 have been determined to contain one molecule of 2.

^c Gibbs free energy difference between the two most stable TSs at 298 K.

^d At 293 K.

^e Potential energy difference between the two most stable TSs.

^f Heat of formation difference between the two most stable TSs.

with the experimentally measured value than those calculated for the unsolvated activated complexes. In particular, the results with the mPW1K-functional, which has been specially developed to model hydrogen transfers [34,35], yields a predicted value of 92% of the (*S*)-enantiomer (entry 1) in close agreement with the experimental value: 90% of (*S*)-**3** [33].

6. ORIGIN OF STEREOSELECTIVITY

In both the optimized unsolvated and mono-solvated activated complexes calculated using mPW1K/6-31 + G(d) (Figs 3 and 4) the proton is more than half-transferred from the carbon to the nitrogen, the carbon–oxygen bond of the epoxide ring is elongated and the carbon–carbon double bond is partially developed. But what interaction differences are causing the stereoselectivity? In the previously postulated activated complexes by Asami, repulsions between a hydrogen in the epoxide (H36) and a hydrogen in the pyrrolidine part (H27) of the lithium amide in (*R*)-TS were suggested to be the origin of the stereoselectivity [4,32]. However, our calculations show that this H–H-repulsion between the epoxide and the lithium amide is absent in the unsolvated (*R*)-TS. Such repulsion is only found in (*R*)-TS·THF and it is absent in the (*S*)-TSs [33]. We have also found that another interaction in (*R*)-TS·THF, between H36 and H9, is of similar magnitude as that found between H36 and H27.

A more detailed analysis of the calculated activated complexes indicates a different major origin of the stereoselectivity than that originally proposed. According to a detailed Natural Bond Orbital (NBO) analysis [33,36,37] of the mPW1K-optimized activated complexes, the major contribution to the calculated energy difference is from the delocalization of the ‘deprotonating’ lone pair on N1. Delocalization into the anti-bonding σ^* -orbital of the C2–H38 bond in (*S*)-TS·THF is more stabilizing than the corresponding delocalization into the anti-bonding orbital of the C5–H38 bond in (*R*)-TS·THF. Destabilizing 4e-interactions between the electron clouds of the bond between C5–H38 and that of the N1–C7 bond in the lithium amide part is larger in (*R*)-TS·THF than the corresponding repulsion (between C2–H38- and N1–C7-bonds) in the (*S*)-TS·THF is also of importance. This effect is, however, somewhat reduced by larger stabilizing 2e-hyperconjugative interactions between the N1–C7 bond and the anti-bonding σ^* -orbital of the C5–H38 bond in (*R*)-TS·THF than the corresponding interaction (N1–C7 and C2–H38) in (*S*)-TS·THF. Also, the destabilizing 4e-interaction between the ‘deprotonating’ lone pair and the bond between C2–H38 in (*S*)-TS·THF is observed to be larger compared with the corresponding interaction (between N1 and C5–H38) in (*R*)-TS·THF.

The developed model for the deprotonation activated complexes described above has been used as a starting point for structural modification of the lithium amide in order to increase the energy difference between the diastereomeric-activated complexes and thus the stereoselectivity. Computational chemistry has been used to predict the stereoselectivity with modified chiral lithium amides. Some of these designed novel lithium amides have been synthesized and investigated experimentally with respect to their stereoselectivity. One of these is the lithium amide **5** (shown in Scheme 8 as monomer **5a**) which, like the previously discussed lithium amides, appear to be a dimer (**5b** or **5c**) in THF solution as shown by multinuclear NMR spectroscopy and computational chemistry [19,38].



Amide **5** appears to be slightly less reactive than **4** in the deprotonation of **2** but as predicted the stereoselectivity was improved. The enantiomer composition of the deprotonation product was now 96.5% (*S*)-alcohol and 3.5% (*R*)-alcohol [19,22]. However, a kinetic investigation revealed that the composition of the activated complexes was different from that assumed in the theoretical model. The reaction orders showed that an activated complex is built from one molecule of chiral lithium amide dimer and one molecule of epoxide **2**. Such activated complexes have been computationally modelled by the use of PM3 and optimized structures are displayed in Fig. 5 [19].

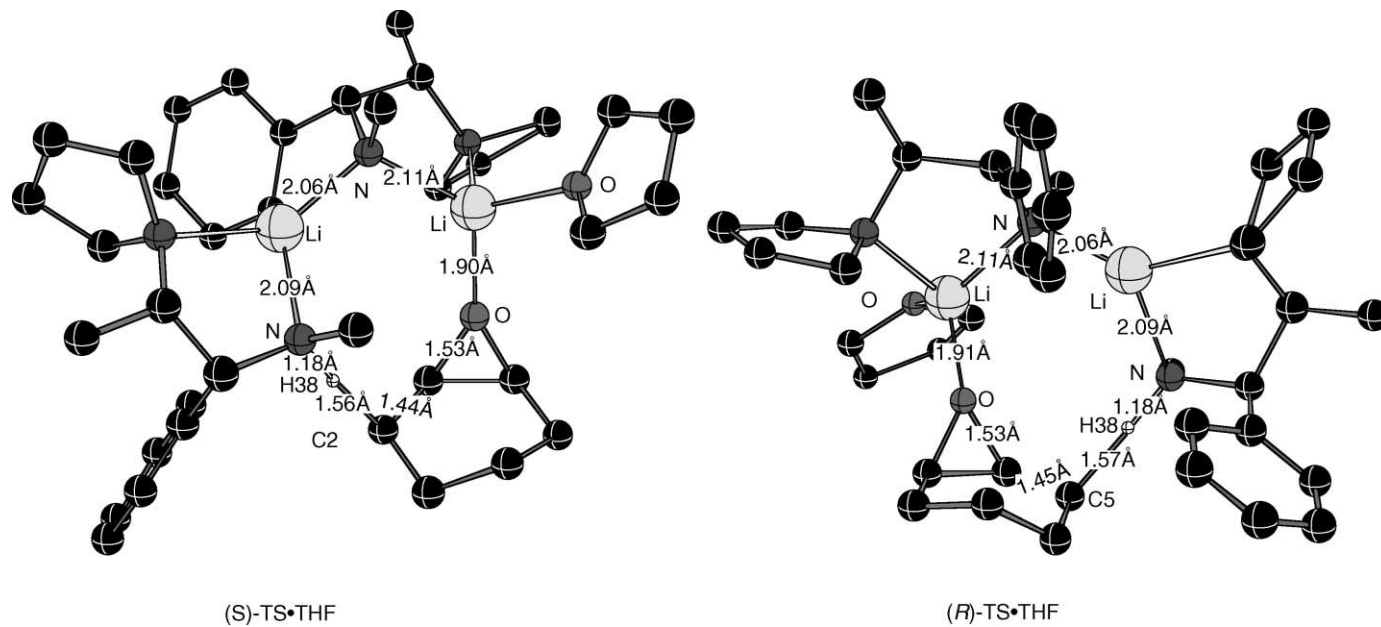


Fig. 5. PM3-optimized THF-solvated diastereoisomeric TSs for deprotonation of **2** with chiral lithium amide **5**. Some hydrogens are omitted for clarity.

Table 2. Calculated energy differences in kcal mol⁻¹ between diastereoisomeric activated complexes with the composition (5a)_x(2)₁(Solvent)₁, and percent (*S*)-3 in the mixture of enantiomeric products, together with experimental values

Entry	Computational method	<i>x</i>	Solvent ^{a,b}	Energy differences	%(<i>S</i>) _{Calc.} / ^d %(<i>S</i>) _{Exp.}
1	B3LYP/6-31 + G(d)//PM3 ^c	2	Calc./Exp. THF/THF	$\Delta E_{\text{Calc.}}^c / \Delta G_{\text{Exp.}}^d$ 1.36/1.96	91/96.5
2		2	None/—	2.38/—	98/—
3	PM3//PM3	2	THF/THF	$\Delta H_{\text{Calc.}}^c / \Delta G_{\text{Exp.}}^d$ 1.82/1.96	95.5/96.5
4		2	None/—	0.23/—	59.5/—
5		1	THF/THF	0.43/1.96	67.5/96.5
6		1	None/—	0.20/—	41.5/—

^a In THF, it has experimentally been determined that *x* = 2 for lithium amide 5.

^b Activated complexes involved in lithium amide deprotonation of 2 have been determined to contain one molecule of 2.

^c Potential energy difference between the two most stable TSs at 298 K.

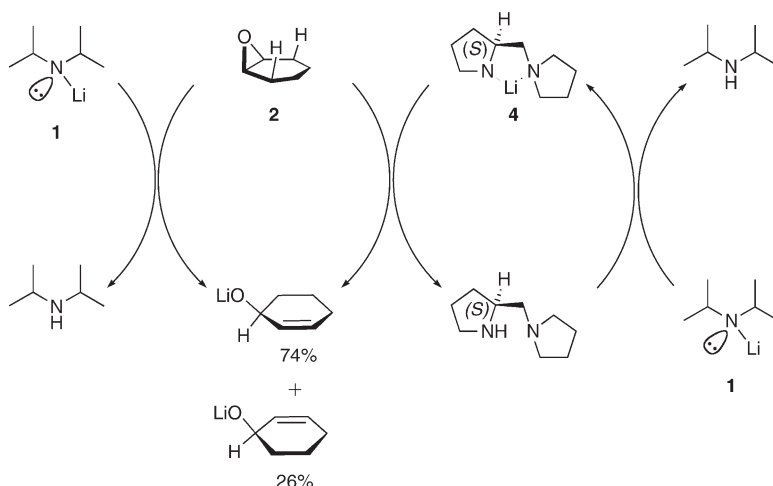
^d At 293 K.

^e Heat of formation difference between the two most stable TSs.

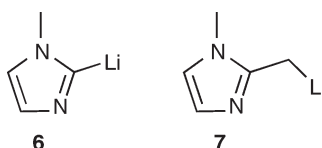
Predicted stereoselectivities are shown in Table 2. Development of other lithium amides with improved reactivity and stereoselectivity using the above-presented approach is in progress. The potential of 5 has been explored in catalytic stereoselective deprotonations and some results are presented below.

8. CATALYTIC STEREOSELECTIVE DEPROTONATIONS

In a lithium amide promoted deprotonation, one lithium amide molecule is consumed for each deprotonated epoxide molecule. Since chiral lithium amides are expensive reagents, there is a strong desire to develop less costly synthetic procedures for stereoselective deprotonations. Catalysis has the potential to solve the problem. What are needed are bulk bases capable of regenerating the chiral lithium amide from the chiral diamine produced in the deprotonation reaction. There have been some attempts along this line, e.g., by Asami and co-workers, who used the non-chiral lithium amide LDA as bulk base and the chiral lithium amide 4 as catalyst [9,12,39–41]. However, the stereoselectivity was considerably lower than what had been achieved in absence of the bulk base, i.e., under stoichiometric conditions. Most likely, the decreased stereoselectivity in the presence of bulk LDA is due to competing deprotonation by LDA to yield racemic product alcohol. The situation is illustrated in Scheme 9.

**Scheme 9.**

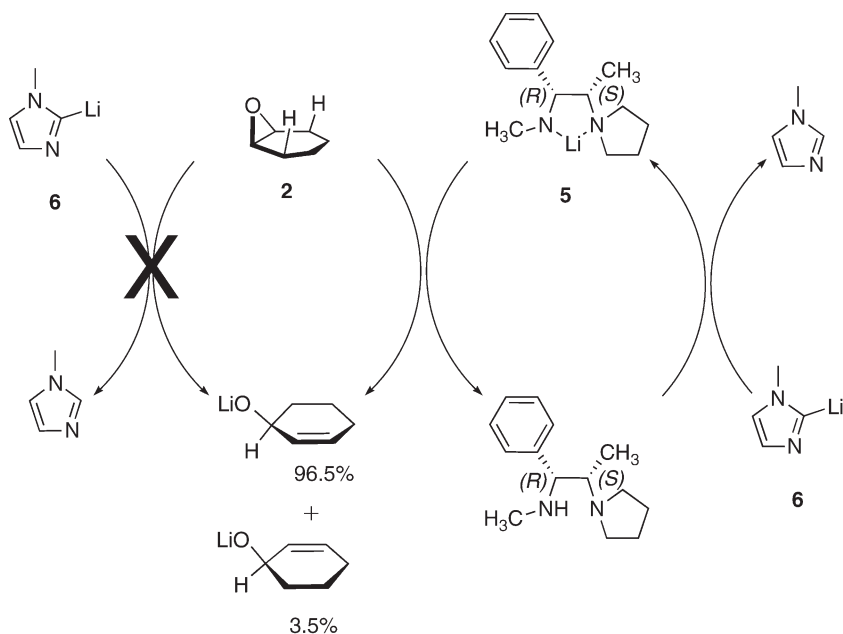
Apparently there is a need for bulk bases that are kinetically much less basic than LDA but that still are capable of efficiently regenerating the chiral lithium amide. Proton transfers to and from electronegative atoms like nitrogen are usually faster than from and to carbon. Therefore, we have explored carbon-based bases for the present purpose [20–22,24]. Indeed, bases like those displayed in Scheme 10 appear to have the predicted behaviour.

**Scheme 10.**

Using either the carbenoid compound **6** or the carbanionic compound **7** as a bulk base in large excess and **5** as catalyst (Scheme 11) gave the same stereoselectivity as the stoichiometric deprotonation of **2** with **5**.

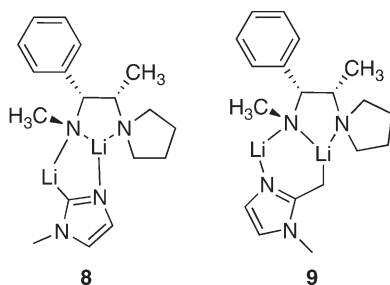
These encouraging results indicate that both bulk bases are functioning as predicted.

However, when another experiment using equimolar amounts of bulk base and **5** was carried out, to our surprise, an increased stereoselectivity was observed [20–22]. The mixture of product enantiomers now contained 98% of the (*S*)-alcohol and only 2% of the (*R*)-alcohol. Apparently the interpretation just made needs some adjustment to account also for these new observations.



Scheme 11.

The results led us to investigate the composition of the reagent solutions by multinuclear NMR spectroscopy. These studies revealed that under these new conditions **5** was no longer present as a homodimer, i.e., a **5** molecule is complexed with another **5** molecule. Instead the results showed new dimers – heterodimers **8** or **9**, respectively. A monomer of **5** forms complex with a monomer of a bulk base and these heterodimers are the new reagents rather than homodimers of the chiral lithium amide (Scheme 12) [20–22].



Scheme 12.

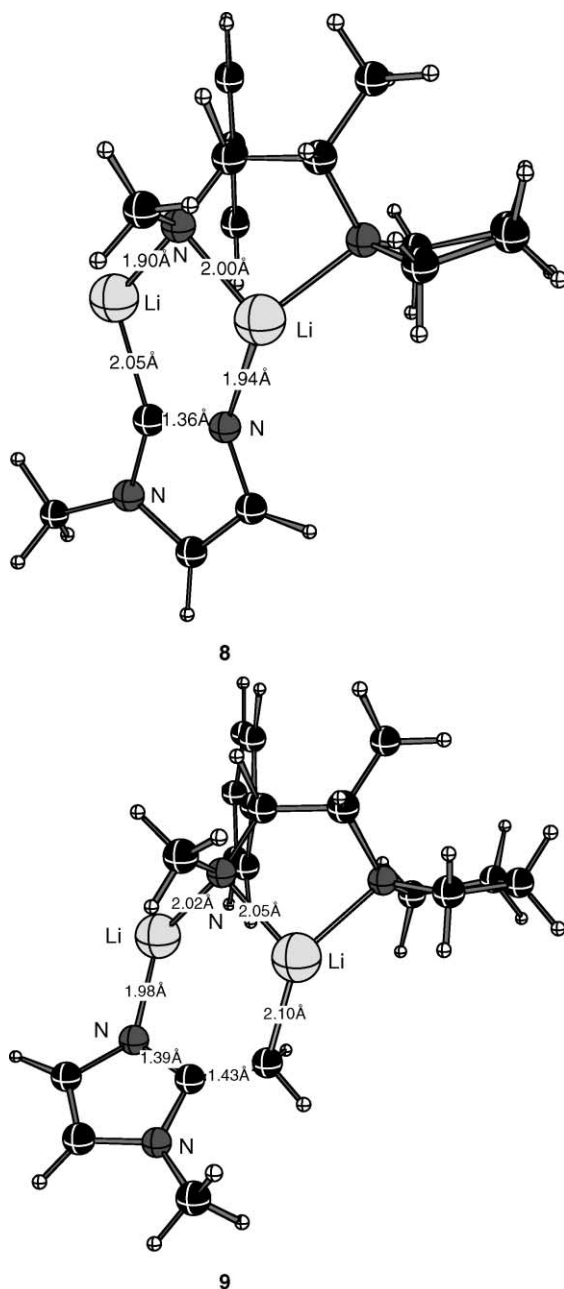


Fig. 6. B3LYP/6-311 + G(d,p) optimized heterodimer **8** and PM3 optimized heterodimer **9**.

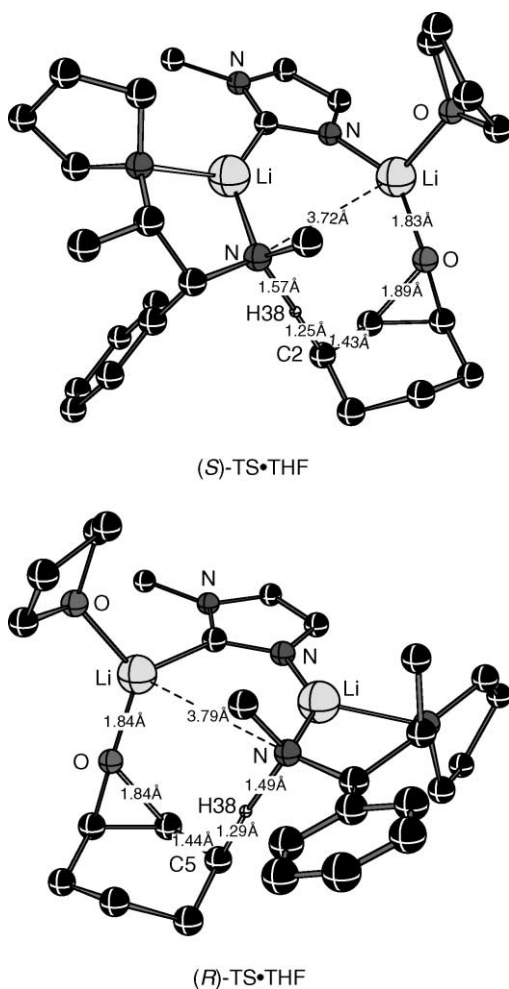


Fig. 7. B3LYP/6-31G(d) optimized THF-solvated TSs for deprotonation of **2** with **8**. Some hydrogens are omitted for clarity.

In Fig. 6, structures of the heterodimers **8** and **9** computationally optimized at the B3LYP/6-311 + G(d,p) or at the PM3-level of theory, respectively, are displayed.

Kinetic investigation of the deprotonation using **8** has been carried out and the reaction orders show that the stereoselecting activated complex is built from one heterodimer molecule and one epoxide molecule [42]. Geometry optimized structures of the stereoselecting activated complexes at the B3LYP/6-31G(d) level of theory are shown in Fig. 7. These results show that

significant advance has been made with respect to our ability to carry out catalyzed reactions with high stereoselectivity. Work is in progress on the design of easily synthesized chiral lithium amides, which in combination with proper bulk bases show even higher reactivity and stereoselectivity. A goal is to make accessible catalysts that find general synthetic use both in the laboratory and in industry.

ACKNOWLEDGEMENTS

We are grateful to the Swedish National Research Council (Vetenskapsrådet) for financial support.

REFERENCES

- [1] H. M. Niemeyer, O. Goscinski and P. Ahlberg, *Tetrahedron*, 1975, **31**, 1699.
- [2] M. B. Huang, O. Goscinski, G. Jonsäll and P. Ahlberg, *J. Chem. Soc., Perkin Trans.*, 1984, **2**, 1327.
- [3] P. Ahlberg, G. Jonsäll, C. Engdahl, M. B. Huang and O. Goscinski, *Preprints – Am. Chem. Soc., Div. Petrol. Chem.*, 1983, **28**, 357.
- [4] M. Asami, *Chem. Lett.*, 1984, 829.
- [5] D. Bhuniya and V. K. Singh, *Synth. Commun.*, 1994, **24**, 375.
- [6] A. Z.-Q. Khan, P. I. Arvidsson and P. Ahlberg, *Tetrahedron: Asymmetry*, 1996, **7**, 399.
- [7] J. K. Whitesell and S. W. Felman, *J. Org. Chem.*, 1980, **45**, 755.
- [8] D. Bhuniya, A. DattaGupta and V. K. Singh, *J. Org. Chem.*, 1996, **61**, 6108.
- [9] J. P. Tierney, A. Alexakis and P. Mangeney, *Tetrahedron: Asymmetry*, 1997, **8**, 1019.
- [10] A. Z.-Q. Khan, R. W. De Groot, P. I. Arvidsson and Ö. Davidsson, *Tetrahedron: Asymmetry*, 1998, **9**, 1223.
- [11] S. E. de Sousa, P. O'Brien and H. C. Steffens, *Tetrahedron Lett.*, 1999, **40**, 8423.
- [12] M. Asami, T. Suga, K. Honda and S. Inoue, *Tetrahedron Lett.*, 1997, **38**, 6425.
- [13] S. K. Bertilsson, M. J. Södergren and P. G. Andersson, *J. Org. Chem.*, 2002, **67**, 1567.
- [14] S. O. Nilsson Lill, P. I. Arvidsson and P. Ahlberg, *Acta Chem. Scand.*, 1998, **52**, 280.
- [15] P. I. Arvidsson, M. Hansson, A. Z.-Q. Khan and P. Ahlberg, *Can. J. Chem.*, 1998, **76**, 795.
- [16] P. I. Arvidsson, G. Hilmersson and P. Ahlberg, *J. Am. Chem. Soc.*, 1999, **121**, 1883.
- [17] S. O. Nilsson Lill, P. I. Arvidsson and P. Ahlberg, *Tetrahedron: Asymmetry*, 1999, **10**, 265.
- [18] R. I. Olsson and P. Ahlberg, *Tetrahedron: Asymmetry*, 1999, **10**, 3991.
- [19] D. Pettersen, M. Amedjkouh, S. O. Nilsson Lill, K. Dahlén and P. Ahlberg, *J. Chem. Soc., Perkin Trans.*, 2001, **2**, 1654.
- [20] M. Amedjkouh, D. Pettersen, S. O. Nilsson Lill and P. Ahlberg, *Chem.-Eur. J.*, 2001, **7**, 4368.
- [21] S. O. Nilsson Lill, D. Pettersen, M. Amedjkouh and P. Ahlberg, *J. Chem. Soc., Perkin Trans.*, 2001, **1**, 3054.
- [22] D. Pettersen, M. Amedjkouh and P. Ahlberg, *Tetrahedron*, 2002, **58**, 4669.
- [23] M. Hansson, P. I. Arvidsson, S. O. Nilsson Lill and P. Ahlberg, *J. Chem. Soc., Perkin Trans.*, 2002, **2**, 763.
- [24] D. Pettersen, M. Amedjkouh, S. O. Nilsson Lill and P. Ahlberg, *J. Chem. Soc., Perkin Trans.*, 2002, **2**, 1397.

- [25] M. Amedjkouh and P. Ahlberg, *Tetrahedron: Asymmetry*, 2002, **13**, 2229.
- [26] J. H. Gilchrist and D. B. Collum, *J. Am. Chem. Soc.*, 1992, **114**, 794.
- [27] J. F. Remenar, B. L. Lucht and D. B. Collum, *J. Am. Chem. Soc.*, 1997, **119**, 5567.
- [28] P. G. Williard and J. M. Salvino, *J. Org. Chem.*, 1993, **58**, 1.
- [29] S. O. Nilsson Lill, PhD Thesis, Organic Chemistry, Department of Chemistry, Göteborg University, Göteborg, Sweden, 2001.
- [30] S. O. Nilsson Lill, U. Köhn and E. Anders, *Eur. J. Org. Chem.*, 2004, **13**, 2868.
- [31] M. Vestergren, J. Eriksson, G. Hilmersson and M. Håkansson, *J. Organomet. Chem.*, 2003, **682**, 172.
- [32] M. Asami, *Bull. Chem. Soc. Jpn*, 1990, **63**, 721.
- [33] S. O. Nilsson Lill, P. Ahlberg, submitted for publication, 2003.
- [34] B. J. Lynch, P. L. Fast, M. Harris and T. G. Donald, *J. Phys. Chem. A*, 2000, **104**, 4811.
- [35] B. J. Lynch and D. G. Truhlar, *J. Phys. Chem. A*, 2001, **105**, 2936.
- [36] A. E. Reed, R. B. Weinstock and F. Weinhold, *J. Chem. Phys.*, 1985, **83**, 735.
- [37] NBO 5.0, Theoretical Chemistry Institute, University of Wisconsin, Madison, WI, 2001.
- [38] M. Amedjkouh and P. Ahlberg, at 11th European Symposium on Organic Chemistry (ESOC 11), Göteborg, Sweden, 1999.
- [39] M. Asami, T. Ishizaki and S. Inoue, *Tetrahedron: Asymmetry*, 1994, **5**, 793.
- [40] T. Yamashita, D. Sato, T. Kiyoto, A. Kumar and K. Koga, *Tetrahedron*, 1997, **53**, 16987.
- [41] A. Magnus, S. K. Bertilsson and P. G. Andersson, *Chem. Soc. Rev.*, 2002, **31**, 223.
- [42] D. Pettersen, P. Dinér, M. Amedjkouth and P. Ahlberg, *Tetrahedron: Asymmetry*, 2004, **15**, 1607.

Proton Insertion in Polycrystalline WO₃ Studied with Electron Spectroscopy and Semi-empirical Calculations

A. Henningsson,¹ A. Stashans,² A. Sandell,¹ H. Rensmo,¹ S. Södergren,³
H. Lindström,⁴ L. Vayssieres,⁴ A. Hagfeldt,⁴ S. Lunell² and H. Siegbahn¹

¹*Department of Physics, Uppsala University, P.O. Box 530, S-751 21 Uppsala, Sweden*

²*Department of Quantum Chemistry, Uppsala University, P.O. Box 518, S-751 20
Uppsala, Sweden*

³*GammaData Scienta AB, P.O. Box 15120, S-750 15 Uppsala, Sweden*

⁴*Department of Physical Chemistry, Uppsala University, P.O. Box 579, S-751 23
Uppsala, Sweden*

Dedicated to Professor Osvaldo Goscinski on the occasion of his 65th birthday.

Abstract

Proton insertion in polycrystalline tungsten oxide has been studied with photoelectron spectroscopy and semi-empirical calculations. The W 4f spectra show growth of W⁵⁺ and W⁴⁺ oxidation states as a function of inserted proton content in the crystal lattice. A concomitant growth of bandgap structure displays two separate peaks. Semi-empirical calculations using the periodic large unit cell (LUC) method suggest the growth of W⁴⁺ states based on the total energy variation with respect to the number of protons/unit cell. At this stage the general picture of insertion is that of a multiphase system containing regions of different x values.

Contents

1. Introduction	24
2. Experimental methods	25
3. Theoretical methods	26
4. Results	27
4.1. Electron spectroscopy	27
4.2. Calculations	30
4.2.1. Geometry of monoclinic WO ₃ with two H atoms	30
4.2.2. W ⁵⁺ and W ⁴⁺ centers in H-inserted WO ₃	31
5. Discussion	32
6. Conclusions	35
Acknowledgements	35
References	35

1. INTRODUCTION

Tungsten oxide (WO_3) was the first discovered electrochromic material [1] and has been by far the most extensively studied one. WO_3 films are often prepared by evaporation or sputtering, but many electrochemical and chemical techniques are also utilized [2]. For example, depositions, using solutions of WCl_6 dissolved in ethanol, *N,N*-dimethylformamide or 2-propanol in the presence of air, have been reported [3–8]. The WO_3 films were crystalline if the substrate temperature was higher than 300 °C during deposition. The crystal structure of WO_3 is of perovskite type, but some atomic displacements and rotations of WO_6 -octahedra normally occur so that, depending on the temperature, tetragonal, orthorhombic, monoclinic, or triclinic symmetries are found. In the present paper, we have prepared monoclinic WO_3 films by a simple deposition technique using WCl_6 solutions.

When ions are inserted into WO_3 , both X-ray photoelectron spectra and electron spin resonance show that W^{5+} as well as W^{6+} are present, and that the W^{5+} density scales with the intensity of the electrochromic absorption peak [2,9]. The picture that emerges is that the inserted electrons are localized at tungsten sites, where they participate in processes responsible for the electrochromism. The insertion/extraction process can then be represented, schematically, by



Interestingly, cyclic voltammograms (CVs) of monoclinic films prepared by chemical vapour deposition (CVD) [10] showed clear peaks both in the cathodic and anodic sweep directions, indicating different electrochemical processes in specific voltage ranges. It was discussed [10] that these features could be due to H^+ from two sources: adsorbed on the oxide surface and in the bulk of the electrolyte. Alternatively, at least two redox waves in the CV can be interpreted by a two-step oxidation of WO_3 , from W^{6+} to W^{5+} and then further to a W^{4+} state. The existence of W^{4+} states during proton insertion in evaporated amorphous WO_3 films for $x > 0.3$ has been discussed by Ottermann *et al.* [11].

In the present chapter, we have studied monoclinic polycrystalline WO_3 films during proton insertion using electron spectroscopy. Several workers [9,11–15] have used electron spectroscopy to investigate both electrochromic tungsten oxides and tungsten bronzes. Features in the W 4f and valence level photoemission spectra show pronounced similarities for the different systems, but the detailed interpretations are still not clearly resolved. In particular, the relation between the observed spectral changes due to ion insertion and the electrochemical conditions has not been fully investigated. The purpose of the present study is, firstly, to connect observed

peaks in the CVs of these films with the electron spectra and, secondly, based on theoretical models using semi-empirical methods, interpret the results.

2. EXPERIMENTAL METHODS

Photoelectron spectroscopy (PES) was performed at the Swedish National Synchrotron Radiation Laboratory, MAX lab. The beamline and the spectrometer are unique in construction since all three phases of matter (gas, liquid, and solid) can be studied ([16] and references therein). This is made possible by means of efficient differential pumping of the analysis chamber of the instrument. To the existing spectrometer we have developed an electrochemical preparation technique where the electrochemistry is performed in a specially designed preparation chamber attached to the analysis chamber of the spectrometer. Thus, all electrochemistry is performed inside the vacuum system of the spectrometer. There are several advantages with this technique. First, the electrochemistry is performed in a controlled atmosphere without any exposure to air. Second, the surface is analyzed within minutes after the electrochemical reaction. Third, the same electrode is analyzed at the same spot for the different electrochemical treatments. The device used for the electrochemical preparations is described in detail elsewhere [17].

The electrodes were prepared from solutions of 0.6 M WCl_6 in ethanol. Conducting SnO_2 glass substrates were spin coated with the WCl_6 solution, and the film turns dark blue within a few seconds. WCl_6 decomposes to WO_3 at 60 °C in the presence of air. Heating the electrode with a heat gun in air at 400 °C for 30 min forms a polycrystalline monoclinic WO_3 film, as determined by X-ray diffraction. The films were visually transparent after the heat treatment. The WCl_6 solution was prepared with dry ethanol (3 Å molecular sieves) at -20 °C. Under these conditions a clear, yellowish solution is obtained. If the solvent was not dry or the preparation of the solution was made at room temperature, a dark blue solution, with some precipitation, was obtained. From blue solutions it was not possible to form reproducible films (cf. Ref. [5]).

All electrochemical preparations were made in argon atmosphere at room temperature in the preparation chamber of the spectrometer using an Eco Chemie PGSTAT10. The electrolyte was 50 mM H_2SO_4 . The electrode was rinsed in water after each electrochemical modification (before each surface analysis). During surface analysis the electrolyte and the rinse bath were stored in a closed compartment in argon atmosphere.

Spectra were recorded with photon energies of 157 eV in the W 4f region and with 80 eV in the valence region. The experimental (photon width and spectrometer resolution) contribution to the energy resolution in the W 4f spectra was 150 meV and in the valence region 100 meV.

3. THEORETICAL METHODS

A quantum-chemical intermediate neglect of differential overlap (INDO) method [18], modified for crystals calculations [19,20], has been used to study theoretically a H-inserted WO_3 crystal. The space group of WO_3 is known to be $C_{2h}^5(P2_1/a)$, and the symmetry of WO_3 , considered at room temperature, is monoclinic, pseudocubic. The W atoms are distorted from their crystallographic sites in the following way: W atoms arranged parallel to the a and b axes are displaced along the c axis in an alternate sense, but W atoms arranged parallel to the c axis show only small displacements. As a result, the W–O bonds form zigzag chains along the three crystallographic axes. The bond lengths are between 1.86 and 1.98 Å (along the a direction), 1.76 and 2.17 Å (along the b direction) and 1.83 and 2.12 Å (along the c direction). In the b and c directions the bonds are alternately long and short while they are similar in length in the a direction. To reproduce such a complex structure, we have to include 32 atoms in the unit cell of WO_3 and use a semi-empirical approach, in which some numerical parameters are used to simplify the *ab initio* Hartree–Fock formalism, thus reducing considerably the computational time. The parametrization scheme for WO_3 is described in detail in Ref. [21]. Here, we shall only note that the computations are carried out using the CLUSTERD computer code [20] in a (non-relativistic) valence basis set of tungsten 6s, 6p, and 5d and oxygen 2s and 2p atomic orbitals (AOs). By fitting our results to the main properties of the electronic band structure of the perfect WO_3 as well as to the structural parameters of the crystalline lattice of monoclinic WO_3 , the parameters are anticipated to partially incorporate relativistic effects, which are sizable in tungsten (see Ref. [21] for more details).

We use a periodic supercell model based on the large unit cell (LUC) method [22] which is free from the limitations of different cluster models applicable mainly to ionic solids, e.g., alkali halides. The main computational equations for calculating the total energy of the crystal within the framework of the LUC have been given in Refs. [22–24]. Here, we shall outline some key elements of the method. The basic idea of the LUC is in computing the electronic structure of the unit cell extended in a special manner at $\mathbf{k} = 0$ in the reduced Brillouin zone (BZ), which is equivalent to a band structure calculation at those BZ \mathbf{k} points, which transform to the reduced BZ center on extending the unit cell [22]. The total energy of the crystal is

$$\begin{aligned}
 E_{\text{LUC}} = & \frac{1}{2} \sum_{A \neq B} \frac{Z_A Z_B}{R_{AB}^{00}} + \frac{1}{2} \sum_{A \in \text{LUC}} E_C^A + \sum_j^{\text{occ}} \varepsilon_j(0) \\
 & + \frac{1}{2} \sum_{\mu, \nu \in \text{LUC}} \rho_{\mu, \nu}(0) Q_{\mu \nu}
 \end{aligned} \tag{2}$$

where $\varepsilon_j(\mathbf{k})$ are the eigenvalues of Fock's matrix, occ is the number of occupied electronic states in the system, and $\rho_{\mu,\nu}(\mathbf{k})$ are the density-matrix elements on the basis of Bloch's combinations of AOs,

$$E_C^A = Z_A \sum_{l \neq 0} \sum_{B \in \text{LUC}} \left[\frac{Z_B}{R_{AB}^{0l}} - \sum_{\mu \in B} \rho_{\mu\mu}(0) (v^{A0})_{\mu\mu}^{0l} \right] \quad (3)$$

$$Q_{\mu\nu} = T_{\mu\mu}^{00} - \sum_{A \in \text{LUC}} Z_A (v^{A0})_{\mu\mu}^{00} + \sum_{l \neq 0} H_{\mu\mu}^{0l}, \quad \text{if } \mu = \nu \quad (4)$$

$$Q_{\mu\nu} = \sum_l H_{\mu\nu}^{0l}, \quad \text{if } \mu \neq \nu \quad (5)$$

where $T_{\mu\mu}^{00}$ are the matrix elements of the kinetic energy operator, $(v^{A0})_{\mu\mu}^{0l}$ are those of the electron–core interaction operator, R_{AB}^{0l} is the distance between the cores of atoms A and B, and Z_A and Z_B are charges of these cores.

The total energy equation (2) is obtained after the introduction of the ‘cut-off function’,

$$\omega(r_{\mu\nu}) = \frac{P_{\mu\nu}^{0l}}{\rho_{\mu\nu}(0)} \quad (6)$$

which is possible due to the fast decrease of the overlap integral $S_{\mu\nu}^{0l}$ with the interatomic distance $r_{\mu\nu}$. We can also note that the Coulomb interaction is treated quite well in the LUC model due to the theory of special \mathbf{k} -points [25].

The theoretical method described above has been used successfully in investigations of various perfect and defective oxide crystals (see Refs. [24, 26–29] and references therein) as well as a number of ionic crystals and different semiconductors.

4. RESULTS

4.1. Electron spectroscopy

Figure 1 shows a CV of a polycrystalline monoclinic WO₃ electrode in 50 mM H₂SO₄, at a scan rate of 1 mV/s, obtained in the electrochemical preparation stage described above. There are two reduction peaks, at -0.10 and -0.34 V vs. saturated calomel electrode (SCE), respectively. The two peaks are characteristic of polycrystalline WO₃ [30–32]. The W 4f lines and the bandgap states for different electrochemical treatments are shown in Fig. 2a,b. Depending on electrochemical treatment the W 4f core level spectrum undergoes substantial changes. For a freshly prepared electrode, the spin–orbit split W 4f_{5/2}, W 4f_{7/2} doublet of WO₃ completely dominates

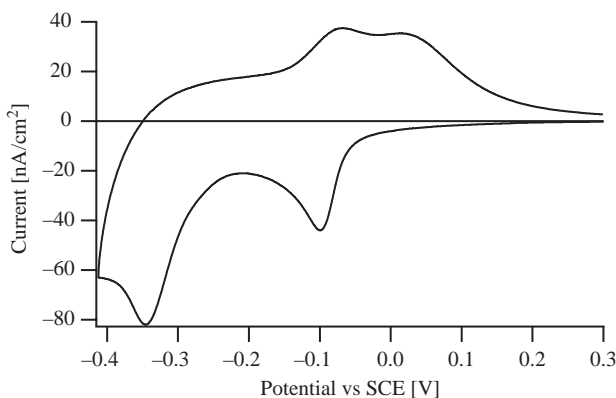


Fig. 1. Cyclic voltammogram of polycrystalline monoclinic WO_3 .

the spectral appearance. These peaks are characteristic of WO_3 with formal valence W^{6+} . The asymmetry at lower binding energy of the W 4f core level and the peaks appearing in the bandgap indicate that the electrode is not completely oxidized.

Inserting protons at -0.10 V for 3 min (the position of the first redox peak in Fig. 1) turns the electrode green. The effect of proton insertion is clearly seen in the photoelectron spectrum, a low binding energy shoulder appears in the W 4f core level region (Fig. 2a). The new state, referred to as W^{5+} , is shifted -1.27 eV relative to W^{6+} , and has a relative intensity of 0.22 with a full width half maximum (FWHM) of 0.91 eV. We also observe that the W^{6+} state increases in FWHM to 1.27 eV. The intensity of the state in the bandgap region has also increased.

Further insertion, at -0.30 V (the beginning of the second reduction peak in the CV), turns the electrode dark blue. At this potential the formation of a second low binding energy shoulder may be observed in W 4f spectrum. This state is shifted -2.51 eV relative to W^{6+} , with a relative intensity of 0.05, and a FWHM of only 0.68 eV. At the same time there is an increase in the width of the W^{5+} state to 1.27 eV, whereas the W^{6+} state is unaffected, 1.28 eV. The relative intensity of the W^{5+} state has increased to 0.32. With increasing insertion the intensities of the bandgap states also increase. Furthermore, at this potential there is a change in the structure of the bandgap states, with an additional peak appearing at 0.15 eV.

Insertion at -0.45 V, beyond the second reduction peak, results in an electrode with a metallic appearance. As can be seen in Fig. 2, the W 4f core level spectrum at this stage of insertion is very complicated. In contrast, the bandgap state features (Fig. 2b) only increase in intensity, while the structure remains similar to that observed at -0.30 V. It was not possible to fit the

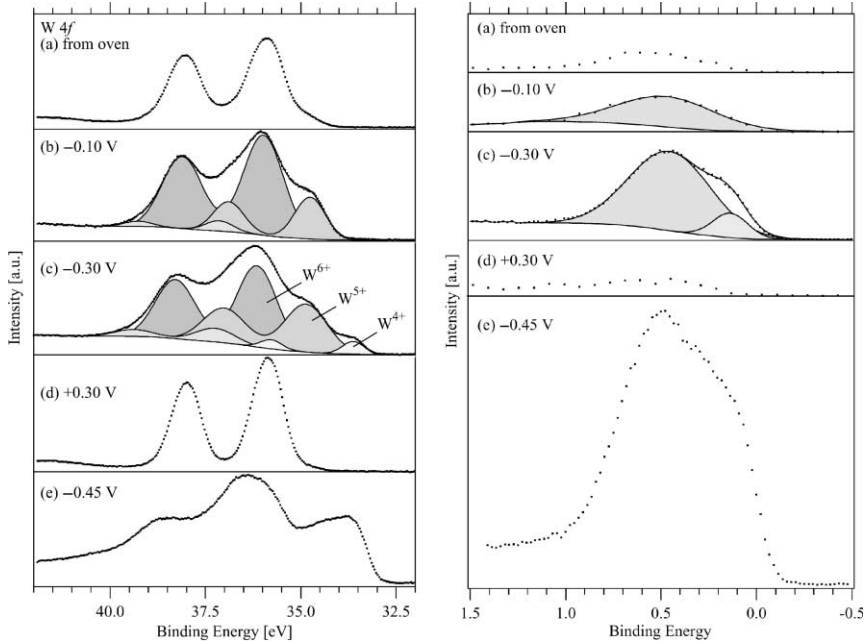


Fig. 2. (a) W 4f core levels for different electrochemical treatments. (b) Bandgap states for different electrochemical treatments.

core level spectrum with the same set of parameters used for the other spectra.

Extraction at +0.30 V turns the electrode transparent. As seen in Fig. 2, the electrode returns to the original W^{6+} state as expected from a reversible insertion reaction. The cycled electrode seems to be more oxidized since the low binding energy states in the core level spectrum and the bandgap states are now almost absent. The width of the W 4f core levels of an electrochemically reoxidized electrode is now 0.95 eV, considerably less than for an ion-inserted electrode.

For all curve fittings we have constrained the line profiles to Gaussians with an intensity ratio of 0.74 and a spin-orbit splitting of 2.14 eV between the $\text{W } 4f_{5/2}$ and $\text{W } 4f_{7/2}$ components. With increasing insertion there is also a build up of a tail in the higher binding energy region. To obtain reasonable curve fits, an additional satellite doublet has been added to include this tail. The results of the curve fits are given in Table 1.

In general, the main component W 4f core level shifts slightly to higher binding energy with increasing insertion. This is probably to be associated with a corresponding shift of the Fermi level due to the filling of the bandgap states associated with the insertion.

Table 1. Results from the curve fitting of the W 4f levels. The potentials given are for different electrochemical treatments. At +0.30 V the electrode is electrochemically oxidized to WO_3

	Potential	+0.30 V	−0.10 V	−0.30 V
W^{6+}	Relative intensity	1	0.73	0.54
	FWHM (eV)	0.95	1.23	1.24
W^{5+}	Shift ^a (eV)		−1.23	−1.28
	Relative intensity		0.23	0.34
W^{4+}	FWHM (eV)		0.93	1.31
	Shift (eV)			−2.52
	Relative intensity			0.05
Satellite	FWHM (eV)			0.66
	Shift (eV)		1.09	1.15
	Relative intensity		0.04	0.07
	FWHM (eV)		0.85	1.09

FWHM, full width half maximum.

^a Relative to W^{6+} .

4.2. Calculations

4.2.1. Geometry of monoclinic WO_3 with two H atoms

Periodic supercells with 32, 64 ($2 \times 1 \times 1$ extended), and 128 ($2 \times 1 \times 1$ extended) atoms were used to study proton insertion in the monoclinic WO_3 crystal. It was shown previously [21] that, when the hydrogen is introduced into the material, it binds to one of the oxygens forming a hydroxyl unit. In the present study, we inserted two H atoms and investigated two different spatial configurations (Fig. 3): (i) two hydrogens, H(1) and H(2), located in different structural voids and bound to two different oxygens, and (ii) two hydrogens, H(2) and H(3), located in the same structural void and bound to two oxygens situated at opposite sites of this void.

The automated geometry optimization procedure, based on the downhill simplex method [33] incorporated into the computer code, was applied to find the total energy minimum in both configurations. As a result, the energetically most favorable configuration was found to be the H(1)–H(2) pair. The 32-atom supercell with two hydrogens at positions 1 and 2 has 1.5 eV lower energy compared to the case of the H(2)–H(3) pair. The interatomic distance between the H and O atoms in the hydroxyl units is 0.99 Å, which is close to the corresponding distance in the free molecule, 0.97 Å.

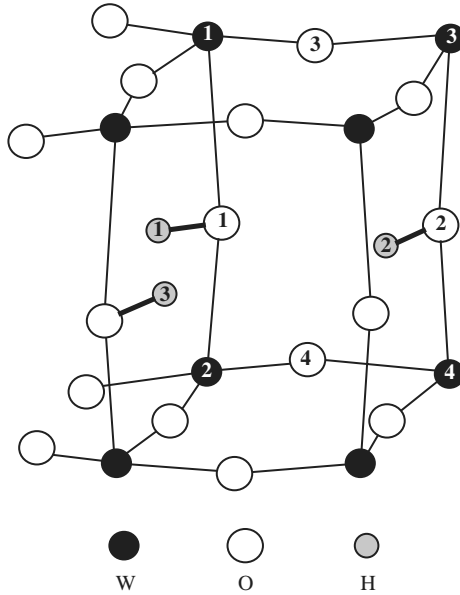


Fig. 3. 32-atom supercell of monoclinic WO_3 crystal with two H atoms placed at different positions. The supercell with H(1)–H(2) pair was found to be the energetically most favorable one, it has lower total energy by 1.5 eV compared to the supercell with the H(2)–H(3) pair.

4.2.2. W^{5+} and W^{4+} centers in H-inserted WO_3

When the hydrogens are inserted into the supercell of WO_3 host atoms, their valence electrons transfer to one or two different W atoms. In the first case, a W^{4+} center is formed and the multiplicity of the system is equal to 1 (singlet) while in the second case, two W^{5+} centers are formed and the multiplicity of the system is equal to 3 (triplet). This pattern is well illustrated by the net atomic charges given in Table 2 for both cases. In calculations of both the singlet and triplet cases, for different size supercells containing two H atoms, it was found that in the larger supercells the triplet state has a lower total energy, while in the smaller supercell the singlet is energetically more favorable.

Our computer simulations of different size supercells correspond to the modeling of different impurity concentrations in the material due to the periodicity of our model. Thus, this implies that W^{5+} centers, which correspond to our triplet state, are formed in H-inserted WO_3 at low concentrations of hydrogen. When the hydrogen concentration exceeds a certain value (see Fig. 4) one should expect the formation of W^{4+} centers. From Fig. 4, the formation of W^{4+} centers begins when the hydrogen to tungsten ratio is about 1/10.

Table 2. The charges on atoms (in elementary charges) in H-inserted WO_3 , 32-atom supercell. Negligible changes of the atomic charges were found in the cases when the two H atoms are inserted into 64-atom and 128-atom supercells. The numeration of the atoms corresponds to that in Fig. 4. Bold numbers refer to atomic charges for W^{4+} (singlet) and W^{5+} (triplet) states

	Perfect WO_3	Singlet	Triplet
H(1)	–	0.63	0.58
H(2)	–	0.67	0.68
W(1)	4.84	2.90	3.86
W(2)	4.79	4.78	4.76
W(3)	4.78	4.57	4.69
W(4)	4.81	4.78	3.83
O(1)	– 1.59	– 1.47	– 1.45
O(2)	– 1.61	– 1.50	– 1.51
O(3)	– 1.64	– 1.60	– 1.63
O(4)	– 1.53	– 1.47	– 1.48

5. DISCUSSION

The present experimental data show similarities with those of previous workers [12,34] but new features appear, which we will discuss in the light of the results from the calculations. Considering first the valence level spectra (Fig. 2b), the growth of bandgap peaks with respect to inserted proton concentration involves two distinct peaks instead of the singular features previously observed. Moreover, the appearance of both peaks may be

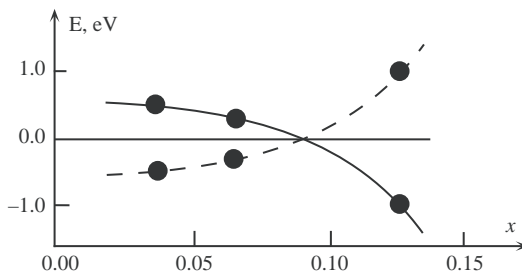


Fig. 4. The pattern of formation of W^{5+} and W^{4+} centers in H-inserted WO_3 crystal. Solid and broken curves denote the energetical preference of W^{4+} and W^{5+} centers in different size supercells, respectively. E denotes the difference of supercell's total energies for singlet (W^{4+} center) and triplet (W^{5+} center) cases for the equivalent hydrogen concentration x . The 'zero' level of the energy corresponds to the hypothetical case when the formation of W^{5+} and W^{4+} centers is energetically equivalent.

directly associated with the onset of maxima in the CV (Fig. 1). We interpret this behavior in terms of the existence of localized states within the bandgap. The localized character of the states is reasonable in a non-conductive region of low x values for the ion-inserted material. The calculations imply that localization occurs to the W sites of the lattice creating either W^{5+} or (at higher x values) W^{4+} states. The detailed nature of the localization should, however, be regarded with some caution since the structure of the material allows at least two possible W sites, with high probability for each inserted proton. Such a proton, according to the calculation, is bound to an oxygen atom which in turn connects to two tungsten atoms. Thus, it is reasonable to expect a rather substantial sensitivity of the localization of the bandgap electron with respect to the bonding geometry of the proton to the oxygen. Inspection of the intensity at the Fermi level (Fig. 2b) shows that at an electrode potential of -0.3 V the density of states (DOS) at this energy is still very small, while at -0.45 V it has become significant. This reflects the general dominance of localized states below the former electrode potentials and the growing importance of itinerant, delocalized electrons above -0.3 V.

Concomitant with the spectral development in the bandgap, the W 4f levels undergo substantial changes as detailed above. At -0.1 V, the extra low-binding energy component appears, which we interpret as due to W^{5+} states and which we associate with the bandgap state at a binding energy of 0.5 eV.

At an insertion potential of -0.3 V, an additional peak appears, shifted even further towards lower binding energy (cf. Fig. 2a). A peak at this position has been observed also by previous workers in the tetragonal hydrogen bronzes [12]. Several interpretations have been suggested [12] involving the coexistence of different crystal structures, the formation of OH^- states or the creation of W^{4+} . The calculations performed here provide strong evidence for the last interpretation in terms of the growth of W^{4+} states above a certain x value. This growth might be intermixed with the increasing importance of itinerant states, leading finally to a conducting state of the material. These are most likely the conditions leading to the complicated spectrum observed for insertion potentials exceeding -0.45 V. Here, the final state (dynamic) effects are probably increasingly important and will significantly distort the distribution among different valence states from expectations based on initial state considerations. At these high x values, it is also highly likely that significant structural changes occur.

The general picture that emerges from the observations in the core and valence spectra for varying degrees of proton insertion is that of a multiphase system, containing regions of different x values. Thus, three different valence states coexist at high average x values. The observed broadening of the W 4f peaks upon insertion corroborates this view.

These mixed-valence systems have been discussed by several authors with respect to final state effects in their core level spectra [12,35]. A distinction is generally made between the cases where the extra electrons occur as itinerant conduction band electrons (metallic case) or whether they are completely localized to single sites. In the former case, the core ionization of one site will in itself lead to the creation of localized levels (by pulling down from the conduction band), whose occupancy in the final state of the ionization process will depend statistically on the conduction electron density. Thus, the final state localized level may be either filled or empty. The net result is a loss of direct correlation between observed relative peak intensities and the number of inserted electrons per formula unit (x value), since the population of the two possible core-hole states is considered to be entirely a final state phenomenon. On the other hand, for the case of complete single-site localization (non-metallic case) the relative intensities are expected to truly represent the relative number of the two possible valence states before ionization and will not be affected by effects due to the final state of the core ionization process.

In the present spectra, we cannot exclude an intermediate case between the two extremes discussed above. On the one hand, there is evidence of localized character of the bandgap states in our spectra. However, at high insertion potentials the core level spectra display final state effects in that the relative intensities of the core level peaks differ from those expected from estimated x values. It should be realized that localization *per se* does not exclude final state effects in the core level spectrum. In fact, we have noted above that localization in this case may well involve two tungsten centers, which provides sufficient grounds to expect significant final state effects. This character of the initial state of the core ionization process leads to a situation akin to those encountered in molecular cases, such as for example adsorbed molecules on metallic substrates. The general behavior may be treated within a common framework, involving the pulling down of a local atomic level on the core-ionized site. Model treatments [36–40] show that, depending on the interaction strength between the participating atomic orbitals, the core ionization may lead to concomitant interatomic charge transfer resulting in a fully relaxed final state. In this case, core ionization of a ($W^{6+}-OH-W^{5+}$) insertion site may lead to a W 4f peak at the low binding energy position corresponding to the W^{5+} peak in either of two ways: by direct ionization of the W^{5+} site or by ionization of the W^{6+} site plus a charge transfer from the W^{5+} site. The conditions for the latter process to occur are favorable in this case in view of the near degeneracy of the two local states on each of the tungsten sites. The general effect on the W 4f spectrum will thus be a net transfer of intensity from the W^{6+} peak over to the W^{5+} peak leading to a deviation from the ratio expected from the x value.

6. CONCLUSIONS

We have investigated monoclinic films of WO₃ under different conditions of electrochemical insertion of protons using electron spectroscopy. The valence and core level data are interpreted in terms of the existence at low x values of localized W⁵⁺ states. At intermediate overall x values, the electron spectra coupled with semi-empirical calculations using the periodic LUC method suggest the additional formation of W⁴⁺ states.

The general picture at this stage of insertion is that of a multiphase system containing regions of different x values. Still higher x values lead to a metallic state of the material, where structural changes and final state effects become important for the appearance of the core level spectrum.

ACKNOWLEDGEMENTS

The present work was supported by the Swedish Research Council (VR) and the Foundation for Strategic Research.

REFERENCES

- [1] S. K. Deb, *Philos. Mag.*, 1973, **27** (4), 801.
- [2] C. G. Granqvist, *Handbook of Inorganic Electrochromic Materials*, Elsevier Science, Amsterdam, 1995.
- [3] D. Craigen, A. Mackintosh, J. Hickman and K. Colbow, *J. Electrochem. Soc.*, 1986, **133** (7), 2529.
- [4] G. H. Zhou, S. A. Wessel and K. Colbow, *J. Phys. D*, 1988, **21** (12), 1802.
- [5] M. A. Habib and D. Glueck, *Sol. Energy Mater.*, 1989, **18** (3–4), 127.
- [6] J. P. Zhang, S. A. Wessel and K. Colbow, *Thin Solid Films*, 1990, **185** (2), 265.
- [7] J. P. Zhang and K. Colbow, *Appl. Phys. Lett.*, 1991, **58** (10), 1013.
- [8] E. Kikuchi, K. Iida, A. Fujishima and K. Itoh, *J. Electroanal. Chem.*, 1993, **351** (1–2), 105.
- [9] R. L. Benbow and Z. Hurych, *Phys. Rev. B: Solid State*, 1978, **17** (12), 4527.
- [10] O. Bohnke, C. Bohnke, A. Donnadiou and D. Davazoglou, *J. Appl. Electrochem.*, 1988, **18** (3), 447.
- [11] C. R. Ottermann, A. Temmink and K. Bange, *Thin Solid Films*, 1990, **193** (1–2), 409.
- [12] G. K. Wertheim, M. Campagna, J.-N. Chazalviel and D. N. E. Buchanan, *Appl. Phys.*, 1977, **13** (3), 225.
- [13] G. Hollinger, P. Pertosa, J. P. Doumerc, F. J. Himpsel and B. Reihl, *Phys. Rev. B: Condens. Matter*, 1985, **32** (4), 1987.
- [14] M. D. Hill and R. G. Egdell, *J. Phys. C*, 1983, **16** (32), 6205.
- [15] S. Hashimoto and H. Matsuoka, *J. Appl. Phys.*, 1991, **69** (2), 933.
- [16] S. Svensson, J. O. Forsell, H. Siegbahn, A. Ausmees, G. Bray, S. Sodergren, S. Sundin, S. J. Osborne, S. Aksela, E. Nommiste, J. Jauhiainen, M. Jurvansuu, J. Karvonen, P. Barta, W. R. Salaneck, A. Evaldsson, M. Logdlund and A. Fahlman, *Rev. Sci. Instrum.*, 1996, **67** (6), 2149.
- [17] S. Södergren, H. Rensmo and H. Siegbahn, *ECASIA 97/7th European Conference on Applications of Surface and Interface Analysis*, Wiley, Chichester, 1997.

- [18] J. A. Pople and D. L. Beveridge, *Approximate MO Theories*, McGraw-Hill, New York, 1970.
- [19] A. Shluger, *Theor. Chim. Acta*, 1985, **66** (6), 355.
- [20] E. Stefanovich, E. Shidlovskaya, A. Shluger and M. Zakharov, *Phys. Status Solidi B*, 1990, **160** (2), 529.
- [21] A. Stashans and S. Lunell, *Int. J. Quantum Chem.*, 1997, **63** (3), 729.
- [22] R. A. Evarestov and V. A. Lovchikov, *Phys. Status Solidi B*, 1977, **79** (2), 743.
- [23] P. V. Smith, J. E. Szymanski and J. A. D. Matthew, *J. Phys. C*, 1985, **18** (16), 3157.
- [24] A. Shluger and E. Stefanovich, *Phys. Rev. B: Condens. Matter*, 1990, **42** (15), 9664.
- [25] R. A. Evarestov, *Quantum-chemical Methods in Solid State Theory*, Leningrad State University Press, Leningrad, 1982.
- [26] A. Stashans, S. Lunell and R. W. Grimes, *J. Phys. Chem. Solids*, 1996, **57** (9), 1293.
- [27] A. Stashans, S. Lunell, R. Bergstrom, A. Hagfeldt and S. E. Lindquist, *Phys. Rev. B*, 1996, **53** (1), 159.
- [28] P. W. M. Jacobs, E. A. Kotomin, A. Stashans and I. A. Tale, *Philos. Mag. B*, 1993, **67** (4), 557.
- [29] A. Stashans, E. Kotomin and J. L. Calais, *Phys. Rev. B*, 1994, **49** (21), 14854.
- [30] L. Y. Berezin and V. P. Malinenko, *Pis'ma Zh. Tekh. Fiz.*, 1987, **13** (7), 401.
- [31] M. Rezrazi, B. Vuillemin and O. Bohnke, *J. Electrochem. Soc.*, 1991, **138** (9), 2770.
- [32] R. H. Jarman and P. G. Dickens, *J. Electrochem. Soc.*, 1982, **129**, 2276.
- [33] W. H. Press, B. P. Flannery, S. A. Teukolsky and W. T. Vetterling, *Numerical Recipes: The Art of Scientific Computing*, Cambridge University Press, Cambridge, 1989.
- [34] A. Temmink, O. Anderson, K. Bange, H. Hantsche and X. Yu, *Thin Solid Films*, 1990, **192** (2), 211.
- [35] P. P. Edwards, R. G. Egdell, I. Fragala, J. B. Goodenough, M. R. Harrison, A. F. Orchard and E. G. Scott, *J. Solid State Chem.*, 1984, **54** (2), 127.
- [36] K. Schonhammer and O. Gunnarsson, *Z. Phys. B*, 1978, **30** (3), 297.
- [37] K. Schonhammer and O. Gunnarsson, *Solid State Commun.*, 1978, **26**, 399.
- [38] K. Schonhammer and O. Gunnarsson, *Solid State Commun.*, 1977, **23** (10), 691.
- [39] O. Gunnarsson and K. Schonhammer, *Phys. Rev. Lett.*, 1978, **41** (23), 1608.
- [40] O. Gunnarsson and K. Schonhammer, *Surf. Sci.*, 1979, **80**, 471.

On the Effects of Spin–Orbit Coupling on Molecular Properties: Dipole Moment and Polarizability of PbO and Spectroscopic Constants for the Ground and Excited States

Björn O. Roos and Per-Åke Malmqvist

*Department of Theoretical Chemistry, Chemical Center, P.O. Box 124,
S-221 00 Lund, Sweden*

Abstract

The lower electronic states of the molecule PbO have been studied using a newly developed basis set of the atomic natural orbital (ANO) type. The method includes scalar relativistic effects through the use of a Douglas–Kroll Hamiltonian. Multiconfigurational wave functions have been used with dynamic correlation included using second-order perturbation theory (CASSCF/CASPT2). Spin–orbit coupling is added *a posteriori* by means of the RASSCF state interaction (RASSI) method, with all electronic states originating from Pb(s^2p^2 , 3P , 1D , 1S) and O(s^2p^4 , 3P) included in the CI expansion.

Computed spectroscopic constants for the 0^+ ground level are: $R_e = 1.926(1.922)$ Å, $D_0 = 4.00(3.83)$ eV, $\omega_e = 723(721)$ cm $^{-1}$, with experimental data within parentheses. Corresponding data for the 11 lowest excited levels are also presented. The dipole moment for the ground state has been computed to be 1.73(1.83) a.u. using finite field perturbation theory. The effect of spin–orbit coupling is to reduce the value with 0.03 a.u. This illustrative calculation shows that an approach that adds scalar relativistic effects to a non-relativistic wave function, and treats spin–orbit coupling by a configuration interaction method, can be used to obtain accurate properties also for molecules containing heavy main group elements.

Contents

1. Introduction	38
2. Details of the calculations	40
3. Results	41
3.1. The ground state potential	41
3.2. The lower excited states of PbO	42
3.3. The dipole moment and polarizability of PbO	46
4. Conclusions	48
Acknowledgements	48
References	49

1. INTRODUCTION

New basis sets of the atomic natural orbital (ANO) type have recently been developed for the alkaline, alkaline earth, main group and rare gas atoms [1,2]. These basis sets include scalar relativistic effects through the use of a Douglas–Kroll Hamiltonian. Multiconfigurational wave functions were used with dynamic correlation included using second-order perturbation theory (CASSCF/CASPT2). The basis sets were applied in calculations of ionization energies, electron affinities, and excitation energies for all atoms and the ground state potentials for the dimers. Spin–orbit coupling (SOC) was included using the RASSCF state interaction (RASSI) method [3]. This approach reproduced the spin–orbit splittings of the lowest atomic terms with an accuracy of better than 0.05 eV, except for the row 5 atoms, where the largest error was 0.27 eV. IPs and EAs had an accuracy better than 0.2 eV and atomic polarizabilities for the spherical atoms were computed with errors smaller than 2.5%. Computed bond energies for the dimers were accurate to better than 0.15 eV in most cases.

This multiconfigurational approach to heavy element chemistry is straightforward but somewhat cumbersome to apply. It includes near-degeneracy effects through the use of the CASSCF method [4] with dynamic electron correlation added using the CASPT2 method [5,6]. The treatment of relativistic effects is based on these non-relativistic wave functions. Scalar relativistic terms are included using the Douglas–Kroll Hamiltonian [7,8]. They are thus included also in the orbital and wave function optimization step. SOC effects do not, however, affect the MOs. Instead these effects are included *a posteriori*, but set up an SOC Hamiltonian matrix on a basis of CASSCF wave functions. An effective one-electron Fock-type spin–orbit Hamiltonian is used to approximate the SOC operator. It is based on atomic mean field integrals (AMFI), which has proven to be an accurate approximation to the true SO Hamiltonian [9,10].

The problem with this approach is that it may converge slowly in the number of basis states used to represent the SO Hamiltonian, in particular for the heaviest main group elements. It was shown in the ANO paper mentioned above that, in order to obtain an SO splitting of the lowest terms of the row 5 main group elements, it was necessary to include in the calculation all terms arising from the ground state electronic configuration, $(6s)^2(6p)^x$. Still, some errors remain. The term splittings for these atoms are given in Table 1. We notice that the error varies between 0.08 and 0.27 eV, becoming larger for the heavier elements. Chemically, it might be more interesting to consider the stabilization of the lowest level due to spin–orbit splitting. These energies are therefore also given in Table 1. They give the largest correction to the bond energy due to SOC (at least for closed shell molecules where SOC is quenched to a large extent at equilibrium geometry) and are afflicted with errors, which are of the same order as the error in the SO splitting.

Table 1. Spin–orbit splitting of the lowest term in the fifth row main group atoms

ΔJ	Atom ^a	SO stabilization ^b
$\frac{3}{2} - \frac{1}{2}$	Tl(² P)	0.60 (67)
	0.89(0.97)	
1–0	Pb(³ P)	1.23 (102)
	0.83(0.97)	
2–0	Po(³ P)	1.14 (63)
	1.20(1.32)	
0–2	Po(³ P)	1.14 (63)
	1.13(0.94)	
1–2	At(² P)	0.84 (33)
	1.82(2.09)	
$\frac{1}{2} - \frac{3}{2}$	At(² P)	0.84 (33)
	2.52(–)	

From Moore’s tables [11].
^aExperimental values within parentheses in eV.
^bStabilization of the ground level due to SOC. Percentage of the SO splitting in parentheses.

An exact estimate of the error is difficult to obtain because we cannot use the simplifications that a Landé interval rule would give. Notice, for example, that the ordering of the levels in Po comes in the order $J = 2,0,1$ instead of the order 2,1,0 given by the Landé rule. In this chapter we will in particular be interested in the SOC for Pb. We can here expect the error in the computed stabilization to be of the same order as the error in the computed SO splitting, about 0.10 eV.

When the present approach is applied to an energy surface of a molecule, one is thus faced with the problem of computing a large number of electronic states. The ground state of the Pb dimer has recently been studied and it was there necessary to include 41 spin-free electronic states [12]. They are all the states that: (1) include the symmetry of the Pb₂ ground state, 0_g⁺, and (2) dissociate to the ³P, ¹D, or ¹S states of the Pb atoms. The number of states increases further if one is also interested in studying potential curves for excited levels. The dimension of the calculation can be decreased substantially if one is only interested in the molecular properties in the neighborhood of the equilibrium geometry where fewer electronic states interact strongly *via* the SO Hamiltonian.

In the present chapter the method is tested for the PbO molecule. This molecule was chosen because a number of properties are known experimentally and because it has recently been studied with other high level quantum chemical methods, which allow a comparison of them with the present approach [13–18]. The molecule has a large dipole moment and polarizability, which can be used to test the importance of SOC on molecular

properties. We shall present results for the ground state potential ($^1\Sigma_g^+, 0^+$) and the lowest excited states. Different approaches to include SOC will be tested: (1) the inclusion of all states that dissociate to $\text{Pb}(^3\text{P}, ^1\text{D}, \text{ or } ^1\text{S})$ plus $\text{O}(^3\text{P})$ in the calculation of the potential curves, (2) CASSCF/CASPT2 calculations on the ground state potential only with the effect of SOC added from (1), and (3) calculations around equilibrium geometry including only the most important SO states, as obtained from the analysis of the results of (1).

2. DETAILS OF THE CALCULATIONS

All calculations reported have been performed using the MOLCAS-5.5 software [19]. The newly developed ANO-RCC basis sets were used with the following primitive/contracted sets: Pb, 25s22p16d12f4g/9s8p6d4f3g; O, 14s9p4d3f2g/5s4p3d2f1g. The active space used in the CASSCF calculations comprised the 6s,6p orbitals of Pb and the 2p orbitals of O (eight electrons in seven orbitals). Our previous studies of the main group dimers have shown that this is an appropriate active space to use for main group elements. Up to the half filled shell one should include also the s-orbital, while it may be left inactive for the p^4 and p^5 atoms. The Pb 5d semi-core electrons were correlated in the CASPT2 calculations, while all other core orbitals were frozen. The calculations were performed in C_2 symmetry, such that degenerate pairs of electronic states could be averaged. Running the calculation in C_{2v} symmetry would break the degeneracy of the Δ and Γ states, because they appear both in irrep 1 and 4, where they can mix with Σ^+ (irrep 1) and Σ^- (irrep 4) states.

Three sets of calculations have been performed:

Case 1: Include in the CASSCF state average calculations all states that dissociate to $\text{Pb}(6s^26p^2; ^3\text{P}, ^1\text{D}, \text{ or } ^1\text{S})$ and $\text{O}(2s^22p^4; ^3\text{P})$. The number of such states in the two irreps are: 5 quintets, 13 triplets and 5 singlets in irrep 1, and 4 quintets, 14 triplets, and 4 triplets in irrep 2, totaling 45 electronic states. Actually the highest singlet state in irrep 1 was excluded due to severe intruder state problems. CASSCF/CASPT2 calculations were performed for these states (separately for each spin and irrep) and the RASSI-SO Hamiltonian used the CASPT2 energies in the diagonal. This calculation gave an accurate SO splitting of the asymptotic states and should describe the SOC in the molecule with the same accuracy. The molecular orbitals will, however, not be the best for the ground electronic state because they have been obtained from a state average CASSCF calculation including five electronic states (degenerate states are counted as two in the above quantifications).

Case 2: Calculations can be performed on the ground and lower excited state potentials using single state CASSCF/CASPT2. This should give a good

representation of the orbitals and the correlation effects. The effect of SOC can then be added from the results obtained in Case 1. This type of calculation was performed for the 0^+ ground state.

Case 3: An alternative, which can be used around the equilibrium geometry, is to include only the electronic states that couple most strongly to the ground state. Which they are can be found from an analysis of the results obtained in Case 1. Again one can expect improved orbitals and wave functions because not so many states are included in the state averaging. The analysis shows that one needs to include only four triplets and one singlet in irrep 1 and 4 triplets in irrep 2, which occur with a weight larger than 10^{-4} in the 0^+ ground state. Thus, no state averaging is included in the ground state wave function.

The results obtained in these trial calculations will be compared with the aim to set a standard for which level of theory one needs in these types of studies.

Electric properties were obtained for the ground state using finite perturbation theory. An electric field, E , along the molecular axis was varied in steps of 0.005 a.u. and the resulting energies were fitted to a fourth-order polynomial in E . The first and second derivative then gave the dipole moment and polarizability along the molecular axis.

Potential curves were generated on a grid with a spacing of 0.05 a.u. around the equilibrium geometries of the different electronic states. Between 20 and 30 points were computed. The spectroscopic constants were obtained using the VIBROT module of the MOLCAS software. VIBROT solves the vibrational–rotational Schrödinger equation by numeric integration. The resulting vibrational energies and wave functions are used to generate the spectroscopic constants.

3. RESULTS

3.1. The ground state potential

The results obtained for the ground state potential are shown in Table 2, which gives the spectroscopic constants for the three different cases. The calculation, which includes all the electronic states (Case 1), gives a dissociation energy (D_0) of 5.08 eV at the CASPT2 level of theory. This is more than 1 eV larger than experiment. Adding the effect of SOC decreases the value to 4.03 eV, 0.2 eV larger than the experimental value quoted in Huber and Herzberg [20]. The computed bond distance is about 0.01 Å longer than the experimental value. All the spectroscopic constants improve when the calculation is restricted to the ground state alone (Case 2), but only marginally. The error in D_0 is reduced to 0.17 eV. The most profound improvement is obtained for the vibrational frequency. The calculation using

Table 2. Spectroscopic constants for the ground state of PbO using three different methods

	Case 1		Case 2		Case 3	
	CASPT2	With SOC	CASPT2	With SOC	With SOC	Expt ^a
R_e (Å)	1.928	1.931	1.923	1.926	1.925	1.922
D_0 (eV)	5.08	4.03	5.05	4.00	4.78	3.83
ω_e (cm ⁻¹)	718	707	732	721	723	721
$\omega_e x_e$ (cm ⁻¹)	3.47	3.60	3.43	3.36	3.09	3.54
$\Delta G_{v+1/2}$ (cm ⁻¹)	711	700	712	715	716	–

Case 1: state average over 44 states. Case 2: only ground state with SOC from Case 1. Case 3: state average over the nine lowest states.

^aFrom Ref. [20].

only the electronic states that interact most strongly with the ground state (Case 3) does not lead to any further improvement. This method can clearly not be used to compute the dissociation energy because the asymptotic energy lowering due to SOC is not accounted for. This value is, however, computed with good accuracy in Case 1. The computed stabilization is 1.22 eV, which should be compared with 1.23 eV obtained in a calculation on the isolated Pb atom. The error in this value can be estimated from the computed atomic SOC to be 0.05–0.1 eV and thus accounts for part of the deviation in the computed bond energy from experiment. We conclude that both Case 1 and Case 2 give a bond energy that deviates not more than 0.1 eV from experiment.

Case 3 also gives satisfactory properties at equilibrium but can obviously not be used to compute the dissociation energy. One may note that a reasonable estimate of this value can be obtained by adding the atomic value for the spin–orbit stabilization to the CASPT2 energy: $5.05 - 1.23 = 3.82$ eV. The effect of SOC at equilibrium is modest: the bond distance is increased by 0.003 Å and the vibrational frequency decreases by 11 cm⁻¹. These effects are minor but not negligible. The only quantity that is strongly affected by SOC for the closed shell molecule PbO is the dissociation energy. This is in line with results obtained in earlier studies (see, e.g., Ref. [17]). The situation is different for the excited states.

3.2. The lower excited states of PbO

As far as we know there has not been any earlier theoretical analysis of the electronic spectrum of PbO. Many of the methods used to study this molecule are such that they cannot be applied to excited states. The present approach, on the other hand, is constructed to be able to deal with complex open shell electronic structures. With the development of the RASSI

methods for SOC it has now become possible to extend that application to complex electronic spectra for heavy element compounds. We have earlier applied the same method to study the excited states of molecules like $\text{Re}_2\text{Cl}_8^{2-}$ [21] and UO_2 [22].

The 44 electronic states of PbO used in Case 1 give rise to 134 spin–orbit states (counting Kramer doublets as two). Fifteen of these have energies smaller than 3 eV ($25,000\text{ cm}^{-1}$). We have computed the spectroscopic constants for them. The seven lowest CASPT2 potentials (no SOC) are presented in Fig. 1. A striking feature of the spectrum is the high density of states in a narrow region around $20,000\text{ cm}^{-1}$ (0.1 a.u.) above the ground state. Five electronic states have T_e values between $19,990$ and $21,430\text{ cm}^{-1}$ (2.48–2.66 eV). They give rise to 10 levels with Ω values ranging from 0 to 3. Analyzing such a complicated spectrum is not without problems and the data given by Huber and Herzberg are also rather incomplete. We shall see that the combination of the experimental data and the present results can put the assignments of the electronic spectrum on a more firm basis.

In Table 3 we present the computed spectroscopic constants for the 10 lowest levels. The corresponding potential curves are shown in Fig. 2.

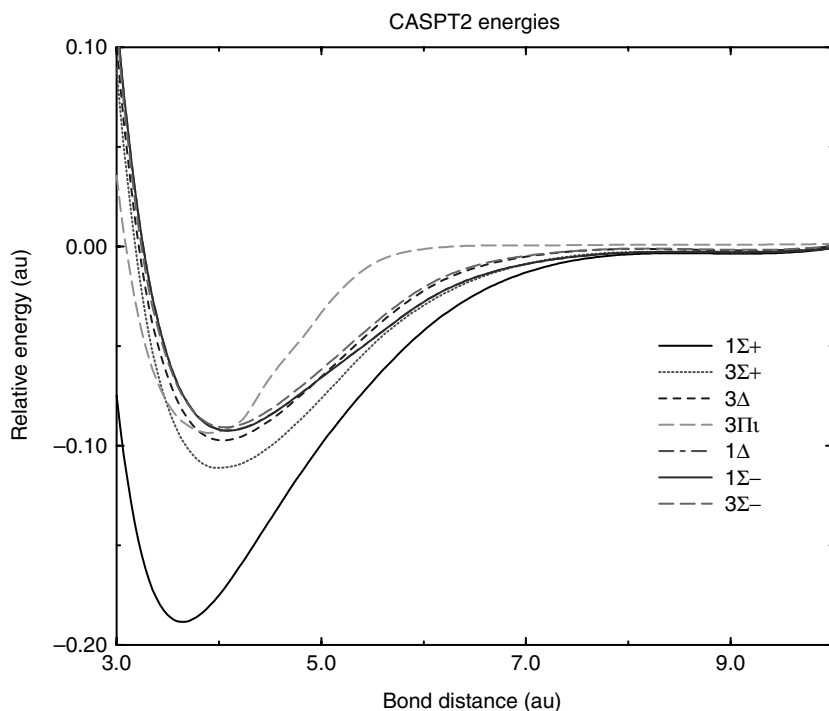


Fig. 1. CASPT2 potential curves (no SOC) for the seven lowest electronic states of PbO .

Table 3. Spectroscopic constants for 11 excited states of PbO including SOC (experimental values within parentheses)

Level	Ω	R_e (Å)	D_0 (eV)	ω_e (cm ⁻¹)	T_e (eV)	Osc. str. ^a	Origin ^b
b	0 ⁻	2.129	2.09	442(441) ^c	1.94(2.04) ^c	—	³ Σ^+ (70%), ¹ Σ^- (19%)
a	1	2.130(2.12)	2.09	496(482)	1.94(1.99)	0.90×10^{-4}	³ Σ^+ (73%), ³ Σ^- (20%)
	2	2.145	1.86	500	2.17	—	³ Δ (56%), ¹ Δ (40%)
	1	2.133	1.85	479	2.20	0.12×10^{-2}	³ Δ (90%)
	0 ⁻	2.073	2.52	564	2.32	—	³ Π (90%), ³ Σ^+ (6%)
A	0 ⁺	2.079(2.09)	1.81	517(444)	2.34(2.46)	0.78×10^{-4}	³ Π (88%), ³ Σ^- (10%)
B	1	2.072(2.07)	2.35	536(498)	2.49(2.76)	0.11×10^{-2}	³ Π (72%), ¹ Π (17%)
C	0 ⁺	2.133(2.11)	2.04	491(532)	2.81(2.95)	0.12×10^{-2}	³ Σ^- (83%), ³ Π (8%)
	0 ⁻	2.151	1.99	476	2.87	—	³ Σ^- (77%), ³ Σ^+ (21%)
C'	1	2.136(2.14)	1.91	458(494)	2.95(3.09)	0.43×10^{-2}	³ Σ^- (71%), ³ Σ^+ (21%)
D	1	2.056(2.05)	1.40	497(531)	3.45(3.74)	0.98×10^{-2}	¹ Π (74%), ³ Π (22%)

From Ref. [20].

^a Oscillator strength computed at the ground state geometry.^b Main electronic state in the SO wave function at the bond distance 4.00 a.u.^c Uncertain.

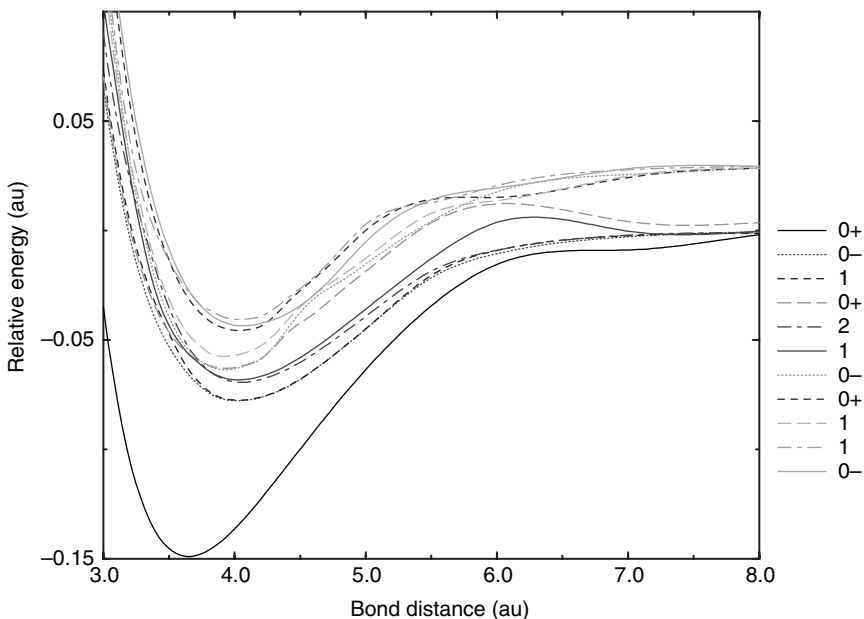


Fig. 2. Potential curves for the 11 lowest spin–orbit states of PbO.

The first two levels (0^- and 1) originate from the $^3\Sigma^+$ state. The two potential curves are almost parallel and the spectroscopic constants are very similar. Experimentally, the T_e values are separated with 0.05 eV (the value for 0^- is, however, uncertain and is given within parentheses), while the calculations give two almost degenerate levels. We note that the difference in vibrational frequency is well reproduced. Huber and Herzberg list five more levels below 4 eV with Ω values 0^+ , 1 , 0^+ , 1 , and 1 (the values that give dipole allowed transitions). In Table 3 we have assigned these levels such that the best agreement is obtained in R_e and T_e values.

A good handle for the assignment is the bond distance. Those levels that originate from the $^3\Pi$ and $^1\Pi$ states (1 , 0^+ , and 0^-) have a bond distance of about 2.07 Å, while other levels have R_e values between 2.13 and 2.15 Å. The assignments presented in Table 3 have used this information and the computed T_e values to assign the levels above the first two, for which the assignment is obvious. As a result, the levels A,B (in the notation of Huber and Herzberg) are assigned to the $^3\Pi$ origin, even if one level with $\Omega = 1$ (originating from the $^3\Delta$ state) appears at a lower energy. With the present assignment all R_e values agree with experiment within 0.02 Å and the transition energies are accurate to better than 0.3 eV. One can probably blame the large number of states used in the state averaging. The error is systematic and is therefore related to the too large value (by 0.20 eV)

obtained for the dissociation energy of the ground state. Correcting the T_e for this error gives agreement with experiment to better than 0.1 eV. One should, however, remember that the method in itself carries an error that can be as large as 0.2 eV for excitation energies.

The vibrational frequencies are not well reproduced, with the exception of the ground state and the two lowest excited levels. We attribute this to the high density of states in the region around 2 eV, with several avoided crossings. Small errors in the relative energies of the different potentials can easily result in large effects on their shape.

3.3. The dipole moment and polarizability of PbO

Many of the earlier studies of PbO have been concerned with the dipole moment and electric polarizability [13,14,18,23]. In 1993 Dolg *et al.* [13] estimated the contribution to SOC for the dipole moment to be between -0.03 and -0.08 a.u. The most recent CCSD(T) study gives a value of 1.764 a.u. for the dipole moment and 62.55 a.u. for the parallel component of the polarizability [18].

These properties have in the present work been computed using finite field perturbation theory (FFPT). Five field strengths were used: -0.01 , -0.005 , 0.0 , 0.005 , and 0.01 a.u. The energies were fitted to a polynomial of degree 4. Two sets of such calculations were performed: one that includes all the 44 states (Case 1) and one that includes the ground state only (Case 2). The latter study will of course give the most accurate value for these properties. It should, however, be possible to use the Case 1 study to estimate the contribution of SOC to them. All calculations were performed at the equilibrium geometry (1.926 Å).

The results are presented in Table 4. Case 1 gives a too small dipole moment. Actually, the expectation value for CASSCF is only 1.32 a.u., showing that the state averaging leads to a ground state electronic structure that is not polar enough (the expectation value and the FFPT result are of course identical in the ground state only calculation). Most of this error is recovered at the CASPT2 level of theory but there remains a difference of 0.06 a.u. between the Case 1 and Case 2 results. The polarizability is less affected with almost identical results at the CASPT2 level in the two sets of calculations. Our final estimate for the dipole moment is 1.756 a.u. without SOC and 1.731 a.u. with. The value obtained without SOC is almost identical to the recent CCSD(T) result. The difference is only 0.008 a.u. The present study concludes that the dipole moment of PbO is decreased with 0.025 a.u. due to SOC. This is due to the inclusion of excited states with smaller polarity into the ground state wave function.

In Fig. 3 we show how the dipole moment varies with the bond distance. These results have been taken as expectation values of the CASPT2 and

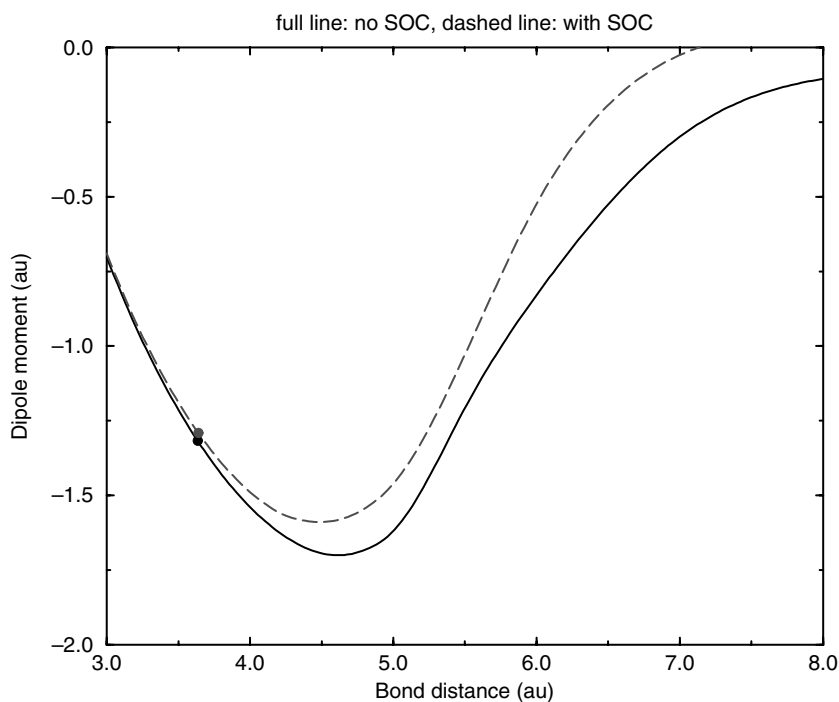
Table 4. Dipole moment and polarizability (α_{zz}) for the ground state of the PbO molecule

	Dipole moment (a.u.)		Polarizability (a.u.)	
	Case 1	Case 2	Case 1	Case 2
CASSCF	1.441	1.692	58.80	62.74
CASPT2	1.699	1.756	61.11	61.21
With SOC	1.674	1.731	60.27	60.37
CCSD(T) ^a		1.764		62.55
Expt ^b		1.83 ± 0.12		

Case 1: state average over 44 states. Case 2: only ground state with SOC from Case 1.

^aFrom Ref. [18].

^bFrom Ref. [20].

**Fig. 3.** Dipole moment curves for PbO. Lower curve: CASPT2, upper curve: with SOC. The dots give the equilibrium geometries in the two cases. The dipole moments have been obtained as expectation values.

CASPT2/SOC wave functions and are therefore not very accurate. However, they give a correct qualitative picture. The difference between the values obtained with SOC and without increases with distance. The curves are quite steep in the neighborhood of equilibrium geometry. The SOC contribution to the dipole moment will therefore also be affected by the change in geometry. In this case it is small (indicated by the two dots in the figure), but in general such considerations cannot be neglected. The experimental value of the dipole moment is 1.83 a.u. with an uncertainty of about 0.1 a.u. One can thus safely conclude that the present, as well as several earlier, results are in agreement with experiment [20,24].

The dipole polarizability along the molecular axis is also decreased; the difference between the results with and without SOC is 0.8 a.u. The spin-free result differs by about 1 a.u. from the CCSD(T) result of Kellö *et al.* [18]. It seems that the present approach is also viable for the calculation of electric properties. Similar results have been obtained also for the excited states, but they will not be presented here.

4. CONCLUSIONS

We have presented results from a theoretical study of the electronic and molecular properties of the PbO molecule. A multiconfigurational approach has been used, which essentially works with non-relativistic wave functions. Relativity is introduced in two steps. First scalar relativistic effects are included through the use of the Douglas–Kroll Hamiltonian and a correspondingly constructed AO basis set. Spin–orbit effects are included by allowing different CASSCF wave functions to mix under the influence of a spin–orbit Hamiltonian.

The results obtained in the present study show that such an approach is capable of yielding molecular properties of an accuracy that is comparable with other sophisticated quantum chemical methods. It is unique in the sense that it treats ground and excited states on an equal footing. This has been amply demonstrated here with a treatment of 11 excited levels, leading to a detailed assignment of the electronic spectrum of PbO below 4 eV.

ACKNOWLEDGEMENTS

This paper is a tribute to Professor Osvaldo Goscinski and his scientific work. Our scientific roads have crossed only occasionally, but there is a seminal paper that had a strong influence on our work on the direct CI method. This is the paper from 1970 on the variational-perturbation approach [25]. Per Siegbahn and I used this approach in the early development of the direct CI method and the convergence rate of the secular problem was increased by an

order of magnitude compared with the simple perturbation approach that was used in the first implementation. The method was later to be known, in a slightly modified version, as the Davidson diagonalization method, but it originates in the work of Brändas and Goscinski.

This work has been supported by a grant from the Swedish Science Research Council, VR and the Swedish Foundation for Strategic Research (SSF). One of us (BOR) would like to thank Professor Vlado Kellö for inspiring this work during a boat trip through northern Norway's waterways.

REFERENCES

- [1] B. O. Roos, V. Veryazov and P.-O. Widmark, *Theor. Chim. Acta*, 2004, **111**, 345.
- [2] B. O. Roos, R. Lindh, P.-Å. Malmqvist, V. Veryzov and P.-O. Widmark, *J. Phys. Chem. A*, 2004, **108**, 2851.
- [3] P.-Å. Malmqvist, B. O. Roos and B. Schimmelpfennig, *Chem. Phys. Lett.*, 2002, **357**, 230.
- [4] B. O. Roos, in *Advances in Chemical Physics; Ab Initio Methods in Quantum Chemistry – II* (ed. K. P. Lawley), Wiley, Chichester, UK, 1987, p. 399, Chapter 69.
- [5] K. Andersson, P.-Å. Malmqvist, B. O. Roos, A. J. Sadlej and K. Wolinski, *J. Phys. Chem.*, 1990, **94**, 5483–5488.
- [6] K. Andersson, P.-Å. Malmqvist and B. O. Roos, *J. Chem. Phys.*, 1992, **96**, 1218–1226.
- [7] N. Douglas and N. M. Kroll, *Ann. Phys.*, 1974, **82**, 89.
- [8] B. Hess, *Phys. Rev. A*, 1986, **33**, 3742.
- [9] B. A. Hess, C. Marian, U. Wahlgren and O. Gropen, *Chem. Phys. Lett.*, 1996, **251**, 365.
- [10] O. Christiansen, J. Gauss and B. Schimmelpfennig, *Chem. Phys. Phys. Chem.*, 2000, **2**, 965.
- [11] C. E. Moore, *Natl Bur. Stand.*, Vol. Circular 467, US Government Printing Office, Washington, DC, 1952.
- [12] B. O. Roos and P.-A. Malmqvist, *Phys. Chem. Chem. Phys.*, 2004, **6**, 2919.
- [13] M. Dolg, A. Nicklass and H. Stoll, *J. Chem. Phys.*, 1993, **99**, 3614.
- [14] V. Kellö, A. J. Sadlej and K. Fægri, Jr., *J. Chem. Phys.*, 1998, **108**, 2056.
- [15] K. G. Dyall and T. Enevoldsen, *J. Chem. Phys.*, 1999, **111**, 10000.
- [16] E. van Lenthe, A. Ehlers and E.-J. Baerends, *J. Chem. Phys.*, 1999, **110**, 8943.
- [17] B. Metz, H. Stoll and M. Dolg, *J. Chem. Phys.*, 2000, **113**, 2563.
- [18] V. Kellö, A. Antušek and M. Urban, *J. Comput. Methods Sci. Eng.*, in press.
- [19] K. Andersson, M. Barysz, A. Bernhardsson, M. R. A. Blomberg, D. L. Cooper, M. P. Fülscher, C. de Graaf, B. A. Hess, G. Karlström, R. Lindh, P.-Å. Malmqvist, T. Nakajima, P. Neogrády, J. Olsen, B. O. Roos, B. Schimmelpfennig, M. Schütz, L. Seijo, L. Serrano-Andrés, P. E. M. Siegbahn, J. Stålring, T. Thorsteinsson, V. Veryazov and P.-O. Widmark, *MOLCAS Version 5.4*, Department of Theoretical Chemistry, Chemical Center, University of Lund, Lund, Sweden, 2002.
- [20] K. P. Huber and G. Herzberg, *Molecular Spectra and Molecular Structure. 4: Constants of Diatomic Molecules*, Van Nostrand Reinhold, Princeton, NJ, 1979.
- [21] L. Gagliardi and B. O. Roos, *Inorg. Chem.*, 2003, **42**, 1599.
- [22] L. Gagliardi, B. O. Roos, P.-Å. Malmqvist and J. M. Dyke, *J. Phys. Chem. A*, 2001, **105**, 10602–10606.
- [23] H. Basch, W. J. Stevens and M. Krauss, *J. Chem. Phys.*, 1981, **74**, 2416.
- [24] Landolt-Börnstein, *Numerical Data and Functional Relationships in Science and Technology, New Series, Vol. 14, Molecular Constants*, Springer, Berlin, 1982.
- [25] E. Brändas and O. Goscinski, *Phys. Rev. A*, 1970, **1**, 552.

This page intentionally left blank

Is There a Favorite Isomer for Hydrogen-Bonded Methanol in Water?

Eudes E. Fileti,¹ Kaline Coutinho² and Sylvio Canuto¹

¹*Instituto de Física, Universidade de São Paulo, CP 66318, 05315-970 São Paulo, SP, Brazil*

²*Universidade de Mogi das Cruzes/CIIB, CP 411, 08701-970 Mogi das Cruzes, SP, Brazil*

Dedicated to Prof. Osvaldo Goscinski on the occasion of his 65th anniversary

Abstract

Sequential Monte Carlo/quantum-mechanical calculations of the interaction energy of hydrogen-bonded methanol in liquid water give the same result for methanol acting either as the proton donor or the proton acceptor. For the complex-optimized cases, methanol acting as the proton acceptor, $\text{CH}_3\text{HO} \cdots \text{H}_2\text{O}$, is more stable than the proton donor, $\text{CH}_3\text{OH} \cdots \text{OH}_2$, by ~ 0.5 kcal/mol. In the case of methanol in liquid water, at room temperature, statistically converged results, using counterpoise corrected MP2/aug-cc-pVDZ calculations, lead to the same binding energy in both cases.

Contents

1. Introduction	51
2. Methods	53
2.1. Monte Carlo simulation	53
2.2. Hydrogen bonds from Monte Carlo simulation	54
2.3. Quantum-mechanical calculations	56
3. Results	57
3.1. Gas-phase interaction	57
3.2. Liquid (1:1) interaction	58
3.3. Statistical convergence	60
4. Final remarks and conclusions	61
Acknowledgements	61
References	62

1. INTRODUCTION

Alcohol–water liquids are among the most interesting liquid mixtures [1–3]. Indeed, alcohol–water exhibits properties that are of great interest in physics, chemistry and biology. To a large extent this is a consequence of

the great ability of both water and alcohol to make hydrogen bonds. They are both proton donors and proton acceptors of hydrogen bonds. The methanol–water system can have two hydrogen-bonded structures corresponding to the two possible heterodimers (or isomers) where methanol is a proton acceptor, $\text{CH}_3\text{HO}\cdots\text{H}_2\text{O}$, or a proton donor, $\text{CH}_3\text{OH}\cdots\text{OH}_2$, of the hydrogen bond (see Fig. 1). The existence of these two isomers is easy to realize and the strengths of the two possible interactions are of great interest. In fact, they are related to several thermodynamic and physico-chemical properties. For instance, the mixture of methanol and water exhibits an entropy value that is considerably smaller than one should expect [1,4,5]. Also there are enormous consequences in the segregation and in the hydrophobic role of the CH_3 group leading to fundamental questions regarding the orientational local order [4,5]. Methanol–water is one of the simplest examples of the amphoteric relation because of the fact that both methanol and water can act as proton donors and proton acceptors of hydrogen bonds. The question of which of the two isomers is the more stable has been a conspicuous one. Early theoretical studies have obtained controversial results [6–10] regarding the relative stability of the two isomers. Even experimental results have missed the $\text{CH}_3\text{OH}\cdots\text{OH}_2$ isomer and obtained only one heterodimer [11]. It was not until very recently that the question has been confidently answered for the gas-phase complexes. Detailed microwave rotation-tunneling spectroscopy [12] has set the issue and established that the complex where methanol is the proton acceptor and water is the proton donor, $\text{CH}_3\text{HO}\cdots\text{H}_2\text{O}$ in Fig. 1 (left), is the more stable isomer in the gas phase. More recent theoretical calculations have indeed confirmed the greater stability of this isomer but obtained a relative stability that is less than 1 kcal/mol [13,14]. Although gas-phase results are of interest in their own right, it is also clear that the liquid situation may find a broader range of interest for alcohol–water mixtures [15–18]. Unfortunately, the results obtained for the gas phase cannot be directly extrapolated to the liquid situation without great risk. The hydrogen bonds in a liquid environment certainly do not satisfy a minimum-energy structure. In fact, a liquid is better

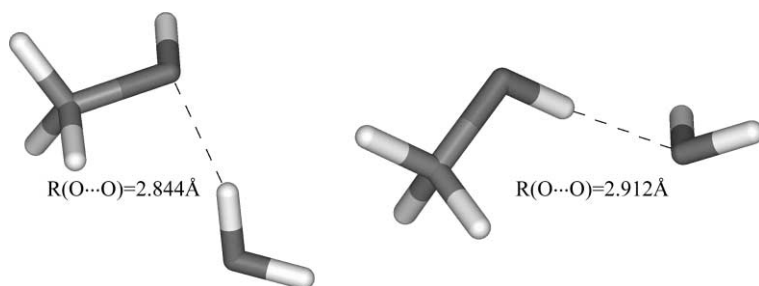


Fig. 1. The two isomers of hydrogen-bonded methanol–water.

described by statistical physics and its structure is represented by a great number of possible configurations or molecular arrangements. The thermal contribution leads to a decrease of the hydrogen bond interaction [19,20]. Hence, the strength of the hydrogen bond formed between methanol and water in the gas phase is not the same as in the liquid case. The focus of this present contribution is to clarify this aspect. In fact, we will make an attempt to obtain the relative strength of the two hydrogen-bonded isomers formed between methanol and water in the liquid environment at room temperature. We use Monte Carlo simulation to generate the structure of the liquid composed of methanol in bulk water. Using the structures of the simulation, we identify the hydrogen bonds in the liquid, in both isomeric possibilities, select the configurations and perform *ab initio* quantum mechanics calculations to obtain the intermolecular strength. These results clarify the relative strengths in the liquid environment and also give a theoretical estimate of the decrease of the hydrogen bond interaction as compared with the gas-phase situation.

2. METHODS

2.1. Monte Carlo simulation

The structure of the liquid is generated by Metropolis Monte Carlo (MC) computer simulation [21], using the DICE Monte Carlo program [22]. The simulations are performed in the canonical (*NVT*) ensemble with one methanol molecule plus 400 water molecules using the experimental density of water, which at $T = 298.15$ K is 0.9966 g/cm^3 . The intermolecular interactions are described by the standard Lennard–Jones plus Coulomb potentials. For the water molecules we use the SPC potential [23] and for methanol we use the all-site OPLS–AA potential [24]. Our sequential Monte Carlo/quantum mechanics procedure for generating liquid structure using MC simulation has been described previously in great detail [19,20,25,26]. The present simulation consisted of an equilibration stage of 2.0×10^6 MC steps, followed by a long averaging stage of 80.0×10^6 MC steps, where the equilibrium configurations are generated. Successive configurations generated in the MC simulations are found to be statistically highly correlated, and will not give important additional information. Therefore, we calculate the interval of statistical correlation using the auto-correlation function of the energy [27]. For the simulations presented here, after the calculation of the auto-correlation of the energy, we obtain that configurations separated by 4.0×10^5 MC steps are statistically relevant ($\sim 20\%$ of statistical correlation). Thus, after the entire simulation, 200 configurations separated by 4.0×10^5 MC steps were sampled.

2.2. Hydrogen bonds from Monte Carlo simulation

An important point is the identification of the hydrogen bonds in the structures generated in the Monte Carlo simulation. Hydrogen bonds are normally extracted from computer simulation using the pair-wise radial distribution function [21]. This gives the coordination of water molecules around the solute, but it cannot be assured that all near-neighbor water molecules are indeed hydrogen bonded. This point has been the subject of previous concern [19,20,26–28]. The definition of a hydrogen bond in a liquid is not unanimously free from ambiguities. However, a very efficient procedure can be obtained using in addition to the geometric, also an energetic criterion [19,20,26,29–31]. Here we identify a hydrogen-bonded structure when the distance $R_{O-O} \leq 3.35$ Å, the angle $\theta(O-OH) \leq 40^\circ$ and the binding energy is larger than 2.5 kcal/mol. These geometric conditions are obtained from the radial and angular distribution functions. For the energetic criterion we look at the pair-wise energy distribution.

First, Fig. 2 shows the pair-wise radial distribution function between the O atom of methanol and the O atom of water. The first peak in this $G_{O-O}(r)$ distribution function starts at 2.45 Å and ends at 3.35 Å, with a maximum at 2.75 Å. Hydrogen bonds can therefore be located for the distance $R_{O-O} \leq 3.35$ Å. Similar analysis gives the criterion for the angle $\theta(O-OH) \leq 40^\circ$. Figure 3, in turn, identifies the hydrogen bonds for pair-wise methanol–water interaction energy at less than -2.5 kcal/mol. Using these three criteria, in the 200 MC configurations we find 287 hydrogen bonds formed in the $CH_3HO \cdots H_2O$ and 160 in the $CH_3OH \cdots OH_2$ isomers.

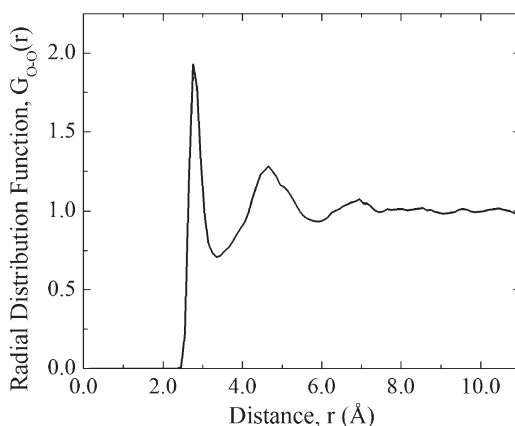


Fig. 2. Pair-wise radial distribution function between the oxygen atoms of methanol and water.

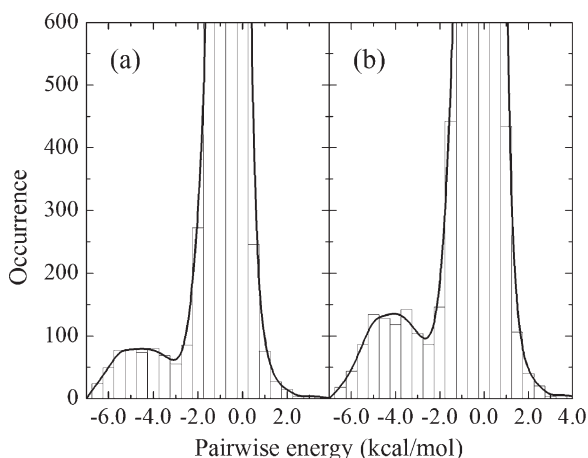


Fig. 3. Histogram of the pair-wise energy interaction between methanol and water: (a) $\text{CH}_3\text{OH}\cdots\text{OH}_2$ isomer and (b) $\text{CH}_3\text{HO}\cdots\text{H}_2\text{O}$ isomer.

Table 1 shows the detailed statistics of hydrogen bonds. For the $\text{CH}_3\text{HO}\cdots\text{H}_2\text{O}$ isomer we find that seven (3.5%) of the configurations do not form any hydrogen bonds, in 103 (51.5%) it forms one, in 86 (43%) it forms two and in only four (2%) it forms three hydrogen bonds. This gives an average of 1.43 hydrogen bonds between methanol and water in the $\text{CH}_3\text{HO}\cdots\text{H}_2\text{O}$ isomer. For the $\text{CH}_3\text{OH}\cdots\text{OH}_2$ the picture is slightly different: 40 (20%) configurations make no hydrogen bond and the rest, 160 (80%), make one hydrogen bond, leading to an average of 0.80 hydrogen bond. Because of the great diversity of structures of the methanol–water mixture [18], an explanation is needed. The physical situation considered here is methanol in extreme dilution in water. Hence, only one methanol molecule is considered. In a liquid mixture with proper proportion there will also be configurations where two methanol molecules acting as proton donor

Table 1. Statistics of the hydrogen bonds formed between methanol and water (see text)

Number of hydrogen bonds	$\text{CH}_3\text{HO}\cdots\text{H}_2\text{O}$	$\text{CH}_3\text{OH}\cdots\text{OH}_2$
0	7 (3.5%)	40 (20.0%)
1	103 (51.5%)	160 (80.0%)
2	86 (43.0%)	–
3	4 (2.0%)	–
Average	1.43	0.80

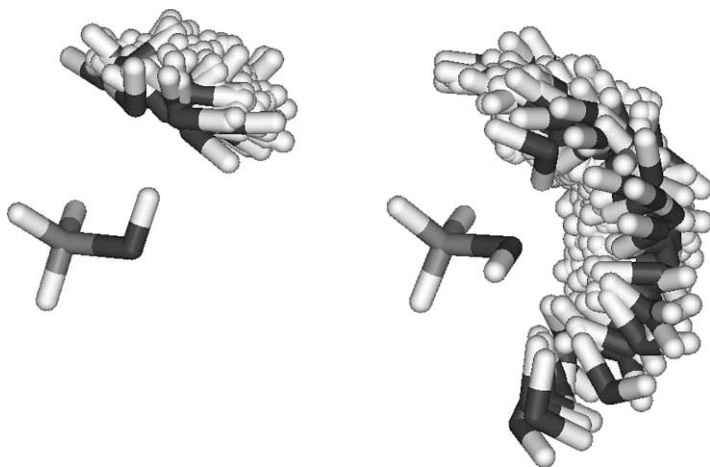


Fig. 4. Superposition of configurations of the hydrogen bonds formed by methanol in aqueous solution.

are hydrogen bonded to a single water molecule. This, however, will not be present here, giving a more simplified picture and a more direct comparison with the (1:1) gas-phase result. Thus, we will focus on the 103 configurations making one hydrogen bond in the $\text{CH}_3\text{HO} \cdots \text{H}_2\text{O}$ and 160 configurations in $\text{CH}_3\text{OH} \cdots \text{OH}_2$. All these (1:1) structures composed of one methanol and one water molecule will be submitted to quantum-mechanical calculations. In fact, statistical convergence is obtained before we use all these hydrogen-bonded structures.

Figure 4 shows, in a single picture, the superposition of all these (1:1) hydrogen bond structures in the liquid for both isomers. It clearly shows the efficiency of the identification and the sampling procedure for obtaining hydrogen bonds formed between methanol and water. Indeed, it can be seen how the configuration space is filled and the water molecules are hydrogen bonded to the methanol. The calculated hydrogen bond distance O–O in the complex is 2.844 Å for the $\text{CH}_3\text{HO} \cdots \text{H}_2\text{O}$ isomer and 2.912 Å for the $\text{CH}_3\text{OH} \cdots \text{OH}_2$ isomer. For comparison, in the (1:1) liquid case, the average distances are calculated as 2.84 ± 0.16 and 2.84 ± 0.15 Å, respectively.

2.3. Quantum-mechanical calculations

The major interest of this paper is the calculation of the binding energy of methanol in liquid water and a comparison with the result obtained for the optimized (1:1) cluster. All binding energies are obtained using counterpoise correction [32] to basis set superposition error (BSSE), i.e.,

$$\Delta E_{\text{AB}}^{\text{CP}} = E_{\text{AB}} - E_{(\text{A})\text{B}} - E_{\text{A}(\text{B})} \quad (1)$$

where, as usual, E_{AB} is the energy of the complex, $E_{A(B)}$ is the energy of the monomer A obtained with the entire basis set, including the basis set of monomer B, and $E_{B(A)}$ is the equivalent for the monomer B.

As the appropriate Boltzmann weights are included in the Metropolis Monte Carlo sampling technique, the average value of the binding energy, or any other property calculated from the MC data, is given as a simple average over a chain of size L of energy values:

$$\langle E \rangle = \frac{1}{L} \sum_i^L E_i \quad (2)$$

The quantum-mechanical energies and properties are calculated individually for each of the (1:1) structures extracted from the MC simulation of the liquid and for the optimized (1:1) complexes using many-body perturbation theory in second order with the Moller–Plesset partitioning [33], using the MP2/aug-cc-pVDZ theoretical model implemented in the Gaussian 98 program [34].

3. RESULTS

3.1. Gas-phase interaction

We first consider the isolated methanol–water system, corresponding to the gas-phase physical circumstance. A full geometry optimization is performed for both isomers using the second-order MP2 and the aug-cc-pVDZ basis set. Figure 1 shows the optimized hydrogen bond O–O distance in both cases. We can note that the $\text{CH}_3\text{HO} \cdots \text{H}_2\text{O}$ isomer has a shorter distance indicating a possible stronger bond. The calculated O–O hydrogen bond distances of 2.844 and 2.912 Å are in good agreement with the previous result [13] of 2.851 and 2.901 Å. Table 2 shows the calculated results for the binding energy of both isomers after taking into account the BSSE *via* counterpoise correction. To analyze the role of electron correlation effects in more detail, higher order calculations, up to the coupled-cluster CCSD(T) level, were performed in the geometries obtained at the MP2/aug-cc-pVDZ level. At the MP2 level the $\text{CH}_3\text{HO} \cdots \text{H}_2\text{O}$ isomer is more stable by 0.7 kcal/mol. This is in good agreement with previous density-functional theory calculations by González *et al.* [13] that obtained the same value for the relative stability of this isomer. With all theoretical results shown in Table 2 we can see that the $\text{CH}_3\text{HO} \cdots \text{H}_2\text{O}$ isomer is more stable but the relative stability is less than 1 kcal/mol. In fact, at the highest level used here, CCSD(T)/aug-cc-pVDZ//MP2/aug-cc-pVDZ, we obtain a relative stability of 0.5 kcal/mol. This agreement between MP2 and CCSD(T) corroborates that MP2/aug-cc-pVDZ is a good theoretical model for obtaining hydrogen bond interaction. If we take

Table 2. Calculated binding energies (kcal/mol) of the two hydrogen-bonded methanol–water isomers in the gas phase

Method	$\text{CH}_3\text{HO} \cdots \text{H}_2\text{O}$	$\text{CH}_3\text{OH} \cdots \text{OH}_2$	Relative stability
MP2/aug-cc-pVDZ	5.2	4.5	0.7
MP3/aug-cc-pVDZ	4.9	4.4	0.5
D-MP4/aug-cc-pVDZ	4.8	4.3	0.5
DQ-MP4/aug-cc-pVDZ	4.7	4.2	0.5
SDQ-MP4/aug-cc-pVDZ	4.8	4.2	0.6
MP4/aug-cc-pVDZ	5.0	4.4	0.6
CCSD/aug-cc-pVDZ	4.7	4.2	0.5
CCSD(T)/aug-cc-pVDZ	5.0	4.5	0.5
B3LYP/6-311 + G(3df,2p)	5.9	5.2	0.7
ZPE	1.9	1.6	–

All present calculations are made using the geometry optimized with MP2/aug-cc-pVDZ. B3LYP stands for the DFT calculations of González *et al.* [13] using the B3LYP/6-311 + G(d,p) optimized geometry. ZPE stands for zero point energy difference between the complex and the separate parts using MP2/aug-cc-pVDZ.

into account the zero-point energy correction that is important in the gas-phase results, the relative stability decreases to 0.5 kcal/mol (MP2) and 0.2 kcal/mol (CCSD(T)). It is clear from these results that high-level *ab initio* calculations systematically predict the existence of both isomers with the $\text{CH}_3\text{HO} \cdots \text{H}_2\text{O}$ one being the most stable. The relative stability is, however, very small, being calculated to be less than 1 kcal/mol and with the best result indicating a relative stability of the $\text{CH}_3\text{HO} \cdots \text{H}_2\text{O}$ isomer by only 0.5 kcal/mol.

3.2. Liquid (1:1) interaction

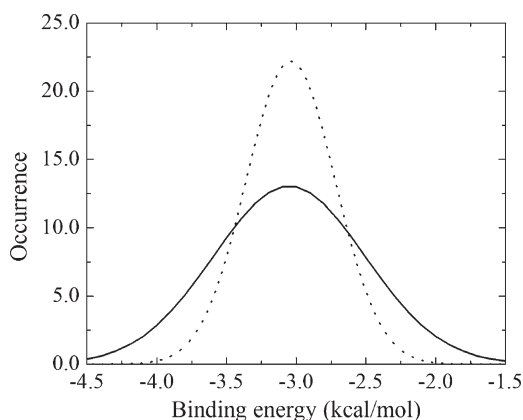
Now we discuss the results obtained using the structures generated by the MC simulation at room temperature. The calculated average binding energies obtained using the (1:1) structures of the MC simulation, sampled according to the statistical correlation as discussed above, are shown in Table 3. These average results include counterpoise correction to BSSE. The results show that the binding energies are the same within 0.01 kcal/mol, which is much smaller than the standard deviation of the calculations. The $\text{CH}_3\text{HO} \cdots \text{H}_2\text{O}$ isomer has an average binding energy of 3.05 ± 1.09 kcal/mol compared with the value of 3.04 ± 0.64 kcal/mol for the $\text{CH}_3\text{OH} \cdots \text{OH}_2$ isomer. It is clear that in the liquid situation at room temperature these results are similar and favor the conclusion that the two possible isomers are equally probable energetically. The largest standard deviation (1.09 vs. 0.64 kcal/mol) obtained for the $\text{CH}_3\text{OH} \cdots \text{H}_2\text{O}$ isomer is a consequence of the larger structural disorder, as can be seen in Fig. 4. The two distributions of

Table 3. Calculated binding energy (kcal/mol) of the two isomers of hydrogen-bonded methanol–water obtained with MP2/aug-cc-pVDZ including counterpoise correction to BSSE

	CH ₃ HO··H ₂ O		CH ₃ OH··OH ₂	
	Liquid	Gas	Liquid	Gas
ΔE	3.05 ± 1.09	5.15	3.04 ± 0.64	4.48
μ	3.68 ± 0.34	2.04	3.42 ± 0.29	2.73
α	31.45 ± 0.09	31.19	31.27 ± 0.18	30.67
$\Delta\alpha$	5.72 ± 0.74	5.90	5.69 ± 1.1	5.25
$\sigma_N (10^{-3})$	4.5 ± 1.1	4.7	4.5 ± 1.8	4.0
$\sigma_P (10^{-3})$	2.2 ± 0.6	2.4	2.3 ± 0.9	2.0
$\sigma_C (10^{-3})$	4.5 ± 1.1	4.7	4.6 ± 1.8	4.0

Results shown for the liquid are averages. Dipole moments are in debye and dipole polarizabilities (average and anisotropic) are in a.u. Rayleigh depolarizations (σ for natural, planar and circular polarizations) are dimensionless. Standard deviations are also shown.

calculated values are shown in Fig. 5. Another aspect worth mentioning is the decrease in binding energy for the liquid situation. As a result of the thermal fluctuation and the ensemble of possible configurations in the liquid, we can note that the final binding energy is reduced to 60–70% of the corresponding value for the minimum-energy configuration of the gas phase. Table 3 also gives the calculated dipole moments. As can be seen, the average dipole moments for the (1:1) liquid situation is considerably larger

**Fig. 5.** Histogram showing the distribution of binding energies between methanol and water. The solid line is for CH₃HO··H₂O and the dashed line is for CH₃OH··OH₂.

than in the (1:1) optimized complex. For completeness, Table 3 also gives the average and anisotropic dipole polarizabilities of the (1:1) structures of the liquid as compared with the gas-phase situation. The inhomogeneity in the electronic distribution leads to depolarization of the light elastically scattered and this Rayleigh depolarization is obtained from the calculated (1:1) dipole polarizabilities. Upon hydrogen bond formation in the aqueous environment, the depolarization ratios become a distribution with the average value being only slightly decreased with respect to the value obtained for the cluster-optimized. The depolarization ratios are essentially the same for both isomers. Table 3 gives the corresponding Rayleigh depolarization ratios for different light polarizations (natural, planar and circular). Rayleigh depolarizations have been analyzed before for the case of pyridine in water with similar results to those found here [20].

3.3. Statistical convergence

The efficient sampling of configurations from the simulation is crucial to ensure fast statistical convergence of the subsequent quantum-mechanical calculations. Instead of performing a quantum-mechanical calculation on every configuration generated by the MC simulation, as discussed in Section 2.1, we used the interval of statistical correlation [27,35] to select the configurations that are statistically relevant [25]. We have shown previously that performing an average over thousands of successive configurations generated in the MC simulation gives the same result as averaging over only a few statistically uncorrelated configurations [36,37]. Using the auto-correlation function of the energy is a very efficient way to sample

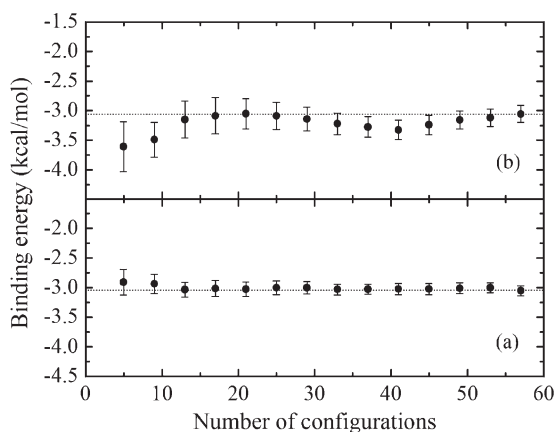


Fig. 6. Convergence of the calculated binding energies for hydrogen-bonded methanol–water: (a) $\text{CH}_3\text{OH}\cdots\text{OH}_2$ and (b) $\text{CH}_3\text{HO}\cdots\text{H}_2\text{O}$. Statistical errors are shown.

configurations and ensure statistically converged results. Indeed, Fig. 6 shows the calculated average binding energy for the increased number of (1:1) configurations used in the liquid case. The results are clearly converged, demonstrating the efficiency of our sampling procedure and the reliability of our average results.

4. FINAL REMARKS AND CONCLUSIONS

Hydrogen bond is a fundamental interaction to understand the thermodynamics of protic liquids, liquid mixtures and several biological phenomena that can only occur in the liquid environment. Hydrogen bonds between biomolecules are perhaps the most significant process regulating functions in living systems. Most understanding of the electronic structure of hydrogen bonds has been derived from studies in optimized complexes. However, the situation found in such clusters is certainly not the same as that in a liquid. Whereas in a cluster the hydrogen bond structure is fixed by a minimum-energy condition, in the liquid environment there are several configurations given by the temperature and the related natural disorder of the liquid. Therefore, the hydrogen-bonded site of a solute molecule in an aqueous environment experiences a great local thermal disorder. Understanding the nature of hydrogen bonds formed between a solute organic molecule and water is crucial for describing several solvation and bio-molecular processes [38]. One system that is very important is the alcohol–water mixture. Methanol–water is among the simplest of these mixtures and we have focused on the adequate treatment of the two possible isomers. In this study we considered the situation of methanol in water in conditions of extreme dilution: one methanol molecule is surrounded by bulk water. This simplified condition precludes the existence of more diversified cluster formation and makes it easier to compare with the (1:1) gas-phase result. Using liquid structures generated by realistic Monte Carlo simulations, we calculated the average interaction energy between methanol and water using first principle calculations at the second-order perturbation theory level, MP2/aug-cc-pVDZ, and counterpoise correction to basis set superposition. We find that the statistically converged binding energies of (1:1) complexes decrease to about 2/3 compared with the minimum-energy structures and that in the liquid environment the two isomers have the same average binding energy.

ACKNOWLEDGEMENTS

SC, in particular, takes great pride in having been one of Prof. Osvaldo Goscinski's graduate students and having the opportunity to pay this modest tribute to a dear friend. This work has been partially supported by CNPq, CAPES and FAPESP (Brazil).

REFERENCES

- [1] F. Franks and J. E. Desnoyers, in *Water Science Reviews*, (ed. F. Franks), Cambridge University Press, Cambridge, 1985, **1**, 171.
- [2] F. Franks and D. J. G. Ives, *Q. Rev.*, 1966, **20**, 1.
- [3] A. K. Soper and J. L. Finney, *Phys. Rev. Lett.*, 1993, **71**, 4346.
- [4] S. Dixit, J. Crain, W. C. K. Poon, J. L. Finney and A. K. Soper, *Nature*, 2002, **416**, 829.
- [5] J.-H. Guo, Y. Luo, A. Augustsson, S. Kashtanor, J.-E. Rubensson, D. K. Shuh, H. Ågren and J. Nordgren, *Phys. Rev. Lett.*, 2003, **91**, 157401.
- [6] J. E. Del Bene, *J. Chem. Phys.*, 1971, **55**, 4633.
- [7] Y. C. Tse, M. D. Newton and L. C. Allen, *Chem. Phys. Lett.*, 1980, **75**, 350.
- [8] G. Bolis, E. Clementi, D. H. Wertz, H. A. Scheraga and C. Tosi, *J. Am. Chem. Soc.*, 1983, **105**, 355.
- [9] S. Kim, M. S. Jho and H. A. Scheraga, *J. Phys. Chem.*, 1988, **92**, 7216.
- [10] N. Bakkas, Y. Bouteiller, A. Loutellier, J. P. Perchard and S. Racine, *J. Chem. Phys.*, 1993, **99**, 3335.
- [11] F. Huisken and M. Stemmler, *Chem. Phys. Lett.*, 1991, **180**, 332.
- [12] P. A. Stockman, G. A. Blakee, F. J. Lovas and R. D. Suenram, *J. Chem. Phys.*, 1997, **107**, 3782.
- [13] L. González, O. Mó and M. Yáñez, *J. Chem. Phys.*, 1998, **109**, 139.
- [14] E. E. Fileti, R. Rivelino and S. Canuto, *J. Phys. B: At. Mol. Opt. Phys.*, 2003, **36**, 399.
- [15] J. L. Finney, D. T. Bowron and A. K. Soper, *J. Phys. Condens. Matter*, 2000, **12**, A123.
- [16] G. Palinkas, E. Hawlicka and K. Heinzeger, *Chem. Phys.*, 1991, **158**, 65.
- [17] H. Tanaka and K. Gubbins, *J. Chem. Phys.*, 1992, **97**, 2626.
- [18] A. Laaksonen, P. G. Kusalik and I. M. Svishchev, *J. Phys. Chem. A*, 1997, **101**, 5910.
- [19] T. Malaspina, K. Coutinho and S. Canuto, *J. Chem. Phys.*, 2002, **117**, 1692.
- [20] E. E. Fileti, K. Coutinho, T. Malaspina and S. Canuto, *Phys. Rev. E*, 2003, **67**, 61504.
- [21] M. P. Allen and D. J. Tildesley, *Computer Simulation of Liquids*, Oxford University Press, Oxford, 1987.
- [22] K. Coutinho and S. Canuto, *DICE (Version 2.8): A General Monte Carlo Program for Liquid Simulation*, University of São Paulo, 2000.
- [23] H. J. C. Berendsen, J. P. M. Postma and W. F. van Gunsteren, in *Intermolecular Forces* (ed. B. Pullman), Reidel, Dordrecht, 1981, p. 331.
- [24] W. L. Jorgensen, D. S. Maxwell and J. T. Rives, *J. Am. Chem. Soc.*, 1996, **118**, 11225.
- [25] K. Coutinho and S. Canuto, *J. Mol. Struct. Theochem*, 2003, **632**, 235.
- [26] S. Canuto and K. Coutinho, *Int. J. Quantum Chem.*, 2000, **77**, 192.
- [27] K. Coutinho, S. Canuto and M. C. Zerner, *J. Chem. Phys.*, 2000, **112**, 9874.
- [28] H. Sato and F. Hirata, *J. Chem. Phys.*, 1999, **111**, 8545.
- [29] F. H. Stiling, *Adv. Chem. Phys.*, 1975, **31**, 1.
- [30] M. Mezei and D. L. Beveridge, *J. Chem. Phys.*, 1981, **74**, 622.
- [31] W. L. Jorgensen, J. M. Briggs and M. L. Contreras, *J. Phys. Chem.*, 1990, **94**, 1683.
- [32] S. F. Boys and F. Bernardi, *Mol. Phys.*, 1970, **19**, 553.
- [33] R. J. Bartlett, *J. Phys. Chem.*, 1989, **93**, 1697.
- [34] M. J. Frisch, G. W. Trucks, H. B. Schlegel, G. E. Scuseria, M. A. Robb, J. R. Cheeseman, V. G. Zakrzewski, J. A. Montgomery, Jr., R. E. Stratmann, J. C. Burant, S. Dapprich, J. M. Millam, A. D. Daniels, K. N. Kudin, M. C. Strain, O. Farkas, J. Tomasi, V. Barone, M. Cossi, R. Cammi, B. Mennucci, C. Pomelli, C. Adamo, S. Clifford, J. Ochterski, G. A. Petersson, P. Y. Ayala, Q. Cui, K. Morokuma, D. K. Malick, A. D. Rabuck, K. Raghavachari, J. B. Foresman, J. Cioslowski, J. V. Ortiz, A. G. Baboul, B. B. Stefanov, G. Liu, A. Liashenko, P. Piskorz, I. Komaromi, R. Gomperts, R. L. Martin, D. J. Fox, T. Keith, M. A. Al-Laham, C. Y. Peng, A. Nanayakkara, C. Gonzalez, M. Challacombe, P. M. W. Gill, B. Johnson, W. Chen, M. W. Wong, J. L. Andres, C. Gonzalez, M. Head-

- Gordon, E. S. Replogle and J. A. Pople, *Gaussian 98, Revision A.6*, Gaussian, Inc., Pittsburgh, PA, 1998.
- [35] K. Coutinho and S. Canuto, *Adv. Quantum Chem.*, 1997, **28**, 89.
- [36] K. Coutinho, M. J. de Oliveira and S. Canuto, *Int. J. Quantum Chem.*, 1998, **66**, 249.
- [37] W. R. Rocha, K. Coutinho, W. B. de Almeida and S. Canuto, *Chem. Phys. Lett.*, 2001, **335**, 127.
- [38] T. W. Bell, A. B. Kksanov and M. G. B. Drew, *J. Am. Chem. Soc.*, 2002, **124**, 14092.

This page intentionally left blank

Validation of the Applicability of Force Fields to Reproduce *Ab Initio* Noncovalent Interactions Involving Aromatic Groups

Guilin Duan,¹ Vedene H. Smith, Jr.¹ and Donald F. Weaver²

¹*Department of Chemistry, Queen's University, Kingston, Ont., Canada K7L 3N6*

²*Departments of Medicine (Neurology) and Chemistry, School of Biomedical Engineering, Dalhousie University, Halifax, NS, Canada B3H 4J3*

Abstract

Noncovalent interactions containing aromatic groups are of important significance to both the structure and function of proteins. It is necessary that modern force fields, especially those designed for biological molecules, are capable of describing these interactions. In this paper, the applicability of the CHARMM force field to the aromatic–amide (side-chain), aromatic–amide (backbone), aromatic–aromatic, aromatic–amine, aromatic–alcohol, aromatic–sulfhydryl and aromatic–aliphatic interactions are evaluated. For the first two interactions, the current CHARMM force field produces their interaction energies in good agreement with BSSE-corrected MP2 interaction energies. For the other four interactions, we found that the current CHARMM force field cannot produce their interaction energies to a satisfactory level of agreement with BSSE-corrected MP2 interactions. To make the CHARMM force field qualified for these interactions and simultaneously avoid changing the already defined parameters in the force field, the Lennard–Jones parameters (well depth and minimum distance) of the specific atom pairs related to these interactions are reparameterized through an automatic least square fitting program. With the new sets of parameters, the CHARMM force field is able to produce the interaction energies of these interactions in good agreement with their BSSE-corrected MP2 interaction energies.

Contents

1. Introduction	66
2. CHARMM force field	67
3. Validation strategies	69
3.1. Model complexes	69
3.2. Calculations of IPESs of model complexes	69
3.3. Choice of parameters to be optimized	70
3.4. Nonlinear least squares fitting	71
3.4.1. General principle	71
3.4.2. Levenberg–Marquardt method	72
3.4.3. Calculation of Gradient and Hessian	73
3.5. Programming the iterative and automatic optimization	74

4. Results and discussion	75
4.1. Aromatic–aliphatic interactions	76
4.2. Aromatic–aromatic interactions	78
4.3. Aromatic–amide(S) interactions	79
4.4. Aromatic–amide(B) interactions	81
4.5. Aromatic–thiol interactions	85
4.6. Aromatic–amine interaction	86
4.7. Aromatic–alcohol interaction	89
5. Conclusion	91
Acknowledgements	91
References	91

1. INTRODUCTION

The molecular mechanics (MM) method has become an increasingly important tool to compute geometries for large biological molecules such as proteins and DNA. In addition to their speed, some MM methods are also as accurate as high-level *ab initio* methods. However, the major obstacle in employing MM methods is the lack of high-quality parameters for many systems. The parameters of a force field are derived from specific physical properties of some selected molecules. Their transferability to other properties or other molecular systems is sometimes not reliable. Therefore, before using a force field to calculate some given property of a new molecular system, it is necessary to validate its applicability for the system by comparing its results to the accurate *ab initio* or experimental values. If there is no satisfactory agreement between them, new parameters should be developed for the force field.

Noncovalent interactions play a key role in determining the structure and function of biological molecules and in controlling the biological processes. Accordingly, it is crucially important that MM force fields, especially those designed for calculating biological systems, are qualified to describe noncovalent forces. Over the past decade, noncovalent interactions involving aromatic groups have been extensively studied and their importance to protein structure has been recognized. These noncolvalent systems include aromatic–cation [1–4], aromatic–aliphatic [5,6], aromatic–aromatic [7–10], aromatic–amide(S) [11,12], aromatic–amide(B) [11,13,14], aromatic–thiol [15], aromatic–amine [16,17], and aromatic–alcohol [18,19]. Throughout this chapter, aromatic–amide(B) stands for the interaction between aromatic and backbone amide groups in proteins; aromatic–amide(S) denotes the interaction between aromatic and side-chain amide groups in proteins.

The major objective of this study is to validate the applicability of a widely used force field (CHARMm) to these noncovalent interactions.

The CHARMM force field [20] was developed particularly for biological macromolecules, and has become a main force field for investigating biological systems. Kollman and co-workers [21,22] have fitted the benzene–cation interaction very accurately with three-body term force fields by including polarizability. Weaver and Donini [23] have also validated the applicability of CHARMM for benzene–cation interaction. Therefore, this study focuses on the aromatic–aliphatic, aromatic–aromatic, aromatic–amide(S), aromatic–amide(B), aromatic–thiol, aromatic–amine, and aromatic–alcohol interactions.

For each of these interactions, a model complex was designed; the BSSE-corrected MP2 interaction potential energy surface (IPES) was calculated; then the CHARMM IPES was validated against the MP2 one. If the CHARMM force field cannot produce a satisfactory IPES, the force field will be reparameterized using an automatic least square optimization program OPTMM written by G.D. in C language [24].

2. CHARMM FORCE FIELD

The CHARMM force field [20] is comprised of a series of function terms for both bonded and nonbonded energies and a set of parameters for these terms. The total energy (E_T) of the system is expressed as

$$\begin{aligned}
 E_T = & \sum_{\text{bonds}} K_b(b - b_0)^2 + \sum_{\text{angles}} K_\theta(\theta - \theta_0)^2 + \sum_{\text{torsions}} K_\phi[1 + \cos(n\phi - \delta)] \\
 & + \sum_{1,3\text{pairs}} K_{\text{UB}}(S - S_0)^2 + \sum_{\text{improper}} K_w(w - w_0)^2 \\
 & + \sum_{\text{nonbonded}} \left\{ \epsilon_{ij} \left[\left(\frac{r_{\text{min},ij}}{R_{ij}^{12}} \right) - \left(2 \frac{r_{\text{min},ij}}{R_{ij}^6} \right) \right] + \frac{q_i q_j}{4\pi D r_{ij}} \right\} \quad (1)
 \end{aligned}$$

In equation (1) the first five terms comprise the internal energies [25]. The first two terms account for bond and angle deformations using a harmonic approximation, where K_b and b_0 are the bond stretching force constant and the equilibrium bond distance, and K_θ and θ_0 are the bond angle stretch force constant and the equilibrium bond angle. The third term is a torsion energy based on a cosine function in which K_ϕ , n , and δ are the torsional force constant, the periodicity, and the phase. The fourth term, the Urey–Bradley term, is a distance constraint used for interactions of the first and third atoms of an angle (1,3 interactions) that are not adequately treated by bond angle bending terms alone. It involves a force constant K_{UB} and 1,3 equilibrium distance S_0 . The fifth term is the improper torsion term that is

designed to maintain planarity about planar atoms. The K_w and w_0 are the torsional force constant and the equilibrium improper torsional angle. The last term includes the nonbonded interactions. The electrostatic interaction is described with the Coulombic term in which q_i is the partial atomic charge located on the nuclear center, r_{ij} the distance between atoms i and j , and D the permittivity of a vacuum. The combination of all other nonbonded interactions is called the van der Waals (vdW) force, and they are incorporated into the familiar Lennard–Jones terms: $r_{\min,ij}$ is the position of the minimum of the potential between the atom pair i – j ; ε_{ij} is the depth of the energy well at the minimum. These two parameters are Lennard–Jones parameters and can be obtained by the Lorentz–Berthelot combination rules [26]

$$\varepsilon_{ij} = \sqrt{\varepsilon_{ii}\varepsilon_{jj}} \quad (2)$$

$$r_{\min,ij} = \frac{r_{\min,ii} + r_{\min,jj}}{2} \quad (3)$$

where ε_{ii} and ε_{jj} are the Lennard–Jones well depth of the individual atoms; $r_{\min,i}$ and $r_{\min,j}$ are the Lennard–Jones radii of the individual atoms.

In CHARMM, the Lennard–Jones well depth and radius for an atom type have been assigned specific values so that the Lennard–Jones parameters for atom pairs can be calculated with these values through the combination rule above. In addition, CHARMM allows the user to modify the vdW interactions between a specific atom pair through setting particular values of Lennard–Jones parameters to the atom pair. The user-specified parameter values overwhelm those from the combination rule in a practical computation.

With the CHARMM force field, the interaction energy (ΔE) for the complex R–T is the summation of the nonbonded interaction energy of all atom pairs between two individual molecules R and T

$$\Delta E = \sum_{a=1}^{N_R} \sum_{b=1}^{M_T} \left\{ \varepsilon_{ab} \left[\left(\frac{r_{\min,ab}}{r_{ab}} \right)^{12} - 2 \left(\frac{r_{\min,ab}}{r_{ab}} \right)^6 \right] + \frac{q_a q_b}{4\pi D r_{ab}} \right\} \quad (4)$$

in which a and b are the atoms of the molecules R and T, respectively; N_R and M_T are the total number of atoms for R and T, respectively; r_{ab} is the distance between atoms a and b ; q_a and q_b are the partial atomic charges of atoms a and b , respectively; ε_{ab} and $r_{\min,ab}$ are the Lennard–Jones parameters for the atom pair a – b which can either be obtained by the combination rule (equations (2) and (3)) or be specified by the user.

3. VALIDATION STRATEGIES

Molecular mechanical parameterization has long been more of an ‘art’ than a science [27]. The problem is twofold: finding and evaluating reference data, and ‘fitting’ parameters to these reference data. In this study, the reference data were obtained through high-level *ab initio* calculations on model complexes; the fitting of the targeted parameters were performed with a nonlinear least squares minimization method.

3.1. Model complexes

Each of the interactions under study was modeled with a complex. The $C_6H_6-CH_4$ complex was used for the aromatic–aliphatic interaction, $C_6H_6-C_6H_6$ for aromatic–aromatic, $C_6H_6-H_2NCOH$ for aromatic–amide(S), $C_6H_6-H_3CCONHCH_2CONH_2$ for aromatic–amide(B), $C_6H_6-HSCH_3$ for aromatic–thiol, $C_6H_6-H_2NCH_3$ for aromatic–amine, and $C_6H_6-HOCH_3$ for aromatic–alcohol. For each model complex, the configuration is defined by a set of intermolecular geometric parameters and its IPES was developed through systematically changing the intermolecular geometries.

3.2. Calculations of IPESs of model complexes

Ab initio interaction energies were used as the reference data for the validation because the experimental IPESs of these interactions are not available. The *ab initio* IPES was calculated through the supermolecular scheme in which the basis set superposition error (BSSE) was corrected with the counterpoise (CP) method [28]. The calculations were performed at the MP2 level with a qualified basis set. For each system, the configurations were systematically selected to reflect the diversity of the interaction. Therefore, although the calculated configurations may not be sufficient for an elaborate IPES, they can reflect the major characteristics of the interaction. All quantum chemical calculations were performed with the Gaussian 94 program [29] on an IBM 8-node SP2 processor.

The force field calculations of the IPES were performed with the CHARMM22/Quanta4.1 package. The dielectric constant was set to one which corresponds to a vacuum. A nonbonded cutoff was not used and the all-atom model was utilized throughout. For all calculations, the geometries of the monomers were kept rigid. The explicit hydrogen bonding energy is not required in the present version of the force field because the parameters have been fitted to describe hydrogen bonding interactions [25,30].

The overall performance of the force field on a given interaction can be evaluated with two statistical properties: average root mean square (RMS)

and average deviation (DEV):

$$\text{RMS} = \sqrt{\frac{1}{N} \sum_{i=1}^N (\text{IEMM}_i - \text{IEQM}_i)^2} \quad (5)$$

$$\text{DEV} = \frac{1}{N} \sum_{i=1}^N (\text{IEMM}_i - \text{IEQM}_i) \quad (6)$$

where N is the number of the calculated configurations.

3.3. Choice of parameters to be optimized

The objective of this study is to improve the ability of the force field to describe the biological molecules by enhancing its quality for treating these interactions involving aromatic groups. Accordingly, the already defined parameters, such as the partial atomic charges, and the Lennard–Jones parameters for the involved individual atoms in these systems should be maintained. To achieve such a maintenance and simultaneously to improve CHARMM's ability to describe these interactions, only the Lennard–Jones parameters for the specific atomic pair (ϵ_{ab} and $r_{\text{min},ab}$) are modified. For example, the modification of $\epsilon_{\text{C6T-C6T}}$ and $r_{\text{min,C6T-C6T}}$ in the CHARMM parameters files affects the energy of aromatic–aromatic interactions, but has no influence over the interaction between an aromatic group and other groups. This is because the Lennard–Jones parameters between a C6T atom and other atoms are obtained through the combination rule and are not to be modified. Note that the symbols CT, C6T, ST, NT, OT represents the atom type for the aliphatic carbon, aromatic carbon, thiol sulfur, amine nitrogen, and alcohol oxygen atom, respectively.

The modification of the Lennard–Jones parameters for the specific atom pairs in a system changes the vdW energy rather than the electrostatic interaction energy. As a result, the improvement may be limited if the electrostatic interaction is a dominant contributor to the total interaction energy. Fortunately, this is not the case for the interactions under study. For these systems, the electrostatic interaction exists but it is not significantly dominant over the dispersion energy. This is true especially for the complexes $\text{C}_6\text{H}_6\text{--C}_6\text{H}_6$, $\text{C}_6\text{H}_6\text{--HSCH}_3$, $\text{C}_6\text{H}_6\text{--HOCH}_3$, and $\text{C}_6\text{H}_6\text{--H}_2\text{NCH}_3$ for which the CHARMM force field is required to be reparameterized.

For the $\text{C}_6\text{H}_6\text{--C}_6\text{H}_6$ interaction, the electrostatic interaction is the relatively weak quadrupole–quadrupole interaction. For the other three, the dispersion interaction between the aromatic ring and S, N or O atom or the --CH_3 group should also be significant. For the sake of simplicity, only the Lennard–Jones parameters for the important atom pair is optimized for

each of these systems. These important atomic pairs are C6T–C6T for C_6H_6 – C_6H_6 , C6T–ST for C_6H_6 – HSCH_3 , C6T–NT for C_6H_6 – H_2NCH_3 , and C6T–OT for C_6H_6 – H_2NCH_3 . The Lennard–Jones potential for the C6T–CT pairs is not chosen for optimization because the CHARMM force field is qualified for the C_6H_6 –($-\text{CH}_3$) interaction (see below). The parameters for an atom pair containing hydrogen atom are also not to be optimized. This is because the dispersion involving a hydrogen atom is relatively less important. The modification of parameters for atom pairs containing hydrogen does not effectively change the interaction of the system, but greatly complicates the optimization process.

3.4. Nonlinear least squares fitting

3.4.1. General principle

The nonlinear least squares fitting is to find a set of optimal parameters (\mathbf{P}) that make the nonlinear model $Y = f(\mathbf{X}; \mathbf{P})$ produce the results for the object (Y) most close to a set of reference values. The overall performance for the parameters can be described with a merit function ($F(\mathbf{P})$), i.e., the sum of squares of all deviations between the reference values and the values from the model

$$F(\mathbf{P}) = \sum_{i=1}^N [Y_i - f(\mathbf{X}_i; \mathbf{P})]^2 \quad (7)$$

where N is the number of values for the object Y .

The deviations in equation (7) should be scaled by weighting factors. Such weighting factors were fixed as one throughout this study; thus it does not appear in the equation. $\mathbf{P} \equiv (P_1, P_2, \dots, P_M)^T$ is the parameter matrix in which P_1, P_2, \dots, P_M are the parameters to be optimized and T means the ‘transpose of matrix’.

In terms of \mathbf{P} and $\Delta\mathbf{P}$, the Taylor expansion of the merit function $F(\mathbf{P})$ is

$$F(\mathbf{P} + \Delta\mathbf{P}) = F(\mathbf{P}) + \sum_{i=1}^n \frac{\partial F}{\partial P_i} \Delta P_i + \frac{1}{2} \sum_{i=1}^n \sum_{j=1}^n \frac{\partial^2 F}{\partial P_i \partial P_j} \Delta P_i \Delta P_j + \dots \quad (8)$$

In the vector form and neglecting the higher terms, equation (8) may be rewritten as

$$F(\mathbf{P} + \Delta\mathbf{P}) = F(\mathbf{P}) + \Delta\mathbf{P}^T \nabla F + \frac{1}{2} \Delta\mathbf{P}^T \mathbf{H} \Delta\mathbf{P} \quad (9)$$

in which $\Delta\mathbf{P}$ is the matrix

$$\Delta\mathbf{P} = (\Delta P_1, \Delta P_2, \dots, \Delta P_M)^T \quad (10)$$

$\nabla \mathbf{F}$ is the Gradient of $F(\mathbf{P})$ with respect to the parameters \mathbf{P} ,

$$\nabla \mathbf{F} = (\beta_1, \beta_2, \dots, \beta_M)^T, \quad \beta_k \equiv \frac{\partial F}{\partial P_k}, \quad k = 1, 2, \dots, M \quad (11)$$

\mathbf{H} is the Hessian of $F(\mathbf{P})$,

$$\mathbf{H} = (\alpha_{ij}), \quad \alpha_{ij} \equiv \frac{\partial^2 F}{\partial P_i \partial P_j}, \quad i = 1, 2, \dots, N \text{ and } j = 1, 2, \dots, M \quad (12)$$

The best set of parameters (\mathbf{P}) is that which minimizes the merit function $F(\mathbf{P})$. Accordingly, efforts should be made to choose $\Delta \mathbf{P}$ in such a way that $F(\mathbf{P})$ is minimized, namely,

$$\frac{\partial F(\mathbf{P} + \Delta \mathbf{P})}{\partial \Delta \mathbf{P}} = 0 \quad (13)$$

Combining equations (9) and (13), one gets

$$\Delta \mathbf{P} = -\mathbf{H}^{-1} \nabla \mathbf{F} \quad (14)$$

Equation (14) can be rewritten as

$$\sum_{l=1}^M \alpha_{kl} \Delta P_l = \beta_k \quad (15)$$

Equation (14) or (15) is usually solved iteratively until $\Delta \mathbf{P}$ is equal to zero or satisfies the convergence criteria required.

3.4.2. Levenberg–Marquardt method

Many approaches have been devised to solve equation (14) or (15). In this study, the Levenberg–Marquardt (LM) method was used. This is because the LM method works well in practice and has become the standard of nonlinear least squares routines [31].

The LM method defines a new matrix $\mathbf{H}' = (\alpha'_{ij})$ as

$$\alpha'_{ii} \equiv \alpha_{ii}(1 + \lambda), \quad (16)$$

$$\alpha'_{ij} \equiv \alpha_{ij}, \quad i \neq j, \quad i = 1, 2, \dots, N \text{ and } j = 1, 2, \dots, M$$

and the equations corresponding to equations (14) and (15) are, respectively,

$$\Delta \mathbf{P} = -\mathbf{H}'^{-1} \nabla \mathbf{F} \quad (17)$$

$$\sum_{l=1}^M \alpha'_{kl} \Delta P_l = \beta_k \quad (18)$$

Given an initial guess for the set of parameters \mathbf{P} , the LM method generates new values for the parameters through solving the linear equation (18) in the following way:

- (i) choose a suitable value for λ . A suitable λ should ensure the new value for each parameter is located within the reasonable range;
- (ii) compute $F(\mathbf{P})$, and the corresponding matrix elements for \mathbf{H}' and $\nabla\mathbf{F}$ using the initial values of the parameters;
- (iii) solve the linear equation (18) for $\Delta\mathbf{P}$;
- (iv) compute $F(\mathbf{P} + \Delta\mathbf{P})$, and the corresponding matrix elements for \mathbf{H}' and $\nabla\mathbf{F}$ using the new values of the parameters;
- (v) if $F(\mathbf{P} + \Delta\mathbf{P}) \geq F(\mathbf{P})$, increase λ by a substantial factor (for instance 10) and go back to (iii). If $F(\mathbf{P} + \Delta\mathbf{P}) \leq F(\mathbf{P})$ and the expected convergence criteria is not satisfactory, decrease λ a substantial factor, update the value of parameter ($\mathbf{P}_{\text{new}} = \mathbf{P}_{\text{old}} + \Delta\mathbf{P}$), and then go back to (iii). If $F(\mathbf{P} + \Delta\mathbf{P}) \leq F(\mathbf{P})$ and, moreover, the expected convergence criteria is satisfactory, update the value of the parameters and then stop.

3.4.3. Calculation of Gradient and Hessian

To solve equation (18), both Gradient $\nabla\mathbf{F}$ and Hessian \mathbf{H} of the merit function $F(\mathbf{P})$ should be derived first. For each of the systems for which the CHARMM force field is required to be reparameterized, only the two Lennard–Jones parameters (ε_{ab} and $r_{\min,ab}$) of a specific atom pair ($a-b$) between two individual molecules (R and T) were optimized. These two parameters are, respectively, denoted as ε and σ in the following equations. Accordingly, the corresponding parameters matrix can be denoted as $\mathbf{P} \equiv (\varepsilon, \sigma)^T$. The merit function can be expressed in terms of MM model values (IEMM) and QM reference values (IEQM) as

$$F(\mathbf{P}) = \sum_{i=1}^N [\text{IEMM}_i(\mathbf{P}) - \text{IEQM}_i]^2 \quad (19)$$

where N is the number of the calculated configurations for the system under validation.

From the equations (11) and (12), the matrix elements for both $\nabla\mathbf{F}$ and \mathbf{H} can be derived

$$\beta_1 = \frac{\partial F}{\partial \varepsilon} = -2 \sum_{i=1}^N \left\{ (\text{IEQM}_i - \text{IEMM}_i) \sum_{a \in R} \sum_{b \in T} \left[\left(\frac{\sigma}{r_{abi}} \right)^{12} - 2 \left(\frac{\sigma}{r_{abi}} \right)^6 \right] \right\} \quad (20)$$

where r_{abi} is the distance between the atom a in the molecule R and the atom b in the molecule T in the i th R-T configuration.

$$\beta_2 = \frac{\partial F}{\partial \sigma} = -2\varepsilon \sum_{i=1}^N \left[(\text{IEQM}_i - \text{IEMM}_i) \sum_{a \in R} \sum_{b \in T} \left(12 \frac{\sigma^{11}}{r_{abi}^{12}} - 12 \frac{\sigma^5}{r_{abi}^6} \right) \right] \quad (21)$$

$$\alpha_{11} = \frac{\partial^2 F}{\partial \varepsilon^2} = 2 \sum_{i=1}^N \left\{ \sum_{a \in R} \sum_{b \in T} \left[\left(\frac{\sigma}{r_{abi}} \right)^{12} - 2 \left(\frac{\sigma}{r_{abi}} \right)^6 \right] \right\}^2 \quad (22)$$

$$\begin{aligned} \alpha_{12} = \alpha_{21} &= \frac{\partial^2 F}{\partial \varepsilon \partial \sigma} \\ &= -2 \sum_{i=1}^N \left\{ \left[(\text{IEQM}_i - \text{IEMM}_i) - \varepsilon \sum_{a \in R} \sum_{b \in T} \left(\left(\frac{\sigma}{r_{abi}} \right)^{12} - \left(\frac{\sigma}{r_{abi}} \right)^6 \right) \right] \right. \\ &\quad \left. \times \sum_{a \in R} \sum_{b \in T} \left(12 \frac{\sigma^{11}}{r_{abi}^{12}} - 12 \frac{\sigma^5}{r_{abi}^6} \right) \right\} \end{aligned} \quad (23)$$

$$\begin{aligned} \alpha_{22} &= \frac{\partial^2 F}{\partial \sigma \partial \sigma} \\ &= -2\varepsilon \sum_{i=1}^N \left\{ (\text{IEQM}_i - \text{IEMM}_i) \sum_{a \in R} \sum_{b \in T} \left(132 \frac{\sigma^{10}}{r_{abi}^{12}} - 60 \frac{\sigma^4}{r_{abi}^6} \right) \right. \\ &\quad \left. - \varepsilon \left[\sum_{a \in R} \sum_{b \in T} \left(12 \frac{\sigma^{11}}{r_{abi}^{12}} - 12 \frac{\sigma^5}{r_{abi}^6} \right) \right]^2 \right\} \end{aligned} \quad (24)$$

3.5. Programming the iterative and automatic optimization

The above LM procedures of iteratively solving equation (18) was implemented in the program OPTMM written in C computer language. The program establishes an interface between the LM method and the CHARMM package. This makes the iterative optimization proceed automatic. Figure 1 gives a schematic outline of the algorithm for the iterative and automatic optimization.

In the actual optimization calculation, the original CHARMM values were used as the initial guess for the parameters. The convergence criteria was defined as $[F_n(\mathbf{P}) - F_{n-1}(\mathbf{P})] \leq -10^{-5}$.

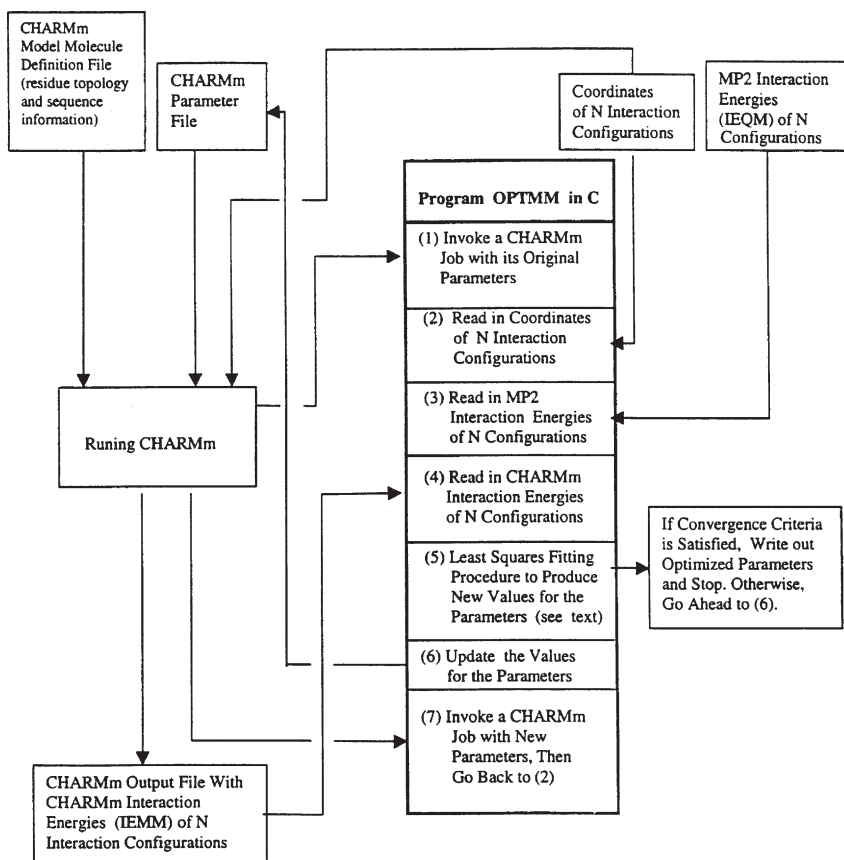


Fig. 1. Schematic flow chart of algorithms for the iterative and automatic optimization of CHARMM force field.

4. RESULTS AND DISCUSSION

As will be shown, the original CHARMM parameters can produce IPESs in good agreement with those calculated by the CP-corrected MP2 method for aromatic–aliphatic, aromatic–amide(S), and aromatic–amide(B) interactions. However, for aromatic–aromatic, aromatic–thiol, aromatic–amine, and aromatic–alcohol interactions, the original parameters cannot reproduce the IPESs which match CP-corrected MP2 results. Therefore, the Lennard–Jones parameters for the important atom pair in these four interactions were selected to be optimized. The original and optimized CHARMM Lennard–Jones parameters for these chosen atom pairs are collected in Table 1 for each of these four interactions.

Table 1. Original and optimized Lennard–Jones parameters ϵ_{ab} and $r_{\min,ab}$ for the chosen atomic pairs in four optimized interactions

Interactions	Atomic pair ($a-b$) for parameter optimization	Original CHARMM		Optimized CHARMM	
		$r_{\min,ab}$	ϵ_{ab}	$r_{\min,ab}$	ϵ_{ab}
Aromatic–aromatic	C6R–C6R	4.08	−0.050	3.50	−0.133
Aromatic–amine	C6R–NT	3.69	−0.087	3.78	−0.139
Aromatic–thiol	C6R–ST	3.93	−0.046	4.04	−0.215
Aromatic–alcohol	C6R–OT	3.59	−0.087	4.03	−0.058

Units are Å for $r_{\min,ab}$ and kcal/mol for ϵ_{ab} . C6R, NT, ST, and OT atom types are aromatic carbon, amine nitrogen, thiol sulfur, and alcohol oxygen atoms, respectively.

4.1. Aromatic–aliphatic interactions

The IPES for this interaction was developed by systematically changing the intermolecular geometric parameters (L and P) of two $\text{C}_6\text{H}_6\text{--CH}_4$ structural patterns (see Fig. 2).

The pattern in which one hydrogen of the methane points toward the benzene ring is denoted as 1H; the other is called 3H because three methane hydrogen atoms point toward the benzene ring. In total, 20 configurations were calculated for the IPES. The geometries for these configurations are given in Table 2.

The agreement of the CHARMM and CP-corrected MP2/6-311G(2d,p) IPESs for this interaction is demonstrated in Fig. 3. Note that for each interacting system under validation, the calculated configurations are numbered in the order of decrease in stabilization energy in their IPESs curves in this chapter.

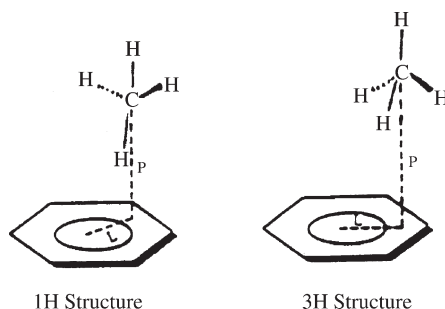
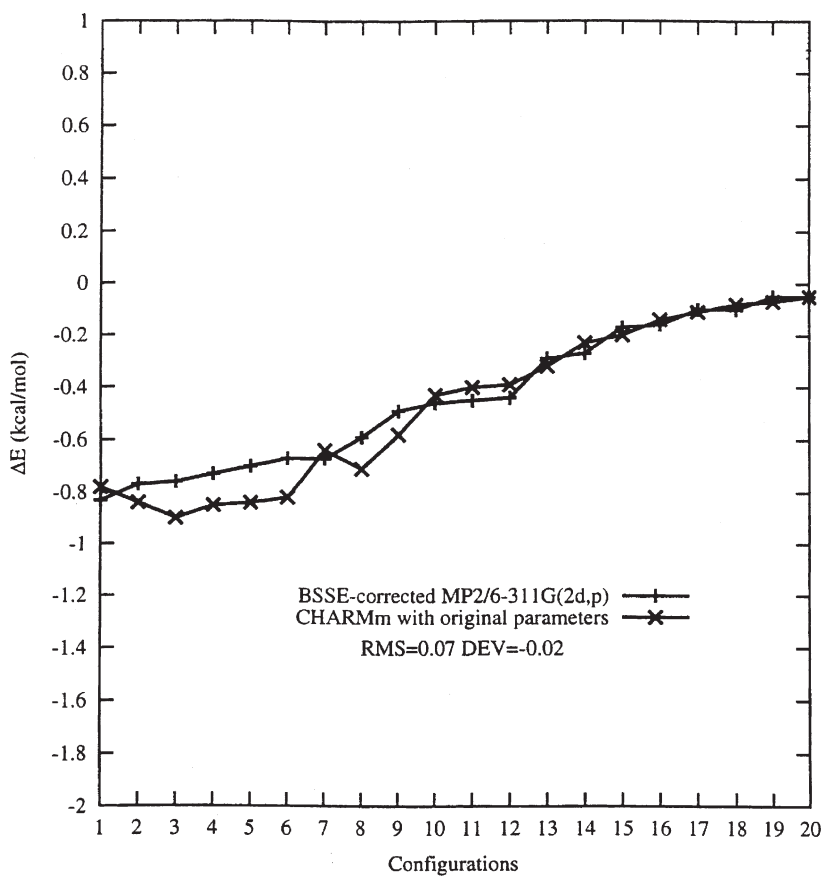
**Fig. 2.** Two $\text{C}_6\text{H}_6\text{--CH}_4$ interaction patterns.

Table 2. Geometries for 20 calculated C₆H₆–CH₄ configurations

#	Pattern	<i>P</i>	<i>L</i>	#	Pattern	<i>P</i>	<i>L</i>	#	Pattern	<i>L</i>	<i>P</i>
1	1H	3.5	1.4	2	1H	4.0	1.9	3	1H	4.0	1.4
4	1H	4.0	2.4	5	3H	4.0	1.4	6	1H	4.0	2.9
7	3H	4.5	1.4	8	1H	4.0	3.4	9	1H	4.5	1.4
10	3H	3.5	1.4	11	1H	4.0	3.9	12	3H	4.5	1.4
13	1H	5.0	1.4	14	3H	5.5	1.4	15	1H	5.5	1.4
16	2H	6.0	1.4	17	1H	6.0	1.4	18	2H	6.5	1.4
19	1H	6.5	1.4	20	2H	7.0					

Units are Å for both *L* and *P*.

**Fig. 3.** CHARMm and MP2 IPESs of C₆H₆–CH₄ interaction.

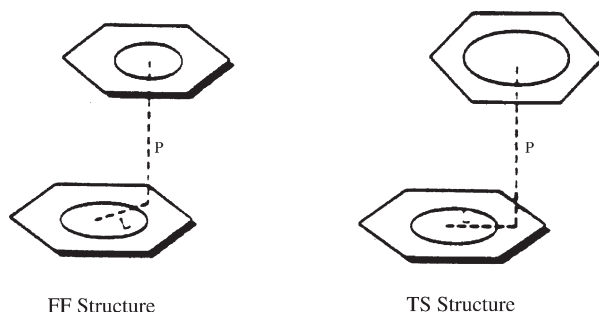


Fig. 4. Two $\text{C}_6\text{H}_6\text{--C}_6\text{H}_6$ interaction patterns.

It can be seen that the existing CHARMM force field can produce the IPES for this interaction in good agreement with the *ab initio* result. It is also reflected by the small RMS and DEV, which are 0.07 and -0.02 kcal/mol, respectively.

4.2. Aromatic–aromatic interactions

To establish the IPES of this interaction, two important $\text{C}_6\text{H}_6\text{--C}_6\text{H}_6$ interaction patterns, face-to-face (FF) and edge-face T-shaped (TS) (Fig. 4), were considered.

Twenty-four configurations were selected for the interaction energy evaluation. Among them, 21 were obtained by systematically varying the intermolecular geometries (P and L); three were the optimized FF or TS structures reported in Ref. [8]. The geometries for these 24 configurations are listed in Table 3.

The IPES from CP-corrected MP2/6-31G(2d,2p), CHARMM with original parameters and CHARMM with optimized parameters are demonstrated in Fig. 5.

The RMS and DEV for the existing CHARMM force field are 0.95 and 0.62 kcal/mol, respectively. In general, the existing parameters underestimate the stabilization energy for the aromatic–aromatic interaction to a noticeable degree. In particular, it fails to produce the stabilization energy of the global energy minimum configuration. The configuration (#1) corresponds to the global minimal energy. It is a displaced face-to-face structure with $L = 1.54$ and $P = 3.40$ Å and has the largest stabilization interaction energy (3.33 kcal/mol [8]). The stabilization interaction energy from the existing CHARMM force field for such a structure is 0.64 kcal/mol. It is unacceptably small. Another significant difference in the stabilization energy between the MP2 and the existing CHARMM occurs in configuration 16. In addition, it is obvious that the discrepancy occurs mainly in configurations with a FF structural pattern. For the TT pattern configurations, the existing CHARMM force field can produce the stabilization interaction energy

Table 3. Geometries for 24 calculated C₆H₆–C₆H₆ configurations

#	Pattern	<i>P</i>	<i>L</i>	<i>DA</i>	#	Pattern	<i>P</i>	<i>L</i>	<i>DA</i>
1 ^{a,b}	FF	3.4	1.54	180	2	TS	5.0	1.20	180
3	TS	5.0	0.80	180	4 ^b	FF	3.8	0.01	90
5	FF	4.0	1.20	180	6 ^b	FF	3.8	0.01	180
7	FF	4.0	0.80	180	8	FF	4.0	2.00	180
9	FF	4.0	0.40	180	10	FF	4.0	0.01	180
11	TS	5.0	0.40	180	12	FF	4.0	2.40	180
13	TS	5.0	0.01	180	14	TS	5.0	2.00	180
15	FF	4.0	2.80	180	16	FF	3.5	0.01	180
17	TS	5.5	0.01	180	18	TS	5.0	2.40	180
19	TS	5.0	2.80	180	20	FF	4.5	0.01	180
21	TS	6.0	0.01	180	22	FF	5.0	0.01	180
23	FF	5.5	0.01	180	24	FF	6.0	0.01	180

Units are Å for distance and degrees for angles.

^a Configuration with global minimal energy.

^b Optimized configurations from Ref. [8].

comparable to those from MP2. The explanation for this is that the existing force field cannot describe the dispersion involved in the interaction, since the dispersion contribution is more important for the FF structures than for the TS structures [32]. The interaction between carbons is the major component for the dispersion energy. This indicates that it is possible to make CHARMM better for this interaction by modifying the Lennard–Jones parameters between the C6T–C6T atom pair.

The optimized $r_{\min,ab}$ and ϵ_{ab} parameters for C6R–C6R atom pair are 3.50 Å and -0.133 kcal/mol, respectively (see Table 1). Compared with the original set, the optimized parameters enlarge the stabilization vdW interaction for this atom pair. This is required to enlarge the dispersion of the FF aromatic–aromatic interaction. With the optimized parameters, the CHARMM IPES for the interaction is noticeably improved. It can produce stabilization energies in good agreement with MP2 results for both the FF and TS arrangements. The magnitude of RMS and DEV for the optimized CHARMM is significantly smaller than those for the existing force field. More importantly, the optimized force field is capable of predicting the global energy minimum structure and its stabilization interaction energy.

4.3. Aromatic–amide(S) interactions

This interaction is modeled by a C₆H₆–H₂NCOH complex. The configuration is specified with five intermolecular geometric parameters, *L*, *P*, *A*, *DA1*, and *DA2*, illustrated in Fig. 6.

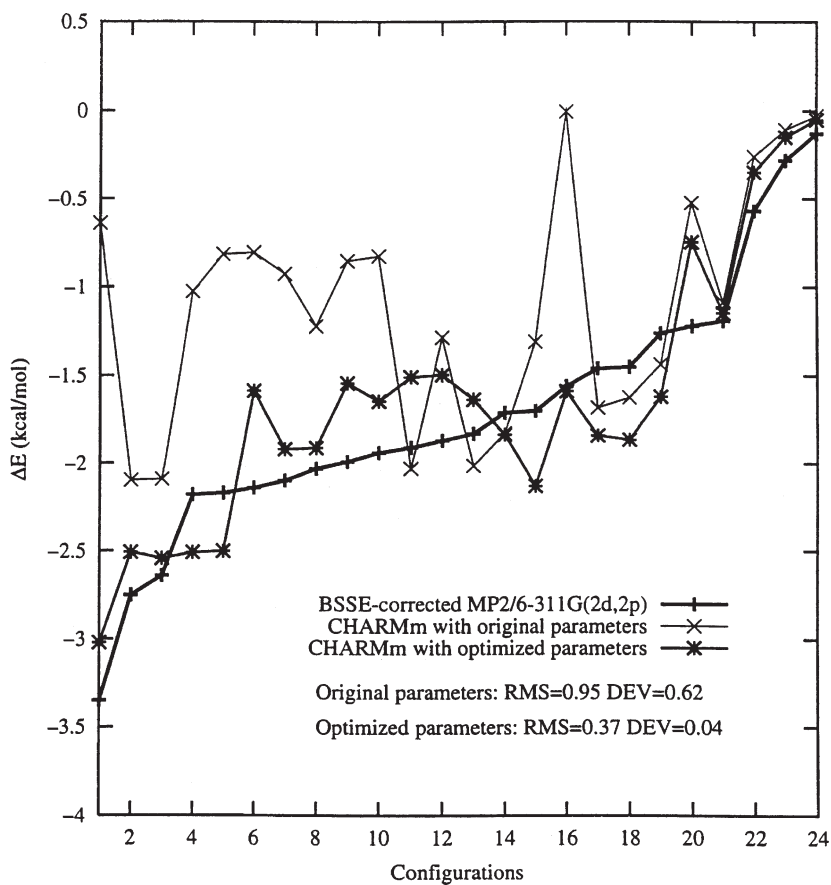


Fig. 5. CHARMM and MP2 IPESs of $C_6H_6-C_6H_6$ interaction.

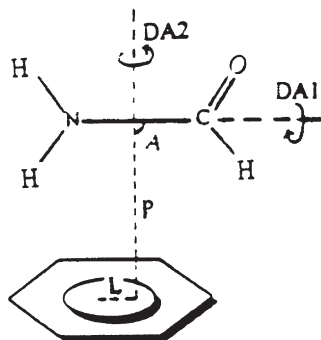


Fig. 6. Intermolecular geometries for $C_6H_6-H_2NCOH$ complex.

The CP-corrected MP2/6-311G(2d,2p) interaction energies for 94 configurations are used to validate the applicability of the existing CHARMM force field for this interaction. The geometries for these configurations are listed in Table 4.

The IPESs from the CP-corrected MP2/6-311G(2d,2p) and the existing CHARMM force field are demonstrated in Fig. 7.

It is shown that the existing force field can produce the IPES in good agreement with that from the MP2 for this interaction. The RMS and DEV are 0.24 and -0.05 kcal/mol, respectively, both of which are rather small in magnitude. For most configurations, the deviation between the CHARMM and MP2 interaction energy is less than 0.5 kcal/mol in magnitude. The force field overestimates the largest stabilization energy which is achieved for the first configuration by 0.6 kcal/mol. However, this should not be a problem due to the overall agreement between the force field and accurate MP2 results. Therefore, the existing CHARMM force field is suitable for the aromatic–amide(S) interaction.

4.4. Aromatic–amide(B) interactions

To model this interaction, the model complex $C_6H_6-H_3CCONHCH_2CONH_2$ was used. The interaction is treated as the interaction between the C_6H_6 and the $H_3CCONHCH_2-$ fragment of the $H_3CCONHCH_2CONH_2$. The configuration is defined by five intermolecular geometric parameters, L , P , A , $DA1$, and $DA2$, illustrated in Fig. 8.

In total, 38 configurations were selected to characterize the IPES of the interaction. Their geometries are given in Table 5.

The CP-corrected MP2/6-31 + G(2d,p) and CHARMM interaction energies for these configurations are shown in Fig. 9.

These calculated interaction energies correspond to the total interaction energy between the C_6H_6 and the entirety of $H_3CCONHCH_2CONH_2$. The interaction energy between C_6H_6 and the $H_3CCONHCH_2-$ fragment should not include the contribution from the interaction between the C_6H_6 and the $-CONH_2$ group. In these 38 configurations, $C_6H_6-(-CONH_2)$ interaction is negligible; thus it is a good approximation to regard the interaction energies indicated in Fig. 9 as those of the $C_6H_6-(H_3CCONHCH_2-)$ interaction. In addition, because the existing CHARMM force field is validated to describe the aromatic–amide(S) interaction as shown above, its suitability for the $C_6H_6-H_3CCONHCH_2CONH_2$ complex implies a suitability for the $C_6H_6-H_3CCONHCH_2-$ which models the aromatic–amide(B) interaction.

Overall, the existing CHARMM force field is capable of producing an IPES comparable to that from the MP2 method for this system. The RMS and DEV is rather small in magnitude and are 0.39 and -0.04 , respectively.

Table 4. Geometries for 94 C₆H₆–H₂NCOH configurations (Å for distance and degrees for angles)

#	<i>P</i>	<i>L</i>	<i>A</i>	<i>DA1</i>	<i>DA2</i>	#	<i>P</i>	<i>L</i>	<i>A</i>	<i>DA1</i>	<i>DA2</i>
1 ^{a,b}			<i>T1Con1</i>			2 ^b			<i>T1Con2</i>		
3	7.5	0.02	135	180	180	4	8.0	0.02	150	180	180
5 ^b			<i>T3Con1</i>			6	7.0	0.02	120	180	180
7	8.5	0.02	165	180	180	8	5.5	0.02	150	0	180
9	6.0	0.02	165	0	180	10	6.5	0.02	105	180	180
11	8.5	0.02	180	180	180	12	5.0	0.02	135	0	180
13 ^b			<i>T2Con2</i>			14 ^b			<i>T2Con1</i>		
15	8.0	0.02	165	90	180	16	4.5	0.02	90	180	180
17	4.5	0.02	120	0	180	18	5.0	0.02	90	180	180
19	4.0	0.02	90	180	180	20	4.0	0.02	90	180	180
21	5.5	0.02	90	180	180	22	0.0	0.02	90	165	180
23	3.5	0.02	90	180	180	24 ^b			<i>T1Con3</i>		
25	5.0	1.40	90	180	30	26	7.5	0.02	150	90	180
27	6.0	0.02	90	180	180	28	6.0	1.40	90	180	60
29	5.5	0.02	75	180	180	30	8.5	0.02	90	150	180
31	6.5	1.40	90	180	75	32	5.0	0.02	60	180	180
33	4.5	0.02	45	180	180	34	6.5	0.02	90	180	180
35	7.0	1.40	90	180	180	36	7.0	1.40	90	180	90
37	6.5	1.40	90	180	165	38	7.5	1.40	90	180	105
39	8.5	0.02	90	135	180	40	7.0	0.02	135	90	180
41	0.0	1.40	90	180	165	42	8.5	1.40	90	180	150
43	8.5	1.40	90	180	135	44	6.0	1.40	90	180	150
45	4.5	0.02	90	180	180	46	7.0	0.02	90	180	180
47 ^b			<i>PaCon2</i>			48	5.5	1.40	90	180	135
49	4.0	0.02	30	180	180	50	8.0	0.02	90	120	180
51	3.5	0.02	90	90	180	52	6.5	0.02	120	90	180
53 ^b			<i>PaCon1</i>			54 ^b			<i>T4Con1</i>		
55	4.5	0.02	90	90	180	56	5.0	1.40	90	180	120
57	4.0	0.02	90	90	180	58 ^b			<i>Coplane</i>		
59	5.0	0.02	90	180	180	60	6.0	0.02	105	90	180
61	5.0	1.40	90	90	30	62	4.0	0.02	90	90	180
63	5.0	0.02	75	90	180	64	8.0	0.02	90	180	180
65	5.5	1.40	90	90	45	66	5.5	0.02	90	180	180
67	4.5	0.02	60	90	180	68	6.0	0.02	90	60	180
69	6.0	1.40	90	90	60	70	5.0	0.02	90	90	180
71 ^b			<i>PaCon3</i>			72 ^b			<i>T5Con1</i>		
73 ^b			<i>T5Con2</i>			74	0.0	1.40	90	90	180
75	6.5	1.40	90	90	75	76	5.0	0.02	90	30	180
77 ^b			<i>T6Con1</i>			78	0.0	1.40	90	90	165
79	7.0	1.40	90	90	90	80	6.0	0.02	90	180	180
81	4.5	0.02	90	0	180	82	7.5	1.40	90	90	105

(continued)

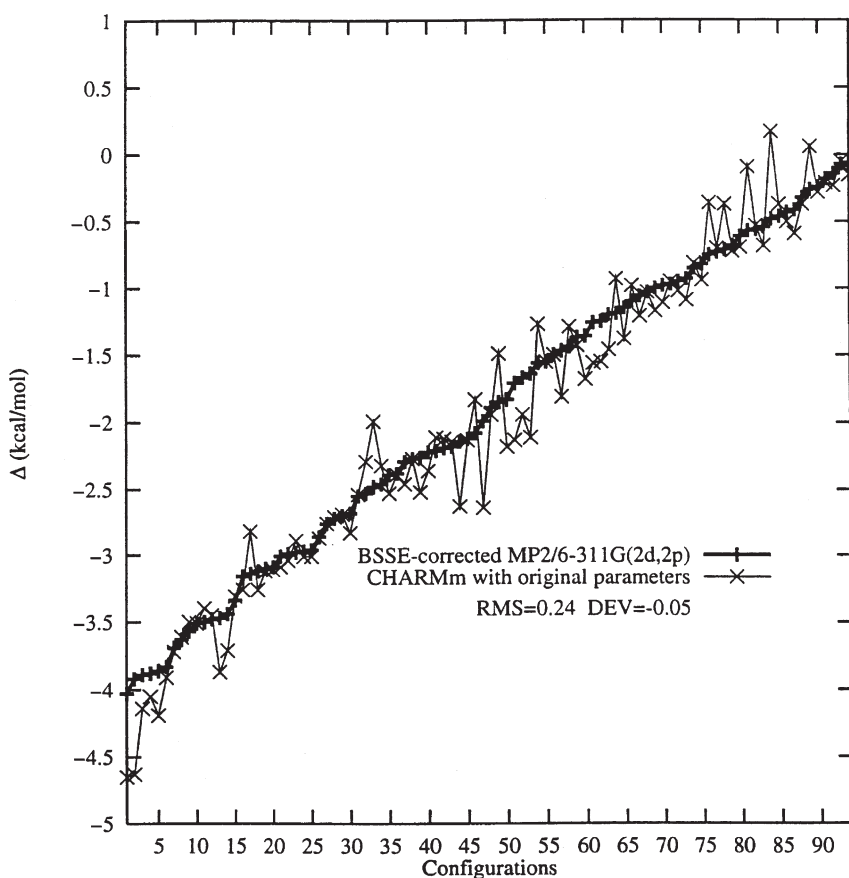
Table 4. Continued

#	<i>P</i>	<i>L</i>	<i>A</i>	<i>DA1</i>	<i>DA2</i>	#	<i>P</i>	<i>L</i>	<i>A</i>	<i>DA1</i>	<i>DA2</i>
83 ^b			<i>T6Con2</i>			84	4.0	0.02	90	0	180
85	8.5	1.40	90	90	135	86	6.5	0.02	90	180	180
87	5.0	0.02	90	90	180	88	7.0	0.02	90	180	180
89	5.0	0.02	90	0	180	90	7.5	0.02	90	180	180
91	8.0	0.02	90	180	180	92	6.0	0.02	90	90	180
93	8.0	0.02	90	90	180	94	6.5	0.02	90	90	180

For a detailed descriptions of these structures, please see Ref. [12].

^a Configuration corresponding to the global minimal energy.

^b These structures are MP2 optimized configurations from Ref. [12].

**Fig. 7.** CHARMM and MP2 on the $\text{C}_6\text{H}_6\text{-H}_2\text{NCOH}$ interaction.

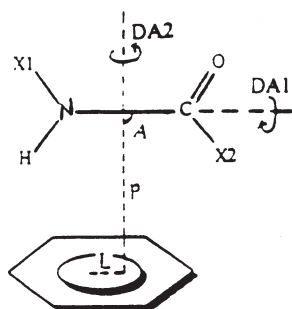


Fig. 8. Intermolecular geometries for $\text{C}_6\text{H}_6\text{-H}_3\text{CCONHCH}_2\text{-}$ interaction. Note that X1 is -CONH_2 and X2 is -CH_3 .

For each of these 38 calculated configurations, the difference in the magnitudes between the CHARMM and MP2 stabilization energy is less than 0.53 kcal/mol. Therefore, the existing CHARMM force field is qualified for the aromatic–amide(B) interaction.

Table 5. Geometries for 38 calculated $\text{C}_6\text{H}_6\text{-H}_3\text{CCONHCH}_2\text{CONH}_2$ configurations

#	<i>P</i>	<i>L</i>	<i>A</i>	<i>DA1</i>	<i>DA2</i>	#	<i>P</i>	<i>L</i>	<i>A</i>	<i>DA1</i>	<i>DA2</i>
1	3.5	0.02	90	90	0	2	5.0	2.20	90	30	180
3	4.0	0.02	90	90	0	4	5.5	0.02	60	150	0
5	4.0	1.40	90	90	90	6	4.5	0.02	120	120	0
7	4.0	2.20	90	90	180	8	4.0	1.40	90	90	0
9 ^a	5.0	1.49	90	150	180	10	4.0	2.20	90	90	90
11	5.5	1.40	60	150	90	12 ^a	5.5	1.40	150	150	180
13	5.0	1.40	90	150	0	14	5.0	0.02	90	150	0
15	5.5	2.20	150	150	0	16 ^a	5.5	1.40	150	150	90
17 ^a	5.0	2.20	90	150	180	18	5.0	2.20	30	90	90
19	4.0	2.20	90	90	0	20	5.0	2.20	90	150	0
21	5.5	2.20	150	90	0	22	5.0	1.40	90	150	180
23	4.5	0.02	90	90	0	24 ^a	5.5	2.20	150	150	90
25	5.0	2.20	30	90	0	26	5.0	2.20	90	150	180
27	5.5	1.40	150	150	0	28	5.5	2.20	60	150	90
29	4.5	0.02	60	60	0	30	5.5	2.20	60	150	0
31	5.5	2.20	150	90	90	32	5.0	2.20	30	90	180
33	5.5	2.20	60	150	180	34	5.0	2.20	30	30	90
35	5.0	2.20	30	30	0	36	5.5	2.20	150	90	180
37	5.0	2.20	30	30	180	38	5.0	2.20	60	30	90

Units are Å for distance and degrees for angles.

^a $\text{H}_3\text{CCONHCH}_2\text{CONH}_2$ in these configurations corresponds to the structure modelWH. It corresponds to the structure modelH in the others. See Ref. [13] for the modelH and modelWH.

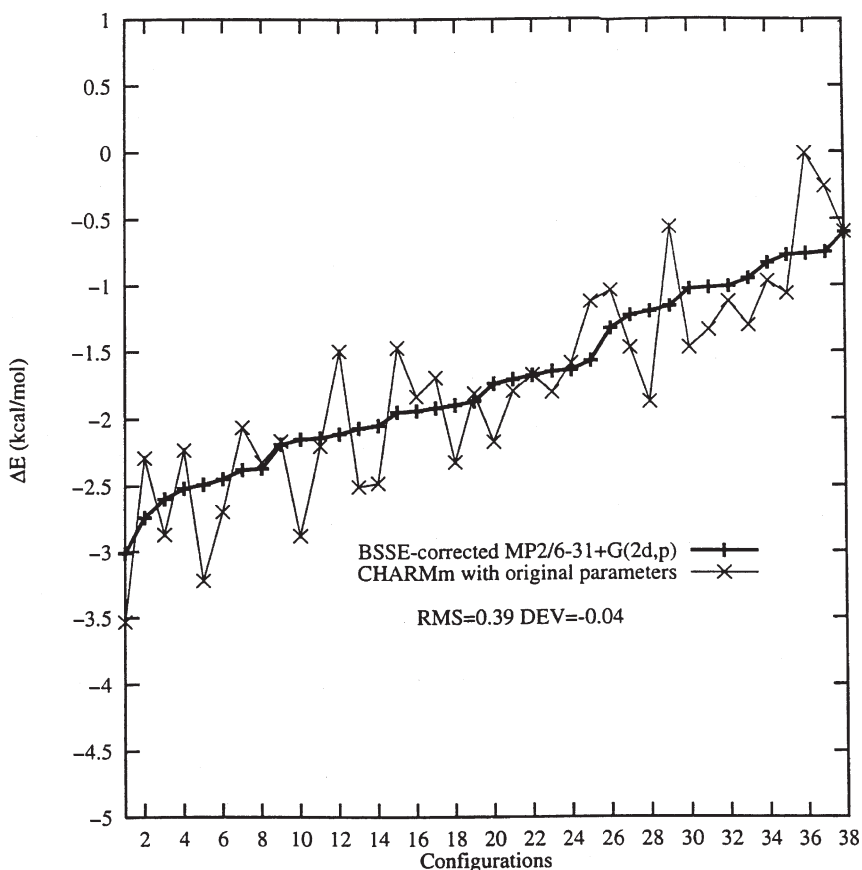


Fig. 9. CHARMM and MP2 on the $C_6H_6-H_3CCONHCH_2CONH_2$ interaction.

4.5. Aromatic-thiol interactions

The model complex used for this interaction is $C_6H_6-HSCH_3$. Its configuration is specified with five intermolecular geometric parameters, L , P , A , $DA1$, and $DA2$, illustrated in Fig. 10.

In total, 68 configurations were selected to characterize its IPES. These configurations were obtained by varying the five intermolecular geometric parameters. Their geometries are listed in Table 6.

In Fig. 11, the IPESs from CP-corrected MP2/6-311G(2d,p), from CHARMM with existing parameters, and with optimized parameters are demonstrated. The existing CHARMM force field cannot yield the IPES in satisfactory agreement with that from MP2. Overall, it underestimates the stabilization energy of the interaction. The RMS and DEV for it are 0.76 and

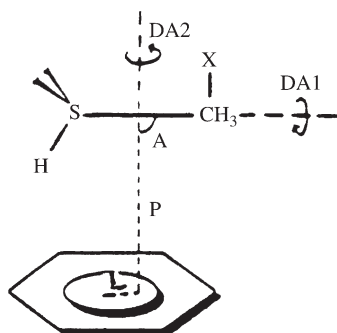


Fig. 10. Definition of $\text{C}_6\text{H}_6\text{--HSCH}_3$ configuration.

0.62 kcal/mol, respectively. For some of the calculated configurations, the underestimation is larger than 1.0 kcal/mol in magnitude. In particular, it underestimates the stability of the first configuration by 1.36 kcal/mol. This configuration is the global energy minimum structure and achieves the largest stabilization energy (3.38 kcal/mol). The Lennard–Jones parameters between aromatic carbon and thiol sulfur (C6R-ST atom pair) were optimized. The new parameters increase the stabilization energy between these two atoms which is reflected by a more negative value for the ϵ_{ab} (see Table 1). With the new parameters, the overall behavior of CHARMM for this interaction is significantly improved. The RMS and DEV for the optimized CHARMM are, respectively, 0.35 and 0.02 kcal/mol which are much less than those for the existing one in magnitude. For most of these calculated configurations, the difference in the stabilization between it and MP2 is less than 0.5 kcal/mol in magnitude. Especially for the global energy minimum configuration (#1) the optimized CHARMM produces a stabilization energy only 0.35 kcal/mol lower than that from the MP2.

4.6. Aromatic–amine interaction

The aromatic–amine interaction is modeled as the interaction between C_6H_6 and H_2NCH_3 . In this work, only the π -type hydrogen bonding structures are considered. In this structure, the amine should reside over the benzene ring with one of its amine hydrogens pointing toward its aromatic π electrons (Fig. 12).

The IPES for this interaction pattern was developed by varying the geometric parameters P . Figure 13 demonstrates the IPESs from CP-corrected MP2/6-311G(2d,p), CHARMM with the original parameters, and optimized parameters.

The MP2 result indicates that the largest stabilization energy is 2.25 kcal/mol and is achieved at $P = 3.5$ Å. According to the interaction

Table 6. Geometries for 68 calculated C₆H₆–HSCH₃ configurations

#	<i>P</i>	<i>L</i>	<i>A</i>	<i>DA1</i>	<i>DA2</i>	#	<i>P</i>	<i>L</i>	<i>A</i>	<i>DA1</i>	<i>DA2</i>
1 ^{a,b}	3.7	0.05	83	180	180	2	4.0	0.05	90	180	180
3	4.0	1.40	90	180	0	4	4.0	1.40	90	180	30
5	4.0	0.05	90	150	180	6	3.5	0.05	90	180	180
7	4.0	1.40	90	180	60	8	4.0	0.05	120	180	180
9	4.0	1.40	90	180	90	10	4.0	0.50	90	180	180
11	4.5	0.05	90	180	180	12	4.0	1.40	90	180	120
13	4.0	1.40	90	180	150	14	4.0	1.40	90	180	180
15	4.0	1.00	90	180	180	16	4.0	0.05	150	180	180
17	4.0	1.50	90	180	180	18	4.0	1.40	90	90	30
19	4.0	1.40	90	90	0	20	4.0	0.05	90	0	180
21	5.0	0.05	90	180	180	22	4.0	1.40	90	90	60
23 ^b	3.9	0.85	90	90	0	24	1.0	5.00	90	0	180
25 ^b	1.1	4.80	97	0	180	26	1.0	5.00	90	0	180
27	4.0	0.85	90	90	180	28	4.0	2.00	90	180	180
29	1.0	5.00	150	0	180	30	4.0	0.05	90	30	180
31	0.5	5.00	90	0	180	32	1.0	5.00	90	30	180
33	1.5	5.00	90	0	180	34	1.0	5.00	60	0	180
35	0.0	5.00	90	0	180	36	1.0	5.00	30	0	180
37	4.0	3.00	90	180	180	38	1.0	5.00	90	60	180
39	2.0	5.00	90	0	180	40	4.2	0.05	180	90	180
41	4.0	0.05	180	180	180	42	4.0	0.02	90	90	180
43	5.5	0.05	90	180	180	44	4.2	0.05	90	90	180
45	4.0	2.50	90	180	180	46	4.0	0.05	60	180	180
47	4.0	0.05	90	60	180	48	4.5	0.85	90	90	180
49	1.0	5.00	90	180	180	50	1.0	5.00	90	90	180
51	1.0	5.00	90	150	180	52	4.0	1.40	90	90	120
53	2.5	5.00	90	0	180	54	4.2	0.05	150	90	180
55	4.0	3.50	90	180	180	56	4.0	0.50	90	90	180
57	6.0	0.05	90	180	180	58	3.0	5.00	90	0	180
59	5.0	0.85	90	90	180	60	6.5	0.05	90	180	180
61	4.0	4.00	90	180	180	62	3.5	0.85	90	90	180
63	5.5	0.85	90	90	180	64	7.0	0.05	90	180	180
65	4.0	1.00	90	90	180	66	6.0	0.85	90	90	180
67	7.5	0.05	90	180	180	68	6.5	0.85	90	90	180

Units are Å for distance and degrees for angles.

^a Configuration corresponding to the global minimal energy.

^b MP2 optimized configurations.

feature of the C₆H₆–CH₄ complex, the contribution from the interaction between C₆H₆ and the –CH₃ should be about 0.80 kcal/mol at such a separation. Therefore, the aromatic–amino(H₂N–) π -hydrogen bonding interaction should have a stabilization energy of about 1.45 kcal/mol. This is

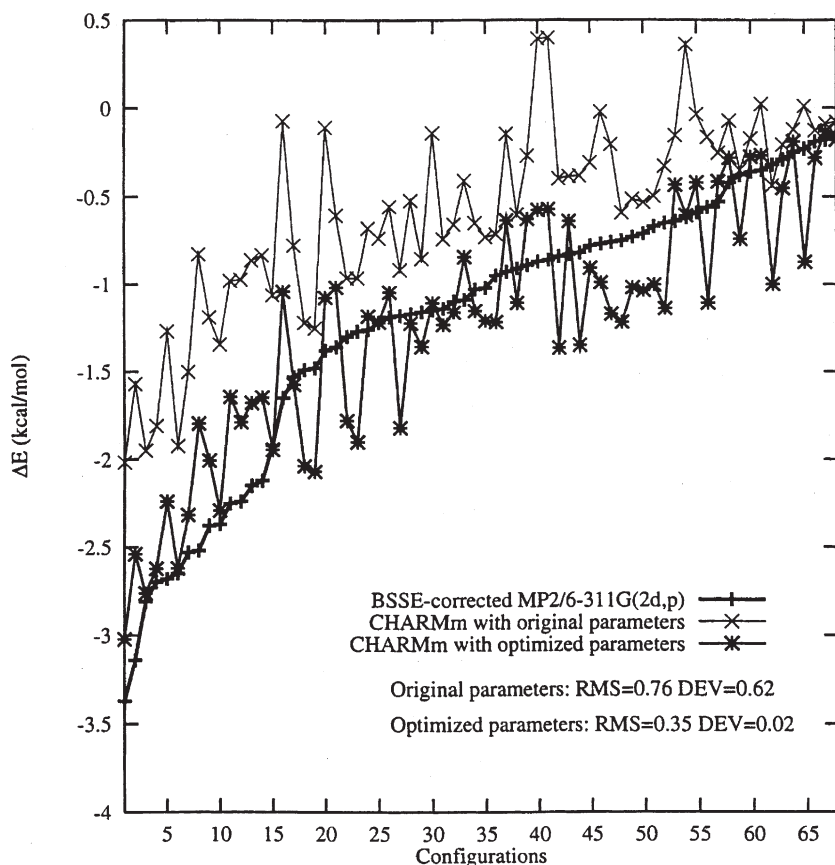


Fig. 11. CHARMm and MP2 on the $C_6H_6-HSCH_3$ interaction.

in agreement with results (about 1.50 kcal/mol) from other theoretical calculations [18,19,33,34] or from experiment [35].

The existing CHARMm parameters can produce a rather good IPES for this interaction. However, its behavior on the interaction can further be improved through modifying the Lennard-Jones parameters between the

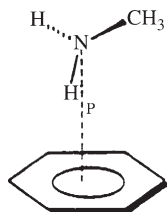


Fig. 12. $C_6H_6-H_2NCH_3$ π -hydrogen bonding structure.

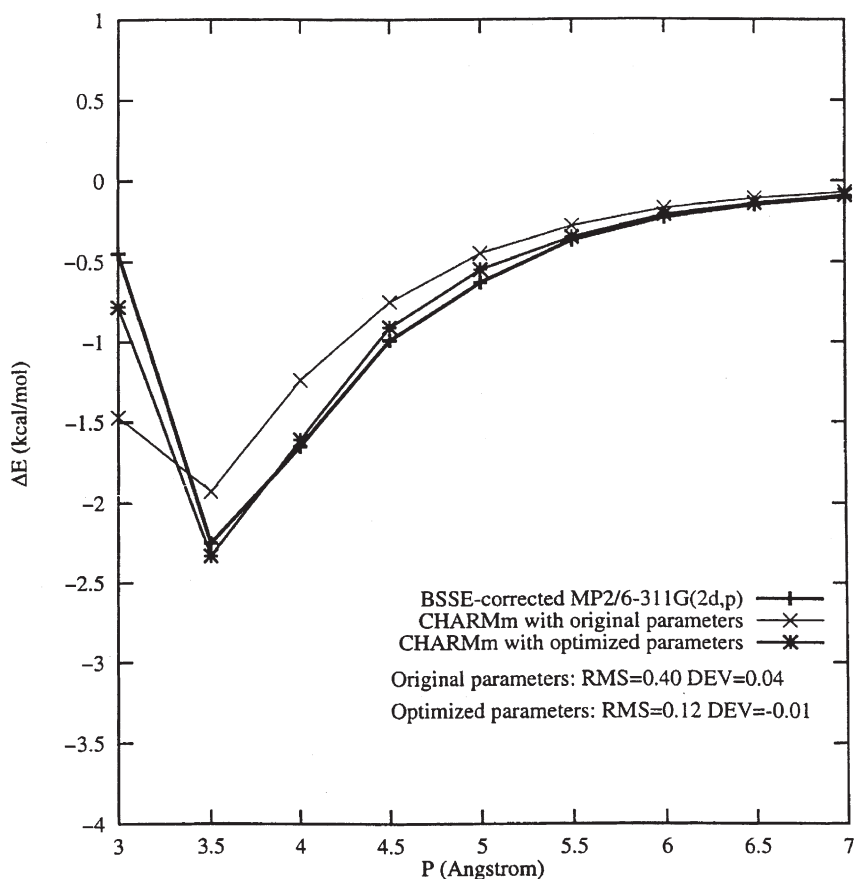


Fig. 13. CHARMM and MP2 IPESs of $C_6H_6-H_2NCH_3$ interaction.

aromatic carbon and the amine nitrogen (C6R-NT atom pair). The improvement is mainly reflected by the fact that the optimized CHARMM can more accurately predict the interaction energy around the global energy minimum structure.

4.7. Aromatic-alcohol interaction

The complex $C_6H_6-HOCH_3$ is a suitable model for this interaction. In this work, the IPES of the π -hydrogen bonding interaction pattern (Fig. 14) was under consideration.

The IPES was developed with respect to the geometric parameters P , which is displayed in Fig. 15.

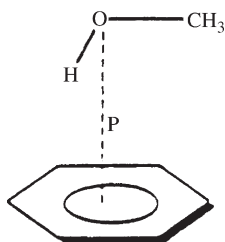


Fig. 14. $\text{C}_6\text{H}_6\text{-HOCH}_3$ π -hydrogen bonding structure.

The MP2 results indicate that the most strong aromatic-hydroxyl(HO-) π -hydrogen bonding interaction is achieved at $P = 3.5$ Å. Its stabilization energy can be approximated as the difference between the total stabilization energy of $\text{C}_6\text{H}_6\text{-HOCH}_3$ interaction (3.27 kcal/mol) and that of $\text{C}_6\text{H}_6\text{-(-CH}_3\text{)}$ interaction (about 0.8 kcal/mol). It is approximately

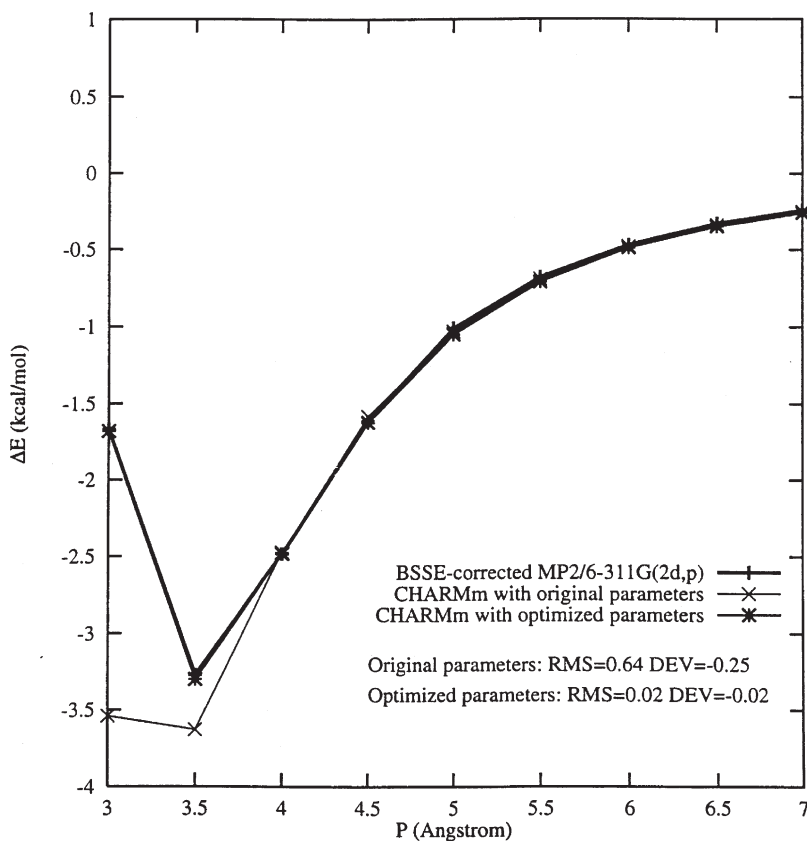


Fig. 15. CHARMM and MP2 IPESs of $\text{C}_6\text{H}_6\text{-HOCH}_3$ interaction.

2.47 kcal/mol. This estimation is close to those previously reported results (about 2.00 kcal/mol) for the aromatic–hydroxyl hydrogen bond [18,19,33].

The existing CHARMM force field severely overestimates the stabilization of the structures around the global energy minimum structure. With the optimized Lennard–Jones parameters between the aromatic carbon and oxygen (C6T–OT atom pair), the optimized CHARMM is capable of producing the IPES for the interaction in excellent agreement with that from MP2.

5. CONCLUSION

In this work, the applicability of the CHARMM force field to model interactions containing aromatics has been validated. An algorithm was developed for fitting CHARMM interaction energies to those produced by accurate *ab initio* calculations. It has been demonstrated that the existing CHARMM force field is able to accurately describe the aromatic–aliphatic, aromatic–amide(S), and aromatic–amide(B) interactions. However, this force field is not capable of satisfactorily producing the IPESs at the MP2 level for aromatic–aromatic, aromatic–thiol, aromatic–amine, and aromatic–alcohol interactions. For these four interactions, the relevant parameters were optimized using the fitting algorithm. With the optimized parameters, CHARMM is suitable to calculate these interactions. Moreover, these new parameters do not modify the interaction between the aromatic and other groups, and thus do not change CHARMM's behavior on other interacting molecular systems. This would make these resultant parameters useful when using the CHARMM force field to study protein structure, protein energetics, and other biological/chemical phenomena.

ACKNOWLEDGEMENTS

V.H.S. and D.F.W. acknowledge operating grants from the Natural Science and Engineering Research Council of Canada. G.D. is thankful to Dr Qizhi Cui for his help in preparing the manuscript of this work. D.F.W. is supported by a Tier 1 Canada Research Chair in Neuroscience. One of us (V.H.S.) wishes to acknowledge the long-standing friendship with Osvaldo Goscinski and to extend best wishes on the occasion of his 65th birthday.

REFERENCES

- [1] C. A. Deakyne and M. Meot-Ner, *J. Am. Chem. Soc.*, 1985, **107**, 474.
- [2] J. Sunner, K. Nishizawa and P. Kebarle, *J. Phys. Chem.*, 1981, **85**, 1814.
- [3] D. A. Dougherty, *Science*, 1996, **271**, 163.
- [4] B. C. Guo, J. W. Purnell and A. W. Castleman, *Chem. Phys. Lett.*, 1990, **168**, 155.
- [5] K. S. Kim, J. Y. Lee, S. J. Lee, T. Ha and D. H. Kim, *J. Am. Chem. Soc.*, 1994, **116**, 7399.

- [6] M. Harel, I. Schalk, L. Ehret-Sabatier, F. Bouet, M. Goeldner, C. Hirth, P. H. Axelsen, I. Silman and J. L. Sussman, *Proc. Natl Acad. Sci. USA*, 1993, **90**, 9031.
- [7] S. K. Burley and G. A. Petsko, *Science*, 1985, **229**, 23.
- [8] R. Jaffe and G. D. Smith, *J. Chem. Phys.*, 1996, **81**, 4871.
- [9] P. Hobza, L. Heinrich and E. W. Schlag, *J. Phys. Chem.*, 1996, **100**, 18790.
- [10] C. Chipot, R. Jaffe, B. Maigret, D. A. Pearlman and P. A. Kollman, *J. Am. Chem. Soc.*, 1996, **118**, 11217.
- [11] G. Duan, V. H. Smith, Jr. and D. F. Weaver, *Chem. Phys. Lett.*, 1999, **310**, 323.
- [12] G. Duan, V. H. Smith, Jr. and D. F. Weaver, *J. Phys. Chem. A*, 2000, **104**, 4521.
- [13] G. Duan, V. H. Smith, Jr. and D. F. Weaver, *Int. J. Quantum Chem.*, 2000, **80**, 44.
- [14] G. Duan, V. H. Smith, Jr. and D. F. Weaver, *Int. J. Quantum Chem.*, 2002, **90**, 669.
- [15] G. Duan, V. H. Smith, Jr. and D. F. Weaver, *Mol. Phys.*, 2001, **99**, 1689.
- [16] M. M. Flocco and S. L. J. Mowbray, *J. Mol. Biol.*, 1994, **211**, 595.
- [17] J. B. O. Mitchell, C. L. Nandi, I. K. McDonald, J. M. Thornton, S. L. Price and J. Singh, *J. Mol. Biol.*, 1994, **239**, 315.
- [18] S. Suzuki, P. G. Green, R. E. Bumgarner, S. Dasgupta, W. A. Goddard and G. A. Blake, *Science*, 1992, **257**, 942.
- [19] J. L. Atwood, F. Hamada, K. D. Robinson, G. W. Orr and R. L. Vincent, *Nature*, 1991, **349**, 683.
- [20] B. R. Brooks, R. E. Bruccoleri, B. D. Olafson, D. J. States, S. Swaminathan and M. Karplus, *J. Comput. Chem.*, 1983, **4**, 187.
- [21] L. X. Dang, J. E. Rice, J. W. Caldwell and P. A. Kollman, *J. Am. Chem. Soc.*, 1991, **113**, 2481.
- [22] J. W. Caldwell, L. X. Dang and P. A. Kollman, *J. Am. Chem. Soc.*, 1990, **112**, 9144.
- [23] O. Donini and D. F. Weaver, *J. Comput. Chem.*, 1998, **13**, 1515.
- [24] B. W. Kernighan and D. M. Ritchie, *The C Programming Language*, 2nd edn., Prentice-Hall, Englewood Cliffs, NJ, 1988.
- [25] A. D. Mackerell, J. Wiorkiewicz and M. Karplus, *J. Am. Chem. Soc.*, 1995, **117**, 11946.
- [26] G. C. Maitland, M. Rigby and W. A. Wakeham, *Intermolecular Forces. Their Origin and Determination*, Clarendon Press, Oxford, 1981.
- [27] J. P. Bowen and N. L. Allinger, in *Molecular Mechanics: The Art and Science of Parameterization* (eds K. B. Lipkowitz and D. B. Boyd), Reviews in Computational Chemistry, VCH, New York, 1991, Vol. 9.
- [28] S. F. Boys and F. Bernardi, *Mol. Phys.*, 1970, **19**, 553.
- [29] M. J. Frische, G. W. Trucks, M. Head-Gordon, P. M. W. Gill, M. W. Wong, J. B. Foresman, B. G. Johnson, H. B. Schlegel, M. A. Robb, E. S. Replogle, R. Gomperts, J. L. Andres, K. Raghavachari, J. S. Binkley, C. Gonzalez, R. L. Martin, D. J. Fox, D. J. DeFrees, J. Baker, J. J. P. Stewart, J. A. Pople, GAUSSIAN 94, Gaussian Inc., Pittsburgh, PA, 1994.
- [30] A. D. Mackerell, D. Bashford, M. Bellott, R. L. Dunbrack, M. J. Field, S. Fischer, J. Cao, H. Gao, S. Ha, D. Joseph, L. Kuchnir, K. Kuczera, F. T. K. Lau, C. Mattos, S. Michnick, T. Ngo, D. T. Nguyen, B. Prodhom, B. Roux, M. Schlenkirch, J. C. Smith, R. Stote, J. Straub, J. Wiorkiewicz-Kuczera and M. Karplus, *FASEB J.*, 1992, **6**, 143.
- [31] W. H. Press, B. P. Flannery, S. A. Teukolsky and W. T. Vetterling, *Numerical Recipes in C*, Cambridge University Press, New York, 1990.
- [32] C. A. Hunter and J. K. M. Sanders, *J. Am. Chem. Soc.*, 1990, **112**, 5525.
- [33] G. Waskman, D. Kominos, S. C. Robertson, N. Pant, D. Baltimore, R. B. Birge, D. Cowburn, H. Hanafusa, B. J. Mayer, M. Overduin, M. D. Resh, C. B. Rios, L. Silverman and J. Kuriyan, *Nature*, 1992, **646**, 358.
- [34] B. F. Henson, G. V. Hartland, V. A. Venturo and P. M. J. Felker, *J. Chem. Phys.*, 1992, **97**, 2189.
- [35] H. Adams, K. D. M. Harris, G. A. Hembury, C. A. Hunler, D. Livingston and J. F. McCabe, *Chem. Commun.*, 1996, 2531.

Are Jordan Blocks Necessary for the Interpretation of Dynamical Processes in Nature?

Erkki J. Brändas

Department of Quantum Chemistry, Uppsala University, Box 518, S-751 20 Uppsala, Sweden

Abstract

We suggest various examples of quantum systems where it seems necessary to include explicitly so-called Jordan blocks in an extended time irreversible dynamical picture. Two types of phenomena are analyzed. First, we illustrate the possibility to map particle–antiparticle pairs by a set of degenerate canonical Jordan forms. Second, we discuss and predict cases of giant Jordan blocks in complex dissipative systems far from equilibrium. The issue of microscopic self-organization is approached and it is demonstrated that degeneracies with higher order Segrè characteristics appear naturally in the generalized dynamical picture.

Contents

1. Introduction	93
2. Hamiltonian level	95
3. Liouvillian level	98
4. Conclusions	102
Acknowledgements	103
Appendix A. Properties of reduced density matrices	103
References	106

1. INTRODUCTION

At the end of the ‘Conference on Irreversible Quantum Dynamics’ in Trieste, in August 2002, Arno Bohm addressed the question of the physical interpretation and the occurrence in Nature of processes related to the appearance of Jordan blocks. He ended the presentation by asking, ‘where are all the Jordan blocks’? The question is not new as the possibility of Jordan canonical forms in an extended quantum dynamical picture has been noticed many times in the past decades, see Refs. [1,2] and references therein. The topic was again resumed at the QSCP workshop in Bratislava a month later.

The question has to be elaborated a bit. Jordan block representations of nilpotent operators are commonly used in quantum mechanics. Well-known examples are so-called transition operators and shift operators, e.g. step

operators in angular momentum algebra or spin dynamics, as well as annihilation and creation operators in second quantization. Obviously Jordan blocks are everywhere!

However, promoting Jordan blocks as wanted by physicists and chemists, implies a different question. The Hamiltonian or Liouvillian serves two purposes, i.e., they are at the same time representatives of a measurable observable and generators of time evolution of the given system. In standard quantum mechanics the Hamiltonian is by necessity self-adjoint. Consequently, the associated differential equation yields real eigenvalues (with the Segrè characteristic equal to one), see Ref. [3] for more information. In other words, representing an observable by a suitable matrix, a standard mathematical theorem says that such matrices can always be diagonalized. Within this framework the answer to the title question changes from yes to no.

Yet, there is something fundamental to discuss here. Recent developments of non-selfadjoint extensions of the Hamiltonian/Liouvillian dynamics, whether the focus is on dilatation analytic, self-adjoint families of operators [4] or concerns semigroup constructions [5] of the associated evolution operator, calls for the immediate incorporation of general classical canonical forms of the Jordan type, see Ref. [3] for details.

In these extended applications, the possible occurrence of degeneracies, with Segrè characteristics larger than one, could result in an unwelcome calculational breakdown – usually considered as a numerical accident brought forward by the self-orthogonality of the transformed vectors. The objective of a successful computation was to stay away from them.

In other situations, however, it was realized that the appearance of a Jordan block in the generator led to interesting consequences for the time evolution. It was in effect realized that one could introduce realistic boundary conditions in order to generate various types of degeneracies and to determine the resulting evolutionary consequences [2,6,7]. The incorporation of higher order Gamow waves in scattering theory was further analyzed by Bohm *et al.* [1]. Other well-known examples include complex representations of the time group and the time translations (see Ref. [8]). These characteristic, triangular reducible, non-decomposable time representations, by way of general Jordan type matrix representation, are here used to describe non-particle ghost degrees of freedom in gauge fields. Other fundamental problems have also been analyzed, e.g. CPT-invariance in antihydrogen [9].

There has not yet been any reported experimental evidence that seems to indicate the need to incorporate Jordan blocks in pure Hamiltonian dynamics. However, if the question is directed towards a more complex situation, i.e., to the thermodynamic domain concerned with a description based on a Liouvillian generator, the appearance of large Jordan blocks has

been shown to lead to surprising consequences with regard to microscopic time evolution including the emergence of self-organizational structures [9].

In this contribution we will consider two examples, first the example of decaying neutral kaons and secondly the possibility of giant Jordan blocks in the domain of complex coherent-dissipative systems. These examples seem to indicate, in contrast to what is believed, that Mother Nature might be rich in Jordan blocks. If this is the case it is our duty to find them!

2. HAMILTONIAN LEVEL

We will first discuss the simple transformation of a 2×2 matrix to complex symmetric form. The model is quite general. We will further establish a simple condition for degeneracy with Segrè characteristic $r = 2$ (see Refs. [6,9,10]). We will consider a specific metric Δ , which in general may not be positive definite. We will distinguish between two principal cases: (1) $\Delta_{11} = \Delta_{22} = 1$; $\Delta_{12} = \Delta_{21} = 0$ and (2) $\Delta_{11} = -\Delta_{22} = 1$; $\Delta_{12} = \Delta_{21} = 0$.

Before introducing any particular models, we realize that the secular problem below, c.f. the Hamiltonian models used in Ref. [9], can be written

$$(\mathbf{H} - E\Delta)\mathbf{c} = 0 \quad (1)$$

or

$$(\tilde{\mathbf{H}} - E1)\mathbf{c} = 0 \quad (2)$$

where several choices for $\tilde{\mathbf{H}}$ can be made, i.e.

$$\tilde{\mathbf{H}} = \Delta^{-1}\mathbf{H}; \quad \tilde{\mathbf{H}} = \Delta^{-\frac{1}{2}}\mathbf{H}\Delta^{-\frac{1}{2}}; \quad \tilde{\mathbf{H}} = \mathbf{H}\Delta^{-1} \quad (3)$$

As already mentioned in the introduction, we will allow non-Hermitian extensions of quantum mechanics and hence it is natural to choose the first of the three forms in equation (3). Note that the formula in the middle is mostly used when working with positive definite metrics and self-adjoint Hamiltonians.

A general theorem in linear algebra, see Ref. [10] for more details, says that any finite matrix representation can be transformed to complex symmetric form. For this reason, we can without loss of generality set up a complex symmetric model for our generalized dynamical picture based entirely on the parameters H_{11} , H_{22} , and v with

$$H_{12} = H_{21} = iv \quad (4)$$

and where the interaction is given by the specific physical situation, c.f. the discussion in Ref. [9].

As usual we will try to diagonalize the matrix H via a suitable similarity transformation, finding that it is not always possible. One obtains with $r = 2$

$$\begin{pmatrix} H_{11} & iv \\ iv & H_{22} \end{pmatrix} \rightarrow \begin{pmatrix} E & 1 \\ 0 & E \end{pmatrix} \quad (5)$$

with the degenerate eigenvalue E given by the condition

$$\lambda_{\pm} = \frac{1}{2}(H_{11} + H_{22}) \pm \frac{1}{2}\sqrt{(H_{11} - H_{22})^2 - 4v^2} \quad (6)$$

requesting the condition of a vanishing discriminant in equation (6). This leads directly to the relations

$$H_{22} = H_{11} \pm 2v; \quad \lambda_+ = \lambda_- = E = \frac{1}{2}(H_{11} + H_{22}) = H_{11} \pm v. \quad (7)$$

The vectors, up to a normalization constant, building up the similarity transformation are

$$\mathbf{c}_1 = \begin{pmatrix} i \\ \pm 1 \end{pmatrix}; \quad \mathbf{c}_2 = \begin{pmatrix} \mp i \\ 1 \end{pmatrix}; \quad \mathbf{c}_1^* = \pm \mathbf{c}_2 \quad (8)$$

where \mathbf{c}_1 in equation (8) is the eigenvector corresponding to the degenerate eigenvalue $H_{11} \pm v$. Any given value of v (or prescribed difference between the two diagonal elements) results in one set of degenerate solutions. However, since we have two ‘ \pm ’ possibilities, one of the choices must be wrong or unphysical. If initially H_{11} is known the other diagonal matrix element must differ by the amount of $\pm 2v$.

One also sees that \mathbf{c}_2 is the eigenvector of the complex conjugate problem and that the ‘upper’ branch of one eigenvector is linearly dependent on the ‘lower’ branch of the other. Also $v \rightarrow -v$ corresponds to the transposition $1 \leftrightarrow 2$. It follows that if \mathbf{c}_1 is the eigenvector then \mathbf{c}_2 would be ‘hidden’ or ‘ghostlike’ and vice versa. Particles that would look different could therefore in principle be each other’s ghost.

Although the 2×2 matrix eigenvalue problem, equations (1–8), stays invariant under the simple transformations indicated, one cannot rule out the possibility that there could exist simultaneously ‘by accident’ two inequivalent solutions, where the ‘+’ and the ‘−’ sign in equations (7) and (8) refers to two different physical situations. For instance, the relation between H_{11} and H_{22} , see equation (7), could refer to two different roots of a secular equation separating two degenerate blocks. In such a case a coupled pair of Jordan blocks could also in principle be physically realizable. In Ref. [9] we looked specifically at the problem of the Lamb shift in

antihydrogen, and the possibility of breaking CPT invariance under

$$p + e \rightarrow \bar{p} + e^+.$$

Reformulating now the model using the non-positive definite metric, the principal case (2), the following changes are incorporated in equations (5)–(7):

$$H_{21} \rightarrow -H_{21}; \quad H_{22} \rightarrow -H_{22}. \quad (9)$$

This is the same as replacing H by $\Delta^{-1}H$ above.

In the present case, we will briefly look at the example of decaying neutral kaons (see Ref. [8]). In an obvious setting we first study the formulation (1), (4)–(9), in the principal case (2) by choosing

$$H_{11} = 0; \quad H_{22} = 2m; \quad H_{12} = i\nu; \quad \nu = m$$

where m represents the mass of the given particle and $2m$ the total mass of the particle–antiparticle pair. It follows that the Jordan block; note the choice of principal case (2),

$$\begin{pmatrix} 0 & im \\ -im & -2m \end{pmatrix} \rightarrow \begin{pmatrix} m & 1 \\ 0 & -m \end{pmatrix}$$

describes in a simplified manner particle–antiparticle pair production.

The representation at hand can easily be applied to the kaon mixing problem. By solving a standard 2×2 eigenvalue problem the kaon and its antiparticle are first combined into their CP eigenstates.

$$2H_{11} = M_L + M_S, \quad H_{12} = i\nu, \quad 2\nu = M_S - M_L,$$

$$M_S = M + \frac{1}{2}m - \frac{i}{2}\Gamma_S, \quad M_L = M - \frac{1}{2}m - \frac{i}{2}\Gamma_L$$

where M is the neutral kaon (particle- and antiparticle) mass (to be more specific the almost equal masses of the short- and long-lived kaons), Δm is the mass difference between K^0 -short and the K^0 -long and Γ_S , Γ_L are the appropriate half-widths, respectively.

Consider now the long- and short-lived neutral kaons as they are observed experimentally with masses as indicated above. It is easy to see that it is not possible here to couple the two kaons as one single particle–ghost pair. However, by noticing the fact that there exist the two possibilities, equations (6–9), one could simply infer that the \pm branches build up two separate Jordan blocks, one with the degenerate eigenvalue $H_{11} + \nu$ and the other one with $H_{11} - \nu$. Hence, we obtain for one of the blocks

$$E = H_{11} + \nu = M_S$$

with the $+$ branch of \mathbf{c}_1 as eigenvector, and for the other

$$E = H_{11} - v = M_L$$

with the $-$ branch of \mathbf{c}_1 as eigenvector. Note that the two vectors correspond to two different spaces and therefore different physical situations. We have not speculated on the dimensions of the various blocks, here they are both two for simplicity. As is well known the longer-lived kaon has three principal- and one CP-violating mode, while the short-lived kaon has two. The CP-violating interaction v conveys two messages, i.e. (i) separates the two matrix blocks and (ii) provides the precise conditions for the exact degeneracy within each block. In this description the kaons K_L^0 and K_S^0 are each associated with a Jordan block of Segrè characteristic 2, their masses and lifetimes given by precise differences *via* the CP-violating interaction as illustrated above. The present model naturally makes clear that ghost of the particle is its antiparticle outlined by the Jordan block canonical form.

A similar model could for example be devised for the neutrino mass problem starting with $M = 0$. It is also tempting to interpret the WMAP collaboration data (see e.g. *Physics Today*, November 2003, p. 42) from our model. As stated, about 4% of the cosmic mass-energy content resides in ordinary baryonic matter, the rest depending on 23% dark matter and 73% dark energy. Suppose now that the universe at some evolutionary stage consisted of (see Eq. (9) and below) no baryonic matter. Then, assuming that the two halves of the baryonic (positive or negative) matter distribute so that the fractions would have been 25% dark matter and 75% dark energy. These numbers would then suggest a fundamental 4×4 Jordan block (Segrè characteristic 4) scenario for our universe.

We will end the discussion here and move on to the case of giant Jordan blocks in coherent-dissipative systems. As the problem is generalized to arbitrary dimensions other possibilities will appear.

3. LIOUVILLIAN LEVEL

In this section, we will generalize the simple 2×2 case and, at the same time, take a closer look at a different type of system, i.e., a quantum system in contact with its environment. Our theoretical formulation includes random-, thermal- and quantum-fluctuations together. This is a fundamentally difficult problem since we are dealing with systems out of equilibrium. We will demonstrate that it is possible to incorporate the temperature in a quasi-equilibrium context and at the same time show that constructive interaction may exist between the environment and the open quantum system.

It is a well-known trick to make time imaginary by formally including temperature in the formulation through the relation

$$t \rightarrow t - i\beta; \quad \beta = \frac{1}{kT} \quad (10)$$

where k is Boltzmann's constant and T the absolute temperature in Kelvin. In the extended dynamical picture to be presented below this analogy no longer holds. We start with the Bloch equation, i.e.

$$-\frac{\partial \rho}{\partial \beta} = \hat{L}_B \rho \quad (11)$$

where \hat{L}_B is the energy super operator appropriately extended to a biorthogonal complex representation

$$\hat{L}_B = \frac{1}{2} \{H| \langle^*| + | \rangle \langle^*| H\}. \quad (12)$$

Note the complex conjugate in the bra position compared to the extended Liouville time generator

$$\hat{L} = H| \langle | - | \rangle \langle H^\dagger. \quad (13)$$

For more details on this construction, see Ref. [9] and references therein.

In Appendix A we have derived a reduced density matrix which exhibits the so-called extreme configuration that may develop off-diagonal long-range order (ODLRO), see equations (A6) and (A7).

$$\Gamma_S^{(2)} = \lambda_S \sum_{k=2}^m |g_k\rangle \langle g_k| = \lambda_S \sum_{k=1}^m \sum_{l=1}^m |h_k\rangle \left(\delta_{kl} - \frac{1}{m} \right) \langle h_l|. \quad (14)$$

Applying now the thermalization procedure to equations (14) it is possible to determine the effects of thermal correlations on the ordered state. One obtains, with E the real part of the energy,

$$e^{-\beta \hat{L}_B} \tilde{\Gamma}_S^{(2)} = \lambda_S e^{-\beta E} \sum_{k=1}^m \sum_{l=1}^m |h_k\rangle e^{i\beta \frac{1}{2}(\varepsilon_k + \varepsilon_l)} \left(\delta_{kl} - \frac{1}{m} \right) \langle h_l^*| \quad (15)$$

where ε_k is the imaginary part of the energy, related to the lifetime in the usual way (\hbar is Planck's constant divided by 2π)

$$\varepsilon_k = \frac{\Gamma_k}{2} = \frac{\hbar}{2\tau_k}. \quad (16)$$

The tilde over the two matrix indicates the extended complex biorthogonal representation according to the analyticity requirements [4,9] given by the resonance formulation.

To appreciate the formulas (14) and (15) we remind the reader of the transformation quoted in Appendix A, see also Ref. [10], i.e., which has

the surprising property below, i.e.

$$\mathbf{Q} = \mathbf{B}^{-1} \mathbf{J} \mathbf{B}. \quad (17)$$

In equation (17) the unitary matrix \mathbf{B} connects the standard Jordan form \mathbf{J}

$$\mathbf{J} = \begin{pmatrix} 0 & 1 & 0 & \cdot & 0 \\ 0 & 0 & 1 & \cdot & \cdot \\ \cdot & \cdot & \cdot & \cdot & 0 \\ \cdot & \cdot & \cdot & \cdot & 1 \\ 0 & \cdot & \cdot & \cdot & 0 \end{pmatrix} \quad (18)$$

with the symmetric representation \mathbf{Q} defined by

$$\mathbf{Q}_{kl} = \left(\delta_{kl} - \frac{1}{m} \right) e^{i \frac{\pi}{m} (k+l-2)}; \quad k, l = 1, 2, \dots, m. \quad (19)$$

Hence, if we can find a relationship between ϵ_k, β with the dimension $r = m$, so that the transformed density operator in equation (15) assumes a Jordan block form (i.e., proportional to \mathbf{Q} or \mathbf{J}), one of the consequences for the related dynamics is the emergence of a dramatically increased lifetime [11]. Matching the thermal and quantum correlations appropriately, i.e.

$$\beta \epsilon_l = 2\pi \frac{l}{r}; \quad l = 1, 2, \dots, r \quad (20)$$

we find that the thermalized density matrix in equation (15) becomes proportional to \mathbf{Q} . A similar analysis with $m = 2$ was obtained for $I_L^{(2)}$. Using equations (10), (11) and (20) one finds that the longest relaxation time τ_{rel} , obtained for $l = 1$, compatible with the smallest dimension or ‘size’ r_{min} is given by

$$\beta \epsilon_l = \frac{\hbar}{2kT \tau_{\text{rel}}} = \frac{2\pi}{r_{\text{min}}}. \quad (21)$$

Thus, the sought after relation between the absolute temperature, the relaxation time and the ‘minimal size’ of our dissipative system is

$$\hbar \tau_{\text{rel}}^{-1} = \frac{4\pi kT}{r_{\text{min}}} \quad (22)$$

where the relaxation time is given by

$$\tau_{\text{rel}} = r_{\text{min}} \tau_{\text{lim}}; \quad \tau_{\text{lim}} = \frac{\hbar}{4\pi kT}. \quad (23)$$

Note that τ_{lim} is the shortest time commensurate with the uncertainty relation.

The relevance of the \mathbf{f} -basis is now clear. It appears through equation (17) and the unitarity property of \mathbf{B} , noting that equations (15) and (20) connects $\Gamma^{(2)}$ with

$$\hat{\mathbf{J}} = |\mathbf{h}\rangle \mathbf{Q} \langle \mathbf{h}| = |\mathbf{h}\rangle \mathbf{B}^{-1} \mathbf{J} \mathbf{B} \langle \mathbf{h}| = |\mathbf{f}\rangle \mathbf{J} \langle \mathbf{f}| = \sum_{k=1}^{r-1} |f_k\rangle \langle f_{k+1}|. \quad (24)$$

The vectors of \mathbf{B}^\dagger express \mathbf{f} in the original basis \mathbf{h} , see Appendix A, while producing the natural basis for the thermalized density matrix. Thus, a quantum system with ODLRO emerging through a dominant macroscopic eigenvalue in the appropriately reduced density matrix may decay through characteristic lifetimes τ . Conversely ordered structures may emerge from the transition from equilibrium to a non-equilibrium situation through constructive thermal fluctuations. This has unexpected consequences for the evolution.

It follows that the operator $\hat{T} = \hat{J}/\tau$ generates the evolution

$$e^{-i\frac{\hat{T}}{\tau}} = \sum_{k=0}^{m-1} \left(\frac{-i\hat{T}}{\tau} \right)^k \frac{1}{k!} \hat{J}^k. \quad (25)$$

Remember that the expression above should be multiplied with $e^{-\frac{t}{\tau}}$ to obtain the full evolution. This leads to the general decay rule, i.e., that the time dependent probability $N(t)$ for finding our system at time t in its initial configuration ordinarily given by

$$dN = -\frac{1}{\tau} N(t) dt \quad (26)$$

becomes modified to, assigning the highest power in the polynomial to $m = r$,

$$N(t) \propto t^{r-1} e^{-\frac{t}{\tau}} \quad (27)$$

and

$$dN = t^{r-2} \left(r - 1 - \frac{t}{\tau} \right) N(t) dt. \quad (28)$$

While we obtain $dN(t) < 0$ for all times in equation (23), the law deduced in equations (24) and (25) yields

$$dN(t) > 0; \quad t < (r - 1)\tau. \quad (29)$$

Hence, instead of the usual disintegration law for the initial state, we find that equation (27) leads to increasing organization during a finite number of lifetimes τ . It is in this context that we can speak of self-organization at the microscopic level.

We have here been very careful to refer to precise constructions and theorems in density matrix theory and resonance formation. It is clear, however, that the present development can be generalized to other more general processes in non-equilibrium quantum statistics, where the two natural basis partners \mathbf{g} and \mathbf{f} refer to density matrices and/or transition matrices [11].

The theory above has been applied to a variety of realistic situations. The range includes ionic conductance in aqueous solutions and molten alkali chlorides, damped spin-wave behaviour in paramagnetic systems, stimulated emission of radiation in masers, the fractional quantum Hall effect and quantum correlations in high- T_c cuprates and other non-BCS superconductors [7,9,11,12].

4. CONCLUSIONS

The subject of the conference referred to initially concerned basic problems of irreversibility and time asymmetry in quantum mechanics. This topic has been an important issue in the history of quantum mechanics, see Ref. [18] for some recent discussions. The Prigogine or Brussels-Austin School, in particular, is well known for its fundamental presentation of the two conflicting views of nature, on one hand the deterministic time reversible exposition and on the other the evolutionary irreversible character of the universe. These considerations prompt the notion of complexity or complex system calling for novel perspectives.

We have confronted the question asked above, first by advocating an embedding of irreversible formulations and standard quantum mechanics into a vaster picture and then by including general Jordan canonical forms explicitly into the formulation. In this setting it becomes natural to ask the question, whether these degenerate blocks of Segrè characteristic larger than one, actually plays a role in the evolution of a quantum complex system. We have looked at two particular problems, i.e., one at the fundamental Hamiltonian level and another one at the Liouvillian mesoscopic level.

It appears natural to map the actual dynamics onto the appropriate processes studied. In both cases one can let the model guide the description towards further explanations and a more fundamental knowledge. Whether the present cases will require a necessary adoption of Jordan blocks in connection with the general interpretation of dynamical processes in Nature remains to be seen. Nevertheless, there are apparent indications, as considered here, that motivates further studies and analysis.

It is evident that self-organization and the emergence of dissipative structures on a Liouvillian meso-macroscopic level seem to support the use of general Jordan forms. At the same time, on the microscopic domain, we have pointed out the possibility to model (i) particle–antiparticle pairs *via*

Jordan blocks and (ii) kaon pairs *via* two coupled Jordan blocks, generated by the ‘CP-violating interaction’. If these models carry some actuality in becoming accepted exemplars to arrive at fundamental irreversible formulations of time asymmetric quantum mechanics, then it is our duty to investigate them further. One would then need suitable means and devices to ‘communicate’ properly with the system, bringing out the essential properties and necessary consequences as well as predicting additional features and associated behaviour.

The application of a new technology at the quantum mechanical level is intrinsically different from traditional practice. Here, the applications are based on non-classical mechanisms. In time asymmetric quantum mechanics one might hence consider supplementary mechanisms based on general properties of correlations and fluctuations in systems far from equilibrium, e.g. in biological systems. Here, one needs to know how to interpret the ghost-like dimensions of the new formulation, where, in addition to the ordinary eigenfunctions, the higher order vectors and their associated degrees of freedom provide a hidden source for new dynamical properties. If this understanding occurs we should be able to extend our answerability to the question posed in the title affirmatively as yes!

ACKNOWLEDGEMENTS

This article is dedicated to Osvaldo Goscinski in honor of his 65th birthday. I am in great debt to him for a very close, for me important, collaboration initially and for later wisdom and guidance, both when we agreed and perhaps more significantly when we did not.

APPENDIX A. PROPERTIES OF REDUCED DENSITY MATRICES

We will review here some definitions and properties of reduced density matrices for fermionic systems. The focus will be on the general density operator ρ and the corresponding Liouville equation

$$i \frac{\partial \rho}{\partial t} = \hat{L} \rho \quad (\text{A1})$$

The historic development has been accounted for in many reviews (see Refs. [9,13]). Important theorems regarding fermionic behaviour was developed by Yang [14], Coleman [15] and Sasaki [16], for a recent review on reduced density matrices and the famous N -representability problem, see Ref. [17].

The N particle (and its p -reduced companions) representable density matrix $\Gamma^{(p)}$ can be defined as follows

$$\begin{aligned} & \Gamma^{(p)}(x_1 \cdots x_p | x'_1 \cdots x'_p) \\ &= \binom{N}{p} \int \Psi^*(x_1 \cdots x_p, x_{p+1} \cdots x_N) \Psi(x'_1 \cdots x'_p, x_{p+1} \cdots x_N) dx_{p+1} \cdots dx_N. \end{aligned} \quad (\text{A2})$$

where the (normalized) wave function $\Psi(x_1 \cdots x_N)$ represents a many-body quantum mechanical system. We will focus on $p=2$.

Note that the definition (A2) normalizes $\rho = \Gamma^{(p)}$ to the number of pairings of N fermions [13]. Other normalizations [14,15] also exists, i.e.

$$\begin{aligned} \text{Löwdin: } & \Gamma^{(p)}; \text{Tr}\{\Gamma^{(p)}\} = \binom{N}{p} \\ \text{Coleman: } & D^{(p)}; \text{Tr}\{D^{(p)}\} = 1 \\ \text{Yang: } & \rho^{(p)}; \text{Tr}\{\rho^{(p)}\} = p! \binom{N}{p}. \end{aligned} \quad (\text{A3})$$

In quantum chemistry the Löwdin normalization appears natural, but other choices are often made depending on the circumstances.

The fundamental concept of ODLRO was introduced by Yang [14] in connection with his celebrated proof of the largest bound for $\Gamma^{(2)}$. He also proved that the manifestation of a macroscopically large eigenvalue $\lambda_L^{(2)}$ in the reduced density matrix led to a new physical order. The emergence of ODLRO through a large macroscopic eigenvalue, e.g. $\lambda_L^{(2)} = N/2$, in the Löwdin normalization, has many interesting consequences, see more below. In the Yang and Coleman normalizations $\lambda_L^{(2)} = N$ and $\lambda_L^{(2)} = 1/N - 1$, respectively.

Although the concept of an extreme state, Coleman [15], is well known in quantum chemistry, it is not fully acknowledged in physics. In condensed matter physics the custom is often to proceed directly to the thermodynamic limit. Nevertheless, ODLRO is of central importance in super-conductivity/fluidity and it will also play a central role here. In connection with this development Coleman [15] identified the precise condition for the so-called extreme state which in certain cases could develop ODLRO.

We start by employing a set of m localized pair functions $\mathbf{h} = (h_1, h_2, \dots, h_m)$ also called geminals, obtained from appropriate pairings of one particle basis spin functions.

Constructing the transformations, the motivation to be given below we obtain

$$\mathbf{B} = \frac{1}{\sqrt{m}} \begin{pmatrix} 1 & \omega & \omega^2 & \cdot & \omega^{m-1} \\ 1 & \omega^3 & \omega^6 & \cdot & \omega^{3(m-1)} \\ \cdot & \cdot & \cdot & \cdot & \cdot \\ \cdot & \cdot & \cdot & \cdot & \cdot \\ 1 & \omega^{2m-1} & \omega^{2(2m-1)} & \cdot & \omega^{(m-1)(2m-1)} \end{pmatrix}; \quad \omega = e^{\frac{i\pi}{m}} \quad (\text{A4})$$

by introducing a coherent and a correlated basis \mathbf{g} and \mathbf{f} , respectively, through

$$|\mathbf{h}\rangle\mathbf{B} = |\mathbf{g}\rangle = |g_1, g_2, \dots, g_m\rangle, \quad |\mathbf{h}\rangle\mathbf{B}^{-1} = |\mathbf{f}\rangle = |f_1, f_2, \dots, f_m\rangle. \quad (\text{A5})$$

We note that the functions in \mathbf{g} are completely delocalized over the region of sites defined by the localized (may be chosen real) basis \mathbf{h} . The \mathbf{f} -basis contains all possible phase shifted contributions from each site in accordance with equation (A5).

Some interconnections can be mentioned here. The first concerns Coleman's so-called extreme state. If \mathbf{h} is the set of two particle determinants and the wave function is constructed from an antisymmetric geminal power, based on g_1 , then the reduced density matrix can be expressed as

$$\Gamma^{(2)} = \Gamma_L^{(2)} + \Gamma_S^{(2)} = \lambda_L |g_1\rangle\langle g_1| + \lambda_S \sum_{k=2}^m |g_k\rangle\langle g_k| \quad (\text{A6})$$

For the exact condition for the extreme state of the two-particle reduced density matrix including the 'tail contribution' resulting from remaining pair configurations, see Ref. [15]. The eigenvalues in equation (A6) may exhibit the (possibly) large eigenvalue λ_L and the degenerate small one λ_S given by

$$\lambda_L = \frac{N}{2} - (m-1)\lambda_S; \quad \lambda_S = \frac{N(N-2)}{4m(m-1)} \quad (\text{A7})$$

Since we have m basis pair functions or geminals and $2m$ spin orbitals, the number of fermion pairings and pair configurations are

$$\binom{N}{2}; \quad \binom{2m}{2},$$

respectively. The dimension of the 'box contribution' defined in equation (A6) is m and consequently the dimension of the missing 'tail contribution' is $2m(m-1)$.

One can prove that the eigenvalue associated with the missing 'tail' is the same as λ_S [15]. For the extreme state one may obtain the large eigenvalue

λ_L and the $(m-1)(2m+1)$ degenerate eigenvalue λ_S . Under specific circumstances one may find that λ_L grows to macroscopic size, i.e., approach $N/2$ (in the Löwdin normalization) developing Yang's ODLRO. Rather than focusing on this transition we will instead consider the precursor level of the extreme state and the importance played by the basis \mathbf{g} .

As pointed out analogous equations can be derived in a statistical framework both for the case of localized fermions in a specific pairing mode and/or bosons subject to a quantum transport environment [7]. The second interconnection regarding the relevance of the basis \mathbf{f} is related to the fact that the transformation (A4) connects the Jordan block (18) to a convenient complex symmetric form. This was explicitly demonstrated in Section 3.

REFERENCES

- [1] A. Bohm, M. Gadella, M. Loewe, S. Maxson, P. Patuleanu and C. Puntmann, Gamow–Jordan vectors and nonreducible density operators from higher order S-matrix poles, *J. Math. Phys.*, 1997, **38**, 1.
- [2] E. Brändas, Resonances and dilatation analyticity in Liouville space, *Adv. Chem. Phys.*, 1997, **99**, 211.
- [3] P. O. Löwdin, *Linear Algebra for Quantum Theory*, Wiley, New York, 1998.
- [4] (a) E. Balslev and J. M. Combes, *Commun. Math. Phys.*, 1971, **22**, 280; (b) C. van Winter, *J. Math. Anal.*, 1974, **47**, 633.
- [5] A. Bohm and M. Gadella, *Dirac Kets, Gamow Vectors and Gel'fand Triplets*, Springer, Berlin, 1989.
- [6] E. Brändas and C. A. Chatzidimitriou-Dreismann, *Resonances*, Lecture Notes in Physics, 1989, Vol. 325, p. 486.
- [7] E. Brändas and C. A. Chatzidimitriou-Dreismann, *Int. J. Quant. Chem.*, 1991, **40**, 649.
- [8] H. Saller and W. Blum, *On the relation between time representations and inner product spaces*, Proceedings from the Jaca Workshop on Rigged Hilbert Spaces and Time Asymmetric Quantum Theory (eds A. Bohm, M. Gadella and P. Kielanowski), *Int. J. Theor. Phys.*, 2003, **42**, 2191.
- [9] E. Brändas, Dissipative systems and microscopic selforganization, *Adv. Quant. Chem.*, 2002, **41**, 121.
- [10] C. E. Reid and E. J. Brändas, Lecture Notes in Physics, 1989, Vol. 325, p. 475.
- [11] E. Brändas, in *Dynamics During Spectroscopic Transitions* (eds E. Lippert and J. D. Macomber), Springer, Berlin, 1995, p. 148.
- [12] E. J. Brändas, *Ber. Bunsen-Ges. Phys. Chem.*, 1992, **96**, 49.
- [13] (a) K. Husimi, *Proc. Phys. Math. Soc. Jpn*, 1940, **22**, 264; (b) See also P. O. Löwdin, *Phys. Rev.*, 1955, **97**, 1474; (c) P. O. Löwdin, *Phys. Rev.*, 1955, **97**, 1490; (d) P. O. Löwdin, *Phys. Rev.*, 1955, **97**, 1509.
- [14] C. N. Yang, *Rev. Mod. Phys.*, 1962, **34**, 694.
- [15] A. J. Coleman, *Rev. Mod. Phys.*, 1963, **35**, 668.
- [16] (a) F. Sasaki, *Uppsala Quantum Chemistry Group, Technical Report 77*, 1962; (b) F. Sasaki, *Phys. Rev.*, 1965, **138B**, 1338.
- [17] A. J. Coleman and V. I. Yukalov, *Reduced Density Matrices Coulson's Challenge*, Lecture Notes in Chemistry 72, Springer, Berlin, 2000.
- [18] I. Prigogine and I. Antoniou, *Science, Evolution and Complexity. Genetics in Europe Open days 2000 (GEOD 2000)*, Sommet européen, Bruxelles, November 16, 2000, 21–36, 2001.

Antisymmetrized Geminal Power Coherent States

Brian Weiner

Department of Physics, Pennsylvania State University, DuBois, PA 15801, USA

Abstract

A detailed analysis of electronic coherent states associated with the one-particle unitary group is presented in terms of coset generators of this group. For even number of electrons these states form non-linear manifolds of antisymmetrized geminal powers (AGPs) that are parameterized by complex coordinates. Different classes of manifolds of AGP states are associated with distinct coset decompositions and produce different restrictions of the time-dependent Schrödinger equation.

Contents

1. Introduction	107
2. Lie algebras	111
3. One-particle groups	112
4. Coherent states	115
4.1. Definition and construction	115
4.2. AGP coherent states	116
4.3. Coset factorization for $U(2s)$	116
4.4. $SU(2)^S$ factors	117
4.5. $USp(\omega_j)$ factors	120
4.6. $SU(2\xi)$ factors	121
4.7. $U(\mathcal{H}^N)/U(1)$ -coherent states	122
5. Summary and discussion	124
Appendix A. AGP states	125
References	126

1. INTRODUCTION

Isolated molecular systems do not interact with their environment and are thus unobservable. In order to have a physical effect and be observed they must respond to external probes, such as electromagnetic fields, and form a composite interacting system whose evolution is described by a joint Hamiltonian. An example of this is the effect of radiation on a molecular

subsystem, which can be monitored by changes in the molecule density and reduced density matrices. If the radiation is weak the behavior of the interaction is well described by the linear response of the molecular system to the radiation, i.e., is linearly proportional to the radiation strength, while if the radiation is intense the molecular system responds in a non-linear way. The interaction of the electromagnetic field with molecules can be approximated in a standard semi-classical fashion by averaging over the photonic degrees of freedom to produce effective one-electron observables. This leads to a reduced Hamiltonian for the molecular subsystem that includes perturbing effective time-dependent one-body potentials, which describe the interaction with the radiation field. In the case of weak intensity radiation, where the linear response regime is sufficient to describe the changes in the molecular system, one needs to only consider responses that are first order in these observables.

The temporal behavior of a state of physical system is completely described by the evolution of its full density matrix, which in turn determines the evolution of all of its reduced density matrices. These variations are conveniently expressed in terms of various propagators, which thus provide a comprehensive formulation of the response of the molecular subsystem to external probes. As is well known exact solutions for quantum evolutions have only been determined for simple model systems, and are not known for multi-electron molecular systems that involve coulombic interactions between electrons. Thus for practical applications the goal is to develop systematic, cost effective, theoretically well-founded and non-arbitrary approximation schemes, that are accurate enough to explain experimental results. A major focus of the illustrious career of professor Osvaldo Goscinski has been the analysis and construction of approximate propagators that fulfill these objectives. In particular the one-electron and polarization propagators, where he effectively used the properties of super operators acting on operator manifolds associated with a given reference state to generate various orders of approximation [1–7]. In this article I will concentrate, for illustrative purposes, on the polarization propagator for a molecular system with a fixed even number of electrons at a fixed geometry. This propagator describes the linear response of the first-order reduced density matrix (FORDM) to electromagnetic radiation.

The polarization propagator is a Hermitian matrix of time-dependent response functions of the matrix elements of the FORDM. If one takes the Laplace transform of this propagator and expresses the resulting matrix in diagonal form, in terms of normal mode operators, one can clearly observe that the poles of this propagator are excitation energies and the associated residues the transition probabilities for excitations generated by one-particle operators between stationary states, $\{|\Psi_k\rangle\}$, of the molecular system. If the initial molecular reference state is stationary (usually the ground state, but not necessarily so) then the poles are the excitation energies and the residues

the transition probabilities from that state. If the transition probability is 100% for a given one-particle operator then this operator produces an excited state from the initial stationary state and is called a state excitation operator. If such an operator produces the excited state $|\Psi_k\rangle$, then its effect on the reference state $\{|\Psi_0\rangle\}$ is the same as the N -particle bra-ket operator $|\Psi_k\rangle\langle\Psi_0|$.

Approximations to the polarization propagator are often based on the following criteria:

- all one-particle operators that diagonalize the propagator matrix are state excitation operators,
- their adjoints annihilate the reference state,
- the reference state is stationary with respect to at least one-particle variations.

If an approximation satisfies these conditions one says that it is a consistent approximation, however, in general, usually one or more of these conditions are not satisfied and the approximation is inconsistent. Some approximations can even lead to propagators that do not correspond to a valid N -particle reference state and thus are not even N -representable.

An important point of note is that it is not necessary that the normal mode one-particle operators actually produce excited states from the reference state, in fact, in the exact case they generally do not. Hence, there is thus some level of ambiguity about polarization propagator approximations, if one is trying to obtain an approximation to a one-particle linear response function, then the annihilation condition is not necessary, though stationarity and N -representability are desirable, while if one is asserting that the polarization propagator is a one-particle approximation to the full N -particle propagator and is used to produce excited states, as well as excitation energies and transition probabilities, then the annihilation condition is necessary for consistency.

In the late 1970s it was found [5,6,8–10] that an antisymmetrized geminal power (AGP) [11] state was the most general $2M$ -electron state that was annihilated by a maximal set of one-electron operators, (for odd number of electrons generalized AGP (GAGP) states [12] are needed but their properties can be derived from AGP states). The $2M$ -electron AGP $|g^M\rangle$ state is an antisymmetrized product of M two-particle geminals

$$|g\rangle = \sum_{1 \leq j < k \leq s} g_{jk} |\varphi_j \varphi_k\rangle, \quad (1)$$

where $\{g_{ij}\}$ are complex coefficients and $\{|\varphi_j\rangle | 1 \leq j \leq r = 2s\}$ is an orthonormal basis for the one-particle Hilbert space \mathcal{H}^1 . However, even when the reference state was an energy optimized AGP state the polarization

propagator approximation failed to be consistent, in that the adjoints of the normal mode excitation operators did not annihilate the reference state, although the numerical results obtained from the application of this approximation scheme agreed well with experimental values of excitation energies and dipole induced transition probabilities, i.e., oscillator strengths, for example, [13–25].

It turns out that the annihilation condition can be naturally expressed in terms of group coherent states (CS) [26–28], where the reference state corresponds to a lowest or highest weight state associated with a representation of the group. The basic ingredients needed for the construction of a family of group CSs in a vector space is the existence of an irreducible representation of a group and a one-dimensional representation of a subgroup. The subgroup is called the isotropy or invariance group of the CSs and the family of CSs is generated by the action of the coset, formed by factoring the group with respect to this subgroup, on the reference state. In the study of electronic systems it is natural to consider the real, compact [29], Lie group $U(r)$ of unitary transformations of the one-electron state space \mathcal{H}^1 (of dimension $r = 2s$), that has irreducible representations on all N -electron state spaces \mathcal{H}^N . The family of CSs in this case are non-linear manifolds, \mathcal{M} , of the N -electron Hilbert space, \mathcal{H}^N , generated by cosets formed by one-particle operators.

One can construct approximate propagators based on stationary states of the restriction of the time-dependent Schrödinger equation (TDSE) to these manifolds. Solutions to such restrictions of the TDSE are obtained by using the time-dependent variational principle (TDVP) [30] or equivalently the stationary phase approximation (SPA) [31] to the path integral expressed in terms of paths on this CS manifold. The resulting equations of motion (EOM) are those of a generalized *classical* system described by a curved phase space, a consequence of the fact that a family of group CSs forms a differentiable manifold [32] whose tangent spaces have an intrinsic symplectic structure [29]. Approximate stationary states of the molecular system then correspond to the special stationary phase ‘paths’ that are critical points of the corresponding classical Hamiltonian. The linear response of these approximate stationary states to external perturbing fields then involves the generators of the Lie algebra of the group, and hence describes the response of the reduced density matrix formed by these operators. Thus the response of the FORDM is determined by generators of one-particle groups.

In this article we will describe how different coset decompositions of the one-particle unitary group $U(2s)$ correspond to different CS manifolds of AGP states and how these manifolds can be parameterized by the coordinates of the subspaces of the direct sum Lie algebra expansions adapted to these coset decompositions. These CS manifolds form generalized curved phase spaces in which classical EOM approximating the TDSE can be formulated,

leading to a classical linear response theory of time-dependent perturbations that extends and clarifies certain aspects of the quantum random phase approximation (RPA) and propagator approximations. However, due to space limitations these considerations will be developed in future manuscripts.

In Section 2 we discuss the Lie algebra structure of Fermi–Fock space, which is the direct sum of all of the state spaces $\{\mathcal{H}^N\}$, in Section 3 we will describe the possible decompositions of the Lie algebra $u(2s)$ of $U(2s)$, the one-particle group associated with \mathcal{H}^1 , and thus the factorizations of $U(2s)$ that lead to manifolds of CSs in \mathcal{H}^N that can be based on $U(2s)$. In Section 4 we study in detail the forms of AGP CSs. We also show how the CS construction applied to the unitary group of N -electron space can reproduce the familiar configurational interaction expansion. We conclude with a summary and discussion in Section 5.

2. LIE ALGEBRAS

The most convenient representation of the generators of the Lie algebra of $U(2s)$ for fermionic quantum mechanics is by second quantized operators acting in Fermi–Fock space, \mathcal{H}_F , which is defined to be the direct sum

$$\mathcal{H}_F = \bigoplus_{0 \leq N \leq r} \mathcal{H}^N, \quad (2)$$

where

$$\mathcal{H}^N = \wedge^N \mathcal{H}^1 \quad (3)$$

is the N -fold antisymmetric tensor product of the one-particle state space \mathcal{H}^1 , a space generated by an orthonormal basis of one-particle functions of position and spin

$$\{\varphi_j | 1 \leq j \leq r\}. \quad (4)$$

The Banach space [29] of bounded operators acting in \mathcal{H}_F is denoted $\mathcal{B}(\mathcal{H}_F)$, and is spanned by a second quantized operator basis

$$\begin{aligned} &\{a_{j_1}^\dagger \cdots a_{j_p}^\dagger a_{k_q} \cdots a_{k_1} | 1 \leq j_1 < \cdots < j_p \leq r; \\ &1 \leq k_1 < \cdots < k_p \leq r; 1 \leq p, q \leq r\}, \end{aligned} \quad (5)$$

where the second quantized operators $\{a_j^\dagger, a_j\}$ act on the zero-particle vacuum $|\phi\rangle$ in the following fashion:

$$a_j |\phi\rangle = 0, \quad a_j^\dagger |\phi\rangle = |\varphi_j\rangle, \quad (6)$$

and satisfy the canonical anti-commutation relationships (CAR)

$$[a_j^\dagger, a_k]_+ = \delta_{jk} I. \quad (7)$$

The operator space $\mathcal{B}(\mathcal{H}_F)$ contains realizations of many classical Lie groups, Lie algebras and universal enveloping algebras [29]. In particular the generators

$$\{a_j^\dagger, a_k, a_j^\dagger a_k - \frac{1}{2} \delta_{jk} I, a_j^\dagger a_k^\dagger, a_j a_k; 1 \leq j \leq k \leq r\} \quad (8)$$

satisfy the commutation relationships of the Lie algebra $\mathfrak{so}(2r+1, \mathbb{R})$, (see Ref. [28], for example, for the definitions of classical Lie groups and algebras), and generate a representation of the universal enveloping algebra $\mathfrak{so}(2r+1, \mathbb{R})$ in $\mathcal{B}(\mathcal{H}_F)$, which is in fact all of $\mathcal{B}(\mathcal{H}_F)$. The subset of these generators

$$\{a_j^\dagger a_k - \frac{1}{2} \delta_{jk} I, a_j^\dagger a_k^\dagger, a_j a_k; 1 \leq j \leq k \leq r\} \quad (9)$$

satisfy the commutation relationships of the Lie algebra of $\mathfrak{so}(2r, \mathbb{R})$ and generate a representation of the universal enveloping algebra of $\mathfrak{so}(2r, \mathbb{R})$ in $\mathcal{B}(\mathcal{H}_F)$. The subset of these generators

$$\{a_j^\dagger a_k - \frac{1}{2} \delta_{jk} I; 1 \leq j \leq k \leq r\} \quad (10)$$

satisfy the commutation relationships of the Lie algebra $u(r)$ and generate a representation of the universal enveloping algebra of $u(r)$ in $\mathcal{B}(\mathcal{H}_F)$.

The representation of $\mathfrak{so}(2r+1, \mathbb{R})$ is irreducible, while the representations of $\mathfrak{so}(2r, \mathbb{R})$ and $u(r)$ are reducible. The irreducible representations of $\mathfrak{so}(2r, \mathbb{R})$ are obtained by restricting to the subspace of even or odd number states in \mathcal{H}_F , while the irreducible representations of $u(r)$ are obtained by restricting to subspaces of states of fixed integer particle number.

3. ONE-PARTICLE GROUPS

In this section we describe the possible direct sum decompositions of the Lie algebra, $u(2s)$, of the group $U(2s)$ of unitary transformations of one-particle state space, \mathcal{H}^1 of dimension $2s$, which lead in a canonical fashion to families of CSs in N -particle state space \mathcal{H}^N . These decompositions are based on the subgroup of special orthogonal transformations. $\mathfrak{SO}(2s, \mathbb{R})$, of a real $2s$ -dimensional Hilbert space, the subgroups $U(N) \times U(2s-N)$, formed by products of unitary transformations of complex N and $(2s-N)$ -dimensional Hilbert spaces and the subgroup, $\mathfrak{USp}(2s)$, of transformations of a complex $2s$ -dimensional Hilbert space, that are simultaneously unitary and symplectic. This latter subgroup is isomorphic to the group of unitary transformations, $U(s, \mathbb{Q})$ of a s -dimensional quaternionic Hilbert space. We signify

the CSs that they induce as G/K -CSs, where, for example, $G = U(2s)$ and the subgroup $K \in \{\text{SO}(2s, \mathbb{R}), U(N) \times U(2s - N), \text{USp}(2s)\}$.

The Lie algebra $u(2s)$ has three direct sum Cartan decompositions [29] which are in terms of the Lie algebras, $\text{so}(2s, \mathbb{R})$, $[u(N) \oplus u(2s - N)]$, and $\text{usp}(2s)$, of its maximal compact [29] subgroups $\text{SO}(2s, \mathbb{R})$, $[U(N) \times U(2s - N)]$, and $\text{USp}(2s)$, respectively, (see Ref. [28] for the definitions of these groups). These decompositions are

$$u(2s) = \text{so}(2s, \mathbb{R}) \oplus \text{so}(2s, \mathbb{R})^\perp, \quad (11a)$$

$$u(2s) = [u(N) \oplus u(2s - N)] \oplus [u(N) \oplus u(2s - N)]^\perp; \quad 0 \leq N \leq 2s, \quad (11b)$$

$$u(2s) = \text{usp}(2s) \oplus \text{usp}(2s)^\perp, \quad (11c)$$

where the orthogonality is with respect to the Killing form inner product [29] of $u(2s)$. The decomposition equations (11a)–(11c) define the following distinct coset decompositions of $U(2s)$

$$U(2s)/U(N) \times U(2s - N); \quad 0 \leq N \leq 2s, \quad (12a)$$

$$U(2s)/\text{USp}(2s), \quad (12b)$$

$$U(2s)/\text{SO}(2s, \mathbb{R}), \quad (12c)$$

and thus three classes of families of CSs (see Section 4).

The motivation of using *maximal* compact subgroups in equations (12a)–(12c) is to produce coset spaces that are irreducible Riemannian manifolds [32] (a Riemannian manifold has tangent spaces that are inner product spaces), i.e., they cannot be factored into a Riemannian product of smaller Manifolds. This technical feature, although important in the classification of Riemannian Manifolds, is too restrictive when considering manifolds of CSs, where we also need to examine decompositions generated by subgroups of these maximal compact groups. We thus enlarge the designation G/K -CS to include subgroups of K .

In order for any of the subgroups

$$\{\text{SO}(2s, \mathbb{R}), \{U(N) \times U(2s - N) | 0 \leq N \leq 2s\}, \text{USp}(2s)\}, \quad (13)$$

or their subgroups, to be isotropy groups of a given N -electron state, the state must carry a one-dimensional unitary representation of that subgroup and not of any larger subgroup containing that subgroup.

There are *no* states in \mathcal{H}^N that produce a one-dimensional representation of $\text{SO}(2s, \mathbb{R})$ and we conjecture that there are *no* subgroups of $\text{SO}(2s, \mathbb{R})$, which *are not* subgroups of $U(N) \times U(2s - N)$ or $\text{USp}(2s)$, that produce one-dimensional representations on \mathcal{H}^N . Thus there are *no* CS manifolds in \mathcal{H}^N based on subgroups of $\text{SO}(2s, \mathbb{R})$ that cannot be described in terms of $U(N) \times U(2s - N)$ or $\text{USp}(2s)$ CSs.

The only subgroup from the set $\{U(N) \times U(2s - N) \mid 0 \leq N \leq 2s\}$ that produces a one-dimensional representation in \mathcal{H}^N is $U(N) \times U(2s - N)$. These $U(2s)/U(N) \times U(2s - N)$ -CSs give the well known Thouless parameterization [33] of the manifold of independent particle states (IPS) and lead to the standard RPA for the linear response function. The subgroup $U(N) \times U(2s - N)$ is actually a subgroup of $\text{USp}(2s)$ and we display in Section 4 that $U(2s)/[U(N) \times U(2s - N)]$ -CSs can in fact be described in terms of the class of $U(2s)/\text{USp}(2s)$ -CSs.

We show by construction in Section 4 that the group $\text{USp}(2s)$ and its subgroups do have one-dimensional representations in $\mathcal{H}^N = \mathcal{H}^{2M}$ and one can form

$$U(2s)/K\text{-coherent states,} \quad \text{where } \text{USp}(2s) \supseteq K, \quad (14)$$

which are manifolds of general AGP states (see Appendix A). All manifolds of CSs in \mathcal{H}^{2M} based on $U(2s)$ can be expressed in terms of the cosets appearing in equation (14), which have the form

$$U(2s)/[\text{USp}(2\omega_1) \times \cdots \times \text{USp}(2\omega_p) \times \text{SU}(2)^\sigma \times \text{SU}(2\xi)], \quad (15)$$

where

$$\text{SU}(2)^\sigma = \overbrace{\text{SU}(2) \times \cdots \times \text{SU}(2)}^{\sigma\text{-factors}}, \quad (16)$$

the index set $\{\sigma, \omega_1, \dots, \omega_p, \xi\}$ characterizes the type of AGP reference state and its elements satisfy

$$2\sigma + 2\omega + 2\xi = r = 2s, \quad \omega = \sum_{1 \leq j \leq p} \omega_j. \quad (17)$$

The index set $\{\sigma, \omega_1, \dots, \omega_p, \xi\}$ is determined by the array $\{c_j \mid 1 \leq j \leq s\}$ of canonical coefficients [34] of the geminal that determines the AGP state according to

- σ = number of non-zero, non-equal $\{c_j\}$ s
- ω_j = number of equal coefficients in the j th set
- ρ = number of sets of equal $\{c_j\}$ s
- ξ = number of zero coefficients.

We now consider a few particular examples. If all the coefficients are different and non-zero, so that $\xi = 0$, $\omega = 0$, $\rho = 0$, the isotropy subgroup is

$$\text{SU}(2)^s = \overbrace{\text{SU}(2) \times \cdots \times \text{SU}(2)}^{s\text{-factors}}, \quad (18)$$

which is the smallest one possible, leading to the biggest coset. In this case the action of coset on the reference AGP generates the manifold containing all AGP states.

If $\xi \neq 0$ the reference AGP is produced by a degenerate geminal and the action of the associated coset only produces a sub-manifold of AGP states, all of which correspond to geminals that have the same null space (see Appendix A) as the reference AGP.

If $\rho \neq 0$ then the geminal has some extreme components and again the coset only generates sub-manifold of AGP's from the reference.

If $\sigma = 0$, $\xi = 0$ and $\rho = s$ then the reference state is an extreme AGP (see Appendix A) and the action of the coset on the reference produces the manifold of *all* extreme AGP states.

All CS manifolds in \mathcal{H}^{2M} based on the one-particle group $U(2s)$ are families of AGP states, some of these manifolds are irreducible Riemannian manifolds and correspond to cosets formed by the maximal compact subgroups $U(2M) \times U(2s - 2M)$ and $USp(2s)$, while others are reducible and correspond to non-maximal compact subgroups $USp(2\omega_1) \times \cdots \times USp(2\omega_p) \times SU(2)^\sigma \times SU(2\xi)$. Each of these manifolds of CSs have certain basic physical properties, e.g., $U(2M) \times U(2s - 2M)$ invariant manifold describes uncorrelated IPSs, the $USp(2s)$ invariant manifold describes highly correlated extreme AGP states that are superconducting, while the $USp(2\omega_1) \times \cdots \times USp(2\omega_p) \times SU(2)^\sigma \times SU(2\xi)$ invariant manifold for general $\{\omega_1, \dots, \omega_p, \sigma, \xi\}$ describe intermediate types of correlation and linear response properties, see, for a particular example, Ref. [35], most of which have not been explored in any depth.

4. COHERENT STATES

4.1. Definition and construction

The CS construction is based on the Hilbert space of states \mathcal{H} that carries unitary irreducible representations $\mathcal{R}(G)$ of a compact group G on \mathcal{H} and a one-dimensional representation of a subgroup $K \subset G$. The groups G we consider are $U(\mathcal{H}^N)$ and $U(\mathcal{H}^1)$ the groups associated with N -electron state space and one-electron state space, respectively. In the finite-dimensional case these groups are the classical matrix groups and $U(\mathcal{H}^N) \equiv U(\binom{r}{N})$ and $U(\mathcal{H}^1) \equiv U(r)$, in general we will use the matrix notation even though in an exact treatment $r = \infty$ and one should be aware of possible infinite-dimensional pathologies. The irreducible representations we consider are $\mathcal{R}(U(\binom{r}{N}))$ and $\mathcal{R}(U(r))$ that are carried by \mathcal{H}^N , unless otherwise stated we will not distinguish between the groups G and K and their representations on \mathcal{H}^N .

A state $|\Phi\rangle \in \mathcal{H}^N$ is a reference state for a group G if there is an isotropy subgroup K , that is contained in G , that has one-dimensional representation on \mathcal{H}^N defined by

$$K = \{g \mid \mathcal{R}(g)|\Phi\rangle = e^{i\theta(g)}|\Phi\rangle; g \in G; \theta(g) \in \mathbb{R}\}. \quad (19)$$

If such isotropy groups exists G can be factored as

$$G = (G/K)K. \quad (20)$$

4.2. AGP coherent states

The group $U(2s)$ has subgroups that leave reference $2M$ -electron AGP states, $|g^N\rangle$ invariant up to an overall phase factor and thus satisfy equation (19). AGP states are given [34] by

$$|g^N\rangle = \sum_{1 \leq j_1 < j_2 < \dots < j_N \leq s} c_{j_1} \dots c_{j_N} |\eta_{j_1} \eta_{j_1+s} \dots \eta_{j_N} \eta_{j_N+s}\rangle, \quad (21)$$

where $\{|\eta_j\rangle | 1 \leq j \leq r\}$ is a complete orthonormal basis for \mathcal{H}^1 , $\{c_j | 1 \leq j \leq s\}$ are positive real numbers called the canonical coefficients of a two electron geminal $|g\rangle$ that has the canonical expansion

$$|g\rangle = \sum_{1 \leq j \leq s} c_j |\eta_j \eta_{j+s}\rangle. \quad (22)$$

The state $|g^N\rangle$ can also be expressed in terms of the coset $\text{SO}(2r, \mathbb{R})/\text{SU}(r)$ of the group $\text{SO}(2r, \mathbb{R})$ acting on the zero-particle vacuum state $|\phi\rangle$ of \mathcal{H}_F [36] as

$$|g^N\rangle = P_N \exp \left\{ \sum_{1 \leq j \leq s} c_j b_j^\dagger b_{j+s}^\dagger \right\} |\phi\rangle, \quad (23)$$

where P_N is the orthogonal projector onto \mathcal{H}^N and $\{b_j^\dagger | 1 \leq j \leq s\}$ are the creators for the one-particle states $\{|\eta_j\rangle | 1 \leq j \leq r\}$, i.e.,

$$b_j^\dagger |\phi\rangle = |\eta_j\rangle. \quad (24)$$

This form has been explored in some detail in Ref. [37]. However, we will not pursue this form of the AGP state further in this article.

4.3. Coset factorization for $U(2s)$

In general the action of $U(2s)$ on a reference AGP, $|g^N\rangle$, state produces a manifold, $\mathcal{M}(\sigma, \omega_1, \dots, \omega_p, \xi)$ of AGP states given by

$$\mathcal{M}(\sigma, \omega_1, \dots, \omega_p, \xi) = \{[U(2s)/K] \times K\} |g^N\rangle, \quad (25)$$

where

$$K = \text{USp}(2\omega_1) \times \cdots \times \text{USp}(2\omega_\rho) \times \text{SU}(2)^\sigma \times \text{SU}(2\xi), \quad (26)$$

and the geminal is of type $(\sigma, \omega_1, \dots, \omega_\rho, \xi)$. Each element of the manifold can be expressed as

$$|g(c)^N\rangle = ck_{\omega_1} \cdots k_{\omega_\rho} k_\sigma k_\xi |g^N\rangle = c|g^N\rangle, \quad (27)$$

where the isotropy subgroup is given by the products $k_{\omega_1} \cdots k_{\omega_\rho} k_\sigma k_\xi$, where

$$\begin{aligned} k_{\omega_j} &\in \text{USp}(2\omega_j), \quad 1 \leq j \leq \rho, & k_\sigma &\in \text{SU}(2)^\sigma, \\ k_\xi &\in \text{SU}(2\xi), c \in U(2s)/K. \end{aligned} \quad (28)$$

The most general AGP manifold is produced when $\sigma = s$, ($\Leftrightarrow (\rho = 0$ and $\xi = 0)$), so it is advantageous to first consider that case.

4.4. $\text{SU}(2)^s$ factors

The isotropy subgroup, K , for an AGP reference state that has non-equal and non-zero canonical coefficients $\{c_j | 1 \leq j \leq s\}$, i.e., $\sigma = s$ and $|g\rangle$ belongs to the class $\{s, 0, 0\}$, is the product group $\text{SU}(2)^s$, which produces the coset decomposition

$$U(2s) = [U(2s)/\text{SU}(2)^s] \times \text{SU}(2)^s. \quad (29)$$

One can express coset representatives in a factored form as the product $G_{+1}G_0G_{-1}$ [38], where $\{G_{+1}, G_0, G_{-1}\}$ are subgroups of the linear group $\text{GL}(2s, \mathbb{C})$, which is the complexification of $U(2s)$, and the group G_{-1} leaves the reference AGP state invariant (note that it is different to the real compact isotropy group). Restricting attention to the connected components of these subgroups, that contain the identity element, one can express this factorization in terms of Lie algebras as

$$U(2s) = e^{N_+} e^{N_0} e^{N_-} e^{\mathcal{K}}, \quad (30)$$

where

$$\mathcal{K} = \overbrace{\text{su}(2) \oplus \cdots \oplus \text{su}(2)}^{s\text{-subspaces}}, \quad (31)$$

$\{N_{+1}, N_0, N_{-1}\}$ are Lie subalgebras of $\text{gl}(2s, \mathbb{C})$, the Lie algebra of $\text{GL}(2s, \mathbb{C})$. The subalgebras $\{N_{-1}, \mathcal{K}\}$ annihilate $|g^N\rangle$, i.e.,

$$b|g^N\rangle = 0 \quad \forall b \in N_{-1} \oplus \mathcal{K}, \quad (32)$$

while the subalgebras $\{N_{+1}, N_0\}$ have the property

$$b|g^N\rangle \neq 0 \quad \forall b \in N_{+1} \oplus N_0. \quad (33)$$

Introducing coordinate systems as $\{\mathbf{z}_+, \lambda, \mathbf{z}_-, \eta\}$ with respect to fixed bases of $\{N_{+1}, N_0, N_{-1}, \mathcal{K}\}$, that depend on the reference AGP state, one can parameterize group elements $u \in U(2s)$ as

$$u(\tilde{\mathbf{z}}, \eta) = \tilde{c}(\tilde{\mathbf{z}})k(\eta) = c_{+1}(\mathbf{z}_+)c_0(\lambda)c_{-1}(\mathbf{z}_-)k(\eta), \quad (34)$$

where $\tilde{\mathbf{z}} \equiv (\mathbf{z}_+, \lambda, \mathbf{z}_-)$. The action of $U(2s)$ on the AGP state is

$$\begin{aligned} u(\tilde{\mathbf{z}}, \eta)|g^N\rangle &= \tilde{c}(\tilde{\mathbf{z}})k(\eta)|g^N\rangle = c_{+1}(\mathbf{z}_+)c_0(\lambda)c_{-1}(\mathbf{z}_-)k(\eta)|g^N\rangle \\ &= c_{+1}(\mathbf{z}_+)c_0(\lambda)|g^N\rangle, \end{aligned} \quad (35)$$

showing that the non-redundant coordinates $\mathbf{z} \equiv (\mathbf{z}_+, \lambda)$ describe a configuration space, that is a sub-manifold \mathcal{M} (in general non-linear) of \mathcal{H}^N with a coordinate system $\{\mathbf{z}\}$, that parameterize the set of $\{|\Phi(\mathbf{z})\rangle\}$ of $U(2s)/\text{SU}(2)^s$ -CSs

$$|\Phi(\mathbf{z})\rangle = c_{+1}(\mathbf{z}_+)c_0(\lambda)|g^N\rangle \equiv c(\mathbf{z})|g^N\rangle, \quad (36)$$

and at the same time represents the coset space $U(2s)/\text{SU}(2)^s$.

The AGP state dependent bases one chooses are

$$\begin{aligned} N_{+1} = \mathbb{C} - \text{linspan}\{ &c_j a_k^\dagger a_j - \sigma(j)\sigma(k)c_k a_{-j}^\dagger a_{-k}; \\ &-s \leq j < k \leq s, |j| \neq |k|; \sigma(j) = \text{sign}(j)\}, \end{aligned} \quad (37a)$$

$$\begin{aligned} N_0 = \mathbb{C} - \text{linspan}\{ &(a_j^\dagger a_j + a_{-j}^\dagger a_{-j}), (a_j^\dagger a_{-j} + a_{-j}^\dagger a_j), \\ &(a_j^\dagger a_j - a_{-j}^\dagger a_{-j}), i(a_j^\dagger a_{-j} - a_{-j}^\dagger a_j); 1 \leq j \leq s\}, \end{aligned} \quad (37b)$$

$$\begin{aligned} N_{-1} = \mathbb{C} - \text{linspan}\{ &c_k a_k^\dagger a_j + \sigma(j)\sigma(k)c_j a_{-j}^\dagger a_{-k}; \\ &-s \leq j < k \leq s, |j| \neq |k|; \sigma(j) = \text{sign}(j)\}, \end{aligned} \quad (37c)$$

$$\begin{aligned} \mathcal{K} = \mathbb{R} - \text{linspan}\{ &i(a_j^\dagger a_{-j} + a_{-j}^\dagger a_j), i(a_j^\dagger a_j - a_{-j}^\dagger a_{-j}), \\ &(a_j^\dagger a_{-j} - a_{-j}^\dagger a_j); 1 \leq j \leq s\}, \end{aligned} \quad (37d)$$

where we have translated the indexing of the canonical general spin orbitals (CGSOs) by

$$|n_j\rangle \rightarrow |n_{j-s}\rangle, \quad 1 \leq j \leq 2s. \quad (38)$$

It is useful to note that

$$N_0 = \{\mathcal{K} \oplus \mathcal{N}\}^{\mathbb{C}}, \quad (39)$$

where

$$\mathcal{N} = \bigoplus_{1 \leq j \leq s} \{\mathbb{R} - \text{linspan}\{(a_j^\dagger a_j + a_{-j}^\dagger a_{-j}) \mid 1 \leq j \leq s\}\}, \quad (40)$$

and $\{\cdot\}^{\mathbb{C}}$ denotes complexification. The factors in the group decomposition are

$$\begin{aligned} c_{+1}(\mathbf{z}_+) &= \exp \left\{ \sum_{\substack{-s \leq j < k \leq s \\ |j| \neq |k|}} z_{+jk} \{c_j a_k^\dagger a_j - \sigma(j) \sigma(k) c_k a_{-j}^\dagger a_{-k}\} \right\} \\ &\equiv \exp \sum_{\substack{-s \leq j < k \leq s \\ |j| \neq |k|}} z_{+jk} q_{jk}^\dagger, \end{aligned} \quad (41)$$

$$\begin{aligned} c_{-1}(\mathbf{z}_-) &= \exp \left\{ \sum_{\substack{-s \leq j < k \leq s \\ |j| \neq |k|}} z_{-jk} \{c_k a_k^\dagger a_j + \sigma(j) \sigma(k) c_j a_{-j}^\dagger a_{-k}\} \right\} \\ &\equiv \exp \sum_{\substack{-s \leq j < k \leq s \\ |j| \neq |k|}} z_{-jk} q_{jk}, \end{aligned} \quad (42)$$

$$c_0(\lambda) = \exp \left\{ \sum_{\substack{1 \leq j \leq s \\ 1 \leq k \leq 4}} \lambda_{jk} n_{jk} \right\}, \quad (43)$$

and

$$h(\eta) = \exp \left\{ \sum_{\substack{1 \leq j \leq s \\ 1 \leq k \leq 3}} \eta_{jk} u_{jk} \right\}, \quad (44)$$

where $\{z_{+jk}, z_{-jk}, \lambda_{jk}\} \in \mathbb{C}$, $\{\eta_{jk}\} \in \mathbb{R}$, and $\{n_{jk}, u_{jk}\}$ are given by equations (37b) and (37d), respectively.

In order that the transformation $c_{+1}(\mathbf{z}_+)c_0(\lambda)c_{-1}(\mathbf{z}_-)k(\eta)$ be unitary the values of $\{\mathbf{z}_+, \lambda, \mathbf{z}_-\}$ must be constrained resulting in dependencies between the variables. The action of such unitary transformations on a normalized

reference state produce normalized CSs that can be expressed in terms of the coset representatives $c_{+1}(\mathbf{z}_+)c_0(\lambda)$. Some of the dependencies between the variables $\{\mathbf{z}_+\}$ and $\{\lambda\}$ can be avoided if one considers unnormalized CSs by modifying the coset representative $c_0(\lambda)$ and explicitly considering the norm of the state in various expectation value expressions.

4.5. $\text{USp}(\omega_j)$ factors

The changes from the $\text{SU}(2)^s$ case can be illustrated by an $\sigma = s - 2, \rho = 1, \omega_1 = 2$ example (in this case $|g\rangle$ belongs to the class $\{s - 2, 2, 0\}$), which clearly leads to the general picture for $\rho > 1$. Here we have $s - 2$ eigenvalues, $\{c_j^2 | 3 \leq j \leq s\}$ of gg^\dagger that are doubly degenerate and one fourfold degenerate eigenvalues, c_1^2 , of gg^\dagger , which is associated with two doubly degenerate eigenvalues, $\{c_1, -c_1\}$ of g affiliated with CGSOs which can be linear combinations of $\{|\eta_1\rangle, |\eta_2\rangle\}$ and $\{|\eta_{-1}\rangle, |\eta_{-2}\rangle\}$, respectively [34]. In this case unitary transformations, $u(\tilde{z}, \eta)$, belonging to $U(2s)$ can be expressed in factored form as

$$\begin{aligned} u(\tilde{z}, \eta) &= c(\tilde{z})k_\sigma(\eta_\sigma)k_\omega(\eta_\omega) \\ &= c_{+1}(\mathbf{z}_{\sigma+})u_{+1}(\mathbf{z}_{\omega+})u_0(\lambda_\omega)c_0(\lambda_\sigma) \\ &\quad u_{-1}(\mathbf{z}_{\omega-})c_{-1}(\mathbf{z}_{-})k_\sigma(\eta_\sigma)k_\omega(\eta_\omega), \end{aligned} \quad (45)$$

where $k_\sigma(\eta_\sigma) \in \text{SU}(2)^{s-2}$ and $c_{\sigma 0}(\lambda_\sigma) \in \exp N_0$ and are expanded in the basis equations (37b) and (37d), respectively, with the operators referring to CGSOs $\{|\eta_j\rangle | j = \pm 1, \pm 2\}$ deleted. The operators $c_{+1}(\mathbf{z}_{\sigma+}) \in \exp N_{+1}$ and $c_{-1}(\mathbf{z}_{\sigma-}) \in \exp N_{-1}$ are expanded in the basis equations (37a) and (37c) with the operators referring to the pairs $\{(|\eta_j\rangle, |\eta_k\rangle) | j = \pm 1, k = \pm 1\}$ of CGSOs deleted.

The factors $u_{+1}(\mathbf{z}_{\omega+}) \in \exp U_{+11}$, $u_{-1}(\mathbf{z}_{\omega-}) \in \exp U_{-11}$, $u_{\omega 0}(\lambda_\omega) \in \exp U_{01}$, $k_\omega(\eta_\omega) \in \text{USp}(4)$, where U_{+1} , U_0 , U_{-1} and $\text{usp}(4)$ are expanded in the following bases:

$$U_{+11} = \mathbb{C} - \text{linspan}\{a_k^\dagger a_j + \sigma(j)\sigma(k)a_{-j}^\dagger a_{-k} ; j = 1, -1; k = 2, -2\}, \quad (46)$$

$$\begin{aligned} U_{01} = \mathbb{C} - \text{linspan}\{ & (a_j^\dagger a_j + a_{-j}^\dagger a_{-j}), (a_j^\dagger a_j - a_{-j}^\dagger a_{-j}), \\ & (a_j^\dagger a_{-j} + a_{-j}^\dagger a_j), i(a_j^\dagger a_{-j} - a_{-j}^\dagger a_j), \\ & i(a_k^\dagger a_j - \sigma(j)\sigma(k)a_{-j}^\dagger a_{-k} - a_j^\dagger a_k + \sigma(j)\sigma(k)a_{-k}^\dagger a_{-j}), \\ & (a_k^\dagger a_j - \sigma(j)\sigma(k)a_{-j}^\dagger a_{-k} + a_j^\dagger a_k - \sigma(j)\sigma(k)a_{-k}^\dagger a_{-j}); \\ & j = 1, -1; k = 2, -2\}, \end{aligned} \quad (47)$$

$$U_{-11} = \mathbb{C} - \text{linspan}\{a_k^\dagger a_j - \sigma(j)\sigma(k)a_{-j}^\dagger a_{-k};$$

$$j = 1, -1; k = 2, -2\}, \quad (48)$$

$$\text{usp}(2\omega_1) = \text{usp}(4)$$

$$= \mathbb{R} - \text{linspan}\{i(a_j^\dagger a_j - a_{-j}^\dagger a_{-j}), i(a_j^\dagger a_{-j} + a_{-j}^\dagger a_j), (a_j^\dagger a_{-j} - a_{-j}^\dagger a_j),$$

$$(a_k^\dagger a_j - \sigma(j)\sigma(k)a_{-j}^\dagger a_{-k} - a_j^\dagger a_k + \sigma(j)\sigma(k)a_{-k}^\dagger a_{-j}),$$

$$i(a_k^\dagger a_j - \sigma(j)\sigma(k)a_{-j}^\dagger a_{-k} + a_j^\dagger a_k - \sigma(j)\sigma(k)a_{-k}^\dagger a_{-j});$$

$$j = 1, -1; k = 2, -2\}, \quad (49)$$

where $\sigma(j) = \text{sign}(j)$. The manifold of $U(2s)/[\text{USp}(4) \times \text{SU}(2)^{s-1}]$ -CSs is then given by

$$|\Phi(\mathbf{z})\rangle = c_{+1}(\mathbf{z}_{+\sigma})u_{+1}(\mathbf{z}_{+\omega})u_{01}(\lambda_{\omega_1})c_0(\lambda_\sigma)|g^N\rangle, \quad (50)$$

where $\mathbf{z} = (\mathbf{z}_{+\sigma}, \mathbf{z}_{+\omega}, \lambda_\omega, \lambda_\sigma)$ and the reference AGP is generated by a geminal $|g\rangle$ in the class $\{s-2, 2, 0\}$.

If $\rho > 2$ then one deletes the appropriate operators in the bases $\{N_{+1}, N_0, N_{-1}, \mathcal{K}\}$ defined in equations (37a)–(37d) and defines new bases $\{\{U_{+1j}, U_{0j}, U_{-1j}, \text{usp}(2\omega_j)\} | 1 \leq j \leq \rho\}$ according to equations (46)–(49). The subalgebras $\{U_{-1j}, \text{usp}(2\omega_j)\} | 1 \leq j \leq \rho\}$ annihilate $|g^N\rangle$, i.e.,

$$b|g^N\rangle = 0 \quad \forall b \in \bigoplus_{1 \leq j \leq \rho} U_{-1j} \oplus \bigoplus_{1 \leq j \leq \rho} \text{usp}(2\omega_j), \quad (51)$$

while the subalgebras $\{U_{+1j}, U_{0j} | 1 \leq j \leq \rho\}$ have the property

$$b|g^N\rangle \neq 0 \quad \forall b \in \bigoplus_{1 \leq j \leq \rho} U_{+1j} \oplus \bigoplus_{1 \leq j \leq \rho} U_{0j}. \quad (52)$$

The $U(2s)/[\prod_{1 \leq j \leq \rho} \text{USp}(2\omega_j) \times \text{SU}(2)^{s-\omega}]$ -CS manifold, $\mathcal{M}(s - \omega, \omega_1, \dots, \omega_\rho, \xi)$, is then given by

$$|\Phi(\mathbf{z})\rangle = c_{+1}(\mathbf{z}_{\sigma+}) \prod_{1 \leq j \leq \rho} \{u_{+1j}(\mathbf{z}_{+j})u_{0j}(\lambda_j)\} c_0(\lambda_\sigma)|g^N\rangle. \quad (53)$$

The manifold of extreme AGPs, $\mathcal{M}(0, s, 0)$, are $U(2s)/\text{USp}(2s)$ -CS, which have been discussed in super conductivity [39] is given by

$$|\Phi(\mathbf{z})\rangle = u_{+11}(\mathbf{z}_{+1})u_{01}(\lambda_1)|g^N\rangle. \quad (54)$$

4.6. $\text{SU}(2\xi)$ factors

The changes from $\text{SU}(2)^s$ can now be illustrated by an $\sigma = s - 1$, $\rho = 0$, $\xi = 1$ example, ($|g\rangle$ belongs to the class $\{s - 1, 0, 1\}$), which also clearly leads to the general picture for $\xi > 1$. Here we have $s - 1$ eigenvalues,

$\{c_j^2 | 2 \leq j \leq s\}$ of gg^\dagger that are doubly degenerate and a doubly degenerate zero eigenvalue of gg^\dagger , which is associated with the CGSOs $\{|\eta_{-1}\rangle, |\eta_1\rangle\}$. In this case unitary transformations, $u(\tilde{\mathbf{z}}, \eta)$, belonging to $U(2s)$ can be expressed in factored form as

$$\begin{aligned} u(\tilde{\mathbf{z}}, \eta) &= c(\tilde{\mathbf{z}})k_\sigma(\eta_\sigma)k_\xi(\eta_\xi) \\ &= c_{+1}(\mathbf{z}_{\sigma+})v_0(\lambda_\xi)c_0(\lambda_\sigma)c_{-1}(\mathbf{z}_{\sigma-})k_\sigma(\eta_\sigma)k_\xi(\eta_\xi), \end{aligned} \quad (55)$$

where $k_\sigma(\eta_\sigma) \in \text{SU}(2)^{s-1}$ and $c_0(\lambda_\sigma) \in \exp N_0$ which are expanded in the basis equations (37b) and (37d) with the operators referring to CGSOs $\{|\eta_j\rangle | j = \pm 1\}$ deleted. The definitions of $c_{+1}(\mathbf{z}_{\sigma+}) \in \exp N_{+1}$ and $c_{-1}(\mathbf{z}_{\sigma-}) \in \exp N_{-1}$ are unchanged and are still expanded in the basis equations (37a) and (37c). The factors $v_0(\lambda_\xi) \in \exp V_0$, $k_\xi(\eta_\xi) \in \text{SU}(2)$, where $\text{su}(2)$ is expanded in the following bases:

$$\begin{aligned} \text{su}(2) &= \mathbb{R} - \text{linspan}\{i(a_1^\dagger a_{-1} + a_{-1}^\dagger a_1), \\ &\quad i(a_1^\dagger a_1 - a_{-1}^\dagger a_{-1}), (a_1^\dagger a_{-1} - a_{-1}^\dagger a_1)\}, \end{aligned} \quad (56)$$

and V_0 is given by

$$\{\text{su}(2) \oplus \mathcal{N}\}^\mathbb{C}, \quad (57)$$

where

$$\mathcal{N} = \mathbb{R} - \text{linspan}\{(a_1^\dagger a_1 + a_{-1}^\dagger a_{-1})\}. \quad (58)$$

The subalgebra $\{\text{su}(2\xi)\}$ annihilates $|g^N\rangle$, i.e.,

$$b|g^N\rangle = 0 \quad \forall b \in \text{su}(\xi). \quad (59)$$

As the class of the reference AGP changes from $\{s-1, 0, 1\}$ to $\{s-p, 0, p\}$ it is clear how the definitions of the factors equation (55) evolve. It is easy to confirm that the class $\{M, 0, s-M\}$ cannot in fact exist, while the class $\{0, M, s-M\}$ does and such reference AGPs are IPSs and the $U(2s)/[\text{USp}(2M) \times \text{SU}(2s-2M)]$ -CS manifold is in fact the Thouless $U(2s)/[U(2M) \times U(2s-2M)]$ -CS manifold.

4.7. $U(\mathcal{H}^N)/U(1)$ -coherent states

It is illuminating and instructive to consider the CS formulation of the manifold, \mathcal{M}_N , of all N -particle states based on the unitary group $U(\mathcal{H}^N) \equiv U(\binom{r}{N})$ of \mathcal{H}^N . In this case the configuration space formed by the coherent states represents all of the states $|\Psi\rangle \in \mathcal{H}^N$ via a parameterization $\{|\Phi(\mathbf{z})\rangle\}$ and the *exact* quantum evolution equations can be expressed in terms of classical EOM, that are equivalent to the full TDSE, for paths belonging

to \mathcal{M}_N . The isotropy subgroup is

$$\begin{aligned} K &= \{g|g \in G, g|\Phi_1\rangle = e^{i\theta(g)}|\Phi_1\rangle\} \\ &= \left\{ \exp(i\lambda(g)|\Phi_1\rangle\langle\Phi_1|) \exp\left(i \sum_{i,j \neq 1} \lambda_{ij}(g)|\Phi_i\rangle\langle\Phi_j|\right) \right\}. \end{aligned} \quad (60)$$

The cost representatives are

$$\begin{aligned} U(\mathcal{H}^N)/K &= \left\{ \exp\left(\sum_{i>1} \eta_i |\Phi_i\rangle\langle\Phi_1|\right) \exp(\eta_1 |\Phi_1\rangle\langle\Phi_1|) \right. \\ &\quad \left. \times \exp\left(-\sum_{i>1} \bar{\eta}_i |\Phi_i\rangle\langle\Phi_1|\right) \right\}, \end{aligned} \quad (61)$$

where $\{|\Phi_i\rangle|1 \leq i \leq \binom{r}{N}\}$ is a complete orthonormal basis for \mathcal{H}^N . The family of CSs associated with this coset is defined as

$$|\Phi(\eta)\rangle = \left\{ \exp\left(\sum_{i>1} \eta_i |\Phi_i\rangle\langle\Phi_1|\right) \exp(\eta_1 |\Phi_1\rangle\langle\Phi_1|) \right\} |\Phi_1\rangle. \quad (62)$$

It is convenient to introduce a new equivalent coordinate system $\{\mathbf{z}\}$ by setting

$$\begin{aligned} \eta_1 = \ln(z_1) &\Leftrightarrow z_1 = e^{\eta_1}, & \eta_j = \frac{z_j}{z_1}; \\ 2 \leq j \leq \binom{r}{N} &\Leftrightarrow z_j = \eta_j e^{\eta_1}, \end{aligned} \quad (63)$$

which leads to the following form for the CSs

$$|\Phi(\mathbf{z})\rangle = \sum_{1 \leq j \leq \binom{r}{N}} z_j |\Phi_j\rangle. \quad (64)$$

Clearly equation (64) is the familiar CI expansion of a general N -fermion state and the parameters $\{z_j\}$ the configurational interaction coefficients. The normalization of these CSs is given by

$$\langle\Phi(\mathbf{z})|\Phi(\mathbf{z})\rangle = \sum_{1 \leq j \leq \binom{r}{N}} |z_j|^2 = |z_1|^2 + \sum_{2 \leq j \leq \binom{r}{N}} |z_j|^2, \quad (65)$$

$$\langle\Phi(\eta)|\Phi(\eta)\rangle = e^{2\text{Re}\eta_1} \left\{ 1 + \sum_{2 \leq j \leq \binom{r}{N}} |\eta_j|^2 \right\}. \quad (66)$$

Hence if one sets η_1 as the function

$$\eta_1 = \eta_1(\eta_2, \dots, \eta_{\binom{r}{N}}) = \frac{1}{2} \ln \left(1 - \sum_{2 \leq j \leq \binom{r}{N}} e^{2 \operatorname{Re} \eta_j} \right), \quad (67)$$

and z_1 as the function

$$z_1 = z_1(z_2, \dots, z_{\binom{r}{N}}) = \left(1 - \sum_{2 \leq j \leq \binom{r}{N}} |z_j|^2 \right)^{1/2} \quad (68)$$

the family of CSs $\{|\Phi(\mathbf{z})\rangle\} \equiv \{|\Phi(\boldsymbol{\eta})\rangle\}$ are normalized if the reference state $|\Phi_1\rangle$ is normalized, i.e., $\langle\Phi_1|\Phi_1\rangle = 1$. If one uses the CS parameters $\{\eta_2, \dots, \eta_{\binom{r}{N}}\}$ or $\{z_2, \dots, z_{\binom{r}{N}}\}$ the CS manifold is the unit sphere in \mathcal{H}^N , while if one uses $\{\boldsymbol{\eta}\}$ or $\{\mathbf{z}\}$ then it is all of \mathcal{H}^N and one explicitly considers the normalization in all expressions.

5. SUMMARY AND DISCUSSION

We have described how there are three possible chains of coset decompositions of the one-particle unitary group $U(r)$ starting from maximal compact subgroups. Each of these chains produce families of cosets $\{U(r)/K\}$. A coset produces a manifold of CSs from a reference state $|\Phi_{\text{ref}}\rangle$ if this state carries a one-dimensional unitary representation of the subgroup K and the Hilbert space that $|\Phi_{\text{ref}}\rangle$ belongs to carries an irreducible representation of $U(r)$. As we are considering $N = 2M$ electron states this condition rules out cosets based on the maximal compact groups $\text{SO}(r)$ and $U(p) \times U(r-p)$ for $p \neq N$, leaving only $\text{USp}(2s)$ and $U(N) \times U(r-N)$. The subgroups $\text{USp}(2\omega_1) \times \dots \times \text{USp}(2\omega_p) \times \text{SU}(2)^\sigma \times \text{SU}(2\xi)$ of $\text{USp}(2s)$ also satisfy this CS condition, but there are no subgroups of $U(N) \times U(r-N)$ that do. The reference state for all of these cosets is an AGP state belonging to the class (see Section 3) $\{\sigma, \omega_1, \dots, \omega_p, \xi\}$ that is determined by the canonical coefficients $\{c_j\}$ of the geminal $|g\rangle$, this index set also classifies the possible isotropy subgroups and hence the cosets. The Lie algebra of $U(r)$ has different direct sum decompositions determined by the different subgroups generating the cosets. The manifolds of AGP CSs $\mathcal{M}\{\sigma, \omega_1, \dots, \omega_p, \xi\}$ have complex coordinate systems \mathbf{z} wrt the reference state dependent bases adapted to these Lie algebra decompositions and these coordinates parameterize AGP states. Different manifolds contain AGP states that describe different physical properties, e.g., extreme AGPs have properties associated with highly correlated systems, such as superconductors.

The manifolds $\mathcal{M}\{\sigma, \omega_1, \dots, \omega_p, \xi\}$ equipped with the coordinate system \mathbf{z} are particularly useful as they have a natural generalized phase space

structure and can be used to construct, *via* the TDVP, approximations of the TDSE as a classical dynamical system. If one used the manifold constituted by whole Hilbert space \mathcal{H}^N (not an AGP manifold) then the classical Hamilton equations plus an equation for a time-dependent phase would be equivalent to the TDSE, and their solutions would provide solutions to the Schrödinger equation. The classical equations restricted to the AGP manifolds produce paths of AGP states that approximate the exact paths. One can consider the classical linear response of approximate stationary states found on these manifolds to external time-dependent perturbations either within the curved phase or in the tangent space at these points [37]. This allows a variety of linear response approximations schemes to be developed that generalize and clarify propagator and RPAs.

APPENDIX A. AGP STATES

The $N = 2M$ electron AGP states, $|g^N\rangle$ can be expanded as

$$|g^N\rangle = \sum_{1 \leq j_1 < j_2 < \dots < j_N \leq s} c_{j_1} \dots c_{j_N} |\eta_{j_1} \eta_{j_1+s} \dots \eta_{j_N} \eta_{j_N+s}\rangle, \quad (\text{A1})$$

where $\{|\eta_j\rangle | 1 \leq j \leq r = 2s\}$ are CGSO which form a complete orthonormal basis for \mathcal{H}^1 , and $\{c_j | 1 \leq j \leq s\}$ are positive real numbers called the canonical coefficients of the two electron geminal $|g\rangle$ that has the canonical expansion

$$|g\rangle = \sum_{1 \leq j \leq s} c_j |\eta_j \eta_{j+s}\rangle. \quad (\text{A2})$$

The canonical coefficients are the square roots of the occupation numbers $\{n_j = n_{j+s} | 1 \leq j \leq s\}$ of the first-order reduced density operator (FORDO) $|g\rangle\langle g|$ of the two-electron state $|g\rangle$. The number, ν , of non-zero $\{n_j | 1 \leq j \leq s\}$ is called the rank of the geminal $|g\rangle$, the dimension of the null space of $|g\rangle$ is equal to $2(s - \nu)$. If all the occupation are equal (hence non-zero) the geminal is called extreme and the state $|g^N\rangle$ an extreme AGP State.

The CGSOs $\{n_j | 1 \leq j \leq s\}$ diagonalize both the FORDO of the geminal state $|g\rangle$ and the AGP state $|g^N\rangle$ and are thus natural general spin orbitals (NGSOs) of these operators, *however*, NGSOs of these operators *are not* necessarily CGSOs! In fact if one multiplies $\{n_j | 1 \leq j \leq r\}$ by arbitrary, but at least some non-equal phase factors a *different* geminal $|g\rangle$ is produced. It is interesting to observe that different geminals produced in such a manner have the same FORDO.

REFERENCES

- [1] O. Goscinski, B. Pickup and G. Purvis, *Chem. Phys. Lett.*, 1973, **22**, 167.
- [2] B. Pickup and O. Goscinski, *Mol. Phys.*, 1973, **26**, 1013.
- [3] O. Goscinski and E. Brandas, *Phys. Rev.*, 1969, **182**, 43.
- [4] O. Goscinski and B. Lukman, *Chem. Phys. Lett.*, 1970, **7**, 573.
- [5] B. Weiner and O. Goscinski, *Int. J. Quantum Chem.*, 1980, **18**, 1109.
- [6] O. Goscinski and B. Weiner, *Phys. Scr.*, 1980, **21**, 385, from conference: Many-body Theory of Atomic Systems. Proceedings of the Nobel Symposium 46, 11–16 June 1979.
- [7] G. Howat, M. Trsic and O. Goscinski, *Int. J. Quantum Chem.*, 1977, **11**, 283.
- [8] B. Weiner and O. Goscinski, *Phys. Rev. A [Gen. Phys.]*, 1980, **22**, 2374.
- [9] J. Linderberg and Y. Öhrn, *Int. J. Quantum Chem.*, 1977, **12**, 161.
- [10] Y. Öhrn and J. Linderberg, *Int. J. Quantum Chem.*, 1979, **15**, 343.
- [11] A. J. Coleman, *Rev. Mod. Phys.*, 1963, **35**, 668.
- [12] A. J. Coleman, *J. Math. Phys.*, 1965, **6**, 1425.
- [13] E. Sangfelt and O. Goscinski, *J. Chem. Phys.*, 1985, **82**, 4187.
- [14] E. Sangfelt, H. Kurtz, N. Elander and O. Goscinski, *J. Chem. Phys.*, 1984, **81**, 3976.
- [15] N. Elander, E. Sangfelt, H. Kurtz and O. Goscinski, *Int. J. Quantum Chem.*, 1983, **23**, 1047, from conference: Proceedings of the Fourth International Congress in Quantum Chemistry, 13–20 June 1982.
- [16] O. Goscinski, B. Weiner and N. Elander, *J. Chem. Phys.*, 1982, **77**, 2445.
- [17] B. Weiner, *J. Math. Phys.*, 1983, **24**, 1791.
- [18] E. Sangfelt, O. Goscinski, N. Elander and H. Kurtz, *Int. J. Quantum Chem., Quantum Chem. Symp.*, 1981, 133–141, from conference: Proceedings of the International Symposium on Atomic, Molecular, and Solid-State Theory, Collision Phenomena, and Computational Quantum Chemistry, 8–14 March 1981.
- [19] B. Weiner and Y. Öhrn, *J. Phys. Chem.*, 1987, **91**, 563.
- [20] E. Sangfelt, R. Chowdhury, B. Weiner and Y. Öhrn, *J. Chem. Phys.*, 1987, **86**, 4523.
- [21] Y. Öhrn, *Int. J. Quantum Chem., Quantum Chem. Symp.*, 1985, 39–50, from conference: Proceedings of the International Symposium on Atomic, Molecular and Solid-State Theory, Scattering Problems, Many Body Phenomena, and Computational Quantum Chemistry, 18–23 March 1985.
- [22] B. Weiner and Y. Öhrn, *J. Chem. Phys.*, 1985, **83**, 2965.
- [23] B. Weiner, H. J. A. Jensen and Y. Öhrn, *J. Chem. Phys.*, 1984, **80**, 2009.
- [24] H. J. A. Jensen, B. Weiner, J. V. Ortiz and Y. Öhrn, *Int. J. Quantum Chem., Quantum Chem. Symp.*, 1982, 615–631, from conference: Proceedings of the International Symposium on Quantum Chemistry, Theory of Condensed Matter, and Propagator Methods in the Quantum Theory of Matter, 1–13 March 1982.
- [25] H. J. A. Jensen, B. Weiner and Y. Öhrn, *Int. J. Quantum Chem.*, 1983, **23**, 65, from conference: Proceedings of the Fourth International Congress in Quantum Chemistry, 13–20 June 1982.
- [26] A. Perelomov, *Generalized Coherent States*, Springer, Berlin, 1986.
- [27] B.-S. S. J. Klauder, *Coherent States*, World Scientific, Singapore, 1985.
- [28] R. Gilmore, *Lie Groups, Lie Algebras, and Some of Their Applications*, Wiley, London, 1974.
- [29] K. Ito, Eds., *Encyclopedia of Mathematics*, 2nd edn., MIT press, Cambridge, 1993, Vol. 2.
- [30] P. Kramer and M. Saraceno, *Geometry of the Time-Dependent Variational Principle in Quantum Mechanics*, Springer, Berlin, 1981.
- [31] L. Schulman, *Techniques and Applications of Path Integration*, Wiley, London, 1981.
- [32] S. Helgason, *Differential Geometry, Lie Groups, and Symmetric Spaces*, Academic Press, London, 1978.

- [33] D. J. Thouless, *Nucl. Phys.*, 1960, **21**, 225.
- [34] B. Weiner and J. V. Ortiz, *Int. J. Quantum Chem.*, 2004, **97**, 896.
- [35] O. Goscinski and B. Weiner, *Phys. Rev. A [Gen. Phys.]*, 1982, **25**, 650.
- [36] E. Deumens, B. Weiner and Y. Öhrn, *Nucl. Phys. A*, 1987, **A466**, 85.
- [37] B. Weiner, E. Deumens and Y. Öhrn, *J. Math. Phys.*, 1994, **35**, 1139.
- [38] W.-M. Zhang, D. H. Feng and R. Gilmore, *Rev. Mod. Phys.*, 1990, **62**, 867.
- [39] A. J. Coleman and V. I. Yukalov, *Reduced Density Matrices*, Springer, Berlin, 2000.

This page intentionally left blank

Current Methods for Coulomb Few-Body Problems

Frank E. Harris

*Department of Physics, University of Utah, Salt Lake City, UT 84112, USA
Quantum Theory Project, P.O. Box 118435, University of Florida,
Gainesville, FL 32611, USA*

Abstract

This contribution examines current approaches to Coulomb few-body problems mainly from a methodological perspective, in contrast to recent reviews which have focused on the results obtained for benchmark problems. The methods under discussion here employ wavefunctions which explicitly involve all the interparticle coordinates and use functional forms appropriate to ‘nonadiabatic’ systems in which all the particles are of comparable mass. The use of such wavefunctions for states of arbitrary angular symmetry is reviewed, and the kinetic-energy operator, written in the interparticle coordinates, is presented in a convenient form. Evaluation of the resultant angular matrix elements is discussed in detail. For exponentially correlated wavefunctions, problems of integral evaluation are surveyed, the relatively new analytical procedures are summarized, and relations among matrix elements are presented. The current status of Gaussian-orbital and Hylleraas methods is also reviewed.

Contents

1. Introduction	130
2. Basis wavefunctions	131
3. Kinetic energy	134
4. Matrix elements	138
5. Four-body exponentially correlated wavefunctions	143
6. Three-body exponentially correlated wavefunctions	145
7. Correlated Gaussian wavefunctions	146
8. Hylleraas methods	146
9. Other methods	148
Acknowledgements	149
Appendix A. Angular Momentum Identities	149
Appendix B. Differential Properties of the \mathcal{Y}_{LM}^{μ}	150
References	153

1. INTRODUCTION

The topic of few-body systems is highly appropriate as a contribution in honor of Professor Osvaldo Goscinski because it is a subject that has historically been of interest at Uppsala University, with contributions by a number of investigators whose scientific development owes much to the Quantum Chemistry Group. This publication also gives the author an opportunity to express his appreciation for the cordial relationship he has had with Osvaldo and the Group over a period of 40 years, starting when he was a guest professor in Uppsala in 1963.

A distinguishing feature found in work on few-body problems (typically meaning those involving no more than four particles) is the use of wavefunctions explicitly involving all the interparticle distances. While this may seem just a convenience for an atom such as He or Li, where expansions in terms of orbital products can be very effective, the situation becomes quite different when all the particles are of comparable mass. In such 'nonadiabatic' systems, there is no natural system 'center', and it is important to treat all particles on an equal footing. This issue becomes especially important for model calculations on small nuclei, where the energetically most important interactions between all pairs of particles are of the same functional form (including its sign).

The earliest precursors to the modern work in the field were the pioneering contributions of Hylleraas [1], who made the first calculations of the He atom by a method that included the interelectron distance as an explicit coordinate, and James and Coolidge [2], who introduced the use of perimetric coordinates in the same problem. These workers used Slater-type orbitals for the two electrons, and included linear (or in some cases higher powers) of the interelectron coordinate to better describe electron repulsion effects. Attention to this approach languished until the landmark paper on He by Pekeris [3] appeared, causing the importance of the Hylleraas approach to become more generally appreciated. This no doubt catalyzed the early work in the field at the Uppsala Quantum Theory Group, which in turn laid a foundation for much of the later work on integrals involving the interparticle coordinates. Work at Uppsala during that era included a paper by Calais and Löwdin [4] in 1962, a contribution by Öhrn and Nordling [5] in 1966, and papers on Li by Larsson [6] in 1968 and by Larsson and Smith [7] in 1969. Outside Uppsala, significant contributions in this same time period included work by Szász [8] and Perkins [9] on integrals, a paper by Sack [10] on the expansions of powers of interparticle coordinates, and a paper that received scant notice at the time, by Delves and Kalotas [11], on the use of exponentials in all the interparticle separations.

The next significant advance in the area after these early investigations did not occur for about a decade, perhaps awaiting a growth in the power of digital computers. In 1977, Thakkar and Smith (an Uppsala alumnus)

[12] described an approach (disguised as an application of the then-trendy ‘generator-coordinate method’) for treating three-body systems using exponentials in all the interparticle coordinates. An essential aspect of the approach was that it contemplated the use of an extensive configuration–interaction wavefunction. Since 1977, the work on few-body problems has in a sense bifurcated, with some investigators following the approach of Thakkar and Smith (sometimes without attribution) or a similar formulation using correlated Gaussians [13], while others have stayed closer to the original method of Hylleraas, using Slater-type orbitals for the electrons, with the interelectron coordinates appearing only in polynomials.

At this point in time, there has been considerable success in the study of the adiabatic three and four-body problems He and Li. We call attention to a review of high-precision He calculations by Drake [14] and one on Li calculations by King [15], the latter including 610 literature references. These reviews focused primarily on the results which have been obtained. In contrast, the focus of the present paper will be on computational methods; we review various current approaches, adding contributions and observations where appropriate. Because these methods have restrictions in their implementations that limit them to three- and four-body systems, the discussion will for the most part be correspondingly restricted. Most of the points we wish to make are already present in nonrelativistic calculations on Coulomb systems, so we make those restrictions as well.

2. BASIS WAVEFUNCTIONS

We consider systems containing $N \leq 4$ particles, of respective masses m_i , with a spatial wavefunction depending on their positions $\mathbf{r}_1, \dots, \mathbf{r}_N$ in a space-fixed coordinate system. These coordinates can be transformed into the position \mathbf{R} of the system’s center of mass and relative coordinates $\mathbf{r}_{1N}, \dots, \mathbf{r}_{N-1,N}$, where \mathbf{r}_{ij} stands for $\mathbf{r}_i - \mathbf{r}_j$; we also define $r_{ij} = |\mathbf{r}_{ij}|$ and $\hat{\mathbf{r}}_{ij} = \mathbf{r}_{ij}/r_{ij}$. We restrict our attention to isolated systems in which it is not necessary to consider the motion of the center of mass, so the wavefunction can be expressed entirely in terms of the $3N - 3$ relative coordinates, of which three (two if $N = 2$) can be chosen to specify the orientation of the entire wavefunction with respect to space-fixed axes, while the remaining coordinates can describe the internal structure of the wavefunction. The restriction to $N \leq 4$ causes the number of internal coordinates to be equal to the number of distinct r_{ij} . Considering also that orbital angular momentum must be conserved, the two-particle system can have the trivial spatial wavefunction

$$\Psi(\mathbf{r}_{12}) = Y_{LM}(\hat{\mathbf{r}}_{12})\phi(r_{12}), \quad (1)$$

where Y_{LM} is a normalized spherical harmonic of quantum numbers L, M , and its argument $\hat{\mathbf{r}}_{ij}$ is interpreted as a shorthand for the corresponding angular coordinates θ_{ij}, ϕ_{ij} .

For a three-particle system, the orientation of the wavefunction depends upon both $\hat{\mathbf{r}}_{13}$ and $\hat{\mathbf{r}}_{23}$, and Ψ can be built from quantities such as

$$g(\mathbf{r}_{13}, \mathbf{r}_{23}) = Y_{lm}(\hat{\mathbf{r}}_{13}) Y_{l'm'}(\hat{\mathbf{r}}_{23}) \phi(r_{12}, r_{13}, r_{23}). \quad (2)$$

In 1961, Schwartz [16] considered three-body spatial wavefunctions of the form

$$\Psi(\mathbf{r}_{13}, \mathbf{r}_{23}) = \mathcal{Y}_{LM}^{ll'}(\mathbf{r}_{13}, \mathbf{r}_{23}) \phi(r_{12}, r_{13}, r_{23}), \quad (3)$$

where $\mathcal{Y}_{LM}^{ll'}$ is an angular momentum eigenfunction of quantum numbers L, M built from solid spherical harmonics of degrees l and l' . Using equation (A1), we write

$$\begin{aligned} \mathcal{Y}_{LM}^{ll'}(\mathbf{r}_{13}, \mathbf{r}_{23}) &= (-1)^{l'-l-M} \sqrt{2L+1} r_{13}^l r_{23}^{l'} \\ &\times \sum_m \begin{pmatrix} l & l' & L \\ m & M-m & -M \end{pmatrix} Y_{lm}(\hat{\mathbf{r}}_{13}) Y_{l',M-m}(\hat{\mathbf{r}}_{23}). \end{aligned} \quad (4)$$

The quantity of the form

$$\begin{pmatrix} a & b & c \\ d & e & f \end{pmatrix}$$

is a Wigner 3- j symbol [17]. An important point in Schwartz's discussion was that the most general angular function could be obtained with l and l' restricted to the range $(0, L)$, with $l + l'$ equal either to L or to $L + 1$. Formulas for basis functions corresponding to equations (3) and (4) were developed by Frolov and Smith [18].

A few comments about equation (4) are in order. Because the range of $\hat{\mathbf{r}}_{23}$ is limited to points consistent with the current values of the r_{ij} , the $\mathcal{Y}_{LM}^{ll'}$ are not normalized even though the values of the coupling coefficients would produce normalized functions if the variables \mathbf{r}_{13} and \mathbf{r}_{23} were independent. For the same reason, $\mathcal{Y}_{LM}^{ll'}$ of different l or l' (but the same L and M) are not in general orthogonal. However, the procedure whereby the individual spherical harmonics are coupled to form an L, M eigenfunction does not depend upon the normalization, but only on the commutation rules for angular momentum operators, so the validity of equation (4) is not in question. One might consider rescaling the $\mathcal{Y}_{LM}^{ll'}$ to make them normalized; it is better not to do so because one would then lose various simplifications arising in the angular-momentum algebra.

Turning now to the four-body problem, a possible starting point would be the generalization of equation (2),

$$g(\mathbf{r}_{14}, \mathbf{r}_{24}, \mathbf{r}_{34}) = Y_{lm}(\hat{\mathbf{r}}_{14}) Y_{l'm'}(\hat{\mathbf{r}}_{24}) Y_{l''m''}(\hat{\mathbf{r}}_{34}) \phi(r_{12}, r_{13}, r_{14}, r_{23}, r_{24}, r_{34}). \quad (5)$$

Yan and Drake [19] proposed the use of these functions in combinations yielding eigenfunctions of the total angular momentum of quantum numbers L, M , presenting their analysis in a form appropriate to the calculations by the Hylleraas method.

At this point we observe that, even for the four-body case, only three coordinates are needed to define the spatial orientation of the wavefunction, and these have been determined once $\hat{\mathbf{r}}_{14}$ and $\hat{\mathbf{r}}_{24}$ have been specified. It might, therefore, seem unnecessary to use a form as complicated as that in equation (5), and one might consider using an angular momentum eigenfunction such as

$$\Psi(\mathbf{r}_{14}, \mathbf{r}_{24}, \mathbf{r}_{34}) = \mathcal{Y}_{LM}''(\mathbf{r}_{14}, \mathbf{r}_{24}) \phi(r_{12}, r_{13}, r_{14}, r_{23}, r_{24}, r_{34}). \quad (6)$$

Such an approach, however, is flawed in that application of the kinetic energy operator to a function of this form for $L \neq 0$ generates a result with components not representable by equation (6), and a starting point like the one given by equation (5) is indeed required if exact energies are to be attained.

A complete specification of the basis requires a choice for the functional form(s) to be used for ϕ . The choice also influences the details of the evaluation of matrix elements, particularly those of the kinetic energy operator. The older work, designed primarily for systems in which particle N is a nucleus and the other particles are electrons, used Slater-type s orbitals in the coordinates r_{iN} and introduced the remaining r_{ij} only as powers. Illustrating for $N = 3$:

$$\phi(r_{12}, r_{13}, r_{23}) = r_{12}^k r_{13}^j r_{23}^{j'} e^{-\alpha_{13}r_{13} - \alpha_{23}r_{23}}. \quad (7)$$

The corresponding form for $N = 4$ is

$$\phi(r_{12}, r_{13}, r_{14}, r_{23}, r_{24}, r_{34}) = r_{12}^k r_{13}^{k'} r_{23}^{k''} r_{14}^j r_{24}^{j'} r_{34}^{j''} e^{-\alpha_{14}r_{14} - \alpha_{24}r_{24} - \alpha_{34}r_{34}}. \quad (8)$$

When functions of the types given in equations (7) and (8) are used in computations, the parameters α_{ij} are usually restricted to one or at most a few sets of values, and flexibility in the basis is obtained by taking many values of the exponents j and k .

An alternative form for the $\phi(r_{12}, \dots)$ is one containing exponentials in all the interparticle distances, with the powers of the r_{ij} omitted, as in

$$\phi(r_{12}, r_{13}, r_{23}) = e^{-\alpha_{12}r_{12} - \alpha_{13}r_{13} - \alpha_{23}r_{23}} \quad (9)$$

or

$$\phi(r_{12}, r_{13}, r_{14}, r_{23}, r_{24}, r_{34}) = e^{-\alpha_{12}r_{12} - \alpha_{13}r_{13} - \alpha_{14}r_{14} - \alpha_{23}r_{23} - \alpha_{24}r_{24} - \alpha_{34}r_{34}}. \quad (10)$$

Difficulties in evaluating the integrals arising from the use of equation (10) have led some investigators to use a corresponding formulation using

Gaussian functions:

$$\phi(r_{12}, r_{13}, r_{14}, r_{23}, r_{24}, r_{34}) = e^{-\alpha_{12}r_{12}^2 - \alpha_{13}r_{13}^2 - \alpha_{14}r_{14}^2 - \alpha_{23}r_{23}^2 - \alpha_{24}r_{24}^2 - \alpha_{34}r_{34}^2}. \quad (11)$$

With bases involving the functions in equation (9), (10) or (11), flexibility is usually obtained by using a large number of functions with different values of the α_{ij} . In some of the recent work, the α_{ij} have been permitted to assume complex values, thereby introducing oscillations into individual basis functions.

3. KINETIC ENERGY

For nonrelativistic Coulomb systems, the potential energy consists of terms proportional to r_{ij}^{-1} and it is obvious how to incorporate these contributions into matrix elements. However, the kinetic energy is much more problematic, as the basis functions contain nonorthogonal coordinates (the r_{ij}) and exhibit redundancy between the r_{ij} and the coordinates occurring in the angular factors. If computations are restricted to spherically symmetric (S) states, this problem is minimal; for states of general angular symmetry, it is not. If radial wavefunctions of the forms in equation (7) or (8) are used, one approach could be to expand all the r_{ij}^k factors in terms of r_{iN} and r_{jN} using formulas such as those of Sack [10], after which each term of the resulting expansion would be a conventional orbital product, for which the kinetic energy could be computed by standard methods. Formulations based on Gaussians also become tractable by standard methods, due in part to the specific properties of the quadratic exponentials. However, these potential simplifications do not apply for radial wavefunctions of the forms in equation (9) or (10), and we therefore continue with an analysis predicated on the impracticality of removing explicit occurrences of any of the r_{ij} from the wavefunction.

A starting point for our present discussion of the kinetic energy operator T is its form in the space-fixed coordinates $\mathbf{r}_1, \mathbf{r}_2, \dots, \mathbf{r}_N$, which we write in a system of units in which $\hbar = 1$:

$$T = -\frac{1}{2m_1} \nabla_1^2 - \frac{1}{2m_2} \nabla_2^2 - \dots - \frac{1}{2m_N} \nabla_N^2. \quad (12)$$

We consider the application of T to functions which formally depend only upon the overcomplete set of relative coordinates $\mathbf{r}_{12}, \mathbf{r}_{13}, \dots, \mathbf{r}_{N-1,N}$, with the result that the contributing portion of ∇_i is

$$\nabla_i = \sum_{j \neq i} \nabla_{ij}. \quad (13)$$

Here we have used the fact that $\nabla_{ji} = -\nabla_{ij}$, and have kept in mind that the \mathbf{r}_{ij} on which the ∇_{ij} act are treated as formally independent, so that, for example, $\nabla_{ij}f(\mathbf{r}_{ik}) = 0$. We can then form each ∇_i^2 and bring T to the form

$$T = -\frac{1}{2} \sum_{ij, i < j} \frac{1}{\mu_{ij}} \nabla_{ij}^2 - \sum_i \frac{1}{m_i} \sum_{jk \neq i, j < k} \nabla_{ij} \cdot \nabla_{ik}, \quad (14)$$

where $\mu_{ij}^{-1} = m_i^{-1} + m_j^{-1}$.

Now, following Frolov and Smith [18], we apply T to wavefunctions Ψ of the form given in equation (3), specializing to the three-body problem because we believe the analysis for the four-body case has not yet been brought to a correspondingly convenient form. Recognizing that Ψ consists of an angular factor $\mathcal{Y}_{LM}^{l'}(\mathbf{r}_{13}, \mathbf{r}_{23})$ and a ‘radial’ factor $\phi(r_{12}, r_{13}, r_{23})$, we apply equation (14) in a more extended form, suppressing for clarity the arguments of \mathcal{Y} and ϕ :

$$\begin{aligned} T\Psi = & - \sum_{i=1,2} \frac{1}{2\mu_{i3}} [(\nabla_{i3}^2 \mathcal{Y}_{LM}^{l'})\phi + 2(\nabla_{i3} \mathcal{Y}_{LM}^{l'}) \cdot \nabla_{i3} \phi] \\ & - \sum_{ij, i < j} \frac{1}{2\mu_{ij}} \mathcal{Y}_{LM}^{l'} \nabla_{ij}^2 \phi - \frac{1}{m_1} [\mathcal{Y}_{LM}^{l'} \nabla_{12} \cdot \nabla_{13} + (\nabla_{13} \mathcal{Y}_{LM}^{l'}) \cdot \nabla_{12}] \phi \\ & - \frac{1}{m_2} [\mathcal{Y}_{LM}^{l'} \nabla_{21} \cdot \nabla_{23} + (\nabla_{23} \mathcal{Y}_{LM}^{l'}) \cdot \nabla_{21}] \phi \\ & - \frac{1}{m_3} [\mathcal{Y}_{LM}^{l'} \nabla_{31} \cdot \nabla_{32} + (\nabla_{31} \mathcal{Y}_{LM}^{l'}) \cdot \nabla_{32} + (\nabla_{32} \mathcal{Y}_{LM}^{l'}) \cdot \nabla_{31} \\ & + (\nabla_{31} \cdot \nabla_{32} \mathcal{Y}_{LM}^{l'})] \phi. \end{aligned} \quad (15)$$

A first step toward simplifying equation (15) is to use the fact that ϕ is a function of only the scalars r_{ij} , so (keeping in mind that $\nabla \cdot \hat{\mathbf{r}}_{ij} = 2/r_{ij}$):

$$\nabla_{ij} \phi = \hat{\mathbf{r}}_{ij} \frac{\partial \phi}{\partial r_{ij}}, \quad (16)$$

$$\nabla_{ij}^2 \phi = \left(\frac{\partial^2}{\partial r_{ij}^2} + \frac{2}{r_{ij}} \frac{\partial}{\partial r_{ij}} \right) \phi. \quad (17)$$

Subexpressions of the form $(\nabla_{ij} \mathcal{Y}_{LM}^{l'}) \cdot \nabla_{\sigma\tau} \phi$ therefore reduce to $(\hat{\mathbf{r}}_{\sigma\tau} \cdot \nabla_{ij} \mathcal{Y}_{LM}^{l'}) (\partial \phi / \partial r_{\sigma\tau})$. We also note, as discussed in Appendix B, that

$$\nabla_{13}^2 \mathcal{Y}_{LM}^{l'} = \nabla_{23}^2 \mathcal{Y}_{LM}^{l'} = \nabla_{31} \cdot \nabla_{32} \mathcal{Y}_{LM}^{l'} = 0, \quad (18)$$

the last equality holding because $l + l' \leq L + 1$. Using the notational convention that in a sum over i , unsummed indices j and k represent in any order the other members of 1, 2, 3, the result of these simplifications of

equation (15) takes the form

$$\begin{aligned}
T\Psi = & - \sum_{ij, i < j} \frac{1}{2\mu_{ij}} \mathcal{Y}_{LM}^{l'l'} \left(\frac{\partial^2 \phi}{\partial r_{ij}^2} + \frac{2}{r_{ij}} \frac{\partial \phi}{\partial r_{ij}} \right) \\
& - \sum_i \frac{1}{m_i} (\hat{\mathbf{r}}_{ij} \cdot \hat{\mathbf{r}}_{ik}) \mathcal{Y}_{LM}^{l'l'} \frac{\partial^2 \phi}{\partial r_{ij} \partial r_{ik}} - \frac{1}{m_1} (\hat{\mathbf{r}}_{12} \cdot \nabla_{13} \mathcal{Y}_{LM}^{l'l'}) \frac{\partial \phi}{\partial r_{12}} \\
& - \frac{1}{m_2} (\hat{\mathbf{r}}_{21} \cdot \nabla_{23} \mathcal{Y}_{LM}^{l'l'}) \frac{\partial \phi}{\partial r_{21}} - \sum_{i=1,2} \frac{1}{\mu_{i3}} (\hat{\mathbf{r}}_{i3} \cdot \nabla_{i3} \mathcal{Y}_{LM}^{l'l'}) \frac{\partial \phi}{\partial r_{i3}} \\
& - \frac{1}{m_3} \left[(\hat{\mathbf{r}}_{31} \cdot \nabla_{32} \mathcal{Y}_{LM}^{l'l'}) \frac{\partial \phi}{\partial r_{31}} + (\hat{\mathbf{r}}_{32} \cdot \nabla_{31} \mathcal{Y}_{LM}^{l'l'}) \frac{\partial \phi}{\partial r_{32}} \right]. \tag{19}
\end{aligned}$$

We now make further simplifications based on the following differential properties of the $\mathcal{Y}_{LM}^{l'l'}$ [18,20], which are also discussed in Appendix B:

$$\hat{\mathbf{r}}_{13} \cdot \nabla_{13} \mathcal{Y}_{LM}^{l'l'} = \frac{l \mathcal{Y}_{LM}^{l'l'}}{r_{13}}, \tag{20}$$

$$\hat{\mathbf{r}}_{32} \cdot \nabla_{31} \mathcal{Y}_{LM}^{l'l'} = \frac{A_L(l, l') \mathcal{Y}_{LM}^{l-1, l'+1}}{r_{23}}, \tag{21}$$

$$\hat{\mathbf{r}}_{12} \cdot \nabla_{13} \mathcal{Y}_{LM}^{l'l'} = \frac{l \mathcal{Y}_{LM}^{l'l'} - A_L(l, l') \mathcal{Y}_{LM}^{l-1, l'+1}}{r_{12}}. \tag{22}$$

Here

$$A_L(l, l') = \left[\frac{(L - l')(L - l + 1)(2l + 1)}{2l' + 3} \right]^{1/2}. \tag{23}$$

Finally, we observe that the quantity $\hat{\mathbf{r}}_{ij} \cdot \hat{\mathbf{r}}_{ik}$ is the cosine of the angle between $\hat{\mathbf{r}}_{ij}$ and $\hat{\mathbf{r}}_{ik}$ and has been denoted $\cos \Theta_{ijk}$. It is a function only of r_{ij} , r_{ik} , and r_{jk} :

$$\hat{\mathbf{r}}_{ij} \cdot \hat{\mathbf{r}}_{ik} = \cos \Theta_{ijk} = \frac{r_{ij}^2 + r_{ik}^2 - r_{jk}^2}{2r_{ij}r_{ik}}. \tag{24}$$

After the use of equations (20)–(22) and similar relations obtained therefrom by interchanging indices ‘1’ and ‘2’ and at the same time

interchanging l and l' , we reach

$$\begin{aligned}
 T\Psi = & - \sum_{ij, i < j} \frac{1}{2\mu_{ij}} \mathcal{Y}_{LM}^{l'l'} \left(\frac{\partial^2 \phi}{\partial r_{ij}^2} + \frac{2}{r_{ij}} \frac{\partial \phi}{\partial r_{ij}} \right) - \sum_i \frac{1}{m_i} \cos \Theta_{ijk} \mathcal{Y}_{LM}^{l'l'} \frac{\partial^2 \phi}{\partial r_{ij} \partial r_{ik}} \\
 & - \left[\left(\frac{l}{m_1} + \frac{l'}{m_2} \right) \mathcal{Y}_{LM}^{l'l'} - \frac{A_L(l, l') \mathcal{Y}_{LM}^{l'-1, l'+1}}{m_1} - \frac{A_L(l', l) \mathcal{Y}_{LM}^{l+1, l'-1}}{m_2} \right] \\
 & \times \frac{1}{r_{12}} \frac{\partial \phi}{\partial r_{12}} - \left[\frac{l \mathcal{Y}_{LM}^{l'l'}}{\mu_{13}} + \frac{A_L(l', l) \mathcal{Y}_{LM}^{l+1, l'-1}}{m_3} \right] \frac{1}{r_{13}} \frac{\partial \phi}{\partial r_{13}} \\
 & - \left[\frac{l' \mathcal{Y}_{LM}^{l'l'}}{\mu_{23}} + \frac{A_L(l, l') \mathcal{Y}_{LM}^{l'-1, l'+1}}{m_3} \right] \frac{1}{r_{23}} \frac{\partial \phi}{\partial r_{23}}. \tag{25}
 \end{aligned}$$

If we introduce operators L^{-+} and L^{+-} which operate only on the angular functions and satisfy

$$L^{-+} \mathcal{Y}_{LM}^{l'l'} = A_L(l, l') \mathcal{Y}_{LM}^{l'-1, l'+1}, \tag{26}$$

$$L^{+-} \mathcal{Y}_{LM}^{l'l'} = A_L(l', l) \mathcal{Y}_{LM}^{l+1, l'-1}, \tag{27}$$

the operator equation equivalent to equation (25) (for application to wavefunctions with $\mathcal{Y}_{LM}^{l'l'}$ angular parts) can be written

$$\begin{aligned}
 T = & - \frac{1}{2} \sum_i \frac{1}{m_i} \sum_{j \neq i} \left[\frac{\partial^2}{\partial r_{ij}^2} + \frac{2}{r_{ij}} \frac{\partial}{\partial r_{ij}} + \sum_{k, k \neq i, j} \cos \Theta_{ijk} \frac{\partial^2}{\partial r_{ij} \partial r_{ik}} \right] \\
 & - \left(\frac{l}{\mu_{13}} + \frac{L^{+-}}{m_3} \right) \frac{1}{r_{13}} \frac{\partial}{\partial r_{13}} - \left(\frac{l'}{\mu_{23}} + \frac{L^{-+}}{m_3} \right) \frac{1}{r_{23}} \frac{\partial}{\partial r_{23}} \\
 & - \left(\frac{l - L^{-+}}{m_1} + \frac{l' - L^{+-}}{m_2} \right) \frac{1}{r_{12}} \frac{\partial}{\partial r_{12}}. \tag{28}
 \end{aligned}$$

The first term of equation (28) is the only part of T that contributes for S states. Looking at the remainder of the equation, we see that the presence of the operators L^{+-} and L^{-+} shows that l and l' are not individually good quantum numbers. However, the value of $l+l'$ is conserved under

application of T , indicative of the fact that the parity of the wavefunction is conserved. Wavefunctions with $l+l'=L$ are referred to as having ‘usual parity’; those with $l+l'=L+1$ are said to have ‘unusual parity’.

We close this section by observing that for S states, the first term of equation (28) is a correct description of the contributing part of T for systems with any number of particles, N . In that case, the i summation is from 1 to N , and the remaining summations are over all index values subject to the indicated restrictions and consistent with the system size.

4. MATRIX ELEMENTS

We consider in this section the matrix elements arising from the use of wavefunctions introduced in earlier sections of this paper, under the assumption that the integrations are to be carried out in a coordinate system that explicitly includes all the interparticle distances r_{ij} . For spherically symmetric states, the integration over the independent angular coordinates is trivial and need not be considered further. However, for states with $L \neq 0$, it will be necessary to perform a nontrivial integration over the three Euler angles describing the overall orientation. We consider angular functions of the type $\mathcal{Y}_{LM}^{l'l'}(\mathbf{r}_{13}, \mathbf{r}_{23})$. The integration is to be carried out with fixed values of the internal coordinates r_{ij} , which cause $\hat{\mathbf{r}}_{13}$ and $\hat{\mathbf{r}}_{23}$ not to be completely independent. Drake [21] has given formulas for general angular integrals. However, for those arising for the nonrelativistic Hamiltonian the necessary results can be obtained by a procedure far less involved than that employed by Drake.

The angular integral, which we designate I_L , is over the directions of $\hat{\mathbf{r}}_{13}$ and the azimuthal angle χ locating $\hat{\mathbf{r}}_{12}$ relative to an axis directed along $\hat{\mathbf{r}}_{13}$. Therefore, we consider

$$\begin{aligned}
 I_L(l, l', \lambda, \lambda') &= \int d\hat{\mathbf{r}}_{13} d\chi [\mathcal{Y}_{LM}^{l'l'}(\mathbf{r}_{13}, \mathbf{r}_{23})]^* \mathcal{Y}_{LM}^{\lambda\lambda'}(\mathbf{r}_{13}, \mathbf{r}_{23}) \\
 &= (2L+1) r_{13}^{l+\lambda} r_{23}^{l'+\lambda'} \sum_{m\mu} \begin{pmatrix} l & l' & L \\ m & M-m & -M \end{pmatrix} \\
 &\quad \times \begin{pmatrix} \lambda & \lambda' & L \\ \mu & M-\mu & -M \end{pmatrix} (-1)^{l'+\lambda'-l-\lambda} \int d\hat{\mathbf{r}}_{13} d\chi \\
 &\quad \times Y_{lm}^*(\hat{\mathbf{r}}_{13}) Y_{\lambda\mu}(\hat{\mathbf{r}}_{13}) Y_{l',M-m}^*(\hat{\mathbf{r}}_{23}) Y_{\lambda',M-\mu}(\hat{\mathbf{r}}_{23}). \quad (29)
 \end{aligned}$$

The final member of equation (29) is obtained by inserting equation (4) for $\mathcal{Y}_{LM}^{l'l'}$ and $\mathcal{Y}_{LM}^{\lambda\lambda'}$.

We now combine the two spherical harmonics of $\hat{\mathbf{r}}_{13}$, and also those of $\hat{\mathbf{r}}_{23}$, by invoking equations (A2) and (A3). We simplify the sign factors using the fact that $l + \lambda + \Lambda$ and $l' + \lambda' + \Lambda'$ are even, and, following Drake [19], we write (l, m, n, \dots) as an abbreviation for $(2l + 1)(2m + 1)(2n + 1) \dots$. The result is

$$\begin{aligned} Y_{lm}^*(\hat{\mathbf{r}}_{13}) Y_{\lambda\mu}(\hat{\mathbf{r}}_{13}) &= \sum_{\Lambda} (-1)^{\Lambda+\mu} \left[\frac{(l, \lambda, \Lambda)}{4\pi} \right]^{1/2} \begin{pmatrix} l & \lambda & \Lambda \\ 0 & 0 & 0 \end{pmatrix} \\ &\quad \times \begin{pmatrix} l & \lambda & \Lambda \\ -m & \mu & m - \mu \end{pmatrix} Y_{\Lambda, \mu-m}(\hat{\mathbf{r}}_{13}), \end{aligned} \quad (30)$$

$$\begin{aligned} Y_{l'M-m}^*(\hat{\mathbf{r}}_{23}) Y_{\lambda'M-\mu}(\hat{\mathbf{r}}_{23}) &= \sum_{\Lambda'} (-1)^{\Lambda'+M-m} \left[\frac{(l', \lambda', \Lambda')}{4\pi} \right]^{1/2} \begin{pmatrix} l' & \lambda' & \Lambda' \\ 0 & 0 & 0 \end{pmatrix} \\ &\quad \times \begin{pmatrix} l' & \lambda' & \Lambda' \\ m - M & M - \mu & \mu - m \end{pmatrix} Y_{\Lambda', \mu-m}^*(\hat{\mathbf{r}}_{23}). \end{aligned} \quad (31)$$

We next perform a rotational transformation to write $Y_{\Lambda', \mu-m}^*(\hat{\mathbf{r}}_{23})$ in a coordinate system whose polar axis is aligned with $\hat{\mathbf{r}}_{13}$. The transformation involves a rotation with Euler angles ϕ_{13} , θ_{13} , γ , with γ arbitrary, and (cf. equation (A5)) corresponds to the equation

$$Y_{\Lambda', \mu-m}^*(\hat{\mathbf{r}}_{23}) = \sum_{\sigma} D_{\mu-m, \sigma}^{\Lambda'}(\phi_{13}, \theta_{13}, 0) Y_{\Lambda' \sigma}^*(\Theta_{312}, \chi). \quad (32)$$

Notice that the θ coordinate of $\hat{\mathbf{r}}_{23}$ in the new system is restricted to the unique value Θ_{312} , and the new ϕ coordinate is the overall rotational coordinate χ .

Substituting equations (30)–(32) into equation (29), we reach

$$\begin{aligned}
 I_L = & (2L+1)r_{13}^{l+\lambda}r_{23}^{l'+\lambda'} \sum_{m\mu\Lambda\Lambda'\sigma} (-1)^{\Lambda+\Lambda'+m+\mu+M} \frac{(l, \lambda, l', \lambda', \Lambda, \Lambda')^{1/2}}{4\pi} \\
 & \times \begin{pmatrix} l & l' & L \\ m & M-m & -M \end{pmatrix} \begin{pmatrix} \lambda & \lambda' & L \\ \mu & M-\mu & -M \end{pmatrix} \begin{pmatrix} l & \lambda & \Lambda \\ 0 & 0 & 0 \end{pmatrix} \\
 & \times \begin{pmatrix} l & \lambda & \Lambda \\ -m & \mu & m-\mu \end{pmatrix} \begin{pmatrix} l' & \lambda' & \Lambda' \\ 0 & 0 & 0 \end{pmatrix} \begin{pmatrix} l' & \lambda' & \Lambda' \\ m-M & M-\mu & \mu-m \end{pmatrix} \\
 & \times \int d\hat{\mathbf{r}}_{13} Y_{\Lambda, \mu-m}(\hat{\mathbf{r}}_{13}) D_{\mu-m, \sigma}^{\Lambda'}(\phi_{13}, \theta_{13}, 0) \int d\chi Y_{\Lambda' \sigma}^*(\Theta_{312}, \chi). \quad (33)
 \end{aligned}$$

We can now integrate over χ , obtaining a zero result unless $\sigma = 0$:

$$\int_0^{2\pi} d\chi Y_{\Lambda' \sigma}^*(\Theta_{312}, \chi) = 2\pi \left(\frac{2\Lambda' + 1}{4\pi} \right)^{1/2} P_{\Lambda'}(\cos \Theta_{312}) \delta_{\sigma 0}. \quad (34)$$

Then, from equation (A6), we have

$$D_{\mu-m, 0}^{\Lambda'}(\phi_{13}, \theta_{13}, 0) = \left(\frac{4\pi}{2\Lambda' + 1} \right)^{1/2} Y_{\Lambda', \mu-m}^*(\hat{\mathbf{r}}_{13}), \quad (35)$$

and the $\hat{\mathbf{r}}_{13}$ integration reduces to

$$\int d\hat{\mathbf{r}}_{13} Y_{\Lambda, \mu-m}(\hat{\mathbf{r}}_{13}) D_{\mu-m, 0}^{\Lambda'}(\phi_{13}, \theta_{13}, 0) = \left(\frac{4\pi}{2\Lambda + 1} \right)^{1/2} \delta_{\Lambda \Lambda'}. \quad (36)$$

Inserting equations (34) and (36) into equation (33), and invoking the identity given in equation (A7), we reach the final result

$$\begin{aligned}
 I_L(l, l', \lambda, \lambda') = & [(2l+1)(2l'+1)(2\lambda+1)(2\lambda'+1)]^{1/2} \\
 & \times r_{13}^{l+\lambda} r_{23}^{l'+\lambda'} (-1)^{L+l+\lambda} \sum_{\Lambda} \frac{2\Lambda+1}{2} \begin{pmatrix} l & \lambda & \Lambda \\ 0 & 0 & 0 \end{pmatrix} \\
 & \times \begin{pmatrix} l' & \lambda' & \Lambda \\ 0 & 0 & 0 \end{pmatrix} \left\{ \begin{matrix} \lambda & \lambda' & L \\ l' & l & \Lambda \end{matrix} \right\} P_{\Lambda}(\cos \Theta_{312}). \quad (37)
 \end{aligned}$$

The quantity of the form

$$\begin{Bmatrix} a & b & c \\ d & e & f \end{Bmatrix}$$

is a Wigner 6- j symbol [17]. Equation (37) can be seen to be in agreement with the similar equation of Frolov and Smith [18] (their equation (15)), because $(-1)^{L+l+\lambda} = (-1)^{L+\Lambda}$. We also note that this result is, as it must be, independent of M , and that the conditions for nonvanishing of the 3- j symbols cause I_L to vanish unless $l + l'$ and $\lambda + \lambda'$ are either both even or both odd (thereby confirming the conservation of parity).

When complete matrix elements of the type $\langle \mathcal{Y}_{LM}^{\mu} \phi | H | \mathcal{Y}_{LM}^{\lambda \lambda'} \phi' \rangle$ are evaluated, with H any operator relevant to the computation, each term of the result will contain one I_L , and therewith a Legendre polynomial in the radial function $P_{\Lambda}(\cos \Theta_{312})$ and powers of r_{13} and r_{23} . The net result is a need for integrals containing powers of the r_{ij} multiplying the radial functions ϕ and ϕ' .

For three-particle systems, the volume element for integration over the interparticle coordinates is $d\tau = r_{12}r_{13}r_{23} dr_{12} dr_{13} dr_{23}$, so if the radial functions ϕ and ϕ' are separable in the r_{ij} , the matrix element can be written in terms of products of single-particle integrals. These integrals, however, are linked because their limits of integration are not independent; r_{12} , r_{13} , and r_{23} must satisfy a triangular condition, which may be written $|r_{13} - r_{23}| \leq r_{12} \leq r_{13} + r_{23}$. Illustrating for the exponential basis of equation (9), a straightforward approach leads to integrals of the form

$$\int_0^{\infty} dr_{13} r_{13}^k e^{-\alpha_{13}r_{13}} \int_0^{\infty} dr_{23} r_{23}^{k'} e^{-\alpha_{23}r_{23}} \int_{|r_{13}-r_{23}|}^{r_{13}+r_{23}} dr_{12} r_{12}^{k''} e^{-\alpha_{12}r_{12}}. \quad (38)$$

Because the volume element contributes a factor $r_{12}r_{13}r_{23}$ to the integrand, all the integrals arising from the kinetic and potential energy will have nonnegative values of k , k' , and k'' , and these integrals will be simple to evaluate.

Although the linkage of the integration limits does not cause serious problems for the function used for illustrative purposes in equation (38), a number of workers have proposed methods for making the integrations completely independent – a virtue if it is intended to use a more general basis or create orthogonality relations among the basis functions. One way to unlink the variables, used by James and Coolidge [2] and Pekeris [3], is to use perimetric coordinates ($r_{13} + r_{23} - r_{12}$ and cyclic index permutations thereof), in terms of which the integration limits all become $(0, \infty)$. Another possibility, used by Goldman [22], is to define three new variables u , v , w according to $u = \max(r_{13}, r_{23})$, $v = \min(r_{13}, r_{23})/u$, $w = (r_{12} - u)/uv$, with respective ranges $(0, \infty)$, $(0, 1)$, and $(1, -1)$. A variant of this which has seen

significant use in problems with two heavy particles (e.g., H_2^+) employs coordinates R, ξ, η , with $R = r_{12}$, $\xi = (r_{13} + r_{23})/R$, $\eta = (r_{13} - r_{23})/R$, with respective ranges $(0, \infty)$, $(1, \infty)$, $(-1, 1)$. The Jacobians of the transformations to these new coordinate systems retain factors that cancel the quantities $1/r_{ij}$ that enter the Hamiltonian, but Goldman's coordinates lose some flexibility with respect to the description of the exponential decay that must characterize exact wavefunctions.

The approaches outlined in the preceding paragraph are interesting and have been exploited successfully, but the bulk of the recent work on three-body systems has used methods based on equation (38), probably because improvements in computer hardware and software have caused less of a premium to be placed on ingenious, but complicated methods.

Extending now to four-body systems, one could, in principle, obtain formulas for general angular states based on the generalization of \mathcal{Y} , to $\mathcal{Y}_{LM}^{ll''}(\mathbf{r}_{14}, \mathbf{r}_{24}, \mathbf{r}_{34})$, or could use the currently available reduction of the angular integrals given by Yan and Drake [19]. At this point most of the work that has been reported is for S states, for which T is given by the first term of equation (28). In any case, four-body matrix elements reduce to integrals over the six radial variables r_{ij} . However, integration over these variables is far more complicated than for three-body systems, as indicated by the following general formula [23]:

$$\int f(r_{12}, r_{13}, r_{14}, r_{23}, r_{24}, r_{34}) d\tau = \int \frac{f(r_{12}, r_{13}, r_{14}, r_{23}, r_{24}, r_{34}) r_{12} r_{13} r_{14} r_{23} r_{24} r_{34} dr_{12} dr_{13} dr_{14} dr_{23} dr_{24} dr_{34}}{[(r_{12}^2 - r_{34}^2)(r_{13}^2 - r_{24}^2)(r_{14}^2 - r_{23}^2) - R_6]^{1/2}}. \quad (39)$$

Here R_6 is the following homogeneous sixth-order polynomial in the r_{ij} :

$$\begin{aligned} R_6 = & r_{12}^2 r_{13}^2 r_{14}^2 + r_{12}^2 r_{23}^2 r_{24}^2 + r_{13}^2 r_{23}^2 r_{34}^2 + r_{14}^2 r_{24}^2 r_{34}^2 + r_{12}^2 r_{34}^2 (r_{12}^2 + r_{34}^2 - r_{13}^2 \\ & - r_{14}^2 - r_{23}^2 - r_{24}^2) + r_{13}^2 r_{24}^2 (r_{13}^2 + r_{24}^2 - r_{12}^2 - r_{14}^2 - r_{23}^2 - r_{34}^2) \\ & + r_{14}^2 r_{23}^2 (r_{14}^2 + r_{23}^2 - r_{12}^2 - r_{13}^2 - r_{24}^2 - r_{34}^2). \end{aligned} \quad (40)$$

It is apparent from equation (39) that matrix elements in four-body systems will be far more complicated than their three-body analogs. These radial matrix elements will be the subject of Section 5.

Extension to more than four particles would be expected to generate even more complexity in the volume element, and would be subject to the additional difficulty that the number of distinct r_{ij} then exceeds the number of

internal degrees of freedom. It seems unlikely that methods dependent on the explicit inclusion of all the r_{ij} will prove practical for such systems.

5. FOUR-BODY EXPONENTIALLY CORRELATED WAVEFUNCTIONS

The complications associated with integrations over all the interparticle distances of a four-body system have caused that approach to be used only when all the interparticle distances occur in exponential functions. Integrals of that kind were thought to be intractable until Fromm and Hill [24] presented a closed analytical formula for the basic four-body integral

$$I_0 = \int d\tau \frac{\exp(-\alpha_{12}r_{12} - \alpha_{13}r_{13} - \alpha_{14}r_{14} - \alpha_{23}r_{23} - \alpha_{24}r_{24} - \alpha_{34}r_{34})}{r_{12}r_{13}r_{14}r_{23}r_{24}r_{34}}, \quad (41)$$

where $d\tau$ is the volume element in the space of the r_{ij} (cf. equation (39)), and the integration is over that entire space. By differentiation of this basic integral with respect to its parameters it is possible to insert arbitrary powers of the r_{ij} into the integrand, and all the integrals needed for nonrelativistic energy computations can be found in this way. A few years later, Remiddi [25] reported closed formulas for a special case of I_0 in which the parameters α_{12} , α_{13} , and α_{23} were set to zero. Remiddi also provided analytical formulas for the derivatives with respect to these zero α_{ij} , so that arbitrary powers of all the r_{ij} could still be reached.

Fromm and Hill's paper, while a sophisticated and almost miraculous application of complex variable theory, produced a formula that exhibited two problems from a practical viewpoint. It contained the dilogarithm function, Li_2 , and squares of logarithmic functions, in combinations that were multiple-valued with respect to both their real and imaginary parts, and no simple recipe was provided to indicate which branches of these functions should be used. Fromm and Hill's provisional solution was to start from a point in the parameter space where the proper branch was known from asymptotic considerations, and then move in steps to the required parameter values. This procedure was referred to as 'branch tracking'.

The second problem was that individual terms of the formula became singular for physically relevant parameter values, with the singularities in the various terms expected on general grounds to combine into a nonsingular result. But there was no analysis of the singularity cancellation, and numerical calculation near the termwise singularities became seriously unstable.

In 1997 the present author addressed these problems [26], showing how a modified definition of the multiply valued functions could eliminate the need

for branch tracking. He also discussed the formal cancellation of the termwise singularities and showed how to obtain stable results in their neighborhoods. Further detail in this area was provided by a recent contribution in collaboration with Smith and Frolov [23], to which the reader is referred for a more complete discussion.

The most extensive use of the analytical formulas for four-body wavefunctions has been by Rebane and associates; in 1992 Rebane and Yusupov [27] presented a preliminary study on model problems; there followed a detailed study of the positronium molecule Ps_2 ($e^+e^-e^+e^-$) by Rebane *et al.* [28] and an application to a number of four-particle mesomolecules by Zotev and Rebane [29]. These authors then refined the branch-tracking procedure so as to make it applicable to complex parameter sets [30,31]. At this point, the use of multiconfiguration exponential wavefunctions has produced results of a quality similar to that from more extensive Gaussian expansions, but with what appears to be a comparable amount of effort. There are at present insufficient data to indicate whether the exponential wavefunctions have significant superiority over the Gaussian functions for short-range (e.g., delta-function) properties.

Looking next at technical details in the calculations, we note that to obtain potential-energy and overlap matrix elements from the basic integral I_0 requires 5- and 6-fold differentiation of rather complicated functional forms, and it would seem that additional derivatives would be needed to obtain the integrals involving $\cos \Theta_{ijk}$ that are needed to evaluate the kinetic energy. This problem was addressed by Rebane [32], who showed that in a basis consisting of exponential functions, all the $\cos \Theta_{ijk}$ integrals could be written as linear combinations of overlap and potential-energy integrals. Rebane's demonstration was rather complicated and relied on the use of several model Hamiltonians; we recently offered a much simpler derivation [23]. Letting $|\alpha\rangle$ stand for a radial function of the form given in equation (10), and $|\beta\rangle$ stand for a similar function in which the parameters α_{ij} are replaced by the corresponding β_{ij} , the central result (for the four-particle systems under discussion) is

$$\langle \alpha | \cos \Theta_{ijk} | \beta \rangle = \frac{(\alpha_{ij} + \beta_{ij})s_{ij} + (\alpha_{ik} + \beta_{ik})s_{ik} - (\alpha_{ip} + \beta_{ip})s_{ip}}{(\alpha_{ij} + \beta_{ij})(\alpha_{ik} + \beta_{ik})}, \quad (42)$$

where the index p has the unique value distinct from those of i, j, k , and

$$s_{ij} = \left\langle \alpha \left| \frac{1}{r_{ij}} \right| \beta \right\rangle - \frac{\alpha_{ij} + \beta_{ij}}{2} \langle \beta | \alpha \rangle. \quad (43)$$

We have one additional observation to add at this time. If wavefunctions of exponential type are used for other than S states, $\cos \Theta$ integrals will occur with powers of the various r_{ij} inserted in their integrands. Such integrals can be generated by differentiation of equation (42) with respect to

the corresponding α_{ij} . The differentiation must take into account not only the explicit appearances of α_{ij} , but also its occurrence in the s_{ij} , both as an explicit coefficient and in the constituent integrals. The derivatives of the constituent integrals will simply be overlap and potential-energy integrals for wavefunctions containing powers of the r_{ij} , so the advantage of not requiring specific development of the $\cos \Theta$ integrals will be maintained.

6. THREE-BODY EXPONENTIALLY CORRELATED WAVEFUNCTIONS

In contrast to the four-body problem, real exponential wavefunctions in the interparticle coordinates led to readily evaluated integrals for three-body systems, and that fact was exploited in the context of extensive configuration interaction for adiabatic systems as long ago as 1977 by Thakkar and Smith [12]. Starting in 1987, this method was also applied to nonadiabatic systems by Petelenz and Smith [33,34], and to many adiabatic and nonadiabatic systems by Frolov, both alone [35,36] and in collaboration with Thakkar [37] and with Smith [38].

In 1990, Rebane and Yusupov [39] pointed out that exponential wavefunctions with complex parameters would lead to no computational problems beyond those encountered with real functions, and shortly thereafter demonstrated [40] that this increased flexibility was particularly valuable for nonadiabatic calculations on systems with two massive particles (e.g., H_2^+ and isotopomers). This line of investigation was also pursued by Frolov and Smith [41], and was used, starting in 1998, in a number of contributions by Frolov [42–48], who obtained extremely accurate results for a number of systems ranging from conventional and muonic molecular ions to highly nonadiabatic quasimolecules such as $\text{pp}\mu$ and less symmetric analogs. An important component of Frolov's work was the avoidance of numerical instabilities by using an arbitrary-precision computation package produced by Bailey [49,50]. In 2000, Korobov [51] reported extremely precise calculations on the He ground state and several other three-body systems. It is unfortunate that Korobov did not make appropriate references to the extensive earlier work.

We add here one technical note about the matrix element evaluation. Evaluation of the kinetic energy involves the quantities $\langle \alpha | \cos \Theta_{ijk} | \beta \rangle$; as for the four-body problem, these matrix elements can be related to overlap and potential-energy integrals. The line of reasoning that led to equation (42) yields the following formula for the three-body problem:

$$\langle \alpha | \cos \Theta_{ijk} | \beta \rangle = (\alpha_{ik} + \beta_{ik})^{-1} \left(2 \left\langle \alpha \left| \frac{1}{r_{ij}} \right| \beta \right\rangle - (\alpha_{ij} + \beta_{ij}) \langle \beta | \alpha \rangle \right). \quad (44)$$

Here i, j, k are 1, 2, 3 in any order. The fact that Θ_{ijk} and Θ_{ikj} are equal enables equation (44) also to be a starting point for the development of additional relations connecting overlap and potential-energy integrals.

7. CORRELATED GAUSSIAN WAVEFUNCTIONS

Although correlated Gaussian functions do not have appropriate behavior either in the short or long-range limits, their convenient analytical properties facilitate their use in massive configuration–interaction computations. The initial, moderate-accuracy computations on H_2 reported in 1990 by Preiskorn *et al.* [13] and in 1991 by Cencek *et al.* [52] were followed up in 1993 by higher-precision computations on Ps_2 by Kinghorn and Poshusta [53] and Kozłowski and Adamowicz [54]. Soon thereafter, Frolov and Smith [55,56] presented Ps_2 computations of slightly higher accuracy, also reporting results on a large number of other four-body systems of the symmetric generic type $X^+X^+Y^-Y^-$. This symmetry is important to the calculations because the ground-state wavefunction will have charge–mass-permutation (CMP) invariance. A small additional gain in accuracy for the ground-state energy of Ps_2 has more recently been reported by Usukura *et al.* [57]. These authors also provided extensive data on the convergence of various properties. The delta functions (relevant for annihilation calculations) seem stable to 2–3 significant figures.

A few correlated Gaussian calculations have been carried out on systems with more than four particles. On example is the recent work of Komasa *et al.* [58] on beryllium isoelectronic ions.

8. HYLLERAAS METHODS

This section refers to methods based on wavefunctions of the types illustrated in equation (7) or (8). Although some work has been carried out on nonseparable functions of the r_{ij} [59,60], we focus here on the simpler basis functions that correspond to the majority of the recent work. We describe the wavefunctions now under discussion as orbitals centered on particle N , multiplied by polynomial correlation factors involving the r_{ij} , where i and j are both less than N . It has been usual to use spherical coordinates for the orbitals (in our present notation with coordinates \mathbf{r}_{iN}), and to expand the correlation factors in terms of the orbital coordinates. This approach makes it unnecessary to analyze the kinetic energy as was done earlier in this work, as each term in the expansion of the r_{ij} is just a conventional orbital product.

For the S states of three-body systems, the Hylleraas-method correlation factor r_{12}^k leads to integrals that can be easily evaluated in r_{ij} coordinates without the need to introduce an expansion. A recent paper by Drake *et al.* [61]

shows that this approach can lead to extremely high accuracy for both adiabatic and nonadiabatic systems.

For systems with four or more particles, expansions of the correlation factors are generally employed. The expansion most frequently used is that of Sack [10]:

$$r_{ij}^k = \sum_{l=0}^{\infty} R_{kl}(r_{iN}, r_{jN}) P_l(\cos \Theta_{Nij}), \quad (45)$$

where the $R_{kl}(r_{iN}, r_{jN})$ are radial functions whose exact form is not needed for the present discussion, and P_l is a Legendre function. The angle Θ_{Nij} has the same meaning as throughout this work; it is the angle between \mathbf{r}_{Ni} and \mathbf{r}_{Nj} .

An alternative to the Sack expansion is the defining equation of the Gegenbauer polynomials,

$$r_{ij}^k = \sum_{l=0}^{\infty} \frac{r_-^l}{r_+^{l-k}} C_l^{(-k/2)}(\cos \Theta_{Nij}), \quad (46)$$

where r_- and r_+ are, respectively, the smaller and larger of r_{iN} and r_{jN} , and $C_l^{(-k/2)}$ is the Gegenbauer polynomial of degree l and order $-k/2$ [62]. The Gegenbauer expansion depends on r_{iN} and r_{jN} in a far simpler way than the Sack expansion, but has been sparingly used, probably because the $C_l^{(-k/2)}$ are not orthogonal when integrated over the angular variables of a spherical coordinate system. The potential advantage of the Gegenbauer expansion is the greater systematization it permits for the radial integrals. We illustrate with the four-body integral

$$I_4 = \int r_{12}^k r_{13}^{k'} r_{23}^{k''} r_{14}^j r_{24}^{j'} r_{34}^{j''} \exp(-\alpha_{14} r_{14} - \alpha_{24} r_{24} - \alpha_{34} r_{34}) d\mathbf{r}_{14} d\mathbf{r}_{24} d\mathbf{r}_{34}, \quad (47)$$

which upon insertion of Gegenbauer expansions for r_{12}^k , $r_{13}^{k'}$, and $r_{23}^{k''}$ becomes

$$I_4 = \sum_{l'l''} J_{l'l''}^{kk'k''} K_{l'l''}, \quad (48)$$

where $J_{l'l''}^{kk'k''}$ is an angular integral of definition

$$\begin{aligned} J_{l'l''}^{kk'k''} = & \int C_l^{(-k/2)}(\cos \Theta_{412}) C_{l'}^{(-k'/2)}(\cos \Theta_{413}) C_{l''}^{(-k''/2)} \\ & \times (\cos \Theta_{423}) d\hat{\mathbf{r}}_{14} d\hat{\mathbf{r}}_{24} d\hat{\mathbf{r}}_{34}, \end{aligned} \quad (49)$$

and K is the radial integral

$$K_{ll'l''} = \int_0^\infty dr_{14} \int_0^\infty dr_{24} \int_0^\infty dr_{34} r_{14}^{j+2} r_{24}^{j'+2} r_{34}^{j''+2} \frac{r_{12-}^l}{r_{12+}^{l-k}} \frac{r_{13-}^{l'}}{r_{13+}^{l'-k'}} \frac{r_{23-}^{l''}}{r_{23+}^{l''-k''}} \times \exp(-\alpha_{14}r_{14} - \alpha_{24}r_{24} - \alpha_{34}r_{34}). \quad (50)$$

Here r_{ij-} and r_{ij+} are, respectively, the smaller and larger of r_{i4} and r_{j4} .

The integral $K_{ll'l''}$ is simpler than the corresponding integral derived from the Sack radial functions, and the virtue of the Gegenbauer approach depends upon the efficiency with which $J_{ll'l''}^{kk'k''}$ can be evaluated. The present author has investigated this question for a variety of integrals [63], with the conclusion that any increased difficulty in evaluating the angular integration appears to be more than offset by simplifications in the radial integral. The simple form of $K_{ll'l''}$ also appears to be desirable when designing convergence acceleration procedures (discussed below).

The radial integrals entering Hylleraas-method computations have been well studied. Some recent contributions are those of King and collaborators [64,65], Yan and Drake [19], and Frolov and Smith [66]. Many of the integrals are slowly convergent, and some exhibit numerical instability. One approach to the latter problem is reported by Frolov and Bailey [67], who made calculations using Bailey's arbitrary-precision computation package [49,50]. Another approach, illustrated in recent work by Pelzl *et al.* [68] and in earlier work referred to therein, is to use convergence accelerators to ameliorate the pathologically slow convergence of some integrals. The cited paper compares a number of accelerator methods; the reader is referred to it for details.

An approach that has received relatively little attention is the use of the closed formulas provided by Remiddi [25]. These formulas are considerably simpler than the more general formulas for fully correlated functions [24,26] and are numerically stable. The only recent example of which the author is aware is in a short contribution by Sims and Hagstrom [69] in 2003.

9. OTHER METHODS

There have been a few studies that do not seem to fit into any of the categories thus far identified. Moss [70] has made a number of high-precision nonadiabatic calculations on H_2^+ both by variational methods that specifically include vibrational wavefunctions and by methods based on scattering theory. The same system has also been studied by Ackermann and Shertzer [71] using finite-element methods. Finally, we mention the very precise variational Monte Carlo studies of Ps_2 and its generalization to four-charge systems of type $M^+m^+M^-m^-$ by Bressanini *et al.* [72].

ACKNOWLEDGEMENTS

The author acknowledges stimulating discussions with Professor Vedene Smith and Dr Alexei Frolov of Queen's University, Kingston, Ontario. The work has been supported by the US National Science Foundation, Grant PHY-0303412.

APPENDIX A. ANGULAR MOMENTUM IDENTITIES

The formulas in this section (and those in the main text that derive therefrom) apply only for integer values of the indices, so no distinction is made between, e.g., $(-1)^m$ and $(-1)^{-m}$. These formulas are equivalent to those in the books by Edmonds [17] and Brink and Satchler [73].

Writing in terms of the Wigner 3- j symbols, two spherical harmonics $Y_{lm}(\hat{\mathbf{r}})$ and $Y_{l'm'}(\hat{\mathbf{r}}')$ couple as follows to form a resultant angular momentum eigenfunction of quantum numbers L, M :

$$Y_{LM}(\hat{\mathbf{r}}, \hat{\mathbf{r}}') = (-1)^{l'-l-M} \sqrt{2L+1} \sum_m \begin{pmatrix} l & l' & L \\ m & M-m & -M \end{pmatrix} \times Y_{lm}(\hat{\mathbf{r}}) Y_{l',M-m}(\hat{\mathbf{r}}'). \quad (\text{A1})$$

The 3- j symbols evaluate to real numbers, so equation (A1) continues to be satisfied if each Y is replaced by the corresponding Y^* .

The product of two spherical harmonics of the same argument can be written as a linear combination of harmonics according to the equation

$$Y_{lm}^*(\hat{\mathbf{r}}) Y_{l'm'}(\hat{\mathbf{r}}) = \sum_{\Lambda} (-1)^{m'} \left[\frac{(2l+1)(2l'+1)(2\Lambda+1)}{4\pi} \right]^{1/2} \times \begin{pmatrix} l & l' & \Lambda \\ 0 & 0 & 0 \end{pmatrix} \begin{pmatrix} l & l' & \Lambda \\ m & -m' & m'-m \end{pmatrix} Y_{\Lambda, m'-m}(\hat{\mathbf{r}}). \quad (\text{A2})$$

Complex conjugate signs can be added or removed using the formula

$$Y_{lm}^*(\hat{\mathbf{r}}) = (-1)^m Y_{l,-m}(\hat{\mathbf{r}}). \quad (\text{A3})$$

We define rotation matrices $D_{\sigma m}^l(R)$ for a rotation R of a coordinate system as the quantities satisfying

$$Y_{lm}(\mathbf{R}\hat{\mathbf{r}}) = \sum_{\sigma} D_{\sigma m}^l(R) Y_{l\sigma}(\hat{\mathbf{r}}). \quad (\text{A4})$$

Because $D_{\sigma m}^l$ is unitary, it is also true that

$$Y_{lm}^*(\hat{\mathbf{r}}) = \sum_{\sigma} D_{m\sigma}^l(R) Y_{l\sigma}^*(\mathbf{R}\hat{\mathbf{r}}). \quad (\text{A5})$$

If R corresponds to a rotation described by Euler angles (α, β, γ) , we may write $D_{m\sigma}^l(R)$ as $D_{m\sigma}^l(\alpha, \beta, \gamma)$. We note that a rotation to a coordinate system with polar axis in the direction $\hat{\mathbf{r}} = (\theta, \phi)$ of the unrotated system will have $\alpha = \phi$ and $\beta = \theta$. For such a rotation, D_{m0}^l will have the special value (independent of γ)

$$D_{m0}^l(\phi, \theta, \gamma) = \left(\frac{4\pi}{2l+1} \right)^{1/2} Y_{lm}^*(\hat{\mathbf{r}}). \quad (\text{A6})$$

A formula relating Wigner 3- j and 6- j symbols [73] is the following, where the right hand side may be evaluated for any M in the range $-L \leq M \leq L$:

$$\begin{aligned} \left\{ \begin{matrix} l & l' & L \\ \lambda' & \lambda & \Lambda \end{matrix} \right\} &= \frac{(-1)^{L+l+\lambda}}{2L+1} \sum_{m\mu} (-1)^{M+m+\mu} \begin{pmatrix} l & l' & L \\ m & M-m & -M \end{pmatrix} \\ &\times \begin{pmatrix} \lambda & \lambda' & L \\ \mu & M-\mu & -M \end{pmatrix} \begin{pmatrix} l & \lambda & \Lambda \\ -m & \mu & m-\mu \end{pmatrix} \\ &\times \begin{pmatrix} l' & \lambda' & \Lambda \\ m-M & M-\mu & \mu-m \end{pmatrix}. \end{aligned} \quad (\text{A7})$$

APPENDIX B. DIFFERENTIAL PROPERTIES OF THE $\mathcal{Y}_{LM}^{l'}$

The $\mathcal{Y}_{LM}^{l'}$ are of the form

$$\mathcal{Y}_{LM}^{l'}(\mathbf{r}_{13}, \mathbf{r}_{23}) = \sum_m C_m r_{13}^l Y_{lm}(\hat{\mathbf{r}}_{13}) r_{23}^{l'} Y_{l', M-m}(\hat{\mathbf{r}}_{23}). \quad (\text{B1})$$

Because $r_{13}^l \mathcal{Y}_{lm}(\hat{\mathbf{r}}_{13})$ is, for any m , a solution of the Laplace equation for the variable \mathbf{r}_{13} [74], it is clear that the summation in equation (B1) will also be

a solution, i.e., that

$$\nabla_{13}^2 \mathcal{Y}_{LM}^{l'l'}(\mathbf{r}_{13}, \mathbf{r}_{23}) = 0. \quad (\text{B2})$$

Similar reasoning leads to the companion result $\nabla_{23}^2 \mathcal{Y}_{LM}^{l'l'}(\mathbf{r}_{13}, \mathbf{r}_{23}) = 0$.

From the relation $\hat{\mathbf{r}} \cdot \nabla = \partial/\partial r$, and the fact that the r_{13} dependence of $\mathcal{Y}_{LM}^{l'l'}(\mathbf{r}_{13}, \mathbf{r}_{23})$ is r_{13}^l , we have

$$\hat{\mathbf{r}}_{13} \cdot \nabla_{13} \mathcal{Y}_{LM}^{l'l'}(\mathbf{r}_{13}, \mathbf{r}_{23}) = \frac{l \mathcal{Y}_{LM}^{l'l'}(\mathbf{r}_{13}, \mathbf{r}_{23})}{r_{13}}. \quad (\text{B3})$$

This is equation (20).

The remaining results needed here depend on the fact that l and l' are restricted to values such that $L = l + l'$ or $L = l + l' - 1$. We also note that the operators $\nabla_{31} \cdot \nabla_{32}$ and $\mathbf{r}_{ij} \cdot \nabla_{ik}$ are rotationally invariant so that their application to $\mathcal{Y}_{LM}^{l'l'}(\mathbf{r}_{13}, \mathbf{r}_{23})$ must leave L and M unchanged. Moreover, we may evaluate the action of these operators for the special case $M = L$ and use the fact that the resulting coefficients will be independent of M .

Our starting point, for the case $l + l' = L$, is the equation

$$r^l Y_l(\hat{\mathbf{r}}) = (-1)^l \left(\frac{(2l+1)!!}{4\pi(2l)!!} \right)^{1/2} (x + iy)^l. \quad (\text{B4})$$

Inserting equation (B4) into $\mathcal{Y}_{l+l', l+l'}^{l'l'}$, which consists of only a single term with coefficient unity, and applying $\nabla_{31} \cdot \nabla_{32}$, written in cartesian coordinates, we have

$$\begin{aligned} \nabla_{31} \cdot \nabla_{32} \mathcal{Y}_{l+l', l+l'}^{l'l'}(\mathbf{r}_{13}, \mathbf{r}_{23}) &= \frac{(-1)^{l+l'}}{4\pi} \left(\frac{(2l+1)!!}{(2l)!!} \frac{(2l'+1)!!}{(2l')!!} \right)^{1/2} \\ &\times \left(\frac{\partial^2}{\partial x_{13} \partial x_{23}} + \frac{\partial^2}{\partial y_{13} \partial y_{23}} \right) \\ &\times (x_{13} + iy_{13})^l (x_{23} + iy_{23})^{l'} = 0. \end{aligned} \quad (\text{B5})$$

We next consider the case $l + l' = L + 1$, for which we need also

$$r^l \mathcal{Y}_{l, l-1}(\hat{\mathbf{r}}) = (-1)^{l-1} \left(\frac{(2l+1)!!}{4\pi(2l-2)!!} \right)^{1/2} (x + iy)^{l-1} z. \quad (\text{B6})$$

The expression for $\mathcal{Y}_{LL}^{l'l'}$ now consists of two terms, and is of the form

$$\begin{aligned} & \mathcal{Y}_{l+l'-1, l+l'-1}^{l'l'}(\mathbf{r}_{13}, \mathbf{r}_{23}) \\ &= \frac{l^{1/2} r_{13}^l Y_l(\hat{\mathbf{r}}_{13}) r_{23}^{l'} Y_{l', l'-1}(\hat{\mathbf{r}}_{23}) - l'^{1/2} r_{13}^l Y_{l, l-1}(\hat{\mathbf{r}}_{13}) r_{23}^{l'} Y_{l'l'}(\hat{\mathbf{r}}_{23})}{(l+l')^{1/2}}. \end{aligned} \quad (\text{B7})$$

A process similar to that shown in equation (B5) leads to

$$\nabla_{31} \cdot \nabla_{32} \mathcal{Y}_{l+l'-1, l+l'-1}^{l,l'}(\mathbf{r}_{13}, \mathbf{r}_{23}) = 0, \quad (\text{B8})$$

showing that for all the L values considered here

$$\nabla_{31} \cdot \nabla_{32} \mathcal{Y}_{LM}^{l'l'}(\mathbf{r}_{13}, \mathbf{r}_{23}) = 0. \quad (\text{B9})$$

The extension of this equation to general M is the result given in equation (18).

We continue now to a discussion of $\mathbf{r}_{23} \cdot \nabla_{13} \mathcal{Y}_{LM}^{l'l'}(\mathbf{r}_{13}, \mathbf{r}_{23})$. Again using equation (B4), we have

$$\begin{aligned} \mathbf{r}_{23} \cdot \nabla_{13} \mathcal{Y}_{l+l', l+l'}^{l'l'}(\mathbf{r}_{13}, \mathbf{r}_{23}) &= \frac{(-1)^{l+l'}}{4\pi} \left(\frac{(2l+1)!!}{(2l)!!} \frac{(2l'+1)!!}{(2l')!!} \right)^{1/2} \\ &\quad \times \left(x_{23} \frac{\partial}{\partial x_{13}} + y_{23} \frac{\partial}{\partial y_{13}} \right) (x_{13} + iy_{13})^l (x_{23} + iy_{23})^{l'} \\ &= \frac{(-1)^{l+l'}}{4\pi} \left(\frac{(2l+1)!!}{(2l)!!} \frac{(2l'+1)!!}{(2l')!!} \right)^{1/2} \\ &\quad \times l(x_{13} + iy_{13})^{l-1} (x_{23} + iy_{23})^{l'+1}. \end{aligned} \quad (\text{B10})$$

Comparing with the similar expansion of $\mathcal{Y}_{LM}^{l-1, l'+1}(\mathbf{r}_{13}, \mathbf{r}_{23})$, which also consists of a single term with coefficient unity, we find

$$\mathbf{r}_{23} \cdot \nabla_{13} \mathcal{Y}_{l+l', l+l'}^{l'l'}(\mathbf{r}_{13}, \mathbf{r}_{23}) = \left(\frac{l(l'+1)(2l+1)}{2l'+3} \right)^{1/2} \mathcal{Y}_{l+l'-1, l+l'-1}^{l-1, l'+1}(\mathbf{r}_{13}, \mathbf{r}_{23}). \quad (\text{B11})$$

We next consider the case $l+l' = L+1$. It is elementary, though somewhat tedious, to apply the operator $\mathbf{r}_{23} \cdot \nabla_{31}$ to $\mathcal{Y}_{l+l'-1, l+l'-1}^{l,l'}$, with $\mathbf{r}_{23} \cdot \nabla_{31}$ in cartesian coordinates and all the spherical harmonics written in the forms given in equations (B4) and (B6). Comparing with the analogous form

for $\mathcal{Y}_{l+l'-1, l+l'-1}^{l'-1, l'+1}$, we find

$$\begin{aligned} \mathbf{r}_{23} \cdot \nabla_{13} \mathcal{Y}_{l+l'-1, l+l'-1}^{l'l'}(\mathbf{r}_{13}, \mathbf{r}_{23}) &= \left(\frac{l'(l-1)(2l+1)}{2l'+3} \right)^{1/2} \\ &\times \mathcal{Y}_{l+l'-1, l+l'-1}^{l'-1, l'+1}(\mathbf{r}_{13}, \mathbf{r}_{23}). \end{aligned} \quad (\text{B12})$$

Equations (B11) and (B12) can be brought to a unified notation utilizing the relationships between l , l' , and L . These two equations are consistent with

$$\begin{aligned} \mathbf{r}_{23} \cdot \nabla_{13} \mathcal{Y}_{LM}^{l'l'}(\mathbf{r}_{13}, \mathbf{r}_{23}) &= \left(\frac{(L-l')(L-l+1)(2l+1)}{2l'+3} \right)^{1/2} \\ &\times \mathcal{Y}_{LM}^{l'-1, l'+1}(\mathbf{r}_{13}, \mathbf{r}_{23}). \end{aligned} \quad (\text{B13})$$

The notation in equation (B13) reflects the fact that the derivation for $M=L$ can be extended to general values of M . If we rewrite the LHS of equation (B13) as the equivalent quantity $r_{23} \hat{\mathbf{r}}_{32} \cdot \nabla_{31}$, we obtain equation (21) with $A_L(l, l')$ as given in equation (23).

The only remaining task of this section is to obtain an expression for $\hat{\mathbf{r}}_{12} \cdot \nabla_{13} \mathcal{Y}_{LM}^{l'l'}$. If we write $\mathbf{r}_{12} = \mathbf{r}_{13} - \mathbf{r}_{23}$, the verification of equation (22) is immediate.

REFERENCES

- [1] E. A. Hylleraas, *Z. Phys.*, 1929, **54**, 347.
- [2] H. M. James and A. S. Coolidge, *Phys. Rev.*, 1936, **49**, 688.
- [3] C. L. Pekeris, *Phys. Rev.*, 1958, **112**, 1649.
- [4] J.-L. Calais and P.-O. Löwdin, *J. Mol. Spectrosc.*, 1962, **8**, 203.
- [5] Y. Öhrn and J. Nordling, *Arkiv Fysik*, 1966, **31**, 471.
- [6] S. Larsson, *Phys. Rev.*, 1968, **169**, 49.
- [7] S. Larsson and V. H. Smith, Jr., *Phys. Rev.*, 1969, **178**, 137.
- [8] L. Szász, *J. Chem. Phys.*, 1961, **35**, 1072.
- [9] J. F. Perkins, *J. Chem. Phys.*, 1968, **48**, 1985.
- [10] R. A. Sack, *J. Math. Phys.*, 1964, **5**, 245.
- [11] L. M. Delves and T. Kalotas, *Aust. J. Phys.*, 1968, **21**, 431.
- [12] A. J. Thakkar and V. H. Smith, Jr., *Phys. Rev. A*, 1977, **15**, 1.
- [13] A. Preiskorn, G. C. Lie, D. Frye and E. Clementi, *J. Chem. Phys.*, 1990, **92**, 4941.
- [14] G. W. F. Drake, *Phys. Scr.*, 1999, **T83**, 83.
- [15] F. W. King, *J. Mol. Struct., Theochem*, 1997, **400**, 7.
- [16] C. L. Schwartz, *Phys. Rev.*, 1961, **123**, 1700.
- [17] A. R. Edmonds, *Angular Momentum in Quantum Mechanics*, Princeton University Press, Princeton, NJ, 1960.
- [18] A. M. Frolov and V. H. Smith, Jr., *Phys. Rev. A*, 1996, **53**, 3853.
- [19] Z.-C. Yan and G. W. F. Drake, *J. Phys. B*, 1997, **30**, 4723.
- [20] (a) V. D. Éfros, *Zh. Eksp. Teor. Fiz.*, 1986, **90**, 10; (b) V. D. Éfros, *JETP*, 1986, **63**, 5.
- [21] G. W. F. Drake, *Phys. Rev. A*, 1978, **18**, 820.
- [22] S. P. Goldman, *Phys. Rev. A*, 1998, **57**, R677.

- [23] F. E. Harris, A. M. Frolov and V. H. Smith, Jr., *J. Chem. Phys.*, 2003, **119**, 8833.
- [24] D. M. Fromm and R. N. Hill, *Phys. Rev. A*, 1987, **36**, 1013.
- [25] E. Remiddi, *Phys. Rev. A*, 1991, **44**, 5492, For errata, see Ref. [69].
- [26] F. E. Harris, *Phys. Rev. A*, 1997, **55**, 1820.
- [27] (a) T. K. Rebane and O. N. Yusupov, *Opt. Spektrosk.*, 1992, **73**, 875; (b) T. K. Rebane and O. N. Yusupov, *Opt. Spectrosc.*, 1992, **73**, 523.
- [28] (a) T. K. Rebane, V. S. Zotev and O. N. Yusupov, *Zh. Eksp. Teor. Fiz.*, 1996, **110**, 55; (b) T. K. Rebane, V. S. Zotev and O. N. Yusupov, *JETP*, 1996, **83**, 28.
- [29] (a) V. S. Zotev and T. K. Rebane, *Opt. Spektrosk.*, 1998, **85**, 935; (b) V. S. Zotev and T. K. Rebane, *Opt. Spectrosc.*, 1998, **85**, 856.
- [30] (a) V. S. Zotev and T. K. Rebane, *Yad. Fiz.*, 2000, **63**, 46; (b) V. S. Zotev and T. K. Rebane, *Phys. At. Nucl.*, 2000, **63**, 40.
- [31] V. S. Zotev and T. K. Rebane, *Phys. Rev. A*, 2002, **65**, 062501.
- [32] (a) T. K. Rebane, *Opt. Spektrosk.*, 1993, **75**, 945; (b) T. K. Rebane, *Opt. Spectrosc.*, 1993, **75**, 557.
- [33] P. Petelenz and V. H. Smith, Jr., *Phys. Rev. A*, 1987, **36**, 4078.
- [34] P. Petelenz and V. H. Smith, Jr., *Phys. Rev. A*, 1987, **36**, 5125.
- [35] (a) A. M. Frolov, *Zh. Eksp. Teor. Fiz.*, 1987, **92**, 1959; (b) A. M. Frolov, *JETP*, 1987, **65**, 1100.
- [36] A. M. Frolov, *Phys. Rev. A*, 1999, **60**, 2834.
- [37] A. M. Frolov and A. J. Thakkar, *Phys. Rev. A*, 1992, **46**, 4418.
- [38] A. M. Frolov and V. H. Smith, Jr., *Phys. Rev. A*, 1994, **49**, 3580.
- [39] (a) T. K. Rebane and O. N. Yusupov, *Zh. Eksp. Teor. Fiz.*, 1990, **98**, 1870; (b) T. K. Rebane and O. N. Yusupov, *JETP*, 1990, **71**, 1050.
- [40] (a) V. S. Zotev and T. K. Rebane, *Opt. Spektrosk.*, 1994, **77**, 733; (b) V. S. Zotev and T. K. Rebane, *Opt. Spectrosc.*, 1994, **77**, 654.
- [41] A. M. Frolov and V. H. Smith, Jr., *J. Phys. B*, 1995, **28**, L449.
- [42] A. M. Frolov, *Phys. Rev. A*, 1998, **57**, 2436.
- [43] A. M. Frolov, *Phys. Rev. E*, 2000, **62**, 8740.
- [44] A. M. Frolov, *Phys. Rev. E*, 2001, **64**, 036704.
- [45] A. M. Frolov, *J. Phys. B*, 2002, **35**, L331.
- [46] D. H. Bailey and A. M. Frolov, *J. Phys. B*, 2002, **35**, 4287.
- [47] A. M. Frolov, *Phys. Rev. E*, 2002, **65**, 046705.
- [48] A. M. Frolov, *Phys. Rev. A*, 2003, **67**, 064501.
- [49] D. H. Bailey, *ACM Trans. Math. Software*, 1995, **21**, 379.
- [50] D. H. Bailey, *Comput. Sci. Engng*, 2000, **2**, 24.
- [51] V. I. Korobov, *Phys. Rev. A*, 2000, **61**, 064503.
- [52] W. Cencek, J. Komasa and J. Rychlewski, *J. Chem. Phys.*, 1991, **95**, 2572.
- [53] D. B. Kinghorn and R. D. Poshusta, *Phys. Rev. A*, 1993, **47**, 3671.
- [54] P. M. Kozłowski and L. Adamowicz, *Phys. Rev. A*, 1993, **48**, 1903.
- [55] A. M. Frolov and V. H. Smith, Jr., *J. Phys. B*, 1996, **29**, L433.
- [56] A. M. Frolov and V. H. Smith, Jr., *Phys. Rev. A*, 1997, **55**, 2662.
- [57] J. Usukura, K. Varga and Y. Suzuki, *Phys. Rev. A*, 1998, **58**, 1918.
- [58] J. Komasa, J. Rychlewski and K. Jankowski, *Phys. Rev. A*, 2002, **65**, 042507.
- [59] K. Frankowski and C. L. Pekeris, *Phys. Rev.*, 1966, **146**, 46.
- [60] D. E. Freund, B. D. Huxtable and J. D. Morgan, III, *Phys. Rev. A*, 1996, **54**, 365.
- [61] G. W. F. Drake, M. M. Cassar and R. A. Nistor, *Phys. Rev. A*, 2002, **65**, 054501.
- [62] M. Abramowitz and I. Stegun (eds), *Handbook of Mathematical Functions*, Dover, New York, 1972.
- [63] F. E. Harris, to be published.
- [64] F. W. King, *Phys. Rev. A*, 1991, **44**, 7108.
- [65] F. W. King, K. J. Dykema and A. D. Lund, *Phys. Rev. A*, 1992, **46**, 5406.

- [66] A. M. Frolov and V. H. Smith, Jr., *Int. J. Quantum Chem.*, 1997, **63**, 269.
- [67] A. M. Frolov and D. H. Bailey, *J. Phys. B*, 2003, **36**, 1857.
- [68] J. Pelzl, G. J. Smethells and F. W. King, *Phys. Rev. E*, 2002, **65**, 036707.
- [69] J. S. Sims and S. A. Hagstrom, *Phys. Rev. A*, 2003, **68**, 016501, errata: **68**, 059903(E).
- [70] R. E. Moss, *J. Phys. B*, 1999, **32**, L89.
- [71] J. Ackermann and J. Shertzer, *Phys. Rev. A*, 1996, **54**, 365.
- [72] D. Bressanini, M. Mella and G. Morosi, *Phys. Rev. A*, 1997, **55**, 200.
- [73] D. M. Brink and G. R. Satchler, *Angular Momentum*, 2nd edn., Clarendon Press, Oxford, 1968.
- [74] See, for example, G. B. Arfken and H. J. Weber, *Mathematical Methods for Physicists*, 5th edn., Harcourt, San Diego, 2001, p. 512.

This page intentionally left blank

Atomic Densities, Polarizabilities, and Natural Orbitals Derived from Generalized Sturmian Calculations

John Avery,¹ James Avery,¹ Vincenzo Aquilanti²
and Andrea Caligiana²

¹*Departments of Chemistry and Computer Science, University of Copenhagen,
Copenhagen, Denmark*

²*Department of Chemistry, University of Perugia, Perugia, Italy*

Abstract

The generalized Sturmian method for atomic and molecular electronic structure calculations is a direct configuration interaction method in which the configurations are chosen to be isoenergetic solutions of an approximate N -electron Schrödinger equation with a weighted potential, $\beta_\nu V_0$. The weighting factors β_ν are especially chosen so that all the configurations in the basis set correspond to the same energy regardless of their quantum numbers. In this paper, the generalized Sturmian method is used to calculate excited states, densities, polarizabilities, and natural orbitals of few-electron atoms and ions.

Contents

1. Introduction	157
2. Generalized Sturmians	160
3. Potential-weighted orthonormality relations	161
4. The generalized Sturmian secular equations	162
5. Atomic calculations	162
6. The generalized Slater–Condon rules	166
7. The first-order density matrix	168
8. Natural orbitals	169
9. Atoms in strong external fields; polarizabilities	171
10. Concluding remarks	174
References	174

1. INTRODUCTION

A basic problem in quantum chemistry is the determination of the wave functions for stationary states of electrons in the presence of fixed nuclei (sometimes including the effects of external fields and perturbations).

The electronic wave functions are obtained by solving a time-independent Schrödinger equation by methods that include the use of monoelectronic functions (orbitals) as basis sets for the approximation of solutions: indeed the kind of functions employed as electronic orbitals strongly affects the convergence rate and accuracy of numerical procedures.

The only chemical system whose electronic Schrödinger equation is analytically solvable is the hydrogen-like atom. In the early days of quantum theory, scientists tried to use hydrogenic functions as orbitals in building up more complex wave functions. These functions, and the closely related variants such as Slater-type orbitals, incurred computational problems when extensive calculations of many-center two-electron integrals were needed. Therefore, in the last decades, linear combinations of Gaussian functions have been used as electronic orbitals, effectively replacing most other types of basis sets: Gaussians have allowed a faster calculation of two-electron integrals and consequently an extension of quantum chemistry towards larger systems, permitted also by impressive improvements of computer performances. At the present time, the main goals of researchers are the implementation of calculations for larger and larger systems, and also a better understanding of excited states.

The alternative on which we focus here is the study of Coulomb Sturmian orbitals and their generalizations, functions of a type which have so far received limited attention in quantum theory. Coulomb Sturmians are formally similar to the well-known hydrogenic functions, but they are isoenergetic; and their use has important and peculiar implications that are worthwhile investigating.

A recent article [1] by Osvaldo Goscinski, to whom this paper is dedicated, outlines early developments and includes a reprint of a 1968 report which, although unpublished, was very influential in further developments. The 1959 landmark paper by Shull and Löwdin [2] introduced the basic ideas in a quantum chemical context, and soon afterwards Rotenberg [3,4] provided a more general framework (including the nomenclature) within an atomic physics context.

Sturmians are not simply an alternative orbital set closely related to hydrogenic functions and to Slater-type orbitals. In the last decade the connection between their use and the ever-increasing exploitation of hyperspherical methods to treat the N -body problem in quantum mechanics was established, for both bound-state and scattering problems in nuclear, atomic and molecular physics; and this became an important source of progress, as recorded in a recent book [5].

In the application of hyperspherical techniques to solve quantum-mechanical problems, solutions to the N -particle Schrödinger equation are searched for in a $3N$ -dimensional space, parametrized as a radius and the $3N - 1$ angles of a hypersphere. Recent years have seen considerable progress in the applications of hyperspherical techniques, notably in atomic,

molecular and nuclear physics, and in chemical reaction dynamics. The mathematical apparatus involves connections among several fields – the theory of hyperspherical harmonics, momentum-space quantum theory, and generalized Sturmian basis functions. These methods permit the solution of many-particle problems directly, avoiding the self-consistent-field approximation. Particular attention has lately been given to many-electron Sturmians based on the choice of the attractive potential of the nuclei in the system as a reference potential. This choice offers as advantages the diagonal matrix representation of the nuclear attraction potential and the vanishing of the kinetic energy term from the secular equation; this enforces the automatic optimization of the Slater exponents of the atomic orbitals. The examples worked out so far, a few of which are reported later in the paper, suggest good convergence properties and prospects that excited states can also be obtained with reasonable accuracy.

There is one important further connection that is proving fruitful in current work: It is with modern advances in angular (and hyperangular) momentum theory, since these basis sets arise naturally as Lie-group representations, and therefore belong to the theory of special functions and orthogonal polynomials. Their dissemination may even provide a breakthrough in computational quantum theory, allowing all integrals to be obtained in closed form, the passage to momentum space being used to solve some multi-center one-electron integrals [6]. Moreover, since there are different types of coordinates suitable for the solution of the hydrogen atom problem in configuration space, there are also different types of hydrogenic Sturmians in momentum space. Symmetry properties and orthonormal transformations among them are available [7].

The properties of Sturmians in momentum space are also highly interesting and useful. Simple and exact relationships between Sturmians and hyperspherical harmonics can be established through a famous projection due to Fock. This property is very interesting in itself, and also because it suggests novel applications of angular momentum theory in quantum chemistry. There are a variety of hydrogenic functions available in momentum space, and symmetry properties and orthogonal transformations among them are interesting, as well as relationships between the two reciprocal spaces [8].

Recent applications of generalized Sturmians as a basis set for atomic structure calculations have been presented, also including the effects of external fields. There has been a treatment of the Sturmian formalism applied to one-electron molecules according to the MO-LCAO method [9], and also a method for exploiting Sturmians in a valence bond approach to the study of molecules [10].

In the present paper, generalized Sturmians are introduced in Section 2. Their potential-weighted orthonormality relations (Section 3) permit us to write down a peculiar secular equation (Section 4). Examples of its solution for atomic problems are given in Section 5. In these calculations, generalized

Slater–Condon rules must be used (Section 6), and an analogous treatment is needed for obtaining the first-order density matrix (Section 7). Section 8 describes the promising role of generalized Sturmians in generating natural orbitals. Section 9 discusses applications to the treatment of atoms in strong external fields, and to the calculation of polarizabilities. Some concluding remarks are given in Section 10.

2. GENERALIZED STURMIANS

Let \mathbf{x} be a $3N$ -dimensional vector, representing the Cartesian coordinates of the electrons in an N -particle system, i.e., let

$$\mathbf{x} = \{\mathbf{x}_1, \mathbf{x}_2, \dots, \mathbf{x}_N\} \quad (1)$$

where

$$\mathbf{x}_j \equiv \{x_j, y_j, z_j\}, \quad j = 1, 2, \dots, N \quad (2)$$

We now suppose that we are able to solve the approximate N -particle Schrödinger equation

$$\left[-\frac{1}{2}\Delta + \beta_\nu V_0(\mathbf{x}) - E_\kappa \right] \Phi_\nu(\mathbf{x}) = 0 \quad (3)$$

where V_0 has some resemblance to the actual potential and where

$$\Delta \equiv \sum_{j=1}^N \frac{1}{m_j} \nabla_j^2 \quad (4)$$

In equation (3), the constants β_ν are especially chosen in such a way as to make all of the eigenfunctions Φ_ν correspond to the same energy, E_κ , regardless of their quantum numbers ν [1,5,11–35]. The isoenergetic configurations Φ_ν can be used to build up solutions to the actual Schrödinger equation

$$\left[-\frac{1}{2}\Delta + V(\mathbf{x}) - E_\kappa \right] \Psi_\kappa(\mathbf{x}) = 0 \quad (5)$$

Thus, we represent the true wave function Ψ_κ as a superposition of isoenergetic (generalized Sturmian) basis functions:

$$\Psi_\kappa(\mathbf{x}) = \sum_{\nu} \Phi_\nu(\mathbf{x}) B_{\nu,\kappa} \quad (6)$$

The advantage of choosing our basis set to be isoenergetic at E_κ (the energy of the true wave function) is that the turning points of all the basis functions will be at the same approximate hyperradius as the turning point of Ψ_κ , and the asymptotic behavior of all the basis functions will be correct in the regions of hyperspace where both V_0 and V become small. In this asymptotic

region, all of the basis functions obey exactly the same wave equation as the true wave function, since

$$\left[-\frac{1}{2}\Delta + \beta_\nu V_0(\mathbf{x}) - E_\kappa \right] \Phi_\nu(\mathbf{x}) = 0 \rightarrow \left[-\frac{1}{2}\Delta - E_\kappa \right] \Phi_\nu(\mathbf{x}) = 0 \quad (7)$$

and

$$\left[-\frac{1}{2}\Delta + V(\mathbf{x}) - E_\kappa \right] \Psi_\kappa(\mathbf{x}) = 0 \rightarrow \left[-\frac{1}{2}\Delta - E_\kappa \right] \Psi_\kappa(\mathbf{x}) = 0 \quad (8)$$

3. POTENTIAL-WEIGHTED ORTHONORMALITY RELATIONS

Like the familiar one-particle Sturmians of Shull and Löwdin, generalized Sturmians obey potential-weighted orthonormality relations. To see this, we move the term in V_0 to the right-hand side of equation (3), multiply by a conjugate function in the basis set, and integrate over the coordinates. This gives us the relation

$$\int d\mathbf{x} \phi_{\nu'}^*(\mathbf{x}) \left[\frac{1}{2}\Delta + E_\kappa \right] \phi_\nu(\mathbf{x}) = \beta_\nu \int d\mathbf{x} \phi_{\nu'}^*(\mathbf{x}) V_0(\mathbf{x}) \phi_\nu(\mathbf{x}) \quad (9)$$

If the indices ν and ν' are interchanged, this becomes

$$\int d\mathbf{x} \phi_\nu^*(\mathbf{x}) \left[\frac{1}{2}\Delta + E_\kappa \right] \phi_{\nu'}(\mathbf{x}) = \beta_{\nu'} \int d\mathbf{x} \phi_\nu^*(\mathbf{x}) V_0(\mathbf{x}) \phi_{\nu'}(\mathbf{x}) \quad (10)$$

Subtracting the complex conjugate of equation (10) from equation (9), and making use of the Hermiticity of the operator on the left, we obtain

$$(\beta_\nu - \beta_{\nu'}) \int d\mathbf{x} \phi_{\nu'}^*(\mathbf{x}) V_0(\mathbf{x}) \phi_\nu(\mathbf{x}) = 0 \quad (11)$$

If the β_ν 's are assumed to be real, this implies that

$$\int d\mathbf{x} \phi_{\nu'}^*(\mathbf{x}) V_0(\mathbf{x}) \phi_\nu(\mathbf{x}) = 0 \quad \text{if } \beta_{\nu'} \neq \beta_\nu \quad (12)$$

We must remember that the subscript ν represents a set of indices, and the constants β_ν may be independent of some of them. Orthogonality with respect to these minor indices must be established or constructed in some other way. Assuming that this has been done, we next need to normalize the generalized Sturmian basis set. It turns out that the most natural and convenient choice of normalization is that which yields the potential-weighted orthonormality relations in the form

$$\int d\mathbf{x} \Phi_{\nu'}^*(\mathbf{x}) V_0(\mathbf{x}) \Phi_\nu(\mathbf{x}) = \delta_{\nu',\nu} \frac{2E_\kappa}{\beta_\nu} \quad (13)$$

In the case of atomic calculations, this choice of normalization does not need to be imposed. It results spontaneously from the form of the generalized Sturmian basis set.

4. THE GENERALIZED STURMIAN SECULAR EQUATIONS

To obtain the generalized Sturmian secular equations, we substitute the superposition (6) into the many-particle Schrödinger equation (5):

$$\left[-\frac{1}{2}\Delta + V(\mathbf{x}) - E_\kappa \right] \sum_\nu \Phi_\nu(\mathbf{x}) B_{\nu,\kappa} = 0 \quad (14)$$

Then, making use of equation (3), we have

$$\sum_\nu [V(\mathbf{x}) - \beta_\nu V_0(\mathbf{x})] \Phi_\nu(\mathbf{x}) B_{\nu,\kappa} = 0 \quad (15)$$

Finally, multiplying from the left by a conjugate function in the basis set, integrating over space and spin coordinates, and making use of the potential-weighted orthonormality relations (13), we obtain the set of secular equations:

$$\sum_\nu \left[\int d\mathbf{x} \phi_{\nu'}^*(\mathbf{x}) V(\mathbf{x}) \phi_\nu(\mathbf{x}) - 2E_\kappa \delta_{\nu',\nu} \right] B_{\nu,\kappa} = 0 \quad (16)$$

Notice that the kinetic energy term has vanished! This remarkable feature of equation (16) results from the fact that we have chosen the energy of our isoenergetic basis set to be the same as the energy of the state that we are trying to represent.

5. ATOMIC CALCULATIONS

In the case of atoms, equation (3) can be solved exactly if we set V_0 equal to the Coulomb attraction potential of the bare nucleus:

$$V_0(\mathbf{x}) = - \sum_{j=1}^N \frac{Z}{r_j} \quad (17)$$

Then the configurations given by the Slater determinants

$$\Phi_\nu(\mathbf{x}) = \left| \chi_{n,l,m,m_s} \chi_{n',l',m',m'_s} \chi_{n'',l'',m'',m''_s} \cdots \right| \quad (18)$$

will be exact solutions to equation (3) if the one-electron spin-orbitals χ_{n,l,m,m_s} are just the familiar one-electron hydrogen-like spin-orbitals

corresponding to the effective nuclear charge

$$Q_\nu = \beta_\nu Z = \left(\frac{-2E_\kappa}{\frac{1}{n^2} + \frac{1}{n'^2} + \cdots} \right)^{1/2} \quad (19)$$

In equation (19), Z is the actual nuclear charge, while n, n', n'', \dots are the principal quantum numbers of the hydrogen-like spin-orbitals in the configuration Φ_ν . To see that Φ_ν will then be a solution of equation (3), we remember that the one-electron hydrogen-like spin-orbitals satisfy

$$\left[-\frac{1}{2} \nabla_j^2 + \frac{Q_\nu^2}{2n^2} - \frac{Q_\nu}{r_j} \right] \chi_{n,l,m,m_s}(\mathbf{x}_j) = 0 \quad (20)$$

Thus, if we act on the configuration Φ_ν with the kinetic energy operator we obtain

$$\begin{aligned} \left[-\frac{1}{2} \Delta \right] \Phi_\nu(\mathbf{x}) &= \left[-\frac{Q_\nu^2}{2} \left(\frac{1}{n^2} + \frac{1}{n'^2} + \cdots \right) + \frac{Q_\nu}{r_1} + \frac{Q_\nu}{r_2} + \cdots \right] \Phi_\nu(\mathbf{x}) \\ &= [E_\kappa - \beta_\nu V_0(\mathbf{x})] \Phi_\nu(\mathbf{x}) \end{aligned} \quad (21)$$

which can be identified with equation (3). It can be shown that the configurations Φ_ν , constructed in this way, obey the potential-weighted orthonormality relations (13), and that they are already normalized in the proper way. Isoenergetic atomic configurations of the type shown in equation (18) were introduced by Professor Osvaldo Goscinski in his pioneering 1968 study [1], and it therefore seems appropriate to call such isoenergetic atomic configurations ‘Goscinskians’.

It is convenient to introduce the variables p_κ and \mathcal{R}_ν defined, respectively, by

$$p_\kappa \equiv \sqrt{-2E_\kappa} \quad (22)$$

and

$$\mathcal{R}_\nu \equiv \sqrt{\frac{1}{n^2} + \frac{1}{n'^2} + \frac{1}{n''^2} + \cdots} \quad (23)$$

In terms of these variables, equation (19) can be rewritten in the form

$$Q_\nu = \beta_\nu Z = \frac{p_\kappa}{\mathcal{R}_\nu} \quad (24)$$

and from equation (22), it follows that

$$E_\kappa = -\frac{p_\kappa^2}{2} \quad (25)$$

We now consider the true Schrödinger equation (5), where V is given by the nuclear attraction term V_0 , plus the interelectron repulsion potential

$$V'(\mathbf{x}) \equiv \sum_{i>j}^N \sum_{i=1}^N \frac{1}{r_{ij}} \quad (26)$$

Thus, we wish to use our set of Goscinskians to build up solutions to equation (5), with

$$V(\mathbf{x}) = V_0(\mathbf{x}) + V'(\mathbf{x}) = - \sum_{j=1}^N \frac{Z}{r_j} + \sum_{i>j}^N \sum_{i=1}^N \frac{1}{r_{ij}} \quad (27)$$

If we introduce the matrix

$$T_{\nu',\nu}^0 \equiv - \frac{1}{p_\kappa} \int d\mathbf{x} \Phi_{\nu'}^*(\mathbf{x}) V_0(\mathbf{x}) \Phi_\nu(\mathbf{x}) \quad (28)$$

then from the potential-weighted orthonormality relations (13) and from equations (24) and (25), it follows that

$$T_{\nu',\nu}^0 = \delta_{\nu',\nu} Z \mathcal{R}_\nu \quad (29)$$

From equation (29), we can see that $T_{\nu',\nu}^0$ is independent of p_κ , and hence also independent of E_κ . Similarly, it can be shown that the matrix

$$T'_{\nu',\nu} \equiv - \frac{1}{p_\kappa} \int d\mathbf{x} \Phi_{\nu'}^*(\mathbf{x}) V'(\mathbf{x}) \Phi_\nu(\mathbf{x}) \quad (30)$$

is also independent of p_κ and E_κ . With the help of equations (28)–(30), the Sturmian secular equations (16) for the atom can be written in the form

$$\sum_\nu [\delta_{\nu',\nu} Z \mathcal{R}_\nu + T'_{\nu',\nu} - p_\kappa \delta_{\nu',\nu}] B_{\nu,\kappa} = 0 \quad (31)$$

where we have divided equation (16) by p_κ as well as making the appropriate substitutions. The secular equation (31) differs in several ways from the usual type of secular equation that one would obtain from diagonalizing the Hamiltonian of a system. The kinetic energy term has disappeared, and the nuclear attraction potential is diagonal. Furthermore, the eigenvalues, p_κ , are not energy values, but are related to the energies by equations (22) and (25). From equation (24), it can be seen that the effective charges Q_ν characterizing the atomic orbitals in the Goscinskians Φ_ν are proportional to p_κ . The largest value of p_κ corresponds to the most tightly bound state, and for this state, the corresponding Q_ν values are also large, with the result that the Goscinskians are localized in the near neighborhood of the nucleus. By contrast, the values of p_κ corresponding to excited states are small, as are the effective charges Q_ν . The small effective charges correspond to diffuse

Goscinskians, and these are more appropriate to represent excited states than highly localized basis functions would be. Thus, the p_κ 's can be interpreted as scaling parameters that automatically adapt the basis set to the type of state being represented. By solving the generalized Sturmian secular equation (31), we obtain at one stroke not only the complete spectrum of energies, but also the optimal basis set for representing each state. The basis set is not completely known before the secular equation has been solved; only its form is known, but not its scale.

To illustrate equation (31), we have used it to calculate some excited states of the two-electron and three-electron isoelectronic series (Table 1).

Table 1. 1D excited state energies (in hartrees) for the two-electron isoelectronic series

	He	Li ⁺	Be ²⁺	B ³⁺	C ⁴⁺	N ⁵⁺
1s3d 1D	-2.0555	-4.7218	-8.4990	-13.388	-19.387	-26.498
Expt	-2.0554	-4.7225	-8.5012	-13.392	-19.396	-26.514
1s4d 1D	-2.0312	-4.6246	-8.2801	-12.998	-18.779	-25.622
Expt	-2.0311	-4.6252	-8.2824	-13.003	-18.788	-25.639
1s5d 1D	-2.0200	-4.5797	-8.1790	-12.818	-18.497	-25.217
Expt	-2.0198	-4.5801	-8.1807		-18.507	-25.234
1s6d 1D	-2.0139	-4.5554	-8.1242	-12.721	-18.345	-24.997
Expt	-2.0137	-4.5557			-18.354	
1s7d 1D	-2.0102	-4.5407	-8.0912	-12.662	-18.253	-24.865
Expt	-2.0100	-4.5409			-18.262	
1s8d 1D	-2.0078	-4.5311	-8.0699	-12.624	-18.194	-24.779
Expt	-2.0076	-4.5314			-18.202	
1s9d 1D	-2.0062	-4.5246	-8.0552	-12.598	-18.153	-24.720
Expt	-2.0060					
1s10d 1D	-2.0050	-4.5199	-8.0447	-12.579	-18.124	-24.678
Expt	-2.0048					
1s11d 1D	-2.0041	-4.5165	-8.0370	-12.566	-18.102	-24.647
Expt	-2.0035					
1s12d 1D	-2.0032	-4.5139	-8.0311	-12.555	-18.086	-24.624
Expt	-2.0033					

In making Table 1, the basis set used consisted of 63 generalized Sturmians. Singlet and triplet states were calculated simultaneously, 0.5 s of 499 MHz Intel Pentium III time being required for the calculation of 154 states. Experimental values are taken from the NIST tables (<http://physics.nist.gov/asd>).

The calculations were performed on a personal computer, and only 0.5 s of 499 MHz Intel Pentium III time was required for the calculation of 154 states. The slow step in the calculation is the construction of the interelectron repulsion matrix, $T'_{\nu, \nu'}$. In the general N -electron case, the construction of this matrix requires some refinements, as we will see in the next section. The calculated excited state energies of helium agree well with experimental energies from the home page of the US National Institute of Standards and Technology. Discrepancies between calculated and experimental energies for the ions may be due to experimental inaccuracies, since, for an isoelectronic series, the accuracy of the generalized Sturmian method increases with increasing atomic number.

6. THE GENERALIZED SLATER–CONDON RULES

In the general N -electron case, calculation of the matrices that enter the generalized Sturmian secular equation (31) is complicated by the fact that orthogonality between the spin-orbitals of different configurations cannot be assumed, since each configuration is characterized by its own effective nuclear charge Q_ν . Thus, the generalized Slater–Condon rules must be used in calculating off-diagonal matrix elements. In order to describe the form of these rules that we have found to be the most computationally rapid and robust [17], we introduce the simplified notation:

$$\Phi_\nu \equiv F \equiv \frac{1}{\sqrt{N!}} \begin{vmatrix} f_1(1) & f_2(1) & \cdots & f_N(1) \\ f_1(2) & f_2(2) & \cdots & f_N(2) \\ \vdots & \vdots & & \vdots \\ f_1(N) & f_2(N) & \cdots & f_N(N) \end{vmatrix} \quad (32)$$

and

$$\Phi_{\nu'} \equiv G \equiv \frac{1}{\sqrt{N!}} \begin{vmatrix} g_1(1) & g_2(1) & \cdots & g_N(1) \\ g_1(2) & g_2(2) & \cdots & g_N(2) \\ \vdots & \vdots & & \vdots \\ g_1(N) & g_2(N) & \cdots & g_N(N) \end{vmatrix} \quad (33)$$

In this notation, $f_1(j)$ stands for the one-electron spin-orbital χ_{n,l,m,m_s} as a function of the space and spin coordinates of electron j . We now let S be the matrix of overlap integrals between the isoenergetic configurations

Φ_ν and $\Phi_{\nu'}$:

$$S \equiv \begin{pmatrix} \langle f_1 | g_1 \rangle & \langle f_1 | g_2 \rangle & \cdots & \langle f_1 | g_N \rangle \\ \langle f_2 | g_1 \rangle & \langle f_2 | g_2 \rangle & \cdots & \langle f_2 | g_N \rangle \\ \vdots & \vdots & & \vdots \\ \langle f_3 | g_1 \rangle & \langle f_3 | g_2 \rangle & \cdots & \langle f_3 | g_N \rangle \end{pmatrix} \quad (34)$$

Then the first generalized Slater–Condon rule states that the scalar product of the two configurations is given by

$$\langle \Phi_\nu | \Phi_{\nu'} \rangle = |S| \quad (35)$$

where $|S|$ is the determinant of the matrix of overlap integrals. (One need not be afraid that evaluation of such a determinant will require a computational time proportional to $N!$, since the elements of S are not algebraic expressions but numbers, and very fast algorithms are available for evaluating the determinants of matrices that involve only numbers.)

The second generalized Slater–Condon rule states that if

$$\mathcal{V} = v(1) + v(2) + \cdots + v(N) \quad (36)$$

then

$$\langle \Phi_\nu | \mathcal{V} | \Phi_{\nu'} \rangle = \sum_{i=1}^N \sum_{j=1}^N (-1)^{i+j} \langle f_i | v | g_j \rangle |S_{ij}| \quad (37)$$

where $|S_{ij}|$ is the minor derived from $|S|$ by deleting the i th row and the j th column.

The third generalized Slater–Condon rule states that for a two-electron operator V'

$$\langle \phi_\nu | V' | \phi_{\nu'} \rangle = \sum_{i=1}^N \sum_{j=i+1}^N \sum_{k=1}^N \sum_{l=k+1}^N (-1)^{i+j+k+l} C_{ij,kl} |S_{ij,kl}| \quad (38)$$

where $|S_{ij,kl}|$ is the double minor derived from $|S|$ by deleting the i th and j th rows and the k th and l th columns. In the special case where V' is the interelectron Coulomb repulsion operator shown in equation (26),

$$C_{ij,kl} \equiv \int d\tau_1 \int d\tau_2 f_i^*(1) f_j^*(2) \frac{1}{r_{12}} [g_k(1)g_l(2) - g_l(1)g_k(2)] \quad (39)$$

7. THE FIRST-ORDER DENSITY MATRIX

Having used the generalized Sturmian method to calculate the wave function Ψ_κ for an N -electron atom, we are in a position to derive both the corresponding density distribution and the first-order density matrix [36–52]. However, because we cannot assume orthonormality between the one-electron spin-orbitals of different configurations, it is necessary to use expressions analogous to the generalized Slater–Condon rules. If we let

$$\rho_\kappa(1, 1') \equiv N \int d\tau_2 \int d\tau_3 \cdots \int d\tau_N \Psi_\kappa^*(1, 2, 3, \dots, N) \Psi_\kappa(1', 2, 3, \dots, N) \quad (40)$$

then

$$\rho_\kappa(1, 1') = \sum_{\nu, \nu'} B_{\nu, \kappa}^* \rho^{\nu, \nu'}(1, 1') B_{\nu', \kappa} \quad (41)$$

where

$$\rho^{\nu, \nu'}(1, 1') = \sum_{i=1}^N \sum_{j=1}^N (-1)^{i+j} f_i^*(1) g_j(1') |S_{ij}| \quad (42)$$

The derivation of equation (42) is similar to that of equation (37). In both cases, one obtains the final result by expanding both Φ_ν and $\Phi_{\nu'}$ in terms of their minors. Taking the scalar product of equation (42) with both $\varphi_a(1)$ and $\varphi_b^*(1')$, we obtain

$$\rho_{ab}^{\nu, \nu'} = \sum_{i,j=1}^N (-1)^{i+j} \langle f_i | \varphi_a \rangle \langle \varphi_b | g_j \rangle |S_{ij}| \quad (43)$$

Here the set of one-electron spin-orbitals φ_a can be any complete orthonormal set. Summing over configurations, we obtain the first-order density matrix corresponding to the state Ψ_κ :

$$\rho_{a,b}^\kappa = \sum_{\nu, \nu'} B_{\nu, \kappa}^* \rho_{a,b}^{(\nu, \nu')} B_{\nu', \kappa} \quad (44)$$

In using equation (44), it is important to remember that in order for the properties of the first-order density matrix to be correct, it is necessary that $\langle \Psi_\kappa | \Psi_\kappa \rangle = 1$. This normalization can be achieved by means of the first generalized Slater–Condon rule, equation (35).

8. NATURAL ORBITALS

The natural spin-orbitals $\alpha_i(1)$ corresponding to a many-electron wave function Ψ_κ are defined to be the set in terms of which the first-order density matrix $\rho_{a,b}^\kappa$ is diagonal [36–52]. Thus, if we solve the secular equation

$$\sum_b [\rho_{a,b}^\kappa - n_i \delta_{a,b}] C_{b,i}^\kappa = 0 \quad (45)$$

the natural spin-orbitals will be given by

$$\alpha_i(1) = \sum_b \varphi_b(1) C_{b,i}^\kappa \quad (46)$$

In terms of the α 's, the first-order density operator $\rho_\kappa(1, 1')$ of equation (33) can be written in the form

$$\rho_\kappa(1, 1') = \sum_i \alpha_i^*(1) n_i \alpha_i(1') \quad (47)$$

In the case where Ψ_κ is a single Slater determinant, the eigenvalues n_i of the first-order density matrix reduce to occupation numbers, with values either 0 or 1. In the more general case, where Ψ_κ is a sum of Slater determinants, the eigenvalues n_i can be shown to obey the relationships

$$0 \leq n_i \leq 1, \quad \sum_i n_i = N \quad (48)$$

To illustrate this method, we have calculated the natural orbitals of the ground state of lithium (Fig. 1). The basis of one-electron orthonormal spin-orbitals φ_a used to represent the first-order density matrix consisted of 25 spin-up and 25 spin-down orthogonalized Coulomb Sturmians. The first-order density matrix thus constructed was block-diagonal. The eigenvalues (occupation numbers) corresponding to the spin-up block were

$$n_1 = 0.998666, 0.996995, 0.001862, 0.000176, 0.000012, 0.000001, \dots$$

while those for the spin-down block were

$$n_1 = 0.998085, 0.001908, 0.000007, 0.000000, \dots$$

As expected, the two spin-up natural orbitals with occupation numbers close to 1 were found to resemble 1s and 2s orbitals, respectively. In Fig. 1, the 2s-like natural orbital can be seen to have a radial distribution function with a maximum at $r = 3.2$ bohrs, while the radial distribution function of the 1s-like natural orbital has almost no amplitude beyond $r = 2$ bohrs. The 1s-like spin-down natural orbital also has an occupation number near to 1,

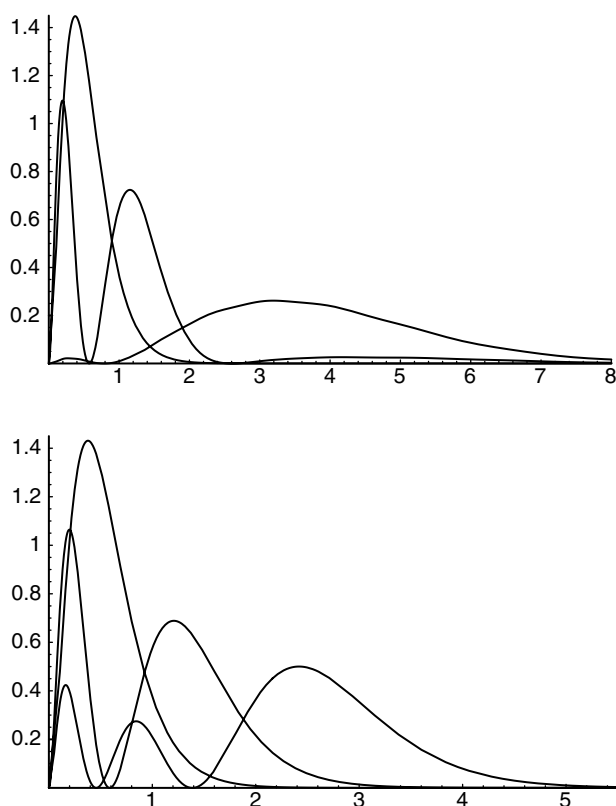


Fig. 1. Radial distribution functions of the most highly occupied spin-up (above) and spin-down (below) natural orbitals of lithium.

and it is almost (but not exactly) identical with the 1s-like spin-up natural orbital. The natural orbitals of a system are especially interesting because it can be shown that the most compact multiconfigurational representation of a state is that based on natural orbitals. A 1-configuration wave function, containing only the single most important configuration based on natural orbitals (that with the 1s-like and 2s-like spin-up natural orbitals occupied and the 1s-like spin-down natural orbital also occupied), was found to correspond to an energy of -7.40813 a.u., while a 24-configuration basis of natural orbitals yielded a ground-state energy of -7.43278 a.u. This value could undoubtedly be improved by projecting out a spin eigenfunction from the approximate 24-configuration ground-state wave function, but we did not attempt this. The original generalized Sturmian calculation from which the first-order density matrix was generated used a basis of 23 Goscinskian configurations, and it yielded a ground-state energy of -7.42623 a.u.

Thus, the 24-configuration natural orbital calculation was an improvement on the original result. Additional improvements could undoubtedly be obtained by including the effects of angular correlation. In a previous publication [17] we have reported the results of a generalized Sturmian calculation using 137 Goscinskian configurations, and including the effects of angular correlation. Using this basis, 36 states of the three-electron isoelectronic series were obtained in 1.49 s of 499 MHz Intel Pentium III CPU time. The ground-state energy obtained for lithium in this calculation was -7.44844 a.u., which should be compared with the experimental value of -7.47798 a.u. Our small pilot configuration interaction calculation using natural spin-orbitals seems to indicate that such calculations are feasible but rather difficult. By contrast, generalized Sturmian atomic calculations with Goscinskian configurations are extremely easy and rapid.

9. ATOMS IN STRONG EXTERNAL FIELDS; POLARIZABILITIES

The generalized Sturmian method is particularly well suited for calculating the spectra of few-electron atoms in strong external fields. In the case of a uniform electric field, the additional term in the potential (in atomic units) is

$$V''(\mathbf{x}) = \sum_{j=1}^N \mathcal{E} r_j \cos \theta_j \quad (49)$$

and the modified Sturmian secular equations have the form:

$$\sum_{\nu} [\delta_{\nu',\nu} Z\mathcal{R} + T'_{\nu',\nu} + \eta T''_{\nu',\nu} - p_{\kappa} \delta_{\nu',\nu}] B_{\nu,\kappa} = 0 \quad (50)$$

In equation (50),

$$T''_{\nu',\nu} \equiv \int d\mathbf{x} \phi_{\nu'}^*(\mathbf{x}) \sum_{j=1}^N p_0 r_j \cos \theta_j \phi_{\nu}(\mathbf{x}) \quad (51)$$

is independent of p_{κ} and

$$\eta \equiv \frac{\mathcal{E}}{p_{\kappa}^2} \quad (52)$$

Having constructed the matrices $T'_{\nu',\nu}$ and $T''_{\nu',\nu}$, we are in a position to calculate the spectra of an isoelectronic series of atoms and ions for all values of the nuclear charge Z , and for all values of the external electric field. We first choose a value of Z . Then, for many values of η we solve the secular equation (46). Finally, making use of the relationship $\eta = \mathcal{E}/p_{\kappa}^2$, we are able to plot atomic spectra, induced dipole moments, induced transition dipole

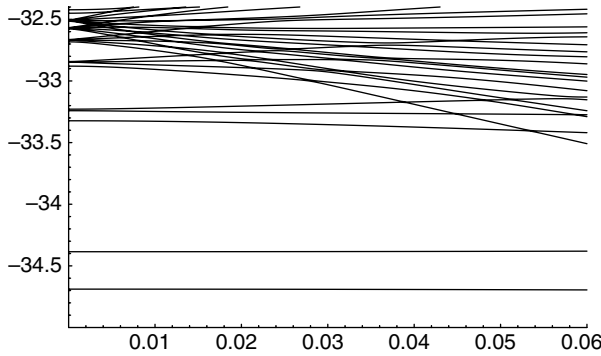


Fig. 2. Spectrum of C^{3+} in strong external electric fields.

moments, etc., as functions of the applied field. Figure 2 shows the spectrum of the C^{3+} ion calculated in this way. Only $m = 0$ states are shown in the figure. The basis set consisted of all singly excited three-electron Goscinskian configurations with the quantum numbers of the outer electron running over the range $n = 2, 3, \dots, 8$, $l = 0, 1, \dots, n - 1$ and $m = 0$. Values of the uniform external electric field, applied in the z -direction, are shown in atomic units on the abscissa of the graph. At the top of Fig. 2, one can observe a number of states which are very sensitive to the external field and which fall rapidly in energy as the field increases in strength. In a previous publication [17], we have shown that these are states in which the outer electron is very distant from the nucleus, and thus they are of course very sensitive to the presence of the external field. A richer basis would show still more of these states, which are in fact infinite in number, and many would be even more sensitive to the external field than those shown in Fig. 2. Close examination shows that what appear to be crossings of states in Fig. 2 are in fact avoided crossings. The states that appear to cross have very little overlap, and therefore the curves to which they correspond come very close to each other before diverging.

From equations (6) and (51) we can see that the dipole moment of the state Ψ_κ will be given by

$$\int dx \Psi_\kappa^* \sum_{j=1}^N z_j \Psi_\kappa = \frac{1}{p_\kappa} \sum_{\nu, \nu'} B_{\nu, \kappa}^* T''_{\nu, \nu'} B_{\nu', \kappa} \quad (53)$$

Since the ground states of atoms and ions have no intrinsic dipole moment, their polarizabilities are given by

$$\frac{1}{\mathcal{E}} \int dx \Psi_1^* \sum_{j=1}^N z_j \Psi_1 = \frac{1}{\eta p_1^3} \sum_{\nu, \nu'} B_{\nu, 1}^* T''_{\nu, \nu'} B_{\nu', 1} \quad (54)$$

Table 2. Static polarizabilities in atomic units for the first few isoelectronic series

	$N = 1$	$N = 2$	$N = 3$	$N = 4$
$Z = 1$	4.50000			
$Z = 2$	0.28125	1.50824		
$Z = 3$	0.05557	0.19281	193.247	
$Z = 4$	0.01758	0.05035	26.8171	39.0524
$Z = 5$	0.00720	0.01849	8.28658	10.9107
$Z = 6$	0.00347	0.00831	3.56008	4.59854
$Z = 7$	0.00187	0.00427	1.84243	2.36406
$Z = 8$	0.00110	0.00241	1.07471	1.37379
$Z = 9$	0.00069	0.00146	0.68124	0.86829
$Z = 10$	0.00045	0.00094	0.45896	0.58401

where p_1 and $B_{\nu,1}$ are, respectively, the lowest eigenvalue and lowest eigenvector of the secular equation (50). Table 2 shows ground-state polarizabilities in atomic units calculated in this way for the first few isoelectronic series of atoms and ions.

It is also possible to calculate field-induced transition dipole moments. When $p_\kappa \approx p_{\kappa'}$, the field-induced transition dipole moment between two states is given approximately by

$$\int \mathrm{d}x \, \Psi_\kappa^* \sum_{j=1}^N z_j \Psi_{\kappa'} \approx \frac{1}{p_\kappa} \sum_{\nu,\nu'} B_{\nu,\kappa}^* T''_{\nu,\nu'} B_{\nu',\kappa'} \tag{55}$$

where the eigenvalues p_κ and eigenvectors $B_{\nu,\kappa}$ are generated by solving the secular equation (50). The field dependence of some induced transition dipole moments of the C^{2+} ion is shown in Table 3 and Fig. 3.

Table 3. Approximate induced transition dipole moments between the ground state and some excited ^1S and ^1D states of C^{2+} for various values of applied electric field

	0.0000	0.0001	0.0002	0.0003	0.0004
$^1\text{S}, 1s^2 2s 4s$	0.00000	0.000659	0.001319	0.001978	0.002637
$^1\text{D}, 1s^2 2s 4d$	0.00000	0.000957	0.001913	0.002869	0.003825
$^1\text{S}, 1s^2 2s 5s$	0.00000	0.002155	0.004306	0.006450	0.008581
$^1\text{D}, 1s^2 2s 5d$	0.00000	0.002794	0.005420	0.007825	0.010038
$^1\text{S}, 1s^2 2s 6s$	0.00000	0.004878	0.009662	0.014264	0.018614
$^1\text{D}, 1s^2 2s 6d$	0.00000	0.001546	0.005251	0.009730	0.014691
$^1\text{S}, 1s^2 2s 7s$	0.00000	0.002612	0.006713	0.010685	0.014439

Values are in atomic units.

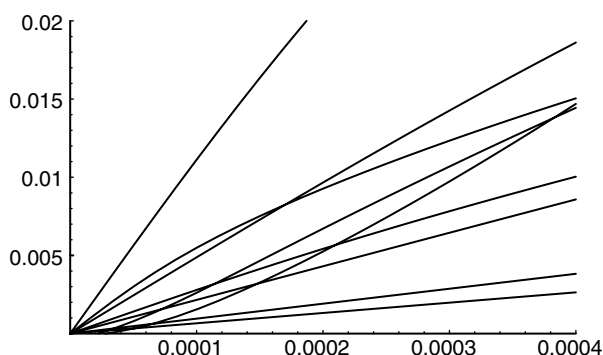


Fig. 3. Approximate induced transition dipole moments between the ground state and the first few excited 1S and 1D states of C^{2+} as a function of external field strength (Table 3).

10. CONCLUDING REMARKS

The generalized Sturmian method can be applied to a wide variety of problems in quantum theory. Using this method, many-particle Schrödinger equations can be solved directly without resorting the usual approximations, such as the Hartree–Fock approximation. The isoenergetic basis sets generated by the solution of the approximate many-particle Schrödinger equation (3) have an advantage over conventional basis functions, since their turning points occur in the right places to contribute usefully to the desired solution of the actual Schrödinger equation. In atomic physics, the method has shown itself to be very well adapted to the calculation of very large numbers of excited states of few-electron atoms and ions in strong external fields.

Programs used in this paper will be made available at the following website: <http://www.ccs.ki.ku.dk/~john/>.

REFERENCES

- [1] (a) O. Goscinski, Preliminary Research Report No. 217, Quantum Chemistry Group, Uppsala University, 1968; (b) O. Goscinski, *Adv. Quantum Chem.*, 2003, **41**, 51–85.
- [2] H. Shull and P. O. Löwdin, *J. Chem. Phys.*, 1959, **30**, 617.
- [3] M. Rotenberg, *Ann. Phys. (NY)*, 1962, **19**, 62.
- [4] M. Rotenberg, *Adv. At. Mol. Phys.*, 1970, **6**, 233–268.
- [5] J. Avery, *Hyperspherical Harmonics and Generalized Sturmians*, Kluwer, Dordrecht, 2000.
- [6] V. Aquilanti and A. Caligiana, *Chem. Phys. Lett.*, 2002, **366**, 157.
- [7] V. Aquilanti, A. Caligiana and S. Cavalli, *Int. J. Quantum Chem.*, 2003, **92**, 99.
- [8] V. Aquilanti, A. Caligiana, S. Cavalli and C. Coletti, *Int. J. Quantum Chem.*, 2003, **92**, 212.

- [9] V. Aquilanti and A. Caligiana in *Fundamental World of Quantum Chemistry: A Tribute to the Memory of P.O. Löwdin*, (eds E. J. Brändas and E. S. Kryachko), Kluwer, Dordrecht, 2003, Vol. I, p. 297.
- [10] V. Aquilanti and A. Caligiana, *J. Mol. Struct. Theochem*, 2004, in press.
- [11] J. Avery and D. R. Herschbach, *Int. J. Quantum Chem.*, 1992, **41**, 673.
- [12] J. Avery, *J. Math. Chem.*, 1997, **21**, 285.
- [13] V. Aquilanti and J. Avery, *Chem. Phys. Lett.*, 1997, **267**, 1.
- [14] J. Avery, *J. Mol. Struct.*, 1999, **458**, 1.
- [15] J. Avery, *Adv. Quantum Chem.*, 1999, **31**, 201.
- [16] J. Avery and R. Shim, *Int. J. Quantum Chem.*, 2001, **83**, 1.
- [17] J. Avery and J. Avery, *J. Math. Chem.*, 2003, **33**, 145–162.
- [18] J. Avery and J. Avery, *Adv. Quantum Chem.*, 2003, **43**, 185–206.
- [19] J. Avery, J. Avery and O. Goscinski, *Adv. Quantum Chem.*, 2003, **43**, 207–216.
- [20] E. J. Weniger, *J. Math. Phys.*, 1985, **26**, 276.
- [21] J. Avery, *J. Math. Chem.*, 1997, **21**, 285.
- [22] J. Avery and F. Antonsen, *J. Math. Chem.*, 1998, **24**, 175.
- [23] J. Avery, *Adv. Quantum Chem.*, 1999, **31**, 201.
- [24] J. Avery, *J. Mol. Struct. Theochem*, 1999, **458**, 1.
- [25] J. Avery and R. Shim, *Int. J. Quantum Chem.*, 2000, **79**, 1.
- [26] J. Avery, *J. Math. Chem.*, 1998, **24**, 169.
- [27] J. Avery and S. Sauer, Many-electron Sturmians applied to molecules. in *Quantum Systems in Chemistry and Physics, Volume 1* (eds A. Hernández-Laguna, J. Maruani, R. McWeeny and S. Wilson), Kluwer, Dordrecht, 2000.
- [28] J. Avery and R. Shim, *Int. J. Quantum Chem.*, 2000, **83**, 1.
- [29] J. Avery, *J. Math. Chem.*, 2000, **4**, 279.
- [30] V. Aquilanti and J. Avery, *Adv. Quantum Chem.*, 2001, **39**, 71.
- [31] V. Aquilanti, S. Cavalli, D. De Fazio and G. Grossi, Hyperangular momentum: applications to atomic and molecular science. in *New Methods in Quantum Theory* (eds C. A. Tsipis, V. S. Popov, D. R. Herschbach and J. S. Avery), Kluwer, Dordrecht, 1996.
- [32] V. Aquilanti, S. Cavalli, C. Coletti and G. Grossi, *Chem. Phys.*, 1996, **209**, 405.
- [33] V. Aquilanti, S. Cavalli and C. Coletti, *Chem. Phys.*, 1997, **214**, 1.
- [34] V. Aquilanti, S. Cavalli and C. Coletti, *Phys. Rev. Lett.*, 1998, **80**, 3209.
- [35] V. Aquilanti, S. Cavalli, C. Coletti, D. Di Domenico and G. Grossi, *Int. Rev. Phys. Chem.*, 2001, **20**, 673.
- [36] P. O. Löwdin, *Appl. Phys. Suppl.*, 1962, **33**, 251.
- [37] (a) P. A. M. Dirac, *Proc. Camb. Phil. Soc.*, 1929, **25**, 62–66; (b) P. A. M. Dirac, *Proc. Camb. Phil. Soc.* 1930, **26**, 376–385; (c) P. A. M. Dirac, *Proc. Camb. Phil. Soc.* 1931, **27**, 240–243.
- [38] P. O. Löwdin, *Phys. Rev.*, 1955, **97**, 1474, 1490, 1510.
- [39] P. O. Löwdin and H. Shull, *Phys. Rev.*, 1956, **101**, 1730.
- [40] C. Coulson, *Rev. Mod. Phys.*, 1960, **32**, 175.
- [41] R. McWeeny, *Rev. Mod. Phys.*, 1960, **35**, 363.
- [42] E. R. Davidson, *J. Chem. Phys.*, 1962, **37**, 577, 2966.
- [43] A. J. Coleman, *Rev. Mod. Phys.*, 1962, **35**, 668–687.
- [44] O. Goscinski and P. Lindner, *Natural Spin Orbitals and Generalized Overlap Amplitudes*, Preliminary Research Report No. 238, Quantum Chemistry Group, Uppsala University, 1969.
- [45] E. R. Davidson, *Reduced Density Matrices*, Academic Press, New York, 1976.
- [46] J. P. Dahl and J. Avery (eds), *Local Density Approximations in Quantum Chemistry and Solid State Physics*, Plenum Press, New York, 1984.
- [47] C. Valdemoro, *Phys. Rev. A*, 1992, **45**, 4462–4467.

- [48] D. E. Ellis (ed.), *Density Functional Theory of Molecules, Clusters and Solids*, Kluwer, Dordrecht, 1995.
- [49] E. K. U. Gross and R. M. Dreizler (eds), *Density Functional Theory*, Plenum Press, New York, 1995.
- [50] A. J. Coleman and V. I. Yukalov, *Reduced Density Matrices: Coulson's Challenge*, Springer, New York, 2000.
- [51] A. J. Coleman, *Int. J. Quantum Chem.*, 2001, **85**, 196–203.
- [52] G. Friesecke, *Proc. Roy. Soc. London A*, 2003, **459**, 47–52.

Electric Field Gradient Effects on Magnetic Susceptibility

Paolo Lazzeretti

*Dipartimento di Chimica, Università degli Studi di Modena e Reggio Emilia,
via G. Campi 183, 41100 Modena, Italy*

Abstract

A general expression for the magnetic susceptibility of a molecule in the presence of a time-independent, spatially uniform magnetic field, and a non-uniform electric field with a uniform gradient is discussed. The molecular response can be described by magnetic susceptibility polarizability tensors that depend on the choice of the origin for the coordinate system to which they are referred. However, the orbital magnetic dipole moment induced by the perturbation and the interaction energy are invariant to a change to the origin of the coordinate system and to the related gauge transformation. Theoretical estimates of the induced magnetic dipole moment obtained *via* single-origin methods are translationally invariant only for optimal variational wavefunctions. Common origin approaches relying on the algebraic approximation yield predictions that depend on the first, second, and third power of the origin shift. Distributed origin methods depend at most on the square of the shift.

Contents

1. Introduction	177
2. The expectation value of the electronic moments in a molecule	179
3. Response tensors by continuous transformation of the origin of the current density	182
4. Polarizabilities of susceptibility in different coordinate systems	183
Acknowledgements	189
References	189

1. INTRODUCTION

A static electric field applied to atoms and molecules distorts their electronic charge distribution and leads to changes in the magnetic properties, e.g., magnetic susceptibility (magnetizability) and magnetic shielding at the nuclei. The non-linear response to a combination of external fields can be rationalized by a Taylor series in powers of the electric and magnetic fields.

The coefficients of the fields in the Taylor series are tensors of increasing rank which are usually referred to as magnetizability polarizability, or hypermagnetizability, and magnetic shielding polarizabilities, or hyper-shieldings. The need for investigating the non-linear response of molecules to multiple electromagnetic perturbations has been emphasized in a series of theoretical papers [1–14].

The experimental parameter that may give quantitative information on the magnetizability polarizability to second order in the electric field is the Cotton–Mouton constant, responsible for the Cotton–Mouton effect (CME), i.e., the birefringence of light in gases in a static magnetic field [15–19].

A theoretical interpretation of CME has been given by Buckingham and Pople, who showed that the Cotton–Mouton constant can be expressed in terms of the anisotropy of the fourth-rank hypermagnetizability, the electric polarizability, and the magnetizability [20], and by Atkins and Miller [21].

Several theoretical papers reported *a priori* estimates of hypermagnetizabilities *via* quantum-mechanical approaches at various levels of accuracy [3,22–32]. Experimental observations of CME have been reported for methyl halides [33], for acetylene [34], and for boron trichloride [35]. Both experimental and theoretical aspects have been discussed in a review by Rizzo *et al.* [36].

Theoretical predictions have been presented for nuclear magnetic shielding polarizabilities in small size molecules, by which the change of shielding to first and second order in a spatially uniform electric field can be evaluated [4,7,23,24,26,28,37–45].

The effects of a non-uniform external electric field on nuclear magnetic shielding have been examined in previous studies [7,46–49]. A number of investigations recently appeared in the literature, studying interesting aspects of molecular response to the electric field gradient (EFG) of an external perturbing field, such as generalized Sternheimer nuclear shielding and electric field polarizabilities [50], and EFG-induced birefringence [51–53].

Allowing for the general procedure presented in a previous paper [54], the present work aims at developing relationships for the third- and fourth-rank hypermagnetizabilities of a molecule responding to three static perturbations, namely the external uniform magnetic field, the external non-uniform electric field (evaluated at the origin of the coordinate system), and the gradient of the electric field (assumed to be uniform in space), see Section 2.

The definition of corresponding molecular tensors arrived at by *continuous transformation* of the *origin* of the *current density*, which formally sets its *diamagnetic* term to *zero* (abbreviated as CT OCD-DZ), is discussed in Section 3. Section 4 deals with the problem of origin dependence of magnetizability polarizabilities of a molecule in the presence of uniform EFG.

2. THE EXPECTATION VALUE OF THE ELECTRONIC MOMENTS IN A MOLECULE

For a molecule with n electrons and N nuclei, charge, mass, position with respect to an arbitrary origin, canonical, and angular momentum of the i th electron are denoted by $-e$, m_e , \mathbf{r}_i , \mathbf{p}_i , $\mathbf{l}_i = \mathbf{r}_i \times \mathbf{p}_i$, $i = 1, 2, \dots, n$. Analogous quantities for nucleus I are $Z_I e$, M_I , \mathbf{R}_I , etc. Capital letters will be used for global electronic operators, e.g., $\mathbf{R} = \sum_{i=1}^n \mathbf{r}_i$, $\mathbf{L} = \sum_{i=1}^n \mathbf{l}_i$, etc. Throughout this paper the Einstein convention of implicit summation over two repeated Greek subscripts is retained.

We assume that the molecule is in the presence of multiple perturbations independent of time: a spatially uniform magnetic field and a non-uniform electric field with uniform gradient. The electronic reference state $|a\rangle \equiv |\Psi_a^{(0)}\rangle$ and the excited states $|j\rangle \equiv |\Psi_j^{(0)}\rangle$ of the molecule are eigenfunctions of the unperturbed time-independent Hamiltonian $H^{(0)}$. The natural transition frequencies are indicated by ω_{ja} .

Molecular properties can be described introducing the following general definitions for response functions

$$\{\hat{A}, \hat{B}\}_{-1} \equiv \frac{2}{\hbar} \sum_{i \neq a} \omega_{ia}^{-1} \Re\{\langle a | \hat{A} | i \rangle \langle i | \hat{B} | a \rangle\}, \quad (1)$$

$$\{\hat{A}, \hat{B}, \hat{C}\}_{-2} \equiv \mathbf{S}(\hat{A}, \hat{B}, \hat{C}) \left(\frac{1}{\hbar^2} \sum_{j \neq a} \sum_{k \neq a} \omega_{ja}^{-1} \omega_{ka}^{-1} \langle a | \hat{A} | j \rangle \langle j | \bar{\hat{B}} | k \rangle \langle k | \hat{C} | a \rangle \right), \quad (2)$$

where barred fluctuation operators are defined

$$\overline{\hat{A}}^{(1)} \equiv \hat{A}^{(1)} - \langle a | \hat{A}^{(1)} | a \rangle, \quad (3)$$

and the symbol $\mathbf{S}(\dots)$ indicates a summation of all the terms in which the operators within brackets are permuted.

The electronic operators for electric dipole, magnetic dipole, and electric quadrupole are denoted by $\hat{\mu}_\alpha$, \hat{m}_α , and $\hat{\mu}_{\alpha\beta}$, respectively [55],

$$\hat{\mu}_\alpha = -e \sum_{i=1}^n r_{i\alpha} = -e R_\alpha, \quad (4)$$

$$\hat{m}_\alpha = -\frac{e}{2m_e c} \sum_{i=1}^n l_{i\alpha} = -\frac{e}{2m_e c} L_\alpha, \quad (5)$$

$$\hat{\mu}_{\alpha\beta} = -\frac{e}{2} \sum_{i=1}^n r_{i\alpha} r_{i\beta} \equiv -\frac{e}{2} \sum_{i=1}^n (r_\alpha r_\beta)_i. \quad (6)$$

A non-traceless form is used for the operator (6) [56]. The electronic interaction Hamiltonians are written

$$\hat{H}^E = -\hat{\mu}_\alpha E_\alpha, \quad (7)$$

$$\hat{H}^{\nabla E} = -\hat{\mu}_{\alpha\beta} E_{\beta\alpha}, \quad (8)$$

$$\hat{H}^B = \frac{e}{m_e c} \sum_{i=1}^n \mathbf{A}_i^B \cdot \hat{\mathbf{p}}_i = -\hat{m}_\alpha B_\alpha, \quad (9)$$

$$\hat{H}^{BB} = \frac{e^2}{2m_e c^2} \sum_{i=1}^n \mathbf{A}_i^B \cdot \mathbf{A}_i^B = -\frac{1}{2} \hat{\chi}_{\alpha\beta}^d B_\alpha B_\beta. \quad (10)$$

In these relationships E_α , B_α , and $E_{\beta\alpha} \equiv \nabla_\beta E_\alpha$ denote electric field, magnetic field, and EFG at the origin of the coordinate system, and the vector potential acting on the i th electron is given by

$$\mathbf{A}_i^B = \frac{1}{2} \mathbf{B} \times \mathbf{r}_i. \quad (11)$$

In a static external uniform magnetic field, without an external electric field, the operator for the total magnetic dipole moment becomes

$$\hat{m}'_\alpha = \hat{m}_\alpha + \hat{\chi}_{\alpha\beta}^d B_\beta, \quad (12)$$

where the relationship

$$\hat{\chi}_{\alpha\beta}^d = -\frac{e^2}{4m_e c^2} \sum_{i=1}^n (r_i^2 \delta_{\alpha\beta} - r_{i\alpha} r_{i\beta}) \quad (13)$$

defines the operator for the diamagnetic contribution to the magnetic susceptibility introduced in equation (10).

When the two external perturbations of uniform magnetic field and non-uniform electric field with uniform gradient are switched on, the electronic energy of a molecule in the $|a\rangle$ reference state contains terms which account for its response. To third order we find

$$\begin{aligned} W_a = W_a^{(0)} &- \frac{1}{2} \alpha_{\alpha\beta} E_\alpha E_\beta - \alpha_{\alpha,\beta\gamma} E_\alpha E_{\beta\gamma} + \cdots - \frac{1}{2} \chi_{\alpha\beta} B_\alpha B_\beta \\ &- \frac{1}{2} \eta_{\alpha\beta,\gamma} B_\alpha B_\beta E_\gamma - \frac{1}{2} \eta_{\alpha\beta,\gamma\delta} B_\alpha B_\beta E_{\delta\gamma} + \cdots \end{aligned} \quad (14)$$

In this expression $\alpha_{\alpha\beta}$ is the electric dipole polarizability, $\alpha_{\alpha,\beta\gamma}$ is the mixed electric dipole–quadrupole polarizability, $\chi_{\alpha\beta}$ is the magnetic susceptibility [56], $\eta_{\alpha\beta,\gamma}$ and $\eta_{\alpha\beta,\gamma\delta}$ can, respectively, be called electric dipole and electric quadrupole polarizability of the magnetic susceptibility. Quantum-mechanical definitions for these quantities within the framework of the Rayleigh–Schrödinger perturbation theory are given later.

The time-independent electric and magnetic moments of the molecule in the presence of the external fields, using definitions (4) and (5) for the operators, are

$$\Delta\langle\hat{\mu}_\alpha\rangle = \alpha_{\alpha\beta}E_\beta + \alpha_{\alpha,\beta\gamma}E_\gamma + \cdots + \frac{1}{2}\eta_{\beta\gamma,\alpha}B_\beta B_\gamma + \cdots, \quad (15)$$

$$\Delta\langle\hat{m}'_\alpha\rangle = \chi_{\alpha\beta}B_\beta + \eta_{\alpha\beta,\gamma}B_\beta E_\gamma + \eta_{\alpha\beta,\gamma\delta}B_\beta E_{\delta\gamma} + \cdots \equiv \chi_{\alpha\beta}(\mathbf{E})B_\beta. \quad (16)$$

In equation (16) the magnetic susceptibility can be described by the relationship

$$\chi_{\alpha\beta}(\mathbf{E}) = \chi_{\alpha\beta} + \eta_{\alpha\beta,\gamma}E_\gamma + \eta_{\alpha\beta,\gamma\delta}E_{\delta\gamma} + \cdots. \quad (17)$$

Explicit definitions for the response tensors are arrived at by quantum-mechanical methods. Allowing for the notation of equations (1) and (2), we used the expressions

$$\alpha_{\alpha\beta} = \{\hat{\mu}_\alpha, \hat{\mu}_\beta\}_{-1}, \quad (18)$$

$$\alpha_{\alpha,\beta\gamma} = \{\hat{\mu}_\alpha, \hat{\mu}_{\beta\gamma}\}_{-1}, \quad (19)$$

for electric polarizabilities. The mixed dipole–quadrupole polarizability tensor (19) has been introduced in Refs. [56,57].

The second-rank tensor appearing in equations (14) and (17),

$$\chi_{\alpha\beta} = \{\hat{m}_\alpha, \hat{m}_\beta\}_{-1} + \langle a | \chi_{\alpha\beta}^d | a \rangle, \quad (20)$$

is the van Vleck magnetic susceptibility, partitioned into paramagnetic and diamagnetic contributions [58]. The higher rank tensors in relationships (14) and (17), $\eta_{\alpha\beta,\gamma}$ and $\eta_{\alpha\beta,\gamma\delta}$, rationalize the non-linear response of the electron cloud to second order in \mathbf{B} , and to first order in \mathbf{E} and $\nabla\mathbf{E}$, respectively.

By analogy with equation (20), it is expedient to split the polarizabilities and hyperpolarizabilities into diamagnetic and paramagnetic contributions,

$$\eta_{\alpha\beta,\gamma} = -\frac{\partial^3 W_a^{(3)}}{\partial B_\alpha \partial B_\beta \partial E_\gamma} = \eta_{\alpha\beta,\gamma}^d + \eta_{\alpha\beta,\gamma}^p, \quad (21)$$

$$\eta_{\alpha\beta,\gamma\delta} = -\frac{\partial^3 W_a^{(3)}}{\partial B_\alpha \partial B_\beta \partial E_{\delta\gamma}} = \eta_{\alpha\beta,\gamma\delta}^d + \eta_{\alpha\beta,\gamma\delta}^p, \quad (22)$$

where

$$\eta_{\alpha\beta,\gamma}^d = \{\hat{\chi}_{\alpha\beta}^d, \hat{\mu}_\gamma\}_{-1}, \quad (23)$$

$$\eta_{\alpha\beta,\gamma}^p = \{\hat{m}_\alpha, \hat{m}_\beta, \hat{\mu}_\gamma\}_{-2}, \quad (24)$$

$$\eta_{\alpha\beta,\gamma\delta}^d = \{\hat{\chi}_{\alpha\beta}^d, \hat{\mu}_{\gamma\delta}\}_{-1}, \quad (25)$$

$$\eta_{\alpha\beta,\gamma\delta}^p = \{\hat{m}_\alpha, \hat{m}_\beta, \hat{\mu}_{\gamma\delta}\}_{-2}. \quad (26)$$

The third-rank properties (21), (23), and (24) have been studied in detail in Refs. [14,43,56]. The fourth-rank tensors (22), (25), and (26), colloquially referred to here as electric quadrupole polarizabilities of magnetic susceptibility, describe the effect of the EFG at the origin of the coordinate system through its coupling with the electronic quadrupole moment, compare, for example, equations (14) and (17).

3. RESPONSE TENSORS BY CONTINUOUS TRANSFORMATION OF THE ORIGIN OF THE CURRENT DENSITY

The CTOCD-DZ definitions for the magnetic susceptibility polarizabilities (23) and (25) can be arrived at by formally annihilating the diamagnetic contribution to the current density induced in the electrons by the uniform external magnetic field in the presence of an external electric field with a uniform EFG.

A much easier route is offered by Geertsen-like procedures [59–61], relying on commutator expressions [62–64]. For instance, the CTOCD-DZ magnetic susceptibility polarizabilities can be obtained *via* equation (10), by using [64]

$$A_{\alpha}^{\mathbf{B}} A_{\alpha}^{\mathbf{B}} = \frac{i}{4\hbar} B_{\gamma} B_{\delta} \epsilon_{\alpha\beta\gamma} [r_{\alpha}, r_{\beta} l_{\delta}], \quad (27)$$

to define a propagator for the diamagnetic contribution to the third-order energy (14), i.e., a response function which formally replaces the expectation value for the diamagnetic terms (23) and (25) of the conventional common-origin (CO) formulation.

Thus, a new definition for the Δ diamagnetic contribution to the magnetic susceptibility quadrupole polarizability is obtained by substituting equation (27) into the Hamiltonian (10) [62]. Introducing the operator

$$\hat{U}_{\alpha\beta}(\mathbf{r}') = \frac{1}{2} \sum_{i=1}^n [(r_{i\alpha} - r'_{\alpha}) \hat{l}_{i\beta}(\mathbf{r}') + \hat{l}_{i\beta}(\mathbf{r}') (r_{i\alpha} - r'_{\alpha})], \quad (28)$$

we obtain the third-rank tensor

$$\eta_{\alpha\beta,\gamma} = \eta_{\alpha\beta,\gamma}^{\mathbf{p}} + \eta_{\alpha\beta,\gamma}^{\Delta}, \quad (29)$$

where

$$\eta_{\alpha\beta,\gamma}^{\Delta} = \frac{e^2}{4m_e^2 c^2} \epsilon_{\beta\lambda\mu} \{ \hat{P}_{\lambda}, \hat{\mu}_{\gamma}, \hat{U}_{\mu\alpha} \}_{-2}. \quad (30)$$

The relationship for the fourth-rank tensor is

$$\eta_{\alpha\beta,\gamma\delta} = \eta_{\alpha\beta,\gamma\delta}^p + \eta_{\alpha\beta,\gamma\delta}^\Delta, \quad (31)$$

where

$$\eta_{\alpha\beta,\gamma\delta}^\Delta = \frac{e^2}{4m_e^2 c^2} \epsilon_{\beta\lambda\mu} \{\hat{P}_\lambda, \hat{\mu}_{\gamma\delta}, \hat{U}_{\mu\alpha}\}_{-2}. \quad (32)$$

The identity of expressions (25) and (32) for exact eigenfunctions of a model Hamiltonian and optimum variational wavefunctions [65] can be proven by the extra-diagonal hypervirial relationship

$$\langle a | \hat{P}_\alpha | i \rangle = -im_e \omega_{ia} \langle a | \hat{R}_\alpha | i \rangle. \quad (33)$$

However, the use of the Δ contributions within the CTOCD-DZ scheme, equation (32), offers some advantages, see below, in practical applications.

4. POLARIZABILITIES OF SUSCEPTIBILITY IN DIFFERENT COORDINATE SYSTEMS

The numerical value of some molecular properties, e.g., the energy $W^{(0)}$, and the permanent electric dipole moment $\mathcal{M}_\alpha^{(0)}$ of a neutral molecule, does not vary with a translation of the coordinate system. Other tensor quantities are similarly described by a set of components that are independent of origin translation. For instance, the electronic operator $\tilde{\mu}_\alpha$ is clearly invariant, and response properties like the electric dipole polarizability, $\alpha_{\alpha\beta} = \{\hat{\mu}_\alpha, \hat{\mu}_\beta\}_{-1}$, equation (18), are obviously independent of the origin of the coordinate system.

The expressions for other molecular quantities depend upon the choice of origin for the coordinate system to which they are referred, for example, in a translation of the origin

$$\mathbf{r}' \rightarrow \mathbf{r}'' = \mathbf{r}' + \mathbf{d}, \quad (34)$$

the definition of operators for the electric dipole and quadrupole of the electrons varies as:

$$\hat{\mu}_\alpha(\mathbf{r}'') = \hat{\mu}_\alpha(\mathbf{r}') + ned_\alpha, \quad (35)$$

$$\tilde{\mu}_{\alpha\beta}(\mathbf{r}'') = \tilde{\mu}_{\alpha\beta}(\mathbf{r}') - \frac{1}{2} [\tilde{\mu}_\alpha(\mathbf{r}') d_\beta + \tilde{\mu}_\beta(\mathbf{r}') d_\alpha], \quad (36)$$

$$\hat{m}_\alpha(\mathbf{r}'') = \hat{m}_\alpha(\mathbf{r}') + \frac{e}{2m_e c} \epsilon_{\alpha\beta\gamma} d_\beta \hat{P}_\gamma, \quad (37)$$

$$\tilde{\chi}_{\alpha\beta}^d(\mathbf{r}'') = \tilde{\chi}_{\alpha\beta}^d(\mathbf{r}') - \frac{e}{4m_e c^2} [2\tilde{\mu}_\gamma(\mathbf{r}') \delta_{\alpha\beta} d_\gamma - \tilde{\mu}_\alpha(\mathbf{r}') d_\beta - \tilde{\mu}_\beta(\mathbf{r}') d_\alpha], \quad (38)$$

$$\hat{U}_{\alpha\beta}(\mathbf{r}'') = \hat{U}_{\alpha\beta}(\mathbf{r}') - d_\gamma \epsilon_{\beta\gamma\delta} \hat{V}_{\alpha\delta}(\mathbf{r}') - d_\alpha \hat{L}_\beta(\mathbf{r}') + d_\alpha d_\gamma \epsilon_{\beta\gamma\delta} \hat{P}_\delta. \quad (39)$$

The Hermitian operator $\hat{V}_{\alpha\beta}$ appearing in the transformation law, equation (39), for $\hat{U}_{\alpha\beta}$, see equation (28), is defined

$$\hat{V}_{\alpha\beta}(\mathbf{r}') = \frac{1}{2} \sum_{i=1}^n [(r_{i\alpha} - r'_{\alpha}) \hat{p}_{i\beta} + \hat{p}_{i\beta} (r_{i\alpha} - r'_{\alpha})]. \quad (40)$$

Some response tensors cannot be uniquely defined. They intrinsically depend upon the origin of the coordinate system, e.g., electric quadrupole polarizability [56,66]. However, there exist translationally invariant molecular properties (that are, in principle, experimentally measurable), although they are expressed in terms of origin-dependent tensors.

As an example, let us discuss the case of the electric moment (15) induced by a static external electric field having a uniform gradient. The equation that describes the change of the mixed third-rank electric polarizability tensor (19) with respect to a change to the origin of the coordinate system is

$$\alpha_{\alpha,\beta\gamma}(\mathbf{r}'') = \alpha_{\alpha,\beta\gamma}(\mathbf{r}') - \frac{1}{2} \alpha_{\alpha\beta} d_{\gamma} - \frac{1}{2} \alpha_{\alpha\gamma} d_{\beta}, \quad (41)$$

and the values of the external electric field at the two origins are related by

$$E_{\beta}(\mathbf{r}'') = E_{\beta}(\mathbf{r}') + d_{\gamma} E_{\gamma\beta}. \quad (42)$$

However, from equations (41), (42), and the Maxwell equation for static fields,

$$\nabla \times \mathbf{E} = \mathbf{0}, \quad (43)$$

the invariance relation

$$\Delta \langle \hat{\mu}_{\alpha}(\mathbf{r}'') \rangle = \Delta \langle \hat{\mu}_{\alpha}(\mathbf{r}') \rangle \quad (44)$$

is proven. Thus, even if the mixed electric polarizability tensor (19) is origin dependent, the induced electric dipole (15) of a molecule in the presence of an external electric field with uniform gradient is invariant to a coordinate transformation. Therefore, the total electric moment of a molecule in the presence of non-uniform external electric field is a measurable physical property.

In much the same way it can be proven that the total energy of a molecule interacting with an electric field with uniform field gradient is origin independent [56].

The case of the ‘quadrupole polarizability’ of magnetic susceptibility is more complicated. There are two aspects that we must take care of, namely, (i) mutual cancellation of paramagnetic and diamagnetic terms, which arise from translation of the origin of the gauge for the vector potential and (ii) intrinsic origin dependence analogous to the case of the mixed third-rank electric polarizability, see equation (41).

These questions will be discussed separately, starting with the first one, and showing that, within the conventional CO formulation of the magnetic response [58,67], exact cancellation takes place only in the case of optimal variational wavefunctions which satisfy hypervirial constraints [65].

On the other hand, even for approximate wavefunctions which do not fulfill the hypervirial theorem, the CTOCD technique guarantees full elimination of terms to third order in the shift of origin, and partial cancellation of terms that depend on it linearly and quadratically.

The equations describing how the third-rank susceptibilities, equations (21) and (29), change in the coordinate transformation (34), accompanied by the *gauge translation*

$$A_\alpha \rightarrow A'_\alpha = A_\alpha + \nabla_\alpha f, \quad f(\mathbf{r}) = -\frac{1}{2} \mathbf{B} \times \mathbf{d} \cdot \mathbf{r}, \quad (45)$$

are [14,56], for the CO paramagnetic contributions,

$$\begin{aligned} \eta_{\alpha\beta,\gamma}^p(\mathbf{r}'') &= \eta_{\alpha\beta,\gamma}^p(\mathbf{r}') - \frac{e^3}{4m_e^2 c^2} [d_\lambda d_\sigma \epsilon_{\alpha\lambda\mu} \epsilon_{\beta\sigma\tau} \{\hat{P}_\mu, \hat{P}_\tau, \hat{R}_\gamma(\mathbf{r}')\}_{-2} \\ &\quad - d_\lambda (\epsilon_{\alpha\lambda\mu} \{\hat{L}_\beta(\mathbf{r}'), \hat{P}_\mu, \hat{R}_\gamma(\mathbf{r}')\}_{-2} \\ &\quad + \epsilon_{\beta\lambda\mu} \{\hat{L}_\alpha(\mathbf{r}'), \hat{P}_\mu, \hat{R}_\gamma(\mathbf{r}')\}_{-2})], \end{aligned} \quad (46)$$

for the CO diamagnetic contributions

$$\eta_{\alpha\beta,\gamma}^d(\mathbf{r}'') = \eta_{\alpha\beta,\gamma}^d(\mathbf{r}') - \frac{e}{4m_e c^2} (2\alpha_\delta \gamma \delta_{\alpha\beta} d_\delta - \alpha_{\alpha\gamma} d_\beta - \alpha_{\beta\gamma} d_\alpha), \quad (47)$$

and for the CTOCD diamagnetic contributions

$$\begin{aligned} \eta_{\alpha\beta,\gamma}^\Delta(\mathbf{r}'') &= \eta_{\alpha\beta,\gamma}^\Delta(\mathbf{r}') + \frac{e^3}{4m_e^2 c^2} \epsilon_{\beta\lambda\mu} (d_\lambda d_\sigma \epsilon_{\alpha\sigma\tau} \{\hat{P}_\mu, \hat{P}_\tau, \hat{R}_\gamma(\mathbf{r}')\}_{-2} \\ &\quad - d_\lambda \{\hat{L}_\alpha(\mathbf{r}'), \hat{P}_\mu, \hat{R}_\gamma(\mathbf{r}')\}_{-2} \\ &\quad - d_\sigma \epsilon_{\alpha\sigma\tau} \{\hat{P}_\mu, \hat{R}_\gamma(\mathbf{r}'), \hat{V}_{\lambda\tau}(\mathbf{r}')\}_{-2}). \end{aligned} \quad (48)$$

A discussion on the invariance conditions for the third-rank tensor is given elsewhere [14,56].

For the paramagnetic contributions to the fourth-rank polarizability we obtain

$$\begin{aligned}
\eta_{\alpha\beta,\gamma\delta}^p(\mathbf{r}'') &= \eta_{\alpha\beta,\gamma\delta}^p(\mathbf{r}') - \frac{1}{2}d_\delta\eta_{\alpha\beta,\gamma}^p(\mathbf{r}') - \frac{1}{2}d_\gamma\eta_{\alpha\beta,\delta}^p(\mathbf{r}') \\
&+ \frac{e}{2m_e c} (d_\lambda\epsilon_{\alpha\lambda\mu}\{\hat{m}_\beta(\mathbf{r}'), \hat{P}_\mu, \hat{\mu}_{\gamma\delta}(\mathbf{r}')\}_{-2} \\
&+ d_\sigma\epsilon_{\beta\sigma\tau}\{\hat{m}_\alpha(\mathbf{r}'), \hat{P}_\tau, \hat{\mu}_{\gamma\delta}(\mathbf{r}')\}_{-2}) \\
&- \frac{e}{4m_e c} [d_\lambda\epsilon_{\alpha\lambda\mu}(d_\delta\{\hat{m}_\beta(\mathbf{r}'), \hat{P}_\mu, \hat{\mu}_\gamma(\mathbf{r}')\}_{-2} \\
&+ d_\gamma\{\hat{m}_\beta(\mathbf{r}'), \hat{P}_\mu, \hat{\mu}_\delta(\mathbf{r}')\}_{-2}) \\
&+ d_\sigma\epsilon_{\beta\sigma\tau}(d_\delta\{\hat{m}_\alpha(\mathbf{r}'), \hat{P}_\tau, \hat{\mu}_\gamma(\mathbf{r}')\}_{-2} \\
&+ d_\gamma\{\hat{m}_\alpha(\mathbf{r}'), \hat{P}_\tau, \hat{\mu}_\delta(\mathbf{r}')\}_{-2})] \\
&+ \left(\frac{e}{2m_e c}\right)^2 d_\lambda d_\sigma\epsilon_{\alpha\lambda\mu}\epsilon_{\beta\sigma\tau}\{\hat{P}_\mu, \hat{P}_\tau, \hat{\mu}_{\gamma\delta}(\mathbf{r}')\}_{-2} \\
&- \frac{1}{2}\left(\frac{e}{2m_e c}\right)^2 d_\lambda d_\sigma\epsilon_{\alpha\lambda\mu}\epsilon_{\beta\sigma\tau}(d_\delta\{\hat{P}_\mu, \hat{P}_\tau, \hat{\mu}_\gamma(\mathbf{r}')\}_{-2} \\
&+ d_\gamma\{\hat{P}_\mu, \hat{P}_\tau, \hat{\mu}_\delta(\mathbf{r}')\}_{-2}), \tag{49}
\end{aligned}$$

for the diamagnetic contributions

$$\begin{aligned}
\eta_{\alpha\beta,\gamma\delta}^d(\mathbf{r}'') &= \eta_{\alpha\beta,\gamma\delta}^d(\mathbf{r}') - \frac{1}{2}d_\delta\eta_{\alpha\beta,\gamma}^d(\mathbf{r}') - \frac{1}{2}d_\gamma\eta_{\alpha\beta,\delta}^d(\mathbf{r}') - \frac{e}{4m_e c^2} \\
&\times [2d_\lambda\alpha_{\lambda,\gamma\delta}(\mathbf{r}')\delta_{\alpha\beta} - d_\alpha\alpha_{\beta,\gamma\delta}(\mathbf{r}') - d_\beta\alpha_{\alpha,\gamma\delta}(\mathbf{r}')] + \frac{e}{8m_e c^2} \\
&\times [2d_\lambda(d_\delta\alpha_{\lambda\gamma} + d_\gamma\alpha_{\lambda\delta})\delta_{\alpha\beta} - d_\alpha(d_\delta\alpha_{\beta\gamma} + d_\gamma\alpha_{\beta\delta}) \\
&- d_\beta(d_\delta\alpha_{\alpha\gamma} + d_\gamma\alpha_{\alpha\delta})], \tag{50}
\end{aligned}$$

and for the CTOCD contributions

$$\begin{aligned}
\eta_{\alpha\beta,\gamma\delta}^{\Delta}(\mathbf{r}'') &= \eta_{\alpha\beta,\gamma\delta}^{\Delta}(\mathbf{r}') - \frac{1}{2}d_{\delta}\eta_{\alpha\beta,\gamma}^{\Delta}(\mathbf{r}') - \frac{1}{2}d_{\gamma}\eta_{\alpha\beta,\delta}^{\Delta}(\mathbf{r}') \\
&\quad - \left(\frac{e}{2m_e c}\right)^2 d_{\mu}\epsilon_{\beta\lambda\mu}\{\hat{L}_{\alpha}(\mathbf{r}'), \hat{P}_{\lambda}, \hat{\mu}_{\gamma\delta}(\mathbf{r}')\}_{-2} \\
&\quad - \left(\frac{e}{2m_e c}\right)^2 d_{\sigma}\epsilon_{\beta\lambda\mu}\epsilon_{\alpha\sigma\tau}\{\hat{P}_{\lambda}, \hat{V}_{\mu\tau}, \hat{\mu}_{\gamma\delta}(\mathbf{r}')\}_{-2} \\
&\quad + \left(\frac{e}{2m_e c}\right)^2 d_{\mu}d_{\sigma}\epsilon_{\beta\lambda\mu}\epsilon_{\alpha\sigma\tau}\{\hat{P}_{\lambda}, \hat{P}_{\tau}, \hat{\mu}_{\gamma\delta}(\mathbf{r}')\}_{-2} \\
&\quad + \frac{1}{2}\left(\frac{e}{2m_e c}\right)^2 d_{\sigma}\epsilon_{\beta\lambda\mu}\epsilon_{\alpha\sigma\tau}(d_{\delta}\{\hat{P}_{\lambda}, \hat{V}_{\mu\tau}, \hat{\mu}_{\gamma}(\mathbf{r}')\}_{-2} \\
&\quad + d_{\gamma}\{\hat{P}_{\lambda}, \hat{V}_{\mu\tau}, \hat{\mu}_{\delta}(\mathbf{r}')\}_{-2}) \\
&\quad + \frac{1}{2}\left(\frac{e}{2m_e c}\right)^2 d_{\mu}\epsilon_{\beta\lambda\mu}(d_{\delta}\{\hat{P}_{\lambda}, \hat{L}_{\alpha}(\mathbf{r}'), \hat{\mu}_{\gamma}(\mathbf{r}')\}_{-2} \\
&\quad + d_{\gamma}\{\hat{P}_{\lambda}, \hat{L}_{\alpha}(\mathbf{r}'), \hat{\mu}_{\delta}(\mathbf{r}')\}_{-2}) \\
&\quad - \frac{1}{2}\left(\frac{e}{2m_e c}\right)^2 d_{\mu}d_{\sigma}\epsilon_{\beta\lambda\mu}\epsilon_{\alpha\sigma\tau}(d_{\delta}\{\hat{P}_{\tau}, \hat{P}_{\lambda}, \hat{\mu}_{\gamma}(\mathbf{r}')\}_{-2} \\
&\quad + d_{\gamma}\{\hat{P}_{\tau}, \hat{P}_{\lambda}, \hat{\mu}_{\delta}(\mathbf{r}')\}_{-2}). \tag{51}
\end{aligned}$$

The expressions for the change of the total CO property (22) and of the total CTOCD property (31) are obtained by summing the RHS of equations (49) and (50) and of equations (49) and (51), respectively.

To understand the difference between the spurious gauge terms (i), which are removed in the ideal case of optimal variational wavefunctions [65], and terms (ii), which account for the *essential* origin dependence of the property, let us first discuss the origin dependence of the quadrupole polarizability of magnetic susceptibility (22) within the conventional common-origin representation.

It can be observed that the expression for the paramagnetic contribution, equation (49), contains terms to third order in \mathbf{d} , which do not appear in the relationship for the diamagnetic contribution (50). Since the total property (22) is invariant in the gauge transformation (45), the coefficients of the third-order terms, i.e., the last term of equation (49) must vanish. In fact, the sum rule

$$\{\hat{P}_{\alpha}, \hat{P}_{\beta}, \hat{\mu}_{\gamma}\}_{-2} = 0 \tag{52}$$

can be directly proved [56], e.g., for optimal variational wavefunctions fulfilling the hypervirial theorem [65].

On the same grounds, we also find that

$$\{\hat{P}_\alpha, \hat{P}_\beta, \hat{\mu}_{\gamma\delta}\}_{-2} = 0, \quad (53)$$

if the hypervirial conditions (33) and

$$\langle a | \hat{P}_\alpha \hat{R}_\beta + \hat{P}_\beta \hat{R}_\alpha | i \rangle = -im_e \omega_{ia} \langle a | \hat{R}_\alpha \hat{R}_\beta | i \rangle \quad (54)$$

are satisfied, so that the last term on the RHS of relationship (49) vanishes.

In many cases, sum rules (52) and (53) may be satisfied for symmetry reasons. However, these conditions are not necessarily met in calculations using the algebraic approximation, i.e., within a finite basis set [68]. For molecules of low symmetry, the closeness to zero of the LHS of equations (52) and (53) is therefore a measure of basis set completeness and accuracy of a calculation of the fourth-rank tensor (22).

By using the hypervirial relation (33), the fourth term of equation (49) gives the fourth term of equation (50) with sign reversed. Analogously, the fifth term of equation (49) is reduced to the opposite of the fifth term of equation (50). The sum rules for the invariance of common-origin polarizabilities of susceptibility (22) in the gauge translation (45), obtained by applying the hypervirial relation (33), and confirmed by comparing the RHS of equations (46) and (47) and of equations (49) and (50), respectively, are

$$\{\hat{m}_\alpha, \hat{P}_\beta, \hat{\mu}_\gamma\}_{-2} = -\frac{1}{2c} \epsilon_{\alpha\beta\delta} \alpha_{\delta\gamma}, \quad (55)$$

$$\{\hat{m}_\alpha, \hat{P}_\beta, \hat{\mu}_{\gamma\delta}\}_{-2} = -\frac{1}{2c} \epsilon_{\alpha\beta\epsilon} \alpha_{\epsilon,\gamma\delta}. \quad (56)$$

In conclusion, summing the RHS of equations (49) and (50), the spurious gauge terms cancel each other out if the hypervirial conditions (33) and (54), and the sum rules for gauge invariance, equations (52), (53), (55), and (56) are fulfilled. Then the CO quadrupole polarizabilities of magnetic susceptibility change according to a relationship analogous to equation (41) for the electric polarizability,

$$\eta_{\alpha\beta,\gamma\delta}(\mathbf{r}'') = \eta_{\alpha\beta,\gamma\delta}(\mathbf{r}') - \frac{1}{2} d_\delta \eta_{\alpha\beta,\gamma}(\mathbf{r}') - \frac{1}{2} d_\gamma \eta_{\alpha\beta,\delta}(\mathbf{r}'). \quad (57)$$

Let us now consider the variation of the total CTOCD fourth-rank tensor (31) obtained by summing the RHS of equations (49) and (51). Observing that the fourth-rank tensor (26) is symmetric in the change $\alpha \leftrightarrow \beta$, we see that terms of the CTOCD expression (51) to third order in the shift \mathbf{d} cancel out with the corresponding ones in the paramagnetic contribution (49). Therefore, third-order terms in \mathbf{d} do not appear in the relationship describing how the total CTOCD fourth-rank tensor (31) changes in a gauge translation.

Similarly, other addenda of equations (49) and (51), having the same magnitude and reversed sign, kill each other: the fourth with the fourth, the tenth with the sixth, the sixth and the seventh with the ninth and the tenth, respectively.

Eighth and ninth addenda of equation (49) cancel with the seventh and eighth addenda of equation (51) if the sum rule [56]

$$\{\hat{L}_\alpha, \hat{P}_\beta, \hat{\mu}_\gamma\}_{-2} = \epsilon_{\alpha\delta\epsilon} \{\hat{P}_\epsilon, \hat{\mu}_\gamma, \hat{V}_{\delta\beta}\}_{-2} \quad (58)$$

is fulfilled. Analogously, the fifth addenda of equations (49) and (51) are the opposite of each other if the calculation satisfies the sum rule

$$\{\hat{L}_\alpha, \hat{P}_\beta, \hat{\mu}_{\gamma\delta}\}_{-2} = \epsilon_{\alpha\epsilon\eta} \{\hat{P}_\eta, \hat{\mu}_{\gamma\delta}, \hat{V}_{\epsilon\beta}\}_{-2}, \quad (59)$$

and relationship (57) is obtained also for the total CTOCD fourth-rank tensor (31).

Then it is easy to show that the induced magnetic dipole moment (16) and the interaction energy are translationally invariant, i.e.,

$$\Delta\langle\hat{m}'_\gamma(\mathbf{r}'')\rangle = \Delta\langle\hat{m}'_\gamma(\mathbf{r}')\rangle \quad (60)$$

and

$$W'(\mathbf{r}'') = W'(\mathbf{r}'), \quad (61)$$

by the use of equations (42), (43), and (57).

On the other hand, the induced magnetic dipole, equation (16), evaluated *via* the CTOCD-DZ method, i.e., *via* equations (26), (31), and (32), is exactly origin independent, because there is complete cancellation of terms on summing the RHS of equations (46) and (48) and of equations (49) and (51), if sum rules (58) and (59) are satisfied.

ACKNOWLEDGEMENTS

The author wishes to thank Dr Jonathan Boyd for helpful discussions. Financial support to the present research from the Italian MURST (Ministero dell'Università e della Ricerca Scientifica e Tecnologica), *via* 60% and FIRB funds, is gratefully acknowledged.

REFERENCES

- [1] A. D. Buckingham, *Can. J. Chem.*, 1960, **38**, 300.
- [2] W. T. Raynes, A. D. Buckingham and H. J. Bernstein, *J. Chem. Phys.*, 1962, **36**, 3481.
- [3] B. Day and A. D. Buckingham, *Mol. Phys.*, 1976, **32**, 343.
- [4] J. P. Riley and W. T. Raynes, *Mol. Phys.*, 1976, **32**, 569.
- [5] M. I. Volodicheva and T. K. Rebane, *Theor. éksp. Khim.*, 1983, **19**, 387, p. 357, Engl. translation, 1984.

- [6] M. I. Volodicheva and T. K. Rebane, *Theor. éksp. Khim.*, 1985, **21**, 391, p. 373, Engl. translation, 1985.
- [7] J. D. Augspurger and C. E. Dykstra, *J. Phys. Chem.*, 1991, **95**, 9230.
- [8] W. T. Raynes, in *Nuclear Magnetic Shielding and Molecular Structure* (ed. J. A. Tossell), NATO ASI Series C, Kluwer, Dordrecht, 1993, Vol. 386, pp. 401–420.
- [9] J. D. Augspurger, C. E. Dykstra, E. Oldfield and J. G. Pearson, in *Nuclear Magnetic Shieldings and Molecular Structure* (ed. J. A. Tossell), NATO ASI Series C, Kluwer, Dordrecht, 1993, Vol. 386, pp. 75–94.
- [10] C. J. Jameson and A. C. de Dios, in *Nuclear Magnetic Shieldings and Molecular Structure* (ed. J. A. Tossell), NATO ASI Series C, Kluwer, Dordrecht, 1993, Vol. 386, pp. 95–116.
- [11] A. C. de Dios and C. J. Jameson, *Ann. Rep. NMR Spectrosc.*, 1994, **29**, 1.
- [12] C. J. Jameson, in *Theoretical and Physical Aspects of Nuclear Shielding* (ed. S. R. G. A. Webb), Specialist Periodical Reports – Nuclear Magnetic Resonance, The Royal Society of Chemistry, Cambridge, 1997, Vol. 26, pp. 46–87.
- [13] W. T. Raynes, in *Encyclopedia of Nuclear Magnetic Resonance* (eds D. M. Grant and R. K. Harris), Wiley, New York, 1996.
- [14] P. Lazzeretti and R. Zanasi, *Mol. Phys.*, 1996, **89**, 157.
- [15] A. Cotton and H. Mouton, *Ct. r. hebd. Séanc. Acad. Sci. Paris*, 1905, **141**, 317, 349.
- [16] A. Cotton and H. Mouton, *Ct. r. hebd. Séanc. Acad. Sci. Paris*, 1906, **142**, 203.
- [17] A. Cotton and H. Mouton, *Ct. r. hebd. Séanc. Acad. Sci. Paris*, 1907, **145**, 229.
- [18] A. Cotton and H. Mouton, *Ann. Chem. Phys.*, 1907, **11**, 145, 289.
- [19] A. Cotton, *Rapp. Cons. Solvay*, 1932, 418.
- [20] A. D. Buckingham and J. A. Pople, *Proc. Phys. Soc. A*, 1956, **69**, 1133.
- [21] P. W. Atkins and M. H. Miller, *Mol. Phys.*, 1968, **15**, 491.
- [22] D. M. Bishop, S. M. Cybulski and J. Pipin, *J. Chem. Phys.*, 1991, **94**, 6686.
- [23] A. Rizzo, T. Helgaker, K. Ruud, A. Barszczewicz, M. Jaszuński and P. Jørgensen, *J. Chem. Phys.*, 1995, **102**, 8953.
- [24] S. Coriani, A. Rizzo, K. Ruud and T. Helgaker, *Mol. Phys.*, 1996, **88**, 931.
- [25] D. Jonsson, P. Norman, O. Vahtras and H. Ågren, *Theor. Chim. Acta*, 1996, **93**, 235.
- [26] S. Coriani, A. Rizzo, K. Ruud and T. Helgaker, *Chem. Phys.*, 1997, **216**, 53.
- [27] K. Ruud, T. Helgaker, A. Rizzo, S. Coriani and K. Mikkelsen, *J. Chem. Phys.*, 1997, **107**, 894.
- [28] S. M. Cybulski and D. M. Bishop, *Mol. Phys.*, 1998, **93**, 739.
- [29] K. Ruud, H. Ågren, P. Dahle, T. Helgaker, A. Rizzo, S. Coriani, H. Koch, K. O. Sylvester-Hvid and K. Mikkelsen, *J. Chem. Phys.*, 1997, **108**, 599.
- [30] A. Rizzo and C. Rizzo, *Mol. Phys.*, 1999, **96**, 973.
- [31] D. Jonsson, P. Norman, H. Ågren, A. Rizzo, S. Coriani and K. Ruud, *J. Chem. Phys.*, 2001, **114**, 8372.
- [32] D. Jonsson, P. Norman, O. Vahtras, H. Ågren and A. Rizzo, *J. Chem. Phys.*, 1997, **106**, 8552.
- [33] M. H. Coonan and G. L. D. Ritchie, *J. Phys. Chem.*, 1991, **95**, 122.
- [34] M. H. Coonan and G. L. D. Ritchie, *Chem. Phys. Lett.*, 1993, **202**, 237.
- [35] D. W. Lamb and G. L. D. Ritchie, *Chem. Phys. Lett.*, 1999, **310**, 150.
- [36] C. Rizzo, A. Rizzo and D. M. Bishop, *Int. Rev. Phys. Chem.*, 1997, **16**, 81.
- [37] H. Fukui, Y. Kitamura and K. Miura, *Mol. Phys.*, 1977, **34**, 593.
- [38] A. J. Sadlej and W. T. Raynes, *Mol. Phys.*, 1978, **35**, 101.
- [39] M. Grayson and W. T. Raynes, *Chem. Phys. Lett.*, 1993, **214**, 473.
- [40] M. Grayson and W. T. Raynes, *Chem. Phys. Lett.*, 1994, **218**, 270.
- [41] M. Grayson and W. T. Raynes, *Mol. Phys.*, 1994, **81**, 533.
- [42] P. E. Hansen, H. Abildgaard and A. Hansen, *Chem. Phys. Lett.*, 1994, **101**, 275.
- [43] M. C. Caputo, M. B. Ferraro and P. Lazzeretti, *J. Chem. Phys.*, 2000, **112**, 6141.

- [44] A. Rizzo and J. Gauss, *J. Chem. Phys.*, 2002, **116**, 869.
- [45] J. Boyd, C. Domene, C. Redfield, M. B. Ferraro and P. Lazzeretti, *J. Am. Chem. Soc.*, 2003, **125**, 9556.
- [46] J. G. Batchelor, *J. Am. Chem. Soc.*, 1975, **97**, 3410.
- [47] J. D. Augspurger, C. E. Dykstra and E. Oldfield, *J. Am. Chem. Soc.*, 1991, **113**, 2447.
- [48] J. D. Augspurger, J. G. Pearson, E. Oldfield, C. E. Dykstra, K. D. Park and D. Schwartz, *J. Magn. Res.*, 1992, **100**, 342.
- [49] T. M. Nymand and P.-O. Åstrand, *J. Chem. Phys.*, 1997, **106**, 8332.
- [50] A. Rizzo, K. Ruud, T. Helgaker and M. Jaszuński, *J. Chem. Phys.*, 1998, **109**, 2264.
- [51] S. Coriani, C. Hättig, P. Jørgensen, A. Rizzo and K. Ruud, *J. Chem. Phys.*, 1998, **109**, 7176.
- [52] S. Coriani, C. Hättig, P. Jørgensen and A. Rizzo, *J. Chem. Phys.*, 1999, **111**, 7828.
- [53] A. Rizzo, S. Coriani, A. Halkier and C. Hättig, *J. Chem. Phys.*, 2000, **113**, 3077.
- [54] P. Lazzeretti, *J. Mol. Struct. Theochem*, 2003, **633**, 105.
- [55] P. Lazzeretti, *Adv. Chem. Phys.*, 1987, **75**, 507.
- [56] P. Lazzeretti, in *Electric and Magnetic Properties of Molecules* (ed. S. Wilson), Handbook of Molecular Physics and Quantum Chemistry, Wiley, Chichester, 2003, Vol. 3, pp. 53–145, Part 1, Chapter 3.
- [57] P. Lazzeretti, *Theor. Chim. Acta*, 1993, **87**, 59.
- [58] J. H. van Vleck, *The Theory of Electric and Magnetic Susceptibilities*, Oxford University Press, Oxford, 1932.
- [59] J. Geertsens, *J. Chem. Phys.*, 1989, **90**, 4892.
- [60] J. Geertsens, *Chem. Phys. Lett.*, 1991, **179**, 479.
- [61] J. Geertsens, *Chem. Phys. Lett.*, 1992, **188**, 326.
- [62] P. Lazzeretti, M. Malagoli and R. Zanasi, *Chem. Phys. Lett.*, 1994, **220**, 299.
- [63] S. Coriani, P. Lazzeretti, M. Malagoli and R. Zanasi, *Theor. Chim. Acta*, 1994, **89**, 181.
- [64] P. Lazzeretti, M. Malagoli and R. Zanasi, *J. Chem. Phys.*, 1995, **102**, 9619.
- [65] S. T. Epstein, *The Variation Method in Quantum Chemistry*, Academic Press, New York, 1974.
- [66] A. D. Buckingham, *Adv. Chem. Phys.*, 1967, **12**, 107.
- [67] N. F. Ramsey, *Phys. Rev.*, 1950, **78**, 699.
- [68] M. C. Caputo and P. Lazzeretti, *Chem. Phys.*, 2003, **288**, 281.

This page intentionally left blank

Singularity Structure of Møller–Plesset Perturbation Theory

David Z. Goodson and Alexey V. Sergeev

*Department of Chemistry and Biochemistry, University of Massachusetts Dartmouth,
North Dartmouth, MA 02747, USA*

*Dedicated to Osvaldo Goscinski
in recognition of his fundamental contributions
to quantum chemistry*

Abstract

Møller–Plesset perturbation theory expresses the energy as a function $E(z)$ of a perturbation parameter, z . This function contains singular points in the complex z -plane that affect the convergence of the perturbation series. A review is given of what is known in advance about the singularity structure of $E(z)$ from functional analysis of the Schrödinger equation, and of techniques for empirically analyzing the singularity structure using large-order perturbation series. The physical significance of the singularities is discussed. They fall into two classes, which behave differently in response to changes in basis set or molecular geometry. One class consists of complex-conjugate square-root branch points that connect the ground state to a low-lying excited state. The other class consists of a critical point on the negative real z -axis, corresponding to a dissociation phenomenon. These two kinds of singularities are characterized and contrasted using quadratic summation approximants. A new classification scheme for Møller–Plesset perturbation series is proposed, based on the relative positions in the z -plane of the two classes of singularities. Possible applications of this singularity analysis to practical problems in quantum chemistry are described.

Contents

1. Introduction	194
2. Functional analysis of the energy	195
2.1. Singularities of the energy function	195
2.2. Convergence classes	197
3. Extracting singularity structure from perturbation series	199
4. Examples	201
4.1. Class A	201
4.2. Class B	202
4.3. Systems with complicated singularity structure	204
5. Discussion	205
References	206

1. INTRODUCTION

The starting point for most *ab initio* calculations of molecular energies is the Hartree–Fock (HF) approximation. Therefore, a central problem of quantum chemistry is the construction of an extrapolation from the HF energy to the true energy eigenvalue of the Schrödinger equation. A particularly straightforward approach, at least in principle, is a perturbation theory proposed by Møller and Plesset [1] in which the HF wavefunction is taken as the zeroth-order approximation for the eigenfunction. The theory can be formulated by partitioning the Hamiltonian according to [2]

$$H = H_0 + (H_{\text{phys}} - H_0)z, \quad (1)$$

where H_0 is the sum of one-electron Fock operators, H_{phys} is the Schrödinger Hamiltonian, and z is a perturbation parameter. The energy is then obtained as a power series $E(z) = E_0 + E_1z + E_2z^2 + \dots$. Thus, in Møller–Plesset (MP) theory the energy is a function of z , in the complex z -plane, such that $E(0)$ is equal to the sum of HF orbital energies and $E(1)$ is the extrapolation to the physical energy.

Traditionally, $E(z)$ is calculated by partial summation, i.e., the power series is truncated at some given order and then evaluated at $z = 1$. Truncation at order n yields the ‘MP n ’ approximation to the energy. Thus, $E(z)$ is evaluated as a polynomial. The power series is an asymptotic series, which is a rigorously correct solution only in the $z \rightarrow 0$ limit [3]. The true functional form of E is much more complicated than a polynomial. In particular, it has a rich structure of singular points, i.e., points in an infinitesimal neighborhood of which the first derivative does not exist. Since a polynomial is a functional form that is nonsingular at any finite z , it cannot describe the true function in the neighborhood of a singularity or outside the convergence radius determined by the nearest singularity to the origin. This is the cause of poor convergence seen in recent high-order MP n studies [4–6].

Knowledge of the singularity structure of $E(z)$ can be used to predict the convergence behavior of an MP series [7–9]. The singularity positions in the MP energy function also affect the convergence of the corresponding coupled-cluster (CC) sequence [10,11]. Since CC theory is another method that extrapolates from the HF approximation to the exact solution, this is not surprising. Although the function $E(z)$ corresponds to the ground state energy, its singularity structure contains information about excited states. If the singularities are not all reasonably far from the points $z = 0$ and 1, then this indicates that a single-determinant HF wavefunction will not be a suitable starting point for describing the true wavefunction.

Our purpose here is to review what is known in advance about the functional form of $E(z)$ and then to describe methods for obtaining detailed

information about the singularities from analysis of MP series. In Section 2 we present existence theorems that tell us what singularity structure to expect. Then in Section 3 we describe methods for ‘empirical’ studies in which information about singularity structure is extracted from high-order series obtained from full configuration–interaction (FCI) calculations. In Section 4 we analyze some representative examples and clarify the connection between singularity structure and convergence ‘class’. MP series convergence is often described in terms of a classification scheme developed by Schmidt *et al.* [12]. Series with monotonic convergence are put in class A while series in which the E_i alternate in sign are put in class B. We suggest a modified classification scheme that explains the behavior of molecules with triple bonds or with distorted geometries, which have previously been considered anomalous [5,6,13]. Finally, we discuss possible applications of MP singularity analysis to practical problems in quantum chemistry.

2. FUNCTIONAL ANALYSIS OF THE ENERGY

2.1. Singularities of the energy function

MP perturbation theory is generally used only for the ground state energy. The zeroth-order approximation for the wavefunction is taken to be the lowest-energy HF determinant. Nevertheless, the function $E(z)$ obtained from this perturbation series, when considered as a function over the complex z -plane, contains within it the full energy spectrum of eigenstates with the same symmetry as the ground state. This is the consequence of a theorem presented by Katz [14]:

Let $E^{(0)}, E^{(1)}, E^{(2)}, \dots$ be the spectrum of energy functions of equation (1) corresponding to a given set of all conserved quantities (e.g., angular momentum). For any i and j there exist complex-conjugate pairs of branch points z_{ij}, z_{ij}^* in the complex z -plane at which $E^{(i)}$ is equal to $E^{(j)}$. In the neighborhood of z_{ij}

$$E^{(i)}(z) = b_{ij} - c_{ij}(1 - z/z_{ij})^{1/2}, \quad E^{(j)}(z) = b_{ij} + c_{ij}(1 - z/z_{ij})^{1/2}, \quad (2)$$

where b_{ij} and c_{ij} are constants, and similarly for z_{ij}^* .

Now consider the ground state function $E^{(0)}(z)$. Starting at the origin, trace a path in the z -plane that circles about the point z_{01} . This point is a branch point singularity, which means that a 360° circuit will lead to a new Riemann sheet corresponding to the function $E^{(1)}(z)$. Similarly, following $E^{(0)}(z)$ on a path that circles z_{02} leads to $E^{(2)}(z)$, and so on.

This phenomenon was studied by Baker [15] using a model two-body problem for which an exact solution for $E(z)$ can be obtained. Depending on the choice of parameters, the complex-conjugate branch points connecting $E^{(0)}$ and $E^{(1)}$ could be in the negative half-plane or in the positive half-plane. If branch cuts were specified from these branch points out to infinity, then there were no other branch points. However, if the branch cut was drawn perpendicular to the real axis, joining the two points, then some of the other branch points predicted by Katz, connecting the ground state with higher excited states, were found. The situation is shown schematically in Fig. 1. If one follows $E^{(0)}(z)$ on a path from the origin along the real axis, there will be an avoided crossing as z passes between the 0–1 branch points and no additional avoided crossings with higher states. However, a path that temporarily leaves the real axis to avoid the 0–1 branch points will show no interaction between $E^{(0)}$ and $E^{(1)}$ but will have an avoided crossing with $E^{(2)}$. Since Katz's analysis does not depend on the specific form of the potential energy function, we expect this behavior to be generic.

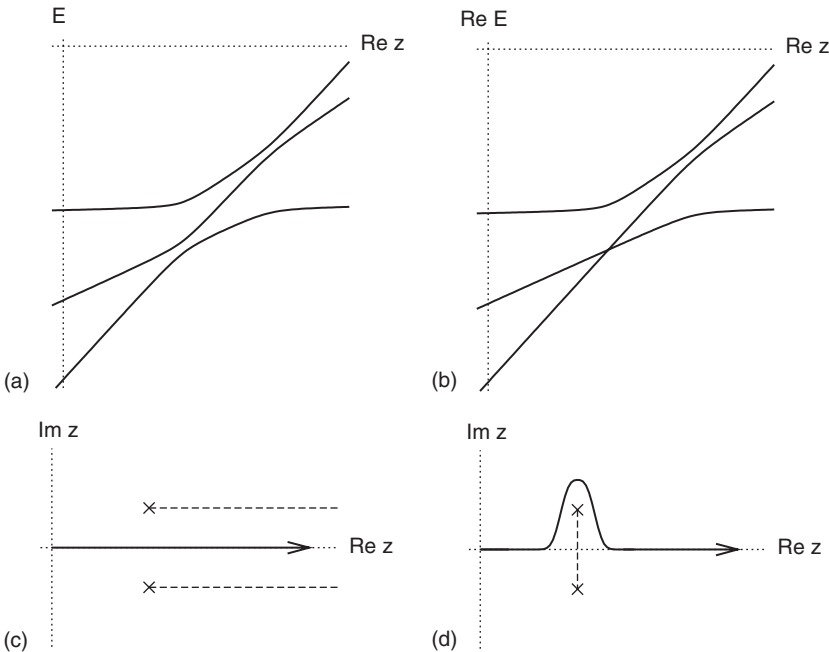


Fig. 1. Schematic representation of energy functions $E^{(0)}$, $E^{(1)}$, and $E^{(2)}$ for two paths in the complex z -plane. Branch cuts (dashed lines) are shown for the branch points z_{01} and z_{01}^* .

These square-root branch points are not the only kind of singularities in the energy function. Baker [15] noted that a many-fermion system in which there are both attractive and repulsive terms in the potential will undergo a spontaneous autoionization at some point on the real z -axis. He suggested this is analogous to a critical point in an (E, z) phase diagram. For z beyond the critical value z_c , there can be no eigenstate in which the system is bound. z_c is a branch-point singularity, although presumably of a more complicated form than equation (2). This was studied by Stillinger [16] for the specific case of an atom. He noted that a negative real z , in equation (1), implies that the r_{12}^{-1} interelectron potential energy terms in H_{phys} are negative, and hence electrons are mutually attractive. At the same time the repulsive mean field central potential in H_0 is, on the negative real axis, increased by a factor of $(1 + |z|)$, which works against the nucleus–electron attraction. For sufficiently large $|z|$ it will be the case that a bound electron cluster infinitely separated from the nucleus will have a lower energy than any state in which the nucleus is bound. Thus, at z_c the nucleus separates from the atom.

The effect of z_c on the behavior of $E^{(0)}(z)$ on the real axis will be rather different from that of the Katz singularities. On a path from the origin along the negative real axis $E^{(0)}(z)$ acquires an imaginary part as it passes through the singularity. This is because the eigenstate then corresponds to a state in the scattering continuum. We expect that the derivative of the function along this path will be continuous.¹ This is due to the fact that when z is only slightly beyond the critical point, there exists a long-range tunneling barrier in the potential, which yields an exponentially small resonance width. Similar behavior is seen in the $1/Z$ expansion, where Z is the nuclear charge, for the two-electron atom [17].

2.2. Convergence classes

It is common practice to classify MP series in terms of their convergence patterns. With class A systems the E_i series coefficients are all of the same sign. The series show monotonic but often rather slow convergence. Class B series, except at the lowest orders, have E_i that alternate in sign. They often converge rapidly but sometimes diverge. A physical interpretation of this classification system was developed by Cremer and He [13]. They examined the terms in the wavefunction that lead to the sign patterns in the E_i and concluded that the class B sign alternation is caused by orbital crowding, as in systems with highly electronegative atoms and closed shells, while class A behavior results from uncrowded orbitals, as in alkanes and radicals.²

¹ The discontinuity of the derivative occurs on paths through z_c that leave the real axis.

² Cremer and coworkers [18] have recently proposed a new nomenclature in which the former classes A and B are now referred to as type I and II, respectively, based on the orbital structure, and with class designations A through E describing a variety of actual convergence patterns seen in practice.

In Ref. [7] it was suggested that these two convergence patterns could be explained in terms of singularity structure. The sign alternation seen for class B would result if the dominant singularity lies on the negative real axis, while class A would result if the dominant singularity is on the positive real axis. The former is consistent with the Stillinger critical point. The Katz analysis predicts complex-conjugate pairs of branch points displaced from the real axis. This would seem to be inconsistent with the class A sign pattern, since a complex-conjugate pair, z_{01}, z_{01}^* in the positive half-plane will give a periodic sign pattern with regions in which successive E_i are negative alternating with regions in which they are positive. However, if the imaginary part of these singularities is small, then the period, given by [17,19]

$$n_0 = \pi / \arctan(|\text{Im } z_{01} / \text{Re } z_{01}|), \quad (3)$$

will be sufficiently large that the series will appear to converge monotonically up to very high orders.

A connection between singularity analysis and the Cremer–He analysis can perhaps be made as follows. If the valence electron orbitals are crowded into a relatively small region of space, then the attractive interaction between the electrons (for negative z) is especially strong, as is the mean-field repulsive perturbation. Both of these effects favor autoionization at small $|z|$. It is not surprising that of the class B systems for which high-order MP series have been calculated, the one with the dominant singularity closest to the origin is F^- , with the aug-cc-pVDZ basis set.

It is interesting that the position of z_c is strongly dependent on the basis set. In the case of F^- if the cc-pVDZ basis, which lacks the diffuse functions of the augmented basis sets, is used instead, then the singularity on the negative real axis seems to disappear [5,7,20]. Apparently, diffuse functions are needed to describe the autoionization.

In contrast, the position of the dominant singularity for class A systems is relatively insensitive to the basis set. This is a Katz branch point pair connecting the ground state with the first excited state. The interaction between these two states can be described reasonably well with a small basis set. The effect of additional polarization functions, representing highly excited configurations, is small. However, changes in molecular geometries can have a large effect on the class A singularity [11], with bond stretching causing the branch points to move in toward the physical point $z = 1$. The distance of these branch points from $z = 1$ is related to the energy gap between the states at $z = 1$. As a bond is stretched the energy gap decreases and the point of avoided crossing along the positive real axis moves closer to $z = 1$.

It is important to note that a path along the *negative* real axis could also show an avoided crossing between the ground state and the first excited state. In Section 4.3, we present empirical evidence indicating that

such a Katz branch point pair, in the negative half-plane, is responsible for the worst examples of MP series divergence. Thus, there are two distinct kinds of class B systems. We suggest that classic class B behavior, with alternating signs in the E_i , is due to a critical point while the complicated sign patterns in systems such as the C_2 molecule or in molecules with bonds stretched well beyond the equilibrium distance are due to the simultaneous effects of Katz degeneracies in both the positive and negative half-planes.

3. EXTRACTING SINGULARITY STRUCTURE FROM PERTURBATION SERIES

There are two general approaches for obtaining information about singularity structure from a perturbation series [21]: asymptotic methods and approximant methods. The former category includes such familiar procedures as the ratio test and the n th-root test as well as some more modern techniques [22,23], all of which are based on a theorem of Darboux that states that in the limit of large order the series coefficients of the function in question become equivalent to the corresponding coefficients of the Taylor series of the *dominant* singularity, i.e., the singularity closest to the origin. The advantage of these methods is that we have for them rigorous convergence proofs. A disadvantage is that they only provide information about the one singularity closest to the origin. More distant singularities can sometimes be studied using conformal mappings [21], but, even for the dominant singularity, convergence can be significantly slowed by interference from other singularities.

For analysis of MP series we have found approximant methods to be more useful than asymptotic methods. The idea is to construct a model function (a *summation approximant*) containing parameters that are chosen so that its Taylor series agrees with the coefficients of the perturbation series up to some given order. Although there are no generally applicable convergence theorems for approximants, if the functional form of the approximant is a reasonable model for the true functional form then the convergence can be rapid. Approximants can simultaneously fit more than one singularity. Furthermore, they provide an analytical continuation to regions of the complex plane where partial sums are poorly convergent or divergent.

A systematic approach to constructing approximants was proposed by Padé [24,25]. A set of polynomials $A_k^{(m)}(z)$, where k indicates the degree of the polynomial, is defined by the asymptotic relation:

$$\sum_{m=0}^M A_{k_m}^m E^m = \mathcal{O}(z^K), \quad K = M + \sum_{m=0}^M k_m. \quad (4)$$

The notation $\mathcal{O}(z^K)$ means that the coefficients of the Taylor series of the left-hand side are equal to zero up through order $K - 1$. E in equation (4) represents the perturbation series of the energy function. Collecting terms according to the power of z yields K linear equations for the $K + 1$ coefficients of the polynomials. The final coefficient is set according to an arbitrary normalization condition, typically, $A^{(M)}(0) = 1$. Once the polynomial coefficients are obtained, equation (4) is solved for $E(z)$.

With $M = 1$ we have rational approximants, $E(z) = A^{(1)}(z)/A^{(0)}(z)$. The application of these to perturbation theories of the Schrödinger equation was pioneered by Brandäs and Goscinski [26]. They proposed using approximants to determine singularity positions. However, the singularity structure of rational approximants is not of the form we expect for the MP energy. They are single-valued functions, containing poles, at the zeros of $A^{(0)}$, but no branch points. Given enough series coefficients, they can model a branch cut with combinations of poles and zeros [7,27] but they cannot model more than one branch.

More appropriate are quadratic approximants [7,27–32], with $M = 2$, which have the double-valued solution

$$E = \frac{1}{2} \left[\frac{A^{(1)}}{A^{(2)}} \pm \frac{1}{A^{(2)}} \sqrt{(A^{(1)})^2 - 4A^{(0)}A^{(2)}} \right], \quad (5)$$

with a square-root branch point as specified by the Katz theorem. It has two branches (\pm) connected by branch points at the values of z at which the discriminant polynomial, $(A^{(1)})^2 - 4A^{(0)}A^{(2)}$, is zero. In principle, one branch describes the ground state and the other, the first excited state. More complicated branch points are, in practice, fit by these approximants with clusters of square-root branch points. Approximants with $M > 2$ can describe additional branches of the function, although the accuracy for higher branches tends to be poor unless the series is known to be quite high order [33–36]. Differential approximants, with the powers of E in equation (4) replaced by derivatives, can describe a wider variety of singularity types [25,37].

Other kinds of approximants can also be used. For example, Olsen *et al.* [20] analyzed MP series convergence using a 2×2 matrix eigenvalue equation [38,39], which implicitly incorporates a square-root branch point. It is of course possible simply to explicitly construct an approximant as an arbitrary function with the singularity structure that $E(z)$ is expected to have. We suggest, for example, approximants of the form³

$$E(z) = \pm P_A(z)[(1 - z/z_{01})(1 - z/z_{01}^*)]^{1/2} + P_B(z)B(z - z_c) + P_C(z), \quad (6)$$

³ This is an example of an Hermite–Padé approximant [27].

where P_A , P_B , and P_C are polynomials and

$$B(z) = \int_0^\infty (1+zt)^{3/2} e^{-t} dt \quad (7)$$

The function $B(z - z_c)$, which can be expressed in terms of an exponential integral, has the behavior we expect for autoionization in that it has a branch point at z_c at which the function becomes complex but with the derivative continuous along the real axis. The coefficients of the polynomials can be chosen so that the Taylor series agrees with the perturbation series.

Note that the gap between the energy of the ground state and that of the first excited state is given by

$$E^{(+)} - E^{(-)} = 2P_A(z)[(1 - z/z_{01})(1 - z/z_{01}^*)]^{1/2}. \quad (8)$$

The value of the gap at $z = 0$ is simply $2P_A(0)$. Since $z = 0$ corresponds to the HF solution, this value is easily calculated. By thus constraining P_A , we can include in the analysis additional information about the singularity structure beyond the information we obtain from the perturbation series. The quadratic approximant, equation (5), can be similarly constrained.

At present, the highest order for which direct calculations of MP series have been carried out is only six [40]. However, MP series to arbitrary order can be computed from elements of the Hamiltonian matrix that are obtained in the course of an FCI calculation [41,42]. As a result, high-order MP series are now available in the literature for a variety of systems with as many as 10 correlated valence electrons [5,6]. In principle, the singularity structure of $E(z)$ can be obtained from an FCI calculation directly, without calculating the perturbation series, by analyzing the characteristic polynomial as a function of z . This is a polynomial of very high degree, which makes a full numerical analysis of the z dependence difficult. However, given an initial estimate of a singularity position one could refine the result with a local analysis of the characteristic polynomial in the neighborhood of that point.

4. EXAMPLES

4.1. Class A

Consider the molecule BH. Since the boron atom is four electrons short of a full octet, this should be a clear example of class A according to the Cremer–He criteria [13]. The MP series has been calculated [5,6] through about 15th order for several of the correlation-consistent basis sets [43] and all the E_i have the same sign.

In principle, the zeros of the discriminant polynomial in equation (5) correspond to branch points of $E(z)$. Since the number of zeros increases

Table 1. Singularity analysis of the energy function of the BH molecule from quadratic approximants

Basis set	Branch point in positive half-plane	Weight	Branch point in negative half-plane	Weight
cc-pVDZ	$1.65 \pm 0.43i$	0.4	-3.6	0.001
cc-pVTZ	$1.60 \pm 0.40i$	0.3	-3.5	0.01
cc-pVQZ	$1.60 \pm 0.31i$	0.4	-3.5	0.04
aug-cc-pVDZ	$1.55 \pm 0.41i$	0.1	-2.5	0.001
aug-cc-pVTZ	$1.59 \pm 0.36i$	0.4	-3	0.01
aug-cc-pVQZ	$1.61 \pm 0.35i$	0.4	-2.1	0.002

The ‘weight’ corresponds to $|c_{ij}|$ of equation (2).

rapidly with the order of the series, we expect most of these branch points to be spurious, and in practice most are unstable from order to order and are often quite distant from the origin or appear as nearly coincident pairs. For BH, the branch points that are stable from order to order are shown in Table 1. They are consistent with the predictions of the functional analysis, with a complex-conjugate pair z_{01}, z_{01}^* with positive real part and a negative real z_c . The former are the dominant singularities, as expected for a class A system. The z_{01} values imply that the period of the sign pattern of the E_i is somewhere between 13 and 17. Since the highest-order coefficients probably contain significant roundoff error, these values are not inconsistent with the lack of apparent sign alternation in the series. The basis sets represent two families, cc-pVXZ and aug-cc-pVXZ. These are equivalent except that the latter are augmented with diffuse functions. The presence of diffuse functions seems to shift z_c toward the origin but has little effect on z_{01} .

In Fig. 2 we plot the two branches of a quadratic approximant as a function of z on the real axis, for BH with the largest basis set. A broad avoided crossing can be seen at $\text{Re } z_{01}$. Also shown is the result from a rational approximant, which agrees very well with the quadratic approximant for the lower branch up to the avoided crossing. It then jumps to the higher branch after passing through the branch cut between z_{01} and z_{01}^* . Very similar behavior is seen with the other five basis sets.

4.2. Class B

In Table 1 we also list a singularity for BH on the negative real axis, which presumably corresponds to the critical point. However, the convergence is rather poor since it is much farther from the origin than are the dominant singularities. For a better example we consider the class B system F^- . Christiansen *et al.* [5] found that the MP series for F^- with the aug-cc-pVDZ

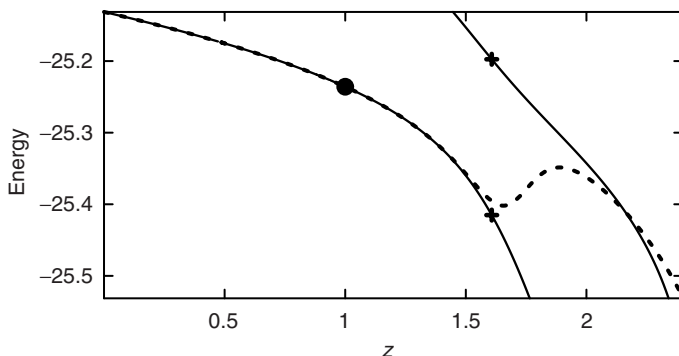


Fig. 2. Energy [44] in E_h for BH with the aug-cc-pVQZ basis as a function of real z , from MP series of Leininger *et al.* [6]. The solid curves are the two branches of the quadratic approximant with polynomial degrees 5, 5, and 5, with the values corresponding to the real part of the branch points marked by crosses. The dashed curve is from the rational approximant with degrees 8 and 8. The filled circle shows the physical point.

basis is divergent. The only stable branch point from quadratic approximants is at -0.60 , which presumably corresponds to the critical point, z_c .

Figure 3 shows $E(z)$ for negative real z . Up until z_c the rational and quadratic approximants are in agreement. After passing through z_c the quadratic approximant gains an imaginary part. The rational approximant, unable to produce a branch point, instead maps out a branch cut

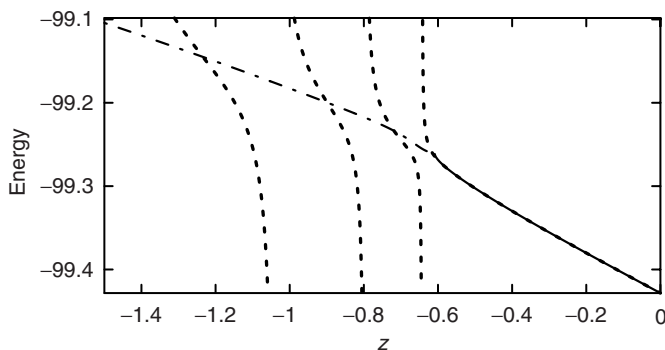


Fig. 3. Energy [44] in E_h for F^- with the aug-cc-pVDZ basis as a function of real z , from MP series of Ref. [5]. The solid curve is the quadratic approximant with degrees 6, 6, and 6. When this approximant is complex, the real part is shown as the dash-dot curve. The dashed curve is the rational approximant with degree 9 for the numerator and 10 for the denominator.

with alternating poles and zeros [27] along the real axis starting slightly beyond z_c .

In Section 2.1 we argued that for a path along the real axis the derivative at z_c should be continuous. By construction, the singularity from a quadratic approximant is a square-root branch point, of the form $P(z_c)(1 - z/z_c)^{1/2}$ where P is nonsingular at z_c . This expression has a discontinuous derivative along any path. However, the quadratic approximant in Fig. 3 restricts the effects of this discontinuity to the immediate neighborhood of z_c by making the weight of the singularity, $|P(z_c)|$, rather small, in this case, 0.03. For this reason, the discontinuity of the derivative is apparent only on close examination of the curve. Similar behavior is seen for z_c of BH, in which case, as shown in Table 1, the weight of z_c is significantly smaller than the weight of z_{01} . Additional evidence for a qualitative difference between the singularity on the negative real axis and the complex-conjugate pair in the positive half-plane is the fact that the quadratic approximants show more clustering of spurious branch points around the former, suggesting that isolated square-root branch points are insufficient to accurately model the function.

4.3. Systems with complicated singularity structure

Molecules such as N_2 , C_2 , and CN^+ , and in general molecules with bonds stretched from the equilibrium geometry, do not fit well into the A/B classification scheme [5,6,13,20,40]. They show irregularities in the sign patterns and poor convergence. This has been attributed to the presence of significant singularity structure in both half-planes [7,9,10].

For C_2 , quadratic approximants show stable branch points at $1.23 \pm 0.35i$ and $-0.95 \pm 0.33i$. The behavior of $E(z)$ in the vicinity of these points is shown in Fig. 4. It is qualitatively similar to the behavior at z_{01} for BH.

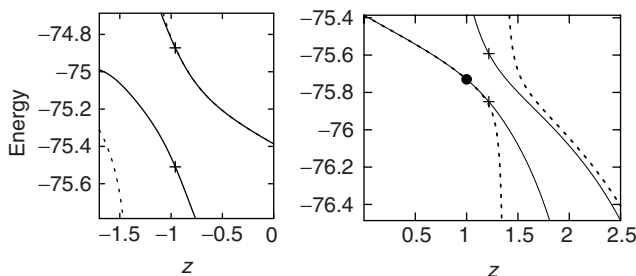


Fig. 4. Energy [44] in E_h of C_2 for real z with the cc-pVDZ basis. The MP series is from Ref. [6]. Solid curves are the branches of the quadratic approximant with degrees 6, 6, and 6. Values corresponding to the real part of the branch points are marked by crosses. The dashed curve is the rational approximant with degrees 9 and 10. The filled circle shows the physical point.

In the case of C_2 we see no singularity on the negative real axis. This may be due to the fact that the basis set (cc-pVDZ) lacks diffuse functions.

The anomalous systems have in common a relatively small weight for the HF reference determinant in the $z = 1$ wavefunction, which suggests that Katz branch points will be especially significant. Stretching a bond decreases the energy gap, which shifts avoided crossings to lower values of $|z|$, causing branch point positions to vary significantly along the potential energy surface. Olsen *et al.* [20] found that the negative real singularity for the hydrogen fluoride molecule, determined from the large-order series, also shifts toward the origin as the bond is stretched, but the effect is small. An analysis [11] of MP4 series found a significant shift of singularities toward $z = 1$ in the positive half-plane and toward $z = 0$ in the negative half-plane as the distances increase toward dissociation. The MP4 analysis could not determine the imaginary part of the singular points, and therefore could not distinguish the nature of the singularity in the negative half-plane.

5. DISCUSSION

The MP energy function $E(z)$ is expected to have a complex-conjugate pair of square-root branch points in the positive half-plane, a branch point on the negative real axis corresponding to a critical point, and, possibly, a complex-conjugate pair of square-root branch points in the negative half-plane. The complex-conjugate branch points in either half-plane result from the same physical phenomenon, avoided crossing between the ground state and a low-lying excited state. They are insensitive to changes in the basis set but shift significantly as bonds are stretched. In contrast, the critical point represents an autoionization process and its position can depend strongly on the basis.

The A/B classification scheme, based on series coefficient sign patterns, is inadequate for describing this situation. It seems more sensible to classify MP series according to singularity structure. We suggest that the complex-conjugate branch points, regardless of the real part, be referred to as ‘class α ’ singularities while the critical point be referred to as ‘class β ’. An atom or molecule in which the class β singularity dominates the perturbation series can be called a class β system. If the class α singularities in the positive half-plane dominate, then we have a class α system. Systems in which the positive class α singularities are approximately the same distance from the origin as the other class α or the class β singularities can be called, respectively, class $\alpha\alpha$ or $\alpha\beta$.

Since for most applications to systems of chemical interest, it is not feasible at present to compute MP series beyond fourth or fifth order, methods will have to be developed for estimating singularity positions from low-order series. For clear class α or class β systems, quadratic

approximants at MP4 can give a reasonably accurate result [7]. Difficulties arise with $\alpha\alpha$ and $\alpha\beta$ systems because the approximants tend to model the multiple singularities with a single branch point halfway between them [9]. One approach for dealing with this is to use a conformal mapping to shift the singular points so that one will always be somewhat closer to the origin than the other [21]. This is the basic idea behind the MP4-q λ method [8], which makes quadratic approximants in most cases a dependable tool for summing the series. In contrast, conformal mappings are less effective with partial summation, since then one must shift all singularities *away* from the origin.

An important potential application to practical quantum chemistry is to use singularity positions as a diagnostic criterion for predicting the accuracy of a calculation. This has already been implemented to some extent, using the MP4-q λ singularity positions to identify cases in which $\alpha\alpha$ and $\alpha\beta$ effects adversely affect energy accuracy. The positions of singularities in the negative half-plane seem to be an excellent diagnostic of the accuracy of the MP energy summation [8,9]. CC calculations with the CCSD(T) method are relatively insensitive to the class β singularity but are affected by $\alpha\alpha$ singularity structure. The MP4-q λ singularity analysis can apparently distinguish, to some extent, between $\alpha\alpha$ and $\alpha\beta$ systems, and thereby serve as an accuracy diagnostic for CC methods [10].

Another application is to multireference perturbation theory (MRPT). A key question in choosing the reference set of eigenstates is the extent of interaction between different states [45–48]. Positions of the complex-conjugate branch points provide a measure of this [49]. One could monitor singularity structure along a path on the potential energy hypersurface, changing the reference set as needed to eliminate harmful branch points. At present, software is readily available only for third-order MRPT [50], which is likely not sufficient for reliable singularity analysis. A fourth-order MRPT with a small reference set might benefit significantly from a quadratic approximant analysis, both for summation and for determining branch point positions.

REFERENCES

- [1] C. Møller and M. S. Plesset, *Phys. Rev.*, 1934, **46**, 618.
- [2] D. Cremer, in *Encyclopedia of Computational Chemistry* (eds P. v. R. Schleyer, N. L. Allinger, T. Clark, J. Gasteiger, P. A. Kollman, H. F. Schaefer III and P. R. Schreiner), Wiley, New York, 1998, 1706–1735.
- [3] C. M. Bender and S. A. Orszag, *Advanced Mathematical Methods for Scientists and Engineers*, McGraw-Hill, New York, 1978.
- [4] (a) K. A. Peterson and T. H. Dunning, Jr., *J. Phys. Chem.*, 1995, **99**, 3898; (b) T. H. Dunning, Jr. and K. A. Peterson, *J. Chem. Phys.*, 1998, **108**, 4761.
- [5] (a) O. Christiansen, J. Olsen, P. Jørgensen, H. Koch and P.-A. Malmqvist, *Chem. Phys. Lett.*, 1996, **261**, 369; (b) J. Olsen, O. Christiansen, H. Koch and P. Jørgensen, *J. Chem. Phys.*, 1996, **105**, 5082.

- [6] M. L. Leininger, W. D. Allen, H. F. Schaefer III and C. D. Sherrill, *J. Chem. Phys.*, 2000, **112**, 9213.
- [7] D. Z. Goodson, *J. Chem. Phys.*, 2000, **112**, 4901.
- [8] D. Z. Goodson, *J. Chem. Phys.*, 2000, **113**, 6461.
- [9] D. Z. Goodson, *Int. J. Quantum Chem.*, 2003, **92**, 35.
- [10] D. Z. Goodson, *J. Chem. Phys.*, 2002, **116**, 6948.
- [11] D. Z. Goodson and M. Zheng, *Chem. Phys. Lett.*, 2002, **365**, 396.
- [12] C. Schmidt, M. Warken and N. C. Handy, *Chem. Phys. Lett.*, 1993, **211**, 272.
- [13] D. Cremer and Z. He, *J. Phys. Chem.*, 1996, **100**, 6173.
- [14] A. Katz, *Nucl. Phys.*, 1962, **29**, 353.
- [15] G. A. Baker, Jr., *Rev. Mod. Phys.*, 1971, **43**, 479.
- [16] F. H. Stillinger, *J. Chem. Phys.*, 2000, **112**, 9711.
- [17] J. D. Baker, D. E. Freund, R. N. Hill and J. D. Morgan III, *Phys. Rev. A*, 1990, **41**, 1247.
- [18] B. Forsberg, Z. He, Y. He and D. Cremer, *Int. J. Quantum Chem.*, 2000, **76**, 306.
- [19] D. Z. Goodson, M. López-Cabrera, D. R. Herschbach and J. D. Morgan III, *J. Chem. Phys.*, 1992, **97**, 8481.
- [20] J. Olsen, P. Jørgensen, T. Helgaker and O. Christiansen, *J. Chem. Phys.*, 2000, **112**, 9736.
- [21] C. J. Pearce, *Adv. Phys.*, 1978, **27**, 89, and references therein.
- [22] D. W. Ninham, *J. Math. Phys.*, 1963, **4**, 679.
- [23] C. Hunter and B. Guerrieri, *SIAM J. Appl. Math.*, 1980, **39**, 248.
- [24] H. Padé, *Ann. de l'Ecole Normale Sup. 3ième Série*, 1892, **9** (Suppl. 1).
- [25] G. A. Baker, Jr. and P. Graves-Morris, *Padé Approximants*, Cambridge University Press, Cambridge, 1996, and references therein.
- [26] (a) E. Brandäs and O. Goscinski, *Phys. Rev. A*, 1970, **1**, 552; (b) E. Brandäs and O. Goscinski, *Int. J. Quantum Chem.*, 1970, **4**, 5718.
- [27] G. A. Baker, Jr., *The Essentials of Padé Approximants*, Academic Press, New York, 1975.
- [28] R. E. Shafer, *SIAM J. Math. Anal.*, 1975, **11**, 447.
- [29] (a) K. D. Jordan, *Int. J. Quantum Chem. Symp.*, 1975, **9**, 325; (b) K. D. Jordan, *Chem. Phys.*, 1975, **9**, 199.
- [30] (a) V. D. Vainberg, V. D. Mur, V. S. Popov and A. V. Sergeev, *Pis'ma Zh. Eksp. Teor. Fiz.*, 1986, **44**, 9; (b) V. D. Vainberg, V. D. Mur, V. S. Popov and A. V. Sergeev, *JETP Lett.*, 1986, **44**, 9.
- [31] A. V. Sergeev, *J. Phys. A: Math. Gen.*, 1995, **28**, 4157.
- [32] D. Z. Goodson and A. V. Sergeev, *J. Chem. Phys.*, 1999, **110**, 8205.
- [33] P. G. Drazin and Y. Tourigny, *SIAM J. Appl. Math.*, 1996, **56**, 1–18.
- [34] A. V. Sergeev and D. Z. Goodson, *J. Phys. A: Math. Gen.*, 1998, **31**, 4301.
- [35] F. M. Fernández and R. H. Tipping, *J. Mol. Struct. Theochem*, 1999, **488**, 157.
- [36] (a) F. M. Fernández and C. G. Diaz, *Eur. Phys. J. D*, 2001, **15**, 41; (b) C. G. Diaz and F. M. Fernández, *J. Mol. Struct. Theochem*, 2001, **541**, 31.
- [37] M. A. H. Khan, *J. Comput. Appl. Math.*, 2002, **149**, 457.
- [38] S. Wilson, K. Jankowski and J. Paldus, *Int. J. Quantum Chem.*, 1985, **28**, 525.
- [39] J. P. Finley, R. K. Chaudhuri and K. F. Freed, *J. Chem. Phys.*, 1995, **103**, 4990.
- [40] Z. He and D. Cremer, *Int. J. Quantum Chem.*, 1996, **59**, 15, see also p. 31, 57, 71.
- [41] W. D. Laidig, G. Fitzgerald and R. J. Bartlett, *Chem. Phys. Lett.*, 1985, **113**, 151.
- [42] (a) P. J. Knowles, K. Somasundram, N. C. Handy and K. Hirao, *Chem. Phys. Lett.*, 1985, **113**, 8; (b) N. C. Handy, P. J. Knowles and K. Somasundram, *Theor. Chim. Acta*, 1985, **68**, 87.
- [43] (a) T. H. Dunning, Jr., *J. Chem. Phys.*, 1989, **90**, 1007; (b) R. A. Kendall, T. H. Dunning, Jr. and R. J. Harrison, *J. Chem. Phys.*, 1992, **96**, 6769.
- [44] The plotted energy here is $E_0 + [E(z) - E_0]/z \sim (E_0 + E_1) + E_2z + E_3z^2 + \dots$.

- [45] G. Hose, *J. Chem. Phys.*, 1986, **84**, 4505.
- [46] (a) S. Zarrabian and R. J. Bartlett, *Chem. Phys. Lett.*, 1988, **153**, 133; (b) S. Zarrabian and J. Paldus, *Int. J. Quantum Chem.*, 1990, **38**, 761.
- [47] J. P. Finley and K. F. Freed, *J. Chem. Phys.*, 1995, **102**, 1306, and references therein.
- [48] J. Olsen and M. P. Fülscher, *Chem. Phys. Lett.*, 2000, **326**, 225.
- [49] M. Warken, *J. Chem. Phys.*, 1995, **103**, 5554.
- [50] H.-J. Werner, *Mol. Phys.*, 1996, **89**, 645.

Approximate Inclusion of the T_3 and R_3 Operators in the Equation-of-motion Coupled-cluster Method

Monika Musiał,¹ Stanisław A. Kucharski²
and Rodney J. Bartlett³

¹*Quantum Theory Project, Department of Chemistry and Physics,
University of Florida, Gainesville, FL 32611, USA*

²*University of Silesia, Institute of Chemistry, Szkolna 9, Katowice, Poland*

³*Quantum Theory Project, Department of Chemistry and Physics, University of Florida,
Gainesville, FL 32611, USA*

Abstract

New iterative triple excitation corrections to the EOM-CCSD based upon the CCSDT-3 method for calculating excitation energies (EE), ionization potentials (IP) and electron affinities (EA) are systematically studied. The methods have been tested by the evaluation of the vertical EEs, IPs, and EAs for the C_2 , O_3 , N_2 and CO molecules. The results have been compared to the respective full models, for all systems and – for one case of the C_2 molecule – were compared to experiment. The most promising variant for IP and EA calculations uses for the ground state the approximate CCSDT-3 scheme with a full, untruncated, approach at the EOM stage. Both steps require n^7 scaling.

Contents

1. Introduction	209
2. Theory	210
3. Approximate variants	212
4. Results and discussion	216
4.1. IP and EA results	219
4.2. EE results	220
5. Conclusions	221
Acknowledgements	221
References	221

1. INTRODUCTION

In coupled-cluster (CC) [1–6] calculations the accuracy of the results depends strongly on the inclusion of the connected triples contributions. The CC formalism offers several possibilities of incorporating the T_3 operator

starting with the very popular noniterative option (CCSD(T)), through various iterative CCSDT- n models ($n = 1, 2, 3, 4$) and ending at the full CCSDT approach. The advantages of the approximate approaches are tied to their computational efficiency: the full CCSDT methods scales as n^8 while the approximate variants scale as n^7 . In situations where the computational efficiency is not compromised by significantly poorer performance, the approximate version may create a reliable computational tool. The experience gained in the process of constructing approximate variants of the CCSDT method for the ground state may be exploited in the search for efficient approximate schemes applicable to the direct calculation of energy differences *via* the equation-of-motion (EOM) technique. The latter approach can be used in the calculation of the excitation energies (EE) [7–14] ionization potentials (IP) [15–19] and electron affinities (EA) [20–22]. There were several attempts to introduce reliable approximate variants in the treatment of the EOM energies [8,9,18]; most of them focused on the electronic EEs [8,9], although the IPs were also addressed [18].

The general conclusion reached on the basis of the EOM EE calculations is that the most reliable variant of the EOM-CC approach with approximate inclusion of the connected triples is that referred to in the literature as CCSDT-3. At the ground state level this approach differs from the full CCSDT method only in the construction of the target T_3 amplitudes, where all the terms containing T_3 contributions to the target amplitude are removed, yet we retain all possible T_1 and T_2 terms. This procedure eliminates any terms that would require more than an $\sim n^7$ procedure. It also bypasses any need to store the $\sim n^6$ T_3 amplitudes as they can be dealt with ‘on-the-fly’.

The analogous strategy can be adopted at the EOM level, i.e., we avoid costly terms involving R_3 to R_3 contributions, which are more difficult computationally. However, in the case of IP and EA calculations another option can also be taken into account which uses the approximate approach at the ground state level, e.g., CCSDT-3 (to avoid costly n^8 scaling) combined with a rigorous, untruncated scheme at the EOM level. This combination makes sense since both scale as n^7 .

The aim of this work is to investigate the performance of various approximate approaches that include connected triple contributions. At the EOM-CC level we have a significantly larger number of options since we may also select various elements of the \bar{H} operator in the R_3 equation. We will investigate the performance of the approximate methods for the EE, IP and EA problems.

2. THEORY

Within the EOM formalism the k -state wave function $|\Psi_k^{XX}\rangle$ ($XX = \text{EE, IP or EA}$) is obtained by the action of the $R^{XX}(k)$ operator on the ground state

wave function $|\Psi_0\rangle$:

$$|\Psi_k^{\text{XX}}\rangle = R^{\text{XX}}(k)|\Psi_0\rangle \quad (1)$$

The $R^{\text{XX}}(k)$ operator is expressed as

$$R^{\text{XX}}(k) = r_0^{\text{XX}}(k) + R_1^{\text{XX}}(k) + R_2^{\text{XX}}(k) + R_3^{\text{XX}}(k) \quad (2)$$

and r_0 is a constant for EE and zero for IP and EA. R_i^{XX} ($i = 1, 2, 3$) is an excitation and/or ionization operator depending on the considered process:

$$\begin{aligned} R^{\text{EE}}(k) = & r_0(k) + \sum_a \sum_i r_i^a(k) a^\dagger i + \frac{1}{4} \sum_{ab} \sum_{ij} r_{ij}^{ab}(k) a^\dagger b^\dagger ji \\ & + \frac{1}{36} \sum_{abc} \sum_{ijl} r_{ijl}^{abc}(k) a^\dagger b^\dagger c^\dagger lji \end{aligned} \quad (3)$$

$$\begin{aligned} R^{\text{IP}}(k) = & \sum_i r_i(k) i + \frac{1}{2} \sum_a \sum_{ij} r_{ij}^a(k) a^\dagger ji \\ & + \frac{1}{12} \sum_{ab} \sum_{ijl} r_{ijl}^{ab}(k) a^\dagger b^\dagger lji \end{aligned} \quad (4)$$

$$\begin{aligned} R^{\text{EA}}(k) = & \sum_a r^a(k) a^\dagger + \frac{1}{2} \sum_{ab} \sum_i r_i^{ab}(k) a^\dagger b^\dagger i \\ & + \frac{1}{12} \sum_{abc} \sum_{ij} r_{ij}^{abc}(k) a^\dagger b^\dagger c^\dagger ji \end{aligned} \quad (5)$$

where the standard notation of indices was used, i.e., indices a, b, \dots (i, j, \dots) refer to virtual (occupied) one-particle levels. Using the normal-ordered Hamiltonian the Schrödinger equation for the ground state ($k = 0$) is

$$H_N |\Psi_0\rangle = \Delta E_0 |\Psi_0\rangle \quad (6)$$

For the k th excited, ionized or electron-attached state the equation $H_N |\Psi_k^{\text{XX}}\rangle = \Delta E_k^{\text{XX}} |\Psi_k^{\text{XX}}\rangle$, can be written as

$$H_N R^{\text{XX}}(k) |\Psi_0\rangle = \Delta E_k^{\text{XX}} R^{\text{XX}}(k) |\Psi_0\rangle \quad (7)$$

Multiplying equation (6) by $R^{\text{XX}}(k)$ and subtracting from equation (7) gives the EOM

$$[H_N, R^{\text{XX}}(k)] |\Psi_0\rangle = \omega_k^{\text{XX}} R^{\text{XX}}(k) |\Psi_0\rangle \quad (8)$$

where $\omega_k^{\text{XX}} = \Delta E_k^{\text{XX}} - \Delta E_0$ is the energy of the particular process (excitation, ionization or electron-attachment). Since $|\Psi_0\rangle = e^T |\Phi_0\rangle$ and both R and T commute, equation (8) may be written as

$$(\bar{H}_N R^{\text{XX}}(k))_c |\Phi_0\rangle = \omega_k^{\text{XX}} R^{\text{XX}}(k) |\Phi_0\rangle \quad (9)$$

Projecting the above equation onto the determinant corresponding to the excited/ionized configurations $|\mathbf{h}\rangle = |\mathbf{h}_1 \mathbf{h}_2 \mathbf{h}_3\rangle$ we obtain matrix eigenvalue equations

$$(\bar{H}_N) R^{\text{XX}}(k) = \omega_k^{\text{XX}} R^{\text{XX}}(k)$$

where \bar{H}_N is the similarity transformed Hamiltonian defined as

$$\bar{H}_N = e^{-T} H_N e^T = (H_N e^T)_c \quad (10)$$

In general we can expand \bar{H}_N into one-body, two-body, three-body, etc. contributions:

$$\bar{H}_N = \sum_{k=0}^2 I_k^1 + \sum_{k=0}^4 I_k^2 + \sum_{k=0}^3 I_k^3 + \sum_{k=0}^3 I_k^4 + \dots$$

where I_k^n represents the n -body element of \bar{H}_N with k annihilation lines. The form of \bar{H}_N which is required for the construction and solution of the EOM equations at the CCSDT level involves up to four-body elements, see Fig. 1. (see our previous works [14,19,22] for details), which would significantly slow down the computations. Table 1 presents this scaling. Thus, in order to build an efficient computational scheme, the construction of these complex elements of \bar{H}_N must be avoided. As we described in Refs. [14,19,22], we fully used a factorization procedure which significantly reduced the scaling factor (see Table 1). Note that this strategy does not introduce any approximation, i.e., the methods are rigorously correct.

3. APPROXIMATE VARIANTS

As we know, states that correspond to the ionized reference can be studied by diagonalizing \bar{H}_N in a basis of determinants containing $N - 1$ electrons (N refers to the number of electrons in $|\Phi_0\rangle$), while the electron attachment states correspond to the diagonal representation of \bar{H} in the $N + 1$ particle Hilbert space, and of course for the electronic excited states we diagonalize \bar{H} in a basis of determinants containing N electrons.

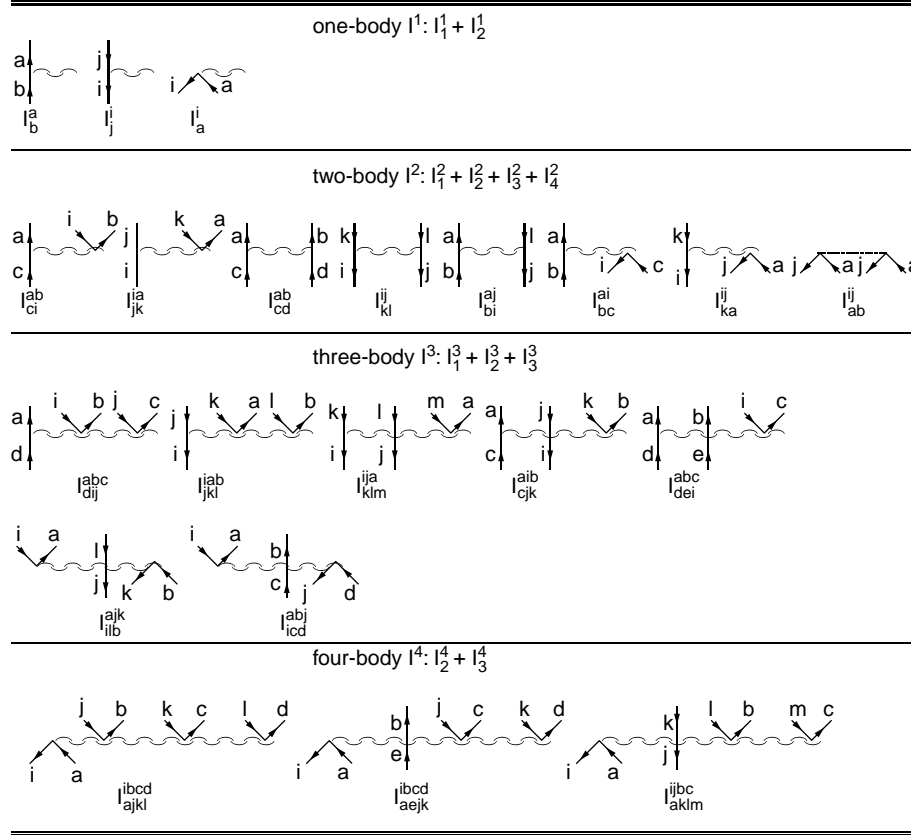


Fig. 1. The diagrammatic representation of the elements of \tilde{H}_N used in the derivation of the IP-, EA-, and EE-EOM-CCSDT equations.

Table 1. Rank of the computational procedure for the EOM-CC variants

Scaling	EOM-CCSD				
	T-3 ^a	T-3a	T-3b	T-3c	T ^b
<i>Ionization potential</i>					
$\bar{H}R$	$n^7(n_0^4n_v^3)^c$	$n^7(n_0^4n_v^3)^c$	$n^7(n_0^4n_v^3)^c$	$n^8(n_0^5n_v^3)^c$	$n^8(n_0^4n_v^4)^c$
	$n^6(n_0^3n_v^3)^d$	$n^6(n_0^3n_v^3)^d$	$n^6(n_0^3n_v^3)^d$	$n^6(n_0^3n_v^3)^d$	$n^7(n_0^3n_v^4)^d$
\bar{H}	$n^7(n_0^3n_v^4)^c$	$n^7(n_0^3n_v^4)^c$	$n^7(n_0^3n_v^4)^c$	$n^9(n_0^5n_v^4)^c$	$n^9(n_0^5n_v^4)^c$
	$n^6(n_0^2n_v^4)^d$	$n^6(n_0^2n_v^4)^d$	$n^6(n_0^2n_v^4)^d$	$n^6(n_0^2n_v^4)^d$	$n^7(n_0^3n_v^4)^d$
<i>Electron affinity</i>					
$\bar{H}R$	$n^7(n_0^2n_v^5)^c$	$n^7(n_0^2n_v^5)^c$	$n^7(n_0^2n_v^5)^c$	$n^8(n_0^3n_v^5)^c$	$n^8(n_0^3n_v^5)^c$
	$n^6(n_0^2n_v^4)^d$	$n^6(n_0^2n_v^4)^d$	$n^6(n_0^2n_v^4)^d$	$n^6(n_0^2n_v^4)^d$	$n^7(n_0^2n_v^5)^d$
\bar{H}	$n^7(n_0^2n_v^5)^c$	$n^7(n_0^2n_v^5)^c$	$n^7(n_0^3n_v^4)^c$	$n^9(n_0^4n_v^5)^c$	$n^9(n_0^4n_v^5)^c$
	$n^6(n_0^2n_v^4)^d$	$n^6(n_0^2n_v^4)^d$	$n^6(n_0^2n_v^4)^d$	$n^6(n_0^2n_v^4)^d$	$n^7(n_0^3n_v^4)^d$
<i>Excitation energy</i>					
$\bar{H}R$	$n^8(n_0^3n_v^5)^c$	$n^8(n_0^3n_v^5)^c$	$n^8(n_0^3n_v^5)^c$	$n^9(n_0^4n_v^5)^c$	$n^9(n_0^4n_v^5)^c$
	$n^7(n_0^3n_v^4)^d$	$n^7(n_0^3n_v^4)^d$	$n^7(n_0^3n_v^4)^d$	$n^7(n_0^3n_v^4)^d$	$n^8(n_0^3n_v^5)^d$
\bar{H}	$n^9(n_0^5n_v^4)^c$	$n^9(n_0^5n_v^4)^c$	$n^9(n_0^4n_v^5)^c$	$n^9(n_0^4n_v^5)^c$	$n^9(n_0^4n_v^5)^c$
	$n^7(n_0^3n_v^4)^d$	$n^7(n_0^4n_v^3)^d$	$n^7(n_0^3n_v^4)^d$	$n^7(n_0^3n_v^4)^d$	$n^8(n_0^4n_v^4)^d$

^aIn case of EE we have one more variant, i.e., EOM-CCSDT-3' which scales as EOM-CCSDT-3.

^bFor all considered schemes (IP, EA, EE) we have one more variant, i.e., EOM-CCSDT' which scales as EOM-CCSDT model.

^cStandard version.

^dFactorized version.

The reference state CCSDT-3 equations take the form

$$\langle \mathbf{h}_1 | (fT_1)_c + \tilde{W} + (\tilde{W}T_3)_c | \Phi_0 \rangle = 0 \quad (11)$$

$$\langle \mathbf{h}_2 | (fT_2)_c + \tilde{W} + (\tilde{W}T_3)_c | \Phi_0 \rangle = 0 \quad (12)$$

$$\langle \mathbf{h}_3 | (fT_3)_c + \tilde{W} | \Phi_0 \rangle = 0 \quad (13)$$

$$\langle \Phi_0 | \bar{H} | \Phi_0 \rangle = \langle \Phi_0 | \tilde{H} | \Phi_0 \rangle = E_{\text{CCSDT-3}} \quad (14)$$

where

$$\bar{H} = \tilde{H} + (\tilde{H}T_3)_c = f + \tilde{W} + (fT_3)_c + (\tilde{W}T_3)_c \quad (15)$$

$$\tilde{H} = e^{-(T_1+T_2)} H e^{T_1+T_2} = f + \tilde{W} \quad (16)$$

$$\begin{aligned}\tilde{W} = & (WT_2)_c + (WT_1T_2)_c + (WT_2^2/2)_c + (WT_1^2T_2/2)_c \\ & + (WT_1T_2^2/2)_c + (WT_1^3T_2/6)_c\end{aligned}\quad (17)$$

and $(fT_3)_c$ becomes $-(e_i + e_j + e_k - e_a - e_b - e_c)t_{ijk}^{abc}$ for a particular triple excitation projection. Thus, the CCSDT-3 approach includes into the T_3 equation all terms which can be evaluated with n^7 scaling. To this group belong all terms but those containing the T_3 operator.

The first of the considered approximate models, termed EOM-CCSDT-3, is defined by the equations (9) and (10):

$$\omega_{\text{CCSDT-3}}\langle \mathbf{h}_1 | R_1 | \Phi_0 \rangle = \langle \mathbf{h}_1 | (fR_1)_c + (\tilde{W}R_1)_c + (\tilde{W}R_2)_c + (\tilde{W}R_3)_c | \Phi_0 \rangle \quad (18)$$

$$\begin{aligned}\omega_{\text{CCSDT-3}}\langle \mathbf{h}_2 | R_2 | \Phi_0 \rangle = & \langle \mathbf{h}_2 | (fR_2)_c + (\tilde{W}R_1)_c + (\tilde{W}R_2)_c + (\tilde{W}R_3)_c \\ & + (\tilde{W}T_3R_1)_c | \Phi_0 \rangle\end{aligned}\quad (19)$$

$$\omega_{\text{CCSDT-3}}\langle \mathbf{h}_3 | R_3 | \Phi_0 \rangle = \langle \mathbf{h}_3 | (fR_3)_c + (\tilde{W}R_1)_c + (\tilde{W}R_2)_c | \Phi_0 \rangle \quad (20)$$

As we see, analogous to the ground state, we do not include into the R_3 equation $(\tilde{W}R_3)_c$ any other R_3 containing terms. This is the general assumptions obeyed in all the approximate models we considered. The diversification of the models results from the several possible schemes for the inclusion of the T_3 operators into the EOM equations. In the equations above, the T_3 operator occurs only in the R_2 equation, see the last term of equation (19). This operator enters the equation either *via* the I_1^2 , which can occur for IP, EA and EE or *via* the I_2^3 element which can happen only for the EE case.

This suggests a possibility to introduce for the EE problem the same treatment of the T_3 operator as in the remaining two cases. In other words we eliminate the T_3 component from the I_2^3 element occurring in the R_2 equations. The variant is denoted in the respective tables as EOM-CCSDT-3'. In this variant the R_1 and R_3 equations are the same as in the EOM-CCSDT-3 method but in the R_2 equation the T_3 operator is added only in the construction of the I_1^2 elements of \tilde{H} , see in Fig. 1, I_{ci}^{ab} and I_{jk}^{ia} components, respectively.

In the next approximate model, EOM-CCSDT-3a, we construct elements of \tilde{H} without T_3 operator. Therefore, the R_1 and R_3 equations are the same as in the EOM-CCSDT-3 variant but we need to modify the R_2 equation which now takes the form:

$$\begin{aligned}\omega_{\text{CCSDT-3a}}\langle \mathbf{h}_2 | R_2 | \Phi_0 \rangle = & \langle \mathbf{h}_2 | (fR_2)_c + (\tilde{W}R_1)_c \\ & + (\tilde{W}R_2)_c + (\tilde{W}R_3)_c | \Phi_0 \rangle\end{aligned}\quad (21)$$

i.e., we skip the last term in equation (19).

In the last two variants, denoted as EOM-CCSDT-3b and EOM-CCSDT-3c, we allow for the T_3 operator in the R_3 equation.

The EOM-CCSDT-3b model for the IP and EA problems has the R_1 and R_2 equations identical as in EOM-CCSDT-3, see equations (18) and (19), but the R_3 equation takes the form

$$\omega_{\text{CCSDT-3b}} \langle \mathbf{h}_3 | R_3 | \Phi_0 \rangle = \langle \mathbf{h}_3 | (fR_3)_c + (\tilde{W}R_1)_c + (\tilde{W}R_2)_c + (\tilde{W}R_1T_3)'_c | \Phi_0 \rangle \quad (22)$$

where the prime indicates that in the construction of the T_3 component of the I_1^3 element (or $(I_{dij}^{abc}, I_{jkl}^{iab})$ of \bar{H}) only certain terms are considered: namely those which make the scaling lower than n^7 . Practically this means that we consider the I_2^1 intermediate. The same model for the EE problem includes one more term:

$$\omega_{\text{CCSDT-3b}} \langle \mathbf{h}_3 | R_3 | \Phi_0 \rangle = \langle \mathbf{h}_3 | (fR_3)_c + (\tilde{W}R_1)_c + (\tilde{W}R_2)_c + (\tilde{W}R_1T_3)''_c + (\tilde{W}R_2T_3)_c | \Phi_0 \rangle \quad (23)$$

Here we include also T_3 in the construction of the I_2^4 element (I_{ajkl}^{ibcd}) (not occurring for IP and EA cases) as well as in the I_1^2 term $(I_{ci}^{ab}, I_{jk}^{ia})$ entering the last term of the above equation. The definition of the particular elements of \bar{H} is given in our previous works [19,22].

Finally, we have considered one more group of approximate variants (denoted as EOM-CCSDT-3c) which is very close to the previous one. In these methods we add within the R_3 equation term or terms (it depends on the objective, i.e., EE, IP, EA) which contain the I_3^4 elements of \bar{H} , see in Fig. 1 $I_{aejk}^{ibcd}, I_{aklm}^{ijbc}$ components.

As a last approach we have investigated the performance of the hybrid method – referred to as CCSDT' – which uses for the ground state the standard CCSDT-3 method and – at the EOM level – it includes the R_3 operator in a rigorous manner. This approach is justified for the IP and EA calculations, since in the full EOM-CCSDT approach the computational bottleneck occurs at the ground state (n^8) step. So approximating the ground state with the CCSDT-3 method we make the scaling for the two steps comparable.

4. RESULTS AND DISCUSSION

To investigate the performance of the new methods in vertical IP, EA, and EE calculations we select four molecules: C_2 , O_3 , N_2 , and CO . The results are collected in Tables 2–6. The experimental geometries used in these calculations for the C_2 , N_2 , and CO molecules are taken from Ref. [23]; in case of the O_3 molecule – from Ref. [24]. In all cases only valence electrons are correlated. For three molecules (C_2 , N_2 , CO) we employ an aug-cc-pVTZ basis set [25]. For the O_3 molecule the results are obtained in the POL1 [26]

Table 2. EOM-CC results (in eV) for C_2 molecule in aug-cc-pVTZ (valence electrons correlated) basis set ($R = 1.243 \text{ \AA}$ [23])

Nominal state	EOM-CCSD						
	T-3	T-3'	T-3a	T-3b	T-3c	T'	T
<i>Vertical ionization potentials</i>							
$^2\Pi_u$	12.412	–	12.454	12.413	12.416	12.564	12.561
$^2\Sigma_u^-$	15.087	–	15.110	15.087	15.087	15.255	15.289
<i>Vertical electron affinities</i>							
$^2\Sigma_g^+$	3.206	–	3.207	3.206	3.201	3.237	3.171
<i>Vertical excitation energies</i>							
$^1\Pi_u$	1.195	1.196	1.157	1.188	1.188	1.230	1.287
$^1\Sigma_u^+$	5.430	5.454	5.357	5.406	5.403	5.459	5.532

basis set. In all cases spherical harmonic polarization functions are used. For each molecule we compare results at the approximate levels, i.e., EOM-CCSDT-3, EOM-CCSDT-3', EOM-CCSDT-3a, EOM-CCSDT-3b, EOM-CCSDT-3c, and EOM-CCSDT' with the full model, i.e., EOM-CCSDT. Then we choose the C_2 molecule and do calculations for larger basis set, i.e., aug-cc-pVQZ [25], in order to compare theoretical results with the experimental data. To attempt to extrapolate we evaluate the complete

Table 3. EOM-CC results (in eV) for O_3 molecule in POL1 (valence electrons correlated) basis set ($R = 1.272 \text{ \AA}$, $\angle 116.8^\circ$, [24])

Nominal state	EOM-CCSD						
	T-3	T-3'	T-3a	T-3b	T-3c	T'	T
<i>Vertical ionization potentials</i>							
2A_1	12.670	–	12.653	12.670	12.671	12.485	12.490
2B_2	12.807	–	12.786	12.807	12.808	12.576	12.584
2A_2	13.300	–	13.243	13.300	13.305	13.354	13.391
<i>Vertical electron affinities</i>							
2B_2	1.617	–	1.677	1.617	1.619	1.537	1.494
<i>Vertical excitation energies</i>							
1B_1	2.293	2.303	2.242	2.293	2.307	2.211	2.246
1B_2	5.211	5.278	5.087	5.168	5.168	5.218	5.282
1A_2	2.230	2.240	2.165	2.229	2.244	2.133	2.170

Table 4. EOM-CC results (in eV) for N₂ molecule in aug-cc-pVTZ (valence electrons correlated) basis set ($R = 1.097685$ Å [23])

Nominal state	EOM-CCSD						
	T-3	T-3'	T-3a	T-3b	T-3c	T'	T
<i>Vertical ionization potentials</i>							
$2\Sigma_g^+$	15.569	–	15.585	15.570	15.571	15.522	15.524
$2\Pi_u$	16.932	–	16.944	16.932	16.934	16.976	16.978
$2\Sigma_u^-$	18.884	–	18.887	18.884	18.885	18.745	18.752
<i>Vertical electron affinities</i>							
$2\Sigma_u^-$	–2.127	–	–2.127	–2.127	–2.127	–2.116	–2.117
$2\Sigma_g^+$	–2.914	–	–2.913	–2.914	–2.914	–2.890	–2.891
$2\Pi_g$	–2.442	–	–2.418	–2.442	–2.442	–2.404	–2.415
$2\Pi_u$	–3.142	–	–3.142	–3.142	–3.142	–3.127	–3.128
<i>Vertical excitation energies</i>							
$1\Pi_g$	9.397	9.399	9.385	9.399	9.400	9.357	9.369
$1\Sigma_u^-$	9.949	9.952	9.928	9.950	9.950	9.936	9.952
$1\Delta_u$	10.369	10.373	10.333	10.368	10.369	10.347	10.362

Table 5. EOM-CC results (in eV) for CO molecule in aug-cc-pVTZ (valence electrons correlated) basis set ($R = 1.128323$ Å [23])

Nominal state	EOM-CCSD						
	T-3	T-3'	T-3a	T-3b	T-3c	T'	T
<i>Vertical ionization potentials</i>							
$1^2\Sigma^+$	13.939	–	13.951	13.939	13.940	13.946	13.944
$2^2\Pi$	17.084	–	17.065	17.085	17.082	17.007	17.016
$2^2\Sigma^+$	19.777	–	19.771	19.777	19.777	19.588	19.601
<i>Vertical electron affinities</i>							
$1^2\Pi$	–1.624	–	–1.617	–1.624	–1.625	–1.600	–1.604
$1^2\Sigma^+$	–1.657	–	–1.657	–1.657	–1.657	–1.660	–1.659
$2^2\Sigma^+$	–2.302	–	–2.302	–2.302	–2.302	–2.266	–2.269
$2^2\Pi$	–3.154	–	–3.137	–3.154	–3.154	–3.114	–3.119
<i>Vertical excitation energies</i>							
1Π	8.554	8.556	8.562	8.562	8.566	8.537	8.540
$1\Sigma^-$	10.086	10.095	10.023	10.085	10.084	10.032	10.044
1Δ	10.217	10.227	10.130	10.214	10.213	10.166	10.180
$1\Sigma^+$	11.012	11.014	11.021	11.026	11.028	10.983	10.982

Table 6. EOM-CC results (energies in eV) for C_2 molecule ($R = 1.243 \text{ \AA}$ [23])

Nominal state	Aug-cc-pVTZ ^a		Aug-cc-pVQZ ^a		Aug-cc-pV ∞ Z ^a		Expt.
	T-3	T	T-3	T	T-3	T	
<i>Vertical ionization potentials</i>							
² Π_u	12.41	12.56	12.45	12.61	12.48	12.65	12.15 ^b
<i>Vertical electron affinities</i>							
² Σ_g^+	3.21	3.17 ^c	3.24	3.21 ^c	3.26	3.24 ^c	3.30 ^d
<i>Vertical excitation energies</i>							
¹ Π_u	1.195	1.287	1.185	1.276	1.178	1.268	1.041 ^e
¹ Σ_u^+	5.430	5.532	5.411	5.514	5.397	5.501	5.361 ^e

^a Valence electrons correlated.^b Ref. [28].^c Ref. [22].^d Ref. [29].^e Ref. [30].

basis set limit (CBS) results presented in Table 6 and compare with the experimental ones. We use the two-point extrapolation formula [27].

4.1. IP and EA results

The general characteristics of the IP and EA results is their low sensitivity to the considered modifications in the EOM equations. In fact we observe two principal groups of results: the first one due to the CCSDT-3a approach and the second involving the rest of the methods. This means that the crucial modification that makes a difference in the results is the presence or absence of the T_3 operator in the R_2 equation (equation (19)). When we construct the R_2 equation according to the formula given in equation (19), the other discussed changes have a minor effect, resulting in corrections on the order of a few thousandth or even below 0.001 eV.

What is interesting is that for most cases results closer to the rigorous method are obtained when the T_3 term in the R_2 equation is omitted. This is true for the C_2 molecule, for all but one state of the CO case, and for the majority of states for the remaining systems (O_3 and N_2). Note that two of the EA states for N_2 and CO do not show any dependence on the form of the EOM equations.

Encouraging results are obtained with the hybrid methods denoted in Tables 2–5 as CCSDT'. The obtained IP and EA values stay very close to the exact results, most below 0.01 eV. This is true for all but one N_2 and CO states, (the single exception is 0.013 eV for the $2^2\Sigma^+$ IP state). The largest deviation for the IP occurs for the $^2\Sigma_u^-$ state of C_2 (0.034 eV) and 2A_2 of O_3

(0.037 eV). For the EA values the largest error occurs for the C_2 molecule (0.066 eV). The above results indicate a useful scheme for the accurate and relatively fast calculations of IP and EA energies. The actual computer effort required for the hybrid method is several times smaller than for the rigorous approach (due to replacing CCSDT with CCSDT-3) with excellent results.

4.2. EE results

For the EE results the differentiation of the obtained data is much greater. The smallest changes are observed for the T-3b and T-3c schemes. Only for the ozone molecule are there differences larger than 0.01 eV; for the remaining cases they stay within 0.000–0.004 eV. Note that the T-3c method differs only by the presence of the I_3^4 four-body term in the R_3 equation, which means that neglecting that term in the EOM scheme has a negligible effect on the results, with the possible exception of systems with significant multiconfiguration reference character like O_3 .

Similar close values are obtained for the T-3 and T-3' method, which differ only by neglecting (in the latter) the T_3 term in the I_2^4 element. For well-behaved molecules (N_2 , CO) the differences do not exceed 0.01 eV; but for the O_3 they amount to 0.067 eV for the 1B_2 state.

Assessing the reliability of the various approximations in the EE calculations, one can exclude from consideration the forms denoted as T-3b and T-3c, (they differ from the rest by the presence of the T_3 operator in the R_3 equation), and they are relatively far from the reference method. To recommend the proper computational scheme for approximate calculations, we have to decide between the approaches denoted as EOM-CCSDT-3 (3') and EOM-CCSDT-3a. For the majority of the molecules considered and states, better results are obtained with the former method. A notable exception is the ozone molecule: two out of the three states considered are better with the T-3a scheme and only one (1B_2) with the T-3' approach.

Using the latter method (or the T-3) for the previous two states would increase the errors by 0.053, and 0.065 eV for the 1B_1 and 1A_2 states, respectively. For 1B_2 , replacing the methods would result in a much larger error (by ca. 0.2 eV). So, on the whole, the test calculations would indicate that the EOM-CCSDT-3 approach is the most reliable approximate variant.

In Table 6 we list the results for the C_2 molecule obtained with the EOM-CCSDT-3 and full T approaches for several basis sets. We observe that the differences between the approximate and the rigorous scheme are stable indicating that the mutual interrelations between the method do not depend on the basis set quality and size. Due to the cancellation of the errors the approximate scheme gives results closer to the experimental values, but – of course – this is not meaningful for the general case.

5. CONCLUSIONS

We studied the behavior of various approximate EOM models based on the CCSDT-3 ground state wavefunction in IP, EA and EE calculations. We assumed that the approximate models should exhibit a lower scaling than the full method, i.e., n^6 for IP and EA problems and n^7 for the EE case, so the bottom line for all approaches is an elimination of the R_3 operator from the R_3 equation in the EOM scheme, cf. equation (20).

The results collected in Tables 2–5 indicate that the inclusion of more terms in the final EOM equations do not necessarily improve the results. For the EE scheme the variants which most closely reproduce the rigorous method are those which either the T_3 operator in the \bar{H} elements (EOM-CCSDT-3a scheme) or allow for it only in the R_2 equation (EOM-CCSDT-3 scheme), see equation (19). Similar conclusions could be presented with respect to the IP and EA problems, although we should be aware that using the approximate versions (i.e., those which require no higher than n^6 scaling) is not so crucial here, since the full approaches need n^7 , which is the same as the CCSDT-3 method employed for the ground state. Hence we recommend using the hybrid methods which – in view of the collected results – seems to be preferable over the rest of the considered schemes.

ACKNOWLEDGEMENTS

Congratulations Osvaldo! It is a pleasure to contribute this paper to a special volume in honour of Osvaldo Goscinski. The senior author has known Osvaldo since he began his graduate work in the Florida, Quantum Theory Project, shortly after Osvaldo had finished his dissertation and moved to Uppsala. His paper Greens' functions approach to IPs and his inner projected super-operator formulation of Greens' functions are routinely used by us and many others today.

This work has been supported by the United States Air Force Office of Scientific Research under Grant Number AFOSR-F49620-95-1-0130 and also by the Committee for Scientific Research (KBN), Poland, under Grant No. 4 T09A 013 24.

REFERENCES

- [1] (a) J. Cizek, *J. Chem. Phys.*, 1966, **45**, 4256; (b) J. Cizek, *Adv. Chem. Phys.*, 1969, **14**, 15; (c) J. Paldus, J. Cizek and I. Shavitt, *Phys. Rev.*, 1974, **A5**, 50.
- [2] (a) R. J. Bartlett, *J. Phys. Chem.*, 1989, **93**, 1697; (b) R. J. Bartlett, in *Modern Electronic Structure Theory, Part I* (ed. D. R. Yarkony), World Scientific, New York, 1995, pp. 1047–1131; (c) R. J. Bartlett and J. F. Stanton, in *Reviews in Computational Chemistry* (eds. K. B. Lipkowitz and D. B. Boyd), VCH Publishers, New York, 1994, Vol. 5, pp. 65–169.

- [3] J. D. Watts and R. J. Bartlett, *J. Chem. Phys.*, 1990, **93**, 6104.
- [4] J. Paldus and X. Li, *Adv. Chem. Phys.*, 1999, **110**, 1.
- [5] S. A. Kucharski and J. Bartlett, *J. Chem. Phys.*, 1992, **97**, 4282.
- [6] (a) M. Musiał, S. A. Kucharski and R. J. Bartlett, *Chem. Phys. Lett.*, 2000, **320**, 542; (b) M. Musiał, S. A. Kucharski and R. J. Bartlett, *J. Chem. Phys.*, 2002, **116**, 4382.
- [7] (a) J. F. Stanton and R. J. Bartlett, *J. Chem. Phys.*, 1993, **98**, 7029; (b) J. Geertsen, M. Rittby and R. J. Bartlett, *Chem. Phys. Lett.*, 1989, **164**, 57; (c) D. C. Comeau and R. J. Bartlett, *Chem. Phys. Lett.*, 1993, **207**, 414; (d) H. Sekino and R. J. Bartlett, *Int. J. Quantum Chem. Symp.*, 1984, **18**, 225.
- [8] (a) J. D. Watts and R. J. Bartlett, *Chem. Phys. Lett.*, 1995, **233**, 81; (b) J. D. Watts and R. J. Bartlett, *Chem. Phys. Lett.*, 1996, **258**, 581; (c) J. D. Watts and R. J. Bartlett, *J. Chem. Phys.*, 1994, **101**, 3073.
- [9] J. D. Watts, S. R. Gwaltney and J. Bartlett, *J. Chem. Phys.*, 1996, **105**, 6979.
- [10] J. D. Watts and R. J. Bartlett, *Spectrochim. Acta, Part A*, 1999, **55**, 495.
- [11] K. Kowalski and P. Piecuch, *J. Chem. Phys.*, 2000, **113**, 8490.
- [12] K. Kowalski and P. Piecuch, *J. Chem. Phys.*, 2001, **115**, 643.
- [13] P. Piecuch and J. Bartlett, *Adv. Quantum Chem.*, 1999, **34**, 295.
- [14] S. A. Kucharski, M. Włoch, M. Musiał and R. J. Bartlett, *J. Chem. Phys.*, 2001, **115**, 8263.
- [15] M. Nooijen and J. G. Snijders, *Int. J. Quantum Chem. Symp.*, 1992, **26**, 55.
- [16] M. Nooijen and J. G. Snijders, *Int. J. Quantum Chem.*, 1993, **48**, 15.
- [17] J. F. Stanton and J. Gauss, *J. Chem. Phys.*, 1994, **101**, 8938.
- [18] J. F. Stanton and J. Gauss, *J. Chem. Phys.*, 1999, **111**, 8785.
- [19] M. Musiał, S. A. Kucharski and R. J. Bartlett, *J. Chem. Phys.*, 2003, **118**, 1128.
- [20] M. Nooijen and R. J. Bartlett, *J. Chem. Phys.*, 1995, **102**, 3629.
- [21] M. Nooijen and R. J. Bartlett, *J. Chem. Phys.*, 1995, **102**, 6735.
- [22] M. Musiał and R. J. Bartlett, *J. Chem. Phys.*, 2003, **119**, 1901.
- [23] K. P. Huber and G. Herzberg, *Molecular Structure and Molecular Spectra. IV. Constants of Diatomic Molecules*, Van Nostrand Reinhold, New York, 1979.
- [24] (a) A. Barbe, C. Secroun and P. Jouve, *J. Mol. Spectrosc.*, 1974, **49**, 171; (b) T. Tanaka and Y. Morino, *J. Mol. Spectrosc.*, 1970, **33**, 538.
- [25] (a) T. H. Dunning, Jr., *J. Chem. Phys.*, 1989, **90**, 1007; (b) R. A. Kendall, T. H. Dunning, Jr. and R. J. Harrison, *J. Chem. Phys.*, 1992, **96**, 6796; (c) D. E. Woon and T. H. Dunning, Jr., *J. Chem. Phys.*, 1995, **103**, 4572.
- [26] A. J. Sadlej, *Collect. Czech. Chem. Commun.*, 1988, **53**, 1995.
- [27] A. Helgaker, T. Helgaker, P. Jørgensen, W. Klopper, H. Koch, J. Olsen and A. K. Wilson, *Chem. Phys. Lett.*, 1998, **286**, 243.
- [28] V. H. Dibeler and S. K. Liston, *J. Chem. Phys.*, 1967, **47**, 4548.
- [29] S. Yang, K. J. Taylor, M. J. Craycraft, J. Conceicao, C. L. Pettiette, O. Cheshnovsky and R. E. Smalley, *Chem. Phys. Lett.*, 1988, **144**, 431.
- [30] O. Christiansen, H. Koch, P. Joergensen and J. Olsen, *Chem. Phys. Lett.*, 1996, **256**, 185.

Operator Algebra: From Franck–Condon to Floquet Theory

Alejandro Palma

*Instituto de Física (BUAP), Apartado Postal J-48, Puebla, Pue. 72570, México
and Instituto Nacional de Astrofísica, Óptica y Electrónica (INAE), México*

Dedicated to Professor Osvaldo Goscinski

Abstract

In this work we discuss some mathematical aspects and important applications of the operator algebra to several problems. Part of the results here presented have been published elsewhere and represent contributions set down along several years of research. We begin by discussing the mathematical structure of the Franck–Condon integral and the associated Lie algebraic formulation, as well as some connections with the concept of squeezed states. We also consider the operator algebra solution of the Schrödinger equation with a time-dependent periodic Hamiltonian by means of standard operator algebra techniques and by using the concept of the Bargmann–Segal space. In the final section of this report we include some unpublished material on the Lie algebraic approach to the Floquet quasi-energies.

Contents

1. Introduction	223
2. Franck–Condon factors and ladder operators	224
3. The Lie algebraic approach to the Franck–Condon integral	226
4. The Lie algebraic approach to the Morse oscillator	227
5. The Franck–Condon overlap and squeezed states	230
6. Operator algebra and Floquet states	232
7. The Lie algebraic approach to Floquet quasi-energies	235
8. Discussion	237
Acknowledgements	237
References	237

1. INTRODUCTION

Operator algebra is a field which has attracted the attention of several authors [1–3]. Among his outstanding contributions, Dirac called it the

symbolic method and advanced that it ‘will probably be increasingly used in the future as it becomes better understood and its own special mathematics gets developed’ [4]. At present this prediction has been partly fulfilled, albeit there is still much work to be done. Several years ago we started exploring applications of the operator algebra to the Franck–Condon (FC) integral [5] although it should be acknowledged that some authors previously considered this problem [6,7]. The main point in treating this problem by operator algebra is not only the simplification and elegance that are achieved, but also to establish connections with other well-known concepts, as for example that of the squeezed states. This can be accomplished when we view such a problem from a very general standpoint and, thus, it is essential to understand the abstract and general mathematical tools that are involved. Perhaps the most important thing when working in this field is to follow Dirac’s advice about the beauty of equations [8], since several implications in physics and chemistry arise as a consequence.

Although the FC principle has a wide range of applications in chemistry and physics, it will not be the subject of discussion in this work. Rather, since very few authors [9,10] – in addition to the ones mentioned above – have looked more closely into the mathematical structure of the integral associated with it, we will devote ourselves to matters related to the latter. We start by considering very naïve methods of operator algebra applied to the evaluation of well-known recurrence and closed relations, then gradually move on by introducing more sophisticated methods to finally arrive at the Lie algebraic approach. We will also consider applications of operator algebra to the solution of the time-dependent Schrödinger equation with a periodic Hamiltonian, which is of paramount importance in Floquet theory. We will conclude this report by discussing this approach to Floquet quasi-energies, where the results obtained hitherto are not yet published.

2. FRANCK–CONDON FACTORS AND LADDER OPERATORS

Within the framework of operator algebra methods, perhaps the simplest approach to treating the FC integral is to consider the ladder operators associated with each of the wells, i.e., the ground (G) and excited (E) states whose minima are shifted with respect to each other by a distance $\ell = x_G - x_E$:

$$\begin{aligned}(1 + \beta^2)a_G &= \sqrt{2}\beta^2\gamma + (1 - \beta^2)a_G^+ + 2\beta a_E \\ (1 + \beta^2)a_E^+ &= -\sqrt{2}\beta\gamma + 2\beta a_G^+ - (1 - \beta^2)a_E\end{aligned}\tag{1}$$

where

$$\beta = \left(\frac{m_E \omega_E}{m_G \omega_G} \right)^{1/2}; \quad \gamma = \left(\frac{m_G \omega_G}{\hbar} \right)^{1/2} \ell$$

Although there exist several relations involving these operators, they are the only ones that lead to recurrence relations which are useful in spectroscopy calculations. The derivation of such relations is much simpler than by using the traditional method, i.e., through recurrence relations between Hermite polynomials, since we need to use only the well-known properties of ladder operators:

$$\begin{aligned} {}_G\langle m|n\rangle_E &= \left(\frac{2}{m} \right)^{1/2} \frac{\beta^2 \gamma}{1 + \beta^2} {}_G\langle m-1|n\rangle_E + \left(\frac{n}{m} \right)^{1/2} \frac{2\beta}{1 + \beta^2} {}_G\langle m-1|n-1\rangle_E \\ &\quad + \left(\frac{m-1}{m} \right)^{1/2} \frac{1 - \beta^2}{1 + \beta^2} {}_G\langle m-2|n\rangle_E \\ {}_G\langle m|n\rangle_E &= -\left(\frac{2}{m} \right)^{1/2} \frac{\beta^2 \gamma}{1 + \beta^2} {}_G\langle m|n-1\rangle_E + \left(\frac{m}{n} \right)^{1/2} \frac{2\beta}{1 + \beta^2} {}_G\langle m-1|n-1\rangle_E \\ &\quad - \left(\frac{n-1}{n} \right)^{1/2} \frac{1 - \beta^2}{1 + \beta^2} {}_G\langle m|n-2\rangle_E \end{aligned} \quad (2)$$

These are the familiar recurrence relations originally derived by Wagner [11] and Ansbacher [12]. Closed formula can also be obtained by means of these techniques, for which we need to introduce the well-known Cauchy relation in the complex variable theory

$$a^{+n} = \frac{n!}{2\pi i} \oint \frac{ds}{s^{n+1}} e^{sa^+} \quad (3)$$

where the contour of integration in the complex plane includes the origin. The use of the Cauchy relation simplifies the derivation a great deal since in the whole procedure all the manipulations are symbolic. By using well-known properties of ladder operators, we obtain

$${}_G\langle m|n\rangle_E = (m!n!)^{-1/2} {}_G\langle 0|a_G^m a_E^{+N}|0\rangle_E \quad (4)$$

The ladder operators a_G and a_E^+ can be written using equation (3) and two complex variables and, after substitution in equation (4) and some algebra,

we obtain the closed formula

$$\begin{aligned}
 {}_G\langle m|n\rangle_E = {}_G\langle O|O\rangle_E & \left(\frac{1-\beta^2}{2(1+\beta^2)} \right)^{m+n/2} (m!n!)^{1/2} \\
 & \times \sum_{k=0}^{[m,n]} \left(\frac{4\beta}{1-\beta^2} \right)^k \frac{(-i)^{m-k}}{k!(m-k)!(n-k)!} \\
 & \times H_{m-k} \left(\frac{i\beta^2\gamma}{(1-\beta^4)^{1/2}} \right) H_{n-k} \left(\frac{\beta\gamma}{(1-\beta^4)^{1/2}} \right) \quad (5)
 \end{aligned}$$

Although this formula could hardly be of any practical use in spectroscopy, its importance lies in the fact that the FC overlap has an analytic closed formula for the harmonic oscillator potential. It was derived for the first time by Ansbacher with a minor mistake, which has inspired some authors [13,14] to derive analogous formulae for other potentials. The above equation is beautiful and elegant because it represents an exact and closed expression for the FC overlap, with the restriction of being valid only for the special case of the harmonic oscillator. The application of this method to matrix elements of monomial, exponential and Gaussian operators is straightforward and has been published elsewhere [15,16].

3. THE LIE ALGEBRAIC APPROACH TO THE FRANCK-CONDON INTEGRAL

The FC integral has been treated above as a two-center integral; however, by using mapping operators it can be transformed into a one-center integral. We define a mapping between the states of the two oscillators where one of them is displaced and distorted with respect to the other [17]

$$|m\rangle = e^{-\gamma \frac{d}{dx}} e^{\ell n \beta x \frac{d}{dx}} |m\rangle \quad (6)$$

where we have changed to a more comfortable notation ${}_G\langle n|m\rangle_E = \langle n|m\rangle$ and γ and β are the same spectroscopic constants defined above. Therefore, the FC integral can be seen as the one-center matrix element of the operator

$$\hat{O} = e^{-\gamma \frac{d}{dx}} e^{\ell n \beta x \frac{d}{dx}}, \quad {}_G\langle n|m\rangle_E = \langle n|e^{-\gamma \frac{d}{dx}} e^{\ell n \beta x \frac{d}{dx}} |m\rangle \quad (7)$$

By defining the two operators:

$$\hat{P} = -x \frac{d}{dx}, \quad \hat{Q} = \frac{d}{dx} \quad (8)$$

It is easy to see that they satisfy the well-known property of the nonabelian two-dimensional algebra

$$[\hat{P}, \hat{Q}] = \hat{Q} \quad (9)$$

So the FC integral is added to the very few physical systems [18] which are realizations of this particular algebra. Using the Taylor theorem for shift operators due to Sack [19], and the Cauchy relation mentioned above, we can apply this very general idea to the specific case of the harmonic oscillator to obtain the closed formula (5). Recurrence relations can also be obtained by noticing that \hat{O} is in reality a superoperator which maps normal ladder operators by the canonical transformation:

$$\hat{A}^\pm = \hat{O} \hat{a}^\pm \hat{O}^{-1} \quad (10)$$

Taking as a particular case the harmonic oscillator ladder operators [20]

$$\hat{a}^\pm = \frac{1}{\sqrt{2}} \left(x \mp \frac{d}{dx} \right) \quad (11)$$

and using the well-known [2] operator identity:

$$e^{\xi A} B e^{-\xi A} = B + \xi [A, B] + \frac{\xi^2}{2!} [A, [A, B]] + \dots \quad (12)$$

we obtain operator relations between the two sets of ladder operators:

$$\hat{A}^\pm = \mp \frac{1 \mp \beta^2}{2\beta} \hat{a}^- \pm \frac{1 \pm \beta^2}{2\beta} \hat{a}^+ - \frac{\beta\gamma}{\sqrt{2}} 1 \quad (13)$$

from which we can obtain equations (1) and the recurrence relations (2) follow directly from

$$\langle m|n \rangle = \frac{1}{\sqrt{m}} \langle m-1|\hat{a}^-|n \rangle, \quad \langle m|n \rangle = \frac{1}{\sqrt{n}} \langle m|\hat{A}^+|n-1 \rangle \quad (14)$$

4. THE LIE ALGEBRAIC APPROACH TO THE MORSE OSCILLATOR

Although the Morse oscillator has been treated algebraically by some other authors [21], it is interesting to explore some other algebras from which we can obtain its eigenvalues and matrix elements. We will follow the constructive approach of Cizek and Paldus [22] to define a so (2,1) algebra. Starting with the time-independent Schrödinger equation corresponding to the Morse potential and after some changes of variables [23], one can reduce

this to

$$\frac{1}{2} \left[yp^2 - \left(\varepsilon + \frac{1}{4} \right) y^{-1} + y \right] \varphi = K \varphi \quad (15)$$

where p is the canonical momentum, ε the energy eigenvalue and K the anharmonicity constant. We define the operators

$$W_1 = y, \quad W_2 = p, \quad W_3 = yp^2 - \left(\varepsilon + \frac{1}{4} \right) y^{-1} \quad (16)$$

from which we can obtain the commutator relations

$$[W_1, W_2] = iW_1, \quad [W_2, W_3] = iW_3, \quad [W_1, W_3] = 2iW_2 \quad (17)$$

By using these operators we can introduce

$$T_3 = \frac{1}{2}(W_1 + W_3), \quad T_{\pm} = \frac{1}{2}(W_3 - W_1) \pm iW_2 \quad (18)$$

which satisfy the commutation relations of a so (2,1) algebra

$$[T_3, T_{\pm}] = \pm T_{\pm}, \quad [T_+, T_-] = -2T_3 \quad (19)$$

we see immediately that ladder operators T_{\pm} shift the potential parameter K , but not the energy ε . We define the corresponding Casimir operator:

$$C^2 = T_3^2 - T_3 - T_{\pm} T_{\mp} = -\varepsilon - \frac{1}{4} \quad (20)$$

So, for any given energy ε there exists a minimum value K for which a solution of the corresponding Schrödinger equation exists. Let this value be K_0 , then eigenfunction φ_0 fulfills:

$$T_3 \varphi_0 = K_0 \varphi_0, \quad T_- \varphi_0 = 0 \quad (21)$$

Using equation (20) and the fact that $T_+ \varphi_K \sim \varphi_{K+1}$ and $K = K_0 + n$ where $n = 0, 1, 2, \dots$, we obtain

$$(T_3^2 - T_3 - C^2) \varphi_0 = \left[\left(K_0 - \frac{1}{2} \right)^2 + \varepsilon \right] \varphi_0 = 0 \quad (22)$$

which finally leads to the energy eigenvalues

$$\varepsilon_n = - \left(K - n - \frac{1}{2} \right)^2 \quad (23)$$

For a fixed K we have $n = 0, 1, 2, \dots, K - \frac{1}{2}$. The largest integer in $K + \frac{1}{2}$ gives the number of bound states.

The calculation of matrix elements between different energy states is awkward using the scheme outlined above. The reason is that two eigenstates

of the Morse oscillator correspond to different irreducible representations (IR) of the group $SO(2,1)$. For this reason it is convenient to explore another operator algebra for this problem. In order to proceed, we introduce another change of variable which transforms the Morse equation into the equation for a two-dimensional harmonic oscillator (HO) [24]:

$$\rho = \sqrt{2K} e^{-u/2} \quad (24)$$

where K is a dimensionless potential strength and u the dimensionless length, so the original Morse equation becomes

$$\frac{1}{\rho} \frac{d}{d\rho} \left(\rho \frac{d\varphi}{d\rho} \right) + \left[\frac{4\varepsilon}{\rho^2} - \rho^2 + 4K \right] \varphi = 0 \quad (25)$$

When comparing with the two-dimensional HO equation in polar coordinates we immediately see that the HO eigenvalue is

$$W = 2K \quad (26)$$

ε corresponds to the square of the angular momentum quantum number

$$\varepsilon = -\frac{1}{4}\ell^2 \quad \text{where} \quad \frac{\partial \Phi}{\partial \phi} = i\ell \Phi \quad (27)$$

and Φ is given by

$$\Phi(\rho, \phi) = \frac{1}{\sqrt{2\pi}} \chi(\rho) e^{i\ell\phi} \quad (28)$$

Since the use of polar coordinates for the HO does not allow for a straightforward operator algebra, it is more convenient to introduce the complex variable:

$$z = \rho e^{i\phi} \quad (29)$$

together with its complex conjugate z^* and their conjugate momenta ρ_z and ρ_{z^*} . The ladder operators

$$A = \frac{1}{2}z + i\rho_{z^*}, \quad B = \frac{1}{2}z^* - i\rho_z \quad (30)$$

fulfill the usual commutation relations. The only nonvanishing commutators are

$$[A, A^+] = [B, B^+] = 1$$

and the corresponding number operators

$$N_1 = A^+A, \quad N_2 = B^+B \quad (31)$$

yield the harmonic oscillator Hamiltonian

$$H_{\text{HO}} = N_1 + N_2 + 1 \quad (32)$$

and the corresponding angular momentum

$$J_o = -i \frac{\partial}{\partial \phi} = B^+ B - A^+ A \quad (33)$$

Using equations (26) and (27) we finally obtain

$$K = \frac{1}{2}(n_1 + n_2 + 1), \quad \varepsilon = -\frac{1}{4}(n_2 - n_1)^2 \quad (34)$$

Identifying n_1 as the Morse oscillator quantum number n we obtain for the energy

$$\varepsilon_n = -\left(K - n - \frac{1}{2}\right)^2 \quad (35)$$

which is exactly equation (23) obtained by the $\text{so}(2,1)$ algebra. The calculation of matrix elements is more easily performed when using these ladder operators and they have been published elsewhere [24].

5. THE FRANCK-CONDON OVERLAP AND SQUEEZED STATES

Several years ago Wheeler [25] advanced a conjecture about the parallelism between the FC and squeezed states. Here, we will outline how the operator algebra formalism can be used to develop a unifying scheme from which both phenomena are obtained as particular cases. The close connection between squeezed and the FC states can be seen by considering the case of amplitude-squared squeezed states [26] or, better yet, by considering the recurrence relations and closed formulas which are common to both phenomena [27].

Let us consider the so-called squeezed operator [28]:

$$\hat{O} = e^{aa^+ - a^*a} e^{\frac{1}{2}(za^{+2} - z^*a^2)} \quad (36)$$

In general this operator will distort a general ket $|m\rangle$

$$|m\rangle = \hat{O}|m\rangle \quad (37)$$

In fact \hat{O} is a superoperator which maps ladder operators from one space of operators to another:

$$A^+ = \hat{O}a^+\hat{O}^+, \quad A = \hat{O}a\hat{O}^+ \quad (38)$$

Using equation (12) we can show that both sets of ladder operators are connected by

$$A^+ = -A \frac{z^*}{|z|} \tanh|z| + a^+ \operatorname{sech}|z| - \alpha^* \operatorname{sech}|z| \quad (39)$$

$$a = A \operatorname{sech}|z| + a^+ \frac{z}{|z|} \tanh|z| + \alpha - \alpha^* \frac{z}{|z|} \tanh|z| \quad (40)$$

From these operator equations there follow recurrence relations. Indeed, there is a correspondence between the algebraic expressions of the two sets of operators and the associated recurrence relations. The latter in FC factors follows immediately by making $z = \ell n \beta$ and $\alpha = \gamma/\sqrt{2}$. In this context, the mathematical treatment of the FC factors thus becomes a particular case of squeezed states at nonzero displacement ($\alpha \neq 0$).

To derive closed formulas, a straightforward and quite general procedure can be followed by writing the operator \hat{O} as

$$\hat{O} = e^{Aa^{+2}} e^{Ba^+} e^{\ell n C a^+ a} e^{Da} e^{Ea^2} \quad (41)$$

where parameters A , B , C , D and E must be determined for each particular case, either FC or squeezed states. The matrix elements for operator O are calculated by employing the relation:

$$\langle m | \hat{O} | n \rangle = \frac{\sqrt{m!n!}}{(2\pi i)^2} \oint \frac{ds}{s^{m+1}} \oint \frac{dt}{t^{n+1}} \langle O | e^{sa} O e^{ta^+} | O \rangle \quad (42)$$

where the contours of integration include the origin. The closed formula for transition intensities can be obtained by using the properties of creation and annihilation boson operators and the integral representation of the Hermite polynomials. After some algebra we obtain

$$\begin{aligned} \langle m | O | n \rangle &= (m!n!)^{1/2} \sum_{k=0}^{[m,n]} \frac{C^k}{k!} \frac{(iA^{1/2})^{m-k}}{(m-k)!} \frac{(iE^{1/2})^{n-k}}{(n-k)!} \\ &\quad \times H_{m-k} \left(\frac{B}{2iA^{1/2}} \right) H_{n-k} \left(\frac{D}{2iE^{1/2}} \right) \end{aligned} \quad (43)$$

where H_n is an n -degree Hermite polynomial and $[m, n]$ denotes the smaller of m and n . This formula contains, as a particular case, the FC and the squeezed states relations, where either identification by comparing the parameters A , B , C , D and E with equation (5) for the FC case or with equation (36) for the squeezed state case. We have thus shown that FC and squeezed states are particular cases of a general common algebraic formulation. This result reveals the mathematical structure of the conjecture advanced several years ago by Wheeler [25].

6. OPERATOR ALGEBRA AND FLOQUET STATES

Floquet theory is becoming increasingly important to describe the interaction of atoms and molecules with time-periodic external fields. Many interesting features of photoionization and photodissociation spectra have been explained by studying Floquet states occurring at some critical values of the field amplitude or frequency. The harmonic oscillator [29] and the parabolic barrier [30] are good and simple models to analyze some of the most important physical and mathematical features of these problems. Although the Floquet quasi-energies and eigenfunctions for these systems have been given previously in the literature, we will show how to derive these results by using operator algebra methods.

We begin by considering the time-dependent Schrödinger equation

$$i \frac{\partial \psi}{\partial t} = H \psi \quad (44)$$

with a time-dependent Hamiltonian:

$$H = -\frac{\partial^2}{\partial t^2} + \omega_0^2 x^2 + \lambda x \cos \omega t \quad (45)$$

This represents a harmonic oscillator of zero-point energy ω_0 interacting with a one-mode laser of angular frequency ω . From the Floquet theory of differential equations, it is well known that the solutions of equation (44) are

$$\psi_F^n(x, t) = e^{-iE_F^n t} \Phi_F^n(x, t) \quad (46)$$

where E_F is called a quasi-energy and Φ_F^n is a periodic function of the time, i.e., with the property

$$\Phi_F^n(x, t + T) = \Phi_F^n(x, t), \quad T = \frac{2\pi}{\omega} \quad (47)$$

In order to find these solutions by operator algebra we use the well-known boson operators to obtain [31]

$$i \frac{\partial U}{\partial t} = \left\{ \omega_0(2a^+a + 1) + \frac{\lambda}{\sqrt{2\omega_0}}(a + a^+)\cos \omega t \right\} U \quad (48)$$

where

$$\psi(x, t) = U(t)\psi(x, 0); \quad U(0) = 1 \quad (49)$$

By using Louisell's technique [2], which introduces the concept of normal order, equation (48) becomes a differential equation involving only complex numbers for the function $U^{(n)}(\alpha, \alpha^*, t)$, where α is a complex number and $U^{(n)}(\alpha, \alpha^*, t)$ is obtained from the normal order form of $U^{(n)}(a, a^+, t)$ through substitution of a by $\alpha + (\partial/\partial \alpha^*)$ and a^+ by α^* . The differential equation

becomes:

$$i \frac{\partial U^{(n)}}{\partial t} = \left\{ \omega_0 \left(2\alpha^* \alpha + 2\alpha^* \frac{\partial}{\partial \alpha^*} + 1 \right) + \frac{\lambda}{\sqrt{2\omega_0}} \left(\alpha + \frac{\partial}{\partial \alpha^*} + \alpha^* \right) \cos \omega t \right\} U^{(n)} \quad (50)$$

whose solution can be written as

$$U^{(n)}(\alpha, \alpha^*, t) = e^{G(\alpha, \alpha^*, t)} \quad (51)$$

where

$$G(\alpha, \alpha^*, t) = A(t) + B(t)\alpha + C(t)\alpha^* + D(t)\alpha^* \alpha \quad (52)$$

with initial conditions: $A(0) = B(0) = C(0) = D(0) = 0$.

Substitution of equation (51) into equation (50) gives a set of four coupled linear differential equations, whose solutions can be obtained by standard procedures. We note that once we have obtained $U^{(n)}(\alpha, \alpha^*, t)$ we recover $U(a, a^+, t)$ by using the definition of normal order operator [2], and finally we obtain

$$U(a, a^+, t) = e^{A(t)} e^{-B^*(t) \exp(-2i\omega_0 t) a^+} e^{-(2i\omega_0 t) a^+ a} e^{B(t) a} \quad (53)$$

By using this operator, one can in principle know the time development of an arbitrary initial wave function. However, we are rather interested in obtaining the Floquet quasi-energies and eigenfunctions for our Hamiltonian, i.e., we are looking for functions $\psi(x, t)$ that satisfy equation (46). Bearing this in mind, we propose the following initial function:

$$\psi(x, 0) = \chi_n(x - x_0) \quad (54)$$

where $\chi_n(x)$ is the harmonic oscillator solution corresponding to the energy eigenvalue $E_n = \omega_0(2n + 1)$, and x_0 is still an indeterminate constant $\psi(x, 0)$ can be rewritten as

$$\psi(x, 0) = e^{-s^2/2} e^{sa^+} e^{-sa} \chi_n(x), \quad S_0 = x_0 \sqrt{\frac{\omega_0}{2}} \quad (55)$$

We substitute $\chi_n(x, 0)$ into equation (49) together with $U(t)$ as given in equation (53) and we straightforwardly apply the commutation properties of boson operators. After some algebra we finally obtain the Floquet quasi-energies:

$$E_F^n = \omega_0(2n + 1) + \frac{\lambda^2}{2(\omega^2 - 4\omega_0^2)} \quad (56)$$

and the corresponding wavefunctions

$$\psi(x, 0) = e^{\beta(t)} e^{\gamma(t)a^+} e^{-\gamma^*(t)a} \chi_n(x) \quad (57)$$

where $\beta(t)$ and $\gamma(t)$ are periodic functions of time, as required by the Floquet theorem.

The case of the parabolic barrier can be solved in a similar fashion; however, the algebraic procedure becomes cumbersome due to the fact that the corresponding ladder operators are not adjoint to each other. A better approach is to use the concept of the Bargmann–Segal space, whereby avoiding long algebraic derivations [32]. We exemplify this method in the case of the harmonic oscillator. Let us consider the time-dependent Hamiltonian:

$$H = \omega_0(2a^+a + 1) + \frac{\lambda}{\sqrt{2\omega_0}}(a + a^+)\cos \omega t \quad (58)$$

When using the Bargmann–Segal space, the corresponding time-dependent Schrödinger equation becomes

$$\left[\omega_0 \left(2z \frac{d}{dz} + 1 \right) + \frac{\lambda}{\sqrt{2\omega_0}} \left(\frac{d}{dz} + z \right) \cos \omega t \right] \psi = i \frac{\partial \psi}{\partial t} \quad (59)$$

The advantage here is that the second-order Schrödinger differential equation has been transformed into a first-order partial differential equation, involving an unknown function ψ and two independent variables z and t . It can be solved by the well-known Lagrange method. So equation (59) can be written as

$$P \frac{\partial \psi}{\partial z} + Q \frac{\partial \psi}{\partial t} = R \quad (60)$$

where P , Q and R are functions of ψ , z and t . Then the solution will be an arbitrary function $\Phi(u, v) = 0$ provided $u(z, t, \psi) = A$ and $v(z, t, \psi) = B$ which are obtained from the auxiliary system:

$$\frac{dz}{P} = \frac{dt}{Q} = \frac{d\psi}{R} \quad (61)$$

where A and B are integration constants. There are two independent Lagrange equations, whose solutions are

$$u(z, t) = (z - \gamma^*)e^{-2i\omega_0 t} = A, \quad u(z, t, \psi)e^{-iEt}e^{\beta+z}\psi^{-1} = B \quad (62)$$

where $E = \omega_0 + (\lambda^2/2(\omega^2 - 4\omega_0^2))$ and β and γ are periodic functions of time.

Now we need to specify the functional form for the general solution $\Phi(u, v)$. Based on the fact that the Floquet functions resulting in our approach become the harmonic oscillator functions when the field amplitude goes to zero, we propose for $\Phi(u, v)$ the form:

$$\Phi(u, v) = u^{-n} - v \quad \text{where } n \text{ is positive integer} \quad (63)$$

This choice of Φ provides us with the Floquet functions $\psi_F^n(z, t)$ in the Bargmann–Segal space, with the Floquet quasi-energies given by

$$E_F^n = \omega_0(2n + 1) + \frac{\lambda^2}{2(\omega^2 - 4\omega_0^2)} \quad (64)$$

where the corresponding functions $\Phi_F^n(z, t)$ are

$$\Phi_F^n(z, t) = e^{\beta(t)} e^{\gamma(t)z} (z - \gamma^*)^n \quad (65)$$

These functions satisfy the condition of periodicity imposed by the Floquet theorem, since both γ and β have period T . On the other hand, the quantization comes here from the analyticity conditions that the functions must satisfy, i.e., they must have derivatives everywhere except at $z = \infty$. It can also be seen that in the limit $\lambda \rightarrow 0$ both γ and β approach zero, so that the functions Φ_F^n approach z^n , and the Floquet quasi-energies E_F^n approach $\omega_0(2n + 1)$.

7. THE LIE ALGEBRAIC APPROACH TO FLOQUET QUASI-ENERGIES

As we have seen from the above discussion, Floquet quasi-energies can be derived by using a variety of methods. Several authors have considered similar systems with time-dependent Hamiltonians, although, to the best of our knowledge, no one has studied Floquet quasi-energies by means of Lie algebra methods. The general problem of time-dependent Hamiltonians has received considerable attention, and the most appropriate method is the one discovered by Wei and Norman [18] and apparently rediscovered by some other authors [33]. The treatment by Lie algebraic methods is more general than others previously proposed and goes deeply into the nature of the solutions. Furthermore, it has been noticed [34] that some analytic methods give wrong solutions, i.e., they cannot reproduce correctly the initial conditions in some well-known cases.

To begin with, let us consider the Hamiltonian (58), which can be written as

$$H = a_1 H_1 + a_2 H_2 + a_3 H_3 + a_4 H_4 \quad (66)$$

where $a_1(t) = 2\omega_0$, $a_2(t) = a_3(t) = (\lambda/\sqrt{2\omega_0})\cos \omega t$, $a_4(t) = \omega_0$

$$H_1 = a^+ a, \quad H_2 = a, \quad H_3 = a^+, \quad H_4 = I \quad (67)$$

The four operators appearing in this Hamiltonian form a Lie algebra

$$L = \{H, H_2, H_3, I\} \quad (68)$$

One can easily see that this algebra is solvable since $L''' = \{0\}$ and from the theorem of Wei and Norman there exists a solution which can be easily found by quadratures. Being able to get information on the solvability of the problem without actually solving it is another important advantage of the Lie algebraic approach. Such a solution can be written as the product of four exponentials

$$U(t) = U_1 U_2 U_3 U_4, \quad U_i(t) = e^{g_i(t)H_i} \quad (i = 1, 2, 3, 4) \quad (69)$$

where $g_i(t)$ are scalar functions of time to be determined from a set of nonlinear (in general) differential equations. Some authors have proposed methods to overcome the problem of nonlinearity in these equations [37].

In this particular case we obtain the four linear differential equations:

$$\begin{aligned} \dot{g}_1 &= -ia_1, & \dot{g}_2 e^{-g_2} &= -ia_2, & \dot{g}_3 e^{g_3} &= -ia_3, \\ g_3 g_2 + \dot{g}_4 &= -ia_4 \end{aligned} \quad (70)$$

where \dot{g} denotes differentiation with respect to the variable t . These equations can be easily integrated to give the desired result. Especially important is the determination of g_4 which will give us the Floquet shift:

$$g_4(t) = -i\omega_0 t - \frac{i\lambda^2 t}{2(\omega^2 - 4\omega_0^2)} + \text{periodic terms} \quad (71)$$

We notice that we have obtained the Floquet eigenfunctions

$$\psi_F^n(x, t) = e^{-iE_F^n t} \Phi_F^n(x, t) \quad (72)$$

and the Floquet quasi-energies

$$E_F^n = \omega_0(2n + 1) + \frac{\lambda^2}{2(\omega^2 - 4\omega_0^2)}$$

in a straightforward way without making assumptions other than the initial conditions and the separability:

$$\psi(x, t) = U(t)\varphi(x) \quad (73)$$

where $\varphi(x)$ is the solution of the corresponding time-independent Schrödinger equation.

Even though there are several systems with time-dependent Hamiltonians, very few of them lead to a solvable Lie algebra. One of these few systems is the so-called unperturbed two-electron Hooke's atom [35] which is a three-dimensional generalization of the case here treated. Another interesting system is the Gordon–Volkov wave function of the Schrödinger equation [36] in the nonrelativistic version. Work along these lines is in progress.

8. DISCUSSION

From the above discussion, we have seen that operator algebra methods not only have the advantage of simplicity and elegance, but also they go deeply into the nature of the problem. An example which illustrates this matter is the discovered connection between the Franck–Condon and the squeezed states, where the operators associated with them give immediately the similarity (parallelism) between the two concepts. In both cases, the operator can be decomposed as the product of two operators, one associated with the distortion and another with the displacement of the states. On the other hand, the use of Lie algebra methods in all examples treated here has shown the simplicity and power rendered by superior mathematics, albeit limited to the cases where it can be applied. This is specially the case in the last problem here discussed: the Floquet quasi-energies and eigenfunctions of a mode field interacting with a harmonic oscillator.

ACKNOWLEDGEMENTS

The author is indebted to all his coauthors, but specially to Professors M. Berrondo and R. Lefebvre for many fruitful discussions during years of collaboration. This work was supported by CONACYT under project 32112-E.

REFERENCES

- [1] P. O. Löwdin, *Linear Algebra for Quantum Theory*, Wiley, New York, 1998.
- [2] N. H. Louisell, *Quantum Statistical Properties of Radiation*, Wiley, New York, 1963.
- [3] O. L. Lange and R. E. Raab, *Operator Methods in Quantum Mechanics*, Clarendon Press, Oxford, 1991.
- [4] P. A. M. Dirac, *The Principles of Quantum Mechanics*, Oxford University Press, 1968.
- [5] A. Palma and J. Morales, *Int. J. Quantum Chem.*, 1983, **S17**, 393–400.
- [6] K. Nishikawa, *Int. J. Quantum Chem.*, 1997, **12**, 589.
- [7] J. Katriel, *J. Phys.*, 1970, **B3**, 1315.
- [8] P. A. M. Dirac, *Sci. Am.*, 1963, **208**, 45–53.
- [9] A. Frank, R. Lemus and F. Pérez-Bernal, *J. Math. Chem.*, 1999, **25**, 383.
- [10] F. Iachello and M. Ibrahim, *J. Phys. Chem. A*, 1998, **102**, 9427.
- [11] M. Wagner, *Z. Naturforsch. Teil A*, 1959, **81**.
- [12] F. Ansbacher, *Z. Naturforsch. Teil A*, 1959, **889**.
- [13] A. Matsumoto and K. Iwamoto, *J. Quantum Spectrosc. Radiat. Transfer*, 1993, **50**(1), 103.
- [14] B. Moreno and A. López-Piñeiro, *J. Chem. Phys.*, 1991, **95** (6), 4327.
- [15] J. Morales, A. Palma and M. Berrondo, *Int. J. Quantum Chem.*, 1984, **S18**, 57.
- [16] J. Morales, L. Sandoval and A. Palma, *J. Math. Phys.*, 1986, **27**, 2966.
- [17] A. Palma and L. Sandoval, *Int. J. Quantum Chem.*, 1988, **S22**, 503.
- [18] J. Wei and E. Norman, *J. Math. Phys.*, 1963, **4**, 575.
- [19] R. A. Sack, *Philos. Mag.*, 1958, **3**, 497.
- [20] L. Sandoval, A. Palma and F. Rivas-Silva, *Int. J. Quantum Chem.*, 1989, **S23**, 183.

- [21] (a) B. G. Wybourne, *Classical Groups for Physicists*, Wiley, New York, 1974; (b) R. Montemayor and L. Urrutia, *Am. J. Phys.*, 1983, **51** (7), 641; (c) P. Cordero and S. Hojman, *Lett. Nuovo Cimento IV*, 1970, **24**, 1123.
- [22] J. Cizek and J. Paldus, *Int. J. Quantum Chem.*, 1977, **12**, 875.
- [23] M. Berrondo and A. Palma, *J. Phys. A: Math. Gen.*, 1980, **13**, 773.
- [24] M. Berrondo, A. Palma and J. L. López-Bonilla, *Int. J. Quantum Chem.*, 1987, **XXXI**, 243.
- [25] J. A. Wheeler, *Lett. Math. Phys.*, 1985, **10**, 201.
- [26] L. Sandoval, M. Martin, J. F. Rivas and A. Palma, *Phys. Rev. A*, 1992, **46**, 6095.
- [27] A. Palma, *Int. J. Quantum Chem.*, 1997, **63**, 229.
- [28] D. F. Walls, *Nature*, 1983, **306**, 141.
- [29] R. Lefebvre and A. Palma, *J. Mol. Struct. (Theochem)*, 1997, **390**, 23.
- [30] R. Lefebvre and A. Palma, *Int. J. Quantum Chem.*, 1997, **65**, 487.
- [31] V. M. Leon, M. Martin, L. Sandoval and A. Palma, *Adv. in Quantum Chem.*, 2001, **39**, 357.
- [32] A. Palma, V. Leon and R. Lefebvre, *J. Phys. A: Math. Gen.*, 2002, **35**, 419.
- [33] A. R. P. Rau, *Phys. Rev. Lett.*, 1998, **81** (22), 4785.
- [34] A. R. P. Rau and K. Unnikrishnan, *Phys. Lett. A*, 1996, **222**, 304.
- [35] D. A. Telnov and S. Chu, *Phys. Rev. A*, 2000, **63**, 12514.
- [36] R. Lefebvre, *Int. J. Quantum Chem.*, 2000, **80**, 110.
- [37] F. M. Fernández, *Phys. Rev. A*, 1989, **40** (1), 41, and references therein.

On the Alleged Nonlocal and Topological Nature of the Molecular Aharonov–Bohm Effect

Erik Sjöqvist

*Department of Quantum Chemistry, Uppsala University, Box 518,
Se-751 20 Uppsala, Sweden*

Abstract

The nonlocal and topological nature of the molecular Aharonov–Bohm (MAB) effect is examined for real electronic Hamiltonians. A notion of preferred gauge for MAB is suggested. The MAB effect in the linear + quadratic $E \otimes \varepsilon$ Jahn–Teller system is shown to be essentially analogues to an anisotropic Aharonov–Casher effect for an electrically neutral spin $-\frac{1}{2}$ particle encircling a certain configuration of lines of charge.

Contents

1. Introduction	239
2. Locality and topology	241
3. Preferred gauge	243
4. Aharonov–Casher analogue	249
5. Conclusions	250
Acknowledgements	251
References	251

1. INTRODUCTION

The molecular Aharonov–Bohm (MAB) effect, first hinted at by Longuet-Higgins *et al.* [1–4], is one of the paradigmatic examples on early anticipations of Berry’s discovery [5] of geometric phase factors accompanying cyclic adiabatic changes. The importance of MAB ranges from testable shifts of the vibronic energy spectrum [6,7], effects on cross-sections in molecular reactions [8–10], and effects on reduction factors [11], to subtle symmetry assignments of vibronic states in Jahn–Teller systems [12–15] and search for conical intersections [4,16–20]. However, it is probably fair to say that interest in the MAB effect itself arose first after it was realized [21,22] its mathematical analogy with the standard Aharonov–Bohm (AB) effect [23]. This mathematical analogy is the independence of

details of the shape of the closed path in a multiply connected region of nuclear configuration space.

In a recent work [24], Sjöqvist has considered the physical nature of this analogue in the case of the $E \otimes \epsilon$ Jahn–Teller system. The question addressed there was: does MAB share all the remarkable properties of AB? The main outcome of this analysis was that although MAB obeys the above-mentioned independence of details of the closed path in nuclear configuration space, it does not share the remaining nonlocal and topological properties of AB. The purpose of the present paper is to develop the local and nontopological nature of MAB further. In particular, we wish to extend [24] to any molecular system with real electronic Hamiltonians. We also wish to propose a notion of preferred gauge for MAB in this case, in terms of a so-called gauge invariant reference section [25,26] that appears naturally in the theory of the open path Berry phase [27,28].

The starting point for the argumentation in Ref. [24] is a set of criteria for a nonlocal and topological phase effect, first explicitly introduced by Peshkin and Lipkin [29]. These are

- A phase effect is nonlocal if
 - (N1) the system experiences no physical field,
 - (N2) no exchange of physical quantity takes place along the system's path.
- A phase effect is topological if
 - (T1) it requires the system to be confined to a multiply connected region,
 - (T2) any assignment of phase shift along the system's path is necessarily gauge dependent and thus neither objective nor experimentally testable.

One can argue that AB fulfills all these criteria for a nonlocal and topological phase effect. On the other hand, in the case of MAB, where the physical system consists of the nuclear configuration and a set of electronic variables, the situation is very different. First, MAB is local in that it obeys neither (N1) nor (N2): the nuclei experiences the Coulomb field from the electrons, and there must be a local exchange of force to create the change in the electronic state necessary for the appearance of points in nuclear configuration space, across which the electronic open path Berry phase factor changes sign discontinuously [30–33]. Secondly, MAB is nontopological in that (T2) fails since there is an objective and experimentally testable open path electronic Berry phase that causes the effect on the nuclear motion. Only (T1) is fulfilled for MAB: the nuclei must be confined to a multiply connected region for the effect to occur. We wish to discuss the above criteria in relation to MAB systems of general kind.

In Section 2, we extend the argumentation of Sjöqvist [24] to the case of arbitrary molecular systems with real electronic Hamiltonians. A notion of preferred gauge for MAB in this case is suggested in Section 3 and applied in detail to the $E \otimes \varepsilon$ Jahn–Teller system. The analogue between the MAB effect in the $E \otimes \varepsilon$ Jahn–Teller system and the Aharonov–Casher (AC) effect [34], as pointed out in Ref. [24], is further developed in Section 4, so as to treat linear and quadratic coupling simultaneously. The paper ends with the conclusions.

2. LOCALITY AND TOPOLOGY

The argumentation in Ref. [24] that MAB is essentially a local and nontopological effect was put forward in the special case of the $E \otimes \varepsilon$ Jahn–Teller system. This raises the question whether the main conclusions arrived at in Ref. [24] also apply to other molecular systems that may be described accurately by real electronic Hamiltonians. In this section, we address this issue and argue that MAB also in the general case is local and nontopological.

For sake of clarity, we focus on the motion in some pseudorotational (internal) nuclear coordinate θ , as described by the vibronic Hamiltonian

$$H = \frac{1}{2}p_\theta^2 + H_e(\theta), \quad (1)$$

where p_θ is the canonical momentum corresponding to θ and $H_e(\theta)$ is the electronic Hamiltonian assumed to be real, traceless, and fulfilling $H_e(\theta + 2\pi) = H_e(\theta)$. Let $\{|n\rangle\}_{n=1}^N$ be a fixed orthonormal basis of the electronic Hilbert space of finite dimension N . Furthermore, let $\{R(\theta)|\theta \in [0, 2\pi)\}$ be a one-parameter set of members of the rotation group $\text{SO}(N)$ in \mathbf{R}^N , in terms of which the orthonormal instantaneous eigenvectors of $H_e(\theta)$ read $|n(\theta)\rangle = R(\theta)|n\rangle_{n=1}^N$. Then, we may write $H_e(\theta) = R(\theta)E(\theta)R^T(\theta)$ with T being transpose and $E(\theta) = \text{diag}[E_1(\theta), \dots, E_N(\theta)]$, where $E_1(\theta), \dots, E_N(\theta)$ are the electronic eigenenergies corresponding to $|1(\theta)\rangle, \dots, |N(\theta)\rangle$.

The Born–Oppenheimer regime is attained when the electronic eigenenergies $\{E_n(\theta)\}_{n=1}^N$ are well separated so that the nuclear motion takes place on a single electronic potential energy surface, let us say $E_n(\theta)$. This may be described by the effective nuclear Hamiltonian

$$H_n = \langle n(\theta)|H|n(\theta)\rangle = \frac{1}{2}p_\theta^2 + E_n(\theta), \quad (2)$$

where we have used that $\langle n|R^T(\theta)p_\theta R(\theta)|n\rangle = 0$. The issue of MAB arises when considering the single-valuedness of the molecular state vector $|\Psi(\theta)\rangle$, which in the Born–Oppenheimer regime is a product of the instantaneous

electronic energy eigenvector $|n(\theta)\rangle$ and a nuclear factor $\chi(\theta)$, i.e., $|\Psi(\theta)\rangle = \chi(\theta)|n(\theta)\rangle$. Here, we use the position representation of the nuclear motion in the pseudorotational angle θ . The single-valuedness of $|\Psi(\theta)\rangle$ requires that any multi-valuedness of the electronic part must be compensated for by the nuclear part. Thus, if $|n(\theta + 2\pi)\rangle = -|n(\theta)\rangle$, $\chi(\theta)$ must fulfill the boundary condition $\chi(\theta + 2\pi) = -\chi(\theta)$. A nontrivial MAB effect arises if and only if there is no phase transformation of the form $|n(\theta)\rangle \rightarrow |\tilde{n}(\theta)\rangle = e^{i\xi(\theta)}|n(\theta)\rangle$ so that the effective vector potential

$$A_n(\theta) \equiv i\langle \tilde{n}(\theta) | \partial_\theta | \tilde{n}(\theta) \rangle = -\partial_\theta \xi(\theta) \quad (3)$$

vanishes everywhere and at the same time retaining single-valuedness for $\chi(\theta)$ under the requirement that $|\Psi(\theta)\rangle$ is single valued.

Under the condition that there is a nontrivial MAB effect, let us ask: what is its physical nature in relation to the standard AB effect? Let us first address the issue of locality. As already indicated, the standard AB effect, which may occur when a charged particle encircles a line of magnetic flux, is nonlocal as it fulfills the criteria (N1) and (N2): the effect arises although the particle experiences no physical field and no exchange of physical quantity takes place along the particle's path. Could the same be said about the MAB effect? One way to address this question is to note that since the electronic Born–Oppenheimer states are eigenstates of $H_e(\theta)$, it may be tempting to replace the electronic motion by the appropriate eigenvalue of $H_e(\theta)$ in the Born–Oppenheimer regime so that the electronic variables can be ignored, creating an illusion that the nontrivial effect of the MAB vector potential on the nuclear motion is nonlocal and topological in the sense of the standard AB effect. However, this argument fails essentially because the electronic variables are dynamical and do not commute among themselves. Thus, there always exist a subset of these variables, namely those that are off-diagonal in the instantaneous electronic eigenbasis $\{|n(\theta)\rangle\}_{n=1}^N$, whose expectation values vanish in the Born–Oppenheimer limit, but whose fluctuations do not. These fluctuations are due to the local interaction between the nuclear variables and the electronic degrees of freedom. Thus, both (N1) and (N2) fail for MAB.

Next, we address the issue of topology. The standard AB effect is topological in that (T1) it may occur although the region of magnetic field is inaccessible to the encircling charged particle and in that (T2) the charged particle only feels the gauge dependent vector potential along the path. In the case of MAB, recall that two types of degrees of freedom are involved: those of the electrons and those associated with the nuclear configuration. Now, any assignment of nuclear phase for open paths in nuclear configuration space is necessarily gauge dependent and therefore unphysical. On the other hand, there is an objective way to relate the origin of the MAB phase effect locally in nuclear configuration space using the open path Berry phase γ_n for

the corresponding electronic Born–Oppenheimer state vector $|\tilde{n}(\theta)\rangle = e^{i\xi(\theta)}|n(\theta)\rangle$. Here, we assume $\xi(\theta)$ to be differentiable along the path but otherwise arbitrary. The noncyclic Berry phase is defined by removing the accumulation of local phase changes from the total phase and is testable in polarimetry [31,35] or in interferometry [36,37]. We obtain for $|\tilde{n}(\theta)\rangle$

$$\begin{aligned}\gamma_n &= \arg\langle\tilde{n}(\theta_0)|\tilde{n}(\theta)\rangle + i \int_{\theta_0}^{\theta} \left\langle \tilde{n}(\theta') \left| \frac{\partial}{\partial \theta'} \right| \tilde{n}(\theta') \right\rangle d\theta' \\ &= \arg\langle n(\theta_0)|n(\theta)\rangle\end{aligned}\quad (4)$$

by using equation (3). Clearly, γ_n is locally gauge invariant as it is independent of $\xi(\theta)$. It corresponds to phase jumps of π at points across which the real-valued quantity $\langle n(\theta_0)|n(\theta)\rangle$ goes through zero and changes sign. In the case where an even number of π phase jumps occurs, the nuclear factor $\chi(\theta)$ is single valued and there is no MAB effect. On the other hand, for an odd number of such jumps, there is a physically nontrivial sign change for such a loop. Thus, the presence of a nontrivial MAB effect could be explained locally as it requires the existence of points along the nuclear path where the electronic states at θ_0 and θ become orthogonal. This assignment of electronic Berry phase shift is gauge invariant at each point along the nuclear path and thus experimentally testable in principle. It shows that MAB does not obey the criterion (T2) for a topological phase effect.

3. PREFERRED GAUGE

The assignment of a gauge invariant electronic Berry phase for any open portion of the closed nuclear path suggests that MAB is not topological and that it might be meaningful to introduce a notion of preferred gauge in this context. The corresponding preferred vector potential is defined as that whose line integral gives the open path Berry phase. This idea can be put forward in terms of a so-called gauge invariant reference section [25,26] as follows.

First, in general terms, let $|\psi(s)\rangle$ be a normalized Hilbert space representative of the pure quantal state $\psi(s)$ tracing out the path $C : s \in [s_0, s_1] \rightarrow \psi(s)$ in projective Hilbert space \mathcal{P} . Now, if $0 \neq |\langle\psi(s_0)|\psi(s_1)\rangle| \leq 1$, then the Berry phase $\gamma[C]$ associated with C is [28]

$$\begin{aligned}\gamma[C] &= \arg\langle\psi(s_0)|\psi(s_1)\rangle - \int_{s_0}^{s_1} \arg\langle\psi(s)|\psi(s+ds)\rangle \\ &= \arg\langle\psi(s_0)|\psi(s_1)\rangle + i \int_{s_0}^{s_1} \langle\psi(s)|\dot{\psi}(s)\rangle ds,\end{aligned}\quad (5)$$

where the first and second term on the right-hand side contain the global phase and the accumulation of local phase changes, respectively. This open path Berry phase is real valued and reparameterization invariant [28]. It is gauge invariant and thereby measurable [31,35–37] in that it is independent of choice of Hilbert space representative. $\gamma[C]$ reduces to the cyclic Berry phase [5] in the particular case where $|\langle\psi(s_0)|\psi(s_1)\rangle| = 1$.

A gauge invariant reference section $|\phi(s)\rangle$ is a nonlinear functional of $|\psi(s)\rangle$ defined as [25,26]

$$|\phi(s; s_0)\rangle = \exp(-i \arg\langle\psi(s_0)|\psi(s)\rangle)|\psi(s)\rangle, \quad (6)$$

which has the image C in \mathcal{P} . $|\phi(s; s_0)\rangle$ is in one to one correspondence with C in that it is gauge invariant under phase transformations of $|\psi(s)\rangle$. Furthermore, by inserting equation (6) into equation (5), we obtain

$$\gamma[C] = \int_{s_0}^{s_1} \mathcal{A}(s; s_0) ds, \quad (7)$$

where the gauge function reads

$$\mathcal{A}(s; s_0) = i\langle\phi(s; s_0)|\partial_s \phi(s; s_0)\rangle. \quad (8)$$

Now, the one to one correspondence between the path C and $\{|\phi_n(s; s_0)\rangle | s \in [s_0, s_1]\}$, and the fact that the open path Berry phase can be directly expressed in terms of the vector potential $\mathcal{A}(s; s_0)$, suggest that the gauge invariant reference section defined in equation (6) has a special status: it is natural to regard $|\phi_n(s; s_0)\rangle$ and $\mathcal{A}(s; s_0)$ to constitute a ‘preferred gauge’ for the measurable open path Berry phase. In doing so, one should take notice that the functional form of the preferred vector potential $\mathcal{A}(s; s_0)$ depends in general upon $\psi(s_0)$, but is otherwise unique up to an additional term whose integral over the interval $[s_0, s_1]$ equals an integral multiple of 2π . In particular, once $\psi(s_0)$ has been chosen the corresponding phase factor is gauge invariant under phase transformations of $|\psi(s)\rangle$.

We next apply this idea and calculate the gauge invariant electronic reference section relevant for MAB and its concomitant vector potential in the case of real electronic Hamiltonians. Let the pseudorotational angle $\theta \in [\theta_0, \theta_0 + 2\pi]$ parameterize a closed path C_N in nuclear configuration space. Let $|n(\theta)\rangle = R(\theta)|n\rangle$ be a Hilbert space representative of a nondegenerate electronic energy eigenstate along this path. Under these assumptions, consider a finite portion ΔC_N of C_N . First, suppose that $\langle n(\theta_0)|n(\theta)\rangle \neq 0$, $\theta \in \Delta C_N$. Along such a ΔC_N , the gauge invariant reference section reads

$$|\phi_n(\theta; \theta_0)\rangle = \exp(-i \arg\langle n(\theta_0)|n(\theta)\rangle)|n(\theta)\rangle = \pm |n(\theta)\rangle, \quad (9)$$

where the sign is independent of θ . This follows since $\langle n(\theta_0)|n(\theta)\rangle$ is real valued and may only change sign where it vanishes. Inserting equation (9) into equation (8), we obtain $\mathcal{A}_n(\theta; \theta_0) = 0$, $\theta \in \Delta C_N$.

Now, suppose there is a single isolated point $\theta_k \in \Delta C_N$ across which $\langle n(\theta_0) | n(\theta_k) \rangle$ goes through zero and changes sign. For such a point, it follows that

$$|\phi_n(\theta; \theta_0)\rangle = \pm \exp(i\pi h_s(\theta - \theta_k)) |n(\theta)\rangle, \quad \theta \in \Delta C_N, \quad (10)$$

where h_s is the unit step function. This yields

$$\mathcal{A}_n(\theta; \theta_0) = -\pi \delta(\theta - \theta_k), \quad \theta \in \Delta C_N, \quad (11)$$

where we have used that $\partial_\theta h_s(\theta - \theta_k) = \delta(\theta - \theta_k)$.

Extending this to the whole closed path C_N , we may assume it contains K angles $\theta_1, \dots, \theta_K$, all across which $\langle n(\theta_0) | n(\theta) \rangle$ goes through zero and changes sign. Then, the gauge invariant reference section reads

$$|\phi_n(\theta; \theta_0)\rangle = \exp\left(i\pi \sum_{k=1}^K h_s(\theta - \theta_k)\right) |n(\theta)\rangle, \quad \theta \in C_N \quad (12)$$

with the corresponding preferred vector potential

$$\mathcal{A}_n(\theta; \theta_0) = -\pi \sum_{k=1}^K \delta(\theta - \theta_k), \quad \theta \in C_N. \quad (13)$$

Notice that $\mathcal{A}_n(\theta; \theta_0)$ is a local quantity as it only depends upon the angles $\theta_1, \dots, \theta_K$, whose location is gauge invariant once the ‘initial’ electronic eigenstate $n(\theta_0)$ has been chosen.

There is a nontrivial MAB effect if and only if K is odd, since

$$\gamma_n[C_N] = \oint_{C_N} \mathcal{A}_n d\theta = -K\pi. \quad (14)$$

It is important to notice that this criterion for a nontrivial MAB is only fulfilled if the effective nuclear motion has physical access to the whole closed path C_N . To see this, let $\langle n(\theta_0) | n(\theta) \rangle$ change sign at the angles $\theta_1, \dots, \theta_K$ along C_N . In the preferred gauge the effective Hamiltonian operator for the nuclear motion in the θ direction reads

$$H_n = \langle \phi_n(\theta; \theta_0) | H | \phi_n(\theta; \theta_0) \rangle = \frac{1}{2} [p_\theta + \mathcal{A}_n(\theta; \theta_0)]^2 + E_n(\theta). \quad (15)$$

Suppose $E_n(\theta)$ comprises an infinite potential barrier over the angular range $\theta \in [\vartheta, \vartheta + \Delta\vartheta]$, $0 < \Delta\vartheta < 2\pi$, creating an inaccessible part $C_N(\Delta\vartheta)$ of C_N for the nuclear motion. Then, it is consistent with the boundary condition $\chi(\vartheta) = \chi(\vartheta + \Delta\vartheta) = 0$ to absorb the vector potential \mathcal{A}_n into the phase of the nuclear factor.

Now, what is the origin of a nontrivial gauge invariant reference section? In part this can be answered in terms of the following relationship between the gauge invariant reference section and degeneracy points where two or more electronic potential energy surfaces cross (for an analysis of the related

connection between degeneracies and singularities of the electronic eigenvectors, see Ref. [38]). Let q_N be the internal nuclear coordinates and consider a line $C^\perp : s \in [0, 1] \rightarrow q_N(s)$ in nuclear configuration space for which $\mathcal{A}(q_N(s); q_N(s_0)) = -\pi\delta(q_N - q_N(s))$, for $0 \leq s < s' < 1$, and $\mathcal{A}(q_N(s); q_N(s_0)) = 0$, for $s' < s \leq 1$ (see Fig. 1). Now, any path C in the Born–Oppenheimer regime that starts and ends at the reference point $q_N(s_0)$ and cross C^\perp once, must be associated with a sign change of the electronic eigenvector and thus must enclose at least one point of degeneracy on any surface that has C as boundary, as implied by the Longuet-Higgins theorem [4]. On the other hand, there is no such sign change originating from C^\perp for a closed path C' that does not cross C^\perp , which implies that there must be one less degeneracy enclosed by such a path than by C . Thus, $q_N(s')$ is a degeneracy point.

To illustrate the gauge invariant reference section for MAB, let us revisit the linear + quadratic $E \otimes \varepsilon$ Jahn–Teller effect, which is known to exhibit a nontrivial MAB structure. There, the symmetry induced degeneracy of two electronic states (E) is lifted by their interaction with a doubly degenerate vibrational mode (ε). In the vicinity of the degeneracy point at the symmetric nuclear configuration, this may be modeled by the vibronic Hamiltonian [39]

$$H = \frac{1}{2}p_r^2 + \frac{1}{2r^2}p_\theta^2 + \frac{1}{2}r^2 + \Delta E(r, \theta)(\cos \alpha(r, \theta)\sigma_x + \sin \alpha(r, \theta)\sigma_z). \quad (16)$$

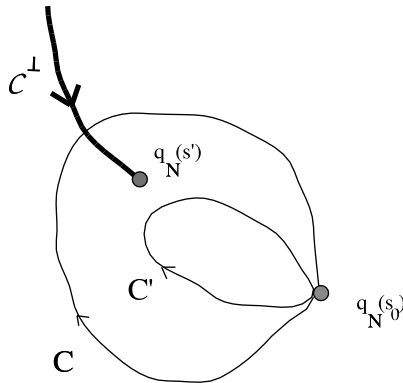


Fig. 1. Single line $C^\perp : s \in [0, 1] \rightarrow q_N(s)$ in nuclear configuration space for which $\mathcal{A}(q_N(s); q_N(s_0)) = -\pi\delta(q_N - q_N(s))$, for $0 \leq s < s' < 1$, and $\mathcal{A}(q_N(s); q_N(s_0)) = 0$, for $s' < s \leq 1$. For any closed path C that cross C^\perp , the electronic eigenvector picks up a sign implying a degeneracy on any surface that has C as boundary. For any closed path C' that does not cross C^\perp , no such sign change occur. From Longuet-Higgins theorem [4] follows that $q_N(s')$ is a point of electronic degeneracy.

Here, (r, θ) are polar coordinates of the vibrational mode, (p_r, p_θ) the corresponding canonical momenta, $k \geq 0$ and $g \geq 0$ are the linear and quadratic vibronic coupling strength, respectively. $\Delta\mathcal{E}$ and α are given by

$$\begin{aligned}\Delta\mathcal{E}(r, \theta) &= \sqrt{k^2 r^2 + kgr^3 \cos 3\theta + \frac{1}{4}g^2 r^4}, \\ \Delta\mathcal{E}(r, \theta)e^{i\alpha(r, \theta)} &= kr \cos \theta + \frac{1}{2}gr^2 \cos 2\theta \\ &\quad + i\left(kr \sin \theta - \frac{1}{2}gr^2 \sin 2\theta\right).\end{aligned}\quad (17)$$

The electronic degrees of freedom are described by Pauli operators defined in terms of the diabatic electronic states $|0\rangle$ and $|1\rangle$ as $\sigma_x = |0\rangle\langle 1| + |1\rangle\langle 0|$, $\sigma_y = -i|0\rangle\langle 1| + i|1\rangle\langle 0|$, and $\sigma_z = |0\rangle\langle 0| - |1\rangle\langle 1|$. Diagonalizing the electronic part of H yields the electronic eigenvectors

$$|+(\alpha)\rangle = \cos\frac{\alpha}{2}|0\rangle + \sin\frac{\alpha}{2}|1\rangle, \quad |-(\alpha)\rangle = -\sin\frac{\alpha}{2}|0\rangle + \cos\frac{\alpha}{2}|1\rangle \quad (18)$$

with corresponding energies $E_\pm = \frac{1}{2}r^2 \pm \Delta\mathcal{E}(r, \theta)$ and where we have put $\alpha \equiv \alpha(r, \theta)$ for brevity. The phase α is undefined only if $\Delta\mathcal{E}(r, \theta) = 0$, corresponding to the degeneracy points at $r = 0$ and $r = 2k/g$ for $\theta = \pi/3$, π , $5\pi/3$.

To calculate the gauge invariant reference section, we may choose $\theta_0 = 0$ so that $\alpha_0 \equiv \alpha(r_0, \theta_0) = 0$, independent of r_0 . In this case, we obtain

$$\langle \pm(\alpha_0) | \pm(\alpha) \rangle = \cos\frac{\alpha}{2}. \quad (19)$$

This vanishes for $\alpha = \pi$ corresponding to

$$kr \sin \theta - \frac{1}{2}gr^2 \sin 2\theta = 0, \quad kr \cos \theta + \frac{1}{2}gr^2 \cos 2\theta < 0, \quad (20)$$

which have the solutions $\theta' = \pi$ for $r < 2k/g$ and $\theta' = \pm \arccos[k/(gr)]$ for $r > 2k/g$. Since the solutions for $r < 2k/g$ are independent of r , they constitute a radial line whose endpoints are the electronic degeneracies at the origin and at $(r, \theta') = (2k/g, \pi)$, see Fig. 2. If $2k/g < r \rightarrow \infty$, we obtain the limit angles $\theta' = \pm \pi/2$ at the infinity. On the other hand, if $r \rightarrow 2k/g^+$, then the lines of sign change terminate at $\theta' = \pm \pi/3$, which are the remaining electronic degeneracies (see Fig. 2).

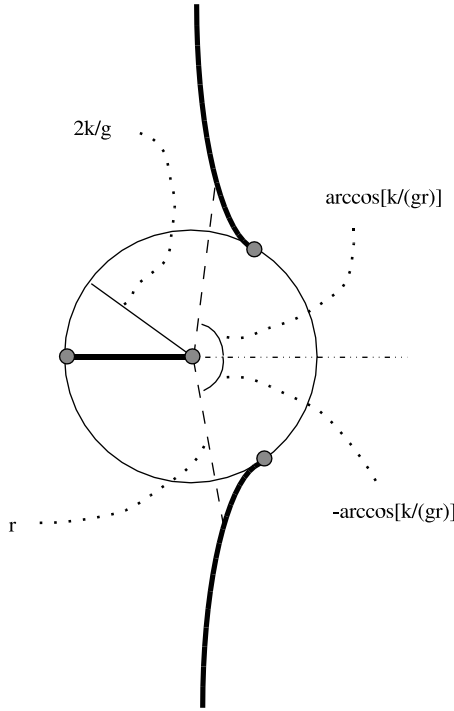


Fig. 2. Lines of sign change and degeneracy points in the linear + quadratic $E \otimes \varepsilon$ Jahn–Teller model for any of the two Born–Oppenheimer states. Degeneracies are indicated by small circles; they occur at the origin and at $r = 2k/g$ for angles $\theta = \pi/3, \pi, 5\pi/3$. The electronic reference state is chosen at an arbitrary point along the dashed–dotted line ($\theta = 0$). The thick continuous lines correspond to points where $\langle \pm(\alpha_0) | \pm(\alpha) \rangle$ goes through zero and changes sign. These lines of sign change end either at infinity or at a degeneracy. For a circular closed path with $r > 2k/g$, there is an even number of jumps for this path, and consequently no MAB effect for the corresponding nuclear motion along the path. On the other hand, for any circular closed path with $r < 2k/g$ there is a single node at $\theta = \pi$, assigning a nontrivial MAB effect.

Next, let us consider the gauge invariant reference section and the corresponding vector potential. For $r < 2k/g$, we have

$$|\phi_{\pm}\rangle = \exp(i\pi h_s(\theta - \pi)) |\pm(\alpha)\rangle, \quad \mathcal{A}_{\pm}(\theta; 0) = -\pi\delta(\theta - \pi), \quad (21)$$

while for $r > 2k/g$, we have

$$\begin{aligned} |\phi_{\pm}\rangle &= \exp(i\pi h_s(\theta - \arccos[k/(gr)]) \\ &\quad + i\pi h_s(\theta + \arccos[k/(gr)])) |\pm(\alpha)\rangle, \\ \mathcal{A}_{\pm}(\theta; 0) &= -\pi\delta(\theta - \arccos[k/(gr)]) - \pi\delta(\theta + \arccos[k/(gr)]). \end{aligned} \quad (22)$$

4. AHARONOV–CASHER ANALOGUE

It was demonstrated in Ref. [24] that for the linear or the quadratic $E \otimes \varepsilon$ Jahn–Teller system, there is a close analogy with the AC phase effect [34] for an electrically neutral spin $-\frac{1}{2}$ particle encircling a line of charge. From this perspective, one may regard the presence (absence) of MAB effect in the linear (quadratic) case as a nontrivial (trivial) $\pi(2\pi)$ AC phase shift. Here, we extend this idea to the linear + quadratic case.

In brief, the AC effect may occur when an electrically neutral spin $-\frac{1}{2}$ particle carrying a magnetic dipole moment μ encircles a straight line of charge. Under the condition that the spin is parallel to the charged line, the particle acquires along the closed path ∂S the phase shift ($\hbar = 1$)

$$\gamma_{AC} = \frac{\mu}{c^2} \oint_{\partial S} (\hat{\mathbf{n}} \times \mathbf{E}) \cdot d\mathbf{r} = \frac{\mu}{c^2} \iint_S \nabla \cdot \mathbf{E} dS = \frac{\mu\lambda}{c^2\epsilon_0} \quad (23)$$

with c the speed of light, $\hat{\mathbf{n}}$ the direction of the dipole, \mathbf{E} the electric field, $d\mathbf{r}$ a line element along this path, S any surface with ∂S as boundary, λ the enclosed charge density, and ϵ_0 the electric vacuum permittivity.

To demonstrate the promised analogy between the MAB effect in the $E \otimes \varepsilon$ Jahn–Teller system and the AC effect, we may use the apparent spin analogy in terms of which we may notice that the electronic Hamiltonian in equation (16) describes a spin $-\frac{1}{2}$ under influence of an effective magnetic field that rotates around the σ_y axis by the angle $\alpha(r, \theta)$. We expect the electronic Hamiltonian be fixed (possibly up to an unimportant r and θ dependent scale factor) in an internal molecular frame that co-moves with this rotation. The essential point here is that, contrary to the usual case of a spin $-\frac{1}{2}$ in a rotating external magnetic field, the rotation angle α of this Jahn–Teller system depends upon the internal variables r and θ . This has the consequence that the vibronic Hamiltonian in the co-moving frame, which reads (omitting the inessential $\frac{1}{2}p_r^2$ and $\frac{1}{2}r^2$ terms)

$$H' = U^\dagger H U = \frac{1}{2r^2} \left[p_\theta - \frac{1}{2} \partial_\theta \alpha(r, \theta) \sigma_y \right]^2 + \Delta \mathcal{E}(r, \theta) \sigma_z \quad (24)$$

with $U = \exp[-i\alpha(r, \theta)\sigma_y/2]$ the unitary spin rotation operator, contains a nontrivial modification of the nuclear kinetic energy operator. Indeed, by using H' and the Heisenberg picture, this modification in turn affects the equations of motion for the electronic variables, which read

$$\begin{aligned} \dot{\sigma}_x &= -\partial_\theta \alpha(r, \theta) \dot{\theta} \sigma_z - 2\Delta \mathcal{E}(r, \theta) \sigma_y, & \dot{\sigma}_y &= 2\Delta \mathcal{E}(r, \theta) \sigma_x, \\ \dot{\sigma}_z &= \partial_\theta \alpha(r, \theta) \dot{\theta} \sigma_x, \end{aligned} \quad (25)$$

where $r^2 \dot{\theta} = p_\theta - \frac{1}{2} \partial_\theta \alpha(r, \theta) \sigma_y$. The Born–Oppenheimer regime is characterized by the condition $\partial_\theta \alpha(r, \theta) |\dot{\theta}| \ll \Delta \mathcal{E}(r, \theta)$ that apparently breaks down

when $\Delta\mathcal{E}(r, \theta)$ is very small, which happens close to the electronic degeneracies. From equation (25), it follows that the electronic motion describes the local torque due to an effective magnetic field $\mathbf{B}_{\text{eff}} = -\partial_\theta \alpha(r, \theta) \dot{\theta} \mathbf{e}_y + 2\Delta\mathcal{E}(r, \theta) \mathbf{e}_z$ seen by the electronic variables in the rotating frame. The large z component of \mathbf{B}_{eff} depends only on the energy difference $\Delta\mathcal{E}(r, \theta)$ between the two electronic states and is thus irrelevant to MAB. On the other hand, the small y component corresponds exactly to the MAB effect and gives rise to a $\boldsymbol{\sigma} \cdot (\mathbf{v} \times \mathbf{E}_{\text{eff}})$ term for the electronic variables in the co-moving frame in the $x - z$ plane. Explicitly, we have

$$\mathbf{E}_{\text{eff}} = \frac{\partial_\theta \alpha(r, \theta)}{2r} \mathbf{e}_r + E_\theta(r, \theta) \mathbf{e}_\theta, \quad (26)$$

where we have left out the explicit form of the θ component of \mathbf{E}_{eff} , as it does not contribute to the MAB phase effect. The effect of this field is equivalent to that of an AC system that consists of four charged lines in the y direction sitting at the four conical intersections at $r = 0$ and $r = 2k/g$ for $\theta = \pi/3, \pi, 5\pi/3$, all of which with the charge per unit length being proportional to $\frac{1}{2}$. Thus, the MAB effect for the $E \otimes \varepsilon$ Jahn–Teller system resembles exactly that of the AC effect for an electrically neutral spin $-\frac{1}{2}$ particle encircling a certain configuration of charged lines perpendicular to the plane of motion.

Note that the phase shift γ_{AC} only depends upon the enclosed charge, but is independent of the shape of the dipole's path. On the other hand, the dipole feels the gauge invariant electric field \mathbf{E} , which defines a preferred gauge in terms of the gauge invariant effective vector potential $(\mu/c^2) \hat{\mathbf{n}} \times \mathbf{E}$ and which causes a nontrivial, essentially local and nontopological autocorrelation among the spin variables, as demonstrated in Ref. [29]. From this perspective, we believe that the present analogy between the AC and MAB effects further strengthens the local and nontopological interpretation of MAB for this Jahn–Teller system.

5. CONCLUSIONS

Arguably one of the most intriguing discoveries of the second half of the 20th century was that of a nonlocal and topological interference effect for a charged particle moving around a magnetic flux line, made by Aharonov and Bohm [23]. Analogues of this remarkable effect have since then been found, such as the AC effect [34] and its Maxwell dual, the so-called He–McKellar–Wilkins (HMW) effect [40,41]. Common to these analogue effects are that they only occur under certain restrictions on some additional degree of freedom: the spin direction for AC and the direction of an electric dipole for HMW. These additional restrictions turn out to make these effects essentially different from the standard AB, in that they do not obey all the properties for being nonlocal and topological.

Does the MAB effect share the fate of these other analogue effects? This question was examined quite recently by Sjöqvist [24] in the particular case of the $E \otimes \varepsilon$ Jahn–Teller system. In identifying the restrictions for this system, which are the conditions of attaining the Born–Oppenheimer regime and the electronic state being in one of two instantaneous energy eigenstates, this issue can be addressed very much along the line of the other analogue effects. The outcome was: the MAB effect for this system is neither nonlocal nor topological in the sense of the standard AB effect. In this paper, this result has been generalized to any molecular system with real electronic Hamiltonian and where a nontrivial MAB effect shows up. In addition, a notion of preferred gauge for such systems, defined by an effective vector potential whose open path integral is the open path Berry phase for the electronic motion, has been suggested.

One of the early motivations preceding the analysis in Ref. [24] was to examine whether there is a relation between the MAB effect in the $E \otimes \varepsilon$ Jahn–Teller system and the AC effect, based upon the simple observation that the original vibronic Hamiltonian for this Jahn–Teller system resembles exactly that of an electrically neutral spin $-\frac{1}{2}$ in a certain field configuration. Indeed, by transforming to a molecular frame that co-moves with the nuclear pseudorotation, this analogue was made explicit in Ref. [24] in the case of either linear or quadratic coupling. In the present paper, this result has been extended to the linear + quadratic case, leading to an anisotropic effective electric field originating from four charged lines sitting at the four conical intersections in nuclear configuration space.

ACKNOWLEDGEMENTS

I wish to express my deep gratitude to Prof. Osvaldo Gosciniski, especially for introducing me to the subject of geometric phases and how they appear in molecular systems, but also for numerous discussions and collaboration during the past 10 years. Osvaldo's great impact on my scientific thinking makes it a very special honour to dedicate this paper on his 65th birthday. I also wish to thank Mauritz Andersson, Henrik Carlsen, Marie Ericsson, Gonzalo García de Polavieja, Magnus Hedström, and Niklas Johansson for discussions and collaboration over the years on issues related to the present paper. This work was supported by the Swedish Research Council.

REFERENCES

- [1] H. C. Longuet-Higgins, U. Öpik, M. H. L. Pryce and R. A. Sack, *Proc. R. Soc. London, Ser. A*, 1958, **244**, 1.
- [2] H. C. Longuet-Higgins, *Adv. Spectrosc.*, 1961, **2**, 429.
- [3] G. Herzberg and H. C. Longuet-Higgins, *Discuss. Faraday Soc.*, 1963, **35**, 77.

- [4] H. C. Longuet-Higgins, *Proc. R. Soc. London, Ser. A*, 1975, **344**, 147.
- [5] M. V. Berry, *Proc. R. Soc. London, Ser. A*, 1984, **392**, 45.
- [6] B. Kendrick, *Phys. Rev. Lett.*, 1997, **79**, 2431.
- [7] H. von Busch, V. Dev, H.-A. Eckel, S. Kasahara, J. Wang, W. Demtröder, P. Sebold and W. Meyer, *Phys. Rev. Lett.*, 1998, **81**, 4584.
- [8] A. Kupperman and Y. M. Wu, *Chem. Phys. Lett.*, 1993, **205**, 577.
- [9] B. Kendrick and R. T. Pack, *J. Chem. Phys.*, 1996, **104**, 7475.
- [10] S. Adhikari and G. D. Billing, *Chem. Phys.*, 2000, **259**, 149.
- [11] E. Sjöqvist and O. Goscinski, *Chem. Phys.*, 1994, **186**, 17.
- [12] F. S. Ham, *Phys. Rev. Lett.*, 1987, **58**, 725.
- [13] F. S. Ham, *J. Phys.: Condens. Matter*, 1990, **2**, 1163.
- [14] P. De Los Rios, N. Manini and E. Tosatti, *Phys. Rev. B*, 1996, **54**, 7157.
- [15] C. P. Moate, M. C. M. O'Brien, J. L. Dunn, C. A. Bates, Y. M. Liu and V. Z. Polinger, *Phys. Rev. Lett.*, 1996, **77**, 4362.
- [16] A. J. Stone, *Proc. R. Soc. London, Ser. A*, 1976, **351**, 141.
- [17] A. J. C. Varandas, J. Tennyson and J. N. Murrell, *Chem. Phys. Lett.*, 1979, **61**, 431.
- [18] S. Xantheas, S. T. Elbert and K. Ruedenberg, *J. Chem. Phys.*, 1990, **93**, 7519.
- [19] M. Ceotto and F. A. Gianturco, *J. Chem. Phys.*, 2000, **112**, 5820.
- [20] N. Johansson and E. Sjöqvist, *Phys. Rev. Lett.*, 2004, **92**, 060406.
- [21] C. A. Mead and D. G. Truhlar, *J. Chem. Phys.*, 1979, **70**, 2284.
- [22] (a) C. A. Mead, *Chem. Phys.*, 1980, **49**, 23; (b) C. A. Mead, *Chem. Phys.*, 1980, **49**, 33.
- [23] Y. Aharonov and D. Bohm, *Phys. Rev.*, 1959, **115**, 485.
- [24] E. Sjöqvist, *Phys. Rev. Lett.*, 2002, **89**, 210401.
- [25] A. K. Pati, *J. Phys. A*, 1995, **28**, 2087.
- [26] A. K. Pati, *Phys. Rev. A*, 1995, **52**, 2576.
- [27] J. Samuel and R. Bhandari, *Phys. Rev. Lett.*, 1988, **60**, 2339.
- [28] N. Mukunda and R. Simon, *Ann. Phys. (NY)*, 1993, **288**, 205.
- [29] M. Peshkin and H. J. Lipkin, *Phys. Rev. Lett.*, 1995, **74**, 2847.
- [30] E. Sjöqvist and M. Hedström, *Phys. Rev. A*, 1997, **56**, 3417.
- [31] G. García de Polavieja and E. Sjöqvist, *Am. J. Phys.*, 1998, **66**, 431.
- [32] R. Englman and A. Yahalom, *Phys. Rev. A*, 1999, **60**, 1802.
- [33] R. Englman, A. Yahalom and M. Baer, *Eur. Phys. J. D*, 2000, **8**, 1.
- [34] Y. Aharonov and A. Casher, *Phys. Rev. Lett.*, 1984, **53**, 319.
- [35] P. Larsson and E. Sjöqvist, *Phys. Rev. A*, 2003, **68**, 042109.
- [36] A. G. Wagh, V. C. Rakhecha, P. Fischer and A. Ioffe, *Phys. Rev. Lett.*, 1998, **81**, 1992.
- [37] E. Sjöqvist, *Phys. Lett. A*, 2001, **286**, 4.
- [38] L. Yin and O. Goscinski, *Int. J. Quantum Chem.*, 1990, **37**, 249.
- [39] J. W. Zwanziger and E. R. Grant, *J. Chem. Phys.*, 1987, **87**, 2954.
- [40] X. G. He and B. H. J. McKellar, *Phys. Rev. A*, 1993, **47**, 3424.
- [41] M. Wilkens, *Phys. Rev. Lett.*, 1994, **72**, 5.

Calculation of Cross Sections in Electron-Nuclear Dynamics

R. Cabrera-Trujillo, John R. Sabin, E. Deumens and Y. Öhrn

*Quantum Theory Project, University of Florida, P.O. Box 118435, Gainesville,
FL 32611-8435, USA*

Abstract

In this work, we present an overview of the study of total and differential cross section calculations within the electron-nuclear dynamics (END). END is a method to solve the time-dependent Schrödinger equation in a non-adiabatic approach to direct dynamics. The method takes advantage of a coherent state representation of the molecular wave function. A quantum-mechanical Lagrangian formulation is employed to approximate the Schrödinger equation, *via* the time-dependent variational principle, to a set of coupled first-order differential equations in time for the END. We obtain the final wave function for the system allowing the determination of collisional properties of interest, as for example, deflection functions, charge exchange probabilities and amplitudes, and differential cross sections. We discuss the use and selection of basis sets for both the electronic description of the colliding systems as well as for their importance in the description of electron capture. As quantum effects are important in many cases and lacking for classical nuclei, we discuss the Schiff methodology and its advantages over other traditional methods for including semiclassical corrections. Time-lapse rendering of the dynamics of the participating electrons and atomic nuclei provides for a detailed view of dynamical and reactive processes. Comparison to experimental and other theoretical results is provided where appropriate data are available.

Contents

1. Introduction	254
2. Minimal electron-nuclear dynamics	255
3. END trajectories	257
3.1. Schiff approximation	258
4. Overview of results	261
4.1. Basis set selection	261
4.2. Deflection function	261
4.3. Direct differential cross section	263
4.4. Charge exchange differential cross section	266
4.4.1. Mulliken population analysis	266
4.4.2. Probability amplitude for electron capture	267
4.5. Total cross sections	268
4.6. State-to-state total cross sections	269

4.7. Trajectories and chemical reactions	271
5. Conclusions	272
References	273

1. INTRODUCTION

Scattering theory has been a subject of interest from the beginning of quantum theory as a way to probe interactions between atoms and molecules. The many-body character of the interaction has proven a very difficult problem to deal with. For a proper description of the interaction, any model should incorporate dynamical effects such as electron transfer, rotations and vibrations, nuclear displacement, bond breaking and bond making (chemical reactions), photon emission and absorption, and ionization.

Theoretical and computational studies of atomic and molecular collisions over a range of energies from a few eV to hundreds of keV offer many challenges. Several stationary electronic states of the system and their potential energy surfaces (PESs) plus non-adiabatic coupling terms are explicitly or implicitly involved. Meaningful comparisons with the best experiments require the determination of absolute differential and integral cross sections for all the processes available to the system. A number of simplifications ranging from the first Born approximation to more elaborate models, such as the Eikonal or sudden approximation, have been used to make the treatment of the interaction between projectiles and targets tractable. Such models commonly impose some restrictions on the number of channels or type of interaction they deal with. For example, the scattering may be limited to rectilinear trajectories, fixed projectile charge, neglect of small terms upon transformation to internal coordinates, and/or approximations of centrifugal terms.

At high projectile energies, perturbative methods such as the first Born approximation or its improvements have been successful in the description of the scattering process. At intermediate projectile energies, when the interaction of the projectile with the target is longer and with stronger coupling, a different approach is required. Of these, we can mention the atomic orbital close coupling method. At low projectile energies, a proper description of the dynamics of the collision requires an accurate electronic wave function that produces an accurate potential landscape with correct barrier heights. Here, adiabatic approaches may be useful, such as the Car–Parinello or, for small systems, a full quantum treatment. However, given the complexities mentioned above, a method suitable for all projectile energies requires a direct, non-adiabatic method. The electron-nuclear dynamics (END) theory offers such a general approach.

In this chapter we describe a procedure to obtain reliable cross sections within the END theory [1] by incorporating a well-known semiclassical treatment by Schiff [2]. This topic requires the combination of classical,

semiclassical, and quantum-mechanical concepts and is particularly suitable for this volume honoring Professor Osvaldo Goscinski, whose contributions to science bridge many subfields.

In Section 2 we briefly outline the salient features of END theory. In Section 3, we discuss the treatment of the END trajectories and their connection to the deflection function and differential cross section, as well as the derivation of the Schiff approximation. In Section 4, we present some simple applications and results of our approach. Finally, Section 5 contains our conclusions.

2. MINIMAL ELECTRON-NUCLEAR DYNAMICS

END theory treats the collisional system in a Cartesian laboratory frame and each level of approximation [3] is defined by a choice of system wave function characterized by a set of time-dependent parameters and choice of basis set. Minimal END employs a system state vector of the form [3]

$$|\psi(t)\rangle = |R(t), P(t)\rangle |z(t), R(t), P(t)\rangle, \quad (1)$$

where the first factor on the right-hand side corresponds to the nuclear wave function

$$\langle X|R(t), P(t)\rangle = \prod_k \exp \left[-\frac{1}{2} \left(\frac{\mathbf{X}_k - \mathbf{R}_k}{w} \right)^2 + i\mathbf{P}_k \cdot (\mathbf{X}_k - \mathbf{R}_k) \right] \quad (2)$$

for distinguishable nuclei $\mathbf{X}_k = (X_{1k}, X_{2k}, X_{3k})$, and the time-dependent average position $\mathbf{R}_k = (R_{1k}, R_{2k}, R_{3k})$ and average momentum $\mathbf{P}_k = (P_{1k}, P_{2k}, P_{3k})$ of nucleus k . In this product, the traveling Gaussians have a common width parameter w . The second factor on the right-hand side in equation (1) corresponds to the electronic wave function (for N electrons)

$$\langle x|z(t), R(t), P(t)\rangle = \det\{\chi_i(\mathbf{x}_j)\}, \quad (3)$$

where the complex and non-orthogonal spin orbitals are expressed as

$$\chi_i = u_i + \sum_{j=N+1}^K u_j z_{ji}, \quad i = 1, 2, \dots, N. \quad (4)$$

The atomic spin orbitals $\{u_j\}_1^K$ are represented in terms of traveling Gaussian basis functions of the form

$$(x - R_{1k})^l (y - R_{2k})^m (z - R_{3k})^n \exp \left[-\alpha(\mathbf{x} - \mathbf{R}_k)^2 - \frac{i}{\hbar} \mathbf{P}_k \cdot (\mathbf{x} - \mathbf{R}_k) \right], \quad (5)$$

centered on the average nuclear position \mathbf{R}_k and moving with momentum \mathbf{P}_k .

Equations (3) and (4) for the electronic wave function describe a Thouless determinant [4] and the time-dependent complex coefficients $z_{ji}(t)$ are called Thouless coefficients. An important quantity is the overlap of two Thouless determinants $S = \langle z, R', P' | z, R, P \rangle$. As the quantum-mechanical Lagrangian $L = \langle \psi | i\hbar(\partial/\partial t) - H | \psi \rangle / \langle \psi | \psi \rangle$, with H the system Hamiltonian, can be expressed in terms of S . In the limit of the width parameter $w \rightarrow 0$ (classical nuclei) one gets

$$L = \sum_{j,k} \left\{ \left[P_{jk} + \frac{i}{2} \left(\frac{\partial \ln S}{\partial R_{jk}} - \frac{\partial \ln S}{\partial R'_{jk}} \right) \right] \dot{R}_{jk} + \left(\frac{\partial \ln S}{\partial P_{jk}} - \frac{\partial \ln S}{\partial P'_{jk}} \right) \dot{P}_{jk} \right\} + \frac{i}{2} \left(\frac{\partial \ln S}{\partial z_{ph}} \dot{z}_{ph} - \frac{\partial \ln S}{\partial z_{ph}^*} \dot{z}_{ph}^* \right) - E, \quad (6)$$

where

$$E = \sum_{jk} \frac{P_{jk}}{2M_k} + \frac{\langle z, R, P | H_{\text{el}} | z, R, P \rangle}{\langle z, R, P | z, R, P \rangle}, \quad (7)$$

with the nuclear–nuclear repulsion terms included in the electronic Hamiltonian H_{el} .

The dynamical variables q for this level of END theory are the complex Thouless coefficient z_{ph}, z_{ph}^* and the Cartesian components of average nuclear positions and momenta R_{jk}, P_{jk} . We combine the Euler–Lagrange equations

$$\frac{d}{dt} \frac{\partial L}{\partial \dot{q}} = \frac{\partial L}{\partial q} \quad (8)$$

into a matrix equation

$$\begin{bmatrix} i\mathbf{C} & \mathbf{0} & i\mathbf{C}_R & i\mathbf{C}_P \\ \mathbf{0} & -i\mathbf{C}^* & -i\mathbf{C}_R^* & -i\mathbf{C}_P^* \\ i\mathbf{C}_R^\dagger & -i\mathbf{C}_R^T & \mathbf{C}_{RR} & -\mathbf{I} + \mathbf{C}_{RP} \\ i\mathbf{C}_P^\dagger & -i\mathbf{C}_P^T & \mathbf{I} + \mathbf{C}_{PR} & \mathbf{C}_{PP} \end{bmatrix} \begin{bmatrix} \dot{\mathbf{z}} \\ \dot{\mathbf{z}}^* \\ \dot{\mathbf{R}} \\ \dot{\mathbf{P}} \end{bmatrix} = \begin{bmatrix} \partial E / \partial \mathbf{z}^* \\ \partial E / \partial \mathbf{z} \\ \partial E / \partial \mathbf{R} \\ \partial E / \partial \mathbf{P} \end{bmatrix}, \quad (9)$$

where the *dynamical metric* contains the coupling elements

$$(C_{XY})_{ik;jl} = -2 \operatorname{Im} \frac{\partial^2 \ln S}{\partial X_{ik} \partial Y_{jl}} \bigg|_{R'=R, P'=P}, \quad (10)$$

$$(C_{X_{ik}})_{ph} = (C_X)_{ph;ik} = \frac{\partial^2 \ln S}{\partial z_{ik}^* \partial X_{ik}} \bigg|_{R'=R, P'=P}, \quad (11)$$

$$C_{ph;qg} = \left. \frac{\partial^2 \ln S}{\partial z_{ph}^* \partial z_{qg}} \right|_{R'=R, P'=P}. \quad (12)$$

One can discern the usual adiabatic coupling terms \mathbf{C}_{RR} and non-adiabatic coupling terms \mathbf{C}_R . This formulation of molecular processes may be characterized as dynamics on a phase space spanned by the wave function parameters [5].

Integration of the system of equations (9) yields trajectories of classical nuclei ‘dressed’ with END. This approach can be characterized as being *direct*, and *non-adiabatic* or as fully non-linear time-dependent Hartree–Fock (TDHF) theory of quantum electrons and classical nuclei. This simultaneous dynamics of electrons and nuclei driven by their mutual instantaneous forces requires a different approach to the choice of basis sets than that commonly encountered in electronic structure calculations with fixed nuclei. This aspect will be further discussed in connection with applications of END.

The solution to equations (9) in its minimal representation is implemented into the *ENDyne* package [6].

3. END TRAJECTORIES

Let us consider a binary molecular collision problem. The reactants are divided into a target system, which is initially at rest at the origin of the laboratory Cartesian coordinate system, and a projectile moving towards the target with an initial momentum corresponding to the collision energy of interest. A given electronic state of each system, say the ground state, is chosen and from that an initial Thouless determinant for the system is constructed in a particular basis. An initial relative orientation of projectile and target is chosen and the projectile is given an impact parameter and initial momentum (or velocity) commensurate with the energy of the collision. The projectile is initially sufficiently distant from the target so that the interaction with it is negligible.

Equations (9) that govern the dynamics of the collision are integrated until a time when the product species are sufficiently separated that there are no further interaction between the products in the dynamics. Depending on the system and on the collision energy, a variety of processes may take place. Each set of initial conditions, such as relative orientation of reactants and impact parameter, b , of the projectile, leads to a particular set of products and states. The simplest situation being that the projectile is simply scattered into a certain solid angle $d\Omega$, gaining some electrons from or losing some electrons to the target.

In these cases, various final electronic states of the total system are calculated in the same basis and projected against the final evolved wave

function to yield a transition probability $P_{fo}(b, E, \varphi) = |\langle f | \psi \rangle|^2$, which depends on collision energy E and on relative initial orientation o of the colliding species and scattering angles (θ, φ) or equivalently (b, φ) .

The classical differential cross section for a particular channel with probability P_{fo} is expressed as

$$\frac{d\sigma_{fo}(E, \theta, \varphi)}{d\Omega} = \sum_i P_{fo}(b_i, E, \varphi) \frac{b_i}{\sin \theta |d\Theta/db_i|}, \quad (13)$$

where the sum runs over all impact parameters that lead to the same scattering angle (θ, φ) . Here, $\Theta(b)$ is the deflection function of the projectile and is defined as the angle between the final and initial projectile momentum. The deflection function contains information concerning the attractive and repulsive region of the interaction of projectile and target. For the first branch of the scattering region, $\theta = |\Theta|$.

A sufficient number of relative initial orientations must be considered in order to achieve a convenient grid in the space of Euler angles so that an accurate average can be taken to yield a cross section for a particular process f , e.g., direct scattering or electron charge exchange

$$\frac{d\sigma_f(E, \theta, \varphi)}{d\Omega} = \left\langle \frac{d\sigma_{fo}}{d\Omega} \right\rangle_o. \quad (14)$$

The recognized deficiencies of equation (13) for the scattering cross section, such as displaying unphysical discontinuities at small angles $\theta = 0$, the so-called glory angle [7], and at angles where $d\Theta/db = 0$, called rainbow angles [7], as well as the lack of the interference between the various trajectories in the sum of equation (13), can be remedied with semiclassical corrections such as the uniform Airy [8,9] or Schiff [2] approximations (*vide infra*).

A classical integral cross section is obtained by integrating the differential cross section over scattering angles or equivalently by mapping the scattering angle to the impact parameter space through the deflection function to obtain

$$\sigma_f(E) = \int_0^\infty db \int_0^{2\pi} d\varphi b P_f(b, E, \varphi). \quad (15)$$

This expression has been successfully applied for reactive scattering down to energies of a fraction of an eV [10].

3.1. Schiff approximation

A more elaborate approach to connect trajectories with classical nuclei to semiclassical cross sections is due to Schiff [2]. The idea is developed in

the context of potential scattering in terms of a potential $U(\mathbf{r})$ with a wave function for a scattered projectile expressed as

$$\psi(\mathbf{r}) = e^{i\mathbf{k}_0 \cdot \mathbf{r}} + \frac{e^{ikr}}{r} f(\mathbf{k}_f, \mathbf{k}_0), \quad (16)$$

with the scattering amplitude

$$f(\mathbf{k}_f, \mathbf{k}_0) = -\frac{1}{4\pi} \int e^{-i\mathbf{k}_f \cdot \mathbf{r}} U(\mathbf{r}) \psi(\mathbf{r}) d\mathbf{r}. \quad (17)$$

The wave vector \mathbf{k}_f points to the detector and $|\mathbf{k}_f| = k$.

Combining equations (16) and (17), one obtains the full Born series

$$\begin{aligned} f(\mathbf{k}_f, \mathbf{k}_0) = & -\frac{1}{4\pi} \sum_{n=0}^{\infty} \int e^{-i\mathbf{k}_f \cdot \mathbf{r}_n} U(\mathbf{r}_n) G(\mathbf{r}_n - \mathbf{r}_{n-1}) U(\mathbf{r}_{n-1}) \\ & G(\mathbf{r}_{n-1} - \mathbf{r}_{n-2}) U(\mathbf{r}_{n-2}) \cdots G(\mathbf{r}_3 - \mathbf{r}_2) U(\mathbf{r}_2) G(\mathbf{r}_2 - \mathbf{r}_1) \\ & U(\mathbf{r}_1) e^{i\mathbf{k}_0 \cdot \mathbf{r}_1} d\mathbf{r}_1 d\mathbf{r}_2 \cdots d\mathbf{r}_n, \end{aligned} \quad (18)$$

with the outgoing Green's function

$$G(\rho) = -\frac{1}{4\pi} \frac{e^{ik\rho}}{\rho}. \quad (19)$$

The Schiff approximation applies only to small scattering angles, such that if R is the range of the potential that contributes significantly to the scattering, then small scattering angles are those that satisfy $\theta \ll (kR)^{-1/2}$. After integration by parts, assuming $1/k$ to be small, i.e., rather high collision energies, each integral factor in a typical term of equation (18) is subjected to the stationary phase approximation. This results in a form of the Born series that can be summed to yield the expression

$$f_o(\mathbf{k}_f, \mathbf{k}_0) = ik_0 \int_0^{\infty} J_0(qb) \{1 - e^{i\delta_o(b, \varphi)}\} b db, \quad (20)$$

where $q = |\mathbf{k}_f - \mathbf{k}_0|$ is the inelastic momentum transfer and $\delta_o(b, \varphi)$ is the semiclassical phase shift for a given target orientation o . Here $J_0(x)$ is the Bessel function of order zero and q depends on the angle between \mathbf{k}_f and \mathbf{k}_0 .

In the original Schiff treatment, the phase shift is given in terms of the static scattering potential $U(\mathbf{r})$ as

$$\delta(b) = \frac{1}{2k} \int_{-\infty}^{\infty} U(b, z) dz. \quad (21)$$

However, according to Mott and Massey [11], one can relate the phase shift to the scattering trajectories (deflection function) by means of the

relation

$$\Theta(b, \phi) = \frac{1}{k_0} \frac{d\delta_o(b, \phi)}{db}. \quad (22)$$

Equation (22) generalizes the treatment of differential cross sections when a time-dependent dynamical trajectory is used in the determination of the deflection function, as in the case of END.

The END trajectories yield q and also the deflection function $\Theta(b, \phi)$ as the angle between \mathbf{k}_0 and \mathbf{k}_f . Thus, integrating equation (22) yields the semiclassical phase shift corresponding to trajectories with the simultaneous dynamics of electrons and nuclei.

With this, the direct differential cross section is obtained as

$$\frac{d\sigma_o(\theta, \phi)}{d\Omega} = \frac{k_f}{k_0} |f_o(\mathbf{k}_f, \mathbf{k}_0)|^2. \quad (23)$$

Equation (23) when modified with the appropriate probability, i.e.,

$$\frac{d\sigma_{of}}{d\Omega} = P_{of}(E, \theta, \phi) \frac{k_f}{k_0} |f_{of}(\mathbf{k}_f, \mathbf{k}_0)|^2, \quad (24)$$

and after averaging over relative reactant orientations o , yields absolute charge exchange differential cross sections in good agreement with the best experiments [12–19] for direct and charge exchange processes f at collision energies ranging from tens of eV to about 100 keV.

However, equation (24) assumes that the probability P_{fo} is independent of the trajectory of the projectile. In order to incorporate interference effects, one introduces into equation (16) the electronic wave function $|\psi\rangle$. Thus, projecting the final wave function onto a final state $|f\rangle$ and repeating the Schiff procedure, one obtains

$$f_{of}(\mathbf{k}_f, \mathbf{k}_0) = ik_0 \int_0^\infty A_{fo}(b, \phi) J_0(qb) \{ \delta_{f\psi} - e^{[i\delta_{of}(b, \phi)]} b db \}, \quad (25)$$

where the complex probability amplitude $A_{fo}(b, \phi)$ for a given target orientation is obtained by projecting a particular product state $|f\rangle$ against the evolved wave function $|\psi(b)\rangle$ for each chosen relative orientation of the reactants.

In Section 4 we present some results employing this choice of scattering amplitude for some simple ion–atom collisions with comparisons to experiment.

4. OVERVIEW OF RESULTS

4.1. Basis set selection

The only approximation involved in the solution of the dynamical equations (9) is the size constraint of the basis set for the electronic structure [equation (4)].

In standard quantum chemistry calculations, basis sets are optimized for ground state energy calculations and not for dynamical properties. Although there are no clear criteria on how to choose a basis set, we have found several conditions that must be fulfilled in order to get a good description of a dynamical process.

Since we are assigning a Thouless coefficient to each orbital, uncontracting the basis sets results in more electronic degrees of freedom, i.e., a larger number of Thouless coefficients, allowing access to a more flexible electron dynamics. Also, adding diffuse orbitals facilitates the description of the charge exchange process in the long-range region of the interaction.

We start by considering a medium size basis set, usually of the Dunning family [20,21]. We uncontract the basis set and add diffuse orbitals in a consistent even-tempered sequence, i.e.,

$$\alpha_i = a\beta^{i-1}, \quad (26)$$

where a and β are determined from the overlap of two Gaussian orbitals, i.e.,

$$S_{ij} = \langle \phi_{\alpha_i} | \phi_{\alpha_j} \rangle = \left(\frac{\sqrt{\alpha_i \alpha_j}}{\alpha_i + \alpha_j} \right)^{5/2} = \left(\frac{2\sqrt{\beta}}{1 + \beta} \right)^{5/2}. \quad (27)$$

We have found that β between 3 and 4, such that S_{ij} is between 0.6 and 0.7, provides a good criteria to add diffuse exponents to a known basis set for s and p type orbitals, although for some systems d orbitals are required.

The criterion we use for the convergence of the basis set is that the total charge transfer cross section does not change when further increasing the size of the basis set. Of course, this criterion depends on the velocity of the projectile. However, once a limit has been reached before the ionization channel opens, the basis set obtained is considered satisfactory.

4.2. Deflection function

In order to obtain the deflection function $\Theta(b)$, i.e., the scattering angle for the projectile as a function of the impact parameter, a range of values in the impact parameter are needed. The impact parameter usually runs from $b = 0.0$ to 20.0 a.u. The impact parameter grid is spaced in steps of 0.1 from $b = 0.0$ to 2.0 , in steps of 0.2 from $b = 2.0$ to 6.0 , in steps of 1.0 from $b = 6.0$ to 10.0 and in steps of 2.0 from $b = 10.0$ to 20.0 . This gives us a total

of 50 dynamical trajectories for a given relative orientation of the target/projectile pair.

For the case of time-independent scattering theory based on a scattering potential, the deflection function is given by [22]

$$\Theta(E_p, b) = \pi - 2 \int_{r_{\min}}^{\infty} \frac{b \, dr}{r \sqrt{r^2 [1 - (U(r)/E_p)] - b^2}}, \quad (28)$$

where r_{\min} is the distance of closest approach. Equation (28) assumes that the internal structure of the projectile does not change during the collision. Therefore, this approach requires the knowledge of PESs to determine the interaction potential.

However, in the END approach, the projectile scattering angle is obtained by projecting the final projectile center of mass momentum on its initial momentum, i.e.,

$$\cos \Theta(E_p, b) = \frac{\mathbf{P}_f(E_p, b) \cdot \mathbf{P}_i}{P_f(E_p, b) P_i}. \quad (29)$$

Thus, the scattering angle contains the consequences of the dynamics of the collision, i.e., of a dynamical potential that involves charge exchange for the projectile and not a stationary potential with a fixed projectile charge as is often done in traditional scattering theory.

In Fig. 1 we present a set of trajectories, as obtained by *ENDyne* and the corresponding deflection function for protons colliding with molecular hydrogen at 200 eV for the orientation where the impact parameter values increase along the molecular hydrogen bond. Of particular interest are the two solid lines on the right-hand side of the figure. Of the two, the one corresponding to the lower impact parameter ($b = 1.8$) corresponds to the glory angle. The second one ($b = 2.7$) corresponds to the rainbow angle, that is the trajectory corresponding to the maximum attraction of the projectile by the target during the interaction.

Also, one observes the envelope produced by the deflection of the trajectories around the classical forbidden region of the potential. On the left-hand side of the figure, one notes the deflection function for these trajectories. At $b = 0.707$ a.u., half the molecule bond length, the scattering angle is $\Theta = \pi$, which corresponds to a head-on collision with one of the target nuclei. Not shown in the figure is the rotation or dissociation of the molecular target produced by this trajectory. At $b = 1.8$ a.u., the deflection function is $\Theta = 0.0$ and the trajectories enter into the attraction region of the interaction potential as b increases, with a minimum around $b = 2.7$ a.u.

As a second example, we show in Fig. 2 the deflection function for protons and hydrogen projectiles colliding with helium atoms at 5.0 keV. From the

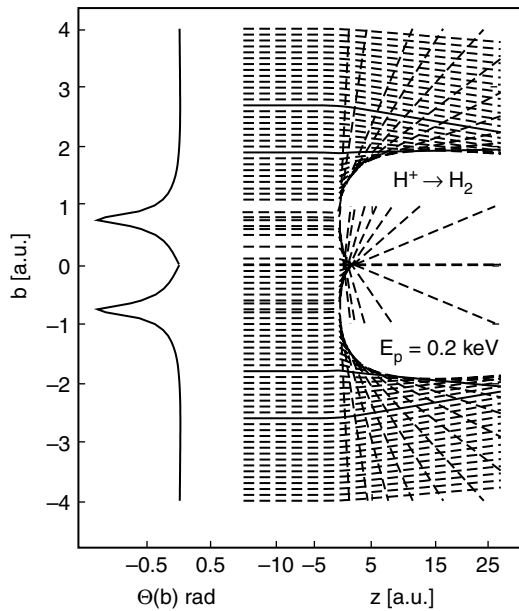


Fig. 1. Trajectories in the collision plane for $H^+ \rightarrow H_2$ and deflection function for H^+ at 200 eV as we have reported in Ref. [16].

deflection function one can distinguish the attractive and repulsive regions of the interaction. The repulsive region is from $b = 0.0$ to 1.1 a.u. At $b = 1.1$ where $\Theta(b_g) = 0.0$, where the point of no deflection, and the transition to the attractive region of the interaction occurs, is the so-called glory angle. From $b = 1.1$ to $b \rightarrow \infty$ is the attractive region which shows a maximum deflection angle for attraction (minimum in the curve) at $b = 1.8$ a.u., the so-called rainbow angle. At the rainbow angle, the deflection function slope is zero, i.e., $d\Theta(b)/db = 0.0$ and therefore the classical cross section diverges [see equation (13)] at this point.

From the relation between the deflection function and the phase shift, equation (22), one obtains the phase shift for the collision as a function of the impact parameter (or angular momentum) necessary for determination of the differential cross section.

4.3. Direct differential cross section

Once the deflection function and the phase shift have been determined for a collisional system, the direct differential cross section is obtained as the classical direct differential cross section when neglecting quantum interference effects [equation (13) with $P_{fo} = 1$] or by introducing semiclassical corrections using the Schiff approximation [equation (20)].

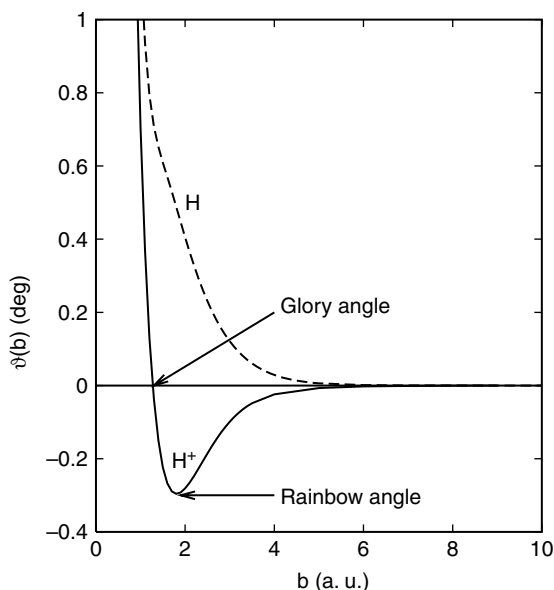


Fig. 2. Deflection function for $H^+ \rightarrow He$ and $H \rightarrow He$ at 5.0 keV as we have reported in Ref. [10].

As an example, in Fig. 3 we show the result for the semiclassical absolute direct differential cross section for neutral helium atoms colliding with neon targets at projectile energies of 0.5, 1.5, and 5.0 keV [12]. Also, for comparison we present the experimental data of Gao *et al.* [23].

The advantage of semiclassical corrections is the inclusion of quantum effects to the differential cross section in the small scattering angle, the so-called forward peak character of the differential cross section. Furthermore, in the particular case of the Schiff approximation, the glory and rainbow angle effects in the interference are accurately represented. This behavior can be observed in Fig. 3, where the absolute direct differential cross section obtained with *ENDyne* goes through the experimentally determined absolute cross sections.

For the case of molecular targets, we show in Fig. 4 the results for the direct differential cross section for protons colliding with molecular hydrogen for proton energies of 0.5, 1.5, and 5.0 keV [18] averaged over all the target orientations. The experimental data are from Gao *et al.* [24]. Also, for comparison, we present the results of Kimura's DIM method (short-dashed line) [24].

The previous examples were for direct scattering processes, i.e., for the channel where the projectile does not alter its charge. In the next section, we will discuss the electron capture cross section.

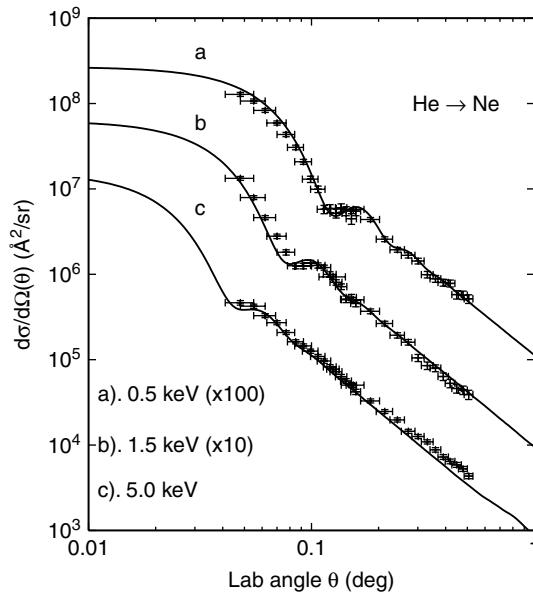


Fig. 3. Direct differential cross section for $\text{He} \rightarrow \text{Ne}$ for He energies from 0.5, 1.5 and 5.0 keV as we have reported in Ref. [12]. The experimental data are from Gao *et al.* [23].

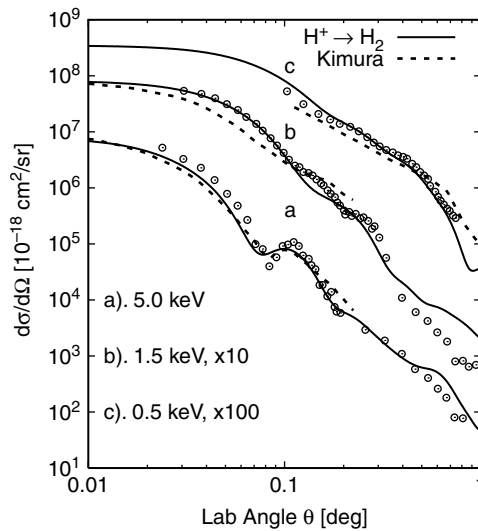


Fig. 4. Direct differential cross section for H^+ and $\text{H} \rightarrow \text{H}_2$ for H^+ energies from 0.5, 1.5 and 5.0 keV. The experimental data are from Gao *et al.* [24] for the molecular case. Note that $d\sigma/d\Omega$ for H_2 is not twice the value that the one for H.

4.4. Charge exchange differential cross section

In order to calculate the charge transfer differential cross section, one requires the probability for electron transfer [see equation (14)] for the case of a classical electron transfer differential cross section, or the probability amplitude for electron transfer [see equation (24)] to include interference effects due to the quantum behavior of the projectile.

4.4.1. Mulliken population analysis

The Mulliken population analysis [25–27] allows us to determine the probability of finding the projectile with certain charge state, independent of the excitation state of the projectile.

From equations (3) and (4), the number of electrons in the system is

$$N = \sum_{\nu,\mu} P_{\mu\nu} \Delta_{\nu\mu} = \sum_{\mu} (\mathbf{P}\Delta)_{\mu\mu} = \text{Tr}(\mathbf{P}\Delta), \quad (30)$$

where $P_{\nu\mu} = \sum_i^N z_{i\nu} z_{i\mu}$ and $\Delta_{\mu\nu}$ is the atomic orbital overlap matrix. It is possible to interpret $(\mathbf{P}\Delta)_{\mu\mu}$ as the number of electrons to be associated with the atomic basis function u_{μ} . From this, $n_A = \sum_{\nu \in A} (\mathbf{P}\Delta)_{\nu\nu}$ is the number of electrons associated with atom A.

Therefore, for example, one determines the probability of electron capture for a proton as the final number of electrons in the projectile according to equation (30). For the case of any other projectile system, the probability for electron transfer (or loss) is given by $N_f - N_i$ normalized to a probability between $\{0,1\}$.

As an example, we show in Fig. 5 the projectile population, or probability for electron capture for protons colliding with molecular hydrogen at 1 keV for the orientation ($\alpha = 0$, $\beta = 90$; molecular bond aligned with the incoming beam) (see Ref. [18]) that corresponds to the projectile trajectory aligned along the target molecular bond and perpendicular to it. Also, for comparison to the DIM model we present the results from Kimura [28] which have been multiplied by 0.1 to show them on the same scale.

From the Mulliken population, we calculate the charge exchange differential cross section. For a more complex system, in Fig. 6, the preliminary results for the direct and charge transfer differential cross section are shown for protons colliding with water at 5.0 keV as obtained by the Mulliken population analysis combined with the Schiff approximation [equation (23)]. Also for comparison we present the experimental results from Lindsay *et al.* [29].

Although the result follows the experimental data closely, the result does not look as good as the direct differential cross section. We attribute this to the need for a finer average grid for the target orientational average.

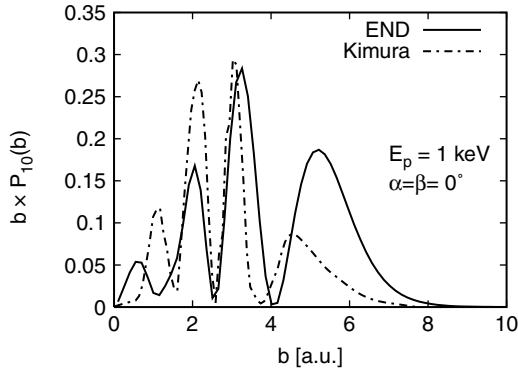


Fig. 5. Probability for electron capture by a proton colliding with molecular hydrogen at 1 keV as obtained by END (solid line). For comparison, we show the results from Kimura's DIM method (short-dotted line) [28] which have been scaled 0.1 times.

4.4.2. Probability amplitude for electron capture

The probability amplitude is determined by projecting the final END electronic wave function, $|\psi\rangle$ for each impact parameter, on a particular determinant in the same basis set, and introducing the result into equation (25) for the charge transfer differential cross section.

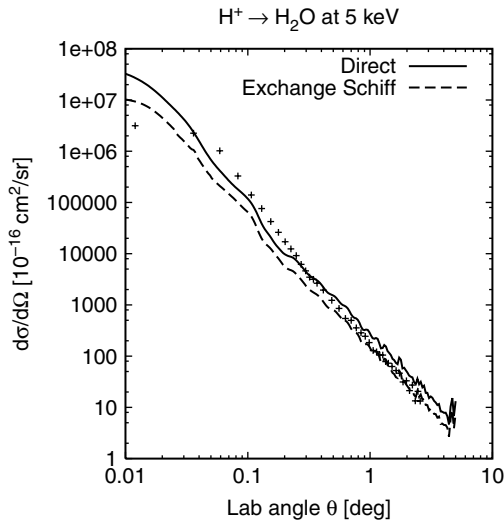


Fig. 6. Preliminary results for the direct and charge exchange differential cross section for $H^+ \rightarrow H_2O$ for H^+ at 5.0 keV. The experimental data for the differential charge exchange cross section are from Lindsay *et al.* [29].

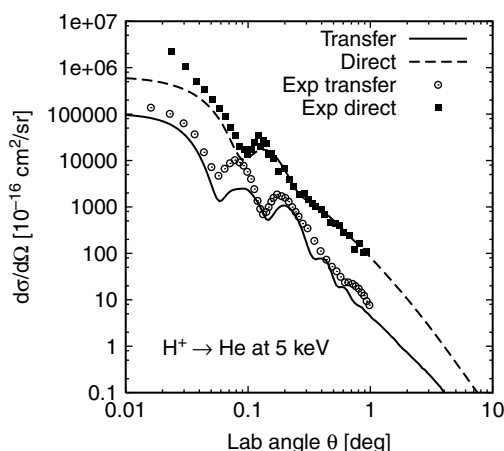


Fig. 7. Direct and charge exchange differential cross section for $H^+ \rightarrow He$ for H^+ at 5.0 keV. The experimental data are from Johnson *et al.* [30].

In Fig. 7, we present preliminary results obtained by this procedure for the direct and electron capture differential cross section for protons colliding with helium atoms at 5 keV. The experimental data are from Johnson *et al.* [30]. Here the quantum effects are evident. The END charge transfer differential cross section is out of phase with the direct differential cross section and in close agreement with the experimental data.

4.5. Total cross sections

Integral properties of the differential cross section are calculated by means of equation (15) or by integrating the differential values over a specified angular range.

In Fig. 8, we show the total cross section for electron capture and electron loss for protons and neutral hydrogen projectiles colliding with atomic and molecular hydrogen, as a function of the projectile energy. The experimental data are from several authors [31–36] and also for comparison we present the theoretical results of Kimura *et al.* [28].

From these results we note the excellent agreement for the atomic target case. For the electron capture for $H^+ \rightarrow H_2$, we need to point out that our results are proportionally lower than those reported by Gealy *et al.* [31] which were normalized to $6.95 \times 10^{-16} \text{ cm}^2$ at $E_p = 2.0 \text{ keV}$. If we normalize the experimental data to our results, the agreement becomes very good.

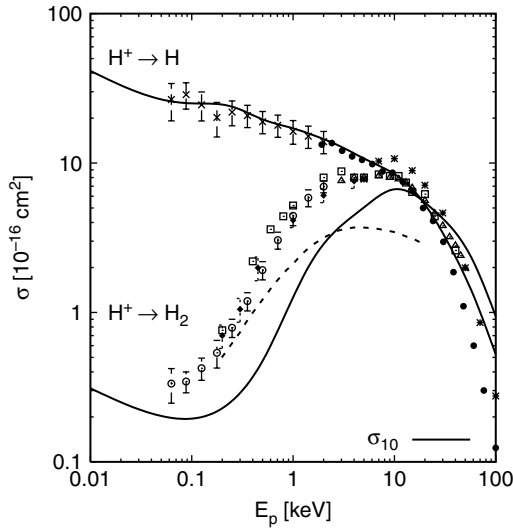


Fig. 8. Charge exchange total cross section for $H^+ \rightarrow H$ and $H^+ \rightarrow H_2$ for projectile energies from 10 eV up to 100 keV as we have reported in Ref. [16]. The experimental data are from: For $H^+ \rightarrow H$, Ref. [31] (\times); Ref. [32] (\bullet). For $H^+ \rightarrow H_2$, Ref. [31] (\circ); Ref. [33] (\square); Ref. [34] (\triangle); Ref. [35] ($*$). For comparison, we also show the results of Kimura [28] for $H^+ \rightarrow H_2$ (short-dashed line).

4.6. State-to-state total cross sections

When the integration is performed over equation (15) when $P_f(b) = |A_f(b)|^2 = |\langle f | \psi(b) \rangle|^2$, we obtain the total cross section to find the system in the final state $|f\rangle$.

In Fig. 9 we present the results for the total cross section for electron excitations in the 2s and 2p states of atomic hydrogen when proton projectiles collide with energies from 100 eV up to 300 keV. In the same figure we compare with some available experimental results [37, 39–41].

For energies between 1 and 300 keV, we note an excellent agreement with the experimental data for the excitation to the 2p state of the target. For lower energies our results are higher than the reported experimental data. Since our time-dependent analysis lacks spontaneous emission, our 2p state have an infinite life (stationary state) in comparison to the experimental data which is measured by quenching the 2p state. For the excitation to the metastable 2s state, we note a discrepancy around 10 keV in our results when compared to the experimental data.

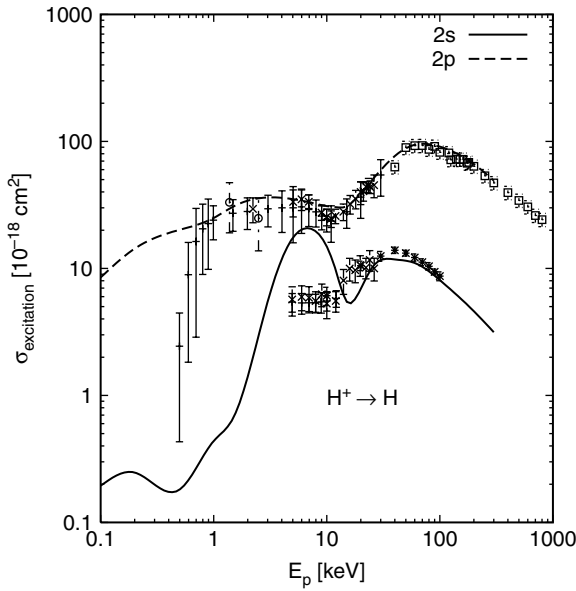


Fig. 9. Total cross section for the excitation of the 2s and 2p hydrogen target states for proton projectiles from 100 eV up to 300 keV. The experimental data are from: ×, Higgins *et al.* [37]; +, Barnett [38]; ×, Morgan *et al.* [39]; □, Detleffsen *et al.* [40]; ○, Stebbings *et al.* [41].

The reason is that the threshold energy around 10 keV is for the ionization channel. As discussed previously, our description of the dynamics lacks a proper account of the continuum channel, thus overestimating some of the state-to-state probabilities. For higher energies, our basis set relaxes to describe properly the 2s excitation, due to some high discretized continuum state of the basis set.

In Fig. 10, we present the results for the total cross section when the electron is captured by the proton projectile in the 2s and 2p state for projectile energies of 100 eV up to 300 keV. The results are compared with experimental data from Refs. [39,42].

For the case of electron capture into the 2s state of the projectile, our results clearly distinguish between the two experimental data of Hill *et al.* [42] and Morgan *et al.* [39] following those of Hill.

For the 2p state, a similar behavior to the 2p excitation of the target is present. Our results are higher for low energies than that reported by the experiment due to the same reason mentioned in the case of the target excitations.

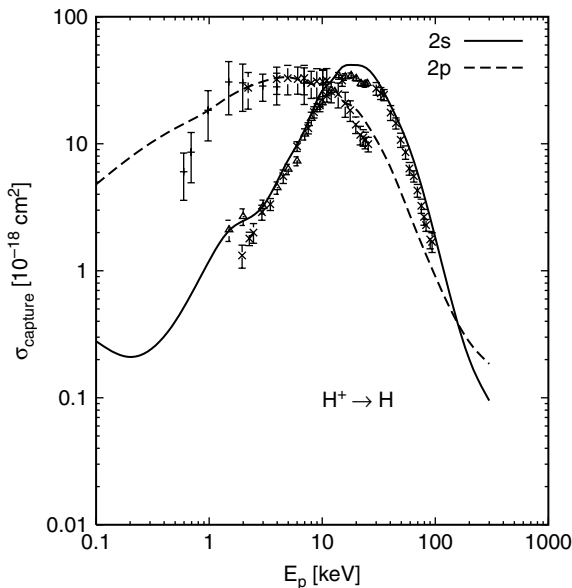


Fig. 10. Total cross section for electron capture in the 2s and 2p states of the hydrogen projectile when colliding with atomic hydrogen from 100 eV up to 300 keV. The experimental data is from: \triangle , Hill *et al.* [42]; $+$, Barnett [38]; \times , Morgan *et al.* [39].

Thus, in general, a good comparison between END theory and experimental is observed for state-to-state total cross sections.

4.7. Trajectories and chemical reactions

As we have mentioned before, END provides a full non-adiabatic description of the dynamics of a collision. Therefore, vibrations, rotations, bond breaking and chemical reactions are described properly during the dynamics. At the end of the time-evolution, we are able to visually render movies of the dynamics.

In Fig. 11, we present a snapshot of such a movie for the case of $\text{H}^+ \rightarrow \text{C}_2\text{H}_6$ at 10 eV for the orientation where the C–C bond is perpendicular to the incoming projectile trajectory. The movie shows the breaking of the C–C bond and the capture of the H^+ by one of the methylene groups. The final channel being $\text{H}^+ + \text{C}_2\text{H}_6 \rightarrow \text{CH}_3^+ + \text{CH}_4$ where the final products are in an excited ro-vibrational state. This rendering provides an intuitive visualization of the chemical reactions, quite different from that of wave packets on a PES.

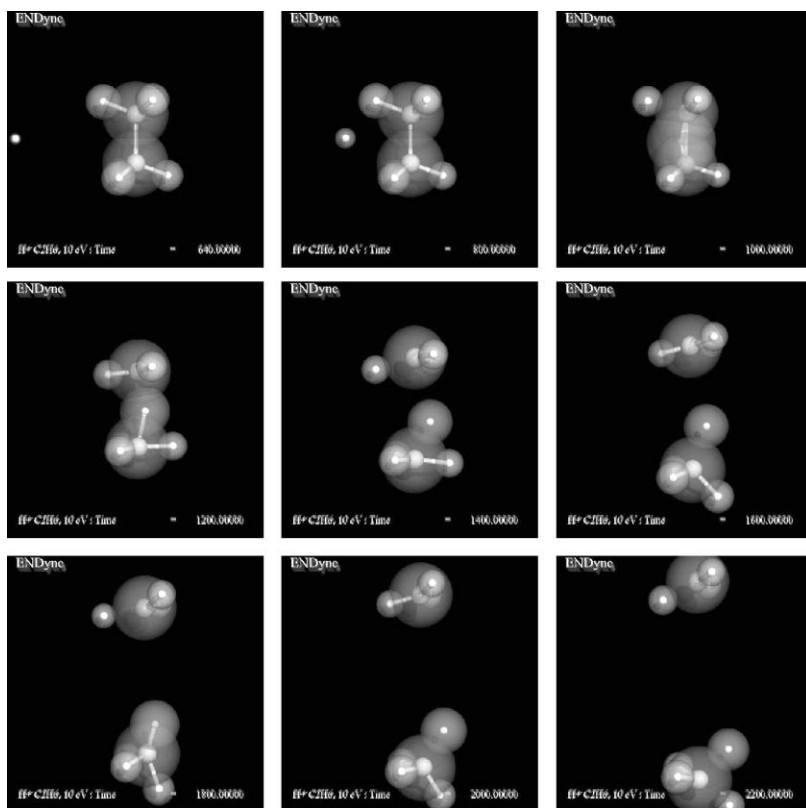


Fig. 11. Snapshots for different times for the dynamics of $\text{H}^+ + \text{C}_2\text{H}_6 \rightarrow \text{CH}_3^+ + \text{CH}_4$. In the second panel, the proton entering from the left has already acquired some electronic charge. The initial time $t = 0.0$ a.u. when the projectile is 15.0 a.u. from the target.

5. CONCLUSIONS

A proper description of the dynamics in a collision is required to obtain absolute differential and total cross section that match the experimental results for a wide range of projectile energies. Here we have shown that the END approach fulfills this requirement. The proper inclusion of non-adiabatic effects, even at the minimal level of END, provides trajectories for the projectile suitable for the calculation of scattering problems. The charge exchange and state-to-state probabilities from the final wave function show excellent agreement with other available theories and/or experiments. Semiclassical corrections are taken into account by means of the Schiff approximation, thus rainbow and glory angle effects are accounted for correctly.

Further extensions of the END method to incorporate ionization channel and time-dependent electromagnetic fields (photon absorption and emission), as well as a multi-configurational SCF for the electronic state, are underway. This will provide the opening of a variety of processes to be treated within the same framework, END.

REFERENCES

- [1] E. Deumens, A. Diz, R. Longo and Y. Öhrn, *Rev. Mod. Phys.*, 1994, **66**, 917.
- [2] L. I. Schiff, *Phys. Rev.*, 1956, **103**, 443.
- [3] E. Deumens and Y. Öhrn, *J. Phys. Chem.*, 2001, **105**, 2660.
- [4] D. J. Thouless, *Nucl. Phys.*, 1960, **21**, 225.
- [5] E. Deumens and Y. Öhrn, *J. Chem. Soc., Faraday Trans.*, 1997, **93**, 919.
- [6] E. Deumens, T. Helgaker, A. Diz, H. Taylor, J. Oreiro, B. Mogensen, J. A. Morales, M. Coutinho-Neto, R. Cabrera-Trujillo and D. Jacquemin, *ENDyne Version 2.8 Software for Electron Nuclear Dynamics*, Quantum Theory Project, University of Florida, Gainesville, FL 32611-8435, 1998.
- [7] K. W. Ford and J. A. Wheeler, *Ann. Phys. (NY)*, 1959, **7**, 259.
- [8] K. W. Ford and J. A. Wheeler, *Ann. Phys.*, 1959, **7**, 259.
- [9] J. A. Morales, A. C. Diz, E. Deumens and Y. Öhrn, *J. Chem. Phys.*, 1995, **103**, 9968.
- [10] Y. Öhrn, J. Oreiro and E. Deumens, *Int. J. Quantum Chem.*, 1996, **58**, 583.
- [11] N. F. Mott and H. S. W. Massey, *The Theory of Atomic Collisions*, Clarendon Press, Oxford, 1965.
- [12] R. Cabrera-Trujillo, J. R. Sabin, Y. Öhrn and E. Deumens, *Phys. Rev. A*, 2000, **61**, 032719.
- [13] R. Cabrera-Trujillo, J. R. Sabin, Y. Öhrn and E. Deumens, *Phys. Rev. Lett.*, 2000, **84**, 5300.
- [14] R. Cabrera-Trujillo, Y. Öhrn, E. Deumens and J. R. Sabin, *Phys. Rev. A*, 2000, **62**, 052714.
- [15] R. Cabrera-Trujillo, E. Deumens, Y. Öhrn and J. R. Sabin, *Nucl. Instrum. Methods*, 2000, **B168**, 484.
- [16] R. Cabrera-Trujillo, J. R. Sabin, E. Deumens and Y. Öhrn, Stopping cross section and charge exchange study of the $\text{He}^+ \rightarrow \text{Ne}$ system, in *Application of Accelerators in Research and Industry, Sixteenth International Conference* (eds J. L. Duggan and I. L. Morgan), American Institute of Physics, Melville, NY, 2001, p. 3.
- [17] R. Cabrera-Trujillo, Y. Öhrn, J. R. Sabin and E. Deumens, *Phys. Rev. A*, 2002, **65**, 024901.
- [18] R. Cabrera-Trujillo, Y. Öhrn, E. Deumens and J. R. Sabin, *J. Chem. Phys.*, 2002, **116**, 2783.
- [19] R. Cabrera-Trujillo, Y. Öhrn, E. Deumens, J. R. Sabin and B. G. Lindsay, *Phys. Rev. A*, 2002, **66**, 042712.
- [20] T. H. Dunning, *J. Chem. Phys.*, 1989, **90**, 1007.
- [21] D. E. Woon and T. H. Dunning, *J. Chem. Phys.*, 1994, **100**, 2975.
- [22] L. D. Landau and E. M. Lifshitz, *Quantum Mechanics*, Addison-Wesley, Reading, MA, 1958.
- [23] R. S. Gao, L. K. Johnson, D. E. Nitz, K. A. Smith and R. F. Stebbings, *Phys. Rev. A*, 1987, **36**, 3077.
- [24] R. S. Gao, L. K. Johnson, G. J. Smith, C. L. Hakes, K. A. Smith, N. F. Lane, R. F. Stebbings and M. Kimura, *Phys. Rev. A*, 1991, **44**, 5599.

- [25] R. S. Mulliken, *J. Chem. Phys.*, 1955, **23**, 1833.
- [26] R. S. Mulliken, *J. Chem. Phys.*, 1955, **23**, 1841.
- [27] R. S. Mulliken, *J. Chem. Phys.*, 1962, **36**, 3428.
- [28] M. Kimura, *Phys. Rev. A*, 1985, **32**, 802.
- [29] B. G. Lindsay, D. R. Sieglaff, K. A. Smith and R. F. Stebbings, *Phys. Rev. A*, 1997, **55**, 3945.
- [30] L. K. Johnson, R. S. Gao, R. G. Dixon, K. A. Smith, N. F. Lane, R. F. Stebbings and M. Kimura, *Phys. Rev. A*, 1989, **40**, 3626.
- [31] M. W. Gealy and B. Van-Zyl, *Phys. Rev. A*, 1987, **36**, 3091.
- [32] G. W. McClure, *Phys. Rev.*, 1966, **148**, 47.
- [33] J. B. Hasted, *Proc. Roy. Soc. (London)*, 1955, **A227**, 466.
- [34] R. K. Curran and T. M. Donahue, Tech. Report ONR-8, Office of Naval Research, 1959.
- [35] M. E. Rudd, R. D. DuBois, L. H. Toburen, C. A. Ratcliffe and T. V. Goffe, *Phys. Rev. A*, 1983, **28**, 3244.
- [36] P. M. Stier and C. F. Barnett, *Phys. Rev.*, 1956, **103**, 896.
- [37] D. P. Higgins, J. Geddes and H. B. Gilbody, *J. Phys. B: At. Mol. Opt. Phys.*, 1996, **29**, 1219.
- [38] C. F. Barnett, Oak Ridge National Laboratory Report No. 6086, Unpublished, 1990.
- [39] T. J. Morgan, J. Geddes and H. B. Gilbody, *J. Phys. B*, 1973, **6**, 2118.
- [40] D. Detleffsen, M. Anton, A. Werner and K.-H. Scharfner, *J. Phys. B: At. Mol. Opt. Phys.*, 1994, **27**, 4195.
- [41] R. F. Stebbings, R. A. Young, C. L. Oxley and H. Ehrhardt, *Phys. Rev.*, 1965, **138**, A1312.
- [42] J. Hill, J. Geddes and H. B. Gilbody, *J. Phys. B: At. Mol. Opt. Phys.*, 1979, **12**, L341.

Generalized Electronic Diabatic Ansatz: A Post-Born–Oppenheimer Approach to Electronuclear Dynamics in External Fields

O. Tapia¹ and Gustavo A. Arteca²

¹*Department of Physical Chemistry, Uppsala University,
Box 579, S-751 23 Uppsala, Sweden*

²*Département de Chimie et Biochimie, Laurentian University, Ramsey Lake Road,
Sudbury, Ont., Canada P3E 2C6*

Abstract

We examine a post-Born–Oppenheimer approach based on a generalized electronic diabatic (GED) ansatz for electronuclear dynamics in external electromagnetic fields. The model is a quantum n -electron system interacting with a set of m classical positive charges located at $\xi = (\xi_1, \dots, \xi_m)$ in laboratory space. The system's Coulomb Hamiltonian is $\mathcal{H}_C = \mathcal{H}_e(\mathbf{q}, \xi) + K(\xi)$, where $\mathcal{H}_e(\mathbf{q}, \xi)$ is its electronic-only part and $K(\xi)$ is the kinetic energy for the background charges. The GED basis set $\{\phi_k(\mathbf{q})\}$ diagonalizes $\mathcal{H}_e(\mathbf{q}, \xi)$, and the diabatic potentials $U(\xi; \phi_k) = U_k(\xi) = \langle \phi_k(\mathbf{q}) | \mathcal{H}_C(\mathbf{q}, \xi) | \phi_k(\mathbf{q}) \rangle_q$ define local effective Hamiltonians, $\langle \phi_k | \mathcal{H}_C | \phi_k \rangle_q = K(\xi) + U_k(\xi)$, whose eigenfunctions $\{\zeta_{kj}(\xi)\}$ represent mass distributions for the positive charge backgrounds. The set $\{\phi_k(\mathbf{q})\zeta_{kj}(\xi)\}$ diagonalizes the model Coulomb Hamiltonian, \mathcal{H}_C . The time evolution of a general quantum state is driven by the operator $H_1(\mathbf{q}, \xi; \mathbf{A})$ that couples the external transverse electromagnetic field \mathbf{A} to the molecular system. The corresponding wave functions $\{\Phi_k(\mathbf{q}, \xi; \mathbf{A})\}$ are represented in the basis $\{\phi_k(\mathbf{q})\zeta_{kj}(\xi)\}$ using the superposition principle, and computed by diagonalizing $\mathcal{H} = \mathcal{H}_C + H_1(\mathbf{q}, \xi; \mathbf{A})$. A chemical reaction is signaled by changes in the amplitudes in the linear superposition. We discuss the implementation of the method for simulation purposes, and illustrate its application in the charge transfer process during $\text{H}(1s) + \text{H}^+$ collisions and a simplified three-state model of a chemical reaction.

Contents

1. Introduction	276
2. GED ansatz	276
3. Post-BO scheme: process description	279
3.1. Charge transfer process in $\text{H}(1s) + \text{H}^+$ collisions	279
3.2. Simple chemical reactions: three-state model	283
3.3. Computer simulation schemes	286
4. Discussion	287
Acknowledgements	290
References	291

1. INTRODUCTION

In the 1970s, Osvaldo Goscinski brought to the attention of the community a number of drawbacks related to the Born–Oppenheimer (BO) approximation, in particular, its handling of symmetry issues [1,2]. Together with other authors [3,4], he showed the severe limitations inherited by molecular quantum mechanics after having introduced elements of classical mechanics early into the theory. In spite of these early warnings, some form of the BO scheme is embedded into standard quantum chemistry, leading to somewhat paradoxical situations, some of which are characterized as ‘non-adiabatic effects.’ We have followed Osvaldo’s footsteps in trying to get beyond these problems [5–9]. We discuss here some recent developments in this trek [10–13].

To start with, we take a fresh look at the separability problem. A generalized electronic diabatic (GED) approach is used as an ansatz to solve a model Schrödinger equation for a set of n electrons interacting with a positive charge background (PCB). This leads to an exactly separable scheme because the PCB is represented as a system of *massless classical test charges*. Bearing in mind the current state of the technology for externally controlled single-molecule manipulations, the approach is thought to offer a useful way to represent electronic and molecular processes under the effects of external (electromagnetic) fields. Section 2 introduces the model Hamiltonian and the GED ansatz. In Section 3, we contrast the above approach to those in more standard quantum-chemical schemes. We examine the scattering during $\text{H}(1s) + \text{H}^+$ collisions, and then apply the GED scheme to a simple model for the formation or breaking of chemical bonds. The chosen examples highlight the advantages of the procedure for treating systems strongly coupled in laser fields, as well as the necessity for transition states (TSs). We close the section with a proposed protocol for computer-assisted simulations based on the GED ansatz. Section 4 contains a detailed discussion that expands on the main differences between the standard BO and the present post-BO approach.

2. GED ANSATZ

Within the present scheme, a general electronuclear system is modeled by a total Hamiltonian \mathcal{H} , associated with a set of n -electrons (with a corresponding electronic Hamiltonian $\mathcal{H}_e(\mathbf{q}, \xi)$), an external PCB consisting of m -charges with position coordinates $\xi = (\xi_1, \dots, \xi_m)$, charge vector $Z = (Z_1, \dots, Z_m)$ in units of the electron charge $|e|$ and a kinetic energy operator $K(\xi)$ allowing for a mass distribution $M = (M_1, \dots, M_m)$ related to the PCB, and finally a transverse vector potential \mathbf{A} provided by an external

electromagnetic field:

$$\mathcal{H} = \mathcal{H}_e(\mathbf{q}, \xi) + K(\xi) + H_1(\mathbf{q}, \xi; \mathbf{A}). \quad (1)$$

The operator $H_1(\mathbf{q}, \xi; \mathbf{A})$ stands for the coupling of the electromagnetic field with the molecular system. The masses included in $K(\xi)$ make it possible to correlate the electronuclear dynamics to the standard molecular approach.

For an essentially self-adjoint operator, a theorem by Kato [14] ensures the existence of a complete set of basis functions, $\{\phi_k(\mathbf{q})\}$, for any partitioning of the molecular Coulombic Hamiltonians. (See Refs. [12,14,15] for detailed discussions.) The present GED ansatz is defined by the existence of a unique set $\{\phi_k(\mathbf{q})\}$ that diagonalizes the Hamiltonian $\mathcal{H}_e(\mathbf{q}, \xi)$ for all ξ [10,12]:

$$\mathcal{H}_e(\mathbf{q}, \xi)\phi_k(\mathbf{q}) = \varepsilon_k(\xi)\phi_k(\mathbf{q}). \quad (2)$$

For each $\phi_k(\mathbf{q})$, the functional $\varepsilon_k(\xi) = U(\xi; \phi_k)$ is a diabatic potential energy:

$$U(\xi; \phi_k) = U_k(\xi) = \langle \phi_k | \mathcal{H}_e(\mathbf{q}, \xi) | \phi_k \rangle_q. \quad (3)$$

Two classes of diabatic electronic basis functions are of interest here:

- (1) those for which $U_k(\xi)$ is a *bound attractor* that defines a single molecular species; and
- (2) those associated with the *asymptotic attractors* for molecular fragments.

Since the $\{\phi_k(\mathbf{q})\}$ basis does not depend on the PCB geometry, the class-1 functions generate $U_k(\xi)$ potentials that are *confining*, i.e., stationary with respect to ξ -displacements around the ξ^k vector of a unique minimum, $\|\partial U(\xi; \phi_k)/\partial \xi\| = 0$ at $\xi = \xi^k$. In other words, there is a single *global attractor* in the \mathfrak{R}^{3m} -space of ξ -configurations that is totally determined by each $\phi_k(\mathbf{q})$ -function. This result also applies to the case of asymptotic attractors.

Using the superposition principle and the GED basis set, we can represent an arbitrary quantum state at a ξ -configuration of the PCB as a scalar product:

$$\Psi(\mathbf{q}; \xi) = (a_0(\xi), a_1(\xi), \dots, a_j(\xi), \dots) \cdot [\phi_0, \phi_1, \dots, \phi_j, \dots]. \quad (4)$$

In equation (4), the $\{\phi_k(\mathbf{q})\}$ -basis is ordered using the attractor energy values $\{U(\xi^k; \phi_k)\}$. Note that quantum state $|\Psi(\mathbf{q}; \xi)\rangle$ depends on the PCB configuration through the row vector coefficients $\{a_j(\xi)\}$. At this level of theory, there is no time evolution (except for the energy phases) once a quantum state is prepared. The $|a_j(\xi)|^2$ is time invariant.

A change of electronic state is mediated by the field operator $H_1(\mathbf{q}, \xi; \mathbf{A})$; this change manifests in the row vector coefficients in equation (4). For

particular ξ values, the general state $|\Psi(\mathbf{q}; \xi)\rangle$ may be dominated by the single chemical species represented by the diabatic state $|\phi_k(\mathbf{q})\rangle$ if $a_k(\xi) \approx 1$. In practice, the quantum state $|\Psi(\mathbf{q}; \xi; A)\rangle$ dressed with the field interaction is obtained after solving the secular equation:

$$\sum_{j \geq 0} [\langle \phi_j | [\mathcal{H}_e(\mathbf{q}, \xi) + H_1(\mathbf{q}, \xi; \mathbf{A})] \phi_i \rangle - E_j(\xi; \mathbf{A}) \delta_{ij}] a_j(\xi; \mathbf{A}) = 0, \quad i \geq 0. \quad (5)$$

A number of chemical processes can be represented by stepwise solutions of equation (5), by choosing particular pathways (or ‘reaction coordinates’) in the laboratory space of the classical PCB. In actual calculations, a finite-dimensional manifold defined by selected electronic diabatic functions may suffice to obtain qualitative and semi-quantitative information. (The reader is referred to Refs. [10–13] for specific examples.) We refer to this as the *quantum-classical* (QC) model. The classical PCB can be used to localize possible reaction events by manipulating charges in laboratory space.

In more quantitative applications, one must also solve the ξ -dynamics for the classical part of the model. Using the GED ansatz, an eigenvalue equation emerges after first performing the integration over the electronic configuration \mathbf{q} -space:

$$[\langle \phi_k(\mathbf{q}) | \mathcal{H}_e(\mathbf{q}, \xi) \phi_k(\mathbf{q}) \rangle + K(\xi)] \zeta_{kj}(\xi) = E_{kj} \zeta_{kj}(\xi). \quad (6)$$

For class-1 states, a simple harmonic representation of $U(\xi; \phi_k)$ leads to a complete set of eigenfunctions $\{\zeta_{kj}^0(\xi)\}$; this harmonic oscillator basis set is used to diagonalize equation (6). In this case, it is sufficient to construct $U(\xi; \phi_k)$ using a standard approach involving mass fluctuation (or ‘nuclear’) coordinates and the corresponding electronic state dependent Hessian. The higher terms in the Taylor expansion define anharmonic contributions to the transition moments. These diabatic states are confining and only one stationary point in ξ -space would be found for each $\phi_k(\mathbf{q})$.

The situation is similar for class-2 states, involving asymptotically free fragments that conserve the total charge and mass. Plasma states can be represented by linear combinations of class-2 basis functions, whereas the individual fragments themselves can be described by class-1 states for a subset of electrons and PCBs.

When using the GED basis and the harmonic oscillator functions for class-1 states, we arrive at what can be characterized as a *quantum–quantum–classical* (Q^2C) scheme, whereby the total wave function for the isolated molecular system becomes

$$\Phi(\mathbf{q}, \xi) = \sum_{k \geq 0} \sum_{s \geq 0} a_{ks} \phi_k(\mathbf{q}) \zeta_{ks}(\xi). \quad (7)$$

The set of basis functions $\{\phi_k(\mathbf{q})\zeta_{k1}(\xi) = \Gamma_{k1}(\mathbf{q}, \xi)\}$ diagonalizes the full Hamiltonian $\mathcal{H}_C = \mathcal{H}_e(\mathbf{q}, \xi) + K(\xi)$, corresponding to the molecular system without the external field.

We can now study the time dependence of the general quantum state $|\Phi\rangle$ as follows. Let $V = H_1(\mathbf{q}, \xi; \mathbf{A})$ be the coupling to the external field; in the Dirac representation, we have $V(t') = \exp(i\mathcal{H}_C t')V \exp(-i\mathcal{H}_C t')$, in units of $\hbar = 1$. Also, the matrix elements of the time evolution operator in the GED basis $\{\Gamma_{ks}(\mathbf{q}, \xi)\}$ are

$$\begin{aligned} \langle \Gamma_{k's'} | U(t, t_0) \Gamma_{ks} \rangle &\approx \delta_{k'k} \delta_{s's} - i \int_{t_0}^t dt' \langle \Gamma_{k's'} | V(t') \Gamma_{ks} \rangle \\ &\quad - \sum_{k'', s''} \int_{t_0}^t dt' \int_{t_0}^{t'} dt'' \langle \Gamma_{k's'} | V(t') \Gamma_{k''s''} \rangle \langle \Gamma_{k''s''} | V(t'') \Gamma_{ks} \rangle + \dots, \end{aligned} \quad (8)$$

where $t_0 < t' < t$. This result permits a rigorous quantum mechanical analysis of time dependent problems in a way that radically differs from the more standard adiabatic and non-adiabatic schemes [16]. Finally, if we start from a set of initial amplitudes $\{a_{ks}(t_0)\}$ at $t = t_0$ corresponding to the Γ_{ks} basis functions, the final state is defined by the following set of coefficients:

$$\begin{aligned} a_{k's'}(t \rightarrow \infty) &\approx i \sum_{k,s} \int_{t_0}^{t \rightarrow \infty} dt' \langle \Gamma_{k's'} | V(t') \Gamma_{ks} \rangle a_{ks}(t_0) \\ &\quad - \sum_{k,s} \sum_{k'', s''} \int_{t_0}^{t \rightarrow \infty} dt' \int_{t_0}^{t'} dt'' \langle \Gamma_{k's'} | V(t') \Gamma_{k''s''} \rangle \langle \Gamma_{k''s''} | V(t'') \Gamma_{ks} \rangle a_{ks}(t_0) + \dots \end{aligned} \quad (9)$$

When using the model functions $\{\zeta_{kj}^0(\xi)\}$ to represent the basis set $\{\Gamma_{ks}(\mathbf{q}, \xi)\}$, the time evolution in equation (9) is essentially determined by Franck–Condon factors involving the overlap between harmonic-oscillator functions for different diabatic electronic attractors. Their actual calculation can be done with the help of the powerful methods developed by Palma [17].

3. POST-BO SCHEME: PROCESS DESCRIPTION

3.1. Charge transfer process in $\text{H}(1s) + \text{H}^+$ collisions

Consider the venerable problem of electron capture in $\text{H}^+ + \text{H}(1s)$ collisions. The standard model describes an encounter in which ‘nucleus 1’, with charge Z_1 and rest mass M , is incident on an atom (or ion) consisting of an electron e bound to ‘nucleus 2’ of charge Z_2 (and a total rest mass $m + M$).

In the impact parameter model (IPM), it is assumed that the position of beam-2 remains fixed while beam-1 moves in a straight line with a constant velocity \mathbf{v} [18,19].

For scattering situations, the beams (represented with local frames) are in motion with respect to specific laboratory frames. Given a beam system, a quantum state is defined in its corresponding inertial frame; electrons and nuclei states will be characterized by the total mass that depends on the relative velocity according to special relativity theory. These frames evolve in real (laboratory) space. The energy levels for the basis states are defined with respect to their rest mass energy $(m + 2M)c^2$; when measured from the laboratory, the levels will be shifted by $\frac{1}{2}M(\mathbf{v}_1 \cdot \mathbf{v}_1)$ for beam 1 and $\frac{1}{2}(m + M)(\mathbf{v}_2 \cdot \mathbf{v}_2)$ for beam 2. The classical beam momenta appear in the phases.

The IPM is a ‘classical’ particle approach. In a post-BO scheme (i.e., where nuclei and electrons are both considered quantum particles), the quantum state of a proton must include electron states belonging to the continuum of the hydrogen atom. We handle the problem by describing the system as if it were a ‘two-electron state’ where the experimentalist manages to keep the real system ionized with only one bound electron for all values of the PCB (i.e., $H^+ + H(1s)$). The resulting basis states are direct products of a hydrogen atom eigenstate (*including its continuum*) and the continuum states characterizing the ‘proton’ in Hilbert space. The latter functions incorporate, so to speak, the ‘boundary condition’ set up by an experiment that focuses on $H^+ + H$. In contrast, the most general basis set would include all direct products between the complete basis of two hydrogen atoms; this aspect is examined later on in this section.

To compare better with the IPM approach, we use a truncated ‘off-diagonal’ basis for the Hilbert space. The simple product for a proton in beam 1 and a bound hydrogen atom state in beam 2 is $\Phi_{klm}^{nlm} = |1; klm\rangle|2; nlm\rangle$, where the index k indicates the kinetic energy above the ionization limit for the proton beam 1. In the case where the protons are in beam 2 and the bound hydrogen atoms in beam 1, the corresponding product function would be $\Phi_{nlm}^{klm} = |1; nlm\rangle|2; klm\rangle$. (The notation uses the superindex for basis states in beam 2 and the subindex for beam 1.) The quantum transitions’ matrix elements $\langle \Phi_{klm}^{nlm} | H_1 | \Phi_{nlm}^{klm} \rangle$ control the electron transfer process. A general quantum state in the QC scheme is

$$\Psi(\mathbf{q}; \xi) = \sum_{n,k,l,m} a_{klm}^{nlm}(\xi) \Phi_{klm}^{nlm} + \sum_{n',k',l',m} b_{n'l'm}^{k'lm}(\xi) \Phi_{n'l'm}^{k'lm}. \quad (10)$$

The asymptotic channel 1 is represented by a set of non-zero coefficients among $\{a_{klm}^{nlm}\}$ and zero for all $\{b_{n'l'm}^{k'lm}\}$. After the interaction, one must perform an appropriate averaging over the ξ -space; the resulting $|b_{n'l'm}^{k'lm}|^2$ coefficients give the probability to measure a charge-transfer process. Equation (9) corresponds to the ξ -averaged case.

The asymptotic Hamiltonian for the system is hence a two-particle model:

$$\begin{aligned}\mathcal{H}_e(1, 2) = & \{K(1)\} + V(|\xi_1 - \mathbf{q}_1|) + \{K(2) + V(|\xi_2 - \mathbf{q}_2|)\} \\ & + V(\mathbf{q}_1, \mathbf{q}_2, \xi_1, \xi_2) = \mathcal{H}_e(1) + \mathcal{H}_e(2) + V(|\mathbf{q}_1 - \mathbf{q}_2|) \\ & + V(|\xi_1 - \mathbf{q}_2|) + V(|\xi_2 - \mathbf{q}_1|) + V(|\xi_1 - \xi_2|).\end{aligned}\quad (11)$$

The interaction potential $V(\mathbf{q}_1, \mathbf{q}_2, \xi_1, \xi_2)$ is a standard sum of Coulomb terms; in what follows it is useful to give it the form: $V(\mathbf{q}_1, \mathbf{q}_2, \xi_1, \xi_2) = V(|\mathbf{q}_1 - \mathbf{q}_2|) + W(\mathbf{q}_1, \mathbf{q}_2; \xi_1, \xi_2)$. The last term includes the Coulomb attraction between negative and positive charges and the repulsion between classical charge elements; this operator has parity $+1$.

We consider now the case $\text{H}(1s)\text{H}^+ \rightarrow \text{H}^+\text{H}(1s)$, i.e., the transition from a basis state in channel 1 to a basis state in channel 2. From parity considerations, we have

$$\langle \Phi_{100}^{k'10} | W(\mathbf{q}_1, \mathbf{q}_2; \xi_1, \xi_2) \Phi_{k'10}^{100} \rangle = 0. \quad (12)$$

During the ionization of the hydrogen atom in the $1s$ -state, the l -angular momentum differs in one unit (allowed dipole transition), whereas the m_l quantum number is conserved. Since $W(\mathbf{q}_1, \mathbf{q}_2; \xi_1, \xi_2)$ has parity $+1$, it follows that the matrix elements $\langle \Phi_{100}^{k'10} | V(|\xi_1 - \mathbf{q}_2|) \Phi_{k'10}^{100} \rangle$ and $\langle \Phi_{100}^{k'10} | V(|\xi_2 - \mathbf{q}_1|) \Phi_{k'10}^{100} \rangle$ will be zero by symmetry.

We can now relate these basis functions to the case of the IPM. Since the latter is an independent-electron model, we can represent it by eliminating the electron–electron repulsion operator in equation (11), $V(|\mathbf{q}_1 - \mathbf{q}_2|) \equiv 0$. The resulting Hamiltonian is

$$\begin{aligned}\mathcal{H}_{\text{eff}} = & \{K(1) + V(|\xi_1 - \mathbf{q}_1|)\} + \{K(2) + V(|\xi_2 - \mathbf{q}_2|)\} \\ & + W(\mathbf{q}_1, \mathbf{q}_2; \xi_1, \xi_2).\end{aligned}\quad (13)$$

This operator is diagonal in the basis set defined by $\{\Phi_{100}^{k'10}, \Phi_{k'10}^{100}\}$ for all proton beams with a kinetic energy k' above the ionization limit of the H-atom. From equation (9), all $a_{ks}(t_o)$ will be zero except $a_{k'10}^{100}(t_o)$. Also, the matrix elements that define the cross section for electron exchange will vanish, $\langle 1; nlm | \langle 2; klm | W(\mathbf{r}') | 1; klm \rangle | 2; nlm \rangle = 0$.

If ε_{100} now denotes the energy of the $1s$ -state of the hydrogen atoms in beam 1, we can represent one of the asymptotic channel states as follows:

$$\langle \Phi_{100}^{k'10} | \{K(1) + V(|\xi_1 - \mathbf{q}_1|) + K(2)\} \Phi_{100}^{k'10} \rangle = \varepsilon_{100} + k' = E_{100}(k'). \quad (14)$$

To recover the viewpoint used in the IPM, we simply integrate over the continuum:

$$\{K(1) + V(|\xi_1 - \mathbf{q}_1|) + k_2 - E_{100}(k')\} \phi_2^1(\mathbf{q}_1) = 0, \quad (15)$$

with $\phi_2^1(\mathbf{q}_1) = \langle \mathbf{q}_2 | \Phi_{100}^{k'10} \rangle$ and where k_2 is the diagonal matrix element of the kinetic energy operator $K(2)$ taken with respect to the continuum basis function associated with beam 2 (i.e., for the hydrogen atoms used to prepare the ‘free’ proton beam). For the permuted asymptotic channel, we have

$$\{K(2) + V(|\xi_2 - \mathbf{q}_2|) + k_1 - E_{100}(k')\}\phi_2^1(\mathbf{q}_2) = 0. \quad (16)$$

These equations correspond to equation (2) in Bates’ paper [19]; also, they can be transformed into equation (20) of Cheshire’ paper [18], after defining $\varepsilon_i = k_2 - E_{100}(k')$ and $\varepsilon_f = k_1 - E_{100}(k')$ as the initial and final eigenvalues for equations (15) and (16). Note that the relative kinetic energy of the proton with respect to the target must be equal to energy above the threshold of the electron-state in the continuum. As a result, the electron capture process under study becomes a two-electron-state problem. In Bates’ paper, this is implicit in the treatment of transition amplitudes, yet the electron is assigned to a single beam as long as one clings to a particle model. In the present post-BO scheme, the particle picture is replaced by infinite basis states in Hilbert space.

Let us now focus on the physical mechanism for charge transfer that emerges from our approach. First, equation (12) predicts a zero probability for the electron exchange $\text{H}(1s)\text{H}^+ \rightarrow \text{H}^+\text{H}(1s)$ as long as one excludes the electron–electron interaction. We can now introduce the latter effect by approximating the two-electron operator as the symmetrized scalar products that couple the electric field of one subsystem with the dipole moment operator of the other subsystem:

$$G(1, 2) = -\frac{1}{2}\mathbf{E}(2_1) \cdot \boldsymbol{\mu}(1) - \frac{1}{2}\mathbf{E}(1_2) \cdot \boldsymbol{\mu}(2). \quad (17)$$

The symbol $\mathbf{E}(2_1)$ stands for the field operator produced by the electron ‘system 2’ onto ‘system 1’, and the factor 1/2 avoids double counting. Since the operators $\mathbf{E}(2_1)$ and $\boldsymbol{\mu}(1)$ have parity ‘ -1 ’, there will be no transition between two basis states of the same parity. Allowed transitions will involve two factors: (i) the matrix element $\langle 2; klm | \mathbf{E}(2_1) | 2; n(l \pm 1)m \rangle$, corresponding to the field produced by an excitation in beam 2 that changes the angular momentum by one unit, and (ii) the integral $\langle 1; nlm | \boldsymbol{\mu}(1) | 1; k(l \pm 1)m \rangle$, corresponding to the transition moment in beam 1 for an excitation that takes a bound to the ionization continuum while also changing the angular momentum by one unit. As a result, the cross section calculated with equation (9) will include nonzero matrix elements $\langle 1; nlm | \langle 2; klm | G(t') | 1; klm \rangle | 2; nlm \rangle$. The asymptotic approximation equation (17)) will couple channel 1 to channel 2 states thereby yielding a mechanism to produce nonzero $b_{n'l'm}^{k'lm}$ amplitudes in equation (10).

Energy conservation imposes an additional selection rule on the matrix elements since *the energy gap for the dipole transition must be compensated by the energy gap from field production*. This can be seen as a form of

microscopic detailed balance. All matrix elements involving two-electron states that conserve the energy would contribute to the electron-transfer mechanism. Thus, if the bound electron is at an s-state ($l = 0$), the free electron state will have $l = 1$ momentum, and *vice versa*.

Recently, electron capture by protons from ground-state hydrogen atoms was analyzed by using Bates's two-state approximation with Cheshire's continuum distorted-wave basis within the context of a one-electron problem [20]. This latter ansatz allows for a representation of the two channels using a coupling operator $\mathbf{x} \cdot \nabla$ that would correspond to the two-electron G -operator in equation (17). The authors then calculate the amplitude for electron capture, indicated by $\sigma_{1s \rightarrow 1s}$, by averaging $|a_2(+\infty)|^2$ over the impact parameter range (cf. equation (13) in Ref. [20]); this term corresponds to $|b_{100}^{k_{10}}|^2$ in our formulation. Note that in the present approach, the integrals over frame amplitudes will not affect the electronic Hilbert space behaviour unless electron-phonon coupling is included (see Refs. [21,22]). The corresponding amplitude will emerge from equation (9), where the second-order term sums over the complete spectra, including the bound ground state $^2\Sigma_g^+$ and the direct products of the ionized electronic states in the continuum. In the present electron transfer scheme, $^2\Sigma_g^+$ is a class-1 bound state. We would expect resonance states to contribute less, as their overlap integrals decrease with an increasing relative energy. A more detailed analysis of this phenomenon will be reported elsewhere.

3.2. Simple chemical reactions: three-state model

In order to compare the present post-BO scheme and the standard approaches, it is useful to analyze electronic models consisting of a finite number of basis states.

Consider the case of a two-state model, comprising two diabatic electronic states $\psi_1(\mathbf{q})$ and $\psi_2(\mathbf{q})$ having the same symmetry with respect to inversion. This situation can be found, for instance, in the isomerization of closed-shell species [10]. If this chemical conversion is regarded as a change of electronic state, the transition integral between these two equal-symmetry diabatic states will be zero. In other words, two diabatic states corresponding to closed-shell isomers are not coupled in the external field: $[\mathcal{H}]_{12} = V_{12} = 0$, where \mathcal{H} is the total in-field Hamiltonian (cf. equation (1)). This implies that the change in electronic amplitude $\psi_1(\mathbf{q}) \rightarrow \psi_2(\mathbf{q})$ requires an additional third state (an actual *transition state* (TS)) in order to build a minimalist model for the reaction. This electronic state must be associated with an open-shell singlet diabatic state $\psi_3(\mathbf{q})$ [10].

Let us consider a model consisting of three bound diabatic basis states $\psi_1(\mathbf{q})$, $\psi_2(\mathbf{q})$, and $\psi_3(\mathbf{q})$ associated with harmonic potential energy functions $U_i(\xi)$. For the sake of simplicity, let us suppose that reactant and product are described by diabatic energy functions in terms of a single

variable ξ , differing only in the location of the respective minima: $U_1(\xi) = 1.25\xi^2$ and $U_2(\xi) = 1.25(\xi - 3)^2$ (in arbitrary units). For the diabatic TS, we consider an attractor nearer to the product $U_3(\xi) = 1.5 + 3(\xi - 2)^2$. The standard BO approximation would yield an artificial ‘transition’ between $\psi_1(\mathbf{q})$ and $\psi_2(\mathbf{q})$ at $\xi = 1.5$, and an effective energy barrier at the diabatic curve crossing $U_1 = U_2 = 2.8125$. In contrast, the GED approach produces also an effective barrier, but its location and height depend on the TS-function and the applied external field.

Total quantum states are represented by linear superpositions of the type

$$\begin{aligned}\Psi(\mathbf{q}; \xi) &= c_1(\xi)\psi_1(\mathbf{q}) + c_2(\xi)\psi_2(\mathbf{q}) + c_3(\xi)\psi_3(\mathbf{q}) \\ &\equiv (c_1(\xi)c_2(\xi)c_3(\xi)) \cdot [\psi_1(\mathbf{q})\psi_2(\mathbf{q})\psi_3(\mathbf{q})].\end{aligned}\quad (18)$$

The ‘pure’ reactant and product states are given by the coefficient vectors $(1\ 0\ 0)$ and $(0\ 1\ 0)$, respectively. A simple view of a chemical process will be elicited by a ξ -path leading over time from one state to the other. The amplitudes in the diabatic basis functions are obtained by diagonalizing the matrix of the complete Hamiltonian operator $\mathcal{H} = \mathcal{H}_e(\mathbf{q}, \xi) + V(\mathbf{q}, \xi; \mathbf{A})$. Using the existing symmetries for functions and operators, the matrix becomes

$$([\mathcal{H}]_{ij}) = \begin{pmatrix} U_1 & 0 & V_{13} \\ 0 & U_2 & V_{23} \\ V_{13} & V_{23} & U_3 \end{pmatrix}. \quad (19)$$

In equation (19), we have considered that (i) $[\mathcal{H}]_{ii} = U_i$, because $V_{ii} = \langle \psi_i(\mathbf{q}) | V \psi_i(\mathbf{q}) \rangle = 0$ given the \mathbf{q} -parity of the interaction operator $V = H_1(\mathbf{q}, \xi; \mathbf{A})$; (ii) $[\mathcal{H}]_{12} = 0$ because $\psi_1(\mathbf{q})$ and $\psi_2(\mathbf{q})$ are *exact* non-degenerate eigenfunctions of the electronic Hamiltonian (i.e., $[\mathcal{H}_e]_{12} = 0$), yet their \mathbf{q} -parity is opposite to V (i.e., $V_{12} = 0$); and (iii) the $\psi_3(\mathbf{q})$ function has the same \mathbf{q} -parity as V , and thus V_{13} and V_{23} need not be zero. By monitoring the lowest eigenvalue of [19], $E(\xi) = \langle \Psi | \mathcal{H} | \Psi \rangle$, we can follow the onset of electronic transitions as a function of the control variable ξ . The corresponding coefficients for the wave function of the total quantum state in the diabatic states are

$$\begin{aligned}|c_1| &= V_{13}c_3/|E - U_1|, & |c_2| &= V_{23}c_3/|E - U_2|, \\ c_3 &= +\{(V_{13}/|E - U_1|)^2 + (V_{23}/|E - U_2|)^2 + 1\}^{-1/2}.\end{aligned}\quad (20)$$

Using these solutions, it is clear that the diabatic curve crossing ($U_1 = U_2$) does not produce a state with the same weight in the reactant and product (i.e., $c_1 = c_2$) *unless* both states are coupled to the TS with the same strength

(i.e., only if $V_{13} = V_{23}$). Note that, since $\psi_i(\mathbf{q})$ is diabatic, the matrix elements V_{ij} are proportional to the intensity of the applied electromagnetic field yet *independent* of the control variable ξ .

Figure 1 shows the results in the case where reactant and product are equally coupled to the TS: $V_{13} = V_{23} = 2$. The diabatic potentials $\{U_i(\xi)\}$ appear in dashed lines; the total energy in the field (after diagonalization), $E(\xi) = \langle \Psi | \mathcal{H} | \Psi \rangle$, appears with thick line. The function $E(\xi)$ is a one-dimensional barrier interpolating between the attractors for reactant and product. In practice, $E(\xi)$ acts as a curve with an effective ‘avoided crossing’

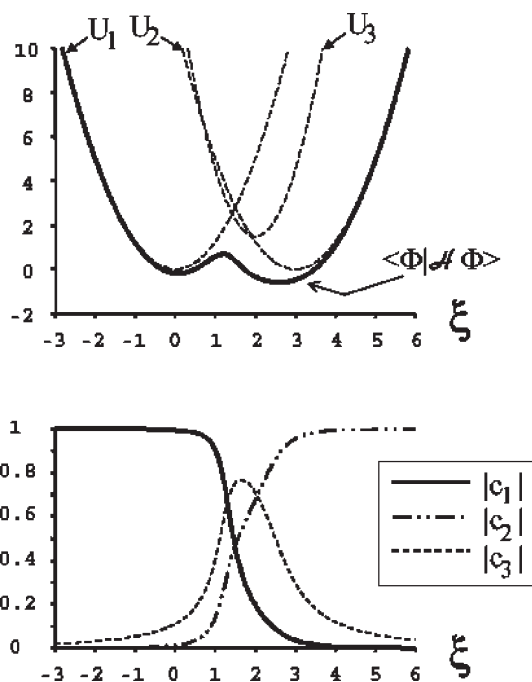


Fig. 1. Evolution of the quantum state $|\Phi\rangle$ for the isomerization of two closed-molecular species. The reactant and product attractors are represented by diabatic potential energy curves U_1 and U_2 which differ only in the ξ value for the location of their minima (dashed lines). A transition between these diabatic states is mediated by the external field and a bound TS with diabatic potential U_3 (also in dashed line). The total energy in the field ($\langle \Phi | \mathcal{H} | \Phi \rangle$, thick line) was computed using equal couplings to the TS, $V_{13} = V_{23} = 1.5$. In this case, the product is effectively stabilized in the field, adopting a quantum state that has a strong contribution from the TS. Note that the effective barrier in $\langle \Phi | \mathcal{H} | \Phi \rangle$ decreases with respect to the diabatic crossing $U_1 = U_2$. In addition, the effective barrier occurs at a ξ -geometry that is closer to the reactant state, in agreement with the Hammond postulate for apparent TSs. The apparent TS corresponds in this case to the local maximum $\langle \Phi | \mathcal{H} | \Phi \rangle \approx 0.701$ at $\xi \approx 1.19$.

between the diabatic potentials $U_1(\xi)$ and $U_2(\xi)$. The bottom diagram in Fig. 1 indicates that the state function Φ evolves slowly from (1 0 0) to (0 1 0) over a range of ξ -configurations. Note that the change $\psi_1(\mathbf{q})$ to $\psi_2(\mathbf{q})$ is to be understood in terms of amplitudes in the post-BO scheme and not as a change of population. The key role of the TS in mediating this electronic transition becomes apparent by the strong, broad maximum in $|c_3|$.

As a result of having three diabatic states coupled by the external field, the $E(\xi)$ function is no longer symmetric with respect to the diabatic crossing at $\xi = 1.5$. The three extrema of $E(\xi)$, denoted by $\xi_1^*(\min) < \xi_2^*(\max) < \xi_3^*(\min)$, are shifted with respect to the barrier that would have been found in the standard two-state BO approximation. In our approach, the product becomes *stabilized*, since the minimum at $E(\xi_3^*)$ is lower than the $E(\xi_1^*)$ value near the reactant; the actual data (not shown) indicates an effective *endothermic* barrier with $E(\xi_3^*) - E(\xi_1^*) = -0.40261$. The barrier maximum at ξ_2^* plays the role of a *pseudo*-transition structure, with its energy value $E(\xi_2^*)$ located below that of the diabatic crossing at $\xi = 1.5$. Moreover, note that the position of the barrier maximum is closer to the reactant ($\xi_2^* - \xi_1^* = 1.12$) than to the product ($\xi_3^* - \xi_2^* = 1.40$). This behaviour is in agreement with the Hammond postulate [23] used in physical organic chemistry. This rule assigns a reactant-like (or ‘early’) TS to most endothermic reactions, whereas a product-like (or ‘late’) TS is expected in most exothermic ones. The present analysis based on a GED ansatz provides a quantitative version of this principle in terms of the $\{c_i(\xi)\}$ coefficients for the projections of the total quantum state to reactant and product basis states. We believe that a measure of similarity based on comparing quantum amplitudes is physically more appealing than the standard approach to the Hammond postulate, based on comparing coordinate values along the conventional reaction paths.

3.3. Computer simulation schemes

In the context of traditional electronic calculations, the GED approach would correspond to a multi-configuration CI wave function written in a complete basis of direct products of one-electron states, as discussed in Section 3.1 [13]. The basis set must be in principle invariant with respect to the choice of electronic Hamiltonian. In practice, however, care must be exercised when using different electronic diabatic states that have been derived from distinct stationary geometries of the PCB.

The linear superposition principle plays a central role in the theory presented here. It should be noted, however, that the standard Copenhagen ‘interpretation’ of quantum mechanics is not well adapted to discuss the notion of state amplitudes and ‘measurements’ in the context required by the GED scheme. A more appropriate theoretical framework for quantum measurement is found in the ideas proposed by Fidler and Tapia [16].

The reader may consult the book by Wimmel [24], where a relevant criticism of the standard interpretation is given.

If a system has reached thermal equilibrium, the amplitudes obtained from equation (9) multiplied with their complex conjugates, $|C_{ks}|^2$ will represent the statistical weight of the corresponding basis state in the equilibrium density matrix. This is a natural result for the Q²C scheme. A statistical approach, however, ignores the role played by the excited states (among them, the present diabatic TSs) through their coupling to closed-shell chemical species represented as electronic class-1 GED states.

Within the QC scheme, regions of the PCB that are relevant to a certain reaction mechanism could be accessed by using, for instance, molecular dynamics methods. Here, any change in PCB configuration in laboratory space would reflect a change in Hilbert space, namely, the quantum amplitudes. One can then use this idea to devise a computational protocol whereby the PCB configuration evolves over time, driven by changes in amplitudes obtained from equation (5).

An operational scheme of the above algorithm would work as follows. First, one would need to identify the relevant stationary geometry states, all in the same coordinate frame. Suppose now that we monitor the evolution of the PCB configuration over time, starting from one diabatic state. Since our model describes the PCB as a set of classical charges, initially only *one* electronic attractor will drive the molecular dynamics and thus the evolution of quantum state. In the neighborhood of ‘crossing’ of two diabatic states, however, the amplitudes of these states could change rapidly. We can now take into account this possibility in a classical simulation, by using a Monte Carlo scheme to decide the odds for changing the electronic attractor, within a specified threshold for the square amplitude in the ‘outgoing’ channel. Since the diabatic electronic states are geometry-invariant but not the diabatic potential energies (cf. equation (5)), the only change will be in a sudden replacement of the forces acting on the mass endowed PCB. Whether the given trajectory would count as a reactive one will depend upon relaxation processes in the new channel and the quantum odds for the re-crossing process.

4. DISCUSSION

The GED approach uses a mixed QC ansatz to construct a separable model for the electronuclear problem. As it corresponds to the case of a set of identical fermions, the electronic part is fully quantized in the GED scheme. The PCB is endowed with a mass distribution allowing for a correspondence with the external potential created by nuclei. The harmonic oscillator model of nuclear dynamics then follows as a quantum extension of the latter model, one where mass fluctuations are described by normal modes related

to specific diabatic electronic states. We refer to latter approach as the Q²C model.

It is clear that the standard molecular approach and the Q²C model are correlated in the sense that their corresponding Hamiltonians are isometric. However, within the Q²C model, the handling of the separation between electrons and nuclei is conceptually different. In the latter, the electrons and a PCB subsystem endowed with mass are coupled *via* electron–phonon operators $H_{e\otimes\text{ph}}$, usually employed for describing Jahn–Teller effects [21,22]. These couplings act as perturbations which provide a mechanism to change the electronic state amplitudes *via* the vibrational degrees of freedom [13]. In the absence of these terms, the electronuclear motions are strictly separable. Note that, for a complete molecular model, one must still include the spin–orbit terms.

Let us highlight some conceptual differences with the standard BO approach. First, in the GED scheme, the operator \mathcal{H}_e is *not* derived from a molecular Hamiltonian using approximations dealing with nuclear masses. Instead, we initially introduce a background of *massless* positive test charges as a tool to build a complete basis set of diabatic electronic functions. Up to this point, the separability is *exact* since the PCB is an *explicitly classical* subsystem. As already noted, the diabatic functions can also be used to represent the general states of the quantized electronuclear system (Q²C). Secondly, nuclear masses do *not* appear in the GED analysis for the *electronic* system either explicitly or implicitly through center-of-mass translations. (Note that this is the case although \mathcal{H}_e is isomorphic to the BO electronic Hamiltonian written in an inertial frame and within the clamped-nuclei approximation [10–13].) These subtle differences are significant as they allow us to circumvent known difficulties associated with interpreting the BO internal electronic Hamiltonian [4,12].

In the present context, the standard BO description corresponds to diagonalizing equation (VIII.12) in Ref. [25] for *all values of the PCB*. In contrast, for the GED scheme, these calculations only make sense *at the stationary geometries* ξ^k . Our approach makes it apparent that there is no actual physical process associated with the ‘crossings’ of electronic states occurring within the BO calculations. In contrast, important conical intersections associated with molecular symmetries still find a natural place in the present post-BO approach, as it incorporates the intersections of diabatic potential energy surfaces.

Nakamura and Truhlar [26] have developed direct calculation techniques to obtain quasi-diabatic states. Yet, a main issue remains: there is no clear quantum-mechanical interpretation as to the meaning of an electronic wave function that depends parametrically on the positive charge positions [4]. The multi-electronic-state molecular dynamics approach by Martinez *et al.* [27] highlights the problems raised by the use of the BO scheme. The crossing points and the uncontrolled coupling of electronic states

having the same symmetry should essentially be seen as *computing artifacts*. Given these issues, we believe that the post-BO protocol sketched in Section 3.3 represents a more reasonable computational compromise. In the GED scheme [10–13], the ‘BO crossings’ merely signal bottleneck zones where the electronic quantum amplitudes change in a way that opens ‘product-state channels’ that would have been energetically inaccessible in the PCB region for the initial ‘reactant states.’ By following diabatic-state amplitudes over time, a mechanistic view for chemical reactions would then emerge naturally.

The most general representation for the quantum states of the complete molecular system of electrons and nuclei in terms of diabatic functions is given as

$$\Psi_i(\mathbf{q}; \xi) = \sum_j B_{ij}(\xi) \psi_j(\mathbf{q}). \quad (21)$$

If the nuclear charges are regarded as classical particles (i.e., the QC approach), the geometry-dependent coefficients $\{B_{ij}(\xi)\}$ result from the coupling between electronic states in the electromagnetic field, yet contain no information on nuclear masses. Note that equation (21) is *not intended to represent a BO wave function*; the fact that $\Psi_i(\mathbf{q}; \xi)$ may not converge rapidly to a BO function is irrelevant to the present approach. The GED ansatz is conceived, by construction, as a scheme that diagonalizes the electronic Hamiltonian; the standard BO approach does not satisfy this property.

When the field is absent and the nuclei are viewed as quantum particles, a complete description requires inclusion of electron–phonon and spin–orbit coupling operators. Now, the $B_{ij}(\xi)$ -coefficients couple electronic states whose diabatic potential energy surfaces yield degenerate functions for the nuclear dynamics. Finally, these geometry-dependent coefficients couple *all* diabatic electronic states whenever a fully quantum-mechanical molecular system is embedded in an external field.

We have also shown that useful concepts commonly employed in the standard BO separation scheme also find their place in the present GED approach, although under a different guise. For instance, avoided crossings in absence of a field are artifacts in the BO approximation resulting from either re-labeling the electronic functions after a diabatic crossing, or from using basis sets that depend on nuclear positions. In contrast, ‘switches’ between (diabatic) electronic states appear naturally in the GED approach of field-mediated transitions. The location and pattern for these switches (effectively ‘avoided crossings’) depend, however, on the geometry of the TS-attractor and on how strongly it is coupled with the diabatic reactant and product through the external field.

An important conceptual point must be stressed here. In the GED ansatz, effective ‘barriers’ are critical points in the sense that they

separate energy domains, but they cannot be obtained by performing variational calculations on the isolated molecule. The reason is simple. A standard quantum-chemical computation using an electronic basis set at a given geometry stationary point will not produce an ‘exact’ electronic diabatic wave function that is independent from the ξ -coordinates. Nevertheless, it is still possible to build *models* of diabatic states, whereby the stationary points (and their corresponding Hessians) are approximated using *harmonically confining* potentials. From the resulting total molecular energy function $\langle \Psi | \mathcal{H} | \Psi \rangle$ for a general quantum state $|\Psi\rangle$, we can then recover the notions of energy barrier, shallow double minima, and the Hammond postulate for the similarity between molecular species along a reaction coordinate. These concepts are legitimately defined in the context of the GED ansatz.

The GED ansatz is also a post-BO scheme in some other important respects. For the BO approach, removing the translational motion involves the introduction of a center of mass and two frames: one parallel to the laboratory frame and rigidly fixed to an ‘equilibrium nuclear configuration,’ and a second one that rotates with the latter assumed to be a rigid body. The molecular system is described as an object that can be ‘observed’ in its states (state population) [28]. Within the GED scheme, an inertial frame eliminates these approximations. The inertial frame with the attractor geometry permits one to define the center of mass and moments of inertia for the particular molecular species; these values will depend of course upon the diabatic electronic state. The six or five degrees of freedom for global classical translation and rotation can still be separated using a Hessian computed in Cartesian coordinates. The global linear momentum and frame angular momentum can be obtained with standard models.

Finally, by emphasizing its relationships to fluctuations in laboratory space, the GED scheme offers a promising line to address aspects of exciting new electronic phenomena. These would include, among others: (i) systems whose structures can be externally controlled by mechanical manipulations, (e.g., designed nanosystems; processes on tailored interfaces; and the steering of chemical reaction paths by scanning force microscopy [28–31]); (ii) quantum mechanical overtones of large, ‘quasi-classical’ systems such as biomolecules; (iii) the energy redistribution in photofragment translational spectroscopy [32].

ACKNOWLEDGEMENTS

This work was supported by grants from the Natural Sciences and Engineering Research Council of Canada and the Canada Research Chairs’ program. We thank N. Grant (Sudbury) for her comments on the manuscript.

REFERENCES

- [1] O. Goscinski and A. Palma, *Int. J. Quantum Chem.*, 1979, **15**, 197.
- [2] O. Goscinski and V. Mujica, in *Density Matrices and Density Functionals* (eds R. Erdahl and V. H. Smith, Jr.), Reidel, Dordrecht, 1987, pp. 597–611.
- [3] R. G. Woolley and B. T. Sutcliffe, *Chem. Phys. Lett.*, 1977, **45**, 393.
- [4] B. T. Sutcliffe, in *Potential Energy Surfaces* (ed. A. F. Sax), Springer, Berlin, 1999, pp. 61–96.
- [5] O. Tapia, in *Quantum Systems in Chemistry and Physics, Vol. II: Advanced Problems and Complex Systems* (eds A. Hernandez-Laguna, J. Maruani, R. McWeeny and S. Wilson), Kluwer, Dordrecht, 2000, pp. 193–212.
- [6] O. Tapia, in *New Trends in Quantum Systems in Chemistry and Physics*, (eds J. Maruani, S. Wilson and Y. G. Smeyers), Kluwer, Dordrecht, 2001, Vol. 2, pp. 23–47.
- [7] O. Tapia, *J. Mol. Struct., Theochem*, 2001, **537**, 89.
- [8] O. Tapia, *Adv. Quantum Chem.*, 2001, **40**, 103.
- [9] O. Tapia and P. Braña, *J. Mol. Struct., Theochem*, 2002, **580**, 9.
- [10] O. Tapia and G. A. Arteca, *Int. Electron. J. Mol. Des.*, 2003, **2**, 454.
- [11] O. Tapia, *J. Int. Quantum Chem.*, 2004, **97**, 637.
- [12] G. A. Arteca and O. Tapia, *J. Math. Chem.*, 2004, **35**, 1.
- [13] O. Tapia, *Int. J. Quantum Chem.*, 2004, in press. DOI.10.1002/qua.20035.
- [14] T. Kato, *Trans. Am. Math. Soc.*, 1951, **70**, 195.
- [15] T. Kato, *Trans. Am. Math. Soc.*, 1951, **70**, 212.
- [16] H. Fidler and O. Tapia, *Int. J. Quantum Chem.*, 2004, **97**, 670.
- [17] A. Palma, *Int. J. Quantum Chem.*, 1997, **63**, 229.
- [18] I. M. Cheshire, *Proc. Phys. Soc.*, 1964, **84**, 89.
- [19] R. D. Bates, *Proc. R. Soc. A*, 1958, **247**, 294.
- [20] M. F. Ferreira da Silva and J. M. P. Serrão, *J. Phys. B: At. Mol. Opt. Phys.*, 2003, **36**, 2357.
- [21] A. Abragam and B. Bleaney, *Electron Paramagnetic Resonance of Transition Ions*, Dover Publications, New York, 1986.
- [22] M. Eriksson, E. Sjöqvist and O. Goscinski, in *Electron–Phonon Dynamics and Jahn–Teller Effect* (eds G. Bevilacqua, L. Martinelli and N. Terzi), World Scientific, Singapore, 1999.
- [23] G. G. Hammond, *J. Am. Chem. Soc.*, 1955, **77**, 334.
- [24] H. Wimmel, *Quantum Physics & Observed Reality*, World Scientific, Singapore, 1992.
- [25] M. Born and K. Huang, *Dynamical Theory of Crystal Lattices*, Clarendon Press, Oxford, 1954.
- [26] H. Nakamura and D. G. Truhlar, *J. Chem. Phys.*, 2001, **115**, 10353.
- [27] T. J. Martinez, M. Ben-Nun and R. D. Levine, *J. Phys. Chem. A.*, 1997, **101**, 6389.
- [28] W. E. Moerner and L. Kador, *Phys. Rev. Lett.*, 1989, **62**, 2535.
- [29] D. T. Chiu and R. N. Zare, *J. Am. Chem. Soc.*, 1996, **118**, 6512.
- [30] B. C. Stipe, M. A. Rezaei, W. Ho, S. Gao, M. Persson and B. I. Lundqvist, *Phys. Rev. Lett.*, 1997, **78**, 4410.
- [31] S. Alavi, B. Larade, J. Taylor, H. Guo and T. Seideman, *Chem. Phys.*, 2002, **281**, 293.
- [32] X.-B. Gu, G.-J. Wang, J.-H. Huang, K.-L. Han, G.-Z. He and N.-Q. Lou, *J. Phys. Chem. A.*, 2001, **105**, 354.

This page intentionally left blank

The Quantum–Classical Density Operator for Electronically Excited Molecular Systems

David A. Micha and Brian Thorndyke

Quantum Theory Project, University of Florida, Gainesville, FL 32611-8435, USA

Abstract

Starting with the Liouville–von Neumann equation for the statistical density operator, a partial Wigner transform is introduced to derive equations coupling quantum degrees of freedom with quasiclassical ones, as frequently encountered in molecular systems undergoing electronic transitions. Further consideration of the limit of short wavelengths in phase space leads to the introduction of effective potentials, and a treatment suitable for calculations of the dynamics of a system with many degrees of freedom. The theory is implemented by numerically introducing an expansion in a basis set of quantal states, and a relax-and-drive time propagation procedure for the density matrix. A model with two coupled states is solved exactly and is compared with the quantal–classical approximation for populations of quantum states, quantal coherence, expectation values of variables and their dispersion in phase space, and the time evolution of a distribution of trajectories in the phase space of quasiclassical variables. Extensions needed to account for dissipation due to interactions with a medium are briefly considered.

Contents

1. Introduction	294
2. The coupled quantum–classical description	295
2.1. Partial Wigner transform	295
2.2. Coupled quantal and classical variables	296
3. Approximations for short wavelengths	297
3.1. Coupled quantum and classical equations	297
3.2. Trajectories from effective potentials and forces	298
4. Numerical propagation method	300
4.1. Propagation in a local interaction picture	300
4.2. The relax-and-drive computational procedure	302
5. Model calculations	303
5.1. Expansions in a basis set and on a phase space grid	303
5.2. Results of model calculations	305
6. Reduced density matrices for dissipative dynamics	309
7. Conclusion	312
Acknowledgements	313
References	313

1. INTRODUCTION

This contribution deals with the description of molecular systems electronically excited by light or by collisions, in terms of the statistical density operator. The advantage of using the density operator instead of the more usual wavefunction is that with the former it is possible to develop a consistent treatment of a many-atom system in contact with a medium (or bath), and of its dissipative dynamics. A fully classical calculation is usually suitable for a many-atom system in its ground electronic state, but is not acceptable when the system gets electronically excited, so that a quantum treatment must then be introduced initially. The quantum mechanical density operator (DOP) satisfies the Liouville–von Neumann (L–vN) equation [1–3], which involves the Hamiltonian operator of the whole system. When the system of interest, or object, is only part of the whole, the treatment can be based on the reduced density operator (RDOP) of the object, which satisfies a modified L–vN equation including dissipative rates [4–7].

The numerical solution of these equations is particularly challenging when dealing with many atoms, and very demanding of computing resources even for a system with a few atoms (10 or fewer). A promising approach is to separate the degrees of freedom of the many-atom system into quantal and classical-like ones, and to develop a consistent treatment of their interaction. In fact, this has been a very active area of research, and the goal has been approached using several formalisms, including wavepackets, path integrals, propagators, and short-wavelength (or eikonal) expansions. References to these approaches as they relate to electronic transitions in molecular systems can be found in our recent publications [8,9]. In addition to these methods, the one which introduces the Wigner transform [7,10] seems the best suited to a formalism based on the density operator. Here, we follow a treatment which introduces a partial Wigner transform (PWT) for molecular systems [11,12].

This is not a review, but a progress report on work we have recently done using the density operator for molecular systems undergoing electronic excitation. The present contribution describes some of our work using a PWT of the DOP, with emphasis on a formulation suitable for numerical work. We have previously employed the DOP to describe electronic rearrangement [13], and in particular for molecular photoexcitation at surfaces [14], collisional excitation in few-atom and many-atom systems [15], and the formulation of a dissipative dynamics in many-atom systems suitable for computational work [9]. Numerical results have been obtained with a time-propagation method we have introduced to deal with coupled equations involving different time scales, named the *relax-and-drive* procedure [16,17], which we have implemented in several applications involving electronic rearrangement in many-electron systems due to collisions or interactions with light [8].

In what follows, we present a general coupled quantum–classical description using the PWT. We describe approximations suitable for short

wavelengths in a phase space of quasiclassical molecular variables, including several choices of effective potentials needed to guide trajectories in phase space. We briefly cover the numerical propagation and present numerical results of a model for two coupled quantum states and one quasiclassical degree of freedom, which illustrates the numerical approach. This includes results for state populations and quantum coherences, expectation values of position and momentum variables and their dispersion of values, and the time evolution of the grid of points in phase space that deforms over time due to the effective potential.

2. THE COUPLED QUANTUM–CLASSICAL DESCRIPTION

2.1. Partial Wigner transform

We consider to begin with an isolated system with a Hamiltonian operator $\hat{H}(t)$. Its state is given by the density operator $\hat{\Gamma}(t)$ which satisfies the L–vN equation of motion,

$$i\hbar\partial\hat{\Gamma}/\partial t = \hat{H}(t)\hat{\Gamma}(t) - \hat{\Gamma}(t)\hat{H}(t) = \hat{\mathcal{H}}\hat{\Gamma}(t) \quad (1)$$

with the initial condition $\hat{\Gamma}(t_{\text{in}}) = \hat{\Gamma}_{\text{in}}$ and normalization $\text{Tr}[\hat{\Gamma}(t)] = 1$. Here, we have introduced a Liouville superoperator shown as a calligraphic symbol, such that $\hat{\mathcal{H}} = [\hat{H}, \bullet]$, a commutator. Expectation values of physical operators \hat{A} of the whole system are obtained from the trace,

$$\langle A(t) \rangle = \text{Tr}[\hat{\Gamma}(t)\hat{A}]/\text{Tr}[\hat{\Gamma}(t)] \quad (2)$$

which also depends on initial conditions. Introducing quantum variables (position and spin variables) $q = (q_1, \dots, q_n)$ and quasiclassical variables (describing nearly classical motions in terms of trajectories) $Q = (Q_1, \dots, Q_N)$, the density operator can be expanded in the quasiclassical coordinate representation using the set of states $\{|Q\rangle\}$, as

$$\hat{\Gamma}(t) = \int dQ \int dQ' |Q\rangle \hat{\Gamma}(Q, Q', t) \langle Q'| \quad (3)$$

where the function $\hat{\Gamma}(Q, Q', t)$ is yet an operator in the quantal variables.

The PWT is obtained by introducing the new coordinates $R = (Q + Q')/2$ and $S = Q - Q'$, in abbreviated notations, and the integral transform [10]

$$\hat{\Gamma}_{\text{W}}(P, R, t) = (2\pi\hbar)^{-N} \int d^N S \exp(iPS/\hbar) \langle R - S/2 | \hat{\Gamma} | R + S/2 \rangle \quad (4)$$

where (P, R) are variables corresponding to momenta and position in a classical limit. The normalization of this density operator is obtained from

a trace over quantum variables and an integral over P and R as

$$\text{Tr}[\hat{I}_W] = \text{Tr}_{\text{qu}} \left[\int dR dP \hat{I}_W(P, R, t) \right] = 1. \quad (5)$$

From this operator it is possible to obtain the quasiclassical phase density

$$\gamma(P, R, t) = \text{Tr}_{\text{qu}}[\hat{I}_W(P, R, t)] \quad (6)$$

and the quantal density operator

$$\hat{I}_{\text{qu}} = \int dR dP \hat{I}_W(P, R, t). \quad (7)$$

A partially Wigner transformed operator \hat{A}_W is similarly defined by

$$\hat{A}_W(P, R) = \int d^N S \exp(iPS/\hbar) \langle R - S/2 | \hat{A} | R + S/2 \rangle \quad (8)$$

and physical properties are obtained from the trace as

$$\langle A \rangle = \text{Tr}(\hat{I}_W \hat{A}_W) = \text{Tr}_{\text{qu}} \left[\int dR dP \hat{I}_W(P, R, t) \hat{A}_W(P, R) \right]. \quad (9)$$

The PWT of a product of two operators \hat{A} and \hat{B} is given by

$$(\hat{A}\hat{B})_W = \hat{A}_W \exp(-i\hbar\vec{\Lambda}/2) \hat{B}_W, \quad \vec{\Lambda} = \frac{\vec{\partial}}{\partial P} \cdot \frac{\vec{\partial}}{\partial R} - \frac{\vec{\partial}}{\partial R} \cdot \frac{\vec{\partial}}{\partial P}, \quad (10)$$

in terms of the Moyal bidirectional operator $\vec{\Lambda}$. In the standard Wigner transform, performed over all the variables, the quantities A_W and B_W are functions and commute, but in our case they are yet operators \hat{A}_W and \hat{B}_W in the quantum variables, and their order must be preserved.

Taking the PWT of the L-vN equation gives the equation of motion

$$i\hbar \partial \hat{I}_W / \partial t = \hat{H}_W(t) \exp(-i\hbar\vec{\Lambda}/2) \hat{I}_W(t) - \hat{I}_W(t) \exp(-i\hbar\vec{\Lambda}/2) \hat{H}_W(t) \quad (11)$$

to be solved with initial conditions given by $\hat{I}_W(P, R, t_{\text{in}}) = \hat{I}_W^{(\text{in})}(P, R)$.

2.2. Coupled quantal and classical variables

This can be further developed for given Hamiltonians. Here, we are interested in the dynamics of coupled quantum and quasiclassical variables that follows from a Hamiltonian operator

$$\hat{H} = H^{(\text{qu})}(\hat{p}, \hat{q}) + H^{(\text{cl})}(\hat{P}, \hat{Q}) + H^{(\text{cq})}(\hat{p}, \hat{q}, \hat{P}, \hat{Q}) \quad (12)$$

with terms corresponding to quantal and quasiclassical Hamiltonian functions of position and momentum operators $\{\hat{p}, \hat{q}\}$ and $\{\hat{P}, \hat{Q}\}$ plus

their coupling energy $H^{(\text{cq})}$, a function of all the variables. Their PWT give $H_W^{(\text{qu})} = H_{\text{qu}}(\hat{p}, \hat{q})$, $H_W^{(\text{cl})} = H_{\text{cl}}(P, R) = P^2/(2M) + V(R)$, and $H_W^{(\text{cq})} = H_{\text{cq}}(\hat{p}, \hat{q}, P, R)$, so that $H_W = \hat{H}_{\text{qu}} + H_{\text{cl}} + \hat{H}_{\text{cq}}$, to be replaced in the equation of motion. This leads to

$$\begin{aligned} \partial \hat{F}_W / \partial t = & (i\hbar)^{-1} [\hat{H}_{\text{qu}}, \hat{F}_W(t)] + (i\hbar)^{-1} [(H_{\text{cl}} + \hat{H}_{\text{cq}}) \exp(-i\hbar \vec{\Lambda}/2) \hat{F}_W(t) \\ & - \hat{F}_W(t) \exp(-i\hbar \vec{\Lambda}/2) (H_{\text{cl}} + \hat{H}_{\text{cq}})]. \end{aligned} \quad (13)$$

The equation of motion for the quasiclassical phase density $\gamma(P, R, t)$ is found by taking the trace of this equation over quantal variables, and the equation of motion for \hat{F}_{qu} follows by instead integrating over R and P .

3. APPROXIMATIONS FOR SHORT WAVELENGTHS

3.1. Coupled quantum and classical equations

The PWT equations can be approximated in a semiclassical limit, obtained to lowest order in $\hbar \vec{\Lambda}$, so that for two operators \hat{A} and \hat{B} ,

$$\hat{A} \exp(-i\hbar \vec{\Lambda}/2) \hat{B} \simeq \hat{A} (1 - i\hbar \vec{\Lambda}/2) \hat{B} \quad (14)$$

which is justified provided the operators are slowly varying functions of phase space variables (P, R) . Further it follows that

$$-\hat{A} \vec{\Lambda} \hat{B} = \frac{\partial \hat{A}}{\partial R} \cdot \frac{\partial \hat{B}}{\partial P} - \frac{\partial \hat{A}}{\partial P} \cdot \frac{\partial \hat{B}}{\partial R} = \{\hat{A}, \hat{B}\} \quad (15)$$

where the last member is their Poisson bracket in the given order. This leads to

$$\begin{aligned} \frac{\partial \hat{F}_W}{\partial t} = & -\frac{i}{\hbar} [\hat{H}_{\text{qu}} + \hat{H}_{\text{cq}}, \hat{F}_W] + \{H_{\text{cl}}, \hat{F}_W\} \\ & + \frac{1}{2} (\{\hat{H}_{\text{cq}}, \hat{F}_W\} - \{\hat{F}_W, \hat{H}_{\text{cq}}\}) \end{aligned} \quad (16)$$

where we find to the right a first term corresponding to quantal motion, followed by a term involving only classical motion, and finally a classical–quantum coupling term which cannot be expressed as a commutator of \hat{F}_W with a Hamiltonian and therefore describes a (*non-intuitive*) new term which does not appear in other treatments based only on physical considerations. This is a partial differential equation for a density operator in the quantum states and of first order in the $2N + 1$ variables (P, R, t) , which must be solved starting with the initial value $\hat{F}_W(P, R, t_{\text{in}})$.

An equation for $\gamma(P, R, t)$ follows from the trace over quantum variables, giving

$$\begin{aligned} \partial \gamma / \partial t - \{H_{\text{cl}}, \gamma\} &= \frac{1}{2} \text{Tr}_{\text{qu}}(\{\hat{H}_{\text{cq}}, \hat{\Gamma}_{\text{W}}\} - \{\hat{\Gamma}_{\text{W}}, \hat{H}_{\text{cq}}\}) \\ &= \text{Tr}_{\text{qu}}(\{\hat{H}_{\text{cq}}, \hat{\Gamma}_{\text{W}}\}). \end{aligned} \quad (17)$$

3.2. Trajectories from effective potentials and forces

It is possible to further simplify the equations taking advantage of the quasiclassical nature of the P and R variables, by introducing effective potentials or forces to guide their motion through phase space, by the approximation $\{\hat{H}_{\text{cq}}, \hat{\Gamma}_{\text{W}}\} \simeq \{V', \hat{\Gamma}_{\text{W}}\}$, with $V'(P, R, t)$ an effective potential function relating to the coupling Hamiltonian of quantal and classical variables. This leads to a new potential $\mathcal{V}(P, R, t) = V(R) + V'(P, R, t)$, and a new classical Hamiltonian $H'_{\text{cl}}(P, R, t) = H_{\text{cl}}(P, R) + V'(P, R, t)$, so that the equation for $\hat{\Gamma}_{\text{W}}$ becomes

$$\frac{\partial \hat{\Gamma}_{\text{W}}}{\partial t} = -\frac{i}{\hbar} [\hat{H}_{\text{qu}} + \hat{H}_{\text{cq}}, \hat{\Gamma}_{\text{W}}(t)] + \{H'_{\text{cl}}, \hat{\Gamma}_{\text{W}}\} \quad (18)$$

which takes the usual form found in the literature, with quantum plus classical terms to the right. This may be justified, for example, if the density operator varies slowly with classical positions and momenta. Possible choices for the effective potential are the *Ehrenfest potential*

$$\mathcal{V}(P, R, t) = V(R) + \text{Tr}_{\text{qu}}[\hat{\Gamma}_{\text{W}}(P, R, t) \hat{H}_{\text{cq}}] / \gamma(P, R, t) \quad (19)$$

or the *average path potential*

$$\mathcal{V}(P, R, t) = V(R) + H_{\text{cq}}[q_{\text{t}}(P, R), p_{\text{t}}(P, R), P, R] \quad (20)$$

with $q_{\text{t}}(P, R) = \text{Tr}_{\text{qu}}[\hat{\Gamma}_{\text{W}}(P, R, t) \hat{q}]$ and similarly for p_{t} , or the potential from the *effective (Hellmann–Feynman) force*

$$\frac{\partial \mathcal{V}(P, R, t)}{\partial R} = \frac{\partial V}{\partial R} + \text{Tr}_{\text{qu}} \left[\hat{\Gamma}_{\text{W}}(P, R, t) \frac{\partial \hat{H}_{\text{cq}}}{\partial R} \right] / \gamma(P, R, t). \quad (21)$$

The same approximation can be made in the equations of motion for γ to obtain

$$\frac{\partial \gamma}{\partial t} = \{H'_{\text{cl}}, \gamma\} \quad (22)$$

which is the usual equation of motion of the purely classical density of phase space.

A more accurate equation includes the quantum–classical operator coupling, after adding and subtracting the V' term, and reads

$$\begin{aligned} \frac{\partial \hat{I}_W}{\partial t} = & -\frac{i}{\hbar} [\hat{H}_{\text{qu}} + \hat{H}_{\text{cq}}, \hat{I}_W] + \{H'_{\text{cl}}, \hat{I}_W\} \\ & + \frac{1}{2} (\{\hat{H}_{\text{cq}} - V', \hat{I}_W\} - \{\hat{I}_W, \hat{H}_{\text{cq}} - V'\}) \end{aligned} \quad (23)$$

where the last term is a first-order quantum–classical coupling correction.

These operator equations become, after expansions of operators in a basis of quantal states, sets of coupled equations for density matrix elements. Other choices have been suggested instead of the effective potential \mathcal{V} , to account in more detail for the different dependence of each density matrix element with time [11,12,18–20], and provide alternative couplings of quantal and classical variables.

Our equations for γ and \hat{I}_W must be solved simultaneously. To proceed, it is convenient to introduce the functions $R(t)$ and $P(t)$, solutions of the Hamiltonian equations

$$\frac{dR}{dt} = \frac{\partial H'_{\text{cl}}}{\partial P}, \quad \frac{dP}{dt} = -\frac{\partial H'_{\text{cl}}}{\partial R} \quad (24)$$

with $H'_{\text{cl}} = P^2/(2M) + \mathcal{V}(P, R, t)$, and initial conditions $R_{\text{in}} = R(t_{\text{in}})$ and $P_{\text{in}} = P(t_{\text{in}})$. Introducing the notation $H'[\hat{p}, \hat{q}, P(t), R(t)] = \hat{H}'(t)$ and

$$\frac{d\hat{I}_W}{dt} = \frac{\partial \hat{I}_W}{\partial t} + \frac{dR}{dt} \cdot \frac{\partial \hat{I}_W}{\partial R} + \frac{dP}{dt} \cdot \frac{\partial \hat{I}_W}{\partial P} \quad (25)$$

and similarly for γ , we find that γ and \hat{I}_W depend on the parameters $\{R_{\text{in}}, P_{\text{in}}\}$. When the first-order coupling correction is neglected, they satisfy the simple equations

$$\frac{d\hat{I}_W}{dt} = \frac{1}{i\hbar} [\hat{H}_{\text{qu}} + \hat{H}_{\text{cq}}(t), \hat{I}_W(t)], \quad d\gamma/dt = 0 \quad (26)$$

with total derivatives with respect to time, instead of the previous partial derivatives, and with the second line indicating conservation of the phase space density. In this way, the many-atom description has been reduced to the simultaneous solution of the above equation for the quantal density operator coupled to the Hamiltonian equations for the classical variables, for given initial classical values. The first-order coupling can be added to the equation for \hat{I}_W if desired.

Expectation values of properties can be obtained from integrals over initial classical values, considering that the element of volume in phase space is

independent of time so that $dR dP = dR_{\text{in}} dP_{\text{in}}$. With this, we find that

$$\langle A \rangle = \text{Tr}(\hat{F}_W \hat{A}_W) = \text{Tr}_{\text{qu}} \left[\int dR_{\text{in}} dP_{\text{in}} \hat{F}_W(P, R, t) \hat{A}_W(P, R) \right] \quad (27)$$

where R and P are known functions of their initial values along the classical trajectories, and the integral can be constructed as the equations of motion are integrated over time for each initial condition.

4. NUMERICAL PROPAGATION METHOD

4.1. Propagation in a local interaction picture

The equation of motion for \hat{F}_W , which involves only a commutator with a Hamiltonian, could be solved by expanding the DOp in terms of density amplitudes satisfying a Schrödinger-like equation. More generally, however, the equation for a reduced DOp would contain dissipative rates, and this would make it necessary to solve the equation directly for the DOp. We therefore develop the numerical propagation method for the general case. The computational procedure starts with a basis set of quantum states, arranged as a row matrix $|\Phi\rangle = [|\Phi\rangle_1, |\Phi\rangle_2, \dots]$, taken here to be orthonormal, and giving the matrix representation $\hat{F}_W = |\Phi\rangle \Gamma_W \langle \Phi|$. Dropping in what follows the subindex W in the matrix, so that $\Gamma_W = \Gamma$, the DM equation is of the form

$$\begin{aligned} \frac{d\Gamma}{dt} = & -\frac{i}{\hbar} \left[\mathbf{H}_{\text{qu}} + \mathbf{H}_{\text{cq}} - i\hbar \left\langle \Phi \left| \frac{d\Phi}{dt} \right\rangle, \Gamma(t) \right] \\ & + \frac{1}{2} (\{\mathbf{H}_{\text{cq}} - V'\mathbf{I}, \Gamma(t)\} - \{\Gamma(t), \mathbf{H}_{\text{cq}} - V'\mathbf{I}\}) \end{aligned} \quad (28)$$

with the full time derivative to the left.

Oscillations in time of quantal states are usually much faster than those of the quasiclassical variables. Since both degrees of freedom are coupled, it is not efficient to solve their coupled differential equations by straightforward time step methods. Instead it is necessary to introduce propagation procedures suitable for coupled equations with very different time scales: short for quantal states and long for quasiclassical motions. This situation is very similar to the one that arises when electronic and nuclear motions are coupled, in which case the nuclear positions and momenta are the quasiclassical variables, and quantal transitions lead to electronic rearrangement. The following treatment parallels the formulation introduced in our previous review on this subject [13]. Our procedure introduces a unitary transformation at every interval of a time sequence, to create a local interaction picture for propagation over time.

The calculation of the density operators over time requires integration of the sets of coupled differential equations for the quasiclassical trajectories and for the density matrix in a chosen expansion basis set. The density matrix could arise from an expansion in many-electron states, or from the one-electron density operator in a basis set of orbitals for a given initial many-electron state; a general case is considered here. The coupled equations are as before $dP/dt = -\partial H/\partial R$, $dR/dt = \partial H/\partial P$ coupled now to

$$\mathbf{H}\mathbf{\Gamma} - \mathbf{\Gamma}\mathbf{H} = i\hbar d\mathbf{\Gamma}/dt, \quad \mathbf{H} = \mathbf{H}_{\text{qu}} + \mathbf{H}_{\text{cq}} - i\hbar\langle\Phi|d\Phi/dt\rangle \quad (29)$$

and must be solved for the initial conditions at $t = t_{\text{in}} : R_{\text{in}} = R(t_{\text{in}})$ and $P_{\text{in}} = P(t_{\text{in}})$, and $\mathbf{\Gamma}_{\text{in}} = \mathbf{\Gamma}(t_{\text{in}})$. To start with, the matrices and trajectory variables are assumed known at a time t_0 ; the density matrices are first obtained as they relax over the interval $t_0 \leq t \leq t_0 + \Delta t$ while keeping the quasiclassical variables fixed. They are the solutions of the equations

$$\mathbf{H}_0\mathbf{\Gamma}^0(t) - \mathbf{\Gamma}^0(t)\mathbf{H}_0 = i\hbar d\mathbf{\Gamma}^0/dt \quad (30)$$

which shows that the density matrix changes with time as it relaxes from its (non-stationary) value at t_0 . The initial conditions in the interval are $\mathbf{\Gamma}^0(t_0) = \mathbf{\Gamma}_0$. Since the Hamiltonian matrix is now constant in time, these coupled equation are simple first-order differential equations with constant coefficients, and can be integrated by diagonalizing the matrix of coefficients. The results are sums of rapidly oscillating functions in time, reflecting the rapid quantal transitions.

In reality the quasiclassical variables are changing and one must account for the driving effect of their displacement and velocity changes within the interval $t_0 \leq t \leq t_1$. Provided this is small, and insofar as the quasiclassical motions are slower than the quantal ones, one can assume that the driving effect will only be corrections to the relaxing densities; this can be verified by shortening the time interval and repeating the calculations. The corrected densities are obtained by writing

$$\mathbf{\Gamma}(t) = \mathbf{\Gamma}^0(t) + \mathbf{U}^0(t)\mathbf{\Gamma}'(t)\mathbf{U}^0(t)^\dagger, \quad \mathbf{U}^0(t) = \exp\left[-\frac{i}{\hbar}\mathbf{H}_0(t-t_0)\right] \quad (31)$$

for the density matrix, where \mathbf{U}^0 defines a unitary transformation to a local interaction picture at each time t_0 .

Replacing this in the L–vN equation, it is found that

$$i\hbar \frac{d\mathbf{\Gamma}'}{dt} = [\mathbf{V}, \mathbf{\Gamma}_0] + [\mathbf{V}, \mathbf{\Gamma}'], \quad \mathbf{V}(t) = \mathbf{U}^0(t)[\mathbf{H}(t) - \mathbf{H}_0]\mathbf{U}^0(t)^\dagger. \quad (32)$$

Here, the matrix \mathbf{V} contains the effect of the quasiclassical displacements; therefore the inhomogeneous first term to the right is a driving term; the second term to the right is of second order in the driving effect, and could be dropped in calculations. Formally, the solution for the density matrix

correction is

$$\begin{aligned}\mathbf{\Gamma}'(t) &= \mathbf{\Delta}'(t) + (i\hbar)^{-1} \int_{t_0}^t dt' [\mathbf{V}(t'), \mathbf{\Gamma}'(t')], \\ \mathbf{\Delta}'(t) &= (i\hbar)^{-1} \int_{t_0}^t dt' [\mathbf{V}(t'), \mathbf{\Gamma}_0]\end{aligned}\tag{33}$$

where the driving term $\mathbf{\Delta}'$ can be obtained from a quadrature, and the second term can usually be neglected.

With the new density matrices known up to time t_1 , it is possible to advance the quasiclassical positions and momenta by integrating their Hamilton equations. This completes a cycle which can be repeated to advance to a later time t_2 . This sequence, based on relaxing the density matrix for fixed nuclei and then correcting it to account for quasiclassical motions, has been called the *relax-and-drive* procedure, and has been numerically implemented in several applications involving electronic rearrangement in atomic collisions [8].

4.2. The relax-and-drive computational procedure

Straightforward stepwise integration of the coupled Hamiltonian and L-vN differential equations would be inefficient and possibly computationally inaccurate, because the fast quantal oscillations demand very small time steps, while the slow quasiclassical motions must be followed over long times, requiring many steps. The accumulation of round-off errors would lead to large inaccuracies. An alternative is to separately do some of the integrations by quadratures. An obvious approach would be to use a perturbation expansion around the initial density matrix $\mathbf{\Gamma}_0$, but this also requires small time intervals because the density matrix relaxes rapidly for fixed quasiclassical variables. An alternative solution which works well is to make a first-order perturbation correction to the relaxing (time-dependent) density matrix.

The correction to the relaxing density matrix can be obtained independently of the Hamiltonian equations, and therefore does not require solving coupled equations for slow and fast functions. This procedure has been successfully applied to several collisional phenomena involving both one and several active electrons, and was observed to show excellent numerical behavior. A simple and yet useful procedure employs the first-order correction $\mathbf{\Gamma}'(t) = \mathbf{\Delta}'(t)$ and an adaptive step size for the quadrature and propagation. The density matrix is approximated in each interval by

$$\mathbf{\Gamma}(t) = \mathbf{\Gamma}^0(t) + \mathbf{U}^0(t)\mathbf{\Delta}'(t)\mathbf{U}^0(t)^\dagger\tag{34}$$

with the first term describing relaxation and the second one giving the driving effect.

To advance from t_0 to $t_1 = t_0 + \Delta t$, the quasiclassical trajectory is first advanced to the time $t_{1/2} = t_0 + \Delta t/2$ and the relaxing density $\Gamma^0(t)$ is calculated at this time; then the correction

$$\Delta'(t_1) = (i\hbar)^{-1} \int_{t_0}^{t_1} dt' [\mathbf{V}(t'), \Gamma_0] \quad (35)$$

is obtained with the (easily improved) quadrature approximation

$$\mathbf{V}(t) = \mathbf{U}^0(t) [\mathbf{H}(t_{1/2}) - \mathbf{H}(t_0)] \mathbf{U}^0(t)^\dagger \quad (36)$$

which allows an analytical integration of each matrix element. This is finally followed by recalculation of the quasiclassical trajectory and full density matrix at time t_1 . To ensure an accurate propagation, the step size Δt is varied to keep the density matrix correction within high and low tolerances in the interval, in accordance with

$$\varepsilon_{\text{low}} \leq \|\Delta'(t)\| / \|\Gamma^0(t)\| \leq \varepsilon_{\text{high}} \quad (37)$$

and the normalization is checked. This leads to an efficient adaptation of the step size, so that for example in a collision it will start large, will then decrease, and later increase again after the interaction forces have disappeared. The propagation accuracy can also be verified by reversing the propagation direction in time.

5. MODEL CALCULATIONS

5.1. Expansions in a basis set and on a phase space grid

In order to test our methods, we consider a model of two quantum states coupled to a quasiclassical variable, suitable for describing the near resonant electron transfer of an alkali atom such as Na as it approaches a metal surface M at thermal energies. The two asymptotic potential energies correspond to a ground state of neutral components $\text{Na} + \text{M}$ (state 1) and an excited state for ionic components $\text{Na}^+ + \text{M}^-$ (state 2), which cross at a short distance. The model consists of two diabatic surfaces and a coupling term given by [21,22]

$$H_{11}(R) = U_0 \exp[-2\alpha(R - R_0)] + 2\exp[-\alpha(R - R_0)] - \epsilon/2, \quad (38)$$

$$H_{22}(R) = U_0 \exp[-2\alpha(R - R_0)] - 2\exp[-\alpha(R - R_0)] + \epsilon/2, \quad (39)$$

$$H_{12}(R) = \beta\epsilon \exp[-\alpha^2(R - R_x)^2]. \quad (40)$$

Here, R is the distance between the surface and the Na atom, and is the quasiclassical variable over which we have taken the PWT. The ionic curve,

$H_{22}(R)$, is a Morse potential with a binding energy U_0 at distance R_0 . The neutral repulsive curve, $H_{11}(R)$, is asymptotically below the ionic one by a potential energy difference ϵ . The strength of the coupling term, $H_{12}(R)$ is characterized by β and peaks at the crossing $R = R_x$ between H_{11} and H_{22} , with a width α^{-1} .

The initial state is formed by approximating the ionic potential well as a harmonic potential around its minimum $R = R_0$, and finding the lowest bound state

$$\psi_1(R) = \left(\frac{1}{\pi\sigma^2} \right)^{1/4} \exp \left[-\frac{(R - R_0)^2}{2\sigma^2} \right] \exp[i\hbar P_0(R - R_0)]. \quad (41)$$

The Wigner density is the PWT over R , giving a Gaussian density in (P, R) ,

$$\Gamma_{11}(P, R) = \frac{1}{\pi} \exp \left[-\left(\frac{R - R_0}{\sigma} \right)^2 - \sigma^2 (P - P_0)^2 \right]. \quad (42)$$

At $t = 0$, the electronic state is promoted by a sudden optical excitation to the repulsive neutral potential, and the simulation follows the spontaneous decay of this state. The parameters used in the calculation are given in Table 1.

In order to propagate the Wigner density numerically, we need to choose a set of initial grid points $(P^{(j)}, R^{(j)})$ in phase space. Having chosen a grid, the quantum–classical Liouville equation with an effective potential (EP-QCLE) becomes a set of uncoupled matrix equations, one for each trajectory:

$$\frac{d\Gamma^{(j)}}{dt} = -\frac{i}{\hbar} [\mathbf{H}^{(j)}, \Gamma^{(j)}], \quad (43)$$

Table 1. Parameters used in the two-state model

Parameter	Value (atomic units)
U_0	0.025
α	0.4
β	0.15
ϵ	0.005
R_0	5.0
R_x	12.5
P_0	0.0
σ	0.233153
M	42,300

where

$$\mathbf{\Gamma}^{(j)}(t) = \mathbf{\Gamma}[P^{(j)}(t), R^{(j)}(t)], \quad \mathbf{H}^{(j)}(t) = \mathbf{H}[P^{(j)}(t), R^{(j)}(t)], \quad (44)$$

and each point in phase space propagates according to the relax-and-drive method combined with the effective Hellmann–Feynman force. In our simulations, we find that starting with a 30×30 uniform grid within the limits $R = [4.2, 5.8]$ a.u. and $P = [-15.0, 15.0]$ a.u. provides convergence for this model.

5.2. Results of model calculations

Because of the simplicity of this model, we were able to generate the precise evolution of the full quantal system using the split-operator FFT method [23, 24] and compare to that obtained with the EP-QCLE. The results are presented in Figs 1–6, where we show the time evolution of neutral (Fig. 1) and ionic (Fig. 2) populations, the coherence between these states (Fig. 3), and the expectation values of the momentum (Fig. 4) and momentum dispersion (Fig. 5), and also the distribution of the grid points at the end of the simulation (Fig. 6). The time propagation was done with the relax-and-drive procedure, using variable time steps regulated by low and high tolerances, which lead to large time intervals at the beginning and end of trajectories, with a substantial reduction in the total number of time intervals. Although we obtained very similar results with a simplified propagation algorithm which used constant time steps and included only the relaxation of

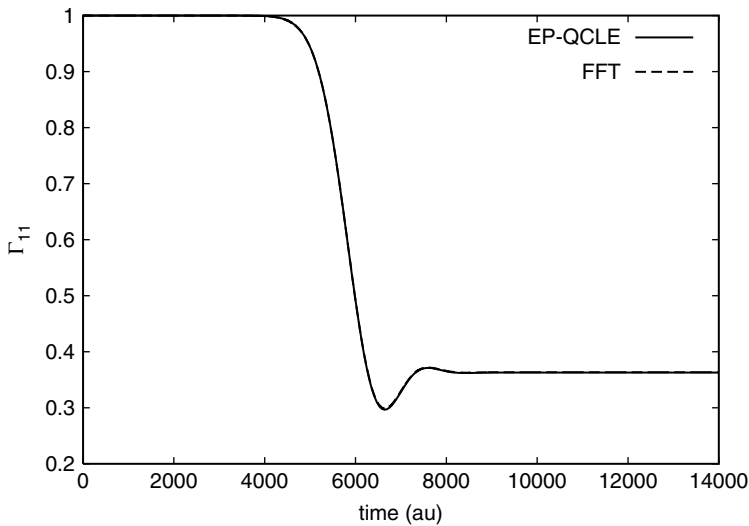


Fig. 1. Population Γ_{11} vs. time.

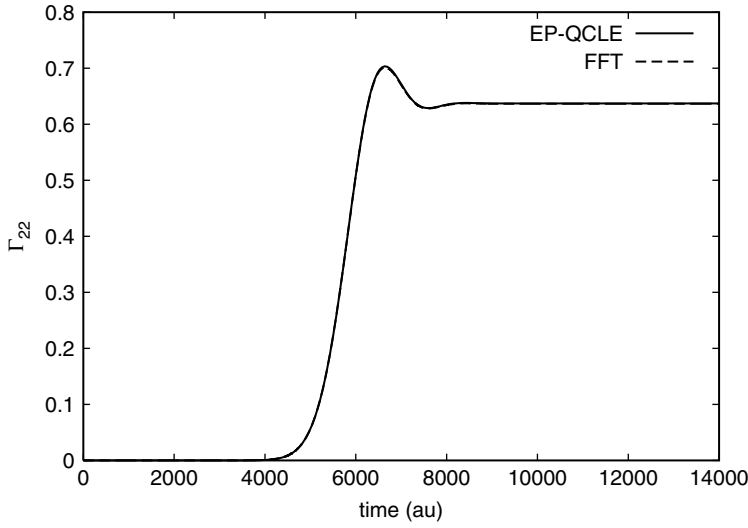


Fig. 2. Population Γ_{22} vs. time.

the Wigner density, the simpler algorithm required over 3.5 times as many time steps as its relax-and-drive counterpart to reach convergence (typically 3500 vs. 1000 steps).

There are a number of interesting things we can glean from these plots. From Figs 1 and 2 we see that as the atom moves away from the metal

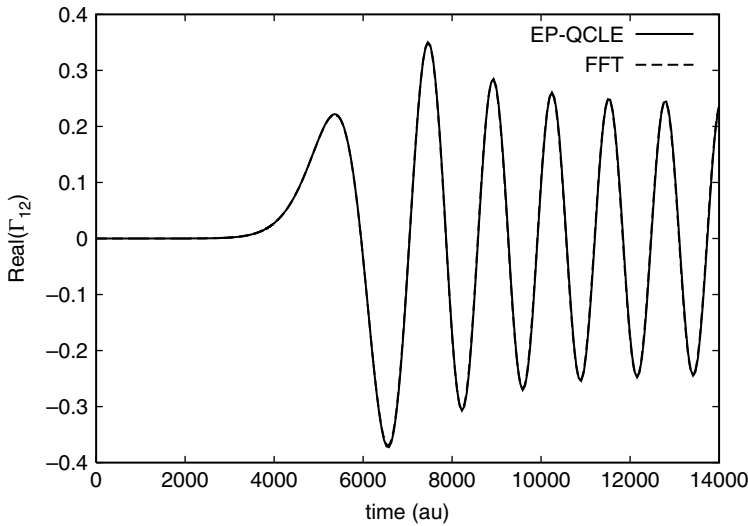


Fig. 3. $\text{Real}(\Gamma_{12})$, the real part of the quantum coherence vs. time.

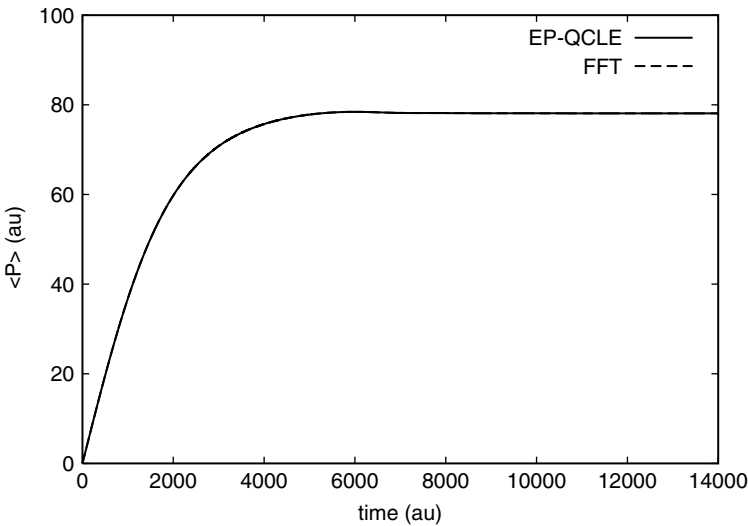


Fig. 4. Momentum vs. time.

surface, between times $t = 4000$ a.u. and $t = 8000$ a.u. about two-thirds of its population shifts from the neutral to ionic state. Figure 3 describes the coherence between the states, which remains large for long times. This is due to the small energy gap at asymptotic distances, as calculations with larger

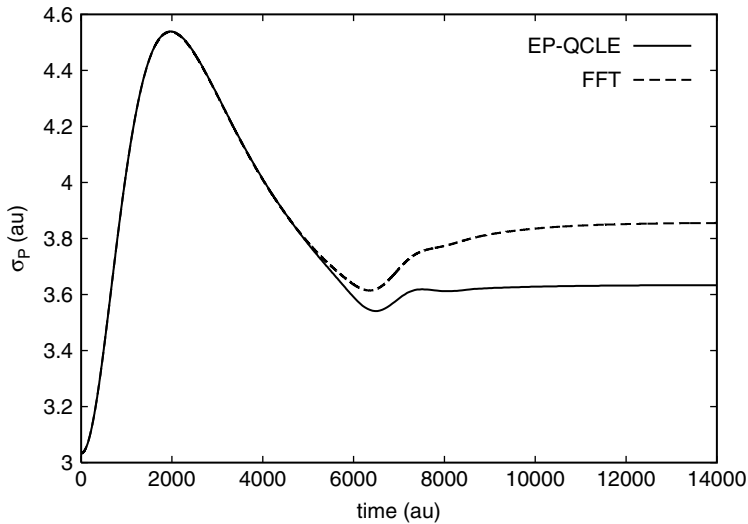


Fig. 5. Momentum dispersion vs. time.

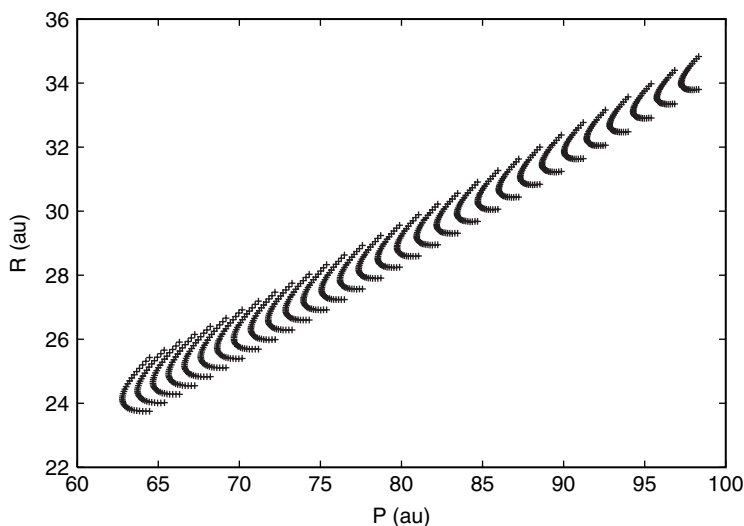


Fig. 6. Final distribution of grid points.

excitation energies lead to more rapidly vanishing coherences. Figure 4 shows the expectation of the momentum increases from $P = 0$ a.u. to about $P = 78$ a.u. by time $t = 6000$ a.u., after which it remains constant. From the population graphs, this reflects the fact that by $t = 6000$ a.u., the Na/surface system has passed halfway through the coupling region, where the mean force on the Na^+ ion quickly vanishes. Figures 1–4 demonstrate the EP-QCLE to be as accurate, to visual resolution, as the full quantal results as far as state-to-state transitions, as well as momentum and position (not shown) expectation values. We see from Fig. 5 that the EP-QCLE calculation of a more demanding observable, the momentum dispersion, deviates from the full quantal results around $t = 6000$ a.u., although the magnitude of this discrepancy is less than 0.3% the magnitude of the momentum in this range. The growing difference at larger times might be attributed to the nature of the EP-QCLE approach, where the asymptotically free ionic and neutral states share the same bundles of trajectories; in the full quantal system, wavepackets on each surface are instead free to propagate independently to infinite distances. Finally, in Fig. 6 we observe the shape of the phase space grid at final time $t = 14,000$ a.u. It is substantially distorted from its initial uniform distribution, and we notice that the points are globally positioned along a straight line in phase space. This reflects the asymptotic state, where each point is subject to a vanishing Hellmann–Feynman force, and thus propagates at constant velocity.

6. REDUCED DENSITY MATRICES FOR DISSIPATIVE DYNAMICS

The extension of the previous treatment to a system in a medium starts from the L–vN equation for $\hat{I}(t)$ to derive the equation of motion of the RDOP $\hat{\rho}$ for the primary (or p-) region, that includes a dissipative term, given by the Liouville superoperator $\hat{\mathcal{L}}_p^{(D)}(t)$. This describes the interaction with a secondary (or s-) region. The PWT is applied only to the p-region so that the quantum and classical Hamiltonians of the previous section refer to the p-region; the s-region is described in terms of its collective motions and a distribution of initial motion amplitudes [9,14].

The dissipative term in the L–vN equation has been derived in several ways. Expressions for the dissipative superoperator $\hat{\mathcal{L}}_p^{(D)}(t)$ can be derived from the dynamics of the s-region, and could therefore be constructed from information about the electronic and atomic structure of this region. Three models of current interest are based on dissipative potentials [14,25], dissipative rate operators [26–29], and a second-order perturbation theory [4,6,30,31,40] with a coupling of p- and s-regions of the bilinear form $\hat{H}_{ps} = \sum_j \hat{A}_p^{(j)} \hat{B}_s^{(j)}$. We develop the PWT treatment in the following, in terms applicable to some of these approaches.

Strong couplings must be expected between p- and s-regions when the latter is activated, for example, by light absorption or atomic collisions, or when there are chemical bonds between atoms in the p- and s-regions. A perturbative treatment for their interaction would not suffice; with this in mind, we will look for solutions to the L–vN equation which can be factorized *after averaging* over the distribution of initial s-region properties, so that the averaged total DOP is

$$\tilde{\hat{I}}(t) = \hat{\rho}(t) \otimes \tilde{\hat{I}}^s(t) \quad (45)$$

at all times, with $\tilde{\hat{I}}^s$ describing the s-region.

To derive an equation for $\hat{\rho}(t)$, we follow the detailed derivation in Ref. [14], which we summarize. The total Hamiltonian is decomposed as $\hat{H} = \hat{F} + \hat{H}_F$, where \hat{F} is a reference SCF Hamiltonian to be defined, and \hat{H}_F is a residual fluctuation coupling. Solving formally the full L–vN equation for the density operator \hat{I} , the solution is replaced in the original differential equation to display energy fluctuation and dissipative memory terms represented by superoperators $\hat{\mathcal{R}}(t)$ and $\hat{\mathcal{M}}(t, t')$, linear and quadratic in the residual coupling \hat{H}_F , respectively. This gives a generalized Langevin equation (GLE) [5,6,33,34], which can be simplified when the s-region can be described as a stochastic medium where fluctuations relax rapidly toward mean values and the delayed portion of the dissipative memory can be neglected. The simplification is done using that

- (i) the fluctuation forces average to zero on the primary time scale, i.e., $\hat{\mathcal{R}}(t)\hat{F}(0) = 0$
- (ii) the memory kernel describes instantaneous dissipation, so that $\hat{\mathcal{M}}(t, t')\hat{F}(t') = \delta(t - t')\hat{\mathcal{W}}(t)\hat{F}(t)$, giving a time-dependent dissipative potential superoperator in the Wigner representation.

It is convenient to make the choice of effective Hamiltonian

$$\hat{F} = \hat{F}_p + \hat{F}_s - \langle\langle \hat{H}_{ps} \rangle\rangle, \quad \hat{F}_p = \hat{H}_p + \hat{G}_p \quad (46)$$

with $\hat{G}_p = \text{Tr}_s[\hat{H}_{ps}\hat{F}^s]$ and $\langle\langle \hat{H}_{ps} \rangle\rangle = \text{Tr}_{ps}[\hat{H}_{ps}\hat{\rho}\hat{F}^s]$, and similarly for the s-operators. This definition leads to $\hat{H}_F = \hat{H}_{ps} - (\hat{G}_p + \hat{G}_s) + \langle\langle \hat{H}_{ps} \rangle\rangle$, a residual coupling due to the non-SCF correlation of motions in the p- and s-regions which averages to zero at all times. The equation for $\hat{\rho}(t)$ is then

$$\partial\hat{\rho}/\partial t = -(i/\hbar)[\hat{F}_p, \hat{\rho}(t)] + \hat{\mathcal{L}}_p^{(D)}\hat{\rho}(t) \quad (47)$$

where $\hat{\mathcal{L}}_p^{(D)} = -\hat{\mathcal{W}}_p(t)/(2\hbar)$ and $\hat{\mathcal{W}}_p(t) = \overline{\text{Tr}_s[\hat{\mathcal{W}}(t)\hat{F}^s(t)]}$ is an instantaneous dissipative potential quadratic in \hat{H}_F , which can be derived from the dynamics of the s-region, and could therefore be constructed from information about the electronic and atomic structure of this region. The dissipative term cannot be written as a commutator of the RDOP with a Hamiltonian, and therefore it is necessary to solve the differential equation directly for the RDOP.

A popular choice for the dissipative superoperator follows from the so-called Lindblad-type expression [26,27], which amounts in our notation to

$$\hat{\mathcal{L}}_p^{(D)}\hat{\rho}(t) = \sum_L \{ \hat{C}_p^{(L)}\hat{\rho}(t)\hat{C}_p^{(L)\dagger} - [\hat{C}_p^{(L)\dagger}\hat{C}_p^{(L)}, \hat{\rho}(t)]_+/2 \} \quad (48)$$

where the $\hat{C}_p^{(L)}$ are operators in the p-region constructed from information about relaxation and decoherence times in the s-region. This form maintains complete positivity and leads to a RDOP $\hat{\rho}(t)$ of constant norm. The operators $\hat{C}_p^{(L)}$ can be constructed as combinations of position and momentum operators in the p-region [35] or from empirical transition rates $k_{\alpha'\leftarrow\alpha}$ between orthonormal eigenstates Φ_α^p and $\Phi_{\alpha'}^p$ of \hat{F}_p [32]. The index L then refers to a given transition $\alpha \rightarrow \alpha'$, and the corresponding operator is $\hat{C}_p^{(L)} = \sqrt{k_{\alpha'\leftarrow\alpha}}|\Phi_{\alpha'}^p\rangle\langle\Phi_\alpha^p|$. This simplifies the form of the Lindblad dissipative rate.

The PWT of the resulting equation of motion can be obtained expressing a product $[\hat{A}\hat{B}\hat{C}]_W$ in terms of each operator PWT, and keeping the first order

in the operator $\hbar\vec{\Lambda}$ so that

$$\begin{aligned} [\hat{A}\hat{B}\hat{C}]_W(P, R) &\simeq \hat{A}_W(P, R)\hat{B}_W(P, R)\hat{C}_W(P, R) \\ &- (i\hbar/2)\{\hat{A}_W(P, R), \hat{B}_W(P, R)\}\hat{C}_W(P, R) \\ &- (i\hbar/2)\hat{A}_W(P, R)\{\hat{B}_W(P, R), \hat{C}_W(P, R)\}. \end{aligned} \quad (49)$$

The resulting equation of motion for $\hat{\rho}_W$ also leads to a new equation for the phase space density γ , after taking the trace over quantum variables.

Alternatively, the equation of motion can be obtained from the PWT Hamiltonian \hat{F}_{pW} , using its eigenstates $|\Phi_I^p(P, R)\rangle$ for quantum states ‘I’ at each phase space point to construct the operators $\hat{C}_p^{(L)}(P, R)$ of the Lindblad expression, with semiempirical rates $k_{J \leftarrow I}(P, R)$. The result is the equation

$$\begin{aligned} \frac{d\hat{\rho}_W}{dt} &= -\frac{i}{\hbar}[\hat{F}_{qu} + \hat{F}_{cq}, \hat{\rho}_W(t)] \\ &- \frac{1}{2} \left\{ \sum_L [\hat{C}_p^{(L)\dagger}(P, R)\hat{C}_p^{(L)}(P, R), \hat{\rho}_W(t)]_+ \right. \\ &\quad \left. - 2\hat{C}_p^{(L)}(P, R)\hat{\rho}_W(t)\hat{C}_p^{(L)\dagger}(P, R) \right\}, \\ \hat{C}_p^{(L)}(P, R) &= \sqrt{k_{J \leftarrow I}(P, R)}|\Phi_I^p(P, R)\rangle\langle\Phi_I^p(P, R)| \end{aligned} \quad (50)$$

which must be solved coupled to the Hamiltonian equations for the quasiclassical variables.

A general procedure for the derivation of dissipative potentials relies on projection operator techniques for the L–vN equation [33,34,36–38]. This has been developed in detail for the case of a medium at equilibrium, and must be modified to account for active media. The results are more general than the SCF results but involve more complicated equations. It introduces a projection superoperator $\hat{\mathcal{P}}_{eq}$ in the Liouville space of density operators. For a bath at equilibrium, with DOp \hat{F}_{eq}^s , the projector is defined by $\hat{F}_p(t) = \hat{\mathcal{P}}_{eq}\hat{F}(t) = \hat{F}^p(t)\hat{F}_{eq}^s/\text{Tr}_s(\hat{F}_{eq}^s)$, where $\hat{F}^p = \text{Tr}_s(\hat{F})$ is as before the RDOP of the p-region, and a complementary projection superoperator is defined by $\hat{\mathcal{Q}}_{eq} = \hat{\mathcal{I}} - \hat{\mathcal{P}}_{eq}$. The projected density operator \hat{F}_p has the factorized form of an SCF approximation, here for a medium at equilibrium, and $\hat{F}_Q(t) = \hat{\mathcal{Q}}_{eq}\hat{F}(t)$ describes correlation corrections. Projecting the L–vN equation with both $\hat{\mathcal{P}}_{eq}$ and $\hat{\mathcal{Q}}_{eq}$, one finds coupled equations of motion for \hat{F}_p and \hat{F}_Q , which can be formally solved to obtain an integrodifferential equation for \hat{F}_p . This has been described in detail, for example in Refs. [33,37,39,40]. This provides a generalization with a non-Markoffian (delayed) dissipative term in the equation for the density operator. It must be followed by a PWT to obtain equations of motion for $\hat{\rho}_W$, which we, however, will not pursue here.

The DM equation for the Lindblad formulation follows along lines similar to the ones mentioned for propagation of the quantum–classical DOP without dissipation. It starts with an expansion of operators in the p-region in terms of a basis set of functions and a discretization of quasiclassical variables in the p-phase space, and leads to a matrix equation which can be written as

$$\begin{aligned} \frac{d\mathbf{\rho}_W}{dt} = & -\frac{i}{\hbar} \left[\mathbf{F}_{qu} + \mathbf{F}_{cq} - i\hbar \left\langle \Phi \left| \frac{d\Phi}{dt} \right\rangle, \mathbf{\rho}_W \right] \\ & - (1/2) \sum_L \{ [\mathbf{C}^{(L)\dagger} \mathbf{C}^{(L)}, \mathbf{\rho}_W]_+ - 2\mathbf{C}^{(L)\dagger} \mathbf{\rho}_W \mathbf{C}^{(L)} \}. \end{aligned} \quad (51)$$

These matrices depend on the initial conditions in phase space, and they must be solved as before on a grid, now constructed in the p-region phase space. The matrix equation is equivalent to a set of coupled linear equations for functions of time, which must be simultaneously integrated with the classical density in phase space, $\gamma(t)$. The propagation of the DM, which generally changes rapidly over time compared to $\gamma(t)$, can again be done with our *relax-and-drive* procedure. This advances time from t_0 to t_1 by first generating a relaxing $\mathbf{\rho}^0(t)$ from $\mathbf{F}(t_0)$ and then correcting it by quadratures to account for the driving term $\Delta\mathbf{F}(t) = \mathbf{F}(t) - \mathbf{F}(t_0)$. Details have been given in Ref. [41].

7. CONCLUSION

A PWT of quasiclassical degrees of freedom provides a rigorous starting point for the treatment of molecular systems with many degrees of freedom. This leads to a convenient numerical procedure to calculate the quantal density operator, when combined with an approximation valid for short wavelengths in phase space. It allows for the introduction of effective potentials to guide the time evolution of quasiclassical trajectories.

The formulation involves a L–vN equation for the quantal density matrix coupled to Hamiltonian equations for quasiclassical trajectories in phase space. The resulting physical picture is one where rapid transitions occur between quantum states, while the phase space more slowly evolves to reflect the coupling of degrees of freedom.

A model has been presented here to illustrate the general approach. This is similar to models used in the near resonant electron transfer of alkali atoms interacting with metal surfaces. It is one of several models introduced in the literature to compare exact results with approximate ones, and we have found that for this model our procedure works very well. The present results are only part of a more thorough study we have undertaken involving other parameters for the system, and also other models with different potentials,

couplings, and crossings, and different initial states and excitation mechanisms [42].

We have also outlined a treatment of systems showing dissipative dynamics. These can be treated with a natural extension of the formulation shown here. The density operator equation differs in a significant way when dissipation is present, because it contains terms which are not derived from a Hamiltonian, and must be written as rates involving superoperators. We have shown here one such situation, with the Lindblad form of the dissipation rate, and other forms can be treated equally well with the present combination of a PWT and a quasiclassical approximation in phase space.

ACKNOWLEDGEMENTS

It is a pleasure to contribute this work in honor of Osvaldo Goscinski, whose elegant theoretical and mathematical treatments have been an inspiration to many of us. The authors acknowledge the financial support of the National Science Foundation of the USA.

REFERENCES

- [1] R. C. Tolman, *The Principles of Statistical Mechanics*, Clarendon Press, Oxford, 1938.
- [2] J. von Neumann, *Mathematical Foundations of Quantum Mechanics*, Princeton University Press, Princeton, NJ, 1955.
- [3] U. Fano, *Rev. Mod. Phys.*, 1957, **29**, 74.
- [4] A. G. Redfield, *Adv. Magn. Reson.*, 1965, **1**, 1.
- [5] K. Blum, *Density Matrix Theory and Applications*, 2nd edn., Plenum Press, New York, 1981.
- [6] C. Cohen-Tannoudji, J. Dupont-Roc and G. Grynberg, *Atom–Photon Interactions*, Wiley, New York, 1992.
- [7] S. Mukamel, *Principles of Nonlinear Optical Spectroscopy*, Oxford University Press, Oxford, 1995.
- [8] D. A. Micha, *J. Phys. Chem.*, 1999, **103**, 7562.
- [9] D. A. Micha and B. Thorndyke, *Int. J. Quantum Chem.*, 2002, **90**, 759.
- [10] M. Hillery, R. F. O’Connell, M. O. Scully and E. P. Wigner, *Phys. Rep.*, 1984, **106**, 121.
- [11] C. C. Martens and J.-Y. Fang, *J. Chem. Phys.*, 1997, **106**, 4918.
- [12] R. Kapral and G. Ciccotti, *J. Chem. Phys.*, 1999, **110**, 8919.
- [13] D. A. Micha, *Adv. Quantum Chem.*, 1999, **35**, 317.
- [14] D. A. Micha, *Int. J. Quantum Chem.*, 2000, **80**, 394.
- [15] D. A. Micha, *Adv. Quantum Chem.*, 2002, **41**, 139.
- [16] E. Q. Feng, D. A. Micha and K. Runge, *Int. J. Quantum Chem.*, 1991, **40**, 545.
- [17] K. Runge, D. A. Micha and E. Q. Feng, *Int. J. Quantum Chem. Symp.*, 1990, **24**, 781.
- [18] A. Donoso and C. C. Martens, *J. Chem. Phys.*, 2000, **112**, 3980.
- [19] C.-C. Wan and J. Schofield, *J. Chem. Phys.*, 2000, **113**, 7047.
- [20] M. Santer, U. Manthe and G. Stock, *J. Chem. Phys.*, 2001, **114**, 2001.
- [21] S.-I. Sawada and H. Metiu, *J. Chem. Phys.*, 1986, **84**, 6293.
- [22] J. M. Cohen and D. A. Micha, *J. Chem. Phys.*, 1992, **97**, 1038.

- [23] M. D. Feit, J. A. Fleck and A. Steiger, *J. Comput. Phys.*, 1982, **47**, 412.
- [24] C. Leforestier, R. Bisseling, C. Cerjan, M. D. Feit and R. Friesner, *J. Comput. Phys.*, 1991, **94**, 59.
- [25] D. Beksic and D. A. Micha, *J. Chem. Phys.*, 1995, **103**, 3795.
- [26] G. Lindblad, *Commun. Math. Phys.*, 1976, **48**, 119.
- [27] V. Gorini, A. Kossakowski and E. C. G. Sudarshan, *J. Math. Phys.*, 1976, **17**, 821.
- [28] K. Kraus, *States, Effects, and Operations*, Springer, New York, 1983.
- [29] R. Alicki and K. Lendi, *Quantum Dynamics Semigroups and Applications*, Springer, New York, 1987.
- [30] S. H. Lin, R. Alden, R. Islampour, H. Ma and A. A. Villaeys, *Density Matrix Methods and Femtosecond Processes*, World Scientific, Singapore, 1991.
- [31] W. T. Pollard and R. A. Friesner, *J. Chem. Phys.*, 1994, **100**, 5054.
- [32] P. Saalfrank and R. Kosloff, *J. Chem. Phys.*, 1996, **105**, 2441.
- [33] R. Kubo, M. Toda and N. Hashitsume, *Statistical Physics II*, 2nd edn., Springer, New York, 1991.
- [34] R. W. Zwanzig, Statistical Mechanics of Irreversibility, in *Lectures in Theoretical Physics* (eds W. E. Brittin, *et al.*), Wiley, New York, 1961, Vol. III, p. 106.
- [35] S. W. Gao, *Phys. Rev. B*, 1998, **57**, 4509.
- [36] B. J. Berne and D. Forster, *Annu. Rev. Phys. Chem.*, 1971, 563.
- [37] J. T. Hynes and J. M. Deutch, in *Physical Chemistry. An Advanced Treatise* (eds H. Eyring, W. Jost and D. Henderson), Nonequilibrium problems – projection operator techniques, Academic Press, New York, 1975, Vol. 11B, p. 729.
- [38] P. O. Lowdin, *Int. J. Quantum Chem.*, 1982, **QCS16**, 485.
- [39] H. Grabert, *Projection Operator Techniques in Nonequilibrium Statistical Mechanics*, Springer, Berlin, 1982.
- [40] V. May and O. Kuhn, *Charge and Energy Transfer Dynamics in Molecular Systems*, Wiley, Berlin, 2000.
- [41] D. A. Micha, *Int. J. Quantum Chem.*, 1994, **51**, 499.
- [42] B. Thorndyke and D. A. Micha, 2004, to be published.

The Generator Coordinate Method for Atomic and Molecular Systems: Revision and Further Developments

Milan Trsic, Wagner F. D. Angelotti and Fábio A. Molfetta

*Instituto de Química de São Carlos, Universidade de São Paulo, CP 780, 13560-970,
São Carlos, SP, Brazil*

Abstract

The generator coordinate method (GCM), as initially formulated in nuclear physics, is briefly described. Emphasis is then given to mathematical aspects and applications to atomic systems. The hydrogen atom Schrödinger equation with a Gaussian trial function is used as a model for former and new analytical, formal and numerical derivations. The discretization technique for the solution of the Hill–Wheeler equation is presented and the generator coordinate Hartree–Fock method and its applications for atoms, molecules, natural orbitals and universal basis sets are reviewed. A connection between the GCM and density functional theory is commented and some initial applications are presented.

Contents

Preface: memories	315
1. Introduction	316
2. The generator coordinate method [3]	317
3. An example of analytical solution for the hydrogen atom [8]	318
4. Further developments for simple systems	319
5. Discretization techniques [12]	323
6. The generator coordinate Hartree–Fock method [10]	323
6.1. Theory	323
6.2. Applications	324
7. A connection between GCM and DFT	326
8. Conclusions	328
Acknowledgements	328
References	329

PREFACE: MEMORIES

I probably first met Osvaldo in 1966 in Abisko, during one of those marvelous Summer Institutes organized by late Per-Olov Löwdin (Pelle

to so many of us). I had my Doctoral degree with Raymond Daudel in Paris in 1966; Daudel was a most considerate and encouraging man and scientist, with deep insight into the foundations of quantum mechanics. I still breathe with the solid concepts from Daudel's teaching. Professor Daudel had been no less than a student of de Broglie (whom I had the privilege to meet personally), one of the men who created quantum mechanics between 1926 and 1930. The Centre de Mecanique Ondulatoire Appliquée, Rue du Maroc, Paris, was created by Daudel and a few other pioneers after the Second World War, with very little resources but with imagination, determination and a solid background in mathematics, chemistry and physics.

On the other hand, Pelle led us to admire (and use) perturbation theory. I was a PD fellow in the Quantum Chemistry Group in Uppsala during 1972–1973. Other than Pelle and Osvaldo, there were other excellent scientists such as Ingve Öhrn, Jean Louis Calais, Erkki Brändas and Sten Lunell, and many, many PDs or visiting scientists; I remember at this moment Vedene Smith and Manuel Berrondo.

My *de facto* scientific interactions in Uppsala were with Osvaldo. We published two papers together [1]. But we had more interactions in personal matters than in science. While about the same age, Osvaldo was more scientifically mature and experienced at that time. He used to be my adviser in many personal matters that I often took to him for his consideration.

Osvaldo and I certainly became friends. We later met many times, in Uppsala, Norway, Florida (where I had also the privilege to meet Professor Slater; I believe he and a few others – Hartree, Fock, Born, Oppenheimer – set the foundations in the 1930s of what we now call quantum chemistry). I remember specially when, in Rio de Janeiro, during the 6th Escola Latinoamericana de Química Teórica in 1988, Osvaldo had very stimulating words on our first results with the generator coordinate method, which I review below.

Milan Trsic

1. INTRODUCTION

The Hartree–Fock (HF) theory [2], at its limit, may provide perhaps 98% of the energy of an atom or molecule. Still, we wish for better, not only in the search of testing quantum mechanics, but also because the ‘small’ 2% error has the magnitude of an ionization potential or an electronic transition.

Several routes are active in the search to recover that missing piece of energy (correlation energy), such as many body perturbation theory (MBPT), density functional theory (DFT) and the variational configuration interaction (CI) method, often at the cost of nontrivial computational efforts.

Wheeler and collaborators [3], in the context of nuclear physics, showed at that time that the limit in the variational procedure potential itself was not reached. Indeed, the Rayleigh–Ritz (RR) variational scheme teaches us how to obtain the best value for a parameter in a trial function, i.e., exponents of Slater (STO) or Gaussian (GTO) type orbital, Roothaan or linear combination of atomic orbitals (LCAO) expansion coefficients and CI coefficients. Instead, the generator coordinate method (GCM) introduces the Hill–Wheeler (HW) equation, an integral transform algorithm capable, in principle, to find the best *functional form* for a given trial function. We present the GCM and the HW equation in Section 2.

On the other hand, as early as 1968, Somorjai [4] had introduced an integral transform method, closely related to GCM, for atomic and molecular systems. An extensive review of this method may be found in Ref. [5]. In this context, accurate correlated functions for two- and three-electron atomic systems were obtained by Thakkar and Smith [6]. Nonetheless, Somorjai used the integration limits of the integral transform as variational parameters. While this was a very innovative option, to some extent it masked the full potential of the HW equation.

It is also worth mentioning that in 1976 a self-consistent GCM was introduced [7] as an improvement over the harmonic approximation in quantum lattice dynamics; applications show an interesting parallelism with the self-consistent random phase approximation.

No doubt, the price to pay for such a powerful tool is high. In Section 3 we show the nontrivial analytical work that was needed to extract from the HW equation the exact 1s function and energy for the hydrogen atom from the deliberately wrong Gaussian trial function [8].

Thus, not surprisingly, applications to nontrivial cases had to rely on either approximations (in nuclear physics, preference was given to the Gaussian overlap approximation [9]) or numerical solutions (see Section 5).

Before discussing atomic and molecular applications, in Section 4 we show some new mathematical findings for simple systems.

In Section 6 we present the GC Hartree–Fock (GCHF) method [10] and review applications to atomic and molecular systems and extensions to relativistic calculations.

Section 7 brings a tentative route for a new application of GCM in junction with DFT, so that ground and excited state energies and wave functions may be generated.

2. THE GENERATOR COORDINATE METHOD [3]

We search the solutions for the Schrödinger equation

$$H(\vec{x})\psi(\vec{x}) = E\psi(\vec{x}) \quad (1)$$

where H is the Hamiltonian operator, E the energy of the system and \vec{x} represents space and spin coordinates. Then, a trial function $\Phi(\vec{x}, \alpha)$ is chosen, where α represents one or several *generator coordinates*. The trial function Φ is generally an approximate solution of equation (1) or the exact solution of a problem similar to equation (1). Next, the GC *ansatz* is built:

$$\psi(\vec{x}) = \int f(\alpha) \Phi(\vec{x}, \alpha) d\alpha. \quad (2)$$

The *weight function* $f(\alpha)$ needs to be determined; we note that if the exact function $f(\alpha)$ is found, then equation (2) is an integral transform leading to the exact function ψ .

The variation of E with reference to f (not α), after a few algebraic steps, leads to the HW equation:

$$\int [H(\alpha, \beta) - ES(\alpha, \beta)] f(\beta) d\beta = 0 \quad (3)$$

where the kernels are defined as

$$H(\alpha, \beta) = \langle \Phi(\vec{x}, \alpha) | \hat{H} | \Phi(\vec{x}, \beta) \rangle = \int d\mathbf{x} \Phi^*(\vec{x}, \alpha) \hat{H} \Phi(\vec{x}, \beta), \quad (4)$$

and

$$S(\alpha, \beta) = \langle \Phi(\vec{x}, \alpha) | \Phi(\vec{x}, \beta) \rangle = \int d\mathbf{x} \Phi^*(\vec{x}, \alpha) \Phi(\vec{x}, \beta). \quad (5)$$

The analytical solution of the HW equation [equation (3)] for many electron atoms and molecules is beyond present mathematical capabilities. There seem to be only a few analytical solutions for the GCM: (a) a solution for the harmonic oscillator [11]; (b) a case in which the weight function was a Heaviside function for the He atom problem [12] and (c) the solution shown below (Section 3).

3. AN EXAMPLE OF ANALYTICAL SOLUTION FOR THE HYDROGEN ATOM [8]

In this mathematical experiment, the trial function was chosen as the (non-normalized) Gaussian

$$\Phi(r, \alpha) = e^{-\alpha r^2}. \quad (6)$$

The calculation of the kernels gives

$$H(\alpha, \beta) = 3\pi^{3/2} \alpha \beta (\alpha + \beta)^{-5/2} - 2\pi(\alpha + \beta)^{-1} \quad (7)$$

and

$$S(\alpha, \beta) = \pi^{3/2}(\alpha + \beta)^{-3/2}. \quad (8)$$

The solution of the HW equation with the kernels above remained elusive for some time [13]. Mohallem and Trsic took advantage of the Laplace transform [14]

$$g(r) = \int_0^\infty e^{-r^2x} G(x) dx \quad (9)$$

with

$$G(x) = \frac{e^{-q^2/4x}}{x^{u+1}} \quad (10)$$

and demonstrated that with the values $q = 1$ and $u = -1/2$ the exact solution for the weight function and the ground state wave function were found

$$e^{-r} = \int_0^\infty f(\alpha) e^{-\alpha r^2} d\alpha \quad (11)$$

with

$$f(\alpha) = \frac{1}{2\sqrt{\pi}} \alpha^{-3/2} e^{-(1/4\alpha)}. \quad (12)$$

The result for the exact ground state energy required some additional effort too. Indeed, the HW equation was then formulated with the exact kernels (7) and (8) and the weight function (12). The change of variables $\beta = \alpha/y$ allowed definite integrable forms (for details see Ref. [8]) and the exact eigenvalue was obtained, $\varepsilon_1 = -1/2$ a.u. It is easy to verify that for $\exp(-\alpha r^2)$ the RR procedure would give the value -0.4243 a.u. for the ground state energy and would not change the functional form.

4. FURTHER DEVELOPMENTS FOR SIMPLE SYSTEMS

The former solution for the hydrogen atom illustrates both the power of the GCM and the mathematical difficulty of its application. Thus, most nuclear, atomic and molecular applications relied on either numerical techniques, approximations, or both. Still, simple systems have always been models for developing new techniques which, when successful, may show new routes for more complicated cases. In this section, we introduce some formal refinements and we continue to rely on the hydrogen atom and the Gaussian function to explore some numerical experiments.

Once the kernels (4) and (5) are calculated, the HW equation (3) becomes an integral equation, from which we should be able to obtain both the weight function and the energy E . Discretization techniques (see Section 5) could be efficient, but alternative mathematical tools should be tested.

Let us first examine where integration by parts could lead. We take that in equation (3) $H(\alpha, \beta)$ and $S(\alpha, \beta)$ are Hermitian and the former as well as $f(\beta)$ belong to class C^1 (meaning basically continuous and that the first derivative exists). Integration by parts of equation (3) gives

$$\begin{aligned} & \int d\beta f(\beta) \frac{\partial}{\partial \beta} [H(\alpha, \beta) - ES(\alpha, \beta)] \\ &= f(\beta)[H(\alpha, \beta) - ES(\alpha, \beta)] - \int d\beta \frac{\partial f(\beta)}{\partial \beta} [H(\alpha, \beta) - ES(\alpha, \beta)] \quad (13) \end{aligned}$$

which we choose to write as

$$\begin{aligned} f(\beta)[H(\alpha, \beta) - ES(\alpha, \beta)] &= \int d\beta f(\beta) \frac{\partial}{\partial \beta} [H(\alpha, \beta) - ES(\alpha, \beta)] \\ &+ \int d\beta \frac{\partial f(\beta)}{\partial \beta} [H(\alpha, \beta) - ES(\alpha, \beta)]. \quad (14) \end{aligned}$$

On the other hand, the derivation of equation (3) leads to

$$\int d\beta \frac{\partial f(\beta)}{\partial \beta} [H(\alpha, \beta) - ES(\alpha, \beta)] + \int d\beta f(\beta) \frac{\partial}{\partial \beta} [H(\alpha, \beta) - ES(\alpha, \beta)] = 0. \quad (15)$$

The comparison of the right-hand side of equations (14) and (15) allows then to obtain $f(\beta)[H(\alpha, \beta) - ES(\alpha, \beta)] = 0$, thus

$$H(\alpha, \beta) - ES(\alpha, \beta) = 0 \quad (16)$$

otherwise the trivial solution $f(\beta) = 0$ would prevail.

Equation (16) may be regarded as the continuous generalization of the secular equation. In fact, in the past we already advocated an intrinsic continuous character of the Roothaan expansion (see Ref. [16b]). Then we may write

$$E = \frac{H(\alpha, \beta)}{S(\alpha, \beta)} \quad (17)$$

with the understanding that $S(\alpha, \beta) \neq 0$ and that E ought to be independent from α and β .

In what follows, we perform a numerical exercise with the same model case described in Section 3.

With equations (7) and (8) for $H(\alpha, \beta)$ and $S(\alpha, \beta)$ we obtain the explicit expression

$$E(\alpha, \beta) = \frac{3\sqrt{\pi}\alpha\beta - 2\alpha(\alpha + \beta)^{1/2} - 2\beta(\alpha + \beta)^{1/2}}{\sqrt{\pi}(\alpha + \beta)}. \quad (18)$$

We plot $E(\alpha, \beta)$ for $\alpha \in (0, 1.0)$ and $\beta \in (0, 1.4)$ in Fig. 1, showing a saddle-like surface. The study of the critical points in Fig. 1 leads to $\alpha_0 = 0.2829421209$ and $\beta_0 = 0.2829421210$, which leads to $E(\alpha_0, \beta_0) = -0.4244131813$. This value is very close to the RR variational value of -0.4243 a.u.

We may further examine equation (18). The previous paragraph indicates that values for α between 0 and 1 produce negative values for the energy. We arbitrarily set $\alpha = 1$ and in Fig. 2 we plot the exact energy $E_n = -1/2n^2$ and $E(1, \beta)$ (a.u.). The similarity between the two curves suggests that not only the ground state energy may be generated by this experiment, but excited state energies as well.

As a continuation of our experiment, we set equation (19), i.e.

$$-\frac{1}{2n^2} = \frac{3\sqrt{\pi}\beta - 2(1 + \beta)^{1/2} - 2\beta(1 + \beta)^{1/2}}{\sqrt{\pi}(1 + \beta)} \quad (19)$$

so we force $E(1, \beta)$ to be equal to the exact expression for the energy. We then scan values of $n = 1, 2, \dots$ and find the respective optimal values of β . These values are used in equation (18) for $E(1, \beta)$ to obtain approximate

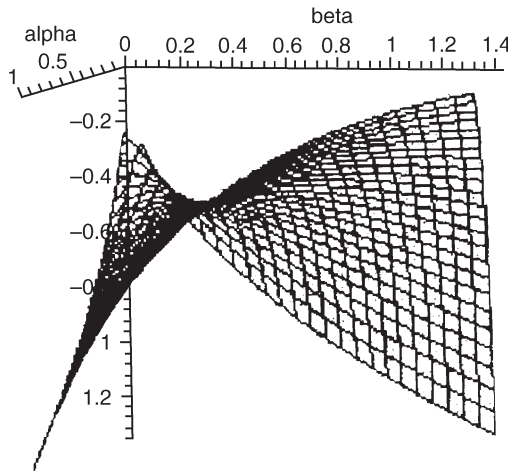


Fig. 1. The $E(\alpha, \beta)$ surface for arbitrary positive values for α and β . Energy in a.u.

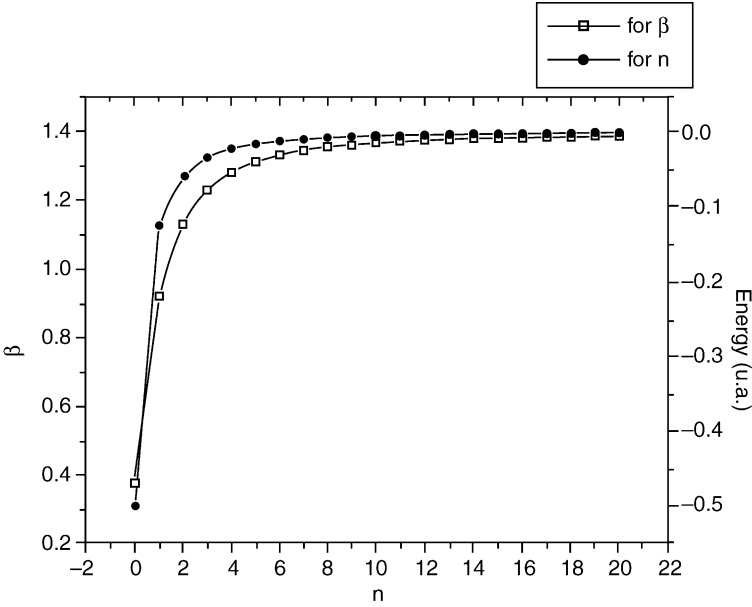


Fig. 2. Plot of $E(1, \beta)$ and E_n for various values of β and n .

eigenvalues for the excited states. We remark that for $n \rightarrow \infty$, β converges to a value of 1.4.

Table 1 shows the values for β and for the eigenvalues. One verifies that the exact and the approximate values are the same for low values of n , while there is some discrepancy for intermediate values.

Table 1. Comparison between exact (E_{exact}) and calculated (E_{calc}) hydrogen atom energies for the ground and the first 11 excited levels

E_{exact} (a.u.)	E_{calc} (a.u.)	β
−0.500000000000	−0.5000000000	0.3795056641
−0.125000000000	−0.1250000000	0.9225340173
−0.055555555556	−0.0555555556	1.128946441
−0.031250000000	−0.0312500000	1.225896227
−0.020000000000	−0.0200000000	1.278060772
−0.013888888889	−0.0138888889	1.308955429
−0.010204081632	−0.0102040816	1.328611873
−0.007812500000	−0.0078125000	1.341829809
−0.006172839506	−0.0061728395	1.351116767
−0.005000000000	−0.0050000000	1.357877624
−0.004132231405	−0.0041322314	1.362945568
−0.003472222222	−0.0034722222	1.366838592

The former mathematical experiment is novel and merits further exploration. The application to two-electron systems is being examined.

5. DISCRETIZATION TECHNIQUES [12]

Probably the first attempt to solve the HW equation by numerical techniques was by Justin et al. [15]. Later, Chattopadhyay et al. [12] discussed in some detail the application of discretization techniques to the integral equations (2) and (3). In that work, various model problems were solved numerically by discretization and some insight into this procedure was provided. Still, at that time the concept of integral discretization (ID) (see Section 6) was not yet introduced, so the conclusions of the authors were somewhat limited with regard to this technique.

6. THE GENERATOR COORDINATE HARTREE-FOCK METHOD [10]

6.1. Theory

During the 1976 Sanibel Symposia, we introduced the GC Hartree-Fock (GCHF) method. This approach is based on choosing as the one-electron function the continuous superpositions

$$\psi_i(1) = \int f_i(\alpha) \varphi_i(1, \alpha) d\alpha, \quad i = 1, \dots, n \quad (20)$$

with φ_i the one-electron generator function, f_i the weight function, and n the size of the basis set. The generator function may be Slater or Gaussian functions (STO or GTO). The use of equation (20) to build the Slater determinant for the many electron wave function and the minimization of the total energy with respect to the generator function leads to the HWHF equation

$$\int [F(\alpha, \beta) - \varepsilon_i S(\alpha, \beta)] f_i(\beta) d\beta = 0 \quad (21)$$

with the kernels $F(\alpha, \beta)$ and $S(\alpha, \beta)$ defined as

$$S(\alpha, \beta) = \langle \varphi_i(1, \alpha) | \varphi_i(1, \beta) \rangle \quad (22)$$

and

$$F(\alpha, \beta) = h(\alpha, \beta) + \sum_j^n [2J_j(\alpha, \beta) - K_j(\alpha, \beta)] \quad (23)$$

where

$$\begin{bmatrix} h(\alpha, \beta) \\ J_j(\alpha, \beta) \\ K_j(\alpha, \beta) \end{bmatrix} = \left\langle \varphi_i(1, \alpha) \left| \begin{array}{c} \hat{h}(1) \\ \hat{J}_j(1) \\ \hat{K}_j(1) \end{array} \right| \varphi_i(1, \beta) \right\rangle. \quad (24)$$

The discretization of the former equation (21) gives

$$\sum_{l=1}^n [F(\alpha_k, \beta_l) - \varepsilon_i S(\alpha_k, \beta_l)] f_i(\beta_l) = 0. \quad (25)$$

The discretization in the first applications for atoms was through the technique called ID [10,16], which includes a relabeling of the generator coordinate space, i.e.

$$\Omega = \frac{\ln \alpha}{A}, \quad A > 1 \quad (26)$$

with A being a scaling factor.

Then the generator coordinate Ω is discretized (for each symmetry) in an equally spaced mesh $\{\Omega_i\}$ so that

$$\Omega_i = \Omega_{\min} + (i - 1)\Delta\Omega, \quad i = 1, \dots, N. \quad (27)$$

In equation (27) N is the number of discretization points, an option which defines the size of the basis set, and $\Delta\Omega$ the numerical integration interval.

6.2. Applications

The very first application of the GCHF method was for the construction of universal atomic basis sets [17], culminating with very accurate Gaussian (GTO) and the construction of Slater (STO) bases for neutral and charged, ground and excited states for atoms H to Xe (see Ref. [18] and references therein). Contracted GTO sets were also introduced [19,20]. The extension of integral transforms other than for 1s functions (Section 3) was also presented [21].

An important point to make on the bases so generated is that the choice of the exponents is not variational, but seeks the best numerical integration of equation (21) [or equation (25)]. We refer to this procedure as ID. This is well

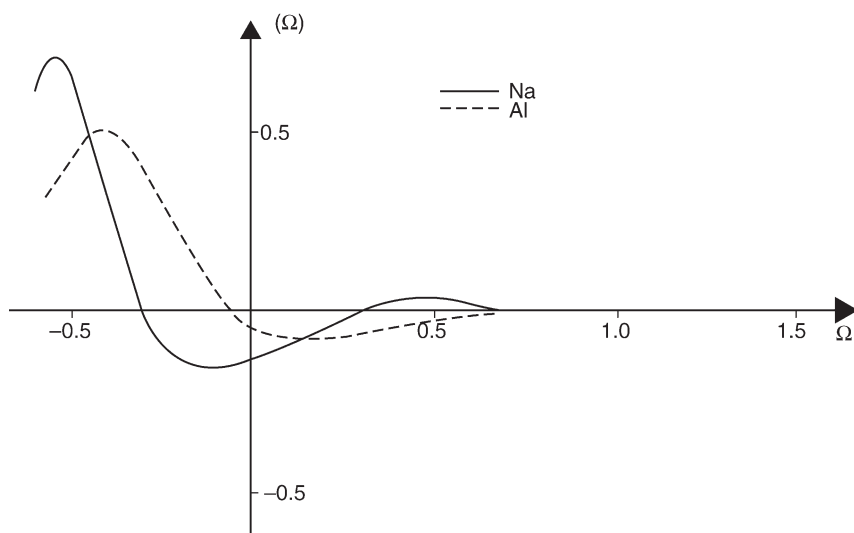


Fig. 3. Weight functions for the 3s and 3p orbitals of Na and Al, respectively. (Reproduced from Ref. [20] with permission of the copyright owner).

illustrated by Fig. 3 (reproduced from Fig. 1 of Ref. [20]). The figure shows the weight functions for the 3s and 3p orbitals of Na and Al, respectively. This kind of plot shows clearly the relevant numerical integration space for the coordinate Ω . Thus, this criterion defines the values of Ω_{\min} and Ω_{\max} , while N (or $\Delta\Omega$) defines the number of basis functions.

Very recently, Barbosa and da Silva [22] proposed a new strategy using polynomial functions for the discretization algorithm of the GCHF method.

A creative application to natural orbitals [23] was also introduced [24] and should certainly deserve further attention in the future.

Other authors adhered to the application of the GCM with ID. A very interesting application was in relativistic HF theory [25], pursued by my collaborator Silva and co-workers (Ref. [26] and references therein). Jorge *et al.* obtained probably the best non-numerical HF energies for the whole Periodic Table with Gaussian functions applying ID segmented for the different s, p, d symmetries [27].

On the other hand, Custodio and co-workers emphasized the optimization of the integration interval within the GCHF method [28], leading to some reminiscence of the work of Somorjai.

Our formulation and first application of GCHF for molecular systems was in 1991 [29]. So far, calculations seem to have been limited to diatomic neutral and charges species (Ref. [30] and references therein). In most of these calculations the HF limit values were obtained.

7. A CONNECTION BETWEEN GCM AND DFT

DFT [31] has gained wide application for the calculation of the electronic energy of atoms and molecules, even being incorporated in currently available computer routines. With this procedure, very accurate energy values are obtained for the ground state, although the extension to excited states is not a trivial task. Moreover, the variety of formulae (and parameters) for the exchange-correlation term (see also Ref. [32]), makes its physics obscure and its meaning elusive.

Very recently, Capelle [33] suggested a connection between GCM and DFT and applied it to the calculation of the ground and excited state energies of two electron atoms. As generator coordinate he used the α constant of the $V_{X\alpha}$ potential of Slater's $X\alpha$ method [34]. This is in fact an extension of the GCM, since in the HW equation the generator coordinate is in the wave function and not in the Hamiltonian. We explore this route, in a preliminary approach to the He atom, with the difference that we employ our previous interpretation for the weight function (see Section 6.2) to gain some insight into the meaning of the α parameter. As early as 1972, Slater raised the point that neither the value $2/3$ nor the value 1 was necessarily optimal.

We initiate a preliminary formulation of this algorithm with a self-consistent field (SCF) HF calculation for the He atom. We first obtain the best HF calculation and then replace the exchange term by Slater's $X\alpha$ potential [34] $V_{X\alpha}$, the simpler expression for DFT, but sufficient for this experiment. We interpret α as the generator coordinate and we weight the exchange-correlation term for different values of the parameter α , i.e.

$$\alpha_i = \alpha_0 + (N - i)\Delta\alpha \quad (28)$$

with $N = 4$, $\alpha_0 = 0.25$ and $\Delta\alpha = 0.25$ in our first experiment.

With the one-electron functions φ_i so generated we construct the determinants

$$\phi_i = |\varphi_i \overline{\varphi_i}|. \quad (29)$$

Table 2. Ground and first excited (1^1S_0 and 2^1S_0) state energies for the He atom (Hartrees)

	E_0	E_1
$N = 4$	-2.903	-2.099
Exact [6]	-2.904	-2.146
Capelle [33]	-2.871	-1.788

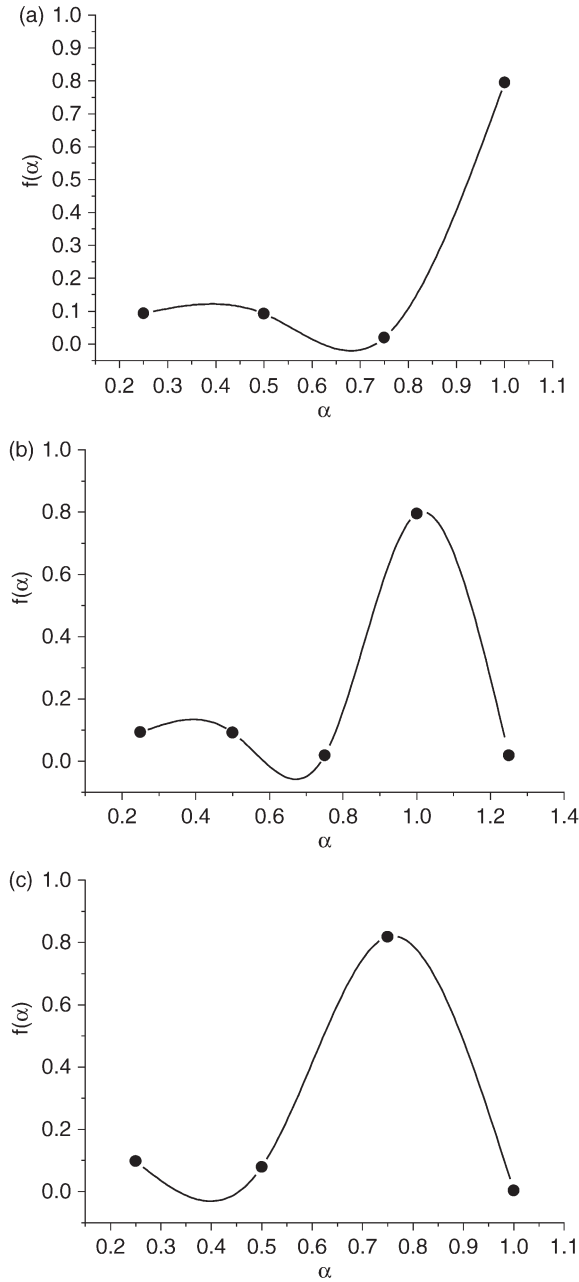


Fig. 4. The weight functions for the ground and the first excited states for the CI calculation for $N = 4$. (a) ground state for $N = 4$ [equation (28)]; (b) ground state for $N = 5$; (c) excited state for $N = 4$.

We then perform a CI calculation leading to the wave function

$$\Psi_0 = \sum C_i |\varphi_i, \overline{\varphi_i}|. \quad (30)$$

Table 2 shows the results for the total energies (E_0 and E_1) for the 1^1S_0 and 2^1S_0 states for $N = 4$.

It is at this point that we bring in the GCM interpretation: thus, we interpret the C_i coefficients (squared) as sample points of a continuous weight function. The behavior of this function (see Section 6.2 and also Ref. [24]) leads us to locate the optimal interval for the α_i values. Figure 4a shows a plot of the weight function for the various values of the α parameter for the 1^1S_0 ground state. One can see that $f(\alpha)$ increases sharply for α close to 1.0. To ensure an understanding of the behavior of this function beyond 1.0 we repeated the calculation for $N = 5$, which shows clearly that values of $\alpha > 1.0$ do not improve the energy values (Fig. 4b). Within the limits of the particular strategy here presented, α values in the region of 1.0 seem optimal for the ground state energy. It may be observed that there is a secondary peak ca. $\alpha = 0.4$ (Figs 4a,b) so that the interval chosen in equation (28) is shown to be efficient.

On the other hand, Fig. 4c shows the shape of the weight function for the excited state, pointing at optimal α values close to 0.7, although in this case also there is a secondary peak for low values of α .

To return to the discussion of Slater in 1972 [34], it seems that, as our results suggest, $\alpha \cong 1.0$ would be best for the ground state, while $\alpha \cong 0.7$ would be indicated for the first excited state with the same symmetry. Perhaps GCM could be an alternative manner to study the exchange-correlation term in DFT.

8. CONCLUSIONS

Certainly, the application of the GCM to atomic, and mainly molecular, systems may gain new perspectives, and GCHF can be further applied, or perhaps surpassed. On the other hand, analytical possibilities, as we show above, could lead to algorithms capable of attaining more complicated situations. Also, the connection with CI and DFT, which we discuss at initial steps, is open to new findings. Perhaps we were able to bring a new perspective to the understanding of the exchange-correlation term in DFT.

ACKNOWLEDGEMENTS

We gratefully acknowledge financial support from the Brazilian agencies CAPES, FAPESP, and CNPq.

REFERENCES

- [1] (a) G. Howat, M. Trsic and O. Goscinski, *Int. J. Quantum Chem.*, 1977, **11**, 283; (b) G. Howat, M. Trsic and O. Goscinski, *Int. J. Quantum Chem.*, 1977, **12**, 963.
- [2] (a) D. R. Hartree, *Proc. Cambridge Philos. Soc.*, 1928, **24**, 89; (b) V. Fock, *Z. Phys.*, 1930, **61**, 126.
- [3] (a) D. L. Hill and J. A. Wheeler, *Phys. Rev.*, 1953, **89**, 1102; (b) J. J. Griffin and J. A. Wheeler, *Phys. Rev.*, 1957, **108**, 311.
- [4] (a) R. L. Somorjai, *Chem. Phys. Lett.*, 1968, **2**, 399; (b) R. L. Somorjai, *Phys. Rev. Lett.*, 1969, **23**, 329.
- [5] D. M. Bishop and B. E. Schneider, *Int. J. Quantum Chem.*, 1975, **9**, 67.
- [6] (a) A. J. Thakkar and V. H. Smith, *Phys. Rev.*, 1977, **A15**, 1; (b) A. J. Thakkar and V. H. Smith, *Phys. Rev.*, 1977, **A15**, 16.
- [7] B. Laskowski and E. Brändas, *Phys. Rev.*, 1976, **C13**, 1741.
- [8] J. R. Mohallem and M. Trsic, *Z. Phys.*, 1985, **A322**, 535.
- [9] (a) J. J. Griffin, *Phys. Rev.*, 1975, **108**, 328; (b) C. C. W. Wong, *Phys. Rev.*, 1975, **108**, 283.
- [10] J. R. Mohallem, R. M. Dreizler and M. Trsic, *Int. J. Quantum Chem. Symp.*, 1986, **20**, 45.
- [11] (a) L. Lathouwers, *Ann. Phys.*, 1976, **102**, 347; (b) L. Lathouwers, P. Van Leuven and M. Bouten, *Chem. Phys. Lett.*, 1977, **52**, 439.
- [12] P. Chattopadhyay, R. M. Dreizler, M. Trsic and M. Fink, *Z. Phys.*, 1978, **A285**, 7.
- [13] (a) L. Lathouwers and P. Van Leuven, *Adv. Chem. Phys.*, 1982, **49**, 115; (b) A. C. Hurley, *Int. J. Quantum Chem. Symp.*, 1967, **1**, 677.
- [14] D. M. Bishop and R. L. Somorjai, *J. Math. Phys.*, 1970, **11**, 1150.
- [15] J. D. Justin, M. D. Mihailovic and M. Rosina, *Nucl. Phys.*, 1971, **A182**, 54.
- [16] (a) J. R. Mohallem, *Z. Phys.*, 1986, **D3**, 339; (b) H. F. M. Dacosta, M. Trsic, A. B. F. da Silva and A. M. Simas, *Eur. Phys. J.*, 1999, **D5**, 375.
- [17] (a) J. R. Mohallem and M. Trsic, *J. Chem. Phys.*, 1987, **86**, 5043; (b) H. F. M. Costa, M. Trsic and J. R. Mohallem, *Mol. Phys.*, 1987, **62**, 91.
- [18] A. B. F. da Silva and M. Trsic, *Can. J. Chem.*, 1996, **74**, 1526.
- [19] J. C. Pinheiro, A. B. F. da Silva and M. Trsic, *J. Mol. Struct. (Theochem)*, 1997, **394**, 107.
- [20] J. C. Pinheiro, A. B. F. da Silva and M. Trsic, *Int. J. Quantum Chem.*, 1997, **63**, 927.
- [21] (a) J. R. Mohallem and M. Trsic, *Int. J. Quantum Chem.*, 1988, **33**, 555; (b) H. F. M. Dacosta, M. Trsic and A. M. Simas, *Int. J. Quantum Chem.*, 1997, **65**, 143.
- [22] R. C. Barbosa and A. B. F. da Silva, *Mol. Phys.*, 2003, **101**, 1073.
- [23] P. O. Löwdin, *Phys. Rev.*, 1955, **97**, 1474.
- [24] H. F. M. Dacosta, A. B. F. da Silva, M. Trsic, A. M. Simas and A. J. A. Aquino, *J. Mol. Struct. (Theochem)*, 1990, **210**, 63.
- [25] Y. Kim, *Phys. Rev.*, 1967, **154**, 17.
- [26] F. E. Jorge, M. T. Barreto and A. B. F. da Silva, *J. Mol. Struct. (Theochem)*, 1999, **394**, 1.
- [27] F. E. Jorge and E. P. Muniz, *Int. J. Quantum Chem.*, 1999, **71**, 307.
- [28] A. S. P. Gómez and R. Custodio, *J. Comp. Chem.*, 2002, **23**, 1007.
- [29] H. F. M. Dacosta, A. B. F. da Silva, J. R. Mohallem, A. M. Simas and M. Trsic, *Chem. Phys.*, 1991, **154**, 379.
- [30] J. C. Pinheiro, M. Trsic and A. B. F. da Silva, *J. Mol. Struct. (Theochem)*, 2001, **539**, 29.
- [31] (a) R. M. Dreizler and E. K. U. Gross, *Density Functional Theory: An Approach to the Quantum Many-Body Problem*, Springer, Berlin, 1990; (b) E. S. Kryachko and E. V. Ludeña, *Energy Density Functional Theory of Many-Electron Systems*, Kluwer Academic, Dordrecht, 1990.
- [32] F. Jensen, *Introduction to Computational Chemistry*, Wiley, Chichester, 1999.
- [33] K. Capelle, *J. Chem. Phys.*, 2003, **119**, 1285.
- [34] J. C. Slater, *Adv. Quantum Chem.*, 1972, **6**, 1.

This page intentionally left blank

Hybrid Quantum/Classical Dynamics Using Bohmian Trajectories

E. Gindensperger, C. Meier and J. A. Beswick

LCAR-IRSAMC, Université Paul Sabatier, Toulouse, France

Abstract

The mixed quantum-classical Bohmian (MQCB) method introduced by Gindensperger, Meier and Beswick [J. Chem. Phys. 113 (2000) 9369] is presented, together with a full derivation of the working equations and their basic properties. It is shown that this approximative method combining quantum and classical dynamics can be derived in a rigorous way from the hydrodynamic formulation of quantum mechanics. The quantum subsystem is described by a wave packet depending on the quantum variables and, *via* the total potential energy of the system, parametrically on the classical trajectories. The wave packet provides de Broglie–Bohm *quantum trajectories* which are used to calculate the force acting on the classical variables. An example of application of the method to a five-dimensional molecule–surface scattering process is presented together with a comparison with full quantum results.

Contents

1. Introduction	332
2. De Broglie–Bohm formulation of quantum mechanics	333
3. From the de Broglie–Bohm formulation to the MQCB method	334
3.1. Derivations of the working equations	334
3.2. Summary of the MQCB equations, initial conditions and basis set representations	337
3.2.1. Adiabatic basis for the quantum problem	338
3.2.2. Diabatic basis for the quantum problem	338
4. Structure of the MQCB equations: initial conditions, reversibility and observables	339
5. An illustrative example: molecule–surface scattering	340
5.1. The MQCB equations	340
5.2. Initial conditions	341
5.3. Observables: diffraction probabilities and rotational energy transfer	342
5.4. Results on the N ₂ /LiF(001) molecule–surface scattering	343
5.4.1. Diffraction probabilities	343
5.4.2. Average rotational energy transfer	343
6. Conclusions	345
Acknowledgements	346
References	346

1. INTRODUCTION

The dynamics of systems containing a large number of degrees of freedom is one of the challenges in contemporary theoretical chemistry. In molecular, condensed phase or surface physics and chemistry, one is often confronted to model processes involving many degrees of freedom some of which have to be treated quantum mechanically. These include proton and electron transfer in isolated polyatomic molecules, liquids, interfaces and biological systems, intramolecular energy redistribution and unimolecular fragmentation, as well as interactions of atoms and molecules with surfaces [1].

In many systems comprising a large number of particles, even though a detailed quantum treatment of all degrees of freedom is not necessary, there may exist subsets that have to be treated quantum mechanically under the influence of the rest of the system. If the typical timescales between system and bath dynamics are very different, Markovian models of quantum dissipation can successfully mimic the influence of the bath onto the system dynamics [2]. However, in the femtosecond regime studied with ultrashort laser pulses, the so-called Markov approximation is not generally valid [3]. Furthermore, very often the bath operators are assumed to be of a special form (harmonic, for instance) which are sometimes not realistic enough.

To perform full quantum mechanical wave packet propagations in several degrees of freedom the multiconfiguration time-dependent Hartree (MCTDH) method [4,5] has proven to be a unique and particularly efficient tool. However, to treat even larger systems like liquids, interfaces or biological systems, a full quantum treatment is still out of reach. In these cases, it is necessary to rest on hybrid quantum/classical schemes in which only the essential degrees of freedom are treated quantum mechanically while all others are described classically. The most popular of these mixed quantum/classical methods are the mean-field approximation [6] and the surface hopping trajectories [7]. In the mean-field treatment, the force for the classical motion is calculated by averaging over the quantum wavefunction. In the surface hopping scheme, the classical trajectories move according to a force derived from a *single quantum state* with the possibility of transitions to other states.

Recently [8–11] an alternative treatment to mix quantum mechanics with classical mechanics, based on Bohmian quantum trajectories was proposed. Briefly, the quantum subsystem is described by a time-dependent Schrödinger equation that depends parametrically on classical variables. This is similar to other approaches discussed above. The difference comes from the way the classical trajectories are calculated. In our approach, which was called mixed quantum-classical Bohmian (MQCB) trajectories, the wave packet is used to define de Broglie–Bohm quantum *trajectories* [12] which in turn are used to calculate the force acting on the classical variables.

Recently, there has been a renewed interest in the de Broglie–Bohm formulation of quantum mechanics as a numerical tool to perform multidimensional wave packet calculations [13–15]. It has also been used to visualize the motion of quantum mechanical wave packets by trajectories and to study the transition from quantum mechanics to classical mechanics [16–18]. Carlsen and Goscinski [16], for instance, have studied fractional and full revivals of circular Rydberg wave packets in the hydrogen atoms using this formulation.

In what follows we shall show that the de Broglie–Bohm formulation can also be used to establish a hybrid quantum/classical scheme to treat the dynamics of systems with a large number of degrees of freedom in which a few need to be described quantum mechanically.

2. DE BROGLIE–BOHM FORMULATION OF QUANTUM MECHANICS

Since the method to mix quantum and classical mechanics to be presented can be considered as an approximate method derived from the de Broglie–Bohm formulation of quantum mechanics, this completely equivalent perspective of quantum mechanics will be briefly reviewed. To this end, we consider a two-dimensional Hilbert space.

Note that considering two dimensions is no restriction to what will be shown below, actually, x, X can be viewed as *collective variables* one of which will comprise all quantum degrees of freedom while the other all classical ones. Writing the wavefunction as $\psi(x, X, t) = R(x, X, t) \exp(iS(x, X, t)/\hbar)$, with R, S being real, the Schrödinger equation can be recast in terms of a continuity equation,

$$\frac{\partial R^2}{\partial t} + \frac{1}{m} \frac{\partial S}{\partial x} \frac{\partial R^2}{\partial x} + \frac{1}{M} \frac{\partial S}{\partial X} \frac{\partial R^2}{\partial X} = -R^2 \left(\frac{1}{m} \frac{\partial^2 S}{\partial x^2} + \frac{1}{M} \frac{\partial^2 S}{\partial X^2} \right) \quad (1)$$

and a quantum Hamilton–Jacobi equation

$$\frac{\partial S}{\partial t} + \frac{1}{2m} \left(\frac{\partial S}{\partial x} \right)^2 + \frac{1}{2M} \left(\frac{\partial S}{\partial X} \right)^2 + V(x, X) + Q(x, X, t) = 0 \quad (2)$$

where $Q(x, X, t)$ is the so-called *quantum potential* [12]

$$Q(x, X, t) = -\frac{\hbar^2}{2m} \frac{1}{R} \frac{\partial^2 R}{\partial x^2} - \frac{\hbar^2}{2M} \frac{1}{R} \frac{\partial^2 R}{\partial X^2} \quad (3)$$

Hence one sees that the phase of $\psi(x, X, t)$ can be viewed as an action function, a solution to the Hamilton–Jacobi equation with an additional

potential term, the quantum potential. This observation led to the definition of *trajectories* $(\mathbf{x}(t), \mathbf{X}(t))$ [12], the conjugate momenta of which are given by the derivative of $S(x, X, t)$:

$$\mathbf{p} = m\dot{\mathbf{x}} = \left. \frac{\partial S}{\partial \mathbf{x}} \right|_{\mathbf{x}=\mathbf{x}(t), X=\mathbf{X}(t)}, \quad \dot{\mathbf{p}} = -\frac{\partial}{\partial \mathbf{x}}(V + Q) \quad (4)$$

$$\mathbf{P} = M\dot{\mathbf{X}} = \left. \frac{\partial S}{\partial \mathbf{X}} \right|_{\mathbf{x}=\mathbf{x}(t), X=\mathbf{X}(t)}, \quad \dot{\mathbf{P}} = -\frac{\partial}{\partial \mathbf{X}}(V + Q) \quad (5)$$

Thus, within the Bohmian formulation of quantum mechanics, *quantum trajectories* move according to the usual Hamilton's equations, subject to the additional quantum potential defined in equation (3). An ensemble of *quantum particles* at positions $(\mathbf{x}(t), \mathbf{X}(t))$ distributed initially according to

$$P([x, x + dx]; [X, X + dX]) = |\psi_0(x, X)|^2 dx dX \quad (6)$$

and propagated alongside using equations (4) and (5), will represent the probability distribution of the quantum mechanical wavefunction at any time [12].

From equations (4) and (5) one sees that whenever the additional force due to the quantum potential is negligible, one has a purely classical motion. Thus, the limit from quantum theory to classical mechanics appears naturally within this theory.

3. FROM THE DE BROGLIE–BOHM FORMULATION TO THE MQCB METHOD

3.1. Derivations of the working equations

In order to establish the mixed quantum-classical method based on Bohmian trajectories (MQCB) [8], we take the same approach as in the de Broglie–Bohm formulation of quantum mechanics, as detailed above. Hence we start from the same, full-dimensional initial wavefunction $\psi_0(x, X)$ alongside with an ensemble of trajectories at initial positions $(\mathbf{x}(t=0), \mathbf{X}(t=0))$ distributed according to $R^2(x, X, t=0) = |\psi_0(x, X)|^2$. After taking derivatives with respect to x and X of equation (2), we neglect the term involving the second derivative of S with respect to X . In addition, we neglect the second derivative of S with respect to X in equation (1) and the second derivative of R with respect to X in equation (3). Considering the simplest case of a free two-dimensional Gaussian wave packet, one sees that these terms describe the dispersion in X -direction. In the limit of large M the wave packet behaves classically and does *not* show much dispersion in the X -direction. Hence, neglecting these terms should be a good approximation

to the real quantum dynamics. In this sense, X will from now on be called the *classical* degrees of freedom. Note that this approximation cannot be made in the original Schrödinger equation (equation (1)) but *only* in the equations for the amplitude and phase! We then have from equation (1)

$$\frac{\partial \tilde{R}^2}{\partial t} + \frac{\partial}{\partial x} \left(\tilde{R}^2 \frac{1}{m} \frac{\partial \tilde{S}}{\partial x} \right) + \frac{1}{M} \frac{\partial \tilde{S}}{\partial X} \frac{\partial \tilde{R}^2}{\partial X} = 0 \quad (7)$$

and from equation (2)

$$\begin{aligned} \frac{\partial}{\partial t} \left(\frac{\partial \tilde{S}}{\partial x} \right) + \left(\frac{1}{m} \frac{\partial \tilde{S}}{\partial x} \right) \left(\frac{\partial^2 \tilde{S}}{\partial x^2} \right) + \left(\frac{1}{M} \frac{\partial \tilde{S}}{\partial X} \right) \left(\frac{\partial^2 \tilde{S}}{\partial x \partial X} \right) \\ = - \frac{\partial}{\partial x} (V + \tilde{Q}) \end{aligned} \quad (8)$$

$$\frac{\partial}{\partial t} \left(\frac{\partial \tilde{S}}{\partial X} \right) + \left(\frac{1}{m} \frac{\partial \tilde{S}}{\partial x} \right) \left(\frac{\partial^2 \tilde{S}}{\partial X \partial x} \right) = - \frac{\partial}{\partial X} (V + \tilde{Q}) \quad (9)$$

where $\tilde{Q} = -(\hbar^2/2m\tilde{R})\partial^2\tilde{R}/\partial x^2$ and tilde quantities stand for the approximate solutions. As in the usual hydrodynamic formulation detailed above, the Bohmian trajectories associated with these approximate equations are

$$\mathbf{p} = m\dot{\mathbf{x}} = \left. \frac{\partial \tilde{S}}{\partial \mathbf{x}} \right|_{x=\mathbf{x}(t), X=\mathbf{X}(t)} \quad (10)$$

$$\mathbf{P} = M\dot{\mathbf{X}} = \left. \frac{\partial \tilde{S}}{\partial \mathbf{X}} \right|_{x=\mathbf{x}(t), X=\mathbf{X}(t)} \quad (11)$$

together with the *same initial conditions* as in the hydrodynamic formulation of quantum mechanics. This does not pose any problem, since within the MQCB method, the full-dimensional initial wavefunction is supposed to be known. Hence, the initial values ($\mathbf{x}(t=0)$, $\mathbf{X}(t=0)$) are chosen according to the distribution as above:

$$P([x, x + dx]; [X, X + dX]) = |\psi_0(x, X)|^2 dx dX \quad (12)$$

The next step consists in evaluating equations (7) and (8) at $X = \mathbf{X}(t)$. Using equation (11) one gets

$$\frac{d\tilde{R}^2}{dt} + \frac{\partial}{\partial x} \left(\tilde{R}^2 \frac{1}{m} \frac{\partial \tilde{S}}{\partial x} \right) = 0 \quad (13)$$

$$\frac{d}{dt} \left(\frac{\partial \tilde{S}}{\partial x} \right) + \left(\frac{1}{m} \frac{\partial \tilde{S}}{\partial x} \right) \left(\frac{\partial^2 \tilde{S}}{\partial x^2} \right) = - \frac{\partial}{\partial x} (V + \tilde{Q}) \quad (14)$$

where d/dt stands for $d\tilde{f}/dt = \partial\tilde{f}/\partial t + \dot{\mathbf{X}} \cdot (\partial\tilde{f}/\partial \mathbf{X})_{X=\mathbf{X}(t)}$.

The important observation at this point is that equations (13) and (14) are rigorously equivalent to a quantum problem in the x subspace with \mathbf{X} being a time-dependent parameter. Thus, the approximate wavefunction $\tilde{\psi}(x, \mathbf{X}(t), t) = \tilde{R}(x, \mathbf{X}(t), t) \exp(i\tilde{S}(x, \mathbf{X}(t), t)/\hbar)$ obeys the Schrödinger equation

$$i\hbar \frac{d\tilde{\psi}(x, \mathbf{X}(t), t)}{dt} = \left(-\frac{\hbar^2}{2m} \frac{\partial^2}{\partial x^2} + V(x, \mathbf{X}(t)) \right) \tilde{\psi}(x, \mathbf{X}(t), t) \quad (15)$$

Note the appearance of the total derivative in the left-hand side of this equation. As it will be shown below, this is important when an adiabatic basis set is used for solving the quantum problem. Since we have only approximated the *equations of motion* and supposed that the initial wavefunction $\psi_0(x, X)$ is known, we have

$$\tilde{\psi}(x, \mathbf{X}(t=0), t=0) = \psi_0(x, X) \Big|_{X=\mathbf{X}(t=0)} \quad (16)$$

as the initial wavefunction in the quantum subspace.

A consistent equation of motion for the classical degrees of freedom is obtained by taking the total derivative with respect to time of equation (11). Noting that this leads to a term $(1/M)(\partial^2 S/\partial X^2)$ which we assumed to be small we can use equation (9) to give

$$\dot{\mathbf{P}} = -\frac{1}{M} \frac{\partial(V(x, X) + \tilde{Q}(x, X))}{\partial X} \Big|_{x=\mathbf{x}(t), X=\mathbf{X}(t)} \quad (17)$$

The fact that at this level of approximation, the quantum potential corresponding to the quantum subsystem remains in the classical equation of motion, is somewhat reminiscent of the Pechukas' force in the surface hopping method [7]. In both the cases, the classical degrees of freedom are directly affected by changes in the quantum subspace. In practice, however, for most of the cases considered so far, we additionally neglect the quantum potential in the classical degrees of freedom. At this level of approximation, the MQCB method is identical to the one proposed independently by Prezhdo *et al.* [9,19,20].

Equation (17), together with equations (10) and (15) provide the working equations of the MQCB method. According to their structure, the position of the classical degrees of freedom, its momentum, the position of the Bohmian particle and the wavefunction in the quantum subspace need to be propagated simultaneously. For clarity, these quantities shall be combined as

$$\Gamma(t) = (\tilde{\psi}(x, \mathbf{X}(t), t), \mathbf{x}(t), \mathbf{X}(t), \mathbf{P}(t)) \quad (18)$$

Note that if one expands $\tilde{\psi}(x, \mathbf{X}(t), t)$ in a basis set, the MQCB equations simply form a set of coupled, first-order ordinary differential equations and $\Gamma(t)$ is a vector of complex numbers, containing the classical position and

momentum, the quantum trajectory and the expansion coefficients of the subspace wavefunction.

3.2. Summary of the MQCB equations, initial conditions and basis set representations

This section gives a concise summary of the working equations of the MQCB method, consisting of the differential equations together with the corresponding initial conditions. As stated above, in order to set up a MQCB calculation, the full-dimensional initial wavefunction $\psi_0(x, X)$ needs to be known. Depending on the physical situation, this can either be a simple asymptotic form or it needs to be calculated or approximated with other techniques like diffusion Monte Carlo or multidimensional relaxation methods for ground states.

First, the initial positions of both the *classical* as well as the *quantum degrees of freedom* $\mathbf{x}(t=0)$ and $\mathbf{X}(t=0)$ are sampled from this full-dimensional initial wavefunction $\psi_0(x, X)$ according to

$$P([x, x + dx]; [X, X + dX]) = |\psi_0(x, X)|^2 dx dX \quad (19)$$

The initial wavefunction $\psi_0(x, X)$ also determines the remaining quantities $\tilde{\psi}(x, \mathbf{X}(t=0), t=0)$ and $\mathbf{P}(t=0)$ of the initial vector $\Gamma(t=0)$:

$$\begin{aligned} \mathbf{P}(t=0) &= \frac{\hbar}{M} \text{Im} \left(\frac{1}{\psi_0(x, X)} \frac{\partial \psi_0(x, X)}{\partial x} \right)_{x=\mathbf{x}(t=0), X=\mathbf{X}(t=0)} \\ \tilde{\psi}(x, \mathbf{X}(t=0), t=0) &= \psi_0(x, X)|_{X=\mathbf{X}(t=0)} \end{aligned} \quad (20)$$

These quantities form the initial vector

$$\Gamma(t=0) = (\tilde{\psi}(x, \mathbf{X}(t=0), t=0), \mathbf{x}(t=0), \mathbf{X}(t=0), \mathbf{P}(t=0)) \quad (21)$$

which is then propagated according to the MQCB equations:

$$i\hbar \frac{d\tilde{\psi}(x, \mathbf{X}(t), t)}{dt} = \left(-\frac{\hbar^2}{2m} \frac{\partial^2}{\partial x^2} + V(x, \mathbf{X}(t)) \right) \tilde{\psi}(x, \mathbf{X}(t), t) \quad (22)$$

$$\dot{\mathbf{x}} = \frac{\hbar}{m} \text{Im} \left(\frac{1}{\tilde{\psi}(x, \mathbf{X}(t), t)} \frac{\partial \tilde{\psi}(x, \mathbf{X}(t), t)}{\partial x} \right)_{x=\mathbf{x}(t)} \quad (23)$$

$$\dot{\mathbf{X}} = \frac{\mathbf{P}}{M}, \quad \dot{\mathbf{P}} = -\frac{1}{M} \frac{\partial (V(x, X) + \tilde{Q}(x, X))}{\partial X} \bigg|_{x=\mathbf{x}(t), X=\mathbf{X}(t)} \quad (24)$$

The MQCB equations need to be solved simultaneously. To this end, the quantum subspace wavefunction can be propagated with any standard propagator that can handle explicit time-dependent Hamiltonians.

A complete simulation consists of a large number of such propagations with different $\mathbf{x}(0)$ and $\mathbf{X}(0)$ in order to represent the probability distribution given by the full-dimensional initial wavefunction.

Very often, diabatic or adiabatic basis sets are very useful, because in these cases, the MQCB equations can be recast in a set of first-order ODE, that are conveniently integrated by any standard integrator.

3.2.1. Adiabatic basis for the quantum problem

An adiabatic basis set can be defined as eigenfunctions of the quantum subspace Hamiltonian for fixed X :

$$\left(-\frac{\hbar^2}{2m}\frac{\partial^2}{\partial x^2} + V(x, X)\right)\phi_k^{(a)}(x; X) = E_k(X)\phi_k^{(a)}(x; X), \quad k = 1, N \quad (25)$$

Hence, the subsystem wavefunction can be expressed as

$$\tilde{\psi}(x, \mathbf{X}(t), t) = \sum_k c_k(t) \phi_k^{(a)}(x; \mathbf{X}(t)) \quad (26)$$

Noting that $d\tilde{f}/dt = \partial\tilde{f}/\partial t + \dot{X}(\partial\tilde{f}/\partial X)_{X=\mathbf{X}(t)}$, equation (22) takes the form:

$$\dot{c}_k = -\frac{i}{\hbar} E_k(\mathbf{X}) c_k - \dot{\mathbf{X}} \sum_{l=1}^N d_{kl}(\mathbf{X}) c_l, \quad k = 1, N \quad (27)$$

with the non-adiabatic coupling elements

$$d_{kl}(X) = \int dx \phi_k^{(a)*}(x; X) \frac{\partial \phi_l^{(a)}(x; X)}{\partial X} \quad (28)$$

This system of equations replace equation (22), and together with equations (23) and (24) we see that the MQCB equations are now a set of first-order ODE.

3.2.2. Diabatic basis for the quantum problem

A diabatic basis set can be defined as eigenfunctions of the quantum subspace Hamiltonian for one fixed value X_0 :

$$\left(-\frac{\hbar^2}{2m}\frac{\partial^2}{\partial x^2} + V(x, X_0)\right)\phi_k^{(d)}(x; X_0) = E_k(X_0)\phi_k^{(d)}(x; X_0), \quad k = 1, N \quad (29)$$

Hence the subsystem wavefunction can be expressed as

$$\tilde{\psi}(x, \mathbf{X}(t), t) = \sum_k c_k(t) \phi_k^{(d)}(x; X_0) \quad (30)$$

Equation (22) is then equivalent to

$$\dot{c}_k = -\frac{i}{\hbar} E_k(X_0) c_k - \frac{i}{\hbar} \sum_{l=1}^N p_{kl}(\mathbf{X}) c_l, \quad k = 1, N \quad (31)$$

with the potential coupling elements

$$p_{kl}(X) = \int dx \phi_k^{(d)*}(x; X_0) (V(x, X) - V(x, X_0)) \phi_l^{(d)}(x; X_0) \quad (32)$$

Together with equations (23) and (24) we see that the MQCB equations are again a set of first-order ODE.

4. STRUCTURE OF THE MQCB EQUATIONS: INITIAL CONDITIONS, REVERSIBILITY AND OBSERVABLES

The mathematical structure of the four MQCB equations (22–24) is such that the time evolution of the combined quantities $\Gamma(t)$ is uniquely determined by the MQCB equations, and reversibility is given in a strict mathematical sense. Upon propagation $\Gamma(0) \rightarrow \Gamma(t)$, changing $\partial/\partial t \rightarrow -\partial/\partial t$ and $\dot{\mathbf{X}}(t) \rightarrow -\dot{\mathbf{X}}(t)$ propagates the state $\Gamma(t)$ backwards to yield the same initial state: $\Gamma(t) \rightarrow \Gamma(0)$.

This simple *mathematical* structure of the quantities $\Gamma(t)$ together with the MQCB equations also need to be connected to *physical* quantities. For the initial conditions, we have shown above that $\Gamma(0)$ can be chosen in a consistent and physically sound way if the full-dimensional initial wavefunction is known.

However, due to the approximate nature of the MQCB equations, the full-dimensional wave packet is in general *not* known at later times. In this sense, the time zero is a special time at which, due to the physical situation considered, the full-dimensional wave packet must be known. However, this is not a severe restriction, since in many physically relevant situations the initial state is either a known asymptotic state like in all collisional processes or an eigenfunction (often the ground state).

The second point is to use the mathematical objects $\Gamma(t)$ to calculate physically measurable observables. Even though the definition of observables is not unique within the MQCB scheme, in all cases considered so far, we use

$$\langle A \rangle = \sum_i \left\langle \tilde{\psi}_i \left| A \left(x, \frac{\partial}{\partial x}, \mathbf{X}_i, \mathbf{P}_i \right) \right| \tilde{\psi}_i \right\rangle \quad (33)$$

where the sum runs over all initially sampled trajectories. Due to the approximate nature of the propagations, the observables obtained by

the MQCB method are approximate as well. In particular, as compared to a full-quantum wave packet calculation, the total energy is not a rigorously conserved quantity.

5. AN ILLUSTRATIVE EXAMPLE: MOLECULE–SURFACE SCATTERING

In this section, we want to illustrate the general methodology by giving a detailed step-by-step outline of a typical MQCB calculation. The five-dimensional model chosen corresponds to molecular diffractive rotational scattering of N_2 from a LiF(001) surface. This problem still allows for a full quantum treatment and thus the MQCB results can be compared to reference calculations [11]. The interaction potential was chosen to be the dumbbell model initially proposed by Gerber *et al.* [21]. Although this is a model surface, it nevertheless has the same features of a realistic surface, in particular a two-dimensional corrugation with periodicity a . We considered energies up to 300 meV. Since at this energies, the first vibrational channel is closed, we approximate the diatomic as a rigid rotator, i.e., keep r fixed. Hence the Hamiltonian reads as

$$H(\mathbf{R}, \theta, \varphi) = \frac{\mathbf{P}_R^2}{2M} + \frac{\hbar^2 \mathbf{J}^2}{2\mu r^2} + V(\mathbf{R}, \theta, \varphi) \quad (34)$$

where M and μ are the total and reduced masses of N_2 , respectively. In this expression, \mathbf{P}_R is the total momentum of the center of mass of N_2 and \mathbf{J} its angular momentum.

5.1. The MQCB equations

The process we are interested in is the rotational energy transfer during the collision as well as the diffraction of the diatomic from the surface that exhibits a two-dimensional corrugation. Since the diffraction is a quantum effect, we treat the whole system classically except for the directions X and Y parallel to the surface. The separation of the total Hamiltonian into a classical and quantum part reads as follows:

$$H(X, Y, Z, \theta, \varphi) = T_q(X, Y) + T_{cl}(Z, \theta, \varphi) + V(X, Y, Z, r, \theta, \varphi) \quad (35)$$

$$T_q(X, Y) = -\frac{\hbar^2}{2M} \frac{\partial^2}{\partial X^2} - \frac{\hbar^2}{2M} \frac{\partial^2}{\partial Y^2}, \quad T_{cl}(Z, \theta, \varphi) = \frac{\mathbf{P}_Z^2}{2M} + \frac{\hbar^2 \mathbf{J}^2}{2\mu r^2} \quad (36)$$

The MQCB equations for this problem are thus given by the Schrödinger equation in the (X, Y) subspace for $\tilde{\psi}(X, Y, \mathbf{q}_\alpha(t), t)$ that depends parametrically on the classical variables $\mathbf{q}_\alpha(t) = \mathbf{Z}(t), \boldsymbol{\theta}(t), \boldsymbol{\varphi}(t)$, the corresponding

equations for the quantum trajectories, as well as Hamilton's equations for the classical degrees of freedom and their conjugate momenta (as explained in Section 2, we have additionally neglected the term \tilde{Q} in the MQCB equations):

$$i\hbar \frac{d\tilde{\psi}}{dt} = \left(-\frac{\hbar^2}{2M} \frac{\partial^2}{\partial X^2} - \frac{\hbar^2}{2M} \frac{\partial^2}{\partial Y^2} + V(X, Y, \mathbf{q}_\alpha(t)) \right) \tilde{\psi} \quad (37)$$

$$\dot{\mathbf{X}}(t) = \frac{\hbar}{M} \text{Im} \left(\frac{1}{\tilde{\psi}} \frac{\partial \tilde{\psi}}{\partial X} \right), \quad \dot{\mathbf{Y}}(t) = \frac{\hbar}{M} \text{Im} \left(\frac{1}{\tilde{\psi}} \frac{\partial \tilde{\psi}}{\partial Y} \right) \quad (38)$$

$$\dot{\mathbf{Z}}(t) = \frac{\mathbf{P}_Z(t)}{M}, \quad \dot{\boldsymbol{\theta}}(t) = \frac{\mathbf{p}_\theta(t)}{\mu r^2}, \quad \dot{\boldsymbol{\varphi}}(t) = \frac{\mathbf{p}_\varphi(t)}{\mu r^2 \sin^2 \boldsymbol{\theta}(t)} \quad (39)$$

$$\dot{\mathbf{P}}_Z(t) = -\frac{\partial V}{\partial Z}, \quad \dot{\mathbf{p}}_\theta(t) = \frac{\mathbf{p}_\varphi^2(t) \cos \boldsymbol{\theta}(t)}{\mu r^2 \sin^3 \boldsymbol{\theta}(t)} - \frac{\partial V}{\partial \theta}, \quad \dot{\mathbf{p}}_\varphi(t) = -\frac{\partial V}{\partial \varphi} \quad (40)$$

evaluated at $X = \mathbf{X}(t)$, $Y = \mathbf{Y}(t)$, $q_\alpha = \mathbf{q}_\alpha(t)$. Starting with initial conditions to be specified below, these equations have to be solved simultaneously. In practice, the Schrödinger equation was solved in a basis of plane waves bearing the periodicity of the surface.

5.2. Initial conditions

As detailed above, the initial conditions for the MQCB equations need to be calculated based on an initial full-dimensional wavefunction. For simplicity, we consider an initially non-rotating molecule approaching the surface at normal incidence with mean momentum \mathbf{P}_Z^0 . Assuming a Gaussian shape for the wavefunction in Z -direction centred around \mathbf{Z}_0 , the full-dimensional initial wavefunction is given by

$$\psi_0(X, Y, Z, \theta, \phi) = \frac{1}{a^2 (2\pi\sigma^2)^{1/4}} e^{-(Z-\mathbf{Z}_0)^2/4\sigma^2} e^{(i/\hbar)\mathbf{P}_Z^0(Z-\mathbf{Z}_0)} Y_{00}(\theta, \phi) \quad (41)$$

with the spherical harmonic $Y_{00}(\theta, \phi)$. According to this wavefunction, *all* initial positions (classical and quantum) are sampled. The initial values of $\mathbf{X}(t=0)$, $\mathbf{Y}(t=0)$, $\mathbf{Z}(t=0)$, $\boldsymbol{\theta}(t=0)$, $\boldsymbol{\varphi}(t=0)$ are hence chosen from the probability distribution

$$\begin{aligned} P([X, X+dX]; [Y, Y+dY]; [Z, Z+dZ]; [\theta, \theta+d\theta]; [\varphi, \varphi+d\varphi]) \\ = |\psi_0(X, Y, Z, \theta, \phi)|^2 dX dY dZ d\cos\theta d\varphi \end{aligned} \quad (42)$$

In our case, using the initial wavefunction (41), one has $\mathbf{P}_Z(t=0) = \mathbf{P}_Z^0$ and $\mathbf{p}_{\theta,i}(t=0) = \mathbf{p}_{\varphi,i}(t=0) = 0$. Hence in this special case, for a given

collision energy E , the initial vertical momentum is given by

$$\mathbf{P}_{Z,i}(t=0) = -\sqrt{2ME} \quad (43)$$

These values form the initial starting vector for the MQCB equations.

From a numerical point of view, equation (40) is integrated with a simple first-order integration method in parallel with the quantum propagation within the low-dimensional Hilbert space. Due to the periodicity of the surface potential, the quantum propagation was performed using a two-dimensional Fourier basis for the X and Y degrees of freedom.

5.3. Observables: diffraction probabilities and rotational energy transfer

In what follows, we are interested in the diffraction probability of the scattered molecule. To this end, we project the final asymptotic wave packet onto scattering states. When this projection is performed with the wave packet being in the asymptotic region, this is equivalent to projecting onto free waves, i.e., the scattering amplitudes are then simply given by the Fourier transform of the asymptotic wave packet [11]. Since in our case, the wavefunction depends parametrically on the classical variables, each trajectory yields a diffraction probability

$$P_i(n, m) = \lim_{t \rightarrow \infty} \left| \int_0^a \int_0^a dX dY \frac{1}{\sqrt{ab}} e^{-i(K_n X + K_m Y)} \tilde{\psi}(X, Y, \mathbf{Z}_i, \boldsymbol{\theta}_i, \boldsymbol{\varphi}_i, t) \right|^2 \quad (44)$$

where $i = 1, N$, $K_n = 2\pi n/a$, and $K_m = 2\pi m/a$. The energy dependence stems from the initial velocities of the classical trajectories according to equation (43). To obtain the total diffraction probability, we average over the whole ensemble of N trajectories:

$$P(n, m) = \frac{1}{N} \sum_{i=1}^N P_i(n, m) \quad (45)$$

The second quantity we are interested in is the rotational energy that is being transferred during the collision. If the initial state is taken to be a $\mathbf{J} = 0$ state, the energy transfer from the translational to the rotational degrees of freedom is simply the rotational energy after the collision

$$E_{\text{rot},i} = \frac{1}{2\mu r^2} \left(\mathbf{p}_{\theta,i}^2 + \frac{\mathbf{p}_{\varphi,i}^2}{\sin^2 \theta_i} \right), \quad i = 1, N \quad (46)$$

The average rotational energy transfer (ARET) is then given by

$$E_{\text{rot}} = \frac{1}{N} \sum_{i=1}^N E_{\text{rot},i} \quad (47)$$

With these definitions, $P(n, m)$ and E_{rot} can directly be compared to full-dimensional quantum wave packet results using the MCTDH method [4,5]. These quantities, which give a detailed information about the rotational diffractive scattering of a diatomic molecule, were calculated with the MQCB method and compared to full-dimensional quantum wave packet results based on the MCTDH method (for details of the calculations see Ref. [22]).

5.4. Results on the $\text{N}_2/\text{LiF}(001)$ molecule–surface scattering

5.4.1. Diffraction probabilities

In this section, we will present the results for the diffraction probability obtained with the MQCB method as compared to 5-d quantum results as a function of collision energy. As detailed above, we have treated the case of normal incidence with the molecule in an initial rotational state $\mathbf{J} = 0$.

In Fig. 1 we compare the results for the final diffraction probabilities of the orders (0,0), (1,1), (2,2) as well as (0,1), (0,2) and (2,1) for different collision energies between 0.1 and 0.3 eV. The solid lines correspond to the quantum result, and the dashed lines represent the results obtained by the approximate MQCB calculations. One clearly sees the very good agreement of our approximate method with the exact results for all orders considered.

At energies higher than about 0.17 eV, the diffraction into the order (0,0), has decreased to only about 1%, while the other diffraction channels are being more and more populated. The diffraction probability $P(1, 1)$ shows a maximum of about 0.15 eV. Taking the symmetry $n \rightarrow -n, m \rightarrow -m$ into account, we see that diffraction into the order $(\pm 1, \pm 1)$ accounts for about 30% of the whole diffraction probability.

Qualitatively and even quantitatively, the exact results are well reproduced. Note that these diffraction probabilities are a pure quantum effect and cannot be obtained directly (i.e., without boxing) by a classical calculation, as it is the case for the ARET to be shown below.

5.4.2. Average rotational energy transfer

In this section, we compare results for the ARET. Since this quantity can be obtained from a purely classical calculation, we can compare the ARET as a function of collision energy obtained by three methods: a purely classical treatment, the mixed MQCB method and the 5-dimensional quantum

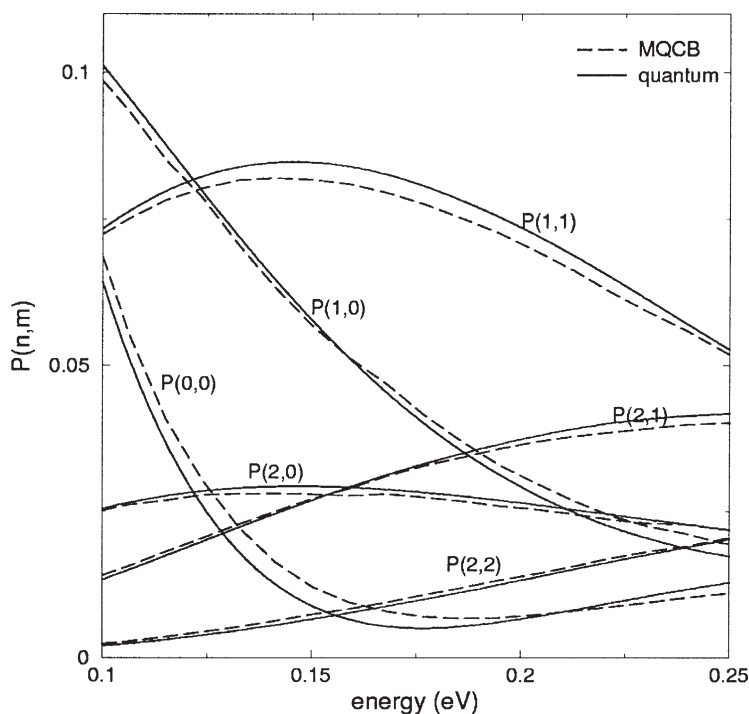


Fig. 1. Diffraction probability as a function of collision energy. Solid line: exact quantum mechanical result obtained by the MCTDH method (from Ref. [22]), dashed line: MQCB results (equation (45)).

treatment. To be able to rigorously test the MQCB method, in all three cases the same 5-dimensional Hamiltonian equation (34) was used.

The pure classical results are readily obtained by integrating the usual Hamilton's equations of classical mechanics, and a solution of the Schrödinger equation in equation (37) is not necessary any more. This again reflects that the MQCB method can be viewed as an extension of classical mechanics by adding quantum effects to certain degrees of freedom. The ARET is then calculated in exactly the same way with equation (47).

Figure 2 shows the ARET as a function of collision energy between 0.1 and 0.3 eV. The solid line is the quantum result, and the dotted line corresponds to the ARET obtained by a purely classical calculation. The MQCB result is shown as dashed lines. For this quantity, we find almost quantitative agreement between all three calculations, showing a monotonically increasing behaviour of the ARET as a function of the collision energy. The classical result is in very good agreement with the correct quantum one, and adding the quantum effects in the X- and Y-direction by

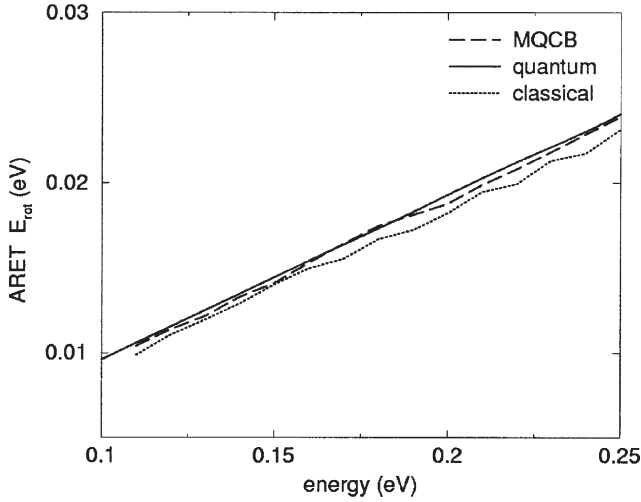


Fig. 2. Average rotational energy transfer (ARET) E_{rot} for different collision energies. Solid line: quantum mechanical wave packet propagation using the MCTDH method (from Ref. [22]); dashed line: MQCB method (equation (47)); dotted line: classical dynamics.

the proposed MQCB scheme does not modify the already very good agreement between classical and quantum results.

However, one should keep in mind that even if the ARET for this system is well described by classical mechanics, the diffraction process, being of purely quantum mechanical nature, cannot be treated by classical mechanics. Thus, one clearly sees how the MQCB method, as a mixed method, really combines classical mechanics with quantum mechanics in some degrees of freedom, when one is interested in effects that are of purely quantum mechanical nature. Comparing the MQCB method with the full quantum results presented in Figs 1 and 2, one clearly sees that both the diffraction probabilities as well as the ARET are extremely well described by the MQCB method.

6. CONCLUSIONS

In this chapter, we have given a full account of the MQCB method as introduced by Gindensperger *et al.* [8]. Especially, technical details about sampling of initial conditions and calculation of observables have been addressed in great detail. Using a five-dimensional model of a molecule–surface collision, the different steps of a MQCB calculation were exemplified. Since full quantum results can be obtained by wave packet propagation techniques, we can give a direct comparison and thus show

the accurateness of the (approximate) MQCB method for the model considered. We find an almost quantitative agreement, which is an encouraging results for possible further applications of the MQCB method in large systems, where inherent quantum effects are required to treat at least parts of the full system quantum mechanically.

ACKNOWLEDGEMENTS

The authors would like to thank M.-C. Heitz and H.-D. Meyer for stimulating discussions as well as for the full quantum results presented for comparison.

REFERENCES

- [1] B. Berne, G. Cicotti and D. Coker (eds), *Classical and Quantum Dynamics in Condensed Phase Simulations*, World Scientific, Singapore, 1998.
- [2] U. Weiss, *Quantum Dissipative Systems*, World Scientific, Singapore, 1993.
- [3] C. Meier and D. Tannor, *J. Chem. Phys.*, 1999, **111**, 3365.
- [4] H.-D. Meyer, U. Manthe and L. S. Cederbaum, *Chem. Phys. Lett.*, 1990, **165**, 73.
- [5] M. H. Beck, A. Jöckle, G. A. Worth and H.-D. Meyer, *Phys. Rep.*, 2000, **324**, 1.
- [6] G. Billing, *Int. Rev. Phys. Chem.*, 1994, **13**, 309.
- [7] J. C. Tully, *Int. J. Quantum Chem.*, 1991, **25**, 299.
- [8] E. Gindensperger, C. Meier and J. A. Beswick, *J. Chem. Phys.*, 2000, **113**, 9369.
- [9] O. V. Prezhdo and C. Brooksby, *Phys. Rev. Lett.*, 2001, **86**, 3215.
- [10] E. Gindensperger, C. Meier and J. A. Beswick, *J. Chem. Phys.*, 2002, **116**, 8.
- [11] E. Gindensperger, C. Meier, J. A. Beswick and M.-C. Heitz, *J. Chem. Phys.*, 2002, **116**, 10051.
- [12] P. R. Holland, *The Quantum Theory of Motion*, Cambridge University Press, Cambridge, 1993.
- [13] C. L. Lopreore and R. E. Wyatt, *Phys. Rev. Lett.*, 1999, **82**, 5190.
- [14] E. R. Bittner, *J. Chem. Phys.*, 2000, **112**, 9703.
- [15] R. E. Wyatt, C. L. Lopreore and G. Parlant, *J. Chem. Phys.*, 2001, **114**, 5113.
- [16] H. Carlsen and O. Goscinski, *Phys. Rev. A*, 1999, **59**, 1063.
- [17] A. S. Sanz, F. Borondo and S. Miret-Artés, *Phys. Rev. B*, 2000, **61**, 7743.
- [18] I. Burghardt and L. S. Cederbaum, *J. Chem. Phys.*, 2001, **115**, 10303.
- [19] L. L. Salcedo, *Phys. Rev. Lett.*, 2003, **90**, 118901.
- [20] O. V. Prezhdo and C. Brooksby, *Phys. Rev. Lett.*, 2003, **90**, 118902.
- [21] R. B. Gerber, L. H. Beard and D. J. Kouri, *J. Chem. Phys.*, 1981, **74**, 4709.
- [22] M.-C. Heitz and H.-D. Meyer, *J. Chem. Phys.*, 2001, **114**, 1382.

The Hückel Model of Polyacetylene Revisited: Asymptotic Analysis of Peierls Instability

Gian Luigi Bendazzoli¹ and Stefano Evangelisti²

¹*Dipartimento di Chimica Fisica e Inorganica, Università di Bologna,
Viale Risorgimento 4, I-40136 Bologna, Italy*

²*Laboratoire de Physique Quantique, UMR 5626, Université Paul Sabatier,
118, Route de Narbonne, 31062 Toulouse Cedex, France*

Abstract

We carry out an analysis of the spectrum the Hückel model of dimerized polyacetylene, both for cyclic and open chain boundary conditions, with special emphasis on the linear polyene with *odd number of π bonds*. We also perform explicit perturbation expansion up to second order in the nuclear displacements. The asymptotic analysis of first- and second-order perturbation theory reveals that some behaviours assumed in the literature are not correct.

Contents

1. Introduction	348
2. The Hückel model for alternating one-dimensional polyenes	348
2.1. The Hamiltonian	348
2.2. The π energy of rings	350
2.3. The π energy for an open chain: even number of bonds	353
2.4. The π energy for an open chain: odd number of bonds	353
3. Perturbation expansion	355
3.1. Even number of bonds	356
3.2. Odd number of bonds	357
4. Discussion and conclusions	360
Acknowledgements	361
Appendix A. The elliptic integral of second kind	361
Appendix B. The roots of equation (25)	362
Appendix C. Asymptotic behaviour of the sums	364
Appendix D. Derivation of equations (48) and (49)	366
Appendix E. Analysis of the first-order perturbation energy	367
References	368

1. INTRODUCTION

Infinite linear polyenes show a bond alternation between successive long and short C–C bonds [1], a consequence of the Peierls theorem on the non-existence of one-dimensional metals [2]. This Peierls distortion (or instability) is very important both from a theoretical and a practical point of view, being a typical example of a metal–insulator transition [3]. Consider an infinite chain of equally spaced sites $-(CH)-$, each of them bearing one electron in a single valence orbital. In this case we have a half-filled band and the system has metallic character. If we distort the chain into an alternating sequence of short and long bonds $-(CH=CH)-$, the half-filled band splits into a lower one completely filled and an upper empty band, separated by a gap. This ‘dimerized’ polyacetylene is an insulator.

Peierls instability in one-dimensional systems has been the subject of several investigations, see Refs. [4,5]. Conjugated hydrocarbons have been treated in the early MO literature at the Hückel level [6,7]. The formulae of the Hückel orbital energies of the conjugated hydrocarbons with alternating long–short bonds are known since long time [6] and it is easy to prove Peierls theorem at this level of theory using periodic boundary conditions [7] and second-order perturbation theory in the distortion coordinate u . The first derivative of the π energy with respect to u is vanishing both for the cyclic and open chain systems, with the exception of the linear polyene with *odd number of bonds*. This feature led some authors [8,9] to assume it as a starting point to treat Peierls distortion in two-dimensional systems. The asymptotic analysis of first- and second-order perturbation theory led us to conclude that some behaviours assumed in Ref. [8] are not correct.

The paper is organized in the following way: in Section 2 the structure of the spectrum of short–long bonds alternating Hückel Hamiltonian is reviewed, and some features are pointed out; in Section 3 we perform an asymptotic analysis of the perturbation treatment of dimerization up to second order; in Section 4 we present our concluding remarks.

2. THE HÜCKEL MODEL FOR ALTERNATING ONE-DIMENSIONAL POLYENES

2.1. The Hamiltonian

Peierls dimerization in polyacetylene is the result of two opposite effects: the σ electrons form a skeleton that opposes dimerization; the π electrons, on the contrary, tend to form alternating bonds [10]. This is modeled by the Hamiltonian (Su–Schrieffer–Heger Hamiltonian [11]):

$$H^{\text{SSH}} = H^{\sigma} + H^{\pi} \quad (1)$$

$$H^\sigma = \frac{K}{2} \sum_l (u_l - u_{l-1})^2 \quad (2)$$

$$H^\pi = \text{Hückel Hamiltonian} \quad (3)$$

composed of a classical, elastic part H^σ and the Hückel Hamiltonian for the π electrons. The σ energy is assumed to be zero when all the C–C bonds have some length d_0 and therefore all C atoms occupy suitable positions. The u_l s in equation (2) are the displacements of the C atoms from these positions and K is a force constant. We consider displacements alternating in sign given by the distortion coordinate u :

$$u_l = (-1)^l u \quad (4)$$

We exclude the case of a ring with odd number of atoms because equation (4) is not compatible with it: we would have a couple of adjacent atoms with a displacement of the same sign, and a bond with unaltered length d_0 . Therefore, our systems belong to the class of *alternant conjugated hydrocarbons*. For even atom rings and odd atom chains the total length is preserved; for even atom chains, the number of bonds is odd, and the extra one can be either short (double) or long (single): the length is preserved only up to $2|u|$. The sum (2) runs over bonds and one has

$$E_\sigma = \frac{K}{2} 4Mu^2, \quad \text{even ring} \quad (5)$$

$$E_\sigma = \frac{K}{2} 4(M-1)u^2, \quad \text{chain} \quad (6)$$

The minimum of the σ energy occurs at $u = 0$ in all cases: short and long bonds have the same σ energy in this model.

The non-vanishing matrix elements of H^π are

$$H_{i,i}^\pi = \alpha \quad (7)$$

$$H_{i,j}^\pi = \beta_{i,j}, \quad j = i \pm 1, \quad \text{i.e., nearest neighbour} \quad (8)$$

We set $\alpha = 0$ without loss of generality; the resonance or hopping integral $\beta_{i,j} < 0$ is a function of the interatomic distance $d_{i,j}$ ($j = i \pm 1$) between nearest-neighbour atoms. We assume a linear dependence of $\beta_{i,j}$ upon the distance:

$$\beta_{i,j} = \beta - 2\kappa u \quad (9)$$

where $\kappa > 0$ is a constant and u can be positive or negative. We have only two values of $\beta_{i,j}$:

$$\beta_\pm = \beta \pm \delta = \beta(1 \pm \tau) \quad (10)$$

In the following we will often use τ as a convenient variable to express the dependence of the resonance integral upon the distance. We point out that $\tau > 0$

means a stronger (short) bond and $|\tau| < 1$. Convenient values of the parameters are: $\beta = -2.5$ eV, $K = 21.0$ eV/Å², $\kappa = 4.1$ eV/Å and $u = 0.04$ Å [11]. However, since we are more interested in *qualitative* aspects of the spectrum, we will use $\beta = -1$ and $\tau = 0.2$.

2.2. The π energy of rings

The simplest way of approaching the limit of the infinite chain is to perform computations on finite systems of increasing number M of atoms and then extrapolate to $M \rightarrow \infty$. This is also the most ‘physical’ in the sense that the finite systems are often real molecules. We will refer to this case as *open chain*. A second, more formal way is to impose periodic boundary conditions to the finite system of M atoms and then let $M \rightarrow \infty$. This choice allows for faster convergence to the limit and it is often preferred in practice. Consider a cyclic polyacetylene molecule (annulene) composed of $M = 2N$ $-\text{CH}-$ units, disposed on a ring in the x, y plane. After dimerization the molecule is composed of N monomers $-\text{CH}=\text{CH}-$; this is the elementary cell of our system. We number the C atoms (or sites) by a cyclic index $i = 0, \dots, 2N - 1$: indexes $2N, 2N + 1, \dots$ coincide with $0, 1, \dots$ respectively. Two families of orbital energies are obtained [7]:

$$\epsilon_{\pm}(k) = \pm \sqrt{\beta_+^2 + \beta_-^2 + 2\beta_+\beta_- \cos k\Theta} \quad (11)$$

$$\epsilon_{\pm}(k) = \pm 2 \sqrt{\beta^2 \cos^2(k\Theta/2) + \delta^2 \sin^2(k\Theta/2)} \quad (12)$$

where $\Theta = 2\pi/N$ and k is an integer defined mod N and referred to as (*pseudo*) *momentum*. The orbital energies defined by equation (12) do not depend upon the sign of k . In order to put in better evidence this degeneracy, the range of k can be written as follows. For an odd number of monomers $N = 2\nu + 1$, the range is $k = 0, \pm 1, \pm 2, \dots, \pm \nu$; all levels, except $k = 0$ are doubly degenerate. For an even number of monomers, $N = 2\nu$, the range is $k = 0, \pm 1, \pm 2, \dots, \pm(\nu - 1), \nu$; the level $k = \pm \nu$ is simple since ν and $-\nu$ differ by N and are therefore identical. Since $\epsilon_-(k)$ is lower than $\epsilon_+(l)$ for any values of k and l , at half filling (one π electron per carbon atom) the orbitals ϕ_- are doubly occupied, while the orbitals ϕ_+ are empty. The energy of the lowest lying molecular orbital is always 2β , unaffected by dimerization. The Fermi momentum k_F is given by

$$k_F = \pm \frac{N - 1}{2} = \nu, \quad N \text{ odd} \quad (13)$$

$$k_F = \frac{N}{2} = \nu, \quad N \text{ even} \quad (14)$$

In the odd case the Fermi level is occupied by four electrons in two degenerate orbitals; in the even case there are two electrons in a non-degenerate level. The π energy $\epsilon_-(k)$ is stabilized by dimerization and a band gap appears; for N odd it is given by

$$\begin{aligned} \epsilon_+(k_F) - \epsilon_-(k_F) \\ = 4\sqrt{\beta^2 \cos^2[(N-1)\pi/2N] + \delta^2 \sin^2[(N-1)\pi/2N]} \end{aligned} \quad (15)$$

The limit value of the gap is 4δ . For N even $k_F\Theta = \pi/2$ and the gap is 4δ already for any finite N . One has

$$2|\delta| = |\beta_+ - \beta_-| \leq |\epsilon_{\pm}(k)| \leq |\beta_+ + \beta_-| = 2|\beta| \quad (16)$$

Indeed, $|\epsilon_{\pm}(k)|$ can be interpreted as the third side of a triangle whose other sides are β_+ and β_- and include the angle $\pi - \Theta$. In Fig. 1 the orbital energies are reported for very large N .

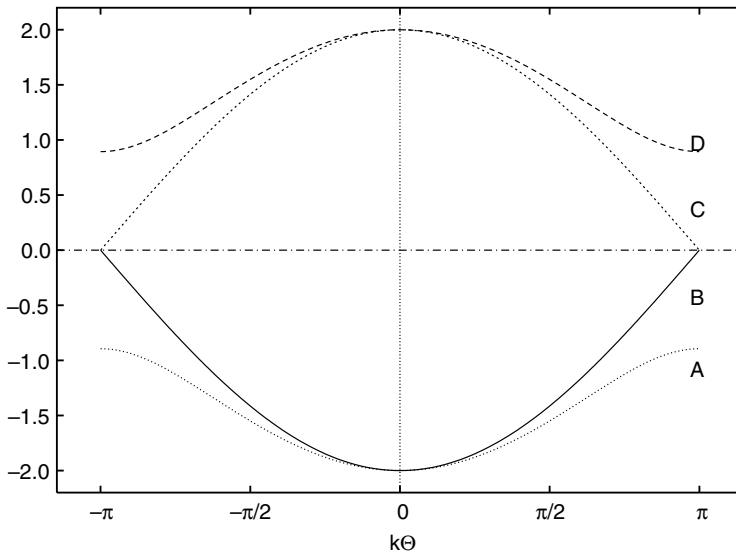


Fig. 1. Eigenvalues of the Hückel Hamiltonian for cyclic polyacetylene as a function of the momentum $k\Theta = 2\pi k/N$, for a non-dimerized case (B,C) and a dimerized case (A,D). ($\alpha = 0$, $\beta = -1$, $\tau = 0.2$, $N = 10,001$).

As concerns the total π energy, we have the sums:

$$E_{\pi}(4\nu + 2) = -4 \sum_{k=-\nu}^{\nu} \sqrt{\beta^2 \cos^2(k\Theta/2) + \delta^2 \sin^2(k\Theta/2)} \quad (17)$$

$$E_{\pi}(4\nu) = -4 \sum_{k=1-\nu}^{\nu-1} \sqrt{\beta^2 \cos^2(k\Theta/2) + \delta^2 \sin^2(k\Theta/2)} - 2\delta \quad (18)$$

In the limit $N \rightarrow \infty$, the π energy per atom can be written as

$$E_{\pi\infty} = \frac{4\beta}{\pi} E\left(\frac{\pi}{2} \middle| \zeta\right) \quad (19)$$

where $E(\frac{\pi}{2}|\zeta)$ is the complete elliptic integral of the second kind [15] and $\cos \zeta = \frac{\delta}{\beta} = \tau$. See Appendix A for the definition of the elliptic integral and other details of the derivation of equation (19). As concerns the asymptotic behaviour of the π energy per atom ($M = 2N$), $E_{\pi}(M)/M$ of equation (17) should approach the value equation (19) as a $O(N^{-2})$ or faster, as shown in Ref. [12] for a ring of N units of more general type. Actually, as seen in the left part of Fig. 2, our numerical data indicate a convergence rate faster than M^{-2} .

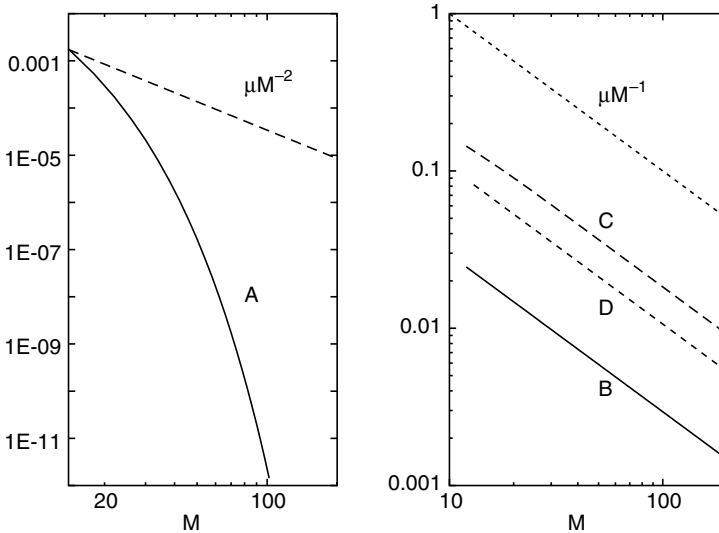


Fig. 2. Asymptotic behaviour of the difference $\Delta_M = E_{\pi}(M)/M - E_{\pi\infty}$ for different boundary conditions. On the left, curve A is $-\Delta_M$ with periodic b.c.; the line $\propto M^{-2}$ is also reported for comparison. On the right, curves 'B' and 'C' are Δ_M for the open chains with N short and $N - 1$ long bonds and vice versa, respectively; curve D is Δ_M for chains with N short and N long bonds; the line $\propto M^{-1}$ is reported for comparison. ($\alpha = 0$, $\beta = -1$ and $\tau = 0.2$; bi-logarithmic scale).

2.3. The π energy for an open chain: even number of bonds

Following Refs. [6,7,13] the Hückel orbital energies λ of an open chain of $M = 2N + 1$ atoms are also arranged in two families:

$$\lambda_{\pm}^{(2N+1)}(k) = \pm \sqrt{\beta_+^2 + \beta_-^2 + 2\beta_+\beta_- \cos k\Theta} \quad (20)$$

$$\lambda_{\pm}^{(2N+1)}(k) = \pm 2\sqrt{\beta^2 \cos^2(k\Theta/2) + \delta^2 \sin^2(k\Theta/2)} \quad (21)$$

separated by an isolated eigenvalue $\lambda_0 = 0$. Equation (20) is similar to equation (12), the only differences being: $\Theta = \pi/(N + 1)$ and $k = 1, 2, \dots, N$. The energy band in the limit $N \rightarrow \infty$ is the same as the $k\Theta > 0$ half of Fig. 1. The energy of the lowest lying molecular orbital is again 2β ; at half filling, the highest doubly occupied MO corresponds to $k = N$ and the band gap for $\delta \neq 0$ is given by

$$\lim_{N \rightarrow \infty} \lambda_+^{(2N+1)}(N) - \lambda_-^{(2N+1)}(N) = 4\delta \quad (22)$$

if we neglect the isolated zero eigenvalue (or consider the positive ion). The total π energy is given by

$$A_{\pi}(2N + 1) = -4 \sum_{k=1}^N \sqrt{\beta^2 \cos^2(k\Theta/2) + \delta^2 \sin^2(k\Theta/2)} \quad (23)$$

Since the HOMO has zero energy, the neutral and the singly ionized polyene molecule have the same energy. We can relate the sum (23) to the periodic case by noticing that $\lambda_{\pm}^{(2N+1)}(k)$ for $M = 2N + 1$ is equal to $\epsilon_{\pm}(k)$ for $M = 2(2N + 2)$. In the linear case $k = 1, 2, \dots, N$, while in the ring $k = 0, \pm 1, \pm 2, \dots, \pm(2N + 1), 2N + 2$

$$2A_{\pi}(2N + 1) = E_{\pi}(4N + 4) - 4\beta - 4\delta \quad (24)$$

Therefore, $A_{\pi}(2N + 1)/(2N + 1)$ tends to the same limit E_{∞}^{π} of equation (19) with asymptotic behaviour of $O(N^{-1})$. This result can also be obtained by the repeat space formalism of Arimoto [14] and it is confirmed by numerical results plotted in curve *D* reported in Fig. 2.

2.4. The π energy for an open chain: odd number of bonds

This case has a lower symmetry than the previous ones, because we can have N short and $N - 1$ long bonds or vice versa, and this implies a difference in energy. This case was first studied by Lennard-Jones [6]: the $\lambda = 0$ eigenvalue is missing, and there are again two families of eigenvalues given

by equation (20) where now $k\Theta$ is replaced by the k th root Z_k of the equation

$$\frac{\beta_+ \sin[(N+1)Z] + \beta_- \sin[NZ]}{\sin Z} = 0 \quad (25)$$

Equation (25) refers to an Hückel matrix of order $2N$ where there are N off diagonal elements equal to β_+ and $N-1$ equal to β_- . The eigenvalues fall in the same intervals as in the previous cases, i.e.

$$2\delta \leq |\lambda_{\pm}(k)| \leq 2|\beta| \quad (26)$$

with two remarkable exceptions. When there are more long than short bonds ($\tau < 0$) and for sufficiently large N , there is also *a couple of isolated eigenvalues* internal to the strip $|\lambda_{\pm}(k)| \leq 2\delta s$, and symmetrically approaching zero for $N \rightarrow \infty$. The contribution of these eigenvalues to the total π energy is asymptotically vanishing. The more stable polyene with $\tau > 0$ does not present this feature. A discussion of equation (25) is given in Appendix B. In Fig. 3 we report computed eigenvalues of the polyene with 40 atoms as functions of k , the ordinal number of the root of equation (25).

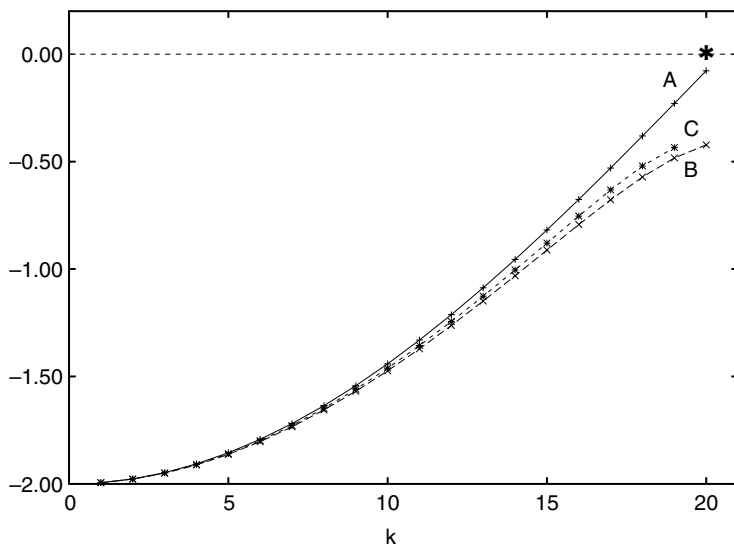


Fig. 3. Lower branch of eigenvalues of the Hückel Hamiltonian ($\alpha = 0$, $\beta = -1$) for linear polyacetylene with 40 atoms as a function of k . Curve A: non-dimerized ($\tau = 0$); curve B: 20 short and 19 long bonds ($\tau = 0.2$); curve C: 20 long and 19 short bonds, 'regular' eigenvalues ($\tau = -0.2$); * is the location of the isolated eigenvalue ($\lambda = -0.00020048597$) for 20 long and 19 short bonds ($\tau = -0.2$).

An equivalent formula has been independently derived by Shin [13] and reads:

$$\lambda_{\pm}^{(2N)}(k) = \pm \sqrt{\beta_+^2 + \beta_-^2 + \beta_+ \beta_- (\eta + \eta^{-1})} \quad (27)$$

where η is a root of the reciprocal algebraic equation:

$$\beta_+ \eta^N + \beta_- \eta^{N-1} + \dots + \beta_- \eta^{1-N} + \beta_+ \eta^{-N} = 0 \quad (28)$$

The equivalence of equations (25) and (28) is obtained by setting $\eta = \exp(iZ)$. In order to determine the limit of the π energy we observe that the Hückel matrix of order $2N + 1$ is obtained by adding one row and one column to that of order $2N$; furthermore, being tridiagonal, all eigenvalues are simple. By the interlace theorem [16], the eigenvalues of the matrix of odd orders $2N \pm 1$ separate those of the matrix of order $2N$. One has explicitly:

$$\begin{aligned} \lambda_-^{(2N+1)}(1) &\leq \lambda_-^{(2N)}(1) \leq \dots \leq \lambda_-^{(2N-1)}(N-1) \leq \lambda_-^{(2N+1)}(N) \\ &\leq \lambda_-^{(2N-1)}(N) \leq \lambda_0 \leq \end{aligned} \quad (29)$$

$$\lambda_+^{(2N)}(1) \leq \lambda_+^{(2N-1)}(1) \leq \dots \leq \lambda_+^{(2N-1)}(N-1) \leq \lambda_+^{(2N)}(N) \quad (30)$$

This ensures that the lowest eigenvalue is again 2β in the limit $N \rightarrow \infty$. Moreover, one has the following inequalities for the total π energies at half filling:

$$A_{\pi}(2N-1) \geq A_{\pi}(2N) \geq A_{\pi}(2N+1) \quad (31)$$

By dividing equation (31) by $2N$ and letting $N \rightarrow \infty$ we show that the limit of the energy in even atom chain is E_{∞}^{π} of equation (19). As concerns the asymptotic behaviour, this is again $O(N^{-1})$ by Arimoto's results [14]. In Fig. 2 we plot $A_{\pi}(2N)/2N - E_{\pi\infty}$ as a function of $M = 2N$: the resulting curves agree with an asymptotic behaviour $\propto 1/M$.

3. PERTURBATION EXPANSION

The dimerization can be treated by perturbation theory by assuming as expansion parameter the displacement u or some quantity related to it. There are two main cases: (i) even number of bonds and (ii) odd number of bonds.

3.1. Even number of bonds

This case occurs in the closed ring or the chain with odd number of atoms. We rewrite the eigenvalues as

$$\epsilon_{\pm}(k) = \pm 2|\beta| \cos(k\Theta/2) \sqrt{1+t^2} \quad \text{where} \quad (32)$$

$$t = \tau \tan\left(\frac{k\Theta}{2}\right) = -\frac{2\kappa u}{\beta} \tan\left(\frac{k\Theta}{2}\right) \quad (33)$$

This equation is also valid for the linear case. The eigenvalues are functions of the displacements, but in the following two cases: (i) $k = 0$ where $\epsilon_{\pm}(0) = \pm 2|\beta|$ and (ii) the isolated zero eigenvalue in the chain with $2N + 1$ atoms. In the ring of $2N = 4\nu$ atoms the orbital energy at the Fermi level has a cusp:

$$\epsilon_{\pm}(k_F) = \pm 2|\delta| \quad (34)$$

i.e., it is not a derivable function of $\delta = -2\kappa u$. All other eigenvalues are even derivable functions of u or δ so the first derivative of the π energy is strictly zero for the ring of $2N = 4\nu + 2$ atoms or the open chain of $2N + 1$ atoms. In the ring $2N = 4\nu$ this is true only if the Fermi level equation (34) is excluded from the sum. Equation (32) can be expanded in a binomial series of t with convergence radius 1. But this implies

$$\tau = \frac{\delta}{\beta} < \cot\left(\frac{k\Theta}{2}\right) \quad (35)$$

so in terms of τ or u the convergence radius shrinks rapidly to zero when k approaches the Fermi momentum. The first two derivatives of the orbital energy are

$$\epsilon_{-}(k) = 2\beta \cos(k\Theta/2) \sqrt{1+t^2} \quad (36)$$

$$\frac{\partial}{\partial t} \epsilon_{-}(k) = 2\beta \cos(k\Theta/2) \frac{t}{\sqrt{1+t^2}} \quad (37)$$

$$\frac{\partial^2}{\partial t^2} \epsilon_{-}(k) = 2\beta \cos(k\Theta/2) \frac{1-t/2+t^2}{(1+t^2)^{3/2}} \quad (38)$$

As concerns the second derivative of the orbital energy $\epsilon_{-}(k)$ for $u = 0$ is given by

$$\frac{\partial^2}{\partial u^2} \epsilon_{-}(k) \Big|_{u=0} = \left(\frac{dt}{du}\right)^2 \frac{\partial^2}{\partial t^2} \epsilon_{-}(k) \Big|_{t=0} = \frac{8\kappa^2 \sin^2(k\Theta/2)}{\beta \cos(k\Theta/2)} < 0 \quad (\beta < 0) \quad (39)$$

where $k = \pm 1, \pm 2, \dots, (N-1)/2$ (ring, N odd), $k = \pm 1, \pm 2, \dots, N/2 - 1$ (ring, N even), and $k = 1, 2, \dots, N$ (chain, $2N + 1$ atoms; the zero eigenvalue does not contribute!). The second derivative of the total¹ π energy is obtained

¹ Except the Fermi level equation (34) for an even ring.

Table 1. Values of $S = \sqrt{2} \sum_{k=1}^{N/2-1} \frac{(\sin k\Theta/2)^2}{\cos k\Theta/2}$, $\frac{S}{N}$ and $\frac{S}{N \ln N}$ as a function of N

N	S	$\frac{S}{N}$	$\frac{S}{N \ln N}$
10	6.460162	0.646016	0.280561
100	167.948233	1.679482	0.364695
1,000	2715.979245	2.715979	0.393178
10,000	37,525.064038	3.752506	0.407423
100,000	478,903.386505	4.789034	0.415970
1,000,000	5,825,561.329295	5.825561	0.421668
10,000,000	68,620,887.935888	6.862089	0.425738
100,000,000	789,861,625.673383	7.898616	0.428791

by summing equation (39) over k ; the second derivative per atom diverges logarithmically for $N \rightarrow \infty$ since

$$E_{2\infty}^{\pi} = \frac{8\kappa^2}{\beta} \sum_{k=1}^{N/2-1} \frac{\sin^2(k\Theta/2)}{\cos(k\Theta/2)} = O(N \ln N), \quad N \rightarrow \infty \quad (40)$$

The proof is given in Appendix C and numerical values are given in Table 1. Therefore, the second derivative at $u = 0$ of the total π energy per atom also diverges logarithmically for $N \rightarrow \infty$.

3.2. Odd number of bonds

In this case the energy is not an even function of the displacement. For a dimerized molecule with $2N$ atoms we have N long and $N - 1$ short bonds or vice versa: switching u from positive to negative interchanges the number of short and long bonds. The energy change ΔE^{sw} associated to the change of sign of u is essentially due to one bond which changes length and it is therefore expected to be asymptotically independent from N for $N \rightarrow \infty$. This means that $\Delta E^{sw}/N$ will asymptotically vanish together with all *odd order perturbative corrections* to the total π energy per atom.

We derived our perturbative expansion from Shin's equation: we rewrite equation (28) as

$$\begin{aligned} & \beta[\eta^N + \eta^{N-1} + \cdots + \eta^{1-N} + \eta^{-N}] \\ &= -\delta[\eta^N - \eta^{N-1} + \cdots - \eta^{1-N} + \eta^{-N}] \end{aligned} \quad (41)$$

$$\beta \frac{1 - \eta^{2N+1}}{\eta^N(1 - \eta)} = -\delta \frac{1 + \eta^{2N+1}}{\eta^N(1 + \eta)}, \quad \eta \neq 0, \quad \eta \neq \pm 1 \quad (42)$$

and note that if η_0 is a root, so is η_0^{-1} : the roots go in pairs. For $\delta = 0$ we recover the well-known solution for the non-dimerized polyene: η is a root of unity, with the exception of ± 1 :

$$\eta_0(k) = \exp\left(\frac{2\pi i k}{2N+1}\right), \quad k = \pm 1, \pm 2, \dots, \pm N \quad (43)$$

$$\eta_0(k) + \eta_0^{-1}(k) = 2\cos\left(\frac{2\pi k}{2N+1}\right) \quad k = 1, 2, \dots, N \quad (44)$$

$$\lambda_{0\pm}(k) = \pm 2\beta \cos\left(\frac{\pi k}{2N+1}\right) = \pm 2\beta \cos\left(\frac{k\Theta_0}{2}\right) \quad (45)$$

where we have $\Theta_0 = 2\pi/(2N+1)$. For $\delta = 0$ the Fermi level is obtained for $k = N$:

$$\lambda_0(N) = 2\beta \sin\left(\frac{\pi}{4N+2}\right) \quad (46)$$

We set up a perturbation expansion in the parameter $\tau = \delta/\beta = -2\kappa u$

$$\eta(k) = \eta_0(k) + \eta_1(k)\tau + \eta_2(k)\tau^2 + \dots \quad (47)$$

and we find (see Appendix D):

$$\eta_1(k) + \eta_1^{-1}(k) = \frac{8}{2N+1} \sin^2\left(\frac{k\Theta_0}{2}\right) \quad (48)$$

$$\eta_2(k) + \eta_2^{-1}(k) = -\frac{4}{(2N+1)^2} \tan^2\left(\frac{k\Theta_0}{2}\right) \left[1 + 2\cos^2\left(\frac{k\Theta_0}{2}\right)\right] \quad (49)$$

and (see Appendix D):

$$\left.\frac{\partial \lambda(k)}{\partial \tau}\right|_{\tau=0} = \frac{2\beta}{2N+1} \sin\left(\frac{k\Theta_0}{2}\right) \tan\left(\frac{k\Theta_0}{2}\right) \quad (50)$$

$$\left.\frac{\partial^2 \lambda(k)}{\partial \tau^2}\right|_{\tau=0} = \frac{4\beta}{(2N+1)^2}$$

$$\left\{ \frac{(4N^2 + 4N - 1) \sin^2\left(\frac{k\Theta_0}{2}\right)}{\cos\left(\frac{k\Theta_0}{2}\right)} - \frac{\tan^2\left(\frac{k\Theta_0}{2}\right) \left[1 + \sin^2\left(\frac{k\Theta_0}{2}\right)\right]}{\cos\left(\frac{k\Theta_0}{2}\right)} \right\} \quad (51)$$

Equation (50) is consistent with equation (7) of Ref. [8]. However, we point out that equation (50) does not describe, even from a *qualitative* point of view the correct behaviour of the orbital energy. Indeed, for a given non-zero displacement u equation (50) predicts a *vanishing band gap*, i.e., a *metallic*

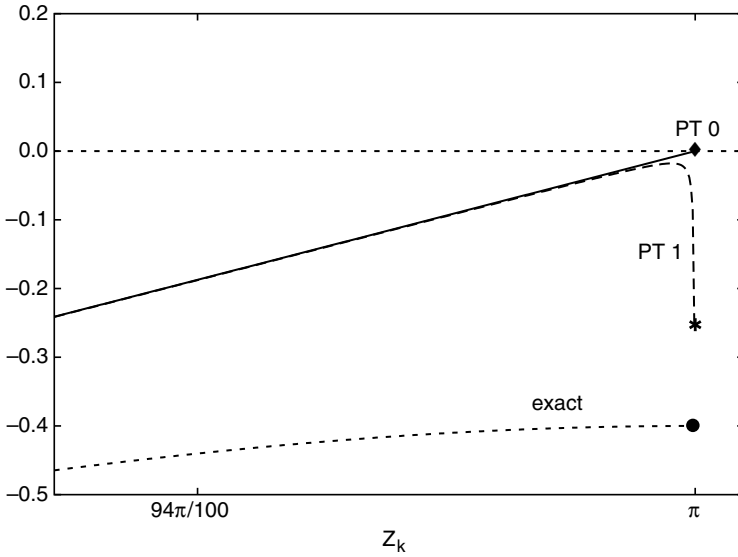


Fig. 4. Eigenvalues of the Hückel Hamiltonian for linear polyacetylene with 10,000 atoms as a function of Z_k ($\alpha = 0$, $\beta = -1$, $\tau = 0.2$): PT 0 is the zeroth order energy, PT 1 is the energy to first order.

chain in the limit $N \rightarrow \infty$. As shown in Appendix E, first-order perturbation theory brings the Fermi level of the undistorted chain *below* other levels having lower values of k . On the other hand, for large enough N , there are always levels *arbitrarily close to zero*. Since the energy spectrum is symmetrical – see equation (27) – the band gap is predicted to be vanishingly small. See Fig. 4, where we report the computed values of the exact orbital energies and their first-order approximations as functions of the root Z of equation (25). Curve PT 0 is the zeroth order ($\tau = 0$) energy and approaches the value 0 for $Z \rightarrow \pi/2$, curve PT 1 is the energy to first order and shows a sharp deviation from PT 0 and approaches the value $-4|\delta|/\pi$ for $Z \rightarrow \pi/2$, while the exact energy goes to $-2|\delta|$. Therefore, the use of equation (50) as a starting point to treat dimerization in two-dimensional systems as done in Refs. [8,9] should be reconsidered in view of this result.

The first- and second-order energies at half filling are obtained by summing over $k = 1, 2, \dots, N$. One has

$$\left(\frac{\partial E_\pi}{\partial u} \right)_{u=0} = E_1 = -\frac{4\kappa}{2N+1} \sum_{k=1}^N \frac{\sin^2\left(\frac{k\Theta_0}{2}\right)}{\cos\left(\frac{k\Theta_0}{2}\right)} \quad (52)$$

and similarly for E_2 :

$$\begin{aligned} \frac{1}{2} \left(\frac{\partial^2 E_\pi}{\partial u^2} \right)_{u=0} = E_2 &= \frac{16\kappa^2}{\beta} \frac{4N(N+1)-1}{(2N+1)^2} \sum_{k=1}^N \frac{\sin^2\left(\frac{k\Theta_0}{2}\right)}{\cos\left(\frac{k\Theta_0}{2}\right)} \\ &+ \frac{16\kappa^2}{\beta(2N+1)^2} \sum_{k=1}^N \frac{\tan^2\left(\frac{k\Theta_0}{2}\right)}{\cos\left(\frac{k\Theta_0}{2}\right)} \left(1 + \sin^2 \frac{k\Theta_0}{2} \right) \quad (53) \end{aligned}$$

By using the arguments given in Appendix C, we see that $E_1 = O(\ln N)$ and $E_2 = O(N \ln N)$. The first-order energy per atom vanishes for $N \rightarrow \infty$, although very slowly, as $O(\ln N/N)$.

The second-order energy per atom has the same asymptotic behaviour as in the periodic or linear $2N+1$ chain: it diverges logarithmically. Therefore, perturbation theory seems to be of very little value in this context. The reason is the shrinking of the convergence radius R of the series expansion of the eigenvalue as k approaches the Fermi value.

4. DISCUSSION AND CONCLUSIONS

The σ energy E_σ has a minimum for $\tau = u = \delta = 0$ where the chain has all the bonds identical; this shows that the σ skeleton opposes dimerization. The second derivative of the σ energy per atom is the force constant, always positive:

$$\frac{\partial^2}{\partial \delta^2} E_\sigma = K, \text{ ring}; \quad \frac{\partial^2}{\partial \delta^2} E_\sigma = \frac{M-1}{M}, \text{ chain} \quad (54)$$

Things are different for the π contribution. Consider first the cases with an even number of bonds. The second derivative of the π energy at $u = 0$ is always negative and diverging for $N \rightarrow \infty$. This is clearly seen in the periodic cases or the odd atom chain, see equation (40). Therefore, for a ring or a $2N+1$ -atom chain large enough, the second derivative of the total energy per atom is certainly negative, and we have dimerization.

It has been shown that Peierls dimerization in both linear and cyclic polyacetylene is predicted already at Hückel level for a sufficiently long chain. This is due to the divergence of the second derivative of the π energy per atom as the chain length is increased, while the corresponding derivative of the σ energy remains constant. Therefore, dimerization is independent from the rigidity of the σ skeleton, provided the hopping integral β has a non-vanishing first derivative at the equilibrium bond distance.

This behaviour can be viewed as a symmetry breaking analogous to the linear Jahn–Teller effect in molecules [17].

In case of a chain with an even number of atoms, the first-order energy is different from zero because there is no symmetry around $u = 0$: going from u to $-u$ interchanges the number of short and long bonds. But this effect is asymptotically vanishing, although rather slowly. Moreover, first-order perturbation theory is also *qualitatively* not correct in this case, because it predicts a zero band gap for the dimerized chain. The second derivative per atom is a sum of terms of opposite signs, but asymptotically one term dominates and gives a diverging second derivative similar to the previous ones.

In any case, perturbation theory cannot provide an estimate of the asymptotic value of the Peierls distortion because the convergence radius of the expansion is rapidly shrinking to zero as N grows large.

ACKNOWLEDGEMENTS

This work was partially supported by the Italian ‘Ministero dell’Istruzione, dell’Università e della Ricerca’ and by the French ‘Centre National de la Recherche Scientifique’ (CNRS).

APPENDIX A. THE ELLIPTIC INTEGRAL OF SECOND KIND

The elliptic integral of the second kind is defined in Ref. [15] as

$$E(\varphi \backslash \alpha) = \int_0^\varphi (1 - \sin^2 \alpha \sin^2 \eta) d\eta \quad (55)$$

The variables φ and α are called the amplitude and the modular angle, respectively; the complete elliptic integral of second kind is $E(\frac{\pi}{2} \backslash \alpha)$.

The reduction of the sum (17) to the complete elliptic integral of the second kind is performed as follows. By using equation (10) and $\frac{\delta}{\beta} = \cos \zeta$ we can rearrange equation (12) as

$$\epsilon_-(k) = \alpha - 2\beta \sqrt{1 - m \sin^2(k\Theta/2)} \quad (56)$$

where

$$m = 1 - \left(\frac{\Delta\beta}{\beta} \right)^2 = \sin^2 \alpha$$

This implies $|\Delta\beta| < |\beta|$; this condition is certainly fulfilled, otherwise either β_+ or β_- would vanish or become positive. Consider a chain of $2N = 4\nu + 2$

atoms and replace the \sum_k by an $\int dk$;² set $\eta = k\Theta/2$. We have $dk = (N/\pi)d\eta$, $-\nu \leq k \leq \nu$ and $-\pi \frac{N-1}{2N} \leq \eta \leq \pi \frac{N-1}{2N}$. The integrand is an even function of η so we replace the integration domain $-\pi/2 \leq \eta \leq \pi/2$ by $0 \leq \eta \leq \pi/2$:

$$E_\pi = \alpha + \frac{4\beta}{\pi} \int_0^{\pi/2} \sqrt{1 - \sin^2 \alpha \sin^2 \eta} d\eta \quad (57)$$

A graph of $E(\frac{\pi}{2}\alpha)$ is found in Ref. [15].

APPENDIX B. THE ROOTS OF EQUATION (25)

The Hückel matrix of order $2N$ is symmetrical and tridiagonal, and therefore has exactly $2N$ non-degenerate real eigenvalues. Since equation (25) is, a part from a constant factor, the secular determinant of the Hückel matrix [6], it has exactly N non-zero distinct roots.

First of all we observe that $\cos Z$ must be real since it is connected to the orbital energy by

$$\lambda_\pm^2 = \beta_+^2 + \beta_-^2 + 2\beta_+\beta_- \cos Z, \quad Z \text{ complex} \quad (58)$$

and λ , β_+ , β_- are all real. Therefore, either Z is real or $Z = i\phi + n\pi$ where ϕ is real and n is an integer. For Z real:

$$2|\delta| = |\beta_+ - \beta_-| \leq |\lambda_\pm| \leq |\beta_+ + \beta_-| = 2|\beta| \quad (59)$$

and we get the ‘regular’ eigenvalues. The case $Z = i\phi + 2n\pi$ is excluded for the following reason. By writing equation (58) as

$$\lambda_\pm^2 = \beta_+^2 + \beta_-^2 + 2\beta_+\beta_- \cosh \phi, \quad \phi \text{ real} \quad (60)$$

we see that $|\lambda_\pm| > 2|\beta|$ as soon as $\phi \neq 0$. But, by Gersgorin’s theorem, the eigenvalues of the Hückel matrix cannot exceed $2|\beta|$ in absolute value: this rules out this case.

Consider now $Z = i\phi + (2n+1)\pi$, equations (58) and (25) become, respectively

$$\lambda_\pm^2 = \beta_+^2 + \beta_-^2 - 2\beta_+\beta_- \cosh \phi, \quad \phi \text{ real} \quad (61)$$

$$\frac{\beta_+ \sinh[(N+1)\phi] - \beta_- \sinh[N\phi]}{\sinh \phi} = 0, \quad \phi \text{ real} \quad (62)$$

By using the standard addition formulae for the hyperbolic functions and

² This derivation is not completely rigorous, but the result is correct. A formal proof can be obtained, e.g., by using the Euler–McLaurin formula [18].

$\beta_{\pm} = \beta(1 \pm \tau)$, equation (62) is rearranged as

$$\frac{\tau \sinh \left[\left(N + \frac{1}{2} \right) \frac{\phi}{2} \right] \cosh \left(\frac{\phi}{2} \right) + \cosh \left[\left(N + \frac{1}{2} \right) \frac{\phi}{2} \right] \sinh \left(\frac{\phi}{2} \right)}{\sinh \phi} = 0 \quad (63)$$

The roots are those of the following equation

$$-\tau \tanh \left[\left(N + \frac{1}{2} \right) \frac{\phi}{2} \right] = \tanh \left(\frac{\phi}{2} \right) \quad (64)$$

with the exclusion of $\phi = 0$. If τ is positive, there is no other crossing point. If $\tau < 0$, there may be another root. The l.h.s of equation (64) starts from 0 at $\phi = 0$ with a slope $-\tau(N/2 + 1/4)$, while the r.h.s. has slope 1/2. If $-\tau(2N + 1) > 1$ the l.h.s. lies above r.h.s. when ϕ is close to zero. But for $\phi \rightarrow \infty$, l.h.s. tends to $-\tau$, while r.h.s. tends to 1. Since $|\tau| < 1$ because $|\delta| < |\beta|$, the two curves cross in a point $\phi_0 > 0$. Since equation (64) is symmetrical in ϕ , there is another root at $-\phi_0$ (see Fig. 5).

From equation (62) we see that ϕ_0 and $-\phi_0$ give rise to the same couple of eigenvalues.

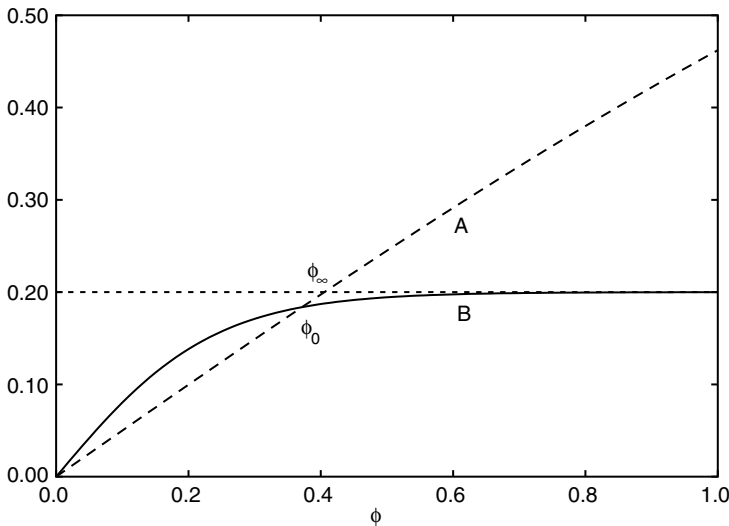


Fig. 5. Graphical solution of equation (64). Curve A: right-hand side; curve B: left-hand side of the equation for $\alpha = 0$, $\beta = -1$, $\tau = -0.2$ and $N = 8$. The root is the abscissa of intersection point ϕ_0 , while ϕ_{∞} is the limiting value of the root for $N \rightarrow \infty$.

Thus, in the case of a linear polyacetylene with N long and $N - 1$ short bonds, i.e., $\tau < 0$, there are two 'extra' eigenvalues corresponding to the root ϕ_0 of equation (64); that root may exist only if $(N + 1/2) > 1/|\tau|$.

We now show that the eigenvalues originated by ϕ_0 approach zero for $N \rightarrow \infty$. First we observe that for any N , ϕ_0 cannot exceed the intersection of the r.h.s. of equation (64) with the line $y = -\tau$, or $\phi_0 < \ln \frac{1+\tau}{1-\tau}$, i.e., ϕ_0 is bounded from above (see Fig. 5). On the other hand, equation (61) can be rearranged as follows:

$$\lambda_{\pm}^2 = 2\beta^2 \cosh^2\left(\frac{\phi_0}{2}\right) \left[\tau^2 - \frac{\sinh^2\left(\frac{\phi_0}{2}\right)}{\cosh^2\left(\frac{\phi_0}{2}\right)} \right] \quad (65)$$

and, taking into account equation (64), we get

$$\lambda_{\pm}^2 = 2\beta^2 \cosh^2\left(\frac{\phi_0}{2}\right) \tau^2 \left\{ 1 - \tanh^2 \left[\left(N + \frac{1}{2} \right) \frac{\phi_0}{2} \right] \right\} \quad (66)$$

Since ϕ_0 is bounded and $\lim_{x \rightarrow \infty} \tanh(x) = 1$ (from below), the proof is complete.

APPENDIX C. ASYMPTOTIC BEHAVIOUR OF THE SUMS

We will use the following results concerning the asymptotic behaviour for $N \rightarrow \infty$ of the following sums where n is an integer [18]:

$$\sum_{j=1}^N j^n = \begin{cases} n \geq 0 : & \text{diverges as } O(N^{n+1}) \\ n = -1 : & \text{diverges as } O(\ln N) \\ n < -1 : & \text{convergent} \end{cases} \quad (67)$$

Similar behaviours are obtained when j is replaced by $j - 1/2$. Moreover we will use the inequalities:

$$\frac{2x}{\pi} \leq \sin x \leq x, \quad 0 \leq x \leq \frac{\pi}{2} \quad (68)$$

$$\frac{1}{x^n} < \frac{1}{\sin^n x} < \frac{\pi}{2x^n}, \quad 0 < x < \frac{\pi}{2}; \quad n \geq 1 \quad (69)$$

$$\left(\frac{N}{j\pi} \right)^n < \left(\sin \frac{j\pi}{N} \right)^{-n} \leq \left(\frac{N}{2j} \right)^n, \quad j = 1, \dots, N/2; \quad n \geq 1 \quad (70)$$

As a consequence of previous equations, we have

$$S(n) = \sum_{j=1}^N \left(\frac{1}{\sin(j\pi/2N)} \right)^n = \begin{cases} n > 1 : & O(N^n) \\ n = 1 : & O(N \ln N) \\ n < 1 : & O(N) \end{cases} \quad (71)$$

Consider e.g. the sum in equation (40):

$$S_1 = \sum_{k=1}^{N/2-1} \frac{\sin^2\left(\frac{k\pi}{N}\right)}{\cos\left(\frac{k\pi}{N}\right)} \quad (72)$$

Let $x = k\pi/N$; we have that $x \rightarrow \pi/2$ for $k = N/2$ and $N \rightarrow \infty$. The origin of the divergence is the pole of the function $1/\cos x$ at $x = \pi/2$. We first move the pole from $\pi/2$ to 0 by changing the variable to $x = k\pi/N$ to $x = \pi/2 - k\pi/N$:

$$j = \frac{N}{2} - k, \quad 1 \leq k \leq \frac{N}{2} - 1, \quad 1 \leq j \leq \frac{N}{2} - 1 \quad (73)$$

$$S_1 = \sum_{j=1}^{N/2-1} \frac{\cos^2\left(\frac{j\pi}{N}\right)}{\sin\left(\frac{j\pi}{N}\right)} \quad (74)$$

Then we break the sum for S_1 in two parts using

$$\frac{\cos^2 x}{\sin x} = \frac{1}{\sin x} - \sin x \quad (75)$$

$$S_1 = \sum_{j=1}^{N/2-1} \sin\left(\frac{j\pi}{N}\right) - \sum_{j=1}^{N/2-1} \frac{1}{\sin\left(\frac{j\pi}{N}\right)} = A + B \quad (76)$$

Sum A is $S(2)$ of equation (71) and therefore is $O(N)$; sum B is $S(1)$ so $B = O(N \ln N)$ and $S = A + B = O(N \ln N)$, $N \rightarrow \infty$.

As concerns the sums appearing in equations (52) and (53), we change summation index from $1 \leq k \leq N$ to $j = N - k + 1$, $1 \leq j \leq N$ and transform cos in sin:

$$\cos\left(\frac{k\pi}{2N+1}\right) = \sin\left(\frac{\pi(j-1/2)}{2N+1}\right) \quad (77)$$

Equation (52) is essentially (40) divided by $2N + 1$; the asymptotic behaviour is $O(\ln N)$. Consider now the two terms on the right of equation (53). The first term is $\frac{4N(N+1)-1}{(2N+1)^2} = O(1)$ times a sum of the same type as S_1 in the previous equation (74) and therefore it is $O(N \ln N)$. The other sums in equation (53) can be rewritten in terms of the following:

$$C = \sum_{k=1}^N \left[\frac{1}{\sin \frac{k\pi}{2N+1}} \right]^3 \rightarrow O(N^3) \quad (78)$$

$$D = \sum_{k=1}^N \frac{1}{\sin \frac{k\pi}{2N+1}} \rightarrow O(N \ln N) \quad (79)$$

$$E = \sum_{k=1}^N \sin \frac{k\pi}{2N+1} \rightarrow O(N) \quad (80)$$

$C/(2N+1)^2$, $D/(2N+1)^2$, $E/(2N+1)^2$ sum up to a $O(N)$ and equation (53) is $O(N \ln N)$.

APPENDIX D. DERIVATION OF EQUATIONS (48) AND (49)

We rearrange equation (42) as

$$(1 + \tau) + (1 - \tau)\eta - (1 - \tau)\eta^{2N+1} - (1 + \tau)\eta^{2N+2} = 0 \quad (81)$$

and set $\eta = \eta_0 + \eta_1\tau + \eta_2\tau^2 + \dots$. The first-order perturbative equation is

$$\begin{aligned} 1 + \eta_1 - \eta_0 - (2N+1)\eta_0^{2N}\eta_1 + \eta_0^{2N+1} \\ - (2N+2)\eta_0^{2N+1}\eta_1 - \eta_0^{2N+2} = 0 \end{aligned} \quad (82)$$

Taking into account $\eta_0^{2N+1} = 1$ we get

$$\eta_1 = \frac{2\eta_0}{2N+1} \frac{1 - \eta_0}{1 + \eta_0} \quad (83)$$

but

$$\frac{1 - \eta_0}{1 + \eta_0} = \frac{\exp\left(-\frac{ik\pi}{2N+1}\right) - \exp\left(\frac{ik\pi}{2N+1}\right)}{\exp\left(-\frac{ik\pi}{2N+1}\right) + \exp\left(\frac{ik\pi}{2N+1}\right)} = -i \tan\left(\frac{k\pi}{2N+1}\right) \quad (84)$$

we get

$$\eta_1(k) = -\frac{2i}{2N+1} \tan\left(\frac{k\pi}{2N+1}\right) \exp\left(\frac{i2k\pi}{2N+1}\right) \quad (85)$$

Since $\eta(k)$ is a derivable function of τ for $\tau = 0$ and $\eta^{-1}(k) = \eta(-k)$ we have also $1/[\eta_1(k)] = \eta_1(-k)$ and

$$\eta_1(k) + \eta_1(-k) = \frac{4}{2N+1} \tan\left(\frac{k\pi}{2N+1}\right) \sin\left(\frac{2k\pi}{2N+1}\right) \quad (86)$$

In a similar fashion one can proceed to the second order. However, the algebra becomes rather cumbersome and we performed the symbolic computations with the program *Mathematica* [19].

APPENDIX E. ANALYSIS OF THE FIRST-ORDER PERTURBATION ENERGY

We consider the orbital energies to first order for a given value of τ and write them as

$$\lambda_0(k) + \lambda_1(k)\tau = 2\beta \left[\cos \phi_k + \frac{\tau \sin^2 \phi_k}{(2N+1)\cos \phi_k} \right] \quad (87)$$

where $\phi_k = k\pi/(2N+1)$, and $0 < \phi_k < \pi/2$. If we replace ϕ_k by a continuous variable ϕ , we get a curve with a maximum at the value ϕ_m fulfilling the equation

$$\frac{\tau(1 + \cos^2 \phi_m)}{2N+1} = \cos^2 \phi_m \quad (88)$$

and therefore $\lim_{N \rightarrow \infty} \phi_m = \pi/2 -$. By inserting equation (88) in equation (87) we have

$$\lambda_0(k_m) + \lambda_1(k_m)\tau = 2\beta \cos \phi_m \left[1 + \frac{\sin^2 \phi_m}{1 + \cos^2 \phi_m} \right] \quad (89)$$

which shows that this orbital energy goes to zero (from below). This maximum of orbital energy is *higher* than the value for $k = N$, which tends to $4\beta\tau/\pi = 4\delta/\pi$ for $N \rightarrow \infty$. The LUMO–HOMO first order energy difference goes to zero for $N \rightarrow \infty$ since the spectrum is symmetrical around zero. We remark that when $\tau < 0$ equation (87) has no stationary point, but assumes values *greater then zero* as k approaches N : it provides an upper bound to the ‘isolated’ eigenvalue $\lambda_0 \rightarrow 0 -$.

REFERENCES

- [1] H. C. Longuet Higgins and L. Salem, *Proc. R. Soc. London, Ser. A*, 1959, **251**, 172.
- [2] R. E. Peierls, *Quantum Theory of Solids*, Clarendon Press, Oxford, 1955.
- [3] J.-L. Calais, *Mott and Peierls Gaps*, Technical Note No. 603, Quantum Chemistry Group, Uppsala University, 1979.
- [4] M. J. Rice and S. Strässler, *Solid State Commun.*, 1973, **13**, 125.
- [5] T. Kennedy and E. H. Lieb, *Phys. Rev. Lett.*, 1987, **59**, 1309.
- [6] (a) J. E. Lennard-Jones, *Proc. R. Soc., Ser. A*, 1937, **158**, 280; (b) C. A. Coulson, *Proc. R. Soc. London, Ser. A*, 1938, **164**, 383.
- [7] L. Salem, *The Molecular Orbital Theory of Conjugated Systems*, W.A. Benjamin, Inc., New York, 1966.
- [8] Y. Aoki and A. Imamura, *J. Chem. Phys.*, 1995, **103**, 9726.
- [9] T. Tada and Y. Aoki, *Int. J. Quantum. Chem.*, 2002, **88**, 401.
- [10] H. C. Longuet-Higgins and L. Salem, *Proc. R. Soc. London, Ser. A*, 1959, **251**, 172.
- [11] (a) W. P. Su, J. R. Schrieffer and A. J. Heeger, *Phys. Rev. Lett.*, 1979, **42**, 1698; (b) W. P. Su, J. R. Schrieffer and A. J. Heeger, *Phys. Rev. B*, 1980, **22**, 2099.
- [12] J. Cioslowski and M. Kertesz, *J. Chem. Phys.*, 1986, **85**, 7193.
- [13] B. C. Shin, *Bull. Aust. Math. Soc.*, 1997, **55**, 249.
- [14] (a) S. Arimoto, *Phys. Lett. A*, 1985, **113**, 126; (b) S. Arimoto, *Phys. Lett. A*, 1987, **124**, 131; (c) S. Arimoto, *Phys. Lett. A*, 1987, **124**, 275.
- [15] M. Abramowitz, I. A. Stegun, *Handbook of Mathematical Functions with Formulas, Graphs and Mathematical Tables*, National Bureau of Standards, Applied Mathematical Series n. 55.
- [16] See, e.g., G. H. Golub, and G. F. van Loan, *Matrix Computations*, North Oxford Academic, Oxford, 1983; in quantum chemical literature this theorem is known as the Hylleraas–Undheim–McDonald’s theorem, but it goes back to Cauchy (1826).
- [17] See, e.g., R. Englman, *The Jahn–Teller Effect in Molecules and Crystals*, Wiley-Interscience, New York, 1972.
- [18] See R. L. Graham, D. E. Knuth and O. Patashnik, *Concrete Mathematics*, Addison-Wesley, Reading, MA, 1989, Chapter 9.
- [19] Wolfram Research Inc., *Mathematica Version 4.2*, Champaign, IL, 2003.

Conjugated Polymers in External DC Fields

Michael Springborg and Yi Dong

Physical Chemistry, University of Saarland, 66123 Saarbrücken, Germany

Abstract

Different aspects related to the theoretical treatment of the electronic properties of infinite, periodic, conjugated polymers exposed to external DC fields are discussed. Various proposed methods are studied within a simple Hückel-like model that includes alternating hopping integrals. It is found that when rewriting the extra term due to the DC field as one that involves the k derivatives of the Bloch functions, one has to be very careful. First, only under certain circumstances one may ignore those parts that are non-diagonal in k , whereas under other circumstances results that depend on the (unphysical) phase factors of the Bloch waves are obtained. On the other hand, an approach based on Wannier functions is found to be mathematically well founded. Based on these results, we subsequently present a density-functional method that uses Wannier functions and that can be used in treating infinite, periodic systems exposed to DC fields. Some first results for an infinite linear chain of carbon atoms are presented and discussed.

Contents

1. Introduction	369
2. General considerations and a simple Hückel-like model	372
3. A first-principles method for polymers	383
4. Conclusions	391
Acknowledgements	391
References	392

1. INTRODUCTION

Theoretical chemistry and physics are partly concerned with the development of new theoretical and computational methods for studying special properties and/or materials and partly concerned with the application of these methods to questions of current interest. Thereby, a central issue is that of exploring new materials or properties that so far has been out of reach with theoretical methods.

Slightly more than 10 years ago one of the present authors together with colleagues in Uppsala, including Osvaldo Goscinski, used one of the simplest possible conjugated polymers, *trans*-polyacetylene, $(\text{CH})_x$, as

a model compound for exploring new computational tools for calculating electronic properties of infinite, periodic, polymeric systems [1,2]. In order to celebrate the 65th birthday of Osvaldo Goscinski, it therefore seems natural to return to a simple conjugated polymer and use it as a model system for studying specific properties of polymeric systems that are of current interest and, simultaneously, pose challenges to theoretical treatments. Thus, we shall here study the response of conjugated polymers to external electrostatic fields. We stress that although this has been the subject of many theoretical studies over the last 1–2 decades (see, e.g., Ref. [3]), there remains still a number of only partly solved problems that warrant more detailed investigations. In this spirit we shall here present results of some simple model calculations together with present and apply a formalism for treating such fields directly in a parameter-free electronic-structure method for infinite, periodic polymers.

Conjugated polymers have been at the focus of a large research activity over more than a quarter of century (see, e.g., Refs. [4–7]). Compared with more traditional plastics, the conjugated polymers contain a backbone with sp^2 - and sp -bonded (and not sp^3 -bonded) carbon atoms. The last valence electron per carbon atom occupies a p orbital and participates in π bonds between the carbon atoms. This has two consequences: the polymers are essentially planar, and the energy gap between occupied and unoccupied orbitals is small (i.e., corresponds to that of conventional semiconductors) with π orbitals appearing closest to the Fermi level.

There is a strong coupling between electrons and phonons (structure) which leads to a lowest-energy structure with alternating C–C bond lengths and to the occurrence of structural defects (i.e., solitons and polarons) when the chains are charged. Both finite oligomers and essentially infinite polymers can be synthesized, and a special class of oligomers is the finite, so-called push–pull systems where the two end-groups are different, so that an excitation involves an internal charge transfer from one end to the other.

Due to the combination of mechanical properties as plastics and electronic properties as crystalline semiconductors, these materials have been considered interesting for many special-purpose applications, including light-emitting diodes, transistors, and sensors. For the present purpose it is, however, most important to observe that the π electrons that are somewhat loosely bound to the backbone, but not so loosely bound that they are free-electron-like, give rise to very large linear and, in particular, non-linear responses to external electric fields. The responses can be quantified through the polarizabilities (α) and hyperpolarizabilities (β, γ, \dots) by expanding either the dipole moment

$$\mu_i = \mu_i^{(0)} + \sum_{j=x,y,z} \alpha_{ij} E_j + \sum_{j,k=x,y,z} \beta_{ijk} E_j E_k + \sum_{j,k,l=x,y,z} \gamma_{ijkl} E_j E_k E_l + \dots \quad (1)$$

or the total energy

$$E_{\text{tot}} = E_{\text{tot}}^{(0)} - \sum_{i=x,y,z} \mu_i^{(0)} E_i - \frac{1}{2} \sum_{i,j=x,y,z} \alpha_{ij} E_i E_j - \frac{1}{3} \sum_{i,j,k=x,y,z} \beta_{ijk} E_i E_j E_k - \frac{1}{4} \sum_{i,j,k,l=x,y,z} \gamma_{ijkl} E_i E_j E_k E_l + \dots \quad (2)$$

in the electric-field components. When AC fields are applied, the (hyper)polarizabilities become frequency dependent,

$$p_{i,j,k,\dots,m}(\omega_i, \omega_j, \omega_k, \dots, \omega_m) \quad \text{with } \omega_i = |\omega_j \pm \omega_k \pm \dots \pm \omega_m|, \quad (3)$$

with p being $\alpha, \beta, \gamma, \dots$. Non-zero values of β and γ lead to effects like second- and third-harmonic generation, four-wave mixing, electric-field-induced second harmonic, the Kerr effects, and the Pockels effect, which are interesting both for basic and for applied science. Accordingly, much effort is put into obtaining maximally large values of these parameters.

In the thermodynamic limit any property Z for a finite system $A-(X)_n-D$ will be either independent of or proportional to n . Experimental [8] and theoretical [9–13] studies have, however, shown that when Z is the polarizability α or the hyperpolarizability γ , $Z(n)/n$ [or $Z(n) - Z(n-1)$] converges only very slowly as a function of n towards the large- n limit and, moreover, the convergence for γ is slower than that for α [10]. On the other hand, since the larger systems tend to have larger values of $Z(n)/n$ than the smaller ones, it is highly relevant to consider the large systems. Thus, considering infinite, periodic systems is a useful alternative.

For finite oligomers of polyacetylene it has been found [12] that the vibrational contribution to the total polarizability amounts to roughly 10% of the total polarizability, and, although it is known that this percentage will increase for the hyperpolarizabilities, we shall here concentrate on the electronic part of the responses.

Most often, (hyper)polarizabilities of polymers are calculated using a perturbation-theoretical approach based on the formalism of Genkin and Mednis [14]. Thereby, both occupied and unoccupied orbitals have to be included in the calculation and the fact that different electronic-structure methods (most notably, Hartree–Fock- and density-functional-based methods) often yield fairly inaccurate results for the unoccupied orbitals may be the reason for the fact that the calculated (hyper)polarizabilities often depend strongly on the method (see, e.g., Refs. [13,15]). Thus, in order to access the accuracy of the different methods or, alternatively, to avoid the problems related to the accuracy of the unoccupied orbitals, one may include a DC field directly in the calculations whereby at least the static (hyper)polarizabilities can be calculated.

However, the inclusion of a static field is a non-trivial endeavor. First, even for the smallest possible system (e.g., an isolated hydrogen atom) and

for the smallest possible external field, the eigenvalue spectrum changes dramatically: there are no bound states, and states that, in the field-free case, were bound change into resonances. And for an infinite system parts of the system will be exposed to a divergent field. On the other hand, for crystalline systems it has been found [16] that the polarization is a bulk property, i.e., is accessible by considering a single unit cell. This can, e.g., be done through the Berry-phase formulation of polarization (see, e.g., Ref. [17]). Moreover, finite-chain calculations have indicated [18,20] that the electron distribution for a chain exposed to a DC field is roughly periodic far away from the boundaries, suggesting that a periodic-chain treatment should be possible. This is what we shall address in this contribution. We shall discuss in detail a simple Hückel-like model that allows for detailed studies of also larger systems and that can give information on the consequences of the different approximations that have been proposed for including an external DC field for an infinite, periodic polymer. Subsequently, we shall present a method for including a DC field in a parameter-free electronic-structure method, and finally we shall present some results using this approach. For the sake of completeness we mention that some preliminary results have been presented previously [19].

We finally mention that one further reason for studying infinite, periodic polymers in external DC fields is the findings [20–22] that currently applied approximate density functionals (like the one we are using) may be inadequate when calculating responses to external DC fields. Thus, studies like the ones of this contribution may provide further insight into the failures of the functionals. On the other hand, we stress that our basic method is, in principle, not dependent on these problems and can be modified easily according to new proposals for approximate density functionals.

2. GENERAL CONSIDERATIONS AND A SIMPLE HÜCKEL-LIKE MODEL

For a single particle of mass m and charge q , moving in the potential $V(\vec{r})$ (e.g., from nuclei), that is being exposed to an external electro-magnetic field, the Hamilton operator becomes

$$\hat{H} = \frac{1}{2m} \left(\hat{\vec{P}} - \frac{q}{c} \vec{A} \right)^2 + V(\vec{r}) + qU(\vec{r}). \quad (4)$$

Here, c is the speed of light and \vec{P} is the momentum conjugate to \vec{r} . The electric and magnetic fields are given by

$$\vec{E} = \frac{\partial \vec{A}}{\partial t} - \vec{\nabla} U, \quad \vec{B} = \vec{\nabla} \times \vec{A}. \quad (5)$$

Whereas \vec{E} and \vec{B} are physical and measurable quantities that are unique, this is not the case for \vec{A} and U and there is some arbitrariness in how these two are chosen, i.e., how the gauge is chosen.

In the electric-dipole approximation, valid for wavelengths of the field much larger than typical distances of the particle, \vec{A} is set equal to 0, giving

$$\hat{H} = \frac{\hat{P}^2}{2m} + V(\vec{r}) + qU(\vec{r}), \quad (6)$$

whereas in the Coulomb gauge, valid for the wavelength of the field being comparable with the typical distances for the particle, U is set to 0, giving

$$\hat{H} = \frac{1}{2m} \left(\hat{P} - \frac{q}{c} \vec{A} \right)^2 + V(\vec{r}). \quad (7)$$

We shall here choose the electric-dipole approximation, but comment on the use of the Coulomb gauge below.

In order to explore the effects of further approximations, we shall study in some detail the Hückel-like Hamiltonian

$$\hat{H} = \hat{H}_{\text{tb}} + \hat{H}_{\text{ext}}, \quad (8)$$

where the last term is caused by the external field, described within the electric-dipole approximation.

The tight-binding part is given by

$$\hat{H}_{\text{tb}} = \sum_i \alpha_i \hat{c}_i^\dagger \hat{c}_i + \sum_i \beta_i (\hat{c}_{i+1}^\dagger \hat{c}_i + \hat{c}_i^\dagger \hat{c}_{i+1}). \quad (9)$$

Here, we have assumed that we have one orbital per site (labeled χ_i with i being the site) and that \hat{c}_i and \hat{c}_i^\dagger are the corresponding annihilation and creation operators. Moreover,

$$\langle \chi_j | \hat{H}_{\text{tb}} | \chi_k \rangle = \begin{cases} \alpha_j & \text{for } j = k \\ \beta_j & \text{for } k = j + 1 \\ \beta_k & \text{for } k = j - 1 \\ 0 & \text{otherwise} \end{cases} \quad (10)$$

We will assume that the external field only affects the diagonal elements,

$$\hat{H}_{\text{ext}} = \sum_i E_i \hat{c}_i^\dagger \hat{c}_i. \quad (11)$$

We will assume that the system has one electron per site, that the on-site energies α_i are site independent (and accordingly can be set equal to 0), and that β_i alternates between $t_- = 0.5$ and $t_+ = 1.5$. For an infinite periodic chain without the external field we will accordingly have an

occupied band between -2 and -1 , a gap between -1 and $+1$, and an unoccupied band between $+1$ and $+2$. These numbers can be used in estimating the strength of a field above which the calculations become meaningless. Considering a finite system with N sites and letting $E_i = Eia/2$, the N th atom experiences a potential of roughly $NEa/2$ higher than the 1st atom does. If this value is larger than the gap, electrons will start flowing from one end of the system to the other. In order to avoid this run-away solution, we must require $E < 4|t_+ - t_-|/aN$. Therefore, we have chosen a fairly large value of the hopping-integral alternation. Another reason is that calculations for a similar model [18] have shown that the polarizability per site converges faster as a function of chain length when the hopping-integral alternation is larger.

We shall now use this model in studying different approximations. We set

$$E_i = (i - M)Ea/2 \quad (12)$$

($a/2$ is the average interatomic distance) and consider a chain of $2M$ sites with periodic boundary conditions, i.e., in effect we assume that atom 1 and atom $2M$ are bonded, too. A very special case is that of $2M = 2$, where we accordingly assume that the external potential has the periodicity of the lattice. For larger values of $2M$ the approximation is that of assuming that the potential has the shape of a sawtooth curve with the periodicity being that of the Born von Kármán zone; i.e., the approximation is equivalent to considering an infinite, periodic system for which an electronic-structure calculation has been performed using M equidistant k points in the first Brillouin zone. Proposing that the external potential due to the field should have this periodicity is not new [23,24], and in fact Resta [25] has shown that one *has* to use an operator with the periodicity of the Born von Kármán zone. These approximations are schematically illustrated in Fig. 1.

Otto [26] and later Kudin and Scusseria [27] realized that the major problem for directly including the field in an electronic-structure calculation is related to the fact that the field destroys the periodicity. On the other hand, as mentioned above, both mathematical arguments and actual calculations have found that the charge distribution inside an extended system remains periodic also in the presence of an external field. Therefore, Otto sought a separation of the form

$$\hat{H}_{\text{ext}} = \hat{H}'_{\text{ext}} + \hat{H}''_{\text{ext}}, \quad (13)$$

where the first term has the periodicity of the lattice and the second is a remainder. Then, only the first term is kept. We stress that this separation may be rather arbitrary (one may add any lattice-periodic term to \hat{H}'_{ext} when simultaneously subtracting it from \hat{H}''_{ext}).

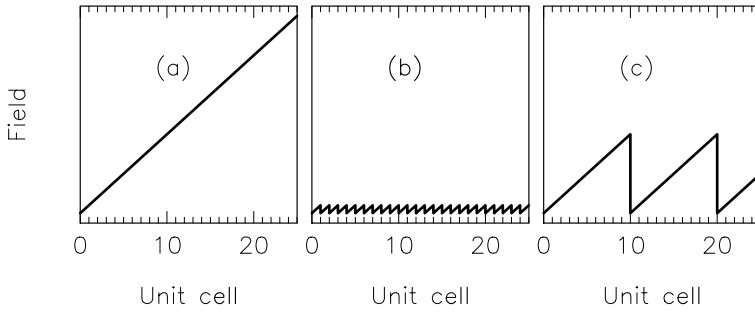


Fig. 1. Schematic representation of the external field for (a) a finite system with the true field, (b) the approximation that the field has the periodicity of the lattice, and (c) that it has the periodicity of the Born von Kármán zone.

According to Bloch, in the absence of the external field any orbital is a Bloch wave of the form

$$\psi_n^{\vec{k}}(\vec{r}) = e^{i\vec{k}\cdot\vec{r}} u_n^{\vec{k}}(\vec{r}), \quad (14)$$

where n is a band index and $u_n^{\vec{k}}$ is lattice-periodic. Then

$$\vec{r}\psi_n^{\vec{k}}(\vec{r}) = ie^{i\vec{k}\cdot\vec{r}}\vec{\nabla}_{\vec{k}}e^{-i\vec{k}\cdot\vec{r}}\psi_n^{\vec{k}}(\vec{r}) - i\vec{\nabla}_{\vec{r}}\psi_n^{\vec{k}}(\vec{r}). \quad (15)$$

By neglecting the second term, only a lattice-periodic term is kept. Maybe the most important problem of this approach is that it is closely tied to the precise definition of the orbitals, equation (14), so that different definitions of the Bloch waves lead ultimately to different definitions of \hat{H}'_{ext} . In order to demonstrate this in detail we shall study our simple Hückel model.

For this model and for a ring of $2M$ sites the Bloch functions for the two bands are given by

$$\psi_n^k = \frac{1}{\sqrt{2M}} \sum_{m=1}^M (\chi_{2m-1} \pm e^{i\phi(k)} \chi_{2m}) e^{ikam} e^{i\theta_n(k)}, \quad (16)$$

where a is the length of one unit cell, $e^{i\theta_n(k)}$ is an, in principle, arbitrary k - and band-dependent phase factor, and

$$e^{i\phi(k)} = \sqrt{\frac{t_+ + t_- e^{ika}}{t_+ + t_- e^{-ika}}}. \quad (17)$$

By using that we have assumed that only on-site overlap matrix elements are non-zero, and that the electrostatic field gives non-zero matrix elements only

for orbitals on the same atom, we obtain after some manipulations

$$\begin{aligned}
 & i \left\langle \psi_{n_1}^{k_1} \left| e^{ik_2 z} \frac{\partial}{\partial k_2} \right| e^{-ik_2 z} \psi_{n_2}^{k_2} \right\rangle \\
 &= -\frac{1}{2M} \sum_m \langle (\chi_{2m-1} \pm e^{i\phi(k_1)} \chi_{2m}) | (am - z) (\chi_{2m-1} \pm e^{i\phi(k_2)} \chi_{2m}) \\
 &\quad \pm e^{i\phi(k_2)} \phi'(k_2) \chi_{2m} + \theta'_{n_2}(k_2) (\chi_{2m-1} \pm e^{i\phi(k_2)} \chi_{2m}) \rangle e^{ia(k_2 - k_1)m} \\
 &\quad \times e^{i(\theta_{n_2}(k_2) - \theta_{n_1}(k_1))} \\
 &= \delta_{k_1, k} \delta_{k_2, k} \left[\frac{1}{2} \langle \chi_1 | z - a | \chi_1 \rangle \pm \frac{1}{2} \langle \chi_2 | z - a | \chi_2 \rangle \mp \frac{1}{2} \phi'(k) \langle \chi_2 | \chi_2 \rangle \right. \\
 &\quad \left. - \frac{1}{2} \theta'_{n_2}(k) (\langle \chi_1 | \chi_1 \rangle \pm \langle \chi_2 | \chi_2 \rangle) \right] e^{i(\theta_{n_2}(k_2) - \theta_{n_1}(k_1))} \\
 &= \delta_{k_1, k} \delta_{k_2, k} e^{i(\theta_{n_2}(k) - \theta_{n_1}(k))} \left[-\frac{a}{4} - \frac{Ma}{4} (1 \pm 1) \mp \frac{1}{2} \phi'(k) \right. \\
 &\quad \left. - \frac{1}{2} \theta'_{n_2}(k) (1 \pm 1) \right] \quad (18)
 \end{aligned}$$

when using that $\langle \chi_p | z | \chi_p \rangle = (p - M)a/2$. Moreover, in the first right-hand side, we choose the same (different) sign in the expressions for the bra and the ket if $n_1 = n_2$ ($n_1 \neq n_2$), whereas the upper (lower) sign is used when $n_1 = n_2$ ($n_1 \neq n_2$) in the subsequent expressions.

This is the term that is kept in the approach by Otto. The one that is neglected is

$$\begin{aligned}
 & -i \left\langle \psi_{n_1}^{k_1} \left| \frac{\partial}{\partial k_2} \right| \psi_{n_2}^{k_2} \right\rangle = \frac{1}{2M} \sum_m \langle (\chi_{2m-1} \pm e^{i\phi(k_1)} \chi_{2m}) | am \\
 &\quad \times (\chi_{2m-1} \pm e^{i\phi(k_2)} \chi_{2m}) \pm e^{i\phi(k_2)} \phi'(k_2) \chi_{2m} + \theta'_{n_2}(k_2) \\
 &\quad \times (\chi_{2m-1} \pm e^{i\phi(k_2)} \chi_{2m}) \rangle e^{ia(k_2 - k_1)m} e^{i(\theta_{n_2}(k_2) - \theta_{n_1}(k_1))} \\
 &= e^{i(\theta_{n_2}(k_2) - \theta_{n_1}(k_1))} \left[\delta_{k_1, k} \delta_{k_2, k} \frac{1}{2} ((1 \pm 1) \theta'_{n_2}(k) \pm \phi'(k)) \right. \\
 &\quad \left. + (1 \pm e^{i(\phi(k_2) - \phi(k_1))}) \frac{a}{2M} \sum_m m e^{iam(k_2 - k_1)} \right]. \quad (19)
 \end{aligned}$$

It is clear that the term neglected by Otto has contributions also from $k_1 = k_2$. Moreover, what is considerably more problematic, the separation into what is kept and what is ignored depends on the phase factors, which often in a practical calculation are out of control. It is also clear that the largest term that is being ignored is comparable to the largest term that is being kept.

When adding the expressions from equations (18) and (19), one obtains

$$\langle \psi_{n_1}^k | \vec{r} | \psi_{n_2}^k \rangle = e^{i(\theta_{n_2}(k) - \theta_{n_1}(k))} \left[-\frac{a}{4} + \delta_{n_1, n_2} \frac{a}{2} \right], \quad (20)$$

i.e., the unsatisfactory dependence on the phase factors is canceled, except as understandable general pre-factors. One may invert equation (16), thereby writing the atom-centered basis functions in terms of the Bloch functions. Subsequently, equations (18) and (19) can be used in identifying $\langle \chi_{m_1} | \hat{H}' | \chi_{m_2} \rangle$. Not surprisingly, it also turns out that this depends on the phase factors.

Alternatively, one may base the discussion on the Bloch waves constructed from the atom-centered basis functions,

$$\chi_1^k = \frac{1}{\sqrt{M}} \sum_{m=1}^M \chi_{2m-1} e^{ikam}, \quad \chi_2^k = \frac{1}{\sqrt{M}} \sum_{m=1}^M \chi_{2m} e^{ikam}, \quad (21)$$

whereby

$$i \left\langle \chi_{n_1}^{k_1} \left| e^{ik_2 z} \frac{\partial}{\partial k_2} \right| e^{-ik_2 z} \chi_{n_2}^{k_2} \right\rangle = \begin{cases} -\frac{(M+1)a}{4} \delta_{k_1, k_2} & \text{for } n_1 = n_2 = 1 \\ -\frac{Ma}{4} \delta_{k_1, k_2} & \text{for } n_1 = n_2 = 2 \\ 0 & \text{otherwise} \end{cases} \quad (22)$$

and

$$-i \left\langle \chi_{n_1}^{k_1} \left| \frac{\partial}{\partial k_2} \right| \chi_{n_2}^{k_2} \right\rangle = \begin{cases} \frac{a}{M} \sum_{m=1}^M m e^{ia(k_2 - k_1)m} & \text{for } n_1 = n_2 \\ 0 & \text{otherwise.} \end{cases} \quad (23)$$

This case corresponds actually to the separation of Fig. 5, to be discussed below, and when only keeping the term \hat{z}_1 that then replaces \hat{H}'_{ext} .

Returning to equations (4) and (5), an electrostatic term may be described in the electric-dipole approximation through

$$U = -\vec{E}_0 \cdot \vec{r}, \quad \vec{A} = \vec{0} \quad (24)$$

or, alternatively, in the Coulomb gauge through

$$U = 0, \quad \vec{A} = t \cdot \vec{E}_0. \quad (25)$$

The latter case involves a potential that is spatially invariant and, accordingly, attractive from a computational point of view. This was the original idea of Genkin and Mednis [14] that recently was taken up by Kirtman *et al.* [28,29]. Since the Coulomb gauge is based on a time-dependent external (vector) potential, the solutions become time dependent, but as argued by Genkin and Mednis they can be written as (time-dependent) Bloch waves characterized by

$$\vec{\kappa} = \vec{k} + \frac{e}{c} \vec{A}(t) \quad (26)$$

with $-e$ being the electronic charge. [Notice that for a polymer, $\vec{k} = (0, 0, k)$, when assuming that the polymer axis is the z -axis.] Thus, the Bloch functions (either in form of Bloch waves constructed from a set of atom-centered basis functions, which is the case in the approach of Kirtman *et al.*, or in form of the exact solutions for the field-free case, which is used by Genkin and Mednis) can be used in studying the case of an external field. Then, one has to study matrix elements between different Bloch waves and the perturbing operator, which, it turns out, is \vec{r} . For this, they arrive ultimately at an expression like equation (13), and also they obtain

$$\hat{H}'_{\text{ext}} = ie^{\vec{k} \cdot \vec{r}} \vec{\nabla}_{\vec{k}} e^{-i\vec{k} \cdot \vec{r}}. \quad (27)$$

This result was based partly on earlier arguments by Blount [30] who discussed how to represent \vec{r} for infinite, periodic crystals. Since this discussion is of fundamental importance to the present study, we shall reproduce it here with some modifications that take into account the procedures of performing band-structure calculations for a polymer.

Usually, a band-structure calculation for a polymer that is considered periodic in the z direction is performed by considering a discrete, equidistant set of k points,

$$\frac{ka}{\pi} = 0, \pm \frac{1}{K}, \pm \frac{2}{K}, \dots, \pm \frac{K-1}{K}, 1 \quad (28)$$

($M = 2K$). Then, all Bloch functions have the periodicity of the Born von Kármán zone, i.e., of the length $2K \cdot a$, with a being the length of one unit cell. With n being the band index, any function with this periodicity can be expanded in the Bloch functions,

$$f(\vec{r}) = \sum_k \sum_n \psi_n^k(\vec{r}) : f_n^k = \sum_k \sum_n e^{ikz} u_n^k(\vec{r}) : f_n^k. \quad (29)$$

With \hat{z} being the sawtooth representation of z , shown in Fig. 1(c), we consider functions that are in its domain, i.e., functions for which $\int_{\text{BvK}} |\hat{z}f(\vec{r})|^2 d\vec{r}$ exists (BvK denotes one Born von Kármán zone). Also $\hat{z}f(\vec{r})$ has the

periodicity of the BvK zone and, accordingly,

$$\hat{z}f(\vec{r}) = \sum_k \sum_n \hat{z}u_n^k(\vec{r})e^{ikz}f_n^k. \quad (30)$$

In contrast to the discussion above, we shall now approach the situation of a real electronic-structure calculation where one does not use an infinite, continuous set of k points, but in most cases a finite set of equidistant points.

We define an operator $\hat{\Delta}$ that is acting on the function $f(\vec{r})$ but whose action is closely linked to the expansion of equation (29), i.e., to the definition of the Bloch functions ψ_n^k . Thus, we define $\hat{\Delta}$ through

$$\begin{aligned} \hat{\Delta}f(\vec{r}) &= \hat{\Delta} \left[\sum_k \sum_n \psi_n^k(\vec{r})f_n^k \right] = \hat{\Delta} \sum_k f_k(\vec{r}) = \sum_k \hat{\Delta}f_k(\vec{r}) \\ &= \sum_k \frac{f_k(\vec{r}) - f_{k-\Delta k}(\vec{r})}{\Delta k}, \end{aligned} \quad (31)$$

with $\Delta k = \pi/aK$. Notice that in the limit of $\Delta k \rightarrow 0$, $\hat{\Delta}$ changes into the differential operator $\partial/\partial k$.

We then have

$$\begin{aligned} -i\hat{\Delta}f(\vec{r}) + ie^{ikz}\hat{\Delta}e^{-ikz}f(\vec{r}) &= \frac{i}{\Delta k} \sum_k \sum_n \{e^{ikz}[u_n^k(\vec{r})f_n^k - u_n^{k-\Delta k}(\vec{r})f_n^{k-\Delta k}] \\ &\quad - [\psi_n^k(\vec{r})f_n^k - \psi_n^{k-\Delta k}(\vec{r})f_n^{k-\Delta k}]\} \\ &= \frac{i}{\Delta k} [1 - e^{i\Delta kz}] \sum_k \sum_n \psi_n^k(\vec{r})f_n^k, \end{aligned} \quad (32)$$

where the first equality is obtained by using that $\hat{\Delta}$ is a linear operator. Only the second term on the left-hand side gives a non-zero contribution, suggesting to keep only this. Hence, in this case taking the limit $\Delta k \rightarrow 0$ one obtains the first term on the right-hand side of equation (15) for \vec{r} acting on some function, except that the function has to be continuous in k and, accordingly, cannot be a Bloch function.

Some comments of caution are required here. First, as also discussed by Blount [30] and by Kirtman *et al.* [29], one has to be careful with the phases of the Bloch functions. Whereas these functions are continuous in \vec{r} space, this may not be the case in k space. Thus, when considering the limit $K \rightarrow \infty$ (i.e., $\Delta k \rightarrow 0$), it is important that the limit exists, i.e., $\psi_n^k f_n^k$ is continuous and differentiable in k space. In that case, one may neglect the first term on the left-hand side and, accordingly, arrive at the approximation of equation (27). On the other hand, only in that limit the expression on the right-hand side corresponds to a Hermitean operator.

A special case occurs when inserting one of the Bloch functions as $f(\vec{r})$, i.e., choosing

$$f_n^k = \delta_{n,n_0} \delta_{k,k_0}. \quad (33)$$

Then

$$-i\hat{\Delta}f(\vec{r}) = 0, \quad ie^{ikz}\hat{\Delta}e^{-ikz}f(\vec{r}) = \frac{i}{\Delta k} [1 - e^{i\Delta kz}] \psi_{n_0}^{k_0}(\vec{r}). \quad (34)$$

Equations (32) and (34) provide an approach for including \vec{r} (or, rather, z) directly in an electronic-structure calculation when using a finite, discrete set of k points. However, only in the limit of an infinite, continuous set, the true z is included, whereas for a discrete set, z is being replaced by

$$\hat{z} = \frac{i}{\Delta k} [1 - e^{i\Delta kz}] \quad (35)$$

that has the periodicity of the Born von Kármán zone, but is not Hermitean.

It shall be emphasized that the operator $\hat{\Delta}$ acts on a function that is expanded in terms of Bloch functions, and that the action is on the expansion coefficients and Bloch functions, specifically on their dependence on k , i.e., it depends strongly on the precise definition of the Bloch functions.

The situation is different when the function depends explicitly on k and this dependence is included in the action. This is, e.g., the case for the operators defined by Otto [26]. His formalism corresponds to define an operator $\hat{\Delta}'$ through

$$\begin{aligned} -i\hat{\Delta}'\psi_{n_0}^{k_0}(\vec{r}) &= -\frac{i}{\Delta k} [\psi_{n_0}^{k_0}(\vec{r}) - \psi_{n_0}^{k_0-\Delta k}(\vec{r})], \\ ie^{ikz}\hat{\Delta}'e^{-ikz}\psi_{n_0}^{k_0}(\vec{r}) &= \frac{i}{\Delta k} [\psi_{n_0}^{k_0}(\vec{r}) - e^{i\Delta kz}\psi_{n_0}^{k_0-\Delta k}(\vec{r})]. \end{aligned} \quad (36)$$

For this, the limits $\Delta k \rightarrow 0$ may exist, provided that the functions ψ_n^k are continuous and differentiable in k space. When only being interested in 'integrated' quantities (e.g., the sum of the operator acting on the different Bloch functions), equations (34) and (36) give – when summed over all contributions – identical results. However, when considering the individual terms, for instance, when including the term in the calculation of the orbital energies, this is not necessarily the case.

Kirtman *et al.* [28,29] implemented this approach in an *ab initio* program for infinite, periodic polymers and calculated subsequently both linear and non-linear responses to external fields. The results were compared with similar results for finite oligomers of increasing size. The results of the two

independent sets of calculations show a convincing agreement, suggesting that it is justified to ignore the formal problem above, although the mathematical rigor for this is lacking.

The discussion makes it obvious that it is a far from trivial problem how to treat \vec{r} in an actual calculation. Therefore, we decided to first study the Hückel-like model numerically, using two different approximations for \vec{r} . In one case we used the full potential of Fig. 1(c), whereas in the other case we considered only the periodic part of Fig. 1(b). As discussed above, the latter case corresponds to use the separation of equations (13) and (15) applied on the Bloch waves formed by the basis functions (i.e., *not* the eigenfunctions).

Figure 2 shows some of the results for the calculations. We considered a ring of 204 sites and the two approximations of Fig. 1(b) and (c) for different field strengths. Since the Hückel model assumes a set of atom-centered orthonormal basis functions, the coefficients to the eigenfunctions give directly information on the number of electrons on the different atoms. From the total number of electrons, depicted in the figure, it is immediately seen that, for the largest fields, the approximation of Fig. 1(c) leads to solutions where parts of the electrons flow from one end to the other, but in the middle part of the chain the two curves seem to be very similar. There are, however, also in this case minor differences that may be important. Thus, simply

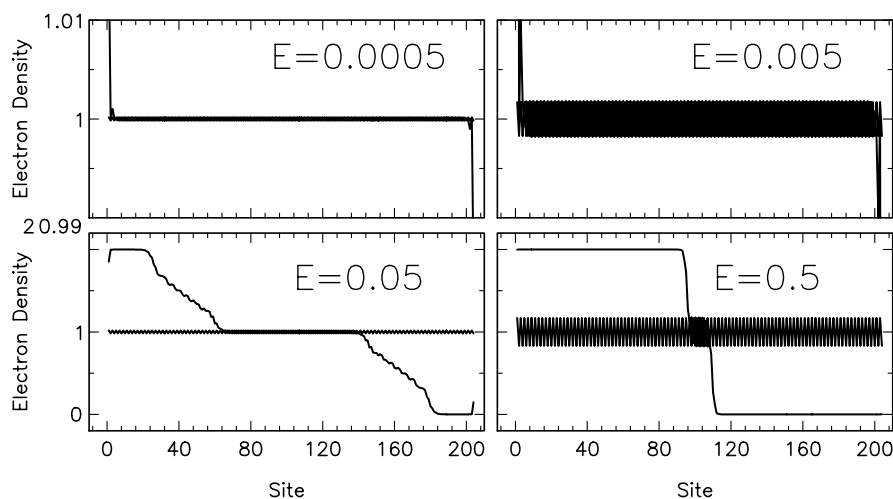


Fig. 2. The number of electrons on the different atoms as found for the Hückel model with a ring of 204 sites exposed to an external field. The field strength is given on the figure, and the two curves in each panel corresponds to the two approximation of Fig. 1(b) and (c).

considering the number of electrons around atom number 101, we find this to be $1 \pm n$ with n being 0.00017, 0.00172, 0.01716, and 0.1687 for the sawtooth curve with the lattice periodicity and for the four different field strengths, respectively, whereas the sawtooth curve with the Born von Kármán periodicity gives n of 0.00018, 0.00182, 0.01821, and around 0.17, respectively, i.e., in general slightly larger.

When looking at the variation of the total energy as a function of field strength (Fig. 3), it is also clear that this depends on the approximation. First, as Fig. 3(a) shows, the energy changes dramatically for field strengths exceeding the value where electrons start flowing from one end to the other [which happens earlier for the approximation of Fig. 1(c) than for that of Fig. 1(b)]. But also for weaker fields, where the electronic distribution is essentially homogeneous throughout the system [cf. Fig. 3(b)], there are clear differences depending on how the system is treated and in general, the approximation of Fig. 1(c) gives a stronger field dependence of the total energy than the approximation of Fig. 1(b), and for the former the dependence increases as a function of system size, also for fairly large sizes.

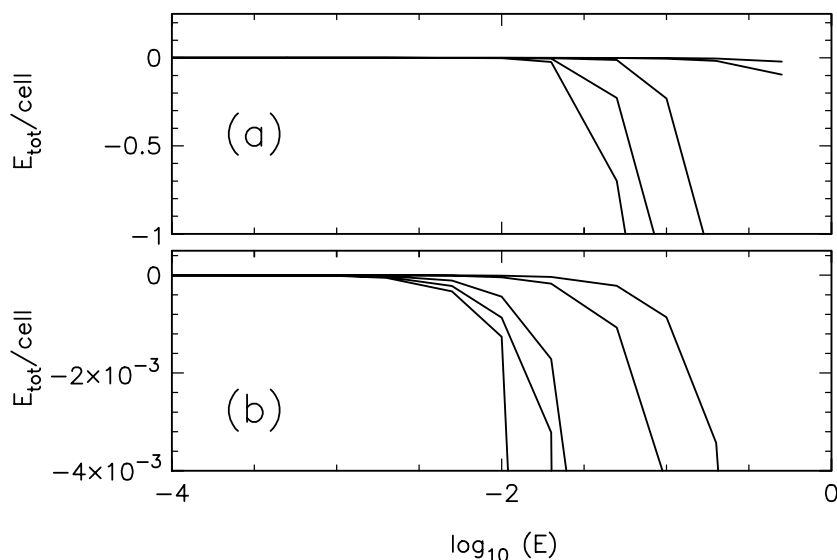


Fig. 3. The total energy per two atoms as a function of field strength for the Hückel model with a ring of 12, 102, 204, and 306 sites (from below) with the sawtooth approximation of Fig. 1(c) together with the results for the same chains with the approximation of Fig. 1(b) (uppermost curve). The two panels differ in the scale of the ordinate.

3. A FIRST-PRINCIPLES METHOD FOR POLYMERS

Ultimately, our goal is to include the effects of the external fields in a parameter-free ground-state calculation of the properties of an infinite, periodic polymer. To this end we apply our own density-functional method that has been described in detail elsewhere [2,31] and, therefore, shall be only briefly discussed here.

The method is based on expanding the eigenfunctions to the Kohn–Sham equations in a basis set of linearized muffin-tin orbitals (LMTOs), which are represented numerically inside non-overlapping, atom-centered, so-called muffin-tin spheres and analytically in the interstitial region outside all spheres. The numerical functions are obtained by considering the spherically symmetric part of the potential inside the muffin-tin spheres and for this solving the Kohn–Sham equations numerically for an orbital energy (denoted ϵ_ν) that is in the energy range where the orbital has its largest support, leading to the atom- and angle-dependent basis function $\phi_{\vec{R},L}$ [L being a short-hand notation for (l,m)]. In addition, we define the energy-derivative $\dot{\phi}_{\vec{R},L} = (\partial/\partial\epsilon_\nu)\phi_{\vec{R},L}$. The analytical functions are decaying, spherical waves [i.e., spherical Hankel functions times harmonic functions, $h_l^{(1)}(|\vec{r} - \vec{R}|\kappa)Y_L(\vec{r} - \vec{R}) \equiv h_{\vec{R},L,\kappa}(\vec{r})$]. The functions are matched continuously and differentially on the sphere boundaries. The basis functions $\chi_{\vec{R},L,\kappa}$ are accordingly eigenfunctions to a muffin-tin potential and, as such, good approximations to the true solutions to the Kohn–Sham equations. It shall, however, be stressed that the full potential is included in the calculations.

In our implementation of the method we consider infinite, periodic, isolated polymer chains. The periodicity is utilized in constructing Bloch functions from the basis functions of different unit cells,

$$\chi_{p,L,\kappa}^k = \lim_{N \rightarrow \infty} \frac{1}{\sqrt{2N+1}} \sum_{n=-N}^N \chi_{\vec{R}_{np},L,\kappa} e^{ik\pi n}, \quad (37)$$

where \vec{R}_{np} is the position of the p th atom in the n th unit cell. We let the z -axis be the polymer axis.

The method has been applied to a number of conjugated polymers over the last almost two decades (see, e.g., Ref. [32]), and as a special application we also studied the case of chains exposed to an external electrostatic field perpendicular to the chain direction. Thereby, the periodicity was not destroyed and, accordingly, the basics of our approach could be kept unchanged.

As one example we show in Fig. 4 results for polycarbonitrile exposed to an external field perpendicular to the chain direction. Polycarbonitrile, $(\text{CHN})_x$, resembles *trans*-polyacetylene but has every second CH group replaced by an N atom. In the figure we show both the band structures and

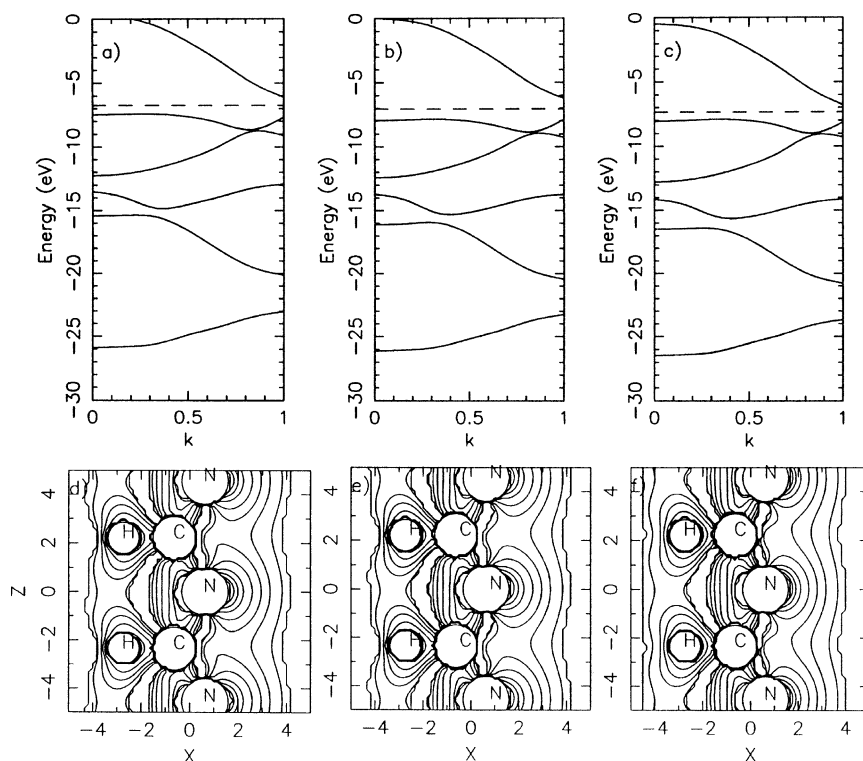


Fig. 4. The (top) band structures and (bottom) electron density for the highest occupied orbital at $k = 0$ for polycarbonitrile $(\text{CHN})_x$ exposed to an external DC field perpendicular to the chain direction but in the plane of the nuclei. The strength of the field is (left) -0.05 , (middle) 0 , and (right) $+0.05$ hartree a.u.

the density of the highest occupied orbital of σ symmetry for different values of the field strength. The largest values, ± 0.05 hartree a.u., are very large compared to typical experimental conditions, so the results of the figure show that the perturbations on the electronic properties due to the field are small. This is an important result because this suggests that the orbitals, etc., calculated for the system without external fields provide good starting points for inclusion of the field. This we shall use.

We shall approximate the scalar potential of the electrostatic field by the sawtooth curve of Fig. 5 that has the periodicity of the Born von Kármán zone, i.e., of the length of one unit cell times the number of k points that is used in a calculation. We have here assumed that the potential takes both positive and negative values. By doing so, the average potential from the field vanishes and we have therefore an optimal starting point for eliminating effects that are linear in the number of k points of the calculation (i.e., in the length of the Born von Kármán zone).

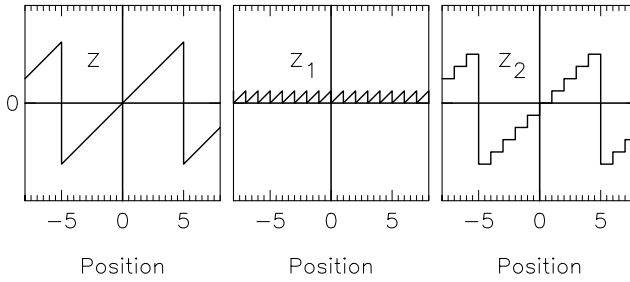


Fig. 5. The left part shows the sawtooth curve \hat{z} that is periodic (and linear) with the periodicity of the Born von Kármán zone. It is decomposed into the lattice-periodic part of the middle part, and the piecewise constant part shown in the right part of the figure, $\hat{z} = \hat{z}_1 + \hat{z}_2$.

In order to make use of the fact that the orbitals of the unperturbed system provide good approximations to those of the perturbed system, we construct Wannier functions from the Bloch orbitals of the unperturbed state. The Bloch functions are given through

$$\begin{aligned} \psi_n^k(\vec{r}) &= \sum_{p,L,\kappa} c_{n;p,L,\kappa}^k \chi_{p,L,\kappa}^k(\vec{r}) \\ &= \begin{cases} \sum_L [a_{n;p,L,\kappa}^k \phi_{\vec{R}_{0p},L}(\vec{r}) + b_{n;p,L,\kappa}^k \dot{\phi}_{\vec{R}_{0p},L}(\vec{r})] \\ \sum_{p,L,\kappa} d_{n;p,l,\kappa}^k \lim_{N \rightarrow \infty} \frac{1}{\sqrt{2N+1}} \sum_{m=-N}^N h_{\vec{R}_{mp},L,\kappa}(\vec{r}), \end{cases} \quad (38) \end{aligned}$$

where the first expression is valid for \vec{r} in sphere at \vec{R}_{0p} and the second is valid for \vec{r} in interstitial region.

Then, the Wannier functions are defined through

$$\begin{aligned} w_{lp}(\vec{r}) &= \frac{1}{\sqrt{2K}} \sum_k \psi_l^k(\vec{r}) e^{i\phi_l(k)} e^{-ik\pi p} \\ &= \lim_{N \rightarrow \infty} \frac{1}{\sqrt{2N+1}} \sum_{n=-N}^N \sum_{j,n,L,\kappa} w_{lp,jnL\kappa} \chi_{\vec{R}_{nj},L,\kappa}(\vec{r}) \\ &= \begin{cases} \sum_L [a_{lp;q,L,\kappa}^w \phi_{\vec{R}_{0q},L}(\vec{r}) + b_{lp;q,L,\kappa}^w \dot{\phi}_{\vec{R}_{0q},L}(\vec{r})] \\ \sum_{p,L,\kappa} d_{lp;q,l,\kappa}^w \lim_{N \rightarrow \infty} \frac{1}{\sqrt{2N+1}} \sum_{m=-N}^N h_{\vec{R}_{mq},L,\kappa}(\vec{r}), \end{cases} \quad (39) \end{aligned}$$

where, once again, the first expression is valid for \vec{r} in sphere at \vec{R}_{0p} and the second is valid for \vec{r} in interstitial region. In addition, $e^{i\phi(k)}$ is a phase factor that can be chosen free (see below), and l is a band index. Moreover, the Wannier functions (that have the periodicity of the Born von Kármán zone) obey the important property

$$w_{l,p+1}(\vec{r}) = w_{lp}(\vec{r} - \vec{a}), \quad (40)$$

with \vec{a} being the lattice vector. A further property is that when the phase factors $e^{i\phi_l(\vec{k})}$ are chosen properly, the Wannier functions take the form of equation (29) with f_l^k being continuous and differentiable, so that the problems discussed at the end of the preceding section vanish.

Using the Wannier functions as basis functions in the electronic-structure calculation means writing any orbital as

$$\psi_i(\vec{r}) = \sum_{lp} c_{i,lp} w_{lp}(\vec{r}). \quad (41)$$

Inserting this expression into the Kohn–Sham equations means, ultimately, that we have to calculate matrix elements $\langle w_{l_1,p_1}(\vec{r}) | \hat{h}_{\text{eff}} | w_{l_2,p_2}(\vec{r}) \rangle$, where \hat{h}_{eff} is the effective Kohn–Sham operator, containing the kinetic-energy operator, the Coulomb potentials from the electrons and from the nuclei, the exchange-correlation potential in some approximation (e.g., a local-density or a generalized-gradient approximation), and, finally, the potential from the external electrostatic field,

$$\hat{h}_{\text{eff}} = -\frac{\hbar^2}{2m_e} \nabla^2 + V_C(\vec{r}) + V_n(\vec{r}) + V_{\text{xc}}(\vec{r}) + V_{\text{DC}}(\vec{r}). \quad (42)$$

Just as for the field-free case where we use the expansion of equation (38), the orbitals, and consequently also the electron density, are expressed in terms of the numerically given functions ϕ and $\dot{\phi}$ inside the muffin-tin spheres and in terms of the analytically given Hankel functions in the interstitial region. Accordingly, the calculation of the matrix elements for all parts of the Kohn–Sham operator except for V_{DC} proceeds just as in for the periodic, field-free case (see Refs. [2,31]). Actually, it is useful to split \hat{h}_{eff} into

$$\hat{h}_{\text{eff}} = \hat{h}_{\text{eff}}^{(0)} + \Delta V_C(\vec{r}) + \Delta V_{\text{xc}}(\vec{r}) + V_{\text{DC}}(\vec{r}), \quad (43)$$

where $\hat{h}_{\text{eff}}^{(0)}$ is the self-consistent Kohn–Sham operator in the field-free case. When expressing the wavefunctions in terms of the Bloch waves of equation (38),

$$\langle w_{l_1,p_1} | \hat{h}_{\text{eff}}^{(0)} | w_{l_2,p_2} \rangle = \delta_{l_1,l_2} \frac{1}{2K} \sum_k \epsilon_{l_1}^k e^{i\pi k(p_1-p_2)}, \quad (44)$$

with ϵ_l^k being the orbital energy of the Bloch wave ψ_l^k in the field-free case. Moreover,

$$\langle w_{l_1 p_1} | w_{l_2 p_2} \rangle = \delta_{l_1, l_2} \delta_{p_1, p_2}. \quad (45)$$

Thus, here we only need to discuss the treatment of V_{DC} . We may write

$$V_{DC}(\vec{r}) = E_x \cdot x + E_y \cdot y + E_z \cdot \hat{z}. \quad (46)$$

The first two terms do not break the translational symmetry and can fairly simply be incorporated into the calculations. The matrix elements can be calculated using the expression of the Wannier functions in terms of the Bloch functions, and subsequently performing the required integrals analytically in the interstitial region and numerically inside the spheres with expressions that are very similar to those we need for the other lattice-periodic parts of the potential (see, e.g., Refs. [2,31]).

For \hat{z} we use the sawtooth function of Fig. 5. Then,

$$\begin{aligned} \langle w_{l_1 p_1} | \hat{z} | w_{l_2 p_2} \rangle &= \lim_{N \rightarrow \infty} \frac{1}{2N+1} \sum_{n_1, n_2 = -2NK+1}^{2NK} \sum_{j_1, j_2} \sum_{L_1, L_2} \sum_{\kappa_1, \kappa_2} w_{l_1 p_1 j_1 n_1 L_1 \kappa_1}^* \\ &\times w_{l_2 p_2 j_2 n_2 L_2 \kappa_2} \langle \chi_{\vec{R}_{n_1 j_1, L_1, \kappa_1}}(\vec{r}) | \hat{z} | \chi_{\vec{R}_{n_2 j_2, L_2, \kappa_2}}(\vec{r}) \rangle. \end{aligned} \quad (47)$$

We write

$$\hat{z} = \hat{z}_1 + \hat{z}_2, \quad (48)$$

where \hat{z}_1 has the periodicity of the lattice, and \hat{z}_2 that of the Born von Kármán zone (cf. Fig. 5). Then,

$$\begin{aligned} \langle w_{l_1 p_1} | \hat{z}_1 + \hat{z}_2 | w_{l_2 p_2} \rangle &= \frac{1}{2K} \sum_{k_1, k_2} \sum_{j_1, j_2} \sum_{L_1, L_2} \sum_{\kappa_1, \kappa_2} c_{l_1 j_1, L_1, \kappa_1}^{k_1*} c_{l_2 j_2, L_2, \kappa_2}^{k_2} e^{i(\phi_{l_2}(k_2) - \phi_{l_1}(k_1))} \\ &\times e^{-i\pi(k_2 p_2 - k_1 p_1)} \langle \chi_{j_1, L_1, \kappa_1}^{k_1} | \hat{z}_1 | \chi_{j_2, L_2, \kappa_2}^{k_2} \rangle. \end{aligned} \quad (49)$$

Here,

$$\begin{aligned} \langle \chi_{j_1, L_1, \kappa_1}^{k_1} | \hat{z}_1 | \chi_{j_2, L_2, \kappa_2}^{k_2} \rangle &= \langle \chi_{j_1, L_1, \kappa_1}^{k_1} | \hat{z}_1 | \chi_{j_2, L_2, \kappa_2}^{k_2} \rangle + \langle \chi_{j_1, L_1, \kappa_1}^{k_1} | \hat{z}_2 | \chi_{j_2, L_2, \kappa_2}^{k_2} \rangle \\ &= \delta_{k_1, k_2} \lim_{N \rightarrow \infty} \sum_{n_1, n_2 = -N}^N e^{ik_1 \pi(n_2 - n_1)} \langle \chi_{\vec{R}_{j_1 n_1, L_1, \kappa_1}} | \hat{z}_1 | \chi_{\vec{R}_{j_2 n_2, L_2, \kappa_2}} \rangle_0 \\ &+ \lim_{N \rightarrow \infty} \frac{1}{2K} \sum_{n_1, n_2 = -N}^N \sum_{n = -K+1}^K e^{i\pi(k_2 n_2 - k_1 n_1)} \\ &\langle \chi_{\vec{R}_{j_1 n_1, L_1, \kappa_1}} | (n-1)a | \chi_{\vec{R}_{j_2 n_2, L_2, \kappa_2}} \rangle_0, \end{aligned} \quad (50)$$

where a is the length of the unit cell. Moreover, the subscript '0' on the bra-kets indicates that the integration is to be taken over the reference unit cell, i.e., whereas x and y are unlimited, the z integration is over the interval of length a .

Since

$$\frac{1}{2K} \sum_{n=-K+1}^K (n-1)a = -\frac{a}{2}, \quad (51)$$

both expressions above can be evaluated by performing an integral over a z interval of length a together with infinite x and y integrations. Except for the basis functions, the integrand is z^m , with $m = 0$ and 1 . We shall also add the integral for $m = 2$ of reasons to be explained below.

Starting with our field-free calculations we have implemented the calculations of these finite- z -interval integrals. It turned out that these were best performed numerically, also in the interstitial region where the basis functions are represented analytically. The reason is that the planar boundary of our integration region is only with great difficulties combined with our representation for the basis functions in spherical coordinates.

The reasons for adding $m = 2$ is that the phases $\phi_l(k)$ of the Wannier functions [cf. equation (39)] at best are determined by requiring that $\langle w_{lp}(\vec{r}) | (z - z_p)^2 | w_{lp} \rangle_0$ is maximized [30] (here, z_p is the z coordinate of the center of the p th unit cell).

We have applied this approach on a linear chain of carbon atoms with alternating bond lengths of 2.7 and 2.5 a.u. In Fig. 6 we show the band structures for this system without any external field. The calculations were done using seven k points in half-part of the Brillouin zone, giving a Born von Kármán zone of 12 unit cells, each with two carbon atoms. Moreover, we included the 20 energetically lowest bands that all are shown in the figure (notice, however, that π and δ bands are pairwise degenerate) and, for the sake of simplicity, we applied a local-density approximation within density-functional theory.

The occupied valence bands consist of two low-lying σ bands and a double degenerate π band just below the Fermi level. Also the lowest unoccupied band is of π symmetry. Thus, without the DC field the four energetically lowest valence bands are double occupied and all other bands are empty. We shall use this information below in quantifying the effects of the external DC field in different approximations, i.e., we shall analyze the occupation of the different bands as a function of band index. Moreover, in order to quantify the electronic distribution, we shall use the number of electrons inside the muffin-tin spheres (with radii of 1.1 a.u.) for the 24 atoms per Born von Kármán zone.

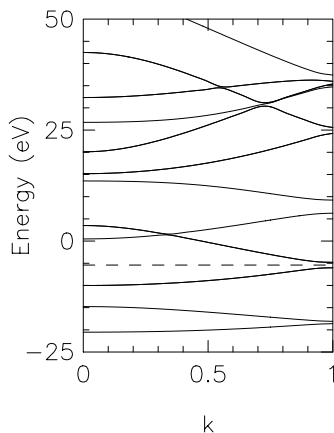


Fig. 6. The band structures for a linear chain of carbon atoms with alternating bond lengths. $k = 0$ and 1 are the center and the edge of the first Brillouin zone, respectively, and the dashed line shows the Fermi level.

We considered two approximate treatments of the DC field, i.e., one where we only included \hat{z}_1 of Fig. 5 and equations (48)–(50), and another where the full sawtooth curve \hat{z} was included. Some representative results are shown in Figs 7 and 8. Since the Wannier functions can be ascribed to individual unit cells, we show in Fig. 7 the number of electrons (relative to the number, 8, for the undistorted system) of each unit cell in the case that the field operator has the symmetry of \hat{z} of Fig. 5. Not surprisingly, the electrons do show an asymmetric distribution, although the flow from one end of the Born von Kármán zone to the other is small. The number of electrons inside the muffin-tin spheres also gives information on the electron redistributions. Thus, for $e \cdot E_z = 0.0002$ hartree these numbers are 3.2403 and 3.2413 for the two carbon atoms per unit cell for the operator \hat{z}_1 of Fig. 5, and 3.2217 and 3.2575 for the operator \hat{z} . Here we also see a larger effect for \hat{z} than for \hat{z}_1 . However, for the \hat{z} all atomic spheres show the same numbers, so that the charge redistribution of Fig. 6 is restricted to the interstitial region.

For the undistorted system, the four lowest bands will contain each 24 electrons, whereas the higher lying bands will contain 0 electrons. Turning on the field will lead to partial occupation of the higher lying bands, and in order to quantify this, we show in Fig. 8 the changes in the band occupancies due to the field both for the field with the operator given by \hat{z} in Fig. 5 and given by \hat{z}_1 of that figure. Two things are immediately clear: the most significant changes occur for the bands closest to the Fermi level, giving support for the calculation based on

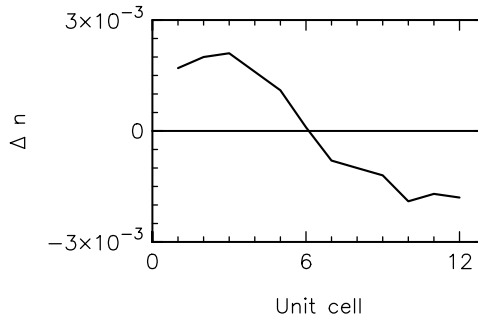


Fig. 7. Changes in the number of electrons ascribed to the different unit cells for the field with the symmetry of the Born von Kármán zone and with a strength of $e \cdot E_z = 0.0002$ hartree.

the Wannier functions, and the operator \hat{z} leads to significantly larger redistributions than the operator \hat{z}_1 does, once the field strength has been fixed.

Finally, also the total energy shows different behaviors depending on how the electric field is being treated. It turned out, however, that the calculations only with great difficulties could be stabilized against oscillations and, therefore, we refrain from presenting results for the total energy.

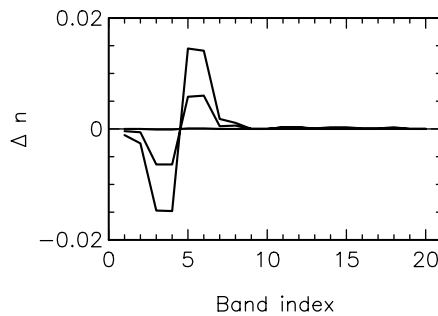


Fig. 8. Changes in the number of electrons for the different bands relative to the numbers for the undistorted system (24 for the first four bands, and 0 for the remaining). The curves are (in order of decreasing amplitude) for field strengths of $e \cdot E_z = 0.0002, 0.0005$, and 0.0002 hartree for (the most oscillating curve) the case of the field with the symmetry of the Born von Kármán zone, and (the other curves) for the case that the field has the lattice periodicity.

4. CONCLUSIONS

In this contribution we have concentrated on presenting some fundamental considerations concerning the theoretical treatment of an infinite, periodic, polymeric chain being exposed to an external electrostatic field. The analysis of a simple Hückel-like model revealed that only under certain circumstances one can base the discussion on Bloch functions and substituting \vec{r} with a derivative with respect to k . Thus, this was not the case when including the field directly in the calculations, but could, e.g., be used when using Wannier functions as basis functions which are continuous functions not only of \vec{r} but also of k .

Subsequently, we presented the general strategy for including the field in a self-consistent electronic-structure method for density-functional studies of infinite, periodic polymers and applied the method for a linear chain of carbon atoms. Here we found similar results, i.e., the response of the system to the external field was significantly stronger when the field was approximated by a sawtooth curve with the periodicity of the Born von Kármán zone than when it possessed the periodicity of the lattice. However, by analyzing the occupancies of the band orbitals for different field strengths, we could see that our approach based on Wannier functions is healthy: the main changes occur for the orbitals closest to the Fermi level.

Finally, we stress that our study does not answer all questions. Thus, the fact that we use an approximate density functional in our parameter-free calculations may be one source of errors in the calculated quantities, although this problem is only marginally related to that of a proper treatment of the external field in an electronic-structure method. Second, our method is still in its infancy and many tests are required before it can be established whether it is a useful approach. Third, we have presented a method for directly including a DC field in the calculations, whereas other approaches, based on perturbation theory, also allow for the treatment of AC fields. Our approach allows for an alternative control of the results of the latter in the limit of vanishing frequencies, but it still is an open question how the results can be used in improving the perturbation-theoretic approaches.

But, as has been the case with much of the work of Osvaldo Gosinski, science proceeds by proposing and trying new approaches. And in this spirit we close this contribution in the honor of Osvaldo Gosinski!

ACKNOWLEDGEMENTS

This work was supported by the German Research Council (DFG) through project Sp 439/11. One of the authors (MS) is grateful to Fonds der

Chemischen Industrie for generous support. Moreover, the authors have benefitted very much from useful discussions with Bernie Kirtman.

REFERENCES

- [1] M. Springborg, J.-L. Calais, O. Goscinski and L. A. Eriksson, *Synth. Met.*, 1991, **41–43**, 3309.
- [2] M. Springborg, J.-L. Calais, O. Goscinski and L. A. Eriksson, *Phys. Rev. B*, 1991, **44**, 12713.
- [3] B. Champagne and D. M. Bishop, *Adv. Chem. Phys.*, 2003, **126**, 41.
- [4] H. Shirakawa, *Angew. Chem.*, 2001, **113**, 2642.
- [5] A. G. MacDiarmid, *Angew. Chem.*, 2001, **113**, 2649.
- [6] A. J. Heeger, *Angew. Chem.*, 2001, **113**, 2660.
- [7] T. A. Skotheim and R. L. Elsenbaumer, J. R. Reynolds (eds), *Handbook of Conducting Polymers*, Marcel Dekker, New York, 1998.
- [8] I. D. W. Samuel, I. Ledoux, C. Dhenaut, J. Zyss, H. H. Fox, R. R. Schrock and R. J. Silbey, *Science*, 1994, **265**, 1070.
- [9] B. Champagne, D. H. Mosley, J. G. Fripiat and J.-M. André, *Int. J. Quantum Chem.*, 1993, **46**, 1.
- [10] D. Lu, B. Marten, M. Ringnald, R. A. Friesner and W. A. Goddard, III, *Chem. Phys. Lett.*, 1996, **257**, 224.
- [11] B. Champagne, D. Jacquemin, J.-M. André and B. Kirtman, *J. Phys. Chem. A*, 1997, **101**, 3158.
- [12] B. Champagne, E. A. Perpète and J.-M. André, *J. Chem. Phys.*, 1994, **101**, 10796.
- [13] D. H. Mosley, B. Champagne and J.-M. André, *Int. J. Quantum Chem. Symp.*, 1995, **29**, 117.
- [14] (a) V. N. Genkin and P. M. Mednis, *Sov. Phys. JETP*, 1968, **27**, 609; (b) V. N. Genkin and P. M. Mednis, *Zh. Eksp. Teor. Fiz.*, 1968, **54**, 1137.
- [15] Z. Shuai and J. L. Brédas, *Phys. Rev. B*, 1992, **46**, 4395.
- [16] R. D. King-Smith and D. Vanderbilt, *Phys. Rev. B*, 1993, **47**, 1651.
- [17] R. Resta, *Rev. Mod. Phys.*, 1994, **66**, 899.
- [18] J.-M. André, J. Delhalle and J.-L. Brédas, *Quantum Chemistry Aided Design of Organic Polymers*, World Scientific, Singapore, 1991.
- [19] Y. Dong and M. Springborg, *Synth. Met.*, 2003, **135–136**, 349.
- [20] B. Champagne, E. A. Perpète, S. J. A. van Gisbergen, E.-J. Baerends, J. G. Snijders, C. Soubra-Ghaoui, K. A. Robins and B. Kirtman, *J. Chem. Phys.*, 1998, **109**, 10489.
- [21] M. van Faassen, P. L. de Boeij, R. van Leeuwen, J. A. Berger and J. G. Snijders, *Phys. Rev. Lett.*, 2002, **88**, 186401.
- [22] M. van Faassen, P. L. de Boeij, R. van Leeuwen, J. A. Berger and J. G. Snijders, *J. Chem. Phys.*, 2003, **118**, 1044.
- [23] K. Kunc and R. Resta, *Phys. Rev. Lett.*, 1983, **51**, 686.
- [24] K. Schmidt and M. Springborg, *Phys. Chem. Chem. Phys.*, 1999, **1**, 1743.
- [25] R. Resta, *Phys. Rev. Lett.*, 1998, **80**, 1800.
- [26] P. Otto, *Phys. Rev. B*, 1992, **45**, 10876.
- [27] K. N. Kudin and G. E. Scuseria, *J. Chem. Phys.*, 2000, **113**, 7779.
- [28] B. Kirtman, F. L. Gu and D. M. Bishop, *J. Chem. Phys.*, 2000, **113**, 1294.
- [29] D. M. Bishop, F. L. Gu and B. Kirtman, *J. Chem. Phys.*, 2001, **114**, 7633.
- [30] E. I. Blount, *Solid State Phys.*, 1962, **13**, 305.
- [31] M. Springborg and O. K. Andersen, *J. Chem. Phys.*, 1987, **87**, 7125.
- [32] M. Springborg, *J. Mol. Struct. Theochem*, 2002, **593**, 155.

Atoms, Molecules, Crystals and Nanotubes in Laser Fields: From Dynamical Symmetry to Selective High-Order Harmonic Generation of Soft X-Rays

Ofir E. Alon, Vitali Averbukh and Nimrod Moiseyev

*Department of Chemistry and Minerva Center for Non-Linear Physics of Complex Systems,
Technion–Israel Institute of Technology, Haifa 32000, Israel*

Abstract

The interaction of atoms, molecules, crystals and nanotubes as well as of artificial nanostructures with time-periodic laser fields can lead to high-order space–time symmetries. These space–time symmetries (also referred to as dynamical symmetries (DSs)) are to the Floquet Hamiltonian what spatial symmetries are to the field-free Hamiltonian. Consequently, DS properties of Floquet states can be studied by group theory. Here we use DSs to characterize the modifications of electronic energy levels induced by circularly polarized laser fields in quantum rings, thin crystals and carbon nanotubes (CNTs). Furthermore, we show that DSs underlie the formulation of selection rules for high-order harmonic generation processes in strong laser fields. This enables one to predict outputs of harmonic generation experiments and even suggests new experiments which would lead to ‘engineered’ spectra. By doing so, we place DS analysis of harmonic generation processes in high-intensity fields on a firm foundation, analogously to that possessed by symmetry analysis in ‘conventional’ spectroscopy. This formalism is applied to single-walled CNTs interacting with circularly polarized laser fields. We find that CNTs can be excellent candidates for a selective and efficient generation of high-order harmonics, up to the soft X-ray regime.

Contents

1. Introduction	394
2. On quantum rings and symmetric molecules in circularly polarized laser fields	394
3. Thin crystals in circularly polarized laser fields	397
4. Nanotubes in circularly polarized laser fields	401
5. Selection rules for the high-order harmonic generation spectra	404
6. High-order harmonic generation of soft x-rays by carbon nanotubes	409
7. Summary and conclusions	419
Acknowledgements	420
References	420

1. INTRODUCTION

Symmetry plays an important role in atomic, molecular and solid-state physics [1]. In particular, it provides the labeling of energy levels and their corresponding *stationary* eigenstates with ‘good’ quantum numbers. Most importantly, it allows the evaluation of matrix elements and therefore provides a general method for determining selection rules (SRs). For instance, the interpretation of electronic and vibrational spectra strongly benefits from such symmetry-based predictions [2]. In ‘conventional’ spectroscopy, one describes transitions between *stationary* (bound) states induced by suitable *time-independent* operators. In fact, such description is appropriate when the laser field used to explore the system is weak and can be considered as a perturbation. In the last two decades, the application of intense laser fields has opened the door to a new realm of non-perturbative and non-linear phenomena in atoms and molecules, among which is high-order harmonic generation (HHG) (for recent reviews, see Refs. [3,4]). It is evident that at such laser intensities time-dependent perturbation theory breaks down, transitions between field-free bound states cannot account for accurate description of these processes and therefore one has to resort to the solution of the time-dependent Schrödinger equation. It turns out that for time-periodic laser fields, the states of the system inside the laser field can be conveniently expanded by the so-called Floquet states [5,6]. In this contribution, we would like to present the application of group theory to the study of laser-system dynamics. More specifically, we show below that the eigenstates of the quantum system inside the laser field possess suitable dynamical symmetries (DSs). Accordingly, the modified energy levels can be classified by ‘good’ quantum numbers [7]. Moreover, the SRs for the HHG phenomena utilize these DSs [8,9,11–20]. In the first part, we begin from Floquet theorem [21] and present few aspects of the theory of DSs of time-periodic Hamiltonians [7]. Specifically, we characterize the symmetry properties of the modified energy levels of (hindered) quantum rings (QRs), thin crystals and single-walled carbon nanotubes (CNTs) in coplanar circularly polarized laser fields (Sections 2–4). In the second part, we briefly describe the HHG phenomena in gases [3,4] and proceed to study the SRs for the HHG spectra (HHGS) by systems possessing high-order DS, in general, [10] and, in particular, by single-walled CNTs in circularly polarized laser fields [12] (Sections 5 and 6). Summary and conclusions are given in Section 7.

2. ON QUANTUM RINGS AND SYMMETRIC MOLECULES IN CIRCULARLY POLARIZED LASER FIELDS

In this section, we would like to characterize the symmetry properties of the modified energy levels in symmetric molecules and nanostructures induced

by time-periodic laser fields (see Ref. [7]). As a generic case, we discuss the application of (monochromatic) coplanar circularly polarized laser fields to (hindered) QRs. To this end, let us first recall the symmetry properties of the field-free energy levels of a QR. Without loss of generality, we consider the following three-dimensional (3D) Hamiltonian, which describes an electron's motion in a hindered QR possessing the N -fold rotational symmetry:

$$\hat{H}(\mathbf{r}) = \frac{\hat{\mathbf{p}}^2}{2m} + V_N(\mathbf{r}), \quad [\hat{H}(\mathbf{r}), \hat{C}_N] = 0, \quad \hat{C}_N = \left(\varphi \rightarrow \varphi + \frac{2\pi}{N} \right). \quad (1)$$

The single-electron eigenstates of the QR can be classified with respect to the rotation operator \hat{C}_N ,

$$\begin{aligned} \hat{H}(\mathbf{r})\psi_{E,p}(\mathbf{r}) &= E\psi_{E,p}(\mathbf{r}), \quad \hat{C}_N\psi_{E,p}(\mathbf{r}) = e^{+ip(2\pi/N)}\psi_{E,p}(\mathbf{r}), \\ p &= 0, 1, \dots, N-1. \end{aligned} \quad (2)$$

Are there non-accidentally degenerate energy levels in this system? The answer is positive. In order to verify this, let us distinguish between two cases. If, in addition to the N -fold rotation symmetry \hat{C}_N , the Hamiltonian is invariant under the reflection symmetry $\hat{\sigma}_y = (y \rightarrow -y) = (\varphi \rightarrow -\varphi)$, one obtains the familiar result reflected by the character table of the point group \mathcal{C}_{Nv} ,

$$\begin{aligned} \text{for } p \neq 0, N/2: \quad & \{\psi_{E,p}, \hat{\sigma}_y\psi_{E,p}\} \text{ span a (real) 2D} \\ & \text{irreducible representation (irrep),} \\ \text{for } p = 0, N/2: \quad & \psi_{E,p} \text{ spans a (real) 1D irrep.} \end{aligned} \quad (3)$$

In the second case (i.e., when $[\hat{H}(\mathbf{r}), \hat{\sigma}_y] \neq 0$) one can still make use of the time-reversal symmetry (TRS) \hat{R} , since for real Hamiltonians $[\hat{H}(\mathbf{r}), \hat{R}] = 0$. Following Wigner's theory of anti-unitary symmetries [22], the result now merely reflects the character table of the point group \mathcal{C}_N ,

$$\begin{aligned} \text{for } p \neq 0, N/2: \quad & \Gamma_p(\hat{C}_N) \text{ is a complex 1D irrep} \Rightarrow \{\Gamma_p(\hat{C}_N), \Gamma_p^*(\hat{C}_N)\} \\ & \text{stick together (case c of Wigner's TRS test),} \\ \text{for } p = 0, N/2: \quad & \Gamma_p(\hat{C}_N) \text{ is a real 1D irrep (case a of Wigner's TRS test).} \end{aligned} \quad (4)$$

$\Gamma_p(\hat{C}_N)$ is the irrep spanned by $\psi_{E,p}$.

Let us add a circularly polarized laser field and inquire what happens to the energy levels of the QR. In the presence of a time-periodic laser field,

the field-free stationary states become quasi-stationary (quasi-energy (QE)) states [5,6]. The time-periodic Hamiltonian is given by

$$\hat{H}(\mathbf{r}, t) = \frac{\hat{\mathbf{p}}^2}{2m} + V_N(\mathbf{r}) + eE_0\rho \cos(\varphi - \omega t), \quad \hat{H}(t) = \hat{H}(t + T), \quad (5)$$

$$T = \frac{2\pi}{\omega},$$

where E_0 and ω are the incident field strength and frequency, respectively. The field propagation direction is assumed to be parallel to the N -fold symmetry axis of the QR. Aiming at solving the time-dependent Schrödinger equation,

$$\hat{H}(\mathbf{r}, t) \Psi(\mathbf{r}, t) = i\hbar \frac{\partial}{\partial t} \Psi(\mathbf{r}, t), \quad (6)$$

one can utilize the periodicity of the Hamiltonian in time. Floquet theorem [21] states that the time-dependent solution $\Psi(\mathbf{r}, t)$ can be decomposed as follows:

$$\Psi_\varepsilon(\mathbf{r}, t) = e^{-(i/\hbar)\varepsilon t} \Phi_\varepsilon(\mathbf{r}, t), \quad \Phi_\varepsilon(\mathbf{r}, t) = \Phi_\varepsilon(\mathbf{r}, t + T). \quad (7)$$

Substituting equation (7) into the time-dependent Schrödinger equation one obtains the Floquet eigenvalue problem

$$\hat{\mathcal{H}}_f(\mathbf{r}, t) \Phi_\varepsilon(\mathbf{r}, t) = \varepsilon \Phi_\varepsilon(\mathbf{r}, t), \quad \hat{\mathcal{H}}_f(\mathbf{r}, t) \equiv \hat{H}(\mathbf{r}, t) - i\hbar \frac{\partial}{\partial t}, \quad (8)$$

where $\hat{\mathcal{H}}_f(\mathbf{r}, t)$ is the Floquet Hamiltonian, $\Phi_\varepsilon(\mathbf{r}, t)$ are the QE or Floquet states and ε are the so-called QEs.

A careful look at the Floquet Hamiltonian reveals that it is invariant under the following N th order DS:

$$\hat{P}_N = \left(\varphi \rightarrow \varphi + \frac{2\pi}{N}, t \rightarrow t + \frac{T}{N} \right). \quad (9)$$

Thus, a complete set of QE states can be found, such that

$$\hat{\mathcal{H}}_f(\mathbf{r}, t) \Phi_{\varepsilon,p}(\mathbf{r}, t) = \varepsilon \Phi_{\varepsilon,p}(\mathbf{r}, t),$$

$$\hat{P}_N \Phi_{\varepsilon,p}(\mathbf{r}, t) = e^{+i(2\pi p/N)} \Phi_{\varepsilon,p}(\mathbf{r}, t), \quad p = 0, 1, \dots, N-1. \quad (10)$$

Having identified the unitary DS associated with the QR-field time-dependent system, it is natural to follow the reasoning used in the field-free case and ask whether there are non-accidentally degenerate Floquet states in this system. One would not expect the existence of non-accidental degeneracies, because the circularly polarized field breaks both the reflection symmetry and the TRS utilized above to characterize such degeneracies in the field-free system. Let us prove with the help of group theoretical analysis

why (and how) this is indeed the case. We first consider the case where the field-free Hamiltonian does not possess the reflection symmetry $\hat{\sigma}_y$. In this case the DS group of the system is cyclic and *unitary*,

$$\mathcal{G}_N \equiv \{\hat{P}_N, \hat{P}_N^2, \dots, \hat{P}_N^{N-1}, \hat{P}_N^N = \mathbf{I}\}. \quad (11)$$

Hence, no non-accidental degeneracies can be found in the QE spectrum of the problem. If, on the other hand, $[\hat{H}(\mathbf{r}), \hat{\sigma}_y]$ then one finds that the Floquet Hamiltonian is invariant under the following generalized TRS (GTRS):

$$\hat{R}_{\varphi t} = (\varphi \rightarrow -\varphi, t \rightarrow -t, *) \equiv \hat{R} \cdot \hat{\sigma}_y. \quad (12)$$

It is, therefore, required to check whether this additional *anti-unitary* symmetry can introduce non-accidental degeneracies into the QE spectrum. To this end, one has to resort to Wigner's theory of anti-unitary symmetries [22] and examine the relation between the irrep $\Gamma_p(\hat{P}_N)$ and the complex conjugate one $\bar{\Gamma}_p(\hat{P}_N) \equiv \Gamma_p^*(\hat{R}_{\varphi t}^{-1} \hat{P}_N \hat{R}_{\varphi t})$. If $\Gamma_p(\hat{P}_N)$ and $\bar{\Gamma}_p(\hat{P}_N)$ are equivalent, i.e., their characters are equal, it is possible to find a similarity transformation B , such that $B^{-1} \Gamma_p(\hat{P}_N) B = \bar{\Gamma}_p(\hat{P}_N)$. In this case two possibilities arise depending on $B^* B$. If $B^* B = \Gamma_p(\hat{R}_{\varphi t}^2)$ then no new degeneracy is introduced (case a). If, on the other hand, $B^* B = -\Gamma_p(\hat{R}_{\varphi t}^2)$ then the degeneracy of $\Gamma_p(\hat{P}_N)$ is doubled (case b). Finally, if $\Gamma_p(\hat{P}_N)$ and $\bar{\Gamma}_p(\hat{P}_N)$ are not equivalent then $\Gamma_p(\hat{P}_N)$ is degenerate with $\bar{\Gamma}_p(\hat{P}_N)$ (case c). In contrast to the field-free case, where $\hat{R}^{-1} \hat{C}_N \hat{R} = \hat{C}_N$, one readily finds that

$$\hat{R}_{\varphi t}^{-1} \hat{P}_N \hat{R}_{\varphi t} = \hat{P}_N^{-1} \Rightarrow \bar{\Gamma}_p(\hat{P}_N) = \Gamma_p^*(\hat{R}_{\varphi t}^{-1} \hat{P}_N \hat{R}_{\varphi t}) = \Gamma_p^*(\hat{P}_N^{-1}) = \Gamma_p(\hat{P}_N) \quad (13)$$

(the last step is valid since $\Gamma_p(\hat{P}_N)$ is a 1D irrep), meaning that all the irrep's $\Gamma_p(\hat{P}_N)$, $p = 0, 1, \dots, N-1$ belong to case a of Wigner's test. Thus, unlike the role played by TRS in the field-free case, $\hat{R}_{\varphi t}$ does not introduce additional degeneracies into the QE spectrum. Is it always the case? In Section 3 we analyze the more intricate case of thin crystals in coplanar circularly polarized fields, where it is demonstrated that GTRS can induce non-accidental degeneracies in the QE band (QEB) spectra.

3. THIN CRYSTALS IN CIRCULARLY POLARIZED LASER FIELDS

Let us consider a thin crystal (e.g., a 2D sheet of graphite; also referred to as graphene) possessing the reflection and rotation symmetries. Without loss of generality, the one-particle, field-free Hamiltonian can be written as

$$\hat{H}_0(\mathbf{r}) = \frac{\hat{p}_x^2 + \hat{p}_y^2}{2m} + V_{\text{cr}}(\mathbf{r}), \quad [\hat{H}_0(\mathbf{r}), \hat{C}_N] = [\hat{H}_0(\mathbf{r}), \hat{\sigma}_y] = 0. \quad (14)$$

Upon shining the thin crystal with (monochromatic) circularly polarized laser field, propagating in parallel to its rotation axes, the corresponding Floquet Hamiltonian is given by

$$\hat{\mathcal{H}}_f(\mathbf{r}, t) = \hat{H}_0(\mathbf{r}) - \frac{eE_0}{m\omega} [\hat{p}_x \sin(\omega t) - \hat{p}_y \cos(\omega t)] - i\hbar \frac{\partial}{\partial t}. \quad (15)$$

Note that $\hat{\mathcal{H}}_f(\mathbf{r}, t)$ is periodic both in time and space; hence, it is referred to as a Floquet–Bloch (FB) Hamiltonian. In other words, the Floquet states can be expressed as FB eigenstates,

$$\begin{aligned} \Phi_{\varepsilon(\mathbf{k}), \mathbf{k}}(\mathbf{r}, t) &= e^{+i\mathbf{k}\mathbf{r}} \phi_{\varepsilon(\mathbf{k}), \mathbf{k}}(\mathbf{r}, t), \\ \hat{\mathcal{H}}_f(\mathbf{r}, t) \Phi_{\varepsilon(\mathbf{k}), \mathbf{k}}(\mathbf{r}, t) &= \varepsilon(\mathbf{k}) \Phi_{\varepsilon(\mathbf{k}), \mathbf{k}}(\mathbf{r}, t). \end{aligned} \quad (16)$$

The energy bands (EBs) $E(\mathbf{k})$ of the field-free Hamiltonian have transformed into the QEBs $\varepsilon(\mathbf{k})$. It is, therefore, natural to inquire what are the symmetries of the QEBs and what is the relation between these symmetries and those of the field-free EBs. The answer lies in the application of the DS operators \hat{P}_N and $\hat{R}_{\varphi t}$ on the FB eigenstates $\Phi_{\varepsilon(\mathbf{k}), \mathbf{k}}(\mathbf{r}, t)$ which gives

$$\begin{aligned} \hat{P}_N \Phi_{\varepsilon(\mathbf{k}), \mathbf{k}}(\mathbf{r}, t) &\equiv e^{+i(C_N^{-1}\mathbf{k})\cdot\mathbf{r}} \phi_{\varepsilon(\mathbf{k}), \mathbf{k}}(C_N\mathbf{r}, t + T/N) \\ &\equiv \Phi_{\varepsilon(\mathbf{k}), C_N^{-1}\mathbf{k}}(\mathbf{r}, t) \Rightarrow \varepsilon(C_N\mathbf{k}) = \varepsilon(\mathbf{k}), \end{aligned} \quad (17)$$

and $(\bar{\sigma}_x = (k_x \rightarrow -k_x))$

$$\begin{aligned} \hat{R}_{\varphi t} \Phi_{\varepsilon(\mathbf{k}), \mathbf{k}}(\mathbf{r}, t) &\equiv e^{+i(-k_x x + k_y y)} \phi_{\varepsilon(\mathbf{k}), \mathbf{k}}^*(\sigma_y \mathbf{r}, -t) \\ &\equiv \Phi_{\varepsilon(\mathbf{k}), \bar{\sigma}_x \mathbf{k}}(\mathbf{r}, t) \Rightarrow \varepsilon(\bar{\sigma}_x \mathbf{k}) = \varepsilon(\mathbf{k}). \end{aligned} \quad (18)$$

In these cases *other* FB states are generated, carrying the *same* QE (since \hat{P}_N and $\hat{R}_{\varphi t}$ are DSs of the FB Hamiltonian) but *transformed* quasimomenta \mathbf{k} . As can be seen, the QEBs exhibit a similar rotational symmetry as the EBs do; however, due to the GTRS, each reflection symmetry σ_y in the *real* space leads to the orthogonal reflection symmetry $\bar{\sigma}_x$ in *reciprocal* space. The results of a similar analysis performed for the 17 plane groups are summarized in Table 1. Analyzing the plane groups with reflection and/or glide planes, we notice that the point groups of the potential (in real space) and QEBs (in reciprocal space) are identical/isomorphic (see the second and sixth columns of Table 1), since they are rotated one with respect to the other by the angle of $\pi/2$. It turns out that for $N = 2, 4, 6$ they are identical (i.e., coincide) while for $N = 1, 3$ they are isomorphic (i.e., they are rotated one with respect to the other by the angle of $\pi/2$). For instance, consider the field-free plane groups $p3m1[x]$ and $p31m[x]$ (the $[x]$ indicates that one of the reflection planes lies along the x -axis). In this case, it is the C_{6v} symmetry of the EBs which contains *both*

Table 1. Comparison between EB and QEB symmetries for 2D lattices in (monochromatic) coplanar circularly polarized fields

Plane group	Point group	EB symmetry	DS plane group	DS point group	QEB symmetry	GTRS
$p1$	C_1	C_2	$g1$	\mathcal{G}_1	C_1	NO
$pm[x]$	$C_s[x]$	C_{2v}	$g1$	\mathcal{G}_1	$C_s[y]$	$\hat{R}_{\varphi t}$
$pg[x]$	$C_s[x]$	C_{2v}	$g1$	\mathcal{G}_1	$C_s[y]$	\hat{R}_{gt}
$cm[x]$	$C_s[x]$	C_{2v}	$g1$	\mathcal{G}_1	$C_s[y]$	$\hat{R}_{\varphi t}$
$p2$	C_2	C_{2v}	$g2$	\mathcal{G}_2	C_2	NO
$p2mg$	C_{2v}	C_{2v}	$g2$	\mathcal{G}_2	C_{2v}	\hat{R}_{gt}
$p2gg$	C_{2v}	C_{2v}	$g2$	\mathcal{G}_2	C_{2v}	\hat{R}_{gt}
$p2mm$	C_{2v}	C_{2v}	$g2$	\mathcal{G}_2	C_{2v}	$\hat{R}_{\varphi t}$
$c2mm$	C_{2v}	C_{2v}	$g2$	\mathcal{G}_2	C_{2v}	$\hat{R}_{\varphi t}$
$p3$	C_3	C_6	$g3$	\mathcal{G}_3	C_3	NO
$p3m1[x]$	$C_{3v}[x]$	C_{6v}	$g3$	\mathcal{G}_3	$C_{3v}[y]$	$\hat{R}_{\varphi t}$
$p31m[x]$	$C_{3v}[x]$	C_{6v}	$g3$	\mathcal{G}_3	$C_{3v}[y]$	$\hat{R}_{\varphi t}$
$p4$	C_4	C_4	$g4$	\mathcal{G}_4	C_4	NO
$p4gm$	C_{4v}	C_{4v}	$g4$	\mathcal{G}_4	C_{4v}	\hat{R}_{gt}
$p4gm$	C_{4v}	C_{4v}	$g4$	\mathcal{G}_4	C_{4v}	$\hat{R}_{\varphi t}$
$p6$	C_6	C_6	$g6$	\mathcal{G}_6	C_6	NO
$p6mm$	C_{6v}	C_{6v}	$g6$	\mathcal{G}_6	C_{6v}	$\hat{R}_{\varphi t}$

The left column lists the 17 plane groups (the $[x]$ indicates that one of the reflection or glide planes lies along the x -axis); the second column lists the point groups of the plane groups; the third column indicates the symmetry of the EBs in reciprocal space; the fourth column lists the symmorphic DS plane groups (primitive translations multiplied by DS point group operations); the fifth column presents the DS point groups of the DS plane groups; the sixth column indicates the symmetry of the QEBs in reciprocal space (the $[y]$ indicates that one of the reflection planes lies along the y -axis); The seventh column lists the relevant GTRS of the FB Hamiltonian (if it exists).

the groups: the $C_{3v}[x]$ of the lattice (in real space) and the rotated group $C_{3v}[y]$ of the QEBs (in reciprocal space). This subgroup relation ‘ensures’ that the application of the circularly polarized field would not induce a higher symmetry in the QEB structure than that of the field-free EBs.

Finally, let us examine whether, analogously to the common situation for EBs, there are non-accidentally degenerate FB states at *specific* values of the quasimomentum \mathbf{k} . We discuss, first, the case of the $\Gamma(\mathbf{k} = 0)$ -point. For this value of the quasimomentum, the FB Hamiltonian (15) is equivalent to the Floquet Hamiltonian of the hindered QR discussed in Section 2. Consequently, no non-accidental degeneracies are possible (compare to the field-free case where 2-fold degeneracies characterize the $\Gamma(\mathbf{k} = 0)$ -point

for $N = 3, 4, 6$). The edge of the Brillouin Zone (BZ) constitutes the second example. Below, we show in the most direct way that sticking together of QEBs can occur along the whole side of the BZ. To this end, consider a field-free Hamiltonian, the non-symmorphic plane group of which is $p2mg$ (see Fig. 1 for an illustration of $p2mg$).

From Table 1, we learn that the corresponding FB Hamiltonian is invariant under the *symmorphic* DS plane group $g2$ and the GTRS operator

$$\begin{aligned}\hat{R}_{gt} &= \left(x \rightarrow x + \frac{a}{2}, y \rightarrow -y, t \rightarrow -t, * \right) = \hat{g} \cdot \hat{R}, \\ \hat{g} &= \left(x \rightarrow x + \frac{a}{2}, y \rightarrow -y \right).\end{aligned}\quad (19)$$

In the following we show that \hat{R}_{gt} does not lift the sticking together *all* EBs exhibit along the edge $\mathbf{k}_Z = (\pi/a, k_y)$, $k_y \in (\pi/b, \pi/b]$. To this end, let us consider the FB state $\Phi_{\varepsilon(Z),Z}(\mathbf{r}, t)$ at the edge point Z . It is evident that the FB state $\hat{R}_{gt}\Phi_{\varepsilon(Z),Z}(\mathbf{r}, t)$ possesses the quasimomentum \mathbf{k}_Z as well. Therefore, one may suppose that

$$\hat{R}_{gt}\Phi_{\varepsilon(Z),Z}(\mathbf{r}, t) = \beta\Phi_{\varepsilon(Z),Z}(\mathbf{r}, t). \quad (20)$$

Next, we calculate the FB state $\hat{R}_{gt}\hat{R}_{gt}\Phi_{\varepsilon(Z),Z}(\mathbf{r}, t)$ in two different ways. Using equation (19) it is found that

$$[\hat{R}_{gt}\hat{R}_{gt}]\Phi_{\varepsilon(Z),Z}(\mathbf{r}, t) = (x \rightarrow x + a)\Phi_{\varepsilon(Z),Z} = -\Phi_{\varepsilon(Z),Z}(\mathbf{r}, t). \quad (21)$$

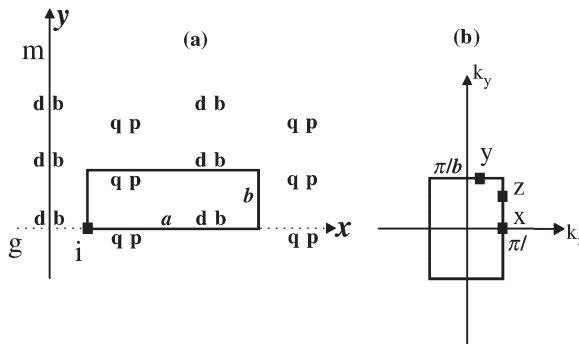


Fig. 1. (a) 2D motif possessing the non-symmorphic plane group symmetry $p2mg$. The relative positions of the mirror plane m , the glide reflection plane g , and the inversion i are shown; (b) The corresponding rectangular first BZ is presented, where \mathbf{k} (quasimomenta) points of the type X , Z and Y are marked.

However, by using equation (20) we obtain

$$\hat{R}_{gt}[\hat{R}_{gt}\Phi_{\varepsilon(Z),Z}(\mathbf{r},t)] = \hat{R}_{gt}\beta\Phi_{\varepsilon(Z),Z}(\mathbf{r},t) = \beta^*\beta\Phi_{\varepsilon(Z),Z}(\mathbf{r},t). \quad (22)$$

Since $\beta^*\beta$ cannot be equal to -1 we encounter a contradiction. Thus, equation (20) must be false and $\hat{R}_{gt}\Phi_{\varepsilon(Z),Z}(\mathbf{r},t)$ and $\Phi_{\varepsilon(Z),Z}(\mathbf{r},t)$ represent two *independent* and degenerate FB states. Consequently, *all* QEBs at the edge Z exhibit sticking together, as is the situation for the EBs of a $p2mg$ -lattice.

4. NANOTUBES IN CIRCULARLY POLARIZED LASER FIELDS

Let us recall, first, the full symmetry of CNTs, the identification of which has been completed recently by Damnjanović *et al.* [23]. The non-symmorphic rod-group [23] describing achiral CNTs with index n can be decomposed in the following manner,

$$\begin{aligned} \mathcal{G}[n] &= \mathcal{L}_{T_z} \times \mathcal{D}_{nh} \times [\mathbf{E} \oplus \mathbf{S}_{2n}] = \mathcal{L}_{T_z} \times \mathcal{D}_{nd} \times [\mathbf{E} \oplus \mathbf{S}_{2n}] \\ &= \mathcal{L}_{T_z} \times [\mathcal{D}_{nh}|_{z=0} \oplus (\mathcal{D}_{nd}|_{z=(T_z/4)} \ominus \mathcal{C}_{nv}) \oplus \mathcal{C}_{nv} \times \mathbf{S}_{2n}], \end{aligned} \quad (23)$$

where the reference point $z = 0$ denotes the crossing of horizontal, σ_h , and vertical, σ_v , reflection planes (see Fig. 2). \mathcal{L}_{T_z} is the 1D translation group with the primitive translation $T_z = |\mathbf{T}_z|$. \mathbf{E} is the identity operation. The screw axis $\mathbf{S}_{2n} = (z \rightarrow z + (T_z/2), \varphi \rightarrow \varphi + (\pi/n))$ involves the lattice smallest non-primitive translation and rotation. The subtraction of the point group \mathcal{C}_{nv} in equation (23) reflects the set relation $\mathcal{D}_{nh}|_{z=0} \cap \mathcal{D}_{nd}|_{z=(T_z/4)} = \mathcal{C}_{nv}$, which is valid for all ns . The glide plane \mathbf{g} is also presented in Fig. 2. It fulfills the multiplication relation $\mathbf{g} = \mathbf{S}_{2n}\sigma_v$. The existence of n distinct glide planes in $\mathcal{G}[n]$ stems from the last term in equation (23). The non-symmorphic rod-group [23] describing the (n, m) -chiral CNT can be decomposed as follows

$$\mathcal{G}[N] = \mathcal{L}_{T_n} \times \mathcal{D}_d \times \left[\sum_{j=0}^{(N/d)-1} \mathbf{S}_{N/d}^j \right] = \mathcal{L}_{T_z} \times \mathcal{D}_1 \times \left[\sum_{j=0}^{N-1} \mathbf{S}_N^j \right]. \quad (24)$$

$N = 2(n^2 + m^2 + nm)/d_R$, where d_R is the greatest common divisor of $2n + m$ and $2m + n$ [24]. d is the greatest common divisor of n and m . $\mathbf{S}_{N/d}$ and \mathbf{S}_N are screw axis operations with the orders of N/d and N , respectively. In general, \mathbf{S}_N can be written as

$$\mathbf{S}_N = (\varphi \rightarrow \varphi + \psi, z \rightarrow z + \tau), \quad \psi = \frac{2\pi R}{N}, \quad \tau = \frac{MT_z}{N}, \quad (25)$$

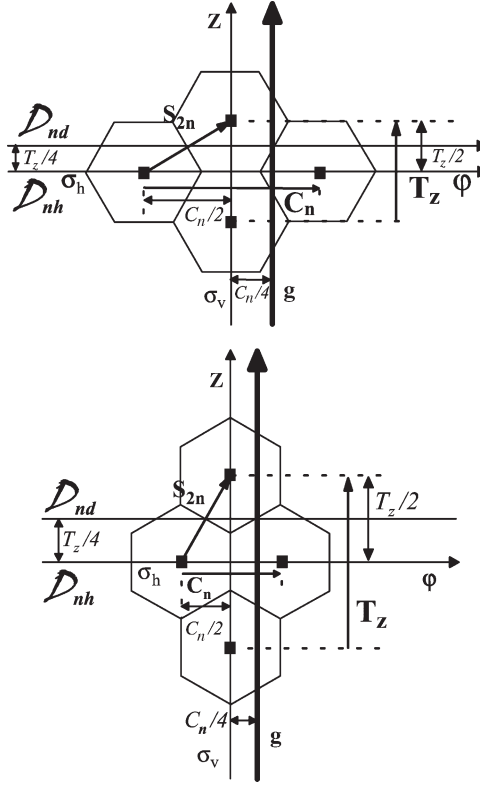


Fig. 2. 2D projection of various symmetries in achiral CNTs (armchair segment, top; zigzag segment, bottom): \mathbf{T}_z is the primitive translation; \mathbf{S}_{2n} is the screw axis with non-primitive translation and rotation, denoted by $T_z/2$ and $C_n/2$, respectively; \mathbf{g} is a glide plane; $\mathcal{D}_{nh}|_{z=0}$ and $\mathcal{D}_{nd}|_{z=(T_z/4)}$ stand for the corresponding point group operations, among which σ_h , σ_v and \mathbf{C}_n are denoted. Note the $T_z/4$ shift between $\mathcal{D}_{nh}|_{z=0}$ and $\mathcal{D}_{nd}|_{z=(T_z/4)}$, that coexist in all achiral CNTs.

where R and M are, respectively, the numbers of complete rotations around and unit cell translations along the nanotube axis obtained after N successive operations of \mathbf{S}_N . For instance, for the achiral CNTs with index n one finds $R = 1$ and $M = N/2 = n$.

Adding the time-dependent laser field, the single-electron Floquet Hamiltonian is given, without loss of generality, by

$$\hat{\mathcal{H}}_{\text{f}}^{\text{nanotube}}(\mathbf{r}, t) = \frac{\left(\hat{\mathbf{p}} - \frac{e}{c}\hat{\mathbf{A}}(\mathbf{r}, t)\right)^2}{2m} + \hat{V}_{\text{nanotube}}(\mathbf{r}) - i\hbar \frac{\partial}{\partial t}. \quad (26)$$

The vector potential $\mathbf{A}(\mathbf{r}, t)$ for the incident circularly polarized plane-wave, propagating along z -axis, is given by

$$\mathbf{A}(\mathbf{r}, t) = \frac{cE_0}{\omega} [\sin(\omega t - k_0 z), -\alpha \cos(\omega t - k_0 z), 0], \quad (27)$$

where k_0 is the wave-vector and α is equal to ± 1 for right or left circular polarizations, respectively. It is quite easy to show that the *interaction term* of the Floquet Hamiltonian transforms like the function

$$\cos[\alpha(\omega t - k_0 z) - \varphi]. \quad (28)$$

Thus, once the circularly polarized field is applied *all* symmetry operations which involve the reflection of φ and/or z ‘collapse’ to the *same* GTRS,

$$\hat{R}_{\varphi z I} = (\varphi \rightarrow -\varphi, z \rightarrow -z, t \rightarrow -t, *) = \hat{R} \cdot \hat{C}_2^x. \quad (29)$$

The *unitary* DSs for a general nanotube involve, therefore, the translation \mathbf{T}_z and screw axis \mathbf{S}_N symmetries only,

$$\hat{P}_N = \left(\varphi \rightarrow \varphi + \psi, z \rightarrow z + \tau, t \rightarrow t + \frac{k_0 \tau}{\omega} + \alpha \frac{\psi}{\omega} \right), \quad (30)$$

and

$$\hat{P}_\infty = \left(z \rightarrow z + T_z, t \rightarrow t + \frac{k_0 T_z}{\omega} \right). \quad (31)$$

Similarly to the result obtained for QRs, these unitary DSs are just the spatial transformations dictated by the symmetry of the nanotube potential and compensated by the appropriate translation in time. It is interesting to examine the quantum numbers associated with the DSs \hat{P}_N and \hat{P}_∞ . Note that the Floquet states $\Phi_\varepsilon(\mathbf{r}, t)$ are eigenstates of \hat{P}_N and \hat{P}_∞ as well. Recall, that for QRs we have $\hat{P}_N^N = \mathbf{I}$ and, therefore, the eigenvalues of \hat{P}_N are the N th order roots of -1 . The situation is more intricate for nanotubes in circularly polarized fields, where we find $\hat{P}_\infty^{-M} \hat{P}_N^N = \mathbf{I}$. Owing to the form of the interaction term, equation (28), and the periodicity embedded in \hat{P}_∞ , it is natural to transform from z and t to another set of orthogonal coordinates: $\omega t - k_0 z$ and $(\omega t + k_0 z)/2$. Afterwards, it is possible to rewrite a Floquet state as

$$\begin{aligned} \Phi_{\varepsilon, q}(\mathbf{r}, t) &= \exp\left(+iq\left(\frac{\omega t + k_0 z}{2k_0}\right)\right) \exp\left(-iq\left(\frac{\omega t - k_0 z}{2k_0}\right)\right) F_{\varepsilon, q}(\mathbf{r}, t) \\ &= \exp(+iqz) F_{\varepsilon, q}(\mathbf{r}, t), \quad -\frac{\pi}{T_z} < q \leq +\frac{\pi}{T_z}, \end{aligned} \quad (32)$$

where

$$\hat{P}_\infty \Phi_{\varepsilon,q}(\mathbf{r}, t) = F_{\varepsilon,q}(\mathbf{r}, t). \quad (33)$$

We, therefore, find that

$$\hat{P}_\infty \Phi_{\varepsilon,q,p}(\mathbf{r}, t) = e^{+iqT_z} \Phi_{\varepsilon,q,p}(\mathbf{r}, t), \quad (34)$$

and

$$\hat{P}_N \Phi_{\varepsilon,q,p}(\mathbf{r}, t) = \exp\left(+iqT_z \frac{M}{N}\right) \exp\left(+i\frac{2\pi R}{N}p\right) \Phi_{\varepsilon,q,p}(\mathbf{r}, t), \quad (35)$$

$$p = 0, 1, \dots, N - 1.$$

Finally, let us discuss briefly the symmetries and degeneracies of the QEBs (a full account for this subject is out of the scope of the present contribution and will be given elsewhere). Due to the lowered symmetry described by the collapse of all reflections to the GTRS $\hat{R}_{\varphi z}$, the reflection symmetry of nanotube EBs with respect to $k \rightarrow -k$ is *lifted*. Moreover, all non-accidental degeneracies of the EBs emanating from the rod-group structure of single-walled CNTs, as well as those added due to TRS, are *lifted* inside the laser field. In Section 6 we shall see that tight-binding-based models, developed to calculate the HHGS by single-walled CNTs within the dipole approximation, may conserve some of the EB symmetries and non-accidental degeneracies.

Summarizing what we have shown so far puts the DS analysis of Floquet states on a firm foundation [7], analogously to that possessed by symmetry analysis of stationary states. More specifically, one can label QEs and their corresponding Floquet states with ‘good’ quantum numbers, determine symmetry properties of QEBs and analyze whether non-accidental degeneracies can be found in the QE spectra following the existence of unitary and anti-unitary DSs. In the following sections we show that evaluating ‘suitable’ matrix elements with the help of DSs suggest a novel perspective and some new applications for the intense-field phenomena of HHG.

5. SELECTION RULES FOR THE HIGH-ORDER HARMONIC GENERATION SPECTRA

HHG is a non-linear phenomena in which high multiplicities of a fundamental frequency are generated by irradiating a non-linear medium, usually composed of rare-gas atoms, with intense lasers [3,4]. As the wavelengths obtained in HHG experiments have become shorter (e.g., 2.7 nm by Chang *et al.* [25] and below 2.5 nm by Schnürer *et al.* [26]), the

maximal order of the harmonics generated in gases has increased dramatically from the first harmonic generation experiments performed by New and Ward [27] and Reintjes *et al.* [28] (3rd and 5th harmonics, respectively) to those of Chang *et al.* [25] and Schnürer *et al.* [26] (about the 300th harmonic). However, *all odd* harmonics are generated in the discrete part of the spectrum in a typical HHG experiment. One property which would make the harmonic radiation particularly useful is the *selectivity* of the generation of high-order harmonics. That is, it would be highly advantageous to ‘design’ a combination of a target system and a laser beam or beams that would lead to the production of, say, the 100th harmonic only. A key component for such a solution lies within the DS properties of the system under study. Below we show that, analogously to ‘conventional’ spectroscopy, the harmonic emission is controlled by SRs, the formulation of which utilizes DSs and ‘suitable’ matrix elements. To see that, let us first understand within the DS formalism a much simpler question – why atoms irradiated by monochromatic, linearly polarized laser fields emit odd harmonics only [29]. Without loss of generality, the Floquet Hamiltonian of the system is given by

$$\hat{\mathcal{H}}_f(\mathbf{r}, t) = \frac{\hat{p}^2}{2m} + V(|\mathbf{r}|) + eE_0 x \cos(\omega t) - i\hbar \frac{\partial}{\partial t}. \quad (36)$$

Next, consider the second-order DS operator

$$\hat{P}_2 = \left(x \rightarrow -x, t \rightarrow t + \frac{T}{2} \right), \quad (\hat{P}_2)^2 = \mathbf{I}. \quad (37)$$

It is straightforward to prove that $[\hat{P}_2, \hat{\mathcal{H}}_f(\mathbf{r}, t)] = 0$. Thus, a complete set of QE states can be found, such that

$$\begin{aligned} \hat{\mathcal{H}}_f(\mathbf{r}, t) \Phi_{\varepsilon, p}(\mathbf{r}, t) &= \varepsilon \Phi_{\varepsilon, p}(\mathbf{r}, t), \\ \hat{P}_2 \Phi_{\varepsilon, p}(\mathbf{r}, t) &= e^{+i\pi p} \Phi_{\varepsilon, p}(\mathbf{r}, t), \quad p = 0, 1. \end{aligned} \quad (38)$$

The intensity of the n th harmonic is given by

$$\begin{aligned} I_\varepsilon^{(n)} &\propto \left| \frac{1}{T} \int_0^T e^{-in\omega t} \frac{d^2}{dt^2} \langle \Phi_{\varepsilon, p} | x | \Phi_{\varepsilon, p} \rangle \right|^2 \\ &= (n\omega)^4 \left| \frac{1}{T} \int_0^T e^{-in\omega t} \langle \Phi_{\varepsilon, p} | x | \Phi_{\varepsilon, p} \rangle \right|^2 \equiv (n\omega)^4 \left| \langle \langle \Phi_{\varepsilon, p} | x e^{-in\omega t} | \Phi_{\varepsilon, p} \rangle \rangle \right|^2, \quad (39) \end{aligned}$$

where we assume that the atomic-field state is described by a Floquet state. The double bra–ket notation

$$\langle\langle \cdots \rangle\rangle = \frac{1}{T} \int_0^T dt \int_{-\infty}^{+\infty} d\mathbf{r}, \quad (40)$$

defined within the extended Hilbert space introduced by Sambe [30] and Howland [31], introduces the ‘suitable’ matrix element relevant for the description of the HHG phenomena: the vectors are the Floquet states and the operator is the Fourier-dipole operator $\hat{x}e^{-in\omega t}$. We now show how the second-order DS \hat{P}_2 can be utilized to evaluate the matrix element defined in equations (39) and (40). By plugging \hat{P}_2 into the above matrix element one finds that the n th harmonic is emitted *iff*

$$\begin{aligned} \langle\langle \Phi_{\varepsilon,p} | x e^{-in\omega t} | \Phi_{\varepsilon,p} \rangle\rangle &= \langle\langle \Phi_{\varepsilon,p} | (\hat{P}_2)^{-1} \hat{P}_2 [\hat{x} e^{-in\omega t}] (\hat{P}_2)^{-1} \hat{P}_2 | \Phi_{\varepsilon,p} \rangle\rangle \\ &= \langle\langle \hat{P}_2 \Phi_{\varepsilon,p} | \hat{P}_2 [\hat{x} e^{-in\omega t}] (\hat{P}_2)^{-1} | \hat{P}_2 \Phi_{\varepsilon,p} \rangle\rangle \\ &= \langle\langle \Phi_{\varepsilon,p} | \hat{P}_2 [\hat{x} e^{-in\omega t}] (\hat{P}_2)^{-1} | \Phi_{\varepsilon,p} \rangle\rangle \neq 0, \end{aligned} \quad (41)$$

where the last step follows from the fact that the Floquet states are eigen states of \hat{P}_2 . Consequently, the non-zero values of $I_{\varepsilon}^{(n)}$ are obtained whenever

$$\hat{P}_2 [\hat{x} e^{-in\omega t}] (\hat{P}_2)^{-1} = -\hat{x} e^{-in\omega(t+\pi/\omega)} = (-1)^{n+1} \hat{x} e^{-in\omega t} = \hat{x} e^{-in\omega t}, \quad (42)$$

i.e., for odd n values only. In other words, the absence of even-harmonic generation in the course of irradiating atoms by monochromatic, linearly polarized lasers is associated here with the second-order DS \hat{P}_2 . It is instructive, at this point, to turn to the case of atoms in (monochromatic) circularly polarized laser fields, where it is known that no high-order harmonics are emitted [29]. The DS formalism enables us to prove very easily why this is so and gain further insight aiming towards our final goal. To this end and without loss of generality, consider the following Floquet Hamiltonian,

$$\hat{\mathcal{H}}_f(\mathbf{r}, t) = \frac{\hat{\mathbf{p}}^2}{2m} + V(|\mathbf{r}|) + eE_0 \rho \cos(\varphi - \omega t) - i\hbar \frac{\partial}{\partial t}. \quad (43)$$

Note that the field-free Hamiltonian is invariant under the ∞ th order (i.e., *continuous*) rotation $C_{\infty} = (\varphi \rightarrow \varphi + \delta\varphi)$, where $\delta\varphi$ is arbitrary. Next, consider the following ∞ th order DS operator,

$$\hat{P}_{\infty} = \left(\varphi \rightarrow \varphi + \delta\varphi, t \rightarrow t + \frac{\delta\varphi}{\omega} \right). \quad (44)$$

It is straightforward to prove that $[\hat{P}_\infty, \hat{\mathcal{H}}_f(\mathbf{r}, t)] = 0$. Therefore, a complete set of QE states can be found, such that

$$\begin{aligned}\hat{\mathcal{H}}_f(\mathbf{r}, t) \Phi_{\varepsilon, p}(\mathbf{r}, t) &= \varepsilon \Phi_{\mathbf{r}, p}(\mathbf{r}, t), \\ \hat{P}_\infty \Phi_{\mathbf{r}, p}(\varphi, t) &= e^{+ip\delta\varphi} \Phi_{\varepsilon, p}(\mathbf{r}, t), \quad p \in \mathbb{Z}.\end{aligned}\quad (45)$$

The intensity of the emitted \mathbf{n} th harmonic is given by

$$I_{\varepsilon, \pm}^{(\mathbf{n})} \propto \mathbf{n}^4 \left| \langle \Phi_{\varepsilon, p} | \rho e^{\pm i\varphi} e^{i\mathbf{n}\omega t} | \Phi_{\varepsilon, p} \rangle \right|^2. \quad (46)$$

The \pm stands for the components of the emitted radiation circularly polarized in the anti-clockwise (clockwise) direction, respectively. The \mathbf{n} th harmonic is, therefore, emitted *iff*

$$\begin{aligned}\hat{P}_\infty [e^{\pm i\varphi} e^{-i\mathbf{n}\omega t}] \hat{P}_\infty^{-1} &= e^{\pm i(\varphi + \delta\varphi)} e^{-i\mathbf{n}\omega(t + (\delta\varphi/\omega))} \\ &= e^{-i\delta\varphi(\mathbf{n} \mp 1)} e^{\pm i\varphi} e^{-i\mathbf{n}\omega t} = e^{\pm i\varphi} e^{-i\mathbf{n}\omega t},\end{aligned}\quad (47)$$

i.e., for $\mathbf{n} = 1$ only. In other words, the total annihilation of HHG in the course of irradiating atoms by circularly polarized laser fields is associated here with the infinite order DS \hat{P}_∞ . Having identified the DSs governing the SRs for the HHGS of atoms in linearly and circularly polarized fields, we have reached the point where SRs for the HHGS by quantum systems possessing the N th order DS \hat{P}_N can be formulated. To this end, we recall that a main principle in constructing a dynamical system possessing the N th order DS \hat{P}_N is the application of a coplanar circularly polarized laser field on a quantum system possessing the N th order rotation axis. All that is left to do is to analyze the matrix element defining the intensity of the emitted \mathbf{n} th harmonic, equation (46), with the finite order DS \hat{P}_N . In this case, one obtains that the \mathbf{n} th harmonic is emitted *iff*

$$\begin{aligned}\hat{P}_N [\exp(\pm i\varphi) \exp(-i\mathbf{n}\omega t)] \hat{P}_N^{-1} \\ &= \exp\left(\pm i\left(\varphi + \frac{2\pi}{N}\right)\right) \exp\left(-i\mathbf{n}\omega\left(t + \frac{T}{N}\right)\right) \\ &= \exp\left(-i\frac{2\pi(\mathbf{n} \mp 1)}{N}\right) \exp(\pm i\varphi) \exp(-i\mathbf{n}\omega t) \\ &= \exp(\pm i\varphi) \exp(-i\mathbf{n}\omega t),\end{aligned}\quad (48)$$

i.e., for

$$\mathbf{n} = 1, N \pm 1, 2N \pm 1, 3N \pm 1, 4N \pm 1, \dots, lN \pm 1, \dots \quad (49)$$

Moreover, for $N > 2$ the $(IN + 1)$ th harmonics are circularly polarized in the anti-clockwise direction (as the incident field is), while the $(IN - 1)$ th harmonics are circularly polarized in the opposite direction.

The proof given above can be easily extended to the case of 3D many-electron systems. The Floquet Hamiltonian for M electrons moving in a potential possessing the N th order rotation symmetry and interacting with a circularly polarized field reads

$$\hat{\mathcal{H}}_{f,M}(\bar{\mathbf{r}}, t) = \sum_{i=1}^M \hat{H}(\mathbf{r}_i, t) + \sum_{i < j=1}^M \frac{e^2}{|\mathbf{r}_i - \mathbf{r}_j|} - i\hbar \frac{\partial}{\partial t}, \quad (50)$$

where $\bar{\mathbf{r}} \equiv (\mathbf{r}_1, \dots, \mathbf{r}_M)$ and $H(\mathbf{r}_i, t)$ is the single-electron, time-dependent Hamiltonian (see equation (5)). The Floquet Hamiltonian (50) is invariant under two mutually disjoint groups: the N th order unitary and cyclic DS group $\mathcal{G}_{N,M}$, and the M -electron permutation group \mathcal{S}_M . The former is generated by the simultaneous rotation of all the electrons and the appropriate translation in time:

$$\hat{P}_{N,M} = \left(\varphi_1 \rightarrow \varphi_1 + \frac{2\pi}{N}, \dots, \varphi_M \rightarrow \varphi_M + \frac{2\pi}{N}, t \rightarrow t + \frac{T}{N} \right). \quad (51)$$

The intensity of the n th harmonic emitted in the M -electron case takes the form

$$I_{\varepsilon, \pm, M}^{(n)} \propto n^4 \left| \left\langle \left\langle \Phi_{\varepsilon, p, M} \right| \left(\sum_{j=1}^M \rho_j e^{\pm i \varphi_j} \right) e^{-i n \omega t} \right| \Phi_{\varepsilon, p, M} \right\rangle \right|^2. \quad (52)$$

As one can see, $\sum_{j=1}^M \rho_j e^{\pm i \varphi_j}$ belongs to the trivial representation of the permutation group \mathcal{S}_M , being a sum of single-particle operators. $|\Phi_{\varepsilon, p, M}|^2$ belongs to this representation as well, owing this property to Pauli's exclusion principle. In case of electrons (which are fermions), $\Phi_{\varepsilon, p, M}$ is an eigenfunction of *any* permutation from \mathcal{S}_M . If the permutation is composed of odd (even) number of transpositions, the corresponding eigenvalue is -1 ($+1$). Therefore, $|\Phi_{\varepsilon, p, M}|^2$ is invariant under all $M!$ M -electron permutations. Thus, the permutational symmetry and the existence of the pairwise interaction do not affect the DS properties of the single-electron Floquet Hamiltonian, equation (5). Moreover, the analysis of the HHG matrix element in equation (52) with respect to the DS operator $\hat{P}_{N,M}$ (equation (51)) results in the SRs *identical* to the ones obtained in the single-electron case with the DS \hat{P}_N (equation (9)).

The HHGS for $N = 100$ is given in Fig. 3 for a simple numerical model. As expected on the basis of the DS-based SRs, the high-order harmonics produced are the 99th, 101st, 199th, 201st, ... ones. For more details, as well as for a discussion of the stability of the HHGS with respect to weak DS-breaking perturbations, see Ref. [10].

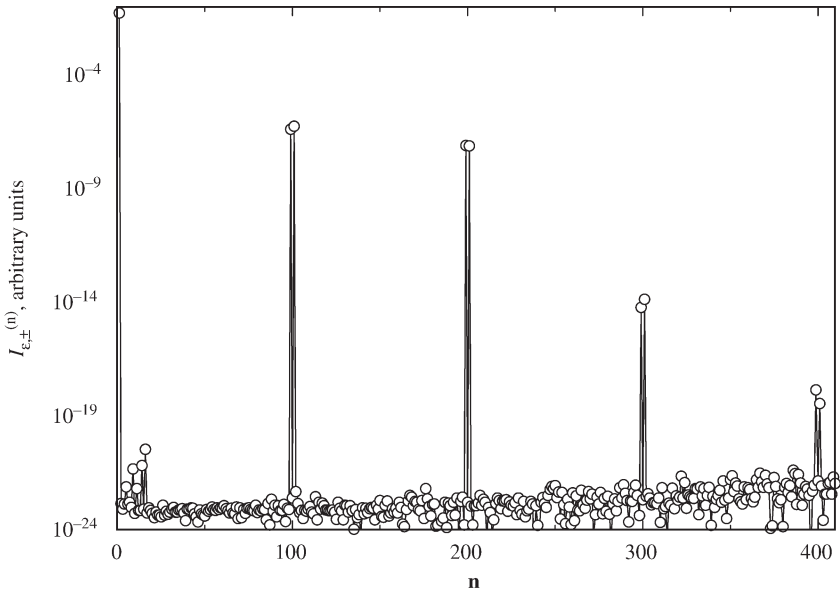


Fig. 3. HHGS for a model of $N = 100$ atoms, which are placed equidistantly on a circle, exposed to (monochromatic) coplanar circularly polarized field of the intensity 1.8×10^{13} W/cm² and frequency $\omega = 0.02$ a.u. ≈ 0.54 eV. The first high-order harmonic has the frequency of $99\omega \approx 2$ a.u.

In conclusion, the higher the DS of the Floquet Hamiltonian is, the lower the wavelength of the first allowed high-order harmonic. Our theoretical search for a method for a short wavelength, almost monochromatic, coherent radiation source would have ended here had we discarded the following practical perspective: if one wishes to design a system the lowest high-order harmonic of which is, say, the 100th, it is required to find a molecular or an artificial system which possesses the 101-fold *rotation* axis. To the best of our knowledge such systems cannot be easily found. Therefore, let us proceed to the study of HHGS from spatially extended targets, such as CNTs, in order to exploit the DS emanating from the *screw axis* spatial symmetry.

6. HIGH-ORDER HARMONIC GENERATION OF SOFT X-RAYS BY CARBON NANOTUBES

The approach to the formulation of the SRs for the HHGS presented in Section 5 is based on the dipole approximation with respect to *both* the incident and the emitted waves. As such, it is not valid for the spatially extended target systems, such as CNTs. Therefore, let us first present a

general and exact method for the formulation of the SRs for HHGS beyond the dipole approximation validity regime and then proceed with applying it to the HHG by single-walled CNTs [12].

According to classical electrodynamics, the intensity of n th harmonic, $I^{(n,k)}$ in HHG processes is associated with the corresponding Fourier component of the time-dependent electron flux $\mathbf{J}(\mathbf{r}, t)$ [32]:

$$I^{(n,k)} \propto |\mathbf{A}^{(n,k)} \times \mathbf{k}|^2, \quad \mathbf{A}^{(n,k)} \propto \int_0^\infty dt \int_{-\infty}^{+\infty} d\mathbf{r} \mathbf{J}(\mathbf{r}, t) e^{-i(n\omega t - \mathbf{k} \cdot \mathbf{r})}, \quad (53)$$

where \mathbf{k} is the harmonic wave-vector. Note that in equation (53) $\mathbf{A}^{(n,k)}$ stands for the (immeasurable) vector potential of the emitted field of the frequency $n\omega$. The (measurable) magnetic and electric fields propagating along the direction of the wave-vector \mathbf{k} are obtained from $\mathbf{A}^{(n,k)}$ by vector multiplication [32]:

$$\mathbf{H}^{(n,k)} = i\mathbf{A}^{(n,k)} \times \mathbf{k}, \quad \mathbf{E}^{(n,k)} = \frac{ic}{n\omega} (\mathbf{k} \times \mathbf{A}^{(n,k)}) \times \mathbf{k}. \quad (54)$$

When dealing with micro- or mesoscopic systems behaving according to the laws of quantum mechanics, one has to use the quantum mechanical expression for the electron flux (current-density operator) [33],

$$\begin{aligned} \hat{\mathbf{J}}(\mathbf{r}, t) &= \frac{e\hbar}{2mi} [\psi^*(\mathbf{r}, t) \hat{\mathbf{p}} \psi(\mathbf{r}, t) - \psi(\mathbf{r}, t) \hat{\mathbf{p}} \psi^*(\mathbf{r}, t)] \\ &\quad - \frac{e^2}{mc} \psi^*(\mathbf{r}, t) \hat{\mathbf{A}}(\mathbf{r}, t) \psi(\mathbf{r}, t) \\ &= \frac{e}{2} [\psi^*(\mathbf{r}, t) \hat{\mathbf{v}} \psi(\mathbf{r}, t) + \psi(\mathbf{r}, t) \hat{\mathbf{v}}^* \psi^*(\mathbf{r}, t)] = e\Re[\psi^*(\mathbf{r}, t) \hat{\mathbf{v}} \psi(\mathbf{r}, t)], \end{aligned} \quad (55)$$

where

$$\hat{\mathbf{v}} = \frac{1}{m} \left[\hat{\mathbf{p}} - \frac{e}{c} \hat{\mathbf{A}}(\mathbf{r}, t) \right]. \quad (56)$$

Consider, for instance, the time-periodic, spatially dependent vector-potential of an incident electromagnetic field, propagating along the z -axis. The Floquet expression for the vector potential of the n th harmonic emitted in the incident field propagation direction (z) is given by

$$\begin{aligned} \mathbf{A}_\varepsilon^{(n,z)} &\propto \langle\langle \Phi_\varepsilon(\mathbf{r}, t) | \hat{\mathbf{A}}^{(n,z)} | \Phi_\varepsilon(\mathbf{r}, t) \rangle\rangle + \langle\langle \Phi_\varepsilon^*(\mathbf{r}, t) | (\hat{\mathbf{A}}^{(n,z)})^{\dagger*} | \Phi_\varepsilon^*(\mathbf{r}, t) \rangle\rangle \\ \hat{\mathbf{A}}^{(n,z)} &= \hat{\mathbf{v}} e^{-in(\omega t - k_0 z)}, \quad (\hat{\mathbf{A}}^{(n,z)})^{\dagger*} = \hat{\mathbf{v}}^* e^{-in(\omega t - k_0 z)}. \end{aligned} \quad (57)$$

In order to determine which harmonics are emitted by nanotubes during the interaction with circularly polarized radiation, it is sufficient to check the invariance of the symmetry-adapted linear combination operators

(see equation (57) with the vector potential in equation (27))

$$\begin{aligned}\hat{A}_{\pm}^{(\mathbf{n},z)} &= \hat{A}_x^{(\mathbf{n},z)} \pm i\hat{A}_y^{(\mathbf{n},z)} \\ &= \left[\frac{\hbar}{i} e^{\pm i\varphi} \left(\frac{\partial}{\partial \rho} \pm \frac{i}{\rho} \frac{\partial}{\partial \varphi} \right) - \frac{eE_0}{\omega} e^{\pm i\alpha(\omega t - k_0 z)} \right] e^{-i\mathbf{n}(\omega t - k_0 z)}, \quad (58)\end{aligned}$$

under the two DSs \hat{P}_N and \hat{P}_{∞} (equations (30) and (31), respectively). It can readily be verified that

$$\hat{P}_{\infty} \cdot \hat{A}_{\pm}^{(\mathbf{n},z)} \cdot (\hat{P}_{\infty})^{-1} = \hat{A}_{\pm}^{(\mathbf{n},z)} \quad \forall \mathbf{n}. \quad (59)$$

The \hat{P}_N DS operator, on the other hand, leaves invariant the vector potential operators $\hat{A}_{\pm}^{(\mathbf{n},z)}$ iff

$$\hat{P}_N \cdot \hat{A}_{\pm}^{(\mathbf{n},z)} \cdot (\hat{P}_N)^{-1} = \exp\left(-i \frac{2\pi R(\alpha \mathbf{n} \mp 1)}{N}\right) \hat{A}_{\pm}^{(\mathbf{n},z)} = \hat{A}_{\pm}^{(\mathbf{n},z)}, \quad (60)$$

i.e., for

$$\mathbf{n} = 1, N \pm 1, 2N \pm 1, \dots, lN \pm 1, \dots \quad (61)$$

The ‘+’ harmonics are circularly polarized as the incident field is, while the ‘−’ harmonics are circularly polarized in the opposite direction. Note that the incident field helicity α does not enter equation (61).

The order N of the screw axis of an achiral CNT is equal to twice the order of its rotation axis n . Consequently, the SRs for the HHGS by achiral CNTs are

$$\mathbf{n} = 1, 2n \pm 1, 4n \pm 1, \dots, 2ln \pm 1, \dots \quad (62)$$

For example, the (9,0)-zigzag ($\rho_0 \approx 6.7$ a.u.) and the (9,9)-armchair CNTs ($N = 2n = 18$) emit only the 17th, 19th, 35th, 37th, ... high-order harmonics of the incident laser frequency. For such a value of N and incident radiation wavelength of $1 \mu\text{m}$ the first emitted high-order harmonic wave-length, λ_{17} , is about 59 nm.

The chiral CNTs can possess the screw axes of much higher orders than the achiral ones (see Ref. [24]), leading to a much more selective HHG by these systems. For example, for the chiral (8,2) ($\rho_0 \approx 6.9$ a.u.) single-walled CNT $N = 28$. Thus, the $(lN \pm 1)$ SRs imply that the first emitted high-order harmonics are the 27th and 29th. In such a case, the wavelength of the first high-order harmonic, generated by a circularly polarized $1 \mu\text{m}$ incident radiation, is about 37 nm. The (8,3) chiral nanotube possessing only a slightly different diameter ($\rho_0 \approx 7.3$ a.u.) but considerably higher order screw axis symmetry ($N = 194$) would generate the first high-order harmonics of the orders 193 and 195!

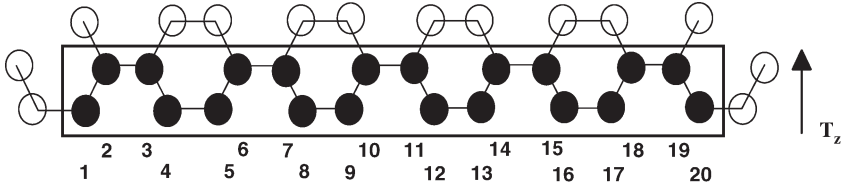


Fig. 4. Unit cell of the (5,5)-armchair CNT. The $2N = 20$ atoms are used to construct the tight-binding Bloch states. $T_z = |\mathbf{T}_z|$ is the unit cell length.

Our discussion of the selectivity of HHG by single-walled CNTs has been limited so far to the formulation of the SRs. It is important, however, to estimate the intensities of the symmetry-allowed harmonics emitted by these systems. To this end, let us consider a model for HHG by single-walled CNTs based on the $2p_z$ -orbital tight-binding approximation to the tube electronic structure [24] and the dipole approximation with respect to the incident and emitted waves. In contrast to our symmetry arguments which are generally valid, this approach is justified only for the low-frequency laser fields, such that the fundamental and high-order harmonic wavelengths are larger than the unit cell length. The Floquet Hamiltonian is represented in the basis of the following tight-binding Bloch states

$$\Psi_p^k(\rho_0, \varphi, z) = \sum_{q=-\infty}^{\infty} e^{ikz_{p,q}} \psi_{2p_z}(\rho_0, \varphi - \varphi_p^{(0)}, z - z_{p,q}) \quad (63)$$

$$z_{p,q} = z_p^{(0)} + qT_z, \quad p = 1, 2, \dots, 2N, \quad q \in \mathbb{Z},$$

where $\{\varphi_p^{(0)}, z_p^{(0)}\}$ are the positions of carbon atoms in the zeroth unit cell and k is the quasimomentum, $-(\pi/T_z) < k \leq +(\pi/T_z)$. Following Hückel approximation, only those field-free Hamiltonian matrix elements that involve the same or adjacent atomic $2p_z$ -orbitals, ψ_{2p_z} , are non-zero. For instance, consider the (5,5)-armchair CNT ($\rho_0 \approx 6.5$ a.u.). In Fig. 4 we show the unit cell used to construct the basis of $2N = 20$ tight-binding Bloch states.

The positions of carbon atoms in the zeroth unit cell are given by (atoms are enumerated from left ($p = 1$) to right ($p = 20$))

$$\varphi_p^{(0)} = \left\{ \begin{array}{ll} \frac{2\pi}{30} + \frac{p-1}{4} \frac{2\pi}{5} : & p = 1, 5, 9, 13, 17 \\ \frac{4\pi}{30} + \frac{p-2}{4} \frac{2\pi}{5} : & p = 2, 6, 10, 14, 18 \\ \frac{8\pi}{30} + \frac{p-3}{4} \frac{2\pi}{5} : & p = 3, 7, 11, 15, 19 \\ \frac{10\pi}{30} + \frac{p-4}{4} \frac{2\pi}{5} : & p = 4, 8, 12, 16, 20 \end{array} \right\}, \quad (64)$$

and

$$z_p^{(0)} = \left\{ \begin{array}{ll} \frac{T_z}{4} : & p = 1, 4, 5, 8, 9, \dots, 20 \\ \frac{3T_z}{4} : & p = 2, 3, 6, 7, 10, \dots, 19 \end{array} \right\}. \quad (65)$$

Finally, the matrix elements of the Hamiltonian $\hat{H}_{\text{nanotube}}^{(5,5)}$ (represented in the $2N = 20$ tight-binding Bloch states) are given by (see also Ref. [24])

$$H_{\text{nanotube}}^{(5,5)}(k) = \beta \begin{pmatrix} 0 & b & 0 & 0 & 0 & \cdots & 0 & 1 \\ b & 0 & 1 & 0 & 0 & \cdots & 0 & 0 \\ 0 & 1 & 0 & b & 0 & \cdots & 0 & 0 \\ 0 & 0 & b & 0 & 1 & \cdots & 0 & 0 \\ 0 & 0 & 0 & 1 & 0 & \cdots & 0 & 0 \\ \vdots & \vdots & \vdots & \vdots & \vdots & \ddots & \vdots & \vdots \\ 0 & 0 & 0 & 0 & 0 & \cdots & 0 & b \\ 1 & 0 & 0 & 0 & 0 & \cdots & b & 0 \end{pmatrix}, \quad (66)$$

where $\beta \approx 2.7$ eV (see in Ref. [34]) is the nearest neighbor tight-binding overlap energy, $T_z = 2.49$ Å, $b = b(k) = 2 \cos(kT_z/2)$ and the energy of each $2p_z$ -orbital, $\langle \psi_{2p_z} | \hat{H}_{\text{nanotube}}^{(5,5)} | \psi_{2p_z} \rangle$, is taken equal to 0.

The interaction term represented in the length gauge is diagonal:

$$\begin{aligned} & \left\langle \Psi_p^k \left| \frac{1}{2} e E_0 \rho_0 (e^{i\omega t} e^{i\varphi} + e^{-i\omega t} e^{-i\varphi}) \right| \Psi_{p'}^k \right\rangle \\ &= \frac{1}{2} e E_0 \rho_0 (e^{i\omega t} e^{i\varphi_p^{(0)}} + e^{-i\omega t} e^{-i\varphi_p^{(0)}}) \delta_{p,p'}. \end{aligned} \quad (67)$$

The solution of the time-dependent Schrödinger equation leads to the FB states which are eigenstates of the translation by a unit cell length, T_z :

$$\Phi_\alpha^k(t) = \sum_{p=1}^{2N} C_{\alpha,p}^k(t) \Psi_p^k, \quad \alpha = 1, 2, \dots, 2N. \quad (68)$$

The corresponding QEs are functions of the quasimomentum, $\varepsilon_\alpha = \varepsilon_\alpha(k)$. In Figs 5 and 6 we show the Π -orbital EB (see equation (4.4) in Ref. [24] for the closed-form formula) and QEB spectra of the (5,5)-armchair CNT, respectively. Note the independent symmetries with respect to $k \leftrightarrow -k$ and $E_i \leftrightarrow -E_i$ all EBs exhibit, as well as the sticking together at the edge

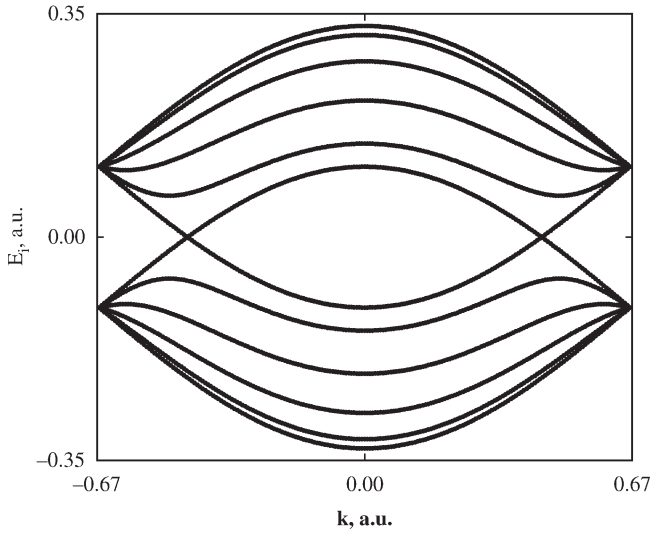


Fig. 5. The Π -orbital (tight-binding approximation) EB spectrum of the (5,5)-armchair CNT. Note the independent symmetries of the EBs with respect to $k \leftrightarrow -k$ and $E_i \leftrightarrow -E_i$.

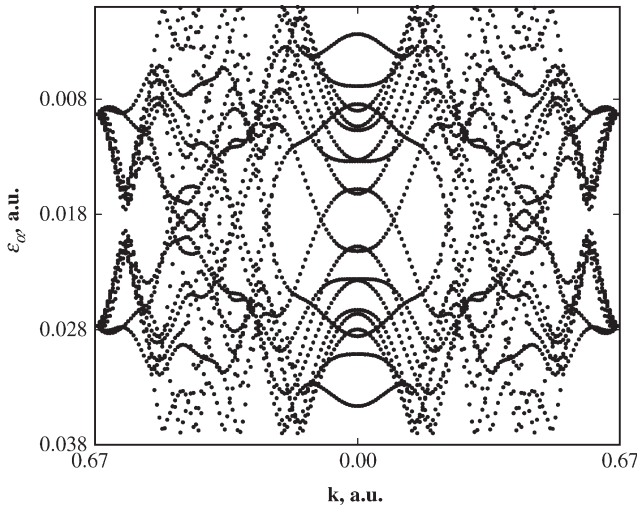


Fig. 6. The Π -orbital (tight-binding approximation) QEB spectrum of the (5,5)-armchair CNT. $\omega = 0.037$ a.u. (≈ 1.0 eV, $\lambda \approx 1.2$ μm) and $E_0 = 0.05$ a.u. ($\approx 9 \times 10^{13}$ W/cm²). Note the independent symmetries of the QEBs with respect to $k \leftrightarrow -k$ and $E_\alpha \leftrightarrow -E_\alpha$ (compare to Fig. 5), which appear due to the dipole and tight-binding approximations employed in the calculation.

of the BZ which remain when the field is turned on. These features can be accounted for by the (full) DSs associated with the dipole and tight-binding approximations employed in the calculation (compare to the discussion in Section 4, after equation (35)) and can be proved by examining the matrix representations of the field-free and Floquet Hamiltonians. Similarly, in Figs 7 and 8 we show the Π -orbital EB (see equation (4.7) in Ref. [24] for the closed-form formula) and QEB spectra of the (9,0)-zigzag CNT, respectively, and in Figs 9 and 10 we show the Π -orbital EB (see equation (4.1) in Ref. [24] for extracting the closed-form formula) and QEB spectra of the (8,2)-chiral CNT, respectively.

The single-electron Fourier components of the time-dependent dipole moment corresponding to the (α, k) th FB state are given by

$$d_{\pm, k}^{(\alpha)}(\mathbf{n}\omega) = \langle\langle \Phi_{\alpha}^k(t) | e \rho_0 e^{-i\mathbf{n}\omega t} e^{\pm i\varphi} | \Phi_{\alpha}^k(t) \rangle\rangle. \quad (69)$$

In order to take into account the generation of harmonics by the electrons filling a number of QEBs, we average the Fourier components of the dipole moment arising from the (α, k) th FB state, $d_{\pm, k}^{(\alpha)}(\mathbf{n}\omega)$, over the quasimomenta and sum them over the filled QEBs (note the symmetry $\varepsilon_{\alpha} \leftrightarrow -\varepsilon_{\alpha}$ of the QEBs in Figs 6 and 8; Fig. 10, on the other hand, lacks this symmetry),

$$d_{\pm}(\mathbf{n}\omega) = \frac{T_z}{2\pi N} \sum_{\alpha=1}^N \int_{k=-(\pi/T_z)}^{+(\pi/T_z)} dk d_{\pm, k}^{(\alpha)}(\mathbf{n}\omega). \quad (70)$$

This procedure is equivalent to the Hartree approximation to the multi-electron FB wavefunction (see Refs. [35,36]). The prefactor of equation (70) reflects the normalization of the Hartree wave function to unity. Such normalization is chosen in order to allow the direct comparison of the nanotube response to the single-atom, single-electron calculations. Indeed, the quantity $|d_{\pm}(\mathbf{n}\omega)|^2$ is fully analogous to the single-atom (microscopic) response of atomic HHG. The model described above, while not being very precise, should give a correct order of magnitude estimate for the high-order harmonic intensities.

In the present calculations we restrict our attention to the intensities low enough so that the ionization is weak. On the basis of the work by Lenzner *et al.* [37], we take the appropriate threshold intensity as $I = 10^{14}$ W/cm². Above this threshold significant ionization is expected to take place, which cannot be accounted for by the present model. Besides an irreversible damage to the CNT sample, the breakdown would be accompanied by the free electrons generation having a negative effect on the propagation of the emitted harmonics. The HHGS of the (5,5)-armchair, the (9,0)-zigzag and the (8,2)-chiral single-walled CNTs interacting with the electric field of the frequency 0.037 a.u. (≈ 1.0 eV, $\lambda \approx 1.2$ μ m) and the strength 0.05 a.u. (corresponding to the intensity of 9×10^{13} W/cm²) are shown in Fig. 11.

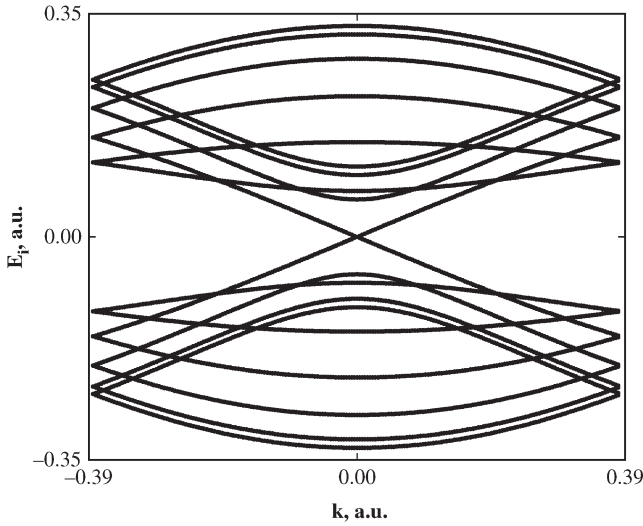


Fig. 7. The Π -orbital (tight-binding approximation) EB spectrum of the (9,0)-zigzag CNT. Note the independent symmetries of the EBs with respect to $k \leftrightarrow -k$ and $E_i \leftrightarrow -E_i$.

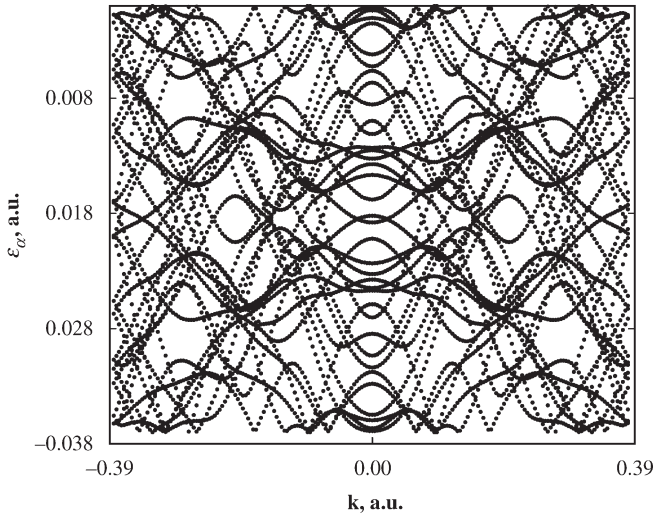


Fig. 8. The Π -orbital (tight-binding approximation) QEB spectrum of the (9,0)-zigzag CNT. $\omega = 0.037$ a.u. (≈ 1.0 eV, $\lambda \approx 1.2$ μm) and $E_0 = 0.05$ a.u. ($\approx 9 \times 10^{13}$ W/cm 2). Note the independent symmetries of the QEBs with respect to $k \leftrightarrow -k$ and $\varepsilon_\alpha \leftrightarrow -\varepsilon_\alpha$ (compare to Fig. 7), which appear due to the dipole and tight-binding approximations employed in the calculation.

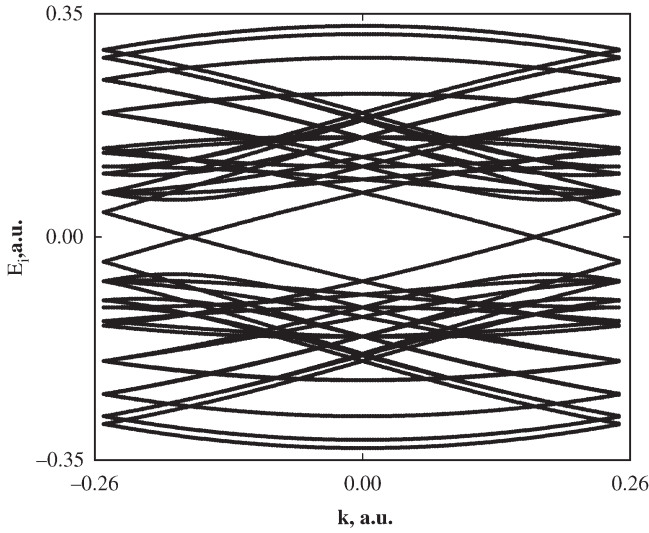


Fig. 9. The Π -orbital (tight-binding approximation) EB spectrum of the (8,2)-chiral CNT. Note the independent symmetries of the EBs with respect to $k \leftrightarrow -k$ and $E_i \leftrightarrow -E_i$.

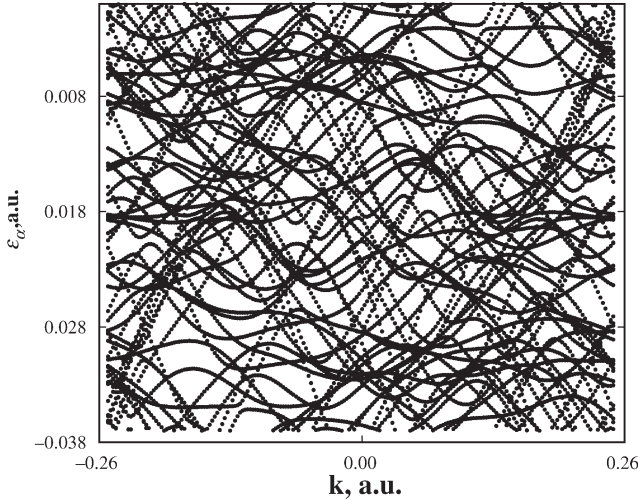


Fig. 10. The Π -orbital (tight-binding approximation) QEB spectrum of the (8,2)-zigzag CNT. $\omega = 0.037$ a.u. (≈ 1.0 eV, $\lambda \approx 1.2$ μm) and $E_0 = 0.05$ a.u. ($\approx 9 \times 10^{13}$ W/cm²). Note the breaking of the symmetry of the QEBs with respect to $k \leftrightarrow -k$, reflecting the removal of the TRS by the laser field. Note, on the other hand, that the *combined* symmetry, $k \leftrightarrow -k$ and $\varepsilon_\alpha \leftrightarrow -\varepsilon_\alpha$ (compare to Fig. 9), is preserved due to the dipole and tight-binding approximations employed in the calculation.

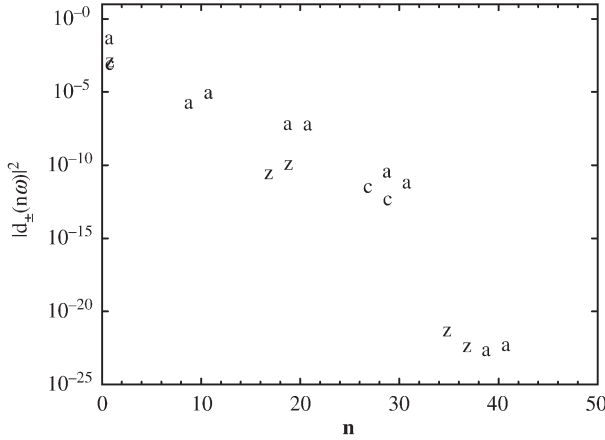


Fig. 11. HHGS of the (5,5)-armchair ('a'), the (9,0)-zigzag ('z') and the (8,2)-chiral ('c') single-walled CNTs based on the $2p_z$ -orbital tight-binding model. $\omega = 0.037$ a.u. (≈ 1.0 eV, $\lambda \approx 1.2$ μm) and $E_0 = 0.05$ a.u. ($\approx 9 \times 10^{13}$ W/cm²).

The SRs for the considered CNTs

$$\begin{aligned}
 (5,5)\text{-armchair } \mathbf{n} &= 1, 9, 11, 19, 21, \dots, \\
 (9,0)\text{-zigzag } \mathbf{n} &= 1, 17, 19, 35, 37, \dots, \\
 (8,2)\text{-chiral } \mathbf{n} &= 1, 27, 29, \dots,
 \end{aligned} \tag{71}$$

are clearly seen. The cutoff in the nanotube HHGS is not sharp and appears at the maximal variation of the interaction energy:

$$\mathbf{n}_{\text{cutoff}} = \frac{2eE_0\rho_0}{\hbar\omega}. \tag{72}$$

Such a cutoff law is a characteristic of the multi-center, ring-like systems driven by (monochromatic) coplanar circularly polarized fields when the interaction energy is much higher than the energy differences of the field-free system [13]. The three nanotubes possess about the same diameter (and hence, about the same value of the interaction energy) which leads to the similar cutoff positions at about $\mathbf{n} = 20$.

The absolute intensities $|d_{\pm}(\mathbf{n}\omega)|^2$ of the plateau harmonics emitted by the above CNTs are of the order of 10^{-5} – 10^{-7} a.u. for the (5,5)-armchair CNT and about 10^{-10} a.u. for the (9,0)-zigzag one. The single pair of high-order harmonics emitted by the (8,2)-chiral CNT is in the cutoff region and possesses an intensity of about 10^{-11} – 10^{-12} a.u. One can see that the armchair CNT leads to the most intense HHGS.

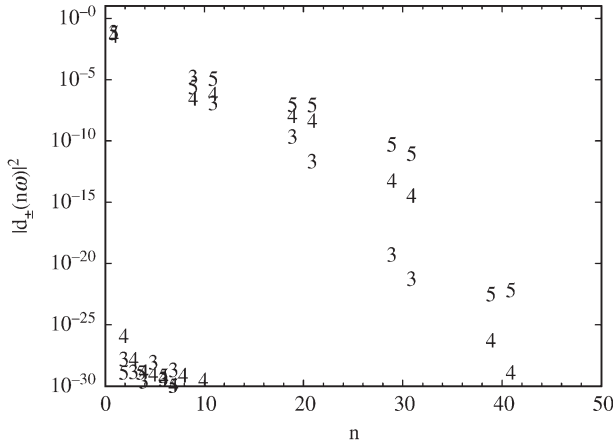


Fig. 12. HHGS of the (5,5)-armchair CNT at the field strengths of $E_0 = 0.03$ a.u. ($\approx 3 \times 10^{13}$ W/cm²), '3', $E_0 = 0.04$ a.u. ($\approx 6 \times 10^{13}$ W/cm²), '4', $E_0 = 0.05$ a.u. ($\approx 9 \times 10^{13}$ W/cm²), '5'. $\omega = 0.037$ a.u. (≈ 1.0 eV, $\lambda \approx 1.2$ μ m). The first two pairs of high-order harmonics (the 9th, 11th and the 19th, 21st) appear in the plateau part of the spectra.

In order to explore further the HHG by the (5,5) armchair CNT we have calculated its HHGS at two additional values of the field strength, $E_0 = 0.03$ and 0.04 a.u., corresponding to the intensities of about 3×10^{13} and 6×10^{13} W/cm², respectively. The HHGS of the (5,5)-armchair nanotube at the three different intensities are shown in Fig. 12. One can see that the first two pairs of high-order harmonics (the 9th, 11th and the 19th, 21st) appear in the plateau part of the spectra. It is instructive to compare the presented harmonic intensities, $|d_{\pm}(\mathbf{n}\omega)|^2$, to those of Fig. 10 of the work by Krause *et al.* [38] in the atomic case for the linear polarization of the incident field at the intensities close to 10^{14} W/cm². One can see that at all the incident intensity values the harmonics generated by the (5,5)-armchair CNT are of the same order of magnitude or stronger than those generated by hydrogen atom [38].

7. SUMMARY AND CONCLUSIONS

1. The combination of the spatial symmetry of a quantum system and the time-periodic, spatially dependent interaction with laser fields brings about the formation of DSs.
2. DS operations form groups and, consequently, DS analysis of Floquet states is analogous to symmetry analysis of stationary states. In particular, one can label QEs and their corresponding Floquet states with appropriate quantum numbers, determine symmetry properties of

- QEBs and analyze whether non-accidental degeneracies can be found in the QEB spectra following the existence of unitary and anti-unitary DSs.
3. DS analysis of HHG processes in high-intensity laser fields has been placed on a firm foundation, analogously to that possessed by symmetry analysis in 'conventional' spectroscopy.
 4. In general, for many-electron, time-periodic Hamiltonians which are invariant under \hat{P}_N only the $\mathbf{n} = 1, N \pm 1, 2N \pm 1, 3N \pm 1, 4N \pm 1, \dots$ harmonics are generated.
 5. The SR derived for *any* single-walled CNT are given by $\mathbf{n} = 1, N \pm 1, 2N \pm 1, 3N \pm 1, 4N \pm 1, \dots$, where N is the number of hexagons in its unit cell. These SRs are invariant with respect to the wavelength of the incident circularly polarized laser radiation, as well as to its helicity. The considered (5,5)-armchair CNT gives rise to the HHGS which is both selective and efficient enough to be of interest to experimentalists. The *chiral* CNTs are the first example of realistic physical systems for which all harmonics but very high-order ones are forbidden by symmetry. We hope that further development of present day technologies of growing arrays of CNTs parallel to each other and preparation of ropes containing CNTs of a single definite symmetry would allow one the experimental verification of the above theory and results in the near future.

ACKNOWLEDGEMENTS

This work is dedicated to Prof. Osvaldo Goscinski on the occasion of his 65th birthday. This work is supported in part by the Basic Research Foundation administered by the Israeli Academy of Sciences and Humanities and by the Fund for the Promotion of Research at Technion. The authors wish to thank Prof. U. Peskin for many helpful discussions and comments. OEA would like to thank the European Community for support (Marie-Curie Fellowship). V.A. would like to thank the Minerva Foundation for financial support. OEA and V.A. would like to acknowledge the hospitality of the Theoretical Chemistry department of Heidelberg University where part of this work has been completed.

REFERENCES

- [1] V. Heine, *Group Theory in Quantum Mechanics*, Dover, New York, 1993.
- [2] D. C. Harris and M. D. Bertolucci, *Symmetry and Spectroscopy: An Introduction to Vibrational and Electronic Spectroscopy*, Dover, New York, 1989.
- [3] P. Salières, A. L'Huillier, P. Antoine and M. Lewenstein, *Adv. At. Mol. Opt. Phys.*, 1999, **4**, 83.
- [4] T. Brabec and F. Krausz, *Rev. Mod. Phys.*, 2000, **72** (2), 745.

- [5] J. H. Shirley, *Phys. Rev.*, 1965, **138**, B979.
- [6] F. H. M. Faisal, *Theory of Multiphoton Processes*, Plenum Press, New York, 1987.
- [7] O. E. Alon, *Phys. Rev. A*, 2002, **66**, 013414.
- [8] N. Ben-Tal, N. Moiseyev and A. Beswick, *J. Phys. B*, 1993, **26**, 3017.
- [9] R. Bavli and H. Metiu, *Phys. Rev. A*, 1993, **47**, 3299.
- [10] O. E. Alon, V. Averbukh and N. Moiseyev, *Phys. Rev. Lett.*, 1998, **80**, 3743.
- [11] V. Averbukh, O. E. Alon and N. Moiseyev, *Phys. Rev. A*, 1999, **60**, 2585.
- [12] O. E. Alon, V. Averbukh and N. Moiseyev, *Phys. Rev. Lett.*, 2000, **85**, 5218.
- [13] V. Averbukh, O. E. Alon and N. Moiseyev, *Phys. Rev. A*, 2001, **64**, 033411.
- [14] F. Ceccherini and D. Bauer, *Phys. Rev. A*, 2001, **64**, 033423.
- [15] F. Ceccherini, D. Bauer and F. Cornolti, *J. Phys. B*, 2001, **34**, 5017.
- [16] V. Averbukh, O. E. Alon and N. Moiseyev, *Phys. Rev. A*, 2002, **65**, 063402.
- [17] P. Ždánká, V. Averbukh and N. Moiseyev, *J. Chem. Phys.*, 2003, **118**, 8726.
- [18] R. Baer, D. Neuhauser, P. Ždánká and N. Moiseyev, *Phys. Rev. A*, 2003, **68**, 043406.
- [19] F. Ceccherini, D. Bauer and F. Cornolti, *Phys. Rev. A*, 2003, **68**, 053402.
- [20] A. K. Gupta, O. E. Alon and N. Moiseyev, *Phys. Rev. B*, 2003, **68**, 205101.
- [21] G. Floquet, *Ann. de l'Ecole Norm. Suppl.*, 1883, **12**, 47.
- [22] E. P. Wigner, *Group Theory and Its Application to Quantum Mechanics of Atomic Spectra*, Academic Press, New York, 1959.
- [23] M. Damjanović, T. Milošević, T. Vuković and R. Sredanović, *Phys. Rev. B*, 1999, **60**, 2728.
- [24] R. Saito, G. Dresselhaus and M. S. Dresselhaus, *Physical Properties of Carbon Nanotubes*, Imperial College Press, London, 1998.
- [25] Z. Chang, A. Rundquist, H. Wang, M. M. Murnane and H. Kapteyn, *Phys. Rev. Lett.*, 1997, **79**, 2967.
- [26] M. Schnürer, Ch. Spielmann, P. Wobrauschek, C. Streli, N. H. Burnett, C. Kan, K. Ferencz, R. Koppitsch, Z. Cheng, T. Brabec and F. Krausz, *Phys. Rev. Lett.*, 1998, **80**, 3236.
- [27] G. H. C. New and F. Ward, *Phys. Rev. Lett.*, 1967, **19**, 556.
- [28] J. Reintjes, R. C. Eckardt, C. Y. She, N. E. Karangelen, R. C. Elton and A. Andrews, *Phys. Rev. Lett.*, 1976, **37**, 1540.
- [29] (a) Y. R. Shen, *The Principles of Non-Linear Optics*, Wiley, New York, 1984; (b) P. N. Butcher and D. Cotter, *The Elements of Nonlinear Optics*, Cambridge University Press, Cambridge, 1990.
- [30] H. Sambe, *Phys. Rev. A*, 1973, **7**, 2203.
- [31] J. Howland, *Math. Ann.*, 1974, **207**, 315.
- [32] L. D. Landau and E. M. Lifschitz, *Classical Theory of Fields*, 4th edn., Butterworth-Heinemann, Oxford, 1975.
- [33] L. I. Schiff, *Quantum Mechanics*, 3rd edn., McGraw-Hill, Singapore, 1987.
- [34] J. W. G. Wildöer, L. C. Venema, A. G. Rinzler, R. E. Smalley and C. Dekker, *Nature*, 1998, **391**, 59.
- [35] F. H. M. Faisal and J. Z. Kamiński, *Phys. Rev. A*, 1996, **54**, R1769.
- [36] F. H. M. Faisal and Z. Kamiński, *Phys. Rev. A*, 1997, **56**, 748.
- [37] M. Lenzner Krüger, S. Sartania, Z. Cheng, Ch. Spielmann, G. Mourou, W. Kautek and F. Krausz, *Phys. Rev. Lett.*, 1998, **80**, 4076.
- [38] J. L. Krause, K. J. Schafer and C. Kulander, *Phys. Rev. A*, 1992, **45**, 4998.

This page intentionally left blank

Small Gold Clusters $\text{Au}_{5 \leq n \leq 8}$ and Their Cationic and Anionic Cousins

F. Remacle¹ and E. S. Kryachko^{1,2}

¹*Department of Chemistry, Bat. B6c, University of Liege, Sart-Tilman, B-4000 Liege 1, Belgium*

²*Bogoliubov Institute for Theoretical Physics, Kiev 03143, Ukraine*

Dedicated to Osvaldo Gocinski on the occasion of his 65th birthday

Abstract

The potential energy surfaces (PESs) of $\text{Au}_{5 \leq n \leq 8}$ gold clusters and their cationic, anionic and metastable dianionic cousins are investigated, as well as the neutral PES of Au_9 . Novel lower energy structures are identified that allow to better define the potential energy landscapes. These findings provide new insights on the early viewpoints on the $2\text{D} \Rightarrow 3\text{D}$ transition in gold clusters. We find that while for cationic clusters almost isoenergetic 2D and 3D structures already coexist for $n = 5$ and 7, for neutral clusters, this occurs at $n = 9$.

Contents

1. A short excursion to gold and alchemy	423
2. 2D–3D transition in small neutral, cationic and anionic gold clusters: early views	426
3. Computational framework	428
4. Five atoms of gold	429
5. Six atoms of gold	437
6. Seven gold atoms	441
7. Eight gold atoms	449
8. The low-energy section of the PES of Au_9	456
9. Summary and outlook	458
Acknowledgements	460
References	460

1. A SHORT EXCURSION TO GOLD AND ALCHEMY

Alchemy aims at transmuting basic metals into gold with the help of the hypothetical substance called the Philosophers' Stone. It emerged from the encounter of the mysticism and practical arts of Egypt (Alexandria) with the rational spirit of Greek philosophers (see, e.g., Refs. [1,2] and references therein, also Ref. [3] for a recent survey and Ref. [4]). Seven metals called

the ‘coinage’ metals: copper, gold, iron, mercury, lead, silver, and tin were known at that time. The ancients related them to certain gods and to certain stellar objects as well. For instance, gold was naturally linked to the Sun due to its bright yellow color (some alchemists even considered gold as ‘condensed sunbeams’ [5] and gave gold the symbol of a circle, the hallmark of mathematical perfection). Silver was linked to Moon, iron to Mars, copper to Venus, tin to Jupiter, lead to Saturn, and mercury obviously to Mercury. The seven days of the week were also associated in the same way with these seven metals [5]: Sunday to gold, Monday to silver, etc.

One of the greatest alchemists, Zosimos of Panopolis, who is reported to have written 28 books on alchemy, alludes to a tincture that transforms silver into gold. The famous Arabian chemist Geber (Abu Musa Jabir ibn Hayyan) thought that gold is composed of sulphur and mercury. On the other hand, Robert Boyle (1627–1691), who is likely to be the first to have introduced the concept of a cluster: “There are Clusters wherein the Particles stick not so close together” (Ref. [6], p. 153), believed that sulphur and mercury cannot be extracted from gold: “I can easily enough sublime Gold into the form of red Crystals of a considerable length; and many other ways may Gold be disguis’d and help to constitute Bodies of very different Natures both from It and from one another, Yellow, Fixt, Ponderous and Malleable Gold it was before its commixture” (Ref. [6], p. 429).

The word ‘gold’ is believed to derive from Sanskrit and means ‘to shine’ [5]. The atom of gold (Au) has the atomic number 79 in the Periodic Table of the Elements with an atomic mass equal to 196.96654. Its ground-state electronic configuration is $(\text{Xe})4f^{14}5d^{10}6s^1$. It has always been considered as the noblest atom. What is the origin of its *nobleness*? It might primarily be a historical reason: gold was found in some river sands in its native metallic form and attracted the man’s attention due to its color and luster and its resilience to tarnish and corrosion [5,7]. Pliny [8] emphasized the latter property of gold by writing that “Those persons are manifestly in error who think that it is the resemblance of its colour to the stars that is so prized in gold.” Gold was mined in more than 95 sites (such as, e.g., Um Rus, Barramiya, Samut, Hamash, El Sid, Atud, El Sukari) in the basement rocks of the Eastern Desert of Egypt, under the dynastic and Roman rules of Egypt [9]. Gold is not subject to rust, verdigris or emanation. In addition, gold steadily resists the corrosive action of salt and vinegar. This was probably the reason why gold was used as a medium of exchange for nearly three thousand years. The first gold coins appeared in Lydia in 700 BC.

The word gold has been used in many different fields, mostly to evoke perfection, like for example the famous ‘gold section’ in geometry. In chemistry, the concept of a ‘gold number’ is used to represent the protective action of colloid (Ref. [10], p. 738). This concept was

introduced by R. A. Zsigmondy (Z. Anal. Chem. XL, 697 (1901)) after the works by J. B. Richter and M. Faraday (Phil. Trans. CXLVII, 145 (1857)) who recognized the protective action of gelatin on the precipitation of colloidal gold. They found that colloidal gold contains finely divided metallic gold and observed the light scattering by them ('Tyndall effect') (Ref. [10], p. 729).

Another side of the *nobleness* of gold has been discovered in the last decade though gold clusters were apparently first studied experimentally in the mid-seventies [11]. As well known, gold is the least reactive of the coinage metals. It is well known too that it exhibits very strong relativistic effects [12] and this is likely to be a key reason for the puzzling and unique behavior (or 'misbehavior') [13] of gold clusters which can be summarized as follows:

- (i) neutral and anionic gold clusters favor 2D structures to unusually large sizes [13,14];
- (ii) small gold clusters exhibit gas phase and catalytic reactivity with, e.g., O_2 [15–19] and CO [20], which, as suggested by Valden *et al.* [21] (see also Ref. [16]), is primarily due to the existence of a band gap;
- (iii) gold possesses a high activation barrier for the H_2 chemisorption [22];
- (iv) finite gold clusters are a very common building 'bricks' for nanostructured materials, electronic devices and novel nanocatalytic systems (Refs. [14,15,23–38] and references therein);
- (v) neutral gold clusters do not follow the typical patterns inherent to Lennard-Jones, Morse, or Gupta systems [35]. For example, the ground-state cluster Au_6 does not have an octahedral structure in the gas phase [14,39–42] although it takes such a geometry for MgO -supported gold nanoclusters [43].

Understanding the reasons of the 2D feature of the *nobleness* of gold clusters is a main concern of the present work. We first review the known low-energy structures of the neutral, anionic and cationic gold clusters $\text{Au}_{5 \leq n \leq 8}$ and previous works on the $2\text{D} \Rightarrow 3\text{D}$ transition. We then carefully study and analyze the potential energy surfaces (PESs) and the $2\text{D} \Rightarrow 3\text{D}$ transition by comparing the results obtained with three most commonly used relativistic effective core potentials (RECP) since, as pointed out in Ref. [44] and clearly shown in the following sections, the structural motifs of the neutral Au_n clusters and their anionic and cationic cousins are strongly dependent on the computational method. While doing so, we identify novel structures and pathways on the PESs, that provide new insights on the $2\text{D} \Rightarrow 3\text{D}$ transition.

2. 2D–3D TRANSITION IN SMALL NEUTRAL, CATIONIC AND ANIONIC GOLD CLUSTERS: EARLY VIEWS

One of the first *ab initio* calculations of small neutral clusters of gold Au_{2-6} , conducted by Bravo-Pérez *et al.* [40] within the second- and fourth-order perturbation Møller-Plesset (MP2 and MP4) method using the Hay-Wadt 19-electron RECP, predicted the most stable Au_5 cluster to be a planar W-shape of C_{2v} symmetry (see Fig. 1). This geometry was later confirmed by Bauschlicher *et al.* [45] and Grünbeck and Andreoni [46]. Regarding 3D Au_5 clusters, two low-energy trigonal bipyramid structures were found 0.42 and 0.95 eV above the W-shape one in Ref. [40] (0.79 eV in Ref. [47]). The LSDA method with the Perdew-Zunger parametrization of the Ceperley-Alder data for the electron gas [46] also favors the trigonal pyramid as the most stable 3D structure of Au_5 , though puts it 0.72 eV higher than the W-form. Somewhat higher in energy, the square pyramid is found at 0.87 eV above the W-form [46]. However, the BLYP density functional (DF) with the same RECP slightly reverses this order: the square pyramid lies at 1.00 eV whereas the trigonal pyramid is 1.03 eV above the W-form [46]. Using the BP86 DF method together with the Stuttgart 19e-RECP, Bonačić-Koutecký *et al.* [44] found that the C_{2v} trigonal bipyramid is 0.930 eV higher than the W-form. For anionic five-gold clusters, the square pyramid becomes more stable compared to the trigonal one (0.88 vs. 1.14 eV for LSDA and 1.05 vs. 1.25 eV for BLYP) [46].

The global minimum of the six-gold cluster possesses a planar, D_{3h} -symmetry triangular structure [40]. The pentagonal pyramid is energetically higher by 0.44 eV [40]. Because of this small energy difference, it was then suggested that “probably at $n = 7$ a 3D form could be the most stable or at least in degeneracy with a planar stable isomer” (Ref. [40b], p. 663). However, as reported in Ref. [44], the pentagonal pyramid lies 0.914 eV higher the triangular cluster.

Häkkinen and Landman [13,14] theoretically predicted that the $2\text{D} \Rightarrow 3\text{D}$ transition occurs for Au_n and Au_n^- if $n \geq 8$ and $n \geq 7$, respectively (see also Ref. [48] for a study of the pyramidal Au_7 cluster with D_{5h} symmetry and Ref. [49] for recent studies of the adsorption of methanol on gold clusters). Häkkinen *et al.* [13] argued that the strong relativistic effects inherent to gold play a key role in the planarity of small gold clusters. It has recently been shown by Bonačić-Koutecký *et al.* [44] that 3D structures appear to be higher than the 2D ones for $n = 7-10$ by 0.528 eV ($n = 7$), 0.530 eV ($n = 8$; for opposite results for $n = 7$ and 8 see the recent work [47] using the LDA-PW91), 0.224 eV ($n = 9$), and 0.285 eV ($n = 10$). Interestingly, the differences in the binding energies per atom between the ground-state 2D and the lowest energy 3D structures calculated in this work [44] fall from

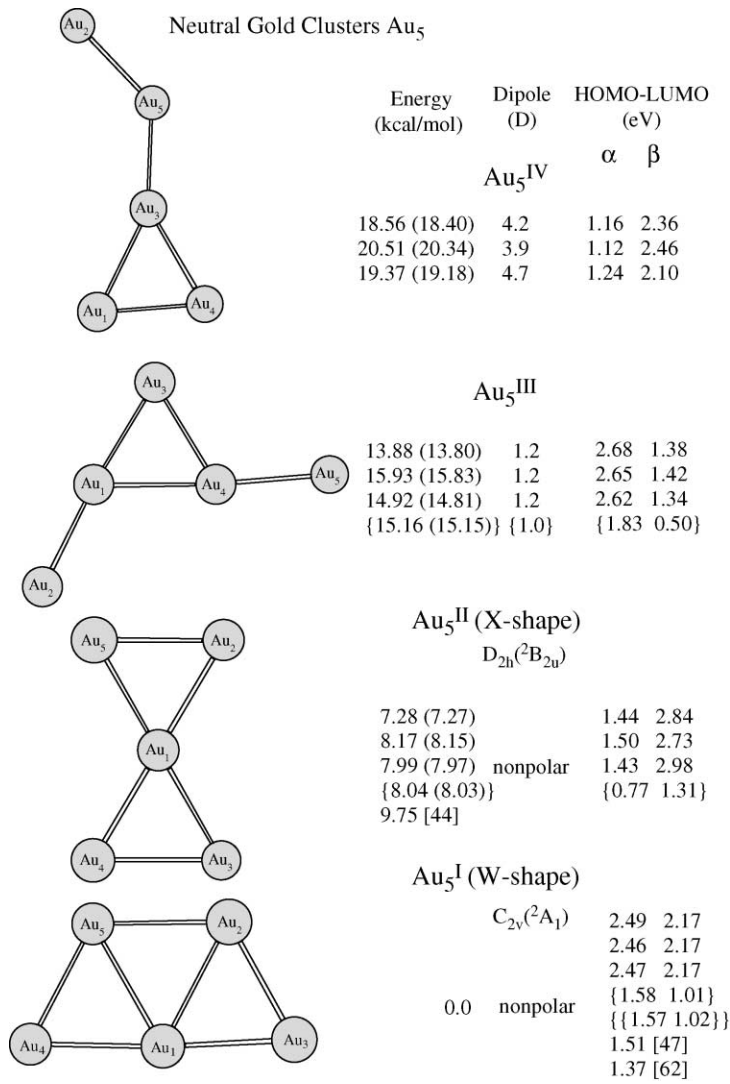


Fig. 1. The low-energy portion of the PES of Au_5 . All quantities are displayed in the following order (from top to bottom): B3LYP/A, B3LYP/B, and B3LYP/C. The quantities in curly brackets correspond to the BP86/A computational level and those in the double curly brackets to the PW91/A.

0.19 eV for $n = 5$ and 0.15 eV for $n = 6$ to 0.02–0.03 eV for $n = 7–9$. Moreover, a simple structural rule, stating that the ground-state structures of $\text{Au}_{4 \leq n \leq 7}$ can be derived by adding a single Au atom to the lowest energy structure Au_{n-1} and forming an additional triangular subunit, has been suggested therein. However, such structural motif disappears for Au_8 where the square is capped by four atoms of gold on each side [44]. The 2D–3D boundary for the neutrals was recently further extended to at least $n = 13$ [13]. The recent gas-phase mobility experiments by Furche *et al.* [50] have demonstrated that planar anionic gold clusters are more stable for sizes as large as $n = 9–11$. On the other hand, similar experiments on the cationic gold clusters, supported by the GGA DF computations with the S-VWN + Becke-Perdew (BP86) parametrization together with the Stuttgart RECP, showed that Au_n^+ are 2D for $n = 3–7$ and 3D for $n = 8–13$ [51]. As concluded therein, the 3D structures of $\text{Au}_{n \geq 7}$ are related to fragments of the bulk phase.

3. COMPUTATIONAL FRAMEWORK

All computations of gold clusters reported here were carried out with the hybrid density functionals B3LYP potential in conjunction with a variety of energy-consistent 19-electron RECPs including the Los Alamos double-zeta type RECP LANL2DZ ($\equiv \text{A}$) [52], the RECP ($\equiv \text{B}$) developed by Ermiler, Christiansen and co-workers [53], and the RECP of the Stuttgart group ($\equiv \text{C}$) [54], using GAUSSIAN 03 package of quantum chemical programs [55]. All optimizations were conducted with the tight keyword.

The B3LYP DF has recently been used for the gold clusters [56–58] along with the others: BP86 [44], BLYP [46], PW91 [16a], BPW91 [59], BPW [60] density functionals. Compared to the MP2 level, the B3LYP was found [57] to give very similar geometries for clusters containing gold atoms, i.e., the Au–Au distances are $\approx 4\%$ longer than the MP2 ones, with the B3LYP ones being more accurate, so that the density functional approach might be more realistic for the gold clusters than MP2 [21]. On the other hand, Bonačić-Koutecký *et al.* [44] and Lee *et al.* [60] have recently pointed out that the DF methods determine relatively small s–d energy gaps and underestimate the gap E_{HL} between the highly occupied molecular orbital (HOMO) and the lowest unoccupied molecular orbital (LUMO). For example, the s–d orbital energy gap between the $d^{10}s^1$ and d^9s^2 configurations of Au^- is estimated in the present work to be equal to 0.88 eV (B3LYP/A), 1.12 eV (B3LYP/B), 1.37 eV (B3LYP/C), 0.23 eV (BP86/A), 0.43 eV (BP86/B), and 0.62 eV (BP86/C). These gaps are smaller than the experimental magnitude of 1.34 eV [61] except for the third estimate demonstrating a good performance

of the B3LYP/C computational level for this task. To further pursue such comparisons for the geometrical, energy, and MO patterns of larger gold clusters and to strengthen the credibility of the present conclusions, the BP86/A and PW91/A methods are also used for some key structures studied in this work.

The harmonic vibrational frequencies and corresponding zero-point vibrational energies (ZPVE) were calculated at all employed B3LYP/X levels ($X = \text{A, B, and C}$) in order to determine the topology of the stationary points. The electronic energies calculated by means of the B3LYP DF with the basis sets A, B, and C are hereby reported in the following order: $\text{Energy}_{\text{B3LYP/A}} (\text{Energy}_{\text{B3LYP/A}} + \text{ZPVE}) [\text{Energy}_{\text{B3LYP/B}} (\text{Energy}_{\text{B3LYP/B}} + \text{ZPVE})]; \text{Energy}_{\text{B3LYP/C}} (\text{Energy}_{\text{B3LYP/C}} + \text{ZPVE})]$. The accepted error of ca. 0.2 eV (4 kcal/mol) of the DF/RECP methods for the gold clusters [44] is taken into account throughout the present work. Similar notations are used for the optimized geometrical parameters. The BP86/A values are given in curly brackets whereas the PW91/A ones appear in the double curly brackets.

The vertical electron detachment energy (VDE) is calculated as the total energy difference between the anionic and neutral clusters, both taken in the anionic optimized geometry without the ZPVE. The adiabatic electron affinity (EA_a) and ionization energy (IE_a) are calculated as the total energy difference between the anionic and cationic clusters, respectively, and the parent neutral cluster in their optimized geometries.

4. FIVE ATOMS OF GOLD

Four low-energy planar structures are identified on the PES of the neutral gold cluster Au_5 (Fig. 1). The global minimum is found to be the nonpolar, trapezoidal W-shape cluster Au_5^{I} of C_{2v} symmetry in the electronic state $^2\text{A}_1$ at all the computational levels used here, in full agreement with all earlier findings [14,16,40,44–47,62]. This geometry is compatible with the triangular motif found in small neutral gold clusters. Au_5^{I} has one 4-coordinated Au atom, two 3- and two 2-coordinated ones. The Au–Au distances in Au_5^{I} , therefore, cluster into four classes (see Table 1): the largest ones, 2.83–2.87 Å, separate 4- and 3-coordinated atoms; the distances between 3-coordinated atoms are 2.74–2.78 Å and 2.72–2.75 Å between 2- and 3-coordinated atoms. The smallest separations, 2.68–2.70 Å, are found between 2- and 4-coordinated atoms. The spin-up and spin-down gaps, $E_{\text{HL}\uparrow}$ and $E_{\text{HL}\downarrow}$, are equal to about 2.5 and 2.2 eV, respectively, at the B3LYP computational levels and ≈ 1.6 and 1.0 eV at BP86/A and PW91/A (see Fig. 1).

Table 1. The bond lengths (in Å) of the low-energy neutral and anionic clusters of five gold atoms

	B3LYP/A	B3LYP/B	B3LYP/C	BP86/A	PW91/A	Early data
Au_5^{I}						
$r(\text{Au}_1-\text{Au}_2)$	2.872	2.831	2.863	2.837	2.829	2.78 [14]; 2.81 [40]; 2.704 [46]
$r(\text{Au}_1-\text{Au}_3)$	2.698	2.678	2.702	2.667	2.666	2.64 [14], 2.72 [40], 2.566 [46]
$r(\text{Au}_2-\text{Au}_3)$	2.750	2.722	2.752	2.723	2.721	2.75 [40]; 2.614 [46]
$r(\text{Au}_2-\text{Au}_5)$	2.777	2.740	2.777	2.734	2.730	2.79 [40]; 2.609 [46]
$\text{Au}_5^{\text{I}-}$						
$r(\text{Au}_1-\text{Au}_2)$	3.001	2.906	2.959			2.82 [14]; 2.725 [46]
$r(\text{Au}_1-\text{Au}_3)$	2.679	2.666	2.685			2.65 [14]; 2.566 [46]
$r(\text{Au}_2-\text{Au}_3)$	2.881	2.831	2.877			2.672 [46]
$r(\text{Au}_2-\text{Au}_5)$	2.676	2.831	2.877			2.582 [46]
Au_5^{II}						
$r(\text{Au}_1-\text{Au}_2)$	2.714	2.689	2.716	2.684		
$r(\text{Au}_2-\text{Au}_5)$	2.751	2.722	2.751	2.723		2.609 [46]

Au_5^{III}				
$r(\text{Au}_1-\text{Au}_2)$	2.619	2.603	2.631	2.594
$r(\text{Au}_1-\text{Au}_3)$	2.731	2.707	2.729	2.684
$r(\text{Au}_1-\text{Au}_4)$	2.793	2.742	2.793	2.742
$r(\text{Au}_4-\text{Au}_5)$	2.619	2.601	2.629	2.586
$\text{Au}_5^{\text{III}-}$				
$r(\text{Au}_1-\text{Au}_2)$	2.628	2.613	2.635	
$r(\text{Au}_1-\text{Au}_3)$	2.719	2.697	2.718	
$r(\text{Au}_1-\text{Au}_4)$	2.922	2.697	2.718	
Au_5^{IV}				
$r(\text{Au}_1-\text{Au}_3)$	2.872	2.814	2.839	
$r(\text{Au}_1-\text{Au}_4)$	2.643	2.640	2.645	
$r(\text{Au}_2-\text{Au}_5)$	2.650	2.626	2.662	
$r(\text{Au}_3-\text{Au}_4)$	2.744	2.701	2.769	
$r(\text{Au}_3-\text{Au}_5)$	2.643	2.617	2.657	

The next structure, by increasing energy, is the X-shape nonpolar cluster Au_5^{II} in the $^2\text{B}_{2u}$ state (D_{2h} symmetry), lying 7.3–8.2 kcal/mol above the ground W-shape state (see Fig. 1 and Table 1). These energies are within the range of earlier results: 7.84–14.53 kcal/mol [46] and 9.75 kcal/mol [44]. Compared to Au_5^{I} , Au_5^{II} is characterized by a narrower spin-up HOMO–LUMO gap (1.4–1.5 eV B3LYP; ≈ 0.8 eV for the BP86/A) and a slightly wider one for the spin-down electrons (2.7–3.0 eV B3LYP; 1.3 eV for BP86/A; see Fig. 1).

Two higher in energy clusters, Au_5^{III} and Au_5^{IV} , are reported in the present work for the first time. They fill the energy gap between the 2D clusters Au_5^{I} and Au_5^{II} and the 3D pyramid which is about 21.4 kcal/mol above Au_5^{I} [44]. Both these two novel structures are less compact, less coordinated, polar (1.2 D and ≈ 4.2 D, respectively) and characterized by rather large polarizabilities (larger by a factor of 1.5–1.6 than that of Au_5^{I}). One of them, Au_5^{III} , is important because it gives rise to the most stable anion $\text{Au}_5^{\text{III-}}$. $\text{Au}_5^{\text{III-}}$ is a novel structure too (see Fig. 2 and Table 1) and is 5.8–7.2 kcal/mol lower in energy than the well-known cluster $\text{Au}_5^{\text{I-}}$ [14,46,50,63], which is certainly beyond the accepted error of ca. 4 kcal/mol of the DF/RECP methods.

The lower energy of $\text{Au}_5^{\text{III-}}$ is readily explained by its larger interatomic distances $r(\text{Au}_2\text{--Au}_5) = 6.807$ [6.803; 6.889] Å and $r(\text{Au}_2\text{--Au}_3) = r(\text{Au}_3\text{--Au}_5) = 5.300$ [5.250; 5.296] Å (Table 1), thus reducing the mutual Coulomb repulsion between the partial excess electron charges that mainly reside on those atoms (the Mulliken charges are equal to -0.37 [-0.49 ; -0.55], -0.23 [-0.28 ; -0.23], and -0.37 [-0.49 ; -0.55] on Au_2 , Au_3 , and Au_5 , respectively). In $\text{Au}_5^{\text{I-}}$ the excess electron spreads over Au_2 (-0.24 [-0.19 ; -0.12]), Au_3 (-0.31 [-0.40 ; -0.26]), Au_4 (-0.31 [-0.40 ; -0.26]), and Au_5 (-0.24 [-0.19 ; -0.12]), which are separated by only 2.72–2.78 Å. Note that $r(\text{Au}_1\text{--Au}_4) = 2.7\text{--}2.9$ Å in $\text{Au}_5^{\text{III-}}$ is smaller than twice the van der Waals radius of Au implying that Au_1 forms an Au–Au bond with Au_4 and hence, $\text{Au}_5^{\text{III-}}$ is distinct from the V-structure shown in Fig. 4 of Ref. [60] (see also Ref. [64]).

$\text{Au}_5^{\text{I-}}$ and $\text{Au}_5^{\text{III-}}$ are also rather different in the MO patterns that determine their catalytic reactivity. The $\text{Au}_5^{\text{I-}}$ HOMO-1–HOMO and HOMO–LUMO gaps are equal to 0.94 [1.01; 1.00] eV (see Ref. [67]) and 1.21 [0.93; 1.09] eV, respectively. In $\text{Au}_5^{\text{III-}}$ the HOMO-1–HOMO gap is substantially narrower, viz., 0.27 [0.23; 0.30] eV while the HOMO–LUMO one is wider and equal to 2.88 [2.39; 2.41] eV. The EA_{as} and VDEs of these anionic clusters are indicated in Fig. 2. The EA_{a} and VDE of $\text{Au}_5^{\text{I-}}$ are comparable with the experimental data and, as shown in Fig. 1, such comparison is fairly satisfactory. The neutral parent of $\text{Au}_5^{\text{I-}}$ is the ground-state cluster Au_5^{I} whereas the neutral parent of $\text{Au}_5^{\text{III-}}$ is the higher energy isomer Au_5^{III} discussed above. On the neutral PES, the transition state between Au_5^{I}

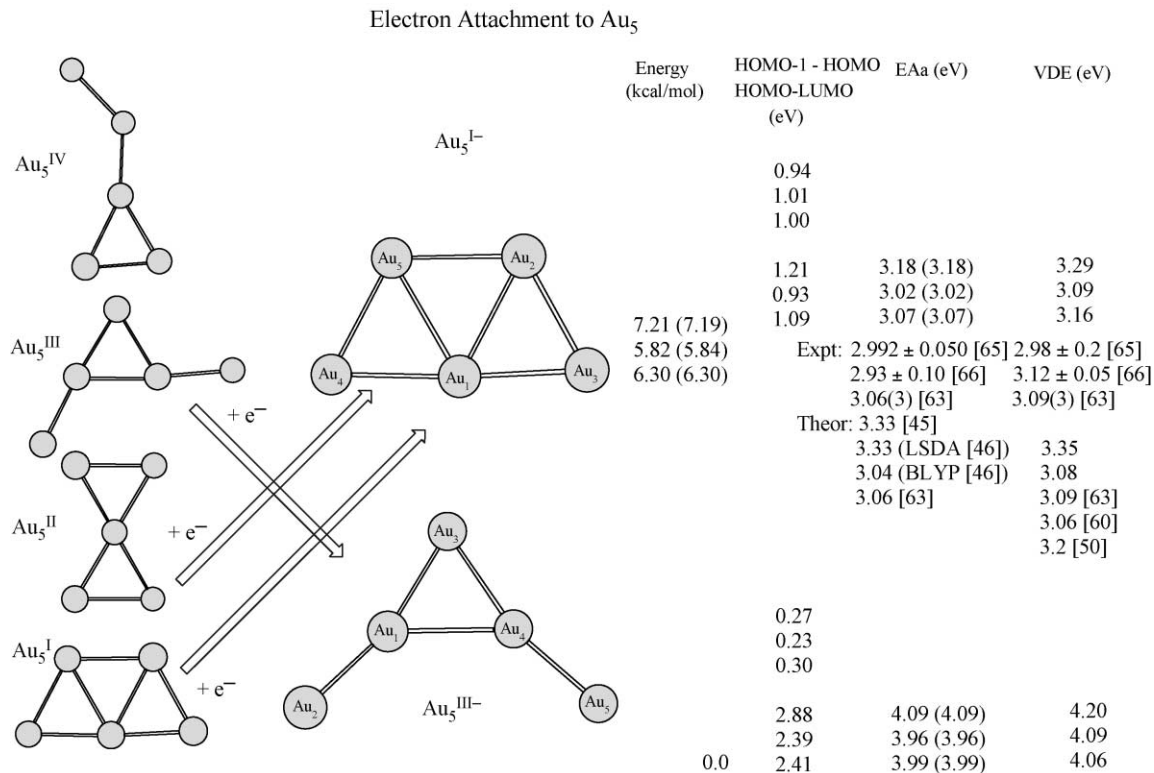


Fig. 2. The low-energy portion of the PES of Au_5^- . All quantities are displayed in the following order (from top to bottom): B3LYP/A, B3LYP/B, and B3LYP/C.

and Au_5^{III} governs the breaking of two Au–Au bonds and its barrier is estimated to be as large as 15 kcal/mol (see Fig. 1). A possible explanation for why it is the $\text{Au}_5^{\text{I}-}$ that is observed experimentally is that it is a long-lived metastable state because of the presence of a similar transition state on the anionic PES. On the other hand, it would be interesting to try to detect experimentally the actual ground-state structure $\text{Au}_5^{\text{III}-}$ reported here.

It is worth mentioning that two electrons can be simultaneously attached to Au_5^{III} to form the dianion $\text{Au}_5^{\text{III}2-}$ shown in Fig. 3. This dianion is stable relative to Au_5^{III} with a total energy difference of 65.6 kcal/mol (65.8 kcal/mol after ZPVE) although it still remains unstable with respect to the corresponding anion $\text{Au}_5^{\text{II}-}$ by 28.8 kcal/mol (28.6 kcal/mol after ZPVE). It is responsible for the second adiabatic electron affinity (see Ref. [68]). This first implies that such a dianion may exist in solvent or condensed phase (see Ref. [69] for current review) and second, that it does not exist in the gas phase and, therefore, there is no contradiction with the statement that the smallest stable dianion is Au_{12}^{2-} [70].

Ionization of all low-energy clusters $\text{Au}_5^{\text{I-IV}}$ yields the same well-known planar X-shape cation $\text{Au}_5^{\text{I}+}$ of D_{2h} symmetry [22] displayed in Fig. 4. The adiabatic ionization energy $\text{IE}_a^{(5)}$ amounts to 7.16 [7.13; 7.09] eV with respect to the global-minimum neutral Au_5^{I} . These estimates are in agreement with the experimental data on $\text{IE}^{(5)} = 8.00$ (upper limit) [71,72]; 7.61 ± 0.20 eV [73] and earlier theoretical data: 7.46 [45], 7.5 [60], 7.68 [74,75], and 7.56 eV [76]. Interestingly, while the ionization pathway from Au_5^{I} and Au_5^{II} to $\text{Au}_5^{\text{I}+}$ is direct although the former is related to the Au_2 – Au_5 bond breaking, the pathway $\text{Au}_5^{\text{III}} \Rightarrow \text{Au}_5^{\text{I}+}$ goes *via* a transition state lying ≈ 15 kcal/mol higher than the product and resembles that between the neutrals Au_5^{I} and Au_5^{III} .

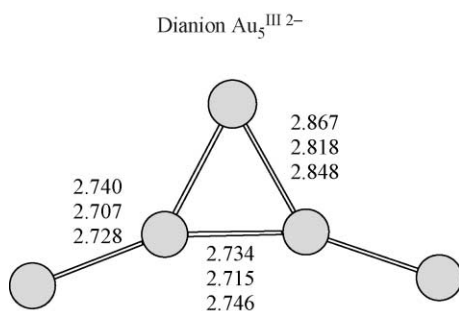


Fig. 3. The structure of the long-lived dianion $\text{Au}_5^{\text{III}2-}$. The bond lengths are given in Å and displayed in the following order (from top to bottom): B3LYP/A, B3LYP/B, and B3LYP/C.

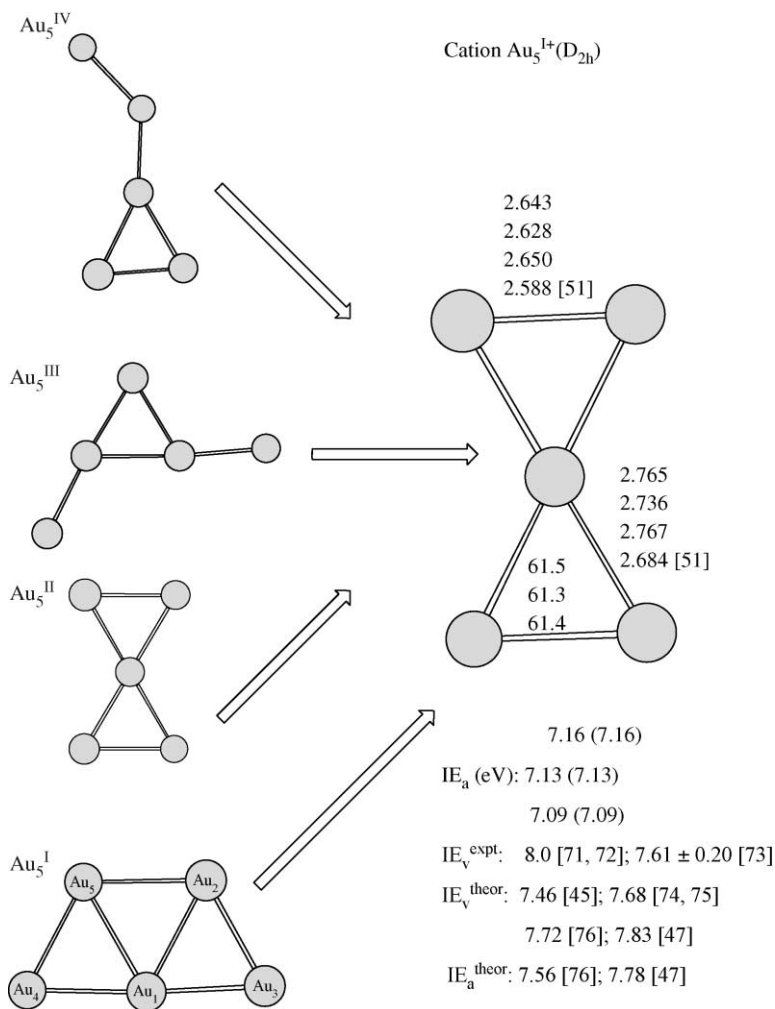
Ionization of Au_5 

Fig. 4. Ionization of the low-energy clusters $\text{Au}_5^{\text{I-IV}}$. The bond lengths are given in Å and displayed in the following order (from top to bottom): B3LYP/A, B3LYP/B, and B3LYP/C.

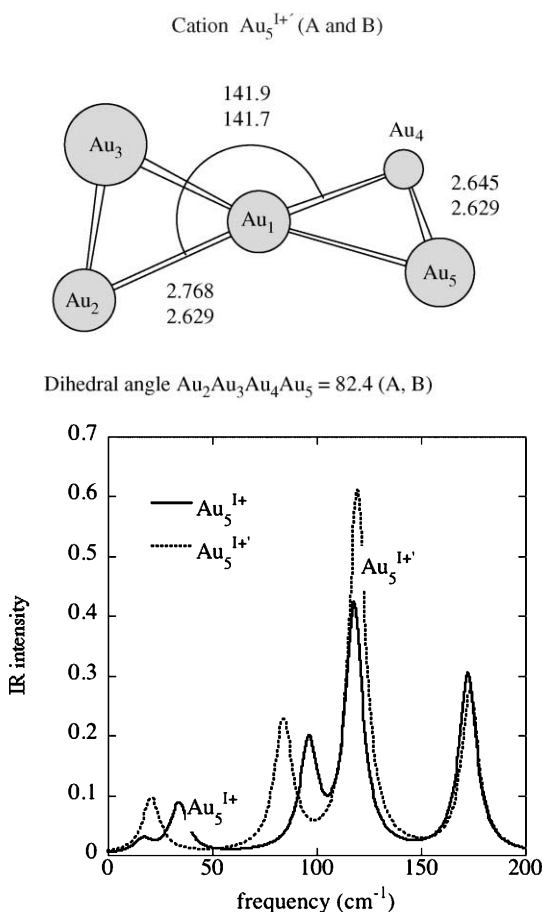


Fig. 5. The 3D cation $\text{Au}_5^{1+'}$ and its IR spectrum. The bond lengths are given in Å and bond angles in degrees: the top value corresponds to the B3LYP/A and the bottom one to the B3LYP/B computational levels.

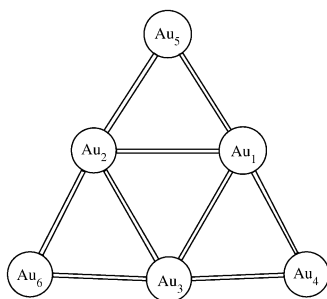
Surprisingly, the cationic PES of the five-gold clusters exhibits the first indication of the co-existence of 2D and 3D structures at the B3LYP/A and B3LYP/B computational levels. Together with the planar Au_5^{1+} , it contains the 3D rotamer $\text{Au}_5^{1+'}$ (see Fig. 5) with a dihedral angle $\angle \text{Au}_2\text{Au}_3\text{Au}_4\text{Au}_5 = 82.4^\circ$ for both the B3LYP/A and B3LYP/B methods (see also Refs. [49b,76]). $\text{Au}_5^{1+'}$ is almost isoenergetic to Au_5^{1+} , i.e., it is 0.28 kcal/mol higher at the B3LYP/A and 0.09 kcal/mol at the B3LYP/B after ZPVE (cf. with 2.08 kcal/mol in Ref. [76]). At the B3LYP/C level the rotamer is energetically equivalent to Au_5^{1+} and characterized by a smaller dihedral

angle, $\angle \text{Au}_2\text{Au}_3\text{Au}_4\text{Au}_5 = 18.0^\circ$. Due to a somewhat larger entropy of the 3D isomer, the B3LYP/A Gibbs energy slightly favors (by ≈ 0.10 kcal/mol) the 3D cluster at room temperature. These clusters have quite different IR spectra shown in Fig. 5 too (computed with a Lorentzian lineshape of half-width equal to 5 cm^{-1}). As seen therein, both Au_5^{I+} and $\text{Au}_5^{I+'}$ have four pronounced peaks in their IR spectra. For Au_5^{I+} , the peaks are centered at 34 (0.4 km/mol; coupled to the mode at 17 cm^{-1} with IR activity of 0.1 km/mol), 96 cm^{-1} (0.9 km/mol), 118 cm^{-1} (2.1 km/mol), and 173 cm^{-1} (1.5 km/mol) (B3LYP/A). The second peak is assigned to the collective mode comprising the coupled scissor $\text{Au}_2\text{--Au}_4$ and $\text{Au}_3\text{--Au}_5$ (see Fig. 5) and the out-of-plane motion of the central atom Au_1 . The rotamer $\text{Au}_5^{I+'}$ shows similar peaks at 21 cm^{-1} (almost degenerate with IR activities both equal to 0.2 km/mol), 84 cm^{-1} , 120 cm^{-1} (3.0 km/mol), and 174 cm^{-1} (1.3 km/mol). The second peak centered at 84 cm^{-1} results from two nearly degenerate vibrational modes. One of them (83 cm^{-1} , 0.5 km/mol) is the coupled scissor $\text{Au}_2\text{--Au}_5$ and $\text{Au}_3\text{--Au}_4$ and the out-of-plane motion of the central atom Au_1 which is IR inactive for Au_5^{I+} . The other (85 cm^{-1} , 0.6 km/mol), the coupled scissor $\text{Au}_2\text{--Au}_4$ and $\text{Au}_3\text{--Au}_5$ and the out-of-plane motion of the central atom Au_1 , is almost identical to the second mode of Au_5^{I+} . The first and second peaks of the rotamer are shifted to lower wavenumbers compared to those of Au_5^{I+} and the second one of rotamer is more IR active (as a doubly degenerate since it results from two almost degenerate vibrational modes). Such distinctive features could be used as their experimental ‘fingerprints’. We do not find similar 3D rotamer on the neutral PES.

5. SIX ATOMS OF GOLD

The global-minimum energy structure Au_6^I retains the triangular motif (Fig. 6 and Table 2) and is well separated from the other isomers, in particular from 3D structures. Structurally, Au_6^I is obtained from Au_5^I by adding another triangle to the $\text{Au}_2\text{--Au}_5$ bond of Au_5^I (Fig. 1). It retains the parent nonpolarity. Note that the BP86/A geometry of Au_6^I is very close to that obtained at the B3LYP/B computational level (see Table 2 for details). The addition of a gold atom stretches the $\text{Au}_2\text{--Au}_5$ bond of Au_5^I by $\approx 0.13\text{--}0.16 \text{ \AA}$ (as the bond between 4-coordinated atoms) and shrinks the $\text{Au}_2\text{--Au}_3$ and $\text{Au}_4\text{--Au}_5$ ones by $0.04\text{--}0.05 \text{ \AA}$. Energetically, the binding energy of Au_6^I relative to the asymptote $\text{Au}_5^I + \text{Au}_1$ is equal to 60.36 (59.96 after ZPVE) [61.29 (60.90); 59.35 (58.95)] kcal/mol. As expected since it is a closed-shell cluster, Au_6^I is more inert than Au_5^I that is indicated by a larger E_{HL} of 2.23 eV (BP86/A) (3.48 [3.35; 3.48] eV at the employed B3LYP

Neutral and Cationic Gold Clusters
 Au_6^{I} and $\text{Au}_6^{\text{I}+}$



Neutral:	Nonpolar	Cation:
	3.48	8.46 (8.45)
HOMO-LUMO (eV): 3.35		IE_a (eV): 8.28 (8.28)
	3.40	8.33 (8.33)
	{2.23}	$\text{IE}_v^{\text{expt}}$: 8.80 [71,72]
2.5 [77]; 2.05 [45]		$\text{IE}_a^{\text{theor}}$: 7.60 [48]; 8.55 [47]
2.06[47]; 1.74[62]		8.37 [74, 75]
	60.36 (59.96)	$\text{IE}_v^{\text{theor}}$: 8.17 [60]
E_{bind} (kcal/mol): 61.29 (60.90)		
	59.35 (58.95)	
50.27 [47]; 63.88 (54.19) [62]		

Fig. 6. The cluster Au_6^{I} and its cationic cousin. All quantities are displayed in the following order (from top to bottom): B3LYP/A, B3LYP/B, and B3LYP/C. The quantities in curly brackets correspond to the BP86/A computational level.

levels). The magnitude of the E_{HL} at BP86/A is very close to the experimental value reported by Taylor *et al.* [77]. The IR strongest Au–Au stretching mode (doublet) is predicted at 167 [174; 167] cm^{-1} and characterized by a small IR activity of 6 [5; 5] km/mol .

As well known [51], under ionization, Au_6^{I} retains its planar triangular structural form. Figure 6 displays the cation $\text{Au}_6^{\text{I}+}$ whose geometry is reported with its neutral parent Au_6^{I} in Table 2. The adiabatic ionization energy $\text{IE}_a^{(6)} = 8.28$ eV is about 1 eV larger than $\text{IE}_a^{(5)}$. The predicted $\text{IE}_a(\text{Au}_6^{\text{I}})$ satisfactorily agrees with the recent experimental data, $\text{IE}_a^{(6)} = 8.80$ eV (upper limit) [71,72], and earlier theoretical computations: 7.60 [48], 8.17 [60], and 8.37 eV [74,75].

Table 2. The bond lengths (in Å) of Au₆^I, Au₆^{I+}, Au₆^{I-}, and Au₆^{II-}

	B3LYP/A	B3LYP/B	B3LYP/C	BP86/A	Early data
Au ₆ ^I					
<i>r</i> (Au ₁ –Au ₂)	2.900	2.856	2.890	2.856	2.81 [14]; 2.84 [40]
<i>r</i> (Au ₁ –Au ₃)	2.900	2.856	2.890	2.855	2.81 [14]; 2.84 [40]
<i>r</i> (Au ₁ –Au ₄)	2.704	2.683	2.706	2.677	2.66 [14]; 2.72 [40]
<i>r</i> (Au ₁ –Au ₅)	2.704	2.683	2.706	2.677	2.66 [14]; 2.72 [40]
<i>r</i> (Au ₃ –Au ₄)	2.704	2.683	2.706	2.677	2.66 [14]; 2.72 [40]
Au ₆ ^{I+}					
<i>r</i> (Au ₁ –Au ₂)	2.732	2.708	3.076		2.915 [51]
<i>r</i> (Au ₁ –Au ₃)	2.997	2.930	2.804		2.752 [51]
<i>r</i> (Au ₁ –Au ₄)	2.728	2.688	2.694		2.623 [51]
<i>r</i> (Au ₁ –Au ₅)	2.700	2.674	2.733		
<i>r</i> (Au ₃ –Au ₄)	2.704	2.679	2.727		
Au ₆ ^{I-}					
<i>r</i> (Au ₁ –Au ₂)	2.810	2.781	2.808	2.784	2.76 [14]
<i>r</i> (Au ₁ –Au ₃)	2.810	2.781	2.808	2.784	2.76 [14]
<i>r</i> (Au ₁ –Au ₄)	2.781	2.746	2.778	2.743	2.71 [14]
<i>r</i> (Au ₁ –Au ₅)	2.781	2.746	2.778	2.743	2.71 [14]
<i>r</i> (Au ₃ –Au ₄)	2.781	2.746	2.778	2.743	2.71 [14]
Au ₆ ^{II-}					
<i>r</i> (Au ₁ –Au ₂)	2.764	2.728	2.765	2.715	
<i>r</i> (Au ₁ –Au ₄)	2.645	2.623	2.654	2.614	

We did not find any new structural motif on the low-energy portion of the PES of Au₆. However, new structures are identified on the cationic and anionic PESs. The anionic PES possesses two low-energy structures (see Fig. 7 and Table 2). One of them is the known planar hexagonal structure Au₆^{I-} [14,39a,60,65,77] which structurally resembles Au₆^I and is characterized by a VDE(Au₆^{I-}) = 2.27 [2.18; 2.20] eV and an EA_a(Au₆^I) = 2.16 [2.09; 2.09] eV (BP86/A predicts 2.43 eV), which satisfactorily agree with the experimental VDE^{(6)expt} = 2.29 eV and EA_a^{(6)expt} = 2.0510 ± 0.0020 [78]; 2.016 ± 0.050 [65]; 2.06(2) eV [63]. The adiabatic electron affinity is slightly smaller than the HOMO–LUMO gap of Au₆^I implying that a rather weak relaxation occurs under electron attachment (of about ± 0.08–0.1 Å). The gap *E*_{H_L↓} of Au₆^{I-} significantly decreases to 0.4 eV (BP86/A) (B3LYP gives 1.11 [1.15; 1.10] eV) compared to the neutral parent whereas the *E*_{H_L↓} stays at approximately the same magnitude 2.09 eV (BP86/A) (3.30 [3.27; 3.27] eV for B3LYP). The electronic energy and enthalpy associated with

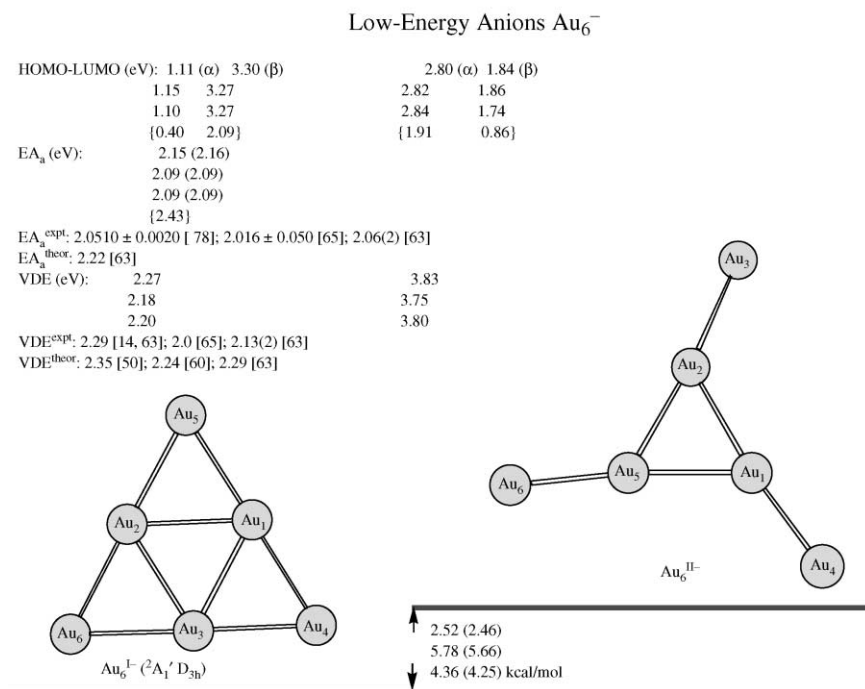


Fig. 7. The low-energy portion of the anionic PES of Au_6 . All quantities are displayed in the following order (from top to bottom): B3LYP/A, B3LYP/B, and B3LYP/C. The quantities in curly brackets correspond to the BP86/A computational level.

the reaction $\text{Au}_5^{\text{I}-} + \text{Au}_1 \Rightarrow \text{Au}_6^{\text{I}-}$ are equal to 36.7 (36.4) and 42.6 kcal/mol (B3LYP/A). Notice that the latter lies within the experimentally measured margin $< 62.5 \pm 9.2$ kcal/mol [79].

The other anion $\text{Au}_6^{\text{II}-}$ (Fig. 7 and Table 2) can be directly linked to the most stable cluster $\text{Au}_5^{\text{III}-}$ on the anionic PES of Au_5 . Actually, adding one Au atom to the Au_3 atom of $\text{Au}_5^{\text{III}-}$ in Fig. 2 yields $\text{Au}_6^{\text{II}-}$ with a gain of energy of 26.9 (26.7) kcal/mol (B3LYP/A). The anion $\text{Au}_6^{\text{II}-}$ is less stable, *viz.*, by 2.52 (2.46) [5.78 (5.66); 4.36 (4.25)] kcal/mol (BP86/A estimates it as equal to 6.67 kcal/mol), than $\text{Au}_6^{\text{I}-}$ and has HOMO–LUMO gaps of 1.91 eV (spin-up, BP86/A) and 1.84 eV (spin-down, BP86/A; the B3LYP values are shown in Fig. 7). Notice that the reaction pathway $\text{Au}_6^{\text{I}-} + \text{e}^- \Rightarrow \text{Au}_6^{\text{II}-}$ is indirect and occurs through a barrier.

The cationic PES exhibits three low-energy clusters displayed in Fig. 8. Two of them, planar $\text{Au}_6^{\text{I}+}$ and $\text{Au}_6^{\text{III}+}$ are known [51] although the

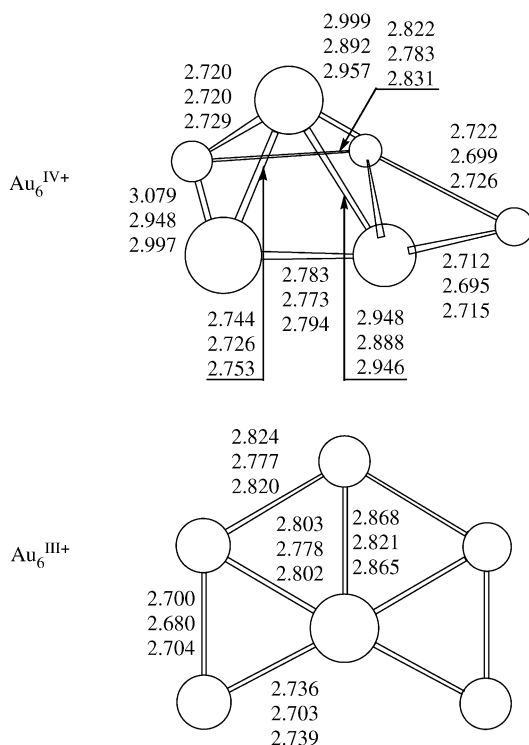


Fig. 8. Two low-energy cationic clusters $\text{Au}_6^{\text{III}+}$ and $\text{Au}_6^{\text{IV}+}$. The bond lengths are given in Å and displayed in the following order (from top to bottom): B3LYP/A, B3LYP/B, and B3LYP/C.

used B3LYP computational level slightly prefers the latter (by 0.93 (0.97) [0.26 (0.33); 1.38 (1.38) kcal/mol]. The third one, $\text{Au}_6^{\text{IV}+}$, is 3D and somewhat less stable (by 5–7 kcal/mol) than $\text{Au}_6^{\text{I}+}$. Interestingly, the cationic clusters $\text{Au}_6^{\text{III}+}$ and $\text{Au}_6^{\text{IV}+}$ are formed *via* the barrier-type ionization of Au_6^{I} .

6. SEVEN GOLD ATOMS

Adding one gold atom to Au_6^{I} and holding the planar triangular motif, one obtains the known global-minimum energy structure Au_7^{I} in the electronic $^2\text{A}'$ state of C_s symmetry with an energy stabilization of 24.56 (24.37) [26.77 (26.55); 24.60 (24.42) kcal/mol. It is shown in Fig. 9 and its optimized geometrical parameters are gathered in Table 3 including those computed within the BP86/A method. Au_7^{I} is an open-shell cluster, slightly polar

Neutral Gold Clusters Au₇

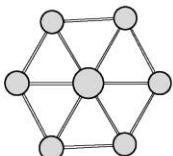
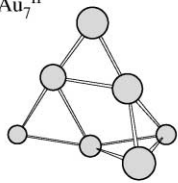
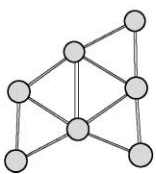
	Dipole (D)	Energy (kcal/mol)	HOMO -LUMO (eV)		E _{bind} (kcal/mol)
			α	β	
Au ₇ ^{III} (D _{2h} (² B _{2g})) 	nonpolar	8.99 (8.82)	1.01	2.76	
		7.69 (7.52)	0.95	2.74	
		8.15 (7.98)	0.97	2.78	
		{8.07 (7.87)}	{0.18 1.73}		
		6.99 [44]	0.87 [62]		
Au ₇ ^{II} 	0.8	5.56 (5.51)	1.83	3.04	
	0.9	6.46 (6.41)	1.74	3.11	
	0.9	5.73 (5.43)	1.78	3.10	
	{0.9}	{5.08 (5.02)}	{0.92 1.79}		
Au ₇ ^I (C _s (² A ₁)) 	0.4		2.24	2.25	24.56 (24.37)
	0.3		2.19	2.20	26.77 (26.55)
	0.3		2.20	2.27	24.60 (24.42)
	{0.4}	0.0	{1.32 1.04}		

Fig. 9. The low-energy portion of the PES of Au₇. All quantities are displayed in the following order (from top to bottom): B3LYP/A, B3LYP/B, and B3LYP/C. The quantities in curly brackets correspond to the BP86/A computational level.

(0.4 [0.3; 0.3] D), characterized by the following spin-up and spin-down HOMO–LUMO gaps: 1.32 and 1.04 eV (BP86/A), respectively (B3LYP gives correspondingly 2.24 [2.19; 2.20] and 2.25 [2.20; 2.27] eV).

Actually, seven is the smallest number of gold atom cluster whose neutral PES contains a low-lying 3D novel structure Au₇^{II} higher in energy than Au₇^I by about 5–6 kcal/mol, *viz.*, 5.56 (5.51) [6.46 (6.47); 5.73 (5.43)] kcal/mol [80]. Figure 9 shows that the three dimensionality arises from capping one of edge triangles of Au₆ with a gold atom (called ‘edge-capped pyramid’ by analogy with Ref. [13]). This 3D structure Au₇^{II} has twice the polarity (0.8 [0.9; 0.9] D) of Au₇^I. Its gap E_{HLL} , equal to 0.92 eV (BP86/A) (B3LYP predicts a wider gap of 1.83 [1.74; 1.78] eV) is responsible for its higher reactivity.

Table 3. The bond lengths (in Å) of the clusters Au₇^{I-III} and their cationic and anionic cousins. The superscript a indicates the bond length equal to 2.714 Å in Ref. [51]

	B3LYP/A	B3LYP/B	B3LYP/C	BP86/A
<hr/>				
Au ₇ ^I				
r(Au ₁ –Au ₂)	2.769	2.734	2.763	2.745
r(Au ₁ –Au ₄)	2.756	2.725	2.762	2.711
r(Au ₂ –Au ₃)	2.717	2.693	2.718	2.683
r(Au ₂ –Au ₄)	2.780	2.753	2.779	2.753
r(Au ₃ –Au ₄)	3.102	3.003	3.065	2.980
r(Au ₃ –Au ₆)	2.868	2.829	2.860	2.843
r(Au ₃ –Au ₇)	2.724	2.702	2.728	2.698
r(Au ₄ –Au ₅)	2.712	2.689	2.715	2.687
r(Au ₄ –Au ₆)	2.845	2.802	2.840	2.794
r(Au ₅ –Au ₆)	2.695	2.674	2.696	2.669
r(Au ₆ –Au ₇)	2.713	2.688	2.713	2.683
<hr/>				
Au ₇ ^{I+ts}				
r(Au ₁ –Au ₂)	2.710			
r(Au ₁ –Au ₄)	2.713			
r(Au ₂ –Au ₃)	2.810			
r(Au ₂ –Au ₄)	2.858			
r(Au ₃ –Au ₄)	2.903			
r(Au ₃ –Au ₆)	2.918			
r(Au ₃ –Au ₇)	2.667			
r(Au ₄ –Au ₅)	2.701			
r(Au ₄ –Au ₆)	2.782			
r(Au ₅ –Au ₆)	2.700			
r(Au ₆ –Au ₇)	2.754			
<hr/>				
Au ₇ ^{II}				
r(Au ₁ –Au ₂)	2.706	2.685	2.708	2.679
r(Au ₁ –Au ₅)	2.701	2.678	2.703	2.674
r(Au ₂ –Au ₃)	2.706	2.685	2.708	2.679
r(Au ₂ –Au ₄)	2.899	2.855	2.890	2.856
r(Au ₂ –Au ₅)	2.899	2.855	2.890	2.856
r(Au ₃ –Au ₄)	2.701	2.678	2.703	2.674
r(Au ₄ –Au ₅)	2.966	2.917	2.948	2.914
r(Au ₄ –Au ₆)	2.756	2.786	2.816	2.777
r(Au ₄ –Au ₇)	2.901	2.786	2.816	2.777
r(Au ₅ –Au ₆)	2.901	2.786	2.816	2.777
r(Au ₅ –Au ₇)	2.756	2.786	2.816	2.777
r(Au ₆ –Au ₇)	2.916	2.869	2.923	2.885
<hr/>				

(continued)

Table 3. Continued

	B3LYP/A	B3LYP/B	B3LYP/C	BP86/A
Au₇^{II+}				
<i>r</i> (Au ₁ –Au ₂)	2.725	2.699	2.726	
<i>r</i> (Au ₁ –Au ₅)	2.671	2.654	2.675	
<i>r</i> (Au ₂ –Au ₃)	2.725	2.699	2.726	
<i>r</i> (Au ₂ –Au ₄)	2.876	2.841	2.871	
<i>r</i> (Au ₂ –Au ₅)	2.871	2.841	2.871	
<i>r</i> (Au ₃ –Au ₄)	2.671	2.654	2.675	
<i>r</i> (Au ₄ –Au ₅)	2.995	2.934	2.979	
<i>r</i> (Au ₄ –Au ₆)	2.861	2.822	2.860	
<i>r</i> (Au ₄ –Au ₇)	2.861	2.822	2.860	
<i>r</i> (Au ₅ –Au ₆)	2.861	2.822	2.860	
<i>r</i> (Au ₅ –Au ₇)	2.861	2.822	2.860	
<i>r</i> (Au ₆ –Au ₇)	2.861	2.670	2.685	
Au₇^{III}				
<i>r</i> (Au ₁ –Au ₂)	2.840	2.725	2.753	2.732
<i>r</i> (Au ₁ –Au ₄)	2.750	2.732	2.805	2.717
<i>r</i> (Au ₃ –Au ₇)	2.910	2.791	2.766	2.854
<i>r</i> (Au ₄ –Au ₅)	2.842	2.860	2.860	2.802
<i>r</i> (Au ₅ –Au ₆)	2.756	2.810	2.905	2.861
<i>r</i> (Au ₆ –Au ₇)	2.755	2.721	2.751	2.733
Au₇^{III+}				
<i>r</i> (Au ₁ –Au ₂) ^a	2.807	2.773	2.790	2.777
<i>r</i> (Au ₁ –Au ₄)	2.779	2.747	2.790	2.750
Au₇^{I–}				
<i>r</i> (Au ₁ –Au ₂)	2.837	2.788	2.830	2.783
<i>r</i> (Au ₁ –Au ₇)	2.648	2.640	2.655	2.634
<i>r</i> (Au ₂ –Au ₃)	2.730	2.712	2.733	2.712
<i>r</i> (Au ₃ –Au ₄)	2.719	2.697	2.719	2.694
<i>r</i> (Au ₃ –Au ₅)	2.874	2.807	2.862	2.802
<i>r</i> (Au ₅ –Au ₇)	2.797	2.753	2.791	2.752
Au₇^{II–}				
<i>r</i> (Au ₁ –Au ₄)	2.692	2.675	2.694	2.670
<i>r</i> (Au ₁ –Au ₅)	2.882	2.822	2.868	2.810
<i>r</i> (Au ₂ –Au ₃)	2.727	2.700	2.729	2.695
<i>r</i> (Au ₂ –Au ₆)	2.622	2.608	2.629	2.597

The 2D–3D transition between the two structures Au_7^{I} and Au_7^{II} appears more clearly on the cationic PES shown in Fig. 10 (see also Table 3). Upon ionization, the 2D cluster Au_7^{I} yields, *via* the 2D barrier $\text{Au}_7^{\text{I}+\text{ts}}$ structurally similar to its parent neutral, to the 3D cation $\text{Au}_7^{\text{II}+}$. The latter is very similar to

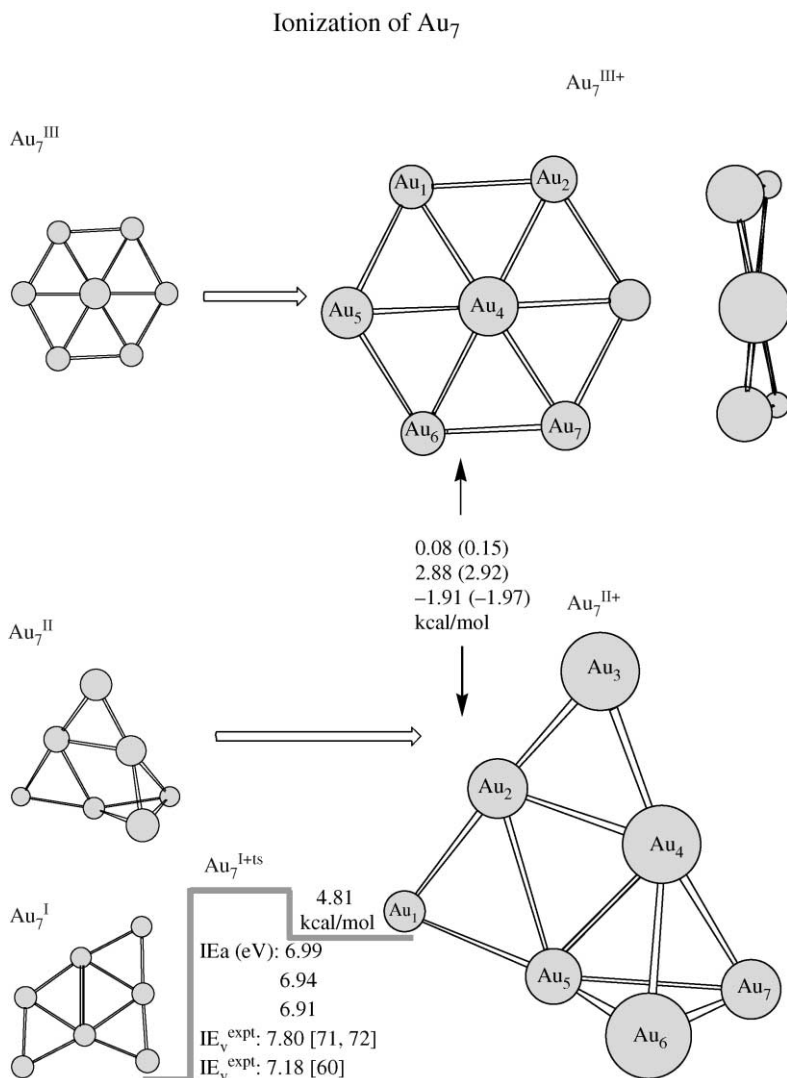


Fig. 10. The low-energy portion of the PES of Au_7^+ . All quantities are displayed in the following order (from top to bottom): B3LYP/A, B3LYP/B, and B3LYP/C. The quantities in curly brackets correspond to the BP86/A computational level.

the 3D neutral Au_7^{II} (Fig. 9). The transition-state linker $\text{Au}_7^{\text{I+ts}}$ is placed 4.81 kcal/mol higher (B3LYP/A). This is one remarkable facet of the cation $\text{Au}_7^{\text{II+}}$. The other is that ionization of Au_7^{II} directly yields $\text{Au}_7^{\text{II+}}$. Such 2D–3D geometry change upon ionization is reported in this work for the first time. The $\text{Au}_7^{\text{I}} \Rightarrow \text{Au}_7^{\text{I+ts}} \Rightarrow \text{Au}_7^{\text{II+}}$ pathway determines an $\text{IE}_a^{(7)} = 6.99$ [6.94; 6.91] eV which is smaller than $\text{IE}_v^{(7)\text{expt}} = 7.80$ eV [71,72]. It might be reasonable to address the following question: what is the reaction product of the attachment to $\text{Au}_7^{\text{II+}}$ of an electron sufficiently slow that the transition barrier $\text{Au}_7^{\text{I+ts}}$ cannot be crossed? Such conditions could directly lead to the 3D cluster Au_7^{II} via the reaction pathway $\text{Au}_7^{\text{II+}} + e^- \Rightarrow \text{Au}_7^{\text{II}}$. This shows that 2D–3D structural conversion of lower energy neutral clusters of seven gold atoms extends to the corresponding cationic PES.

The low-energy 3D cluster Au_7^{II} identified in this work exhibits a 3D to 2D conversion upon electron attachment, which leads to the planar structure $\text{Au}_7^{\text{II-}}$, shown in Fig. 11 (see also Table 3 for its geometry) and characterized

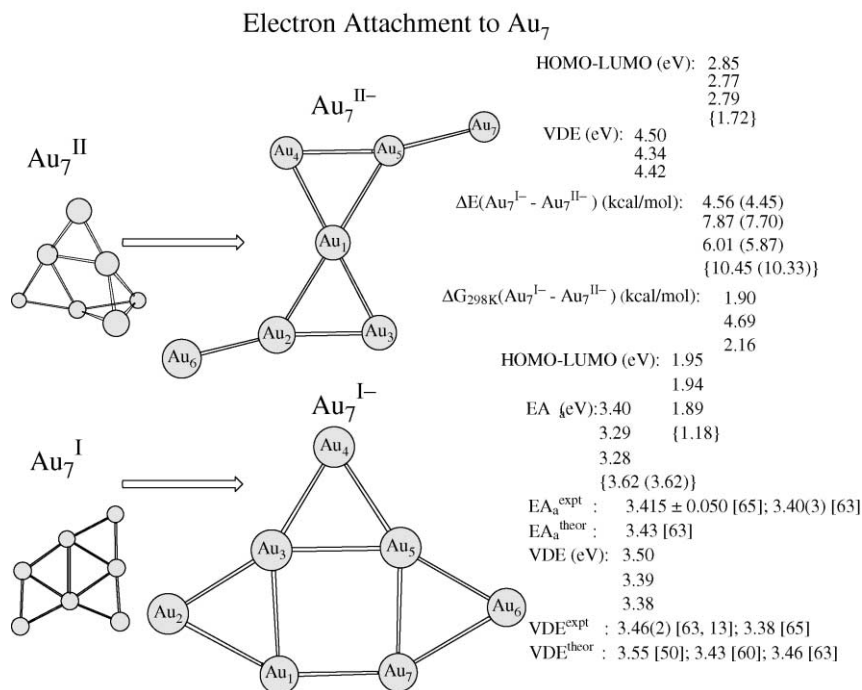


Fig. 11. The low-energy portion of the PES of Au_7^- . All quantities are displayed in the following order (from top to bottom): B3LYP/A, B3LYP/B, and B3LYP/C. The quantities in curly brackets correspond to the BP86/A computational level.

by quite a large $\text{VDE}(\text{Au}_7^{\text{II}-}) = 4.50$ [4.34; 4.42] eV. This clearly indicates that a 3D structure for the anion is less stable than a less strained 2D one. The HOMO–LUMO gap equals to 1.72 eV (BP86/A) (B3LYP provides 2.85 [2.77; 2.79] eV). The $\text{Au}_7^{\text{II}-}$ structure is also reported in the present work for the first time. However, it is not the global minimum on the anionic PES of Au_7 . It lies above the well-known ground-state structure $\text{Au}_7^{\text{I}-}$ [13,63] by 4.56 (4.45) [7.87 (7.70); 6.01 (5.87)] kcal/mol. Due to a large entropy effect, the difference in the B3LYP Gibbs free energies evaluated at $T = 298$ K is rather low 1.90 [4.69; 2.16] kcal/mol, reflecting the floppy nature of the bottom of the anionic PES.

The anionic PES exhibits two energetically almost degenerate 2D structures: $\text{Au}_7^{\text{I}-}$ with the known edge-capped square [13,63] and $\text{Au}_7^{\text{III}-}$ shown in Fig. 12 (see Ref. [81]). The latter is a novel structure obtained by adding a single gold atom to one of the edge atoms of $\text{Au}_6^{\text{I}-}$. It is actually lying 2.51 (2.50) [1.71 (1.73); 2.44 (2.44)] kcal/mol below $\text{Au}_7^{\text{I}-}$ and characterized by a $\text{VDE}(\text{Au}_7^{\text{I}-}) = 3.87$ [3.74; 3.74] eV. Its parent neutral

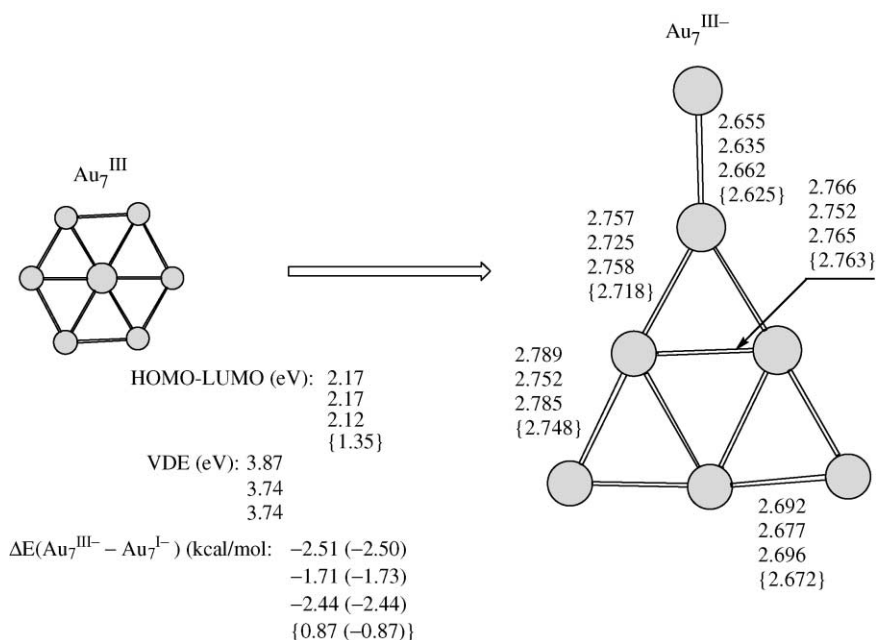


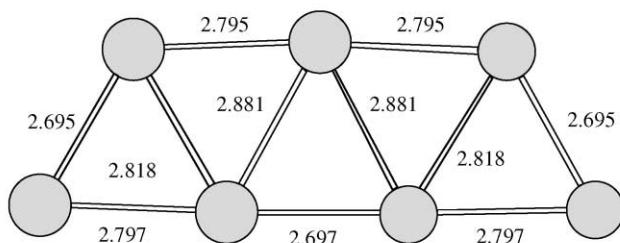
Fig. 12. The anion $\text{Au}_7^{\text{III}-}$ and its neutral parent. The bond lengths are given in Å. All quantities are displayed in the following order (from top to bottom): B3LYP/A, B3LYP/B, and B3LYP/C. The quantities in curly brackets correspond to the BP86/A computational level.

cluster is the honeycomb Au_7^{III} in the state $^2\text{B}_{2g}$ of D_{2h} symmetry [44]. On the neutral PES, Au_7^{III} is, however, 8.99 (8.82) [7.69 (7.52); 8.99 (8.82)] kcal/mol above the bottom (cf. with 6.99 kcal/mol in Ref. [44]; see also Ref. [82]). In contrast to Au_7^{I} , Au_7^{III} is nonpolar and its spin-split HOMO–LUMO gaps are equal to 0.18 and 1.73 eV (BP86/A) (cf. with the B3LYP predictions: 1.01 [0.95; 0.97] and 2.76 [2.76; 2.78] eV), respectively.

Compared to $\text{Au}_7^{\text{II-}}$, $\text{Au}_7^{\text{I-}}$ is more reactive due to a smaller E_{HL} gap = 1.18 eV (BP86/A) (the B3LYP estimates are equal to 1.95 [1.94; 1.89] eV) and is characterized by an $\text{EA}_a^{(7)} = 3.40$ (3.40) [3.29 (3.29); 3.28 (3.28)] eV and a VDE = 3.50 [3.39; 3.38] eV. Both these computed values are fairly close to $\text{EA}_a^{(7)\text{expt}} = 3.415 \pm 0.050$ [65] and 3.40(3) eV [63] and $\text{VDE}^{(7)\text{expt}} = 3.46(2)$ eV [13,63], respectively.

Let us return to the cationic PES of Au_7 shown in Fig. 10. We have identified two novel different structures on its lowest portion. One, as described above, is the cation $\text{Au}_7^{\text{I+}}$ and the other is a 3D honeycomb-type $\text{Au}_7^{\text{III+}}$ (see Table 3 and Ref. [83]). The difference between $\text{Au}_7^{\text{I+}}$ and $\text{Au}_7^{\text{III+}}$ amounts to 0.08 (0.15) [2.88 (2.92); -1.91 (-1.97)] kcal/mol

Au_7^{IV}



$\text{Au}_7^{\text{IVts}}$

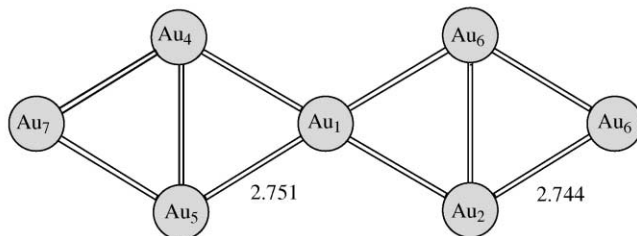


Fig. 13. Two low-energy structures Au_7^{IV} and $\text{Au}_7^{\text{IVts}}$. The B3LYP/A bond lengths are given in Å.

[84]. In summary, it is demonstrated for the first time that the cationic $2\text{D} \Rightarrow 3\text{D}$ conversion also takes place on the cationic PES of seven gold atoms, in a way similar to the five gold atom cationic PES.

To end this section, let us mention another neutral structure Au_7^{IV} in the $^2\text{A}_1$ state of C_{2v} symmetry (Fig. 13) lying 8.48 (8.58) kcal/mol (B3LYP/A) above Au_7^{III} (cf. with 8.27 kcal/mol reported in Ref. [44]). It possesses spin-up and spin-down HOMO–LUMO gaps of 1.52 and 1.50 eV, respectively. The related transition-state double-rhombus structure $\text{Au}_7^{\text{IVts}}$ is also shown in Fig. 13 and determines a barrier of about 17.67 kcal/mol.

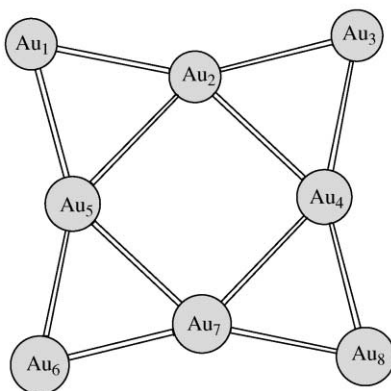
7. EIGHT GOLD ATOMS

It is known that the Au_8 cluster is the smallest catalytically active size of gold clusters [30].

Binding a single gold atom Au_1 to the Au_4 – Au_5 bond of the Au_7^{I} cluster leads to the planar and nonpolar cluster Au_8^{I} (Fig. 14) which is the global minimum on the PES of eight atom gold clusters. Such a structure has recently been reported by Bonačić-Koutecký *et al.* [44,74] as the true global minimum, assigned to the $^1\text{A}_{1g}$ state of D_{4h} symmetry, in contrast to earlier findings. The binding energy of Au_8^{I} , taken relative to the infinitely separated Au_7^{I} and Au_1 , is equal to 55.95 (55.59) [56.82 (56.46); 54.57 (54.18)] eV. Its E_{HL} gap width is 1.31 eV (BP86/A) (B3LYP gives 2.77 [2.72; 2.67] eV).

Geometrically, Au_8^{I} is composed of two kinds of coordinated gold atoms: the four-edged atoms are 2-coordinated while the other four are 4-coordinated. The Au–Au bond length between 2- and 4-coordinated atoms is about 1.6–1.7 Å (see Table 4) shorter than between each pair of 4-coordinated atoms. Each pair of opposite atoms belonging to the internal square are unbounded, thus forming a sort of hole since the corresponding distances of ca. 4.0 Å exceed twice the van der Waals radius of gold (3.32 Å). It is worth noticing that the formation of Au_8^{I} from $\text{Au}_7^{\text{I}} + \text{Au}_1$ requires to break an Au–Au bond of length ≈ 3.0 Å (< 3.32 Å) in the internal rhombus of Au_7^{I} .

The two following low-energy structures, Au_8^{II} and Au_8^{III} , have almost the same energy but differ by their 2D–3D character (see Figs 15 and 16). They lie about 12 kcal/mol above Au_8^{I} : $\Delta E(\text{Au}_8^{\text{II}} - \text{Au}_8^{\text{I}}) = 12.53$ (12.44) [10.77 (10.72); 11.01 (10.94)] kcal/mol and $\Delta E(\text{Au}_8^{\text{III}} - \text{Au}_8^{\text{I}}) = 12.66$ (12.57) [13.90 (13.83); 12.83 (12.73)] kcal/mol and are of the same polarity (≈ 0.9 D). One of them, Au_8^{II} , is a planar C_{2v} structure and possesses a 6-coordinated atom at the center. The other, Au_8^{III} , is a 3D cluster formed by a Au_2 dimer attached to the six-gold most stable cluster Au_6^{I} along its symmetry axis. It is partially composed of four 5-coordinated atoms of gold. It is reported for the first time in the present work. Their difference is also

Gold Clusters Au_8^{I} , $\text{Au}_8^{\text{I}+}$, and $\text{Au}_8^{\text{I}-}$ 

HOMO-LUMO (eV):

 Au_8^{I} : 2.77 [2.72; 2.67] {1.64} $\text{Au}_8^{\text{I}-}$: 1.69 [1.73; 1.68] {1.01} (α); 2.51 [2.53; 2.44] {1.31} (β) E_{bind} (kcal/mol): 55.95 (55.59) [56.82 (56.46); 54.57 (54.18)] IE_a (eV): 7.88 [7.71; 7.72] $\text{IE}_v^{\text{expt}}$ (eV): 8.65 [71] EA_a (eV): 2.78 [2.74; 2.72] $\text{EA}_a^{\text{expt}}$ (eV): 2.764 ± 0.050 [65]; 2.73(2) [63] $\text{EA}_a^{\text{theor}}$ (eV): 2.88 [63] VDE (eV): 2.88 [2.82; 2.82] VDE_{expt} (eV): 2.79 [65]; 2.79(2) [63] $\text{VDE}_{\text{theor}}$ (eV): 3.0 [50]; 2.94 [63]

Fig. 14. The ground-state cluster Au_8^{I} and cationic and anionic cousins and their properties. The quantities in curly brackets correspond to the BP86/A computational level.

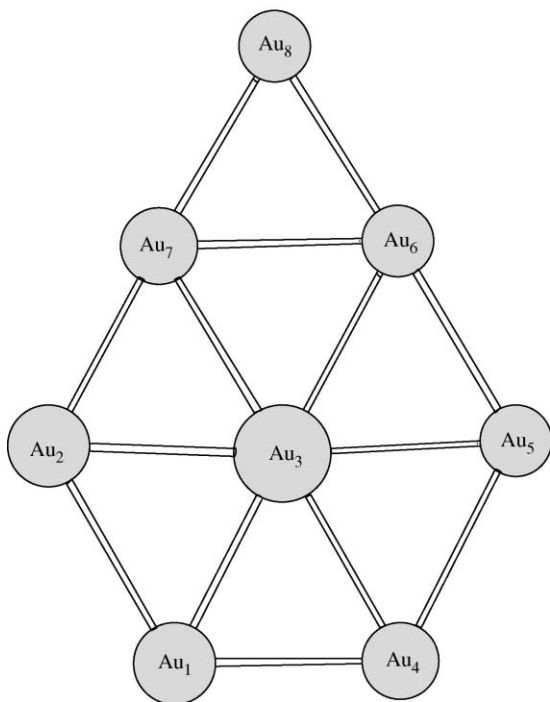
manifested in the width of E_{HL} : if for the 3D cluster Au_8^{III} , it is closer to that of Au_8^{I} , viz., 1.86 eV (BP86/A) (B3LYP: 2.95 [2.85; 2.94] eV), its 2D counterpart has a narrower one, i.e., 0.87 eV (BP86/A) (B3LYP: 1.76 [1.71; 1.72] eV). These two structures are slightly below (ca. 3–4 kcal/mol depending on the computational level) a pair of less stable 3D clusters, Au_8^{IV} and Au_8^{V} (Fig. 16) formed, respectively, by attaching a gold dimer to Au_6^{I} along its 3-atom bond and by adding a gold trimer parallel to Au_5^{I} (see Fig. 4). Both these structures are also novel.

Table 4. The bond lengths (in Å) of the neutral, cationic and anionic clusters Au₈^I and Au₈^{II}

	B3LYP/A	B3LYP/B	B3LYP/C	BP86/A
Au ₈ ^I				
r(Au ₁ –Au ₂)	2.697	2.675	2.698	2.670
r(Au ₁ –Au ₅)	2.697	2.675	2.698	2.670
r(Au ₂ –Au ₄)	2.870	2.826	2.860	2.819
r(Au ₄ –Au ₅)	4.066	4.003	4.045	3.980
Au ₈ ^{I+}				
r(Au ₁ –Au ₂)	2.722	2.695	2.720	
r(Au ₁ –Au ₅)	2.704	2.679	2.711	
r(Au ₂ –Au ₄)	2.844	2.805	2.840	
r(Au ₄ –Au ₅)	3.004	2.919	2.990	
Au ₈ ^{I–}				
r(Au ₁ –Au ₂)	2.754	2.722	2.752	2.721
r(Au ₁ –Au ₅)	2.754	2.722	2.752	2.721
r(Au ₂ –Au ₄)	2.782	2.752	2.780	2.751
r(Au ₄ –Au ₅)	3.940	3.893	3.931	3.895
Au ₈ ^{II}				
r(Au ₁ –Au ₂)	2.946	2.866	2.924	2.866
r(Au ₂ –Au ₃)	2.771	2.743	2.766	2.764
r(Au ₃ –Au ₄)	2.809	2.766	2.805	2.758
r(Au ₃ –Au ₆)	2.877	2.827	2.866	2.816
r(Au ₅ –Au ₆)	2.733	2.714	2.736	2.706
r(Au ₆ –Au ₇)	2.839	2.804	2.832	2.822
r(Au ₇ –Au ₈)	2.772	2.705	2.729	2.700
Au ₈ ^{II+}				
r(Au ₁ –Au ₂)	2.828	2.782	2.822	
r(Au ₂ –Au ₃)	2.813	2.782	2.806	
r(Au ₃ –Au ₄)	2.789	2.756	2.787	
r(Au ₃ –Au ₆)	2.819	2.774	2.816	
r(Au ₅ –Au ₆)	2.886	2.730	2.759	
r(Au ₆ –Au ₇)	2.886	2.852	2.875	
r(Au ₇ –Au ₈)	2.724	2.699	2.728	
Au ₈ ^{II–}				
r(Au ₁ –Au ₂)	2.890	2.829	2.877	
r(Au ₂ –Au ₃)	2.739	2.716	2.740	
r(Au ₃ –Au ₄)	2.857	2.811	2.877	
r(Au ₃ –Au ₆)	2.927	2.869	2.910	
r(Au ₅ –Au ₆)	2.723	2.706	2.728	
r(Au ₆ –Au ₇)	3.008	2.940	2.979	
r(Au ₇ –Au ₈)	2.744	2.717	2.745	

Despite the fact that the 3D cluster Au_8^{IV} is lying rather far from the minimum of the neutral PES, on the cationic PES, it competes with Au_8^{I} and Au_8^{II} , where the three lie at its very bottom (see Fig. 17). To be more

Gold Clusters Au_8^{II} , $\text{Au}_8^{\text{II}+}$, and $\text{Au}_8^{\text{II}-}$



HOMO-LUMO (eV):

Au_8^{II} : 1.76 [1.71; 1.72] {0.87}; 0.74 [62]

$\text{Au}_8^{\text{II}-}$: 1.75 [1.75; 1.74] (α); 1.46 [1.39; 1.39] (β)

$\Delta E(\text{Au}_8^{\text{I}}-\text{Au}_8^{\text{II}})$ (kcal/mol): -12.53 (12.44) [-10.77 (-10.72); -11.01 (-10.94)]
{-9.67 (-9.62)}

IE_a (eV): 7.41 [7.27; 7.26]

VDE (eV): 3.10 [2.97; 2.98]

Fig. 15. The cluster Au_8^{II} and cationic and anionic cousins and their properties. The quantities in curly brackets correspond to the BP86/A computational level.

specific, $\text{Au}_8^{\text{IV}+}$ is only 0.09 (0.06) [2.34 (2.27); 1.22 (1.17)] kcal/mol above $\text{Au}_8^{\text{I}+}$ which in turn is only 1.71 (1.68) [0.63 (0.61); 0.38 (0.37)] kcal/mol lower than $\text{Au}_8^{\text{II}+}$ [85]. Overall, this is in fact a manifestation of the $2\text{D} \leftrightarrow 3\text{D}$ transition occurring on the cationic PES of eight atoms of gold.

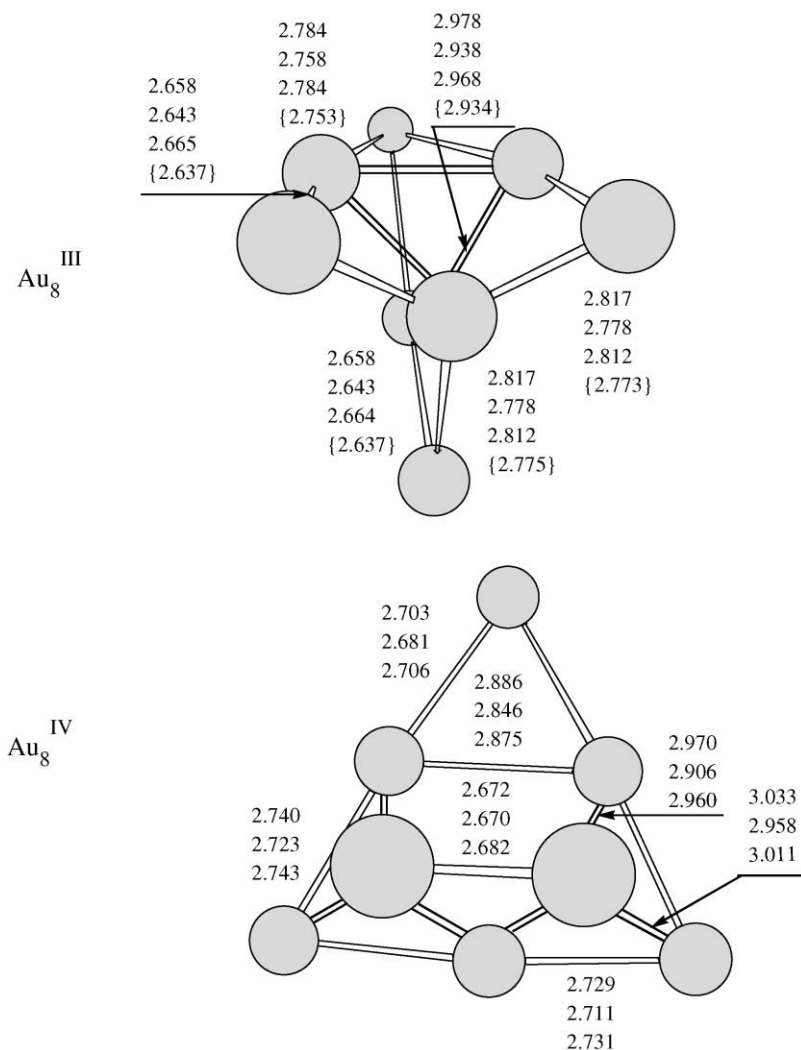


Fig. 16. The low-energy 3D structures on the PES of Au_8 . Their bond lengths are given in Å and displayed in the following order (from top to bottom): B3LYP/A, B3LYP/B, and B3LYP/C.

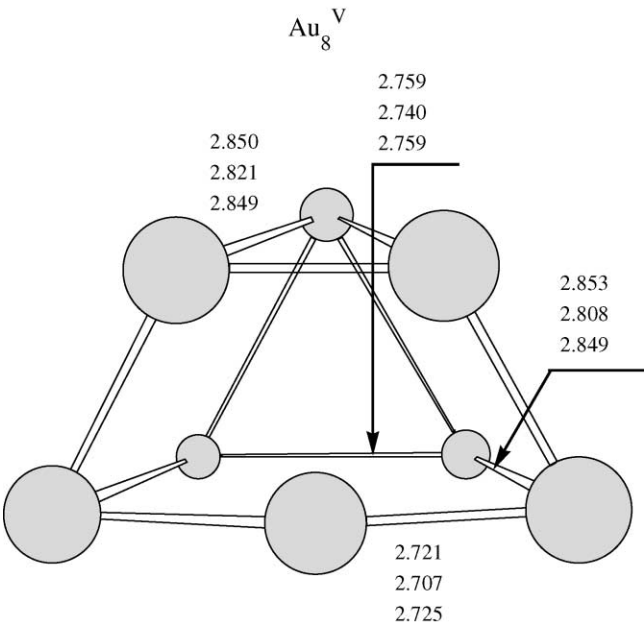


Fig. 16. (continued)

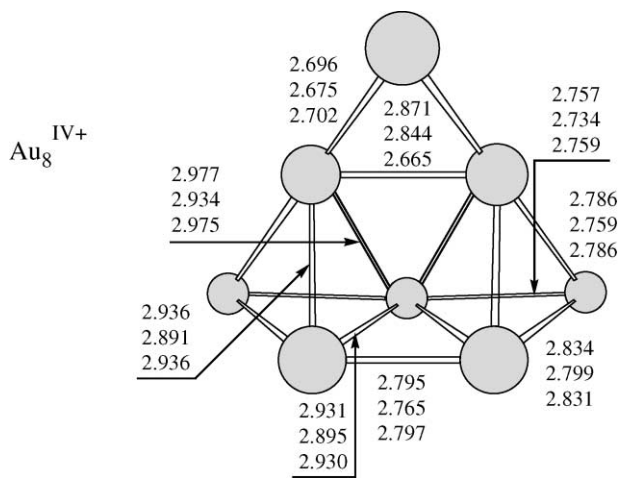


Fig. 17. The low-energy 3D cation $\text{Au}_8^{\text{IV+}}$. Its bond lengths are given in Å and displayed in the following order (from top to bottom): B3LYP/A, B3LYP/B, and B3LYP/C.

The optimized geometries and some other properties of these three cationic clusters are displayed in Figs 14, 15 and 17. It is worth mentioning that the $\text{IE}_a(\text{Au}_8^{\text{I}}) = 7.88$ [7.71; 7.72] eV which correlates with the experimental upper limit of 8.65 eV [68].

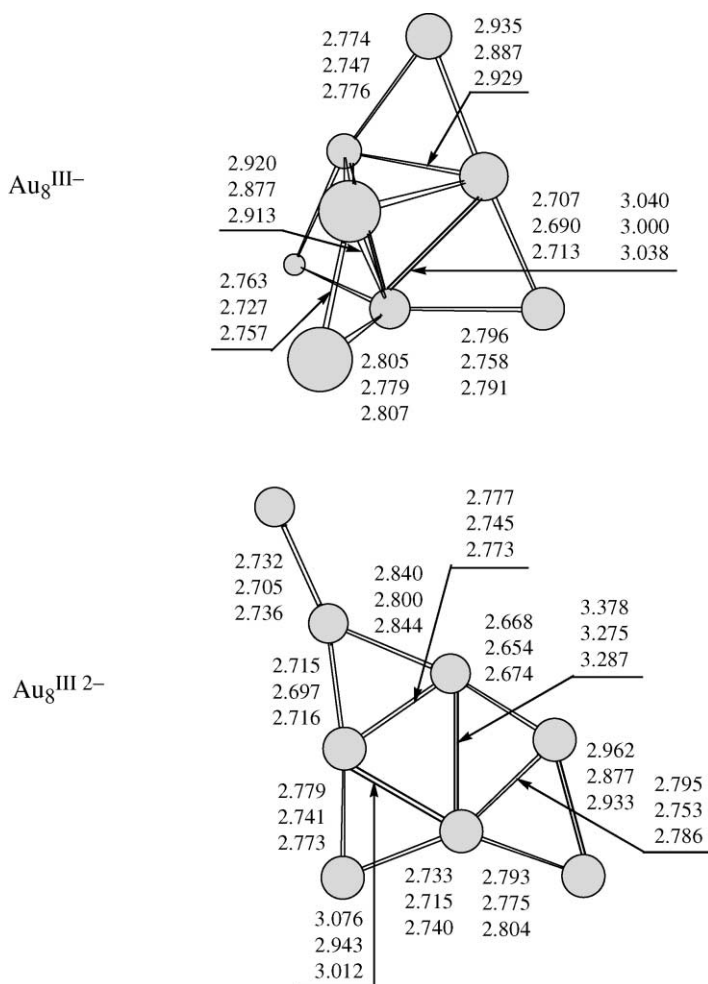


Fig. 18. The anion $\text{Au}_8^{\text{III}-}$ and long-lived dianion $\text{Au}_8^{\text{III}2-}$. The bond lengths are given in Å and displayed in the following order (from top to bottom): B3LYP/A, B3LYP/B, and B3LYP/C.

That $\text{Au}_8^{\text{I}-}$ is the most stable anionic cluster is a well-established fact [50]. It is displayed in Fig. 14. Two other low-energy clusters: the planar $\text{Au}_8^{\text{II}-}$ (7.11 (7.02) [6.90 (6.82); 6.63 (6.55)] kcal/mol higher than $\text{Au}_8^{\text{I}-}$) and the three-dimensional $\text{Au}_8^{\text{III}-}$ (21.08 (20.86) [23.44 (23.24); 21.02 (20.79)] kcal/mol higher than $\text{Au}_8^{\text{I}-}$) are shown in Figs 15 and 18, respectively. The HOMO–LUMO gaps of the open-shell cluster $\text{Au}_8^{\text{I}-}$ amount to 1.01 eV (BP86/A) (cf. B3LYP: 1.69 [1.73; 1.68] eV) (spin- \uparrow) and 1.31 eV (BP86/A) (cf. B3LYP: 2.51 [2.53; 2.44] eV) (spin- \downarrow), respectively. The computed adiabatic electron affinity is equal to 2.78 [2.74; 2.72] eV in agreement with the experimental magnitude of 2.764 ± 0.050 eV [65]. The VDE of $\text{Au}_8^{\text{I}-}$ amounts to 2.88 [2.82; 2.82] eV. Note that the 3D anion $\text{Au}_8^{\text{III}-}$ is stable under attaching e^- . Put in other words, the dianion $\text{Au}_8^{\text{III}2-}$, which becomes 2D and whose structure is displayed in Fig. 18 as well, lies lower than $\text{Au}_8^{\text{III}-}$ by 14.50 (14.49) [11.84 (11.85); 12.23 (12.22)] kcal/mol and therefore exists as a long-lived metastable dianion.

8. THE LOW-ENERGY SECTION OF THE PES OF Au_9

As we have seen in the previous sections, the planar triangular motif, which states that for a given ground-state cluster, Au_n , an additional Au atom forms only two new Au–Au bonds to yield the most stable Au_{n+1} , works for the neutral and anionic ground-state clusters $\text{Au}_{6-8}^{\text{I}}$ but not for the cationic ones. Does it mean that it is applicable for all larger clusters or is there some threshold number of Au atoms for which this motif is no longer valid?

In this section we show that $n = 9$ is in fact such a threshold. The structure of the low-energy nine gold atom clusters, shown in Fig. 19 (see also Table 5), demonstrate this point: three of them, Au_9^{I} , Au_9^{III} , and Au_9^{IV} are 2D whereas Au_9^{II} is 3D. The clusters Au_9^{I} , Au_9^{II} and Au_9^{IV} are novel and found in the present work for the first time (cf. the clusters in Refs. [14,44]; see Ref. [86]). All these four clusters are within ≈ 4 kcal/mol energy range (see Fig. 19). This is precisely the range (ca. 0.2 eV), mentioned already in Section 3, that corresponds to the accepted error of the DF/RECP methods for the gold clusters [44] meaning that all reported four structures can be considered as nearly isoenergetic.

Comparing the neutral PESs of 6–9 gold atoms, we conclude that the three planar low-energy structures Au_9^{I} , Au_9^{III} and Au_9^{IV} derive from Au_8^{I} , Au_7^{I} or Au_6^{I} by adding one, two or three planar triangles, respectively. On the other hand, the almost isoenergetic 3D structure Au_9^{II} is directly obtained from Au_8^{I} by adding (capping) one gold atom to its central square and forming four new Au–Au bonds, instead of two as demanded by the planar

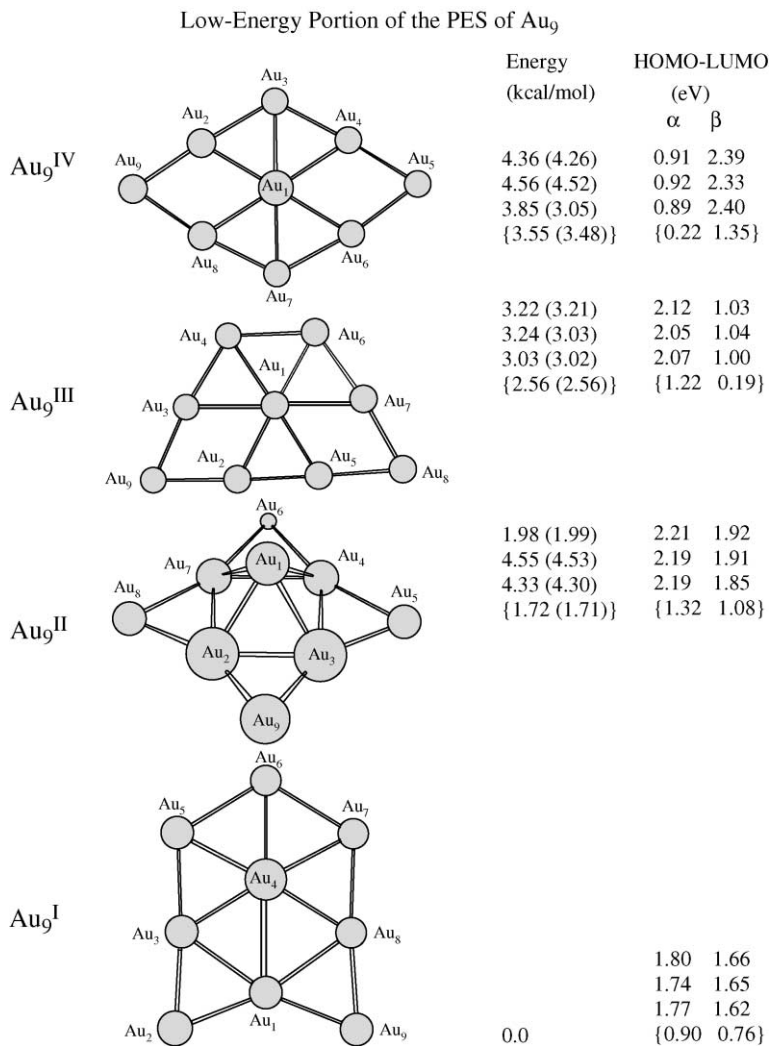


Fig. 19. The lower energy portion of the neutral PES of nine atoms of gold. The bond lengths of the displayed clusters are listed in Table 5.

triangular motif. This means that $n = 9$ is actually the minimal number of gold atoms for which the above rule is no longer fully valid. The neutral PES markedly demonstrates a co-existence of 2D and 3D structures in its low-energy portion.

Table 5. The bond lengths (in Å) of the low-energy neutral clusters of nine gold atoms

	B3LYP/A	B3LYP/B	B3LYP/C	BP86/A
Au₉^I				
$r(\text{Au}_1-\text{Au}_2)$	2.719	2.698	2.726	2.694
$r(\text{Au}_1-\text{Au}_3)$	2.902	2.850	2.885	2.857
$r(\text{Au}_1-\text{Au}_4)$	3.161	3.033	3.092	2.991
$r(\text{Au}_3-\text{Au}_4)$	2.776	2.745	2.775	2.747
$r(\text{Au}_4-\text{Au}_5)$	2.769	2.753	2.774	2.764
$r(\text{Au}_4-\text{Au}_6)$	2.788	2.746	2.787	2.748
$r(\text{Au}_6-\text{Au}_7)$	2.868	2.810	2.851	2.805
Au₉^{II}				
$r(\text{Au}_1-\text{Au}_2)$	2.912	2.856	2.909	2.851
$r(\text{Au}_3-\text{Au}_4)$	2.922	2.887	2.919	2.880
$r(\text{Au}_4-\text{Au}_6)$	2.710	2.688	2.711	2.684
Au₉^{III}				
$r(\text{Au}_1-\text{Au}_2)$	2.761	2.733	2.758	2.737
$r(\text{Au}_1-\text{Au}_3)$	2.956	2.882	2.930	2.884
$r(\text{Au}_1-\text{Au}_4)$	2.779	2.751	2.782	2.753
$r(\text{Au}_3-\text{Au}_4)$	2.752	2.725	2.756	2.709
$r(\text{Au}_3-\text{Au}_9)$	2.670	2.658	2.677	2.650
$r(\text{Au}_4-\text{Au}_6)$	2.891	2.831	2.868	2.849
$r(\text{Au}_2-\text{Au}_5)$	2.706	2.687	2.711	2.676
$r(\text{Au}_5-\text{Au}_7)$	2.950	2.885	2.930	2.905
$r(\text{Au}_5-\text{Au}_8)$	2.802	2.759	2.797	2.755
Au₉^{IV}				
$r(\text{Au}_1-\text{Au}_3)$	2.876	2.729	2.793	2.830
$r(\text{Au}_2-\text{Au}_3)$	2.745	2.729	2.746	2.703
$r(\text{Au}_1-\text{Au}_4)$	2.876	2.840	2.866	2.798
$r(\text{Au}_1-\text{Au}_6)$	2.844	2.755	2.834	2.796
$r(\text{Au}_1-\text{Au}_7)$	2.844	2.842	2.837	2.833
$r(\text{Au}_4-\text{Au}_5)$	2.729	2.753	2.726	2.674
$r(\text{Au}_4-\text{Au}_6)$	3.019	2.928	3.023	3.015
$r(\text{Au}_5-\text{Au}_6)$	2.679	2.645	2.686	2.675

9. SUMMARY AND OUTLOOK

Many novel low-energy structures have been found in the present work on the neutral, cationic and anionic PESs of small gold clusters $\text{Au}_{5 \leq n \leq 8}$ and on the neutral PES of Au_9 . On the neutral PES of Au_5 , we discover two new

planar forms, Au_5^{III} and Au_5^{IV} , that fill the gap of ≈ 21 kcal/mol between the 2D ground-state W-form and the 3D pyramid reported in Ref. [44]. The existence of the novel 3D cluster Au_7^{II} on the PES of Au_7 significantly lowers this 2D–3D gap to ≈ 6 kcal/mol. For $n = 9$, the 2D–3D gap is essentially closed: the 3D structure Au_9^{II} , reported in the present work for the first time, co-exists on almost equal energy footing with three 2D structures, two of which, including the slightly most stable one Au_9^{I} , are new as well.

The 2D–3D co-existence is inherent only to small odd-numbered gold clusters and the even-numbered ones behave differently, particularly Au_8 for which the lowest energy 3D cluster Au_8^{III} is above the 2D ground-state one by ca. 13 kcal/mol. Another feature related to the 2D–3D transition in small odd gold clusters emerges in the present work. This is the behavior of the E_{HL} gap. The spin-up gap $E_{\text{HL}\uparrow}$ of the ground-state 2D clusters narrows as n increases from 1.57 eV (Au_5^{I}) to 1.32 (Au_7^{I}) and 0.90 eV (Au_9^{I}). On the contrary, for the lowest energy 3D clusters Au_7^{II} and Au_9^{II} ($n = 7$ and 9), it widens from 0.92 to 1.32 eV. Also note that $E_{\text{HL}\uparrow}$ of the 3D cluster Au_7^{II} is less (by 0.4 eV) than that of the 2D one Au_7^{I} . This implies that the former has a higher catalytic activity despite its smaller binding energy and it would, therefore, deserve to be experimentally engineered on specific metal supporters.

The novel neutral clusters also exhibit interesting features on the charged PESs. For instance, the novel cluster Au_5^{III} is the parent of the anion $\text{Au}_5^{\text{III}-}$ which appears to be the most stable one, in contrast to the long-standing belief in that the ground anionic state is the W-shape structure $\text{Au}_5^{\text{I}-}$. This discrepancy can be explained by the presence of transition states between the ground-state W-form Au_5^{I} and higher energy cluster Au_5^{III} on the neutral PES and between $\text{Au}_5^{\text{I}-}$ and $\text{Au}_5^{\text{III}-}$ on the anionic one. These transition states govern the breaking of two Au–Au bonds and are characterized by high barriers (of at least 16 kcal/mol on the neutral PES) which lead to a lifetime for $\text{Au}_5^{\text{I}-}$ sufficiently long to be experimentally observed. On the other hand, the $\text{Au}_5^{\text{III}-}$ isomer, though less reactive than $\text{Au}_5^{\text{I}-}$ due to a larger E_{HL} , would be interesting to detect as well for two reasons. First, as demonstrated in Section 4, it gives rise to the long-lived metastable 5-gold dianion whose structural pattern is still present in the 8-gold dianion $\text{Au}_8^{\text{III}2-}$. Second, the bonding of a single gold atom to the atom Au_3 of $\text{Au}_5^{\text{III}-}$ results in the formation of the anionic cluster $\text{Au}_6^{\text{II}-}$ which lies only 3–5 kcal/mol higher than the ground-state anion $\text{Au}_6^{\text{I}-}$. Note that both of them are built, by analogy with the triangular motif rule for neutrals, *via* bonding of Au to the respective 5-gold anions.

As discussed above, the 2D–3D transition for the neutral clusters occurs at $n = 9$. For cationic gold atoms, it already develops for odd $n = 5$ and 7 gold atoms although the ways it does for these two n values are essentially different. For $n = 5$, the transition is associated to the existence of two nearly

isoenergetic rotamers, one, $\text{Au}_5^{\text{I}+}$, being 2D and the other, $\text{Au}_5^{\text{I}+'}$, 3D. Moreover, $\text{Au}_5^{\text{I}+'}$ lacks its neutral 3D parent. The case $n = 7$ is directly related to the ionization of the ground-state neutral 2D cluster Au_7^{I} . We predict that the ionization pathway goes *via* the intermediate planar transition state $\text{Au}_7^{\text{I}+\text{ts}}$ that relaxes to the 3D cluster $\text{Au}_7^{\text{II}+}$. In contrast to the $n = 5$ case and the 3D cation $\text{Au}_5^{\text{I}+'}$, $\text{Au}_7^{\text{II}+}$ possesses its 3D parent image Au_7^{II} on the neutral PES which, however, as already noticed above, is less stable than Au_7^{I} .

By analogy with the neutral case, the cationic 2D–3D co-existence for odd-numbered cationic gold clusters is straightforward. However, the cationic trend of this co-existence is quite different from the neutral case for even n values. For example, the novel 3D cation $\text{Au}_6^{\text{IV}+}$ lies only 5–7 kcal/mol higher than the almost degenerate ground-state cations $\text{Au}_6^{\text{I}+}$ and $\text{Au}_6^{\text{III}+}$. At $n = 8$, the energy offset between the 2D ground-state cluster $\text{Au}_8^{\text{II}+}$ and 3D one $\text{Au}_8^{\text{IV}+}$ reduces to ≈ 1 kcal/mol which falls within the DF/RECP computational error. One may, therefore, anticipate that the even $n = 10$ gold clusters might exhibit the 2D–3D co-existence.

Finally, anions of the studied gold clusters hardly manifest the 2D–3D transition. The most stable 3D cluster is $\text{Au}_8^{\text{III}-}$ and is reported here for the first time. However, it is much higher in energy (about 21–23 kcal/mol) than the 2D ground-state one $\text{Au}_8^{\text{I}-}$. This conclusion is in full agreement with the earlier findings by Landman and co-workers [14,63].

ACKNOWLEDGEMENTS

This work was supported by the Region Wallonne (RW. 115012) and used the computational facilities of NIC (University of Liege).

REFERENCES AND NOTES

- [1] F. Sherwood Taylor, *The Alchemists*, Frogmore, St Albans, Herts, 1976.
- [2] R. Pearsall, *The Alchemists*, Weidenfeld and Nicolson, London, 1986.
- [3] R. Morris, *The Last Sorcerers: The Path from Alchemy to the Periodic Table*, Joseph Henry Press, New York, 2003.
- [4] J. Hogan, *New Scientist*, 2003, **23**, 10.
- [5] J. Newton, *Friend, Man and the Chemical Elements from Stone-Age Hearth to the Cyclotron*, Ch. Griffin, London, 1951.
- [6] R. Boyle, *The Sceptical Chymist: or Chymico-Physical Doubts & Paradoxes, touching the Spagyrist's Principles commonly call'd Hypostatical, as they are wont to be Propos'd and Defended by the Generality of Alchymists*, London, 1661. Reprinted in the Everyman Series. See also T. Birch, *Life of Boyle*, Works, 1744 and L. M. Principe, *The Aspiring Adept: Robert Boyle and His Alchemical Quest*, Princeton University Press, Boston, 2000.

- [7] J. R. Partington, *A Short History of Chemistry*, Macmillan, London, 1957.
- [8] Pliny, *Natural History*, Translation by Bostock and Riley, Bonn, 1857. Book 33, Ch. 19.
- [9] A. El-Taher, K.-L. Kratz, A. Nossair and A. H. Azzam, *Radiat. Phys. Chem.*, 2003, **68**, 751.
- [10] J. R. Partington, *A History of Chemistry*, Macmillan, London, 1964, Vol. 4.
- [11] (a) Ph. Buffat and J.-P. Borel, *Phys. Rev. A*, 1976, **13**, 2287; (b) S.-T. Lee, G. Apai, M. G. Mason, R. Benbow and Z. Hurych, *Phys. Rev. B*, 1981, **23**, 505; (c) I. Katakuse, T. Ichihara, T. Matsuo and H. Matsuda, *Adv. Mass Spectrom.*, 1985, **10B**, 1073; (d) I. Katakuse, T. Ichihara, Y. Fujita, T. Matsuo, T. Sakurai and H. Matsuda, *Int. J. Mass Spectrom. Ion Proc.*, 1985, **67**, 229.
- [12] (a) P. Pykkö, *Chem. Rev.*, 1988, **88**, 563; (b) P. Pykkö, *Angew. Chem. Int. Ed.*, 2002, **41**, 3573.
- [13] H. Häkkinen, M. Moseler and U. Landman, *Phys. Rev. Lett.*, 2002, **89**, 033401.
- [14] H. Häkkinen and U. Landman, *Phys. Rev. B*, 2000, **62**, R2287.
- [15] H. Häkkinen and U. Landman, *J. Am. Chem. Soc.*, 2001, **123**, 9704.
- [16] (a) G. Mills, M. S. Gordon and H. Metiu, *Chem. Phys. Lett.*, 2002, **359**, 493; (b) G. Mills, M. S. Gordon and H. Metiu, *J. Chem. Phys.*, 2003, **118**, 4198.
- [17] W. T. Wallace, A. J. Leavitt and R. L. Whetten, *Chem. Phys. Lett.*, 2003, **368**, 774.
- [18] S. A. Varganov, R. M. Olson, M. S. Gordon, G. Mills and H. Metiu, *Chem. Phys. Lett.*, 2003, **368**, 778.
- [19] W. T. Wallace and R. L. Whetten, *J. Am. Chem. Soc.*, 2002, **124**, 7499.
- [20] W. T. Wallace and R. L. Whetten, *J. Phys. Chem. B*, 2000, **104**, 10964.
- [21] M. Valden, X. Lai and D. W. Goodman, *Science*, 1998, **281**, 1647.
- [22] B. Hammer and J. K. Nørskov, *Nature*, 1995, **376**, 238.
- [23] U. Landman, W. D. Laedtke, N. A. Burnham and R. J. Colton, *Science*, 1990, **248**, 454.
- [24] H. Häkkinen, R. N. Barnett, A. G. Scherbakov and U. Landman, *J. Phys. Chem.*, 2000, **104**, 9063.
- [25] H. Häkkinen, R. N. Barnett and U. Landman, *Phys. Rev. Lett.*, 1999, **82**, 3264.
- [26] C. L. Cleveland, U. Landman, T. G. Schaaff, M. N. Shafiguillin, P. W. Stephens and R. L. Whetten, *Phys. Rev. Lett.*, 1997, **79**, 1873.
- [27] A. Sanchez, S. Abbet, U. Heiz, W.-D. Schneider, H. Häkkinen, R. N. Barnett and U. Landman, *J. Phys. Chem. A*, 1999, **103**, 9573.
- [28] A. P. Alivisatos, *Science*, 1996, **271**, 933.
- [29] Z. Xu, F.-S. Xiao, S. K. Purnell, O. Alexeev, S. Kawi, S. E. Deutsch and B. C. Gates, *Nature*, 1994, **372**, 346.
- [30] A. Sanchez, S. Abbet, U. Heiz, W.-D. Schneider, H. Häkkinen, R. N. Barnett and U. Landman, *J. Phys. Chem. A*, 1999, **103**, 9573.
- [31] F. C. Fritschij, H. B. Brom, L. J. de Jongh and G. Schmid, *Phys. Rev. Lett.*, 1999, **82**, 2167.
- [32] T. G. Schaaff and R. L. Whetten, *J. Phys. Chem. B*, 2000, **104**, 2630.
- [33] O. Dag, *J. Phys. Chem. B*, 2000, **104**, 6983.
- [34] Z. Xu, F.-S. Xiao, S. K. Purnell, O. Alexeev, S. Kawi, S. E. Deutsch and B. C. Gates, *Nature*, 1994, **372**, 346.
- [35] P. Schwerdtfeger, *Angew. Chem. Int. Ed.*, 2003, **42**, 1892.
- [36] H. Häkkinen, S. Abbet, A. Sanchez, U. Heiz and U. Landman, *Angew. Chem. Int. Ed.*, 2003, **42**, 1297.
- [37] Z. Li, S.-W. Chung, J.-M. Nam, D. S. Ginger and C. A. Mirkin, *Angew. Chem. Int. Ed.*, 2003, **42**, 2306.
- [38] J.-M. Nam, C. S. Thaxton and C. A. Mirkin, *Science*, 2003, **301**, 1884.
- [39] (a) K. Balasubramanian and D. W. Liao, *J. Chem. Phys.*, 1991, **94**, 5233; (b) D. W. Liao and K. Balasubramanian, *J. Chem. Phys.*, 1992, **97**, 2548.

- [40] (a) G. Bravo-Pérez, I. L. Garzón and O. Novaro, *J. Mol. Struct.*, 1999, **493**, 225; (b) G. Bravo-Pérez, I. L. Garzón and O. Novaro, *Chem. Phys. Lett.*, 1999, **313**, 655.
- [41] (a) O. D. Häberlen, S.-C. Chung and N. Rösch, *Int. Quant. Chem.: Quant. Chem. Symp.*, 1994, **28**, 595; (b) O. D. Häberlen, H. Schmidbaur and N. Rösch, *J. Am. Chem. Soc.*, 1994, **116**, 8241; (c) O. D. Häberlen, S.-C. Chung, M. Stener and N. Rösch, *J. Chem. Phys.*, 1997, **106**, 5189.
- [42] R. Arratia-Perez and L. Hernandez-Acevedo, *J. Mol. Struct. Theochem*, 1993, **101**, 131.
- [43] J. Guzman and B. C. Gates, *Nano Lett.*, 2001, **12**, 689.
- [44] V. Bonačić-Koutecký, J. Burda, R. Mitrić, M. Ge, G. Zampella and P. Fantucci, *J. Chem. Phys.*, 2002, **117**, 3120.
- [45] C. W. Bauschlicher, S. R. Langhoff and H. Partridge, *J. Phys. Chem.*, 1990, **93**, 8133.
- [46] H. Grünbeck and W. Andreoni, *Chem. Phys.*, 2000, **262**, 1.
- [47] J. Wang, G. Wang and J. Zhao, *Phys. Rev.*, 2002, **66**, 035418.
- [48] E. Van Lenthe, A. van der Avoird and P. E. S. Wormer, *J. Chem. Phys.*, 1998, **108**, 4783.
- [49] (a) R. Rousseau, G. Dietrich, S. Krückeberg, K. Lützenkirchen, D. Marx, L. Schweikhard and C. Walther, *Chem. Phys. Lett.*, 1998, **295**, 41; (b) R. Rousseau, D. Marx and J. J. Chem. Phys., 2000, **112**, 761; (c) M. Vogel, K. Hansen, A. Herlert, L. Schweikhard and C. Walther, *J. Chem. Phys.*, 2002, **116**, 9658.
- [50] F. Furche, R. Ahlrichs, P. Weis, C. Jacob, S. Gilb, T. Bierweiler and M. M. Kappes, *J. Chem. Phys.*, 2002, **117**, 6982.
- [51] S. Gilb, P. Weis, F. Furche, R. Ahlrichs and M. Kappes, *J. Chem. Phys.*, 2002, **116**, 4094.
- [52] (a) P. J. Hay and W. R. Wadt, *J. Chem. Phys.*, 1985, **270**, 299; (b) W. R. Wadt and P. J. Hay, *J. Chem. Phys.*, 1985, **82**, 284.
- [53] R. B. Ross, J. M. Powers, T. Atashroo, W. C. Ermler, L. A. LaJohn and P. A. Christiansen, *J. Chem. Phys.*, 1990, **93**, 6654.
- [54] D. Andrae, U. Haeussermann, M. Dolg, H. Stoll and H. Preuss, *Theor. Chim. Acta*, 1990, **77**, 123.
- [55] M. J. Frisch, G. W. Trucks, H. B. Schlegel, G. E. Scuseria, M. A. Robb, J. R. Cheeseman, J. A. Montgomery Jr., T. Vreven, K. N. Kudin, J. C. Burant, J. M. Millam, S. S. Iyengar, J. Tomasi, V. Barone, B. Mennucci, M. Cossi, G. Scalmani, N. Rega, G. A. Petersson, H. Nakatsuji, M. Hada, M. Ehara, K. Toyota, R. Fukuda, J. Hasegawa, M. Ishida, T. Nakajima, Y. Honda, O. Kitao, H. Nakai, M. Klene, X. Li, J. E. Knox, H. P. Hratchian, J. B. Cross, C. Adamo, J. Jaramillo, R. Gomperts, R. E. Stratmann, O. Yazyev, A. J. Austin, R. Cammi, C. Pomelli, J. W. Ochterski, P. Y. Ayala, K. Morokuma, G. A. Voth, P. Salvador, J. J. Dannenberg, V. G. Zakrzewski, S. Dapprich, A. D. Daniels, M. C. Strain, O. Farkas, D. K. Malick, A. D. Rabuck, K. Raghavachari, J. B. Foresman, J. V. Ortiz, Q. Cui, A. G. Baboul, S. Clifford, J. Cioslowski, B. B. Stefanov, G. Liu, A. Liashenko, P. Piskorz, I. Komaromi, R. L. Martin, D. J. Fox, T. Keith, M. A. Al-Laham, C. Y. Peng, A. Nanayakkara, M. Challacombe, P. M. W. Gill, B. Johnson, W. Chen, M. W. Wong, C. Gonzalez and J. A. Pople, Gaussian Inc., Pittsburgh, PA, 2003.
- [56] D. H. Wells, Jr, W. N. Delgass and K. T. Thomson, *J. Chem. Phys.*, 2002, **117**, 10597.
- [57] H. Tanaka, S. Neukermans, E. Janssens, R. E. Silverans and P. Lievens, *J. Chem. Phys.*, 2003, **119**, 7115.
- [58] H. Basch and M. A. Ratner, *J. Chem. Phys.*, 2003, **119**, 11926, 11943.
- [59] L. Andrews and X. Wang, *J. Am. Chem. Soc.*, 2003, **125**, 11751.
- [60] H. M. Lee, M. Ge, B. R. Sahu, P. Tarakeshwar and K. S. Kim, *J. Phys. Chem. B*, 2003, **107**, 9994.
- [61] (a) T. Leisner, S. Vajda, S. Wolf and L. Woste, *J. Chem. Phys.*, 1999, **111**, 1017; (b) D. W. Boo, Y. Ozaki, L. H. Andersen and W. C. Lineberger, *J. Phys. Chem. A*, 1997, **101**, 6688.

- [62] J. Zhao, J. Yang and J. G. Hou, *Phys. Rev. B*, 2003, **67**, 085404.
- [63] H. Häkkinen, B. Yoon, U. Landman, X. Li, H.-J. Zhai and L.-S. Wang, *J. Phys. Chem. A*, 2003, **107**, 6168.
- [64] $\text{Au}_5^{\text{III}-}$ is distinguished from the V-shaped chain, found in Ref. [50] and placed 0.13 eV higher than $\text{Au}_5^{\text{I}-}$, due to the presence of the additional bond Au_1-Au_4 (see Fig. 2).
- [65] K. J. Taylor, C. L. Pettiette-Hall, O. Cheshnovsky and R. E. Smalley, *J. Chem. Phys.*, 1992, **96**, 3319.
- [66] J. Ho, K. M. Ervin and W. C. Lineberger, *J. Chem. Phys.*, 1990, **93**, 6987.
- [67] These estimates better match the experimentally measured gap of 1.0 eV (Ref. [63], p. 6172).
- [68] The neutral highly symmetric structure resembling the anion $\text{Au}_5^{\text{III}-}$ lies, as shown in Ref. [40], 1.45 eV above Au_5^{I} .
- [69] A. Dreuw and L. S. Cederbaum, *Chem. Rev.*, 2002, **102**, 181.
- [70] (a) C. Yannouleas and U. Landman, *Phys. Rev.*, 2000, **61**, R10587; (b) C. Yannouleas, U. Landman, A. Herlert and L. Schweikhard, *Phys. Rev. Lett.*, 2001, **86**, 2996.
- [71] C. Jackschath, I. Rabin and W. Schulze, *Ber. Bunsenges. Phys. Chem.*, 1992, **96**, 1200.
- [72] K.-i. Sugawara, F. Sobott and A. B. Vakhit, *J. Chem. Phys.*, 2003, **118**, 7808.
- [73] M. A. Cheeseman and J. R. Eyler, *J. Phys. Chem.*, 1992, **96**, 1082.
- [74] R. Mitrić, C. Bürgel, J. Burda, V. Bonačić-Koutecký and P. Fantucci, *Eur. Phys. J. D*, 2003, **24**, 41.
- [75] W. T. Wallace, R. B. Wyrwas, R. L. Whetten, R. Mitrić and V. Bonačić-Koutecký, *J. Am. Phys. Soc.*, 2003, **125**, 8408.
- [76] D. Krüger, H. Fuchs, R. Rousseau, D. Marx and M. Parrinello, *J. Chem. Phys.*, 2001, **115**, 4776.
- [77] K. J. Taylor, C. Jin, J. Conceicao, L.-S. Wang, O. Cheshnovsky, B. R. Johnson, P. J. Nordlander and R. E. Smalley, *J. Chem. Phys.*, 1990, **93**, 7515.
- [78] G. F. Gantefür, D. M. Cox and A. Kaldor, *J. Chem. Phys.*, 1992, **96**, 4102.
- [79] V. A. Spasov, Y. Shi and K. M. Ervin, *Chem. Phys.*, 2000, **262**, 75.
- [80] Notice that the planar structure II reported to be lying 2.26 kcal/mol higher relative to Au_7^{I} on the PES of Au_7 in Ref. [44] or 0.1 kcal/mol lower in Ref. [13] (see Fig. 1 therein), has not been found in the present work at the B3LYP/A computational level. On the contrary, when taken as the initial geometry, it converges to Au_7^{I} under the tight optimization.
- [81] Notice that the anionic structure 7B reported in Ref. [63] and resembling actually the structure of the neutral cluster Au_7^{I} , lying 0.12 kcal/mol higher than $\text{Au}_7^{\text{I}-}$ on the PES of Au_7^- has not been found in the present work at the B3LYP/A computational level. Similarly with Ref. [80], when taken as the initial guess, it converges to $\text{Au}_7^{\text{I}-}$ under the tight optimization.
- [82] This is a difference between the results for the ground-state structure on the PES of the neutral gold cluster of seven atoms, presented in Refs. [14,44] and this work. Note that in Ref. [14], Au_7^{III} was predicted to be the global minimum.
- [83] In a certain sense, $\text{Au}_7^{\text{III}+}$ resembles the 2D structure of the cation Au_7^+ with the D_{6h} symmetry obtained in Ref. [51]. However, all present calculations show that $\text{Au}_7^{\text{III}+}$ is undoubtedly a 3D highly symmetric structure.
- [84] It is suggested in Ref. [51] (p. 4099) that "... several three dimensional structures...can be ruled out since the lowest is almost 0.5 eV higher in energy and the cross sections also disagree with measurement – the pentagonal bipyramid (the lowest 3D structure we found) for example, has a cross-section of 61.7 \AA^2 ...". The experimental and computed cross-sections of $\text{Au}_7^{\text{III}+}$ are correspondingly equal to 65.8 and 65.9 \AA^2 [51]. It would be interesting to calculate the collisional cross-section of $\text{Au}_7^{\text{I}+}$.

- [85] Notice that Gilb *et al.* [51] have recently reported two clusters at the bottom of the PES of Au_8^+ . The global minimum is occupied by $\text{Au}_8^{\text{II}+}$ which is 1.61 kcal/mol lower compared to $\text{Au}_8^{\text{IV}+}$. As suggested in Ref. [51], the mobility data (69.4 \AA^2) rules out ‘the planar isomer’ ($\text{Au}_8^{\text{II}+}$, in the present notations). “The measured cross-section agrees to within 1% with that of the three-dimensional structure” ($\text{Au}_8^{\text{IV}+}$), “which means that in this case the lowest energy DFT structure is *not* found in the experiment”. We assume that the structure which might be determined in such ion mobility experiments is referred to $\text{Au}_8^{\text{I}+}$ (probably with some partial weight of $\text{Au}_8^{\text{IV}+}$) which is actually a novel cationic cluster. This assumption could be verified by evaluating the cross-section of $\text{Au}_8^{\text{I}+}$.
- [86] Due to the absence of the structures Au_9^{I} and Au_9^{II} in Ref. [44], the most stable cluster was assigned to Au_9^{III} .

Positron–Electron Annihilation in Hydrogen–Antihydrogen Collisions

P. Froelich,¹ S. Jonsell,² A. Saenz,³ S. Eriksson,¹ B. Zygelman⁴
and A. Dalgarno⁵

¹*Department of Quantum Chemistry, Uppsala University, Box 518, 75120 Uppsala, Sweden*

²*Theoretical Physics, Umeå University, SE-90187 Umeå, Sweden*

³*AG Moderne Optik, Institut für Physik, Humboldt-Universität zu Berlin, Haus-vogteiplatz 5-7, D-10117 Berlin, Germany*

⁴*Department of Physics, University of Nevada, Las Vegas, NV 89154, USA*

⁵*Harvard-Smithsonian Center for Astrophysics, 60 Garden Street, Cambridge, MA 02138, USA*

Abstract

The rate of direct positron–electron annihilation in cold hydrogen–antihydrogen collisions has been calculated and compared to the rate of proton–antiproton annihilation. We show that the lepton annihilation rate in $\bar{H}H$ collisions depends on the relative orientation of spins of the electron and positron. In the low-energy limit of hydrogen–antihydrogen scattering, the presence of leptonic annihilation introduces an absorptive, imaginary component to the hydrogen–antihydrogen scattering length; this component is $\beta_+ = 1.4 \times 10^{-4} a_0$ for the singlet state of the leptonic spins, and $\beta_- = 1.2 \times 10^{-7} a_0$ for the triplet state. Leptonic annihilation turns out to be about three orders of magnitude slower than proton–antiproton annihilation.

Contents

1. Introduction	465
2. Leptonic annihilation in the hydrogen–antihydrogen system	467
2.1. The scattering wave function in the initial channel	470
2.2. The electron–positron coalescence probability	471
2.3. Asymptotic behavior of the leptonic coalescence probability	473
3. Numerical results	474
4. Conclusions	477
Acknowledgements	479
References	479

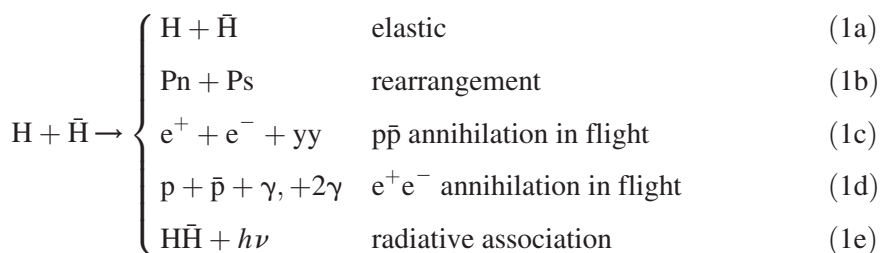
1. INTRODUCTION

The simplest blocks of neutral antimatter in the form of cold antihydrogen atoms have been recently obtained at CERN [1,2]. There are plans to use them

for probing of the charge–parity–time (CPT) symmetry of Nature. The abundance of cold antiatoms opens also the possibility to study the interaction between matter and antimatter, including the gravitational interaction.

What happens when an antiatom comes in contact with matter, e.g., meets an ordinary atom or impinges on a material surface? The quick intuitive answer is that it will disappear in a flash of light in the act of annihilation. However, more careful analysis reveals that a low-energy encounter of an antiatom with matter is a much more intricate process.

It turns out that during hydrogen–antihydrogen collisions a number of reactions are possible; the ones that we have studied so far are [3–8]



We have found that in certain range of low collisional energies, the rate of annihilation in flight is comparable to the rate of rearrangement into positronium and protonium. The latter process can be looked upon as an atom–antiatom chemical reaction which can be radiationless or occur with emission of photons. The radiative association leads to the formation of a meta-stable atom–antiatom molecule. We have seen that in certain energy ranges the elastic scattering may compete successfully with annihilation, which might find applications in collisional cooling of antiatoms. Even more surprisingly, we have been able to show that a sufficiently cold antiatom will be reflected by a material surface rather than being annihilated [9].

Since the electromagnetic interaction is much weaker than the strong nuclear force, one might expect that, in an atom–antiatom collision, proton–antiproton annihilation will be the dominant process. However, the strong force is characterized by a very short interaction range. The electromagnetic interaction between the atoms, on the other hand, is characterized by the effective long-range van der Waals interactions. Processes of an electromagnetic nature, such as rearrangement into positronium and protonium, can, therefore, occur over a much larger range of internuclear distances. Indeed, our previous results show that the cross-section for the rearrangement collision is surprisingly large and only slightly smaller than that for proton–antiproton annihilation in flight. This finding conforms with other calculations of the rearrangement process [10–12].

Large rearrangement implies strong inter-particle correlation. This correlation is of attractive type, i.e., unlike the H_2 system where the electrons

avoid each other, the positron and electron in the $\bar{H}H$ system are attracted to each other (there is neither Coulomb nor Fermi ‘hole’). The presence of attractive inter-leptonic correlation, combined with the slow approach of ultracold $\bar{H}H$ atoms implicates that the leptons might have plenty of time ‘to find each other’. The present chapter is devoted to the question: how fast is the positron–electron annihilation? Could that be so that during the slow $\bar{H} + H$ collision the leptons will annihilate before the hadrons do?

Our previous calculations of the cross-section for proton–antiproton annihilation have been performed in the distorted wave approximation, using the adiabatic interaction in the initial channel [3]. This means that the approaching nuclei are assumed to move in the field of the surrounding leptons. Such assumption would turn out to be a wishful thinking in case the leptons, instead of creating the interaction potential, would directly annihilate each other as the atoms come close. The leptonic screening and the leptonic potential would cease to exist and the hadrons would move under the influence of the bare-nuclei interaction. Most importantly, if direct leptonic annihilation would turn out to occur with large probability, this would be an important loss channel for antihydrogen when interacting with ordinary matter. In the present work we show that this is *not* the case, i.e., during the collision the leptons annihilate on a very different time scale compared with the hadrons. Therefore, direct leptonic annihilation is a negligible loss channel in cold hydrogen–antihydrogen collisions and the leptonic potential is a useful concept in considering atom–antiatom collisions.

The leptonic annihilation is nevertheless observable in hydrogen–antihydrogen collisions. Its main appearance is, however, due to indirect processes, namely the intermediate formation of positronium as a consequence of rearrangement collisions. In that case the leptons are likely to annihilate with a certain time delay after hadronic annihilation. This is because regardless the final state of positronium its life time is longer than that of the most probable final state of protonium with $N = 23$.

2. LEPTONIC ANNIHILATION IN THE HYDROGEN–ANTIHYDROGEN SYSTEM

The direct leptonic annihilation in hydrogen–antihydrogen collisions occurs according to



If this process happens during the collisional approach, the hadrons get stripped from their leptons and start to interact as bare nuclei *via* the Coulomb and strong interactions.

The probability of leptonic annihilation in flight may be obtained in the contact approximation, i.e., assuming that electron–positron annihilation occurs at the exact point of coalescence of the two leptons. The rate of annihilation is obtained as a product of the leptonic probability density for coalescence and the positron–electron annihilation rate constant, integrated over all space. Within this approximation the direct leptonic annihilation rate is given by

$$\lambda_a^{\text{e}\bar{\text{e}}} = \langle \Psi_{\mathbf{k}_i}^{(+)}(\mathbf{r}_e, \mathbf{r}_{\bar{e}}, \mathbf{R}) | A^{\text{e}\bar{\text{e}}} \delta(\mathbf{r}_e - \mathbf{r}_{\bar{e}}) | \Psi_{\mathbf{k}_i}^{(+)}(\mathbf{r}_e, \mathbf{r}_{\bar{e}}, \mathbf{R}) \rangle, \quad (3)$$

where $\Psi_{\mathbf{k}_i}^{(+)}(\mathbf{r}_e, \mathbf{r}_{\bar{e}}, \mathbf{R})$ is the four-body scattering wave function in the initial channel. The latter is an eigenfunction of the total Hamiltonian H in the initial channel,

$$H \Psi_{\mathbf{k}_i}^{(+)}(\mathbf{r}_e, \mathbf{r}_{\bar{e}}, \mathbf{R}) = E_i \Psi_{\mathbf{k}_i}^{(+)}(\mathbf{r}_e, \mathbf{r}_{\bar{e}}, \mathbf{R}), \quad (4)$$

and asymptotically describes two atoms colliding with energy ε_i . E_i is the total energy of the collisional system and thus equal to the sum of the internal energies of the two atoms (-1.0 a.u. in the case of hydrogen and antihydrogen in their $1s$ ground states) and the kinetic energy ε_i . Here and in the following atomic units (Hartree) are used, if not specified otherwise.

The annihilation constant $A^{\text{e}\bar{\text{e}}}$ is given as the number of annihilation events per unit density and unit time. It is obtained from the life time of positronium, which for the singlet state (*para*-positronium) is $\tau_{2\gamma} = 1.25 \times 10^{-10}$ s [13], and for the triplet state (*ortho*-positronium) is $\tau_{3\gamma} = 1.42 \times 10^{-7}$ s [14]. The positronium decay rate is related to the decay constant *via*

$$\lambda = \frac{1}{\tau} = A^{\text{e}\bar{\text{e}}} |\phi_{100}^{\text{Ps}}(0)|^2, \quad (5)$$

which yields $A_+^{\text{e}\bar{\text{e}}} = 8\pi/\tau_{2\gamma} = 4.86 \times 10^{-6}$ a.u. for *para*-positronium and $A_-^{\text{e}\bar{\text{e}}} = 8\pi/\tau_{3\gamma} = 4.28 \times 10^{-9}$ a.u. for *ortho*-positronium.

The reason for the different decay rates of *ortho*- and *para*-positronium is the conservation of the charge conjugation symmetry C by the electromagnetic interaction. For the electron–positron system the leptonic charge conjugation operator can be related to the electron–positron exchange operator $P_{e\bar{e}}$ by $C_l = -P_{e\bar{e}}$. The minus sign comes from the anti-commutativity of the fermionic field operators [15]. Hence, we find that *ortho*-positronium has negative parity under charge conjugation, while *para*-positronium has positive parity. The photon can be regarded as having an intrinsic charge conjugation parity -1 . *Para*-positronium may then decay into two photons, while *ortho*-positronium can only decay into three photons, which is a much slower process. Hence, the longer life time of *ortho*-positronium.

The hydrogen–antihydrogen system is invariant under charge conjugation of all four particles, but it is *not* invariant under charge conjugation of the leptons only. Therefore, we cannot expect our initial state $\Psi_{\mathbf{k}_i}^{(+)}$ to be in an eigenstate of the C_l or $P_{e\bar{e}}$ operator. However, it is possible to relate the decay properties of the $H + \bar{H}$ system to the known decay properties of the positronium. We may construct an effective potential for electron–positron annihilation by projecting out the parts of the wavefunction with positive and negative charge conjugation parity. In addition, we approximate annihilation as a contact interaction, i.e., it occurs only when $\mathbf{r}_{e\bar{e}} = \mathbf{r}_{\bar{e}} - \mathbf{r}_e = 0$. Expressed in terms of the electron–positron exchange operator the effective potential for leptonic annihilation is

$$V_a^{e\bar{e}}(\mathbf{r}_{e\bar{e}}) = \delta(\mathbf{r}_{e\bar{e}}) \left[A_+^{e\bar{e}} \frac{1 - P_{e\bar{e}}}{2} + A_-^{e\bar{e}} \frac{1 + P_{e\bar{e}}}{2} \right]. \quad (6)$$

The initial-state wave function $\Psi_{\mathbf{k}_i}^{(+)}$ can be expressed in terms of the coordinates $\mathbf{r}_{e\bar{e}}$, $\mathbf{r}_{e\bar{e}}^{\text{cm}} = (\mathbf{r}_e + \mathbf{r}_{\bar{e}})/2$, and \mathbf{R} . We may then expand it in partial waves even or odd under exchange of the leptons [$P_{e\bar{e}} Y_{lm}(\Omega_{r_{e\bar{e}}}) = (-1)^l Y_{lm}(\Omega_{r_{e\bar{e}}})$] as

$$\Psi_{\mathbf{k}_i}^{(+)}(\mathbf{R}, \mathbf{r}_{e\bar{e}}^{\text{cm}}, \mathbf{r}_{e\bar{e}}) = \sum_{lm} \Theta_{lm}(\mathbf{R}, \mathbf{r}_{e\bar{e}}^{\text{cm}}, \mathbf{r}_{e\bar{e}}) Y_{lm}(\Omega_{r_{e\bar{e}}}). \quad (7)$$

If the function above is to be single valued, the $r_{e\bar{e}} \rightarrow 0$ limit should be angle independent. This will happen only if all terms $\Theta_{lm}(\mathbf{R}, \mathbf{r}_{e\bar{e}}^{\text{cm}}, 0)$ vanish except the one for $l = 0$. Hence, we conclude that, in the contact-interaction approximation, only the even $l = 0$ partial wave contributes to electron–positron annihilation. Taking also the symmetry under exchange of the leptonic spins χ_{S, M_S} into account we find that

$$\delta(\mathbf{r}_{e\bar{e}})(1 - P_{e\bar{e}}) \Psi_{\mathbf{k}_i}^{(+)} \chi_{1M_S} = 0, \quad \delta(\mathbf{r}_{e\bar{e}})(1 + P_{e\bar{e}}) \Psi_{\mathbf{k}_i}^{(+)} \chi_{00} = 0. \quad (8)$$

We thus see that the leptonic part of the molecular state in the $r_{e\bar{e}} \rightarrow 0$ limit has the symmetry properties of the positronium. Hence, even though the hydrogen–antihydrogen system is not an eigenstate with respect to charge conjugation of the leptons, the same selection rules as for the positronium ground state apply, i.e., the molecular singlet will decay with emission of two photons whereas the triplet state will decay emitting three photons. The annihilation rate of the molecular $H + \bar{H}$ system can be expressed either in terms of the annihilation rate constant for *para*-positronium (for collisions in the molecular singlet state) or *ortho*-positronium (for the molecular triplet collisions).

The ratio of triplet collisions to singlet collisions will depend on the experimental conditions. For a statistical mixture the ratio is 3:1. In a magnetic trap only the spin-polarized states can be held, i.e., the electron spin will be parallel to the magnetic field, while the positron spin, being

parallel to the magnetic moment, will point in the opposite direction. Hence, unlike the case of H + H collisions, the spin-polarized $\bar{\text{H}}\text{-H}$ system corresponds to $M_s = 0$ and the collisions will be in the singlet and triplet states in equal proportions.

In order to obtain the annihilation cross-section the annihilation rate in equation (3) is divided by the flux F of the on-coming atoms

$$\sigma_a^{\text{e}\bar{\text{e}}} = \frac{\lambda_a^{\text{e}\bar{\text{e}}}}{F} = \frac{(2\pi)^3}{k_i^2} A^{\text{e}\bar{\text{e}}} \int |\Psi_{\mathbf{k}_i}^{(+)}(\mathbf{R}, \mathbf{r}_e, \mathbf{r}_{\bar{e}})|^2 \delta(\mathbf{r}_e - \mathbf{r}_{\bar{e}}) d\tau, \quad (9)$$

where the integration $d\tau$ is over all space coordinates.

As is apparent from equation (9), in order to calculate the cross-section for leptonic annihilation in flight we need the scattering wave function in the initial channel of the colliding system, $\Psi_{\mathbf{k}_i}^{(+)}$. The latter may be obtained by means of the formalism developed in our previous work [3,5].

2.1. The scattering wave function in the initial channel

We solve the hydrogen–antihydrogen scattering problem in a distorted wave approximation based on the separation of the leptonic and hadronic motions as implied by the Born–Oppenheimer approximation. The total wave function of the system is written as

$$\Psi_{\mathbf{k}_i}^{(+)}(\mathbf{r}_e, \mathbf{r}_{\bar{e}}, \mathbf{R}) = \psi_i(\mathbf{r}_e, \mathbf{r}_{\bar{e}}; R) \chi_{\mathbf{k}_i}(\mathbf{R}), \quad (10)$$

where the leptonic wave function $\psi_i(\mathbf{r}_e, \mathbf{r}_{\bar{e}}; R)$ depends on the interhadronic distance in a parametric way. In this approximation, the solution of the problem separates into two parts. One first calculates the leptonic potential for the hadronic motion. This is done by solving the leptonic eigenvalue problem

$$H_i^{\text{lep}} \psi_i = V_i^{\text{lep}}(R) \psi_i, \quad (11)$$

where the leptonic Hamiltonian H_i^{lep} is given by

$$\begin{aligned} H_i^{\text{lep}} = & -\frac{1}{2} \nabla_e^2 - \frac{1}{2} \nabla_{\bar{e}}^2 - \frac{1}{|\mathbf{r}_p - \mathbf{r}_e|} - \frac{1}{|\mathbf{r}_{\bar{p}} - \mathbf{r}_{\bar{e}}|} + \frac{1}{|\mathbf{r}_p - \mathbf{r}_{\bar{e}}|} \\ & + \frac{1}{|\mathbf{r}_{\bar{p}} - \mathbf{r}_e|} - \frac{1}{|\mathbf{r}_e - \mathbf{r}_{\bar{e}}|}. \end{aligned} \quad (12)$$

The leptonic potential $V_i^{\text{lep}}(R)$ is then used for solving the Schrödinger equation describing the nuclear motion,

$$\left(-\frac{1}{m_p} \nabla_R^2 + V_i(R) \right) \chi_{\mathbf{k}_i} = E_i \chi_{\mathbf{k}_i} \quad (13)$$

with $V_i(R) = V_i^{\text{lep}}(R) - (1/R)$.

The leptonic eigenvalue problem (11) is solved by means of the variational method [5] expanding wavefunction ψ as a linear combination of (N) basis functions φ ,

$$\psi = \sum_{j=1}^N c_j \varphi_j. \quad (14)$$

The trial wavefunctions φ_j are expressed in prolate spheroidal coordinates, properly symmetry adapted, and of the same explicitly correlated form as introduced by Kolos *et al.* [16]

$$\begin{aligned} \varphi_j = & \left(\frac{2r_{e\bar{e}}}{R} \right)^{\mu_j} [\exp(-\alpha_1 \xi_e - \alpha_2 \xi_{\bar{e}} + \beta_1 \eta_e + \beta_2 \eta_{\bar{e}}) \xi_e^{p_j} \xi_{\bar{e}}^{\bar{p}_j} \eta_e^{q_j} \eta_{\bar{e}}^{\bar{q}_j} \\ & + (-1)^{(q_j + \bar{q}_j)} \exp(-\alpha_2 \xi_e - \alpha_1 \xi_{\bar{e}} + \beta_2 \eta_e + \beta_1 \eta_{\bar{e}}) \xi_e^{p_j} \xi_{\bar{e}}^{\bar{p}_j} \eta_e^{q_j} \eta_{\bar{e}}^{\bar{q}_j}], \end{aligned} \quad (15)$$

where the rational numbers α_i and β_i and the positive integers p_j , q_j , and μ_j characterize the basis set. α_i and β_i were optimized variationally as a function of the internuclear distance R .

2.2. The electron–positron coalescence probability

The factorization of the wave function due to the Born–Oppenheimer approximation in equation (10) allows to structure the annihilation rate given in equation (3),

$$\lambda_a^{e\bar{e}} = \langle \Psi_{\mathbf{k}_i}^{(+)}(\mathbf{R}; \mathbf{r}_e, \mathbf{r}_{\bar{e}}) | A^{e\bar{e}} \delta(\mathbf{r}_e - \mathbf{r}_{\bar{e}}) | \Psi_{\mathbf{k}_i}^{(+)}(\mathbf{R}; \mathbf{r}_e, \mathbf{r}_{\bar{e}}) \rangle \quad (16)$$

$$\lambda_a^{e\bar{e}} = \langle \chi_{\mathbf{k}_i}(\mathbf{R}) \psi_i(\mathbf{R}; \mathbf{r}_e, \mathbf{r}_{\bar{e}}) | A^{e\bar{e}} \delta(\mathbf{r}_e - \mathbf{r}_{\bar{e}}) | \chi_{\mathbf{k}_i}(\mathbf{R}) \psi_i(\mathbf{R}; \mathbf{r}_e, \mathbf{r}_{\bar{e}}) \rangle \quad (17)$$

$$\lambda_a^{e\bar{e}} = A^{e\bar{e}} \int dV_R |\chi_{\mathbf{k}_i}(\mathbf{R})|^2 \int dV_e \int dV_{\bar{e}} |\psi_i(\mathbf{R}; \mathbf{r}_e, \mathbf{r}_{\bar{e}})|^2 \delta(\mathbf{r}_e - \mathbf{r}_{\bar{e}}) \quad (18)$$

$$\lambda_a^{e\bar{e}} = A^{e\bar{e}} \int dV_R |\chi_{\mathbf{k}_i}(\mathbf{R})|^2 P(R). \quad (19)$$

In the equation above, $P(R)$ denotes the conditional probability density for the electron and positron to coalesce (at any place in the leptonic coordinate space) while the hadrons are at a distance R apart. The quantity $P(R)$ that is to be calculated is thus defined as

$$P(R) = \int |\psi_i(\mathbf{R}; \mathbf{r}_e, \mathbf{r}_{\bar{e}})|^2 \delta(\mathbf{r}_e - \mathbf{r}_{\bar{e}}) dV_{\bar{e}} dV_e. \quad (20)$$

Using expansion (14) in equation (20) one gets

$$P(R) = \int dV_e \int dV_{\bar{e}} \sum_{j,i} c_j^* c_i \varphi_j^*(R; \mathbf{r}_e, \mathbf{r}_{\bar{e}}) \varphi_i(R; \mathbf{r}_e, \mathbf{r}_{\bar{e}}) \delta(\mathbf{r}_e - \mathbf{r}_{\bar{e}}). \quad (21)$$

Since the basis functions φ_i are expressed in prolate spheroidal coordinates both the volume element and the delta function must be accordingly transformed. One has

$$dV_e dV_{\bar{e}} = \left(\frac{R^3}{8} \right)^2 (\xi_e^2 - \eta_e^2) (\xi_{\bar{e}}^2 - \eta_{\bar{e}}^2) d\xi_e d\eta_e d\phi_e d\xi_{\bar{e}} d\eta_{\bar{e}} d\phi_{\bar{e}}, \quad (22)$$

and, keeping \mathbf{r}_e fixed,

$$\delta(\mathbf{r}_e - \mathbf{r}_{\bar{e}}) = \delta(\xi_e - \xi_{\bar{e}}) \delta(\eta_e - \eta_{\bar{e}}) \delta(\phi_e - \phi_{\bar{e}}) \frac{8}{R^3} (\xi_{\bar{e}}^2 - \eta_{\bar{e}}^2)^{-1}. \quad (23)$$

Using equations (15) and (22) in equation (21) together with the properties of the delta function (23), interchanging integration and summation, and integrating over the positron coordinates $V_{\bar{e}}$,

$$P(R) = \frac{R^3}{8} \sum_{j,i} c_j^* c_i \int_0^{2\pi} d\phi_e \int_{-1}^{+1} d\eta_e \int_{+1}^{\infty} d\xi_e \varphi_j^*(R; \mathbf{r}_e, \mathbf{r}_e) \varphi_i(R; \mathbf{r}_e, \mathbf{r}_e) (\xi_e^2 - \eta_e^2) \quad (24)$$

is obtained. Using equation (15) the coalescence wavefunctions $\varphi_j(R; \mathbf{r}_e, \mathbf{r}_e)$ are given by

$$\varphi_j(R; \mathbf{r}_e, \mathbf{r}_e) = \begin{cases} 2 \left(\frac{2r_{ee}}{R} \right)^{\mu_j} \exp[-(\alpha_1 + \alpha_2)\xi_e + (\beta_1 + \beta_2)\eta_e] \xi_e^{p_j + \bar{p}_j} \eta_e^{q_j + \bar{q}_j} & \text{for } q_j + \bar{q}_j \text{ even} \\ 0 & \text{for } q_j + \bar{q}_j \text{ odd.} \end{cases} \quad (25)$$

In the present case of Σ symmetry the leptonic wavefunctions are real and thus the complex conjugation can be skipped. A further simplification arises from the fact that the basis functions φ_j contain the prefactor $(2r_{ee}/R)^{\mu_j}$ (see equations (15) and (25)). Since $r_{ee}^{\mu} = 0$ for $\mathbf{r}_{\bar{e}} = \mathbf{r}_e$ and $\mu \neq 0$, the integrand in equation (24) is zero, if either μ_i or μ_j is non-zero. For the remaining

case $\mu_i + \mu_j = 0$ the integration over ϕ_e is trivial and one obtains

$$P(R) = \sum_{i,j}^N c_j c_i \pi R^3 \delta_{\mu_j + \mu_i} (A_{p_j + \bar{p}_j + p_i + \bar{p}_i + 2(2[\alpha_1 + \alpha_2])} B_{q_j + \bar{q}_j + q_i + \bar{q}_i(2[\beta_1 + \beta_2])} - A_{p_j + \bar{p}_j + p_i + \bar{p}_i} (2[\alpha_1 + \alpha_2]) B_{q_j + \bar{q}_j + q_i + \bar{q}_i + 2(2[\beta_1 + \beta_2])}) \quad (26)$$

for $q_j + \bar{q}_j$ and $q_i + \bar{q}_i$ even, and $P(R) = 0$ if either $q_j + \bar{q}_j$ or $q_i + \bar{q}_i$ odd. In equation (26) δ_μ is the Kronecker delta function (non-zero for $\mu = 0$ only) and A and B are given by

$$A_p(\alpha) = \int_{+1}^{\infty} \xi^p e^{-\alpha\xi} d\xi \quad (27)$$

$$B_q(\beta) = \int_{-1}^{+1} \eta^q e^{\beta\eta} d\eta. \quad (28)$$

Both integrals can be solved with the aid of recurrence relations as they are, e.g., given in equations (5.1.15) and (5.1.16) of Ref. [17] (where $\alpha_n(z)$ and $\beta_n(z)$ correspond to $A_p(\alpha)$ and $B_q(-\beta)$, respectively).

The hadronic wavefunction $\chi_{\mathbf{k}_i}$ in equation (13) is obtained numerically after performing a partial-wave decomposition, as is described in Ref. [5]. With the aid of $\chi_{\mathbf{k}_i}(\mathbf{R})$ and $P(R)$ the direct leptonic annihilation rate can be calculated according to equation (19).

2.3. Asymptotic behavior of the leptonic coalescence probability

It is instructive and helpful for assessing the correctness of the numerical apparatus to investigate the asymptotic behavior of the leptonic coalescence density $P(R)$. In the limit $R \rightarrow \infty$ the ground-state $\text{H}\bar{\text{H}}$ system dissociates into separated $\text{H}(1s)$ and $\bar{\text{H}}(1s)$ atoms. In this case the electron and positron densities are spatially separated and do not overlap. Necessarily, $\lim_{R \rightarrow \infty} P(R) = 0$.

In the limit $R \rightarrow 0$ one may choose the origin of the coordinate system at the position of the two hadrons, so that $\mathbf{r}_p = \mathbf{r}_{\bar{p}} = 0$, and hence the leptonic Hamiltonian (12) reduces to

$$H_i^{\text{lep}} = -\frac{1}{2} \nabla_e^2 - \frac{1}{2} \nabla_{\bar{e}}^2 - \frac{1}{|\mathbf{r}_e - \mathbf{r}_{\bar{e}}|}, \quad \text{at } R = 0, \quad (29)$$

the Hamiltonian describing a freely moving positronium. It is now more suitable to transform the coordinates into a center of mass and a relative coordinate,

$$\mathbf{r}_{e\bar{e}} = \mathbf{r}_e - \mathbf{r}_{\bar{e}}, \quad \mathbf{r}_{\text{cm}} = (\mathbf{r}_e + \mathbf{r}_{\bar{e}})/2. \quad (30)$$

In these coordinates the $R \rightarrow 0$ limit of the leptonic Hamiltonian reads

$$H_i^{\text{lep}} = -\frac{1}{4} \nabla_{\text{cm}(\text{e}-\bar{\text{e}})}^2 - \nabla_{\text{e}\bar{\text{e}}}^2 - \frac{1}{r_{\text{e}\bar{\text{e}}}}, \quad \text{at } R = 0 \quad (31)$$

and describes separately the center of mass (first term) and internal motion of positronium (second and third terms). Therefore, at $R = 0$, the solutions to the leptonic eigenvalue problem equation (11) are of the product form

$$\psi_i(\mathbf{r}_{\text{cm}}, \mathbf{r}_{\text{e}\bar{\text{e}}}; 0) = \phi_{nlm}^{\text{Ps}}(\mathbf{r}_{\text{e}\bar{\text{e}}}) \Phi_{\mathbf{k}_i}(\mathbf{r}_{\text{cm}}). \quad (32)$$

Here ϕ_{nlm}^{Ps} is the positronium state defined by the usual hydrogenic quantum numbers n, l, m , and $\Phi_{\mathbf{k}_i}$ is a plane wave with wave vector \mathbf{k}_i corresponding to the motion of the positronium with respect to the origin of coordinates. The corresponding leptonic energy is $V_i^{\text{lep}}(0) = -1/(4n^2) + k_i^2/4$. The lowest adiabatic state of the hydrogen–antihydrogen system correlates to the ground state of positronium, i.e., $n = 1$.

We now use the form (32) of the adiabatic wavefunction at $R = 0$ in order to calculate the coalescence probability density at $R = 0$. According to the definition of P in equation (20) one finds

$$\begin{aligned} P(0) &= \int dV_{\text{e}} \int dV_{\bar{\text{e}}} |\psi_i(\mathbf{r}_{\text{e}}, \mathbf{r}_{\bar{\text{e}}}; 0)|^2 \delta(\mathbf{r}_{\text{e}} - \mathbf{r}_{\bar{\text{e}}}) \\ &= \int dV_{\text{e}\bar{\text{e}}} |\phi_{100}^{\text{Ps}}(\mathbf{r}_{\text{e}\bar{\text{e}}})|^2 \delta(\mathbf{r}_{\text{e}\bar{\text{e}}}) \int dV_{\text{cm}} |\Phi_{\mathbf{k}_i}(\mathbf{r}_{\text{cm}})|^2 = |\phi_{100}^{\text{Ps}}(0)|^2. \end{aligned} \quad (33)$$

Not surprisingly, the coalescence density in the limit $R \rightarrow 0$ is simply given by the coalescence density of positronium. Using the explicit form of the positronium ground-state wavefunction one obtains

$$P(0) = \left| \frac{1}{\sqrt{4\pi}} \frac{2}{2^{3/2}} \right|^2 = \frac{1}{8\pi}. \quad (34)$$

3. NUMERICAL RESULTS

The leptonic coalescence density $P(R)$ has been evaluated as a function of the internuclear distance R in the interval $0.8 \leq R \leq 8.0a_0$ using equation (26) and up to 908 basis functions φ . The $P(R)$ calculated this way clearly goes to zero for $R \rightarrow \infty$. For small R -distances we might expect inaccuracies related to the limitation of the presently employed basis functions to correctly represent positronium [5]. The exponential behavior of the correct positronium wavefunction in equation (32) is approximated by a polynomial in $r_{\text{e}\bar{\text{e}}}^\mu$ when using the basis functions in equation (15). As the present code allows only $\mu \leq 3$, a limited accuracy is obtained. An error of about 5% is found

for the positronium energy when solving equation (32) with the present variational procedure employing the basis functions in equation (15).

The error in the expectation value of energy is typically quadratic as compared to the error in the wave function. Therefore, we might expect an error of about 20% for $P(R)$ at the distances where the positronium character of the $H\bar{H}$ wavefunction becomes dominant. This happens below the critical distance $R_c \approx 0.74a_0$ where the \bar{p} – p pair does not bind the leptons [18,19]. Because of that, leptonic coalescence density $P(R)$ has been smoothly extrapolated from its value at $R \approx 0.8a_0$ to the correct positronium value at $R = 0$ given in equation (33). The resulting $P(R)$ is shown in Fig. 1. Such a procedure is justified if the final result does not critically depend on the extrapolation of the leptonic coalescence density for $R \leq 0.8a_0$. Fortunately, the importance of this R range turns out to be small. Even if one disregards the interval $R \leq 0.8a_0$ completely there is no more than a 7% difference between this result and the one obtained when using a constant value of the integrand in equation (19) (e.g., the value it takes at $R = 0.8a_0$) for all $R < 0.8a_0$. The reason is the small probability density of the hadronic scattering wavefunction in this R range.

As an example, the hadronic radial density is shown for a collisional energy $\varepsilon_i = 10^{-7}$ a.u. in Fig. 1. As is apparent from equation (19), the direct leptonic annihilation rate depends on the product of the hadronic density and $P(R)$. This product is shown in Fig. 2. Clearly, the range with $R < 0.8a_0$ adds only a minor, though non-negligible, part to the integral in equation (19). According to the test calculation mentioned above we estimate this contribution to be in the order of 10%. This accuracy is sufficient for the purpose of this work which is to give a reliable order-of-magnitude estimate of the role of the leptonic annihilation channel in the hydrogen–antihydrogen scattering.

The result of the present calculation of the direct leptonic annihilation rate is presented in Fig. 3. This figure shows (on a logarithmic scale) the cross-section as a function of the collisional energy. The two curves for the leptonic annihilation rate correspond to the two different annihilation constants, $A_+^{e\bar{e}} = 4.9 \times 10^{-6}$ a.u. for the singlet state and $A_-^{e\bar{e}} = 4.3 \times 10^{-9}$ a.u. for the triplet state. As one would expect, the cross-section increases for decreasing collision energies, since the leptons have more time to interact (and annihilate). In the low-energy limit the cross-section for leptonic annihilation shows the behavior characteristic for inelastic collisions as expected from the Wigner’s threshold law. The cross-section is $\sigma_+^{e\bar{e}} = (4.0 \times 10^{-5} / \sqrt{\varepsilon_i}) a_0^2$ for the singlet state and $\sigma_-^{e\bar{e}} = (3.5 \times 10^{-8} / \sqrt{\varepsilon_i}) a_0^2$ for the triplet state. The inelasticity due to leptonic annihilation induces an imaginary component in the hydrogen–antihydrogen scattering length. This component can be obtained as $\beta = 4\pi\sigma_a^{e\bar{e}}$ and is $\beta_+ = 1.4 \times 10^{-4} a_0$ for the singlet and $\beta_- = 1.2 \times 10^{-7} a_0$ for the triplet case, respectively.

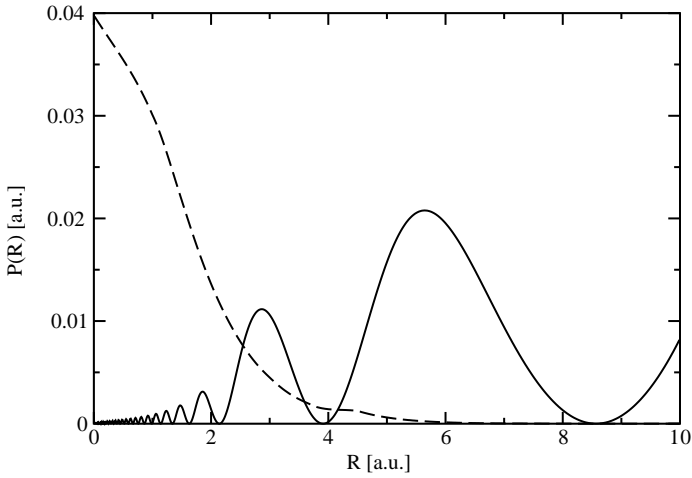


Fig. 1. The leptonic coalescence probability density $P(R)$ in atomic units (dashed) is shown together with the hadronic radial density $|f_0(R)|^2 = |\chi_{k_i}(R)|^2 R^2$ (solid, scaled to fit into plot) for a collision energy of 10^{-7} a.u.

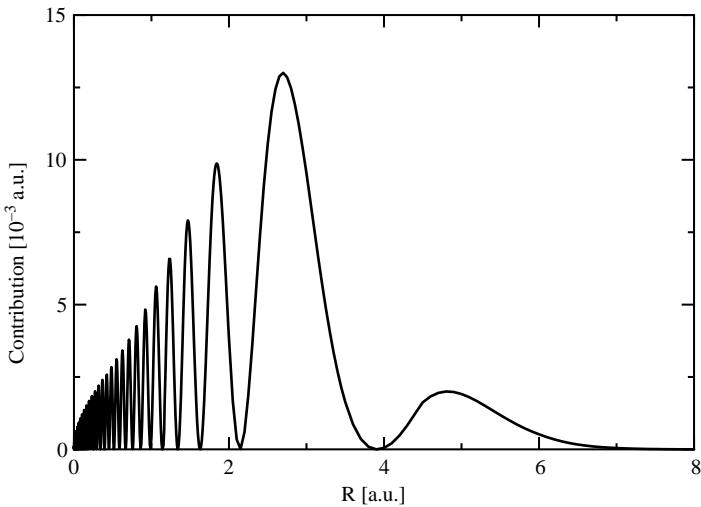


Fig. 2. Contribution to the leptonic annihilation for different interhadronic distances, i.e., the product of the hadronic radial density $|\chi_{k_i}(R)|^2 R^2 = |f_0(R)|^2$ and the leptonic coalescence density $P(R)$ (cf. equation (19)). The presented result is for a collision energy of 10^{-7} a.u.

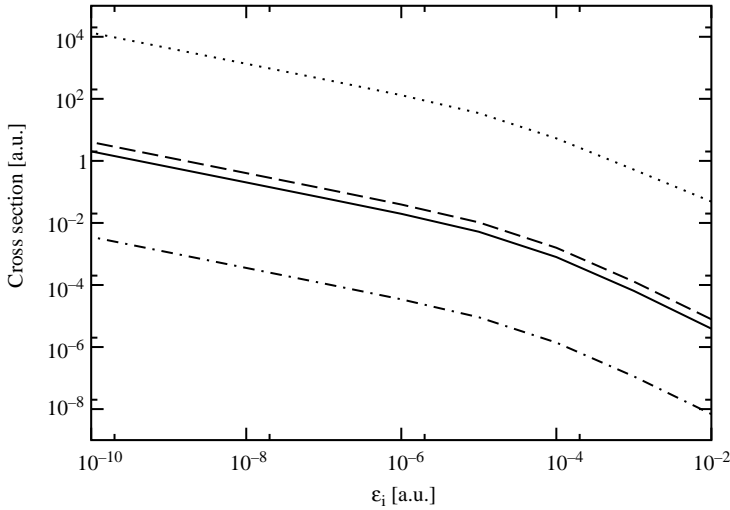


Fig. 3. The cross-section for annihilation in flight in $H + \bar{H}$ collisions (in atomic units). Dashed curve: leptonic annihilation in the collisional singlet state, $\sigma_+^{\bar{e}e} = (4.0 \times 10^{-5}/\sqrt{\epsilon_i})a_0^2$. Dash-dotted curve: leptonic annihilation in the collisional triplet state, $\sigma_-^{\bar{e}e} = (3.5 \times 10^{-8}/\sqrt{\epsilon_i})a_0^2$. Solid line: the total leptonic annihilation rate for spin-polarized $H + \bar{H}$ collisions (e.g., in the magnetic trap), taken as the statistical average of the cross-sections mentioned above. The upper curve (dotted) represents the cross-section $\sigma^{\bar{p}p} = (0.14/\sqrt{\epsilon_i})a_0^2$ for the hadronic annihilation in flight.

The cross-sections $\sigma_+^{\bar{e}e}$ and $\sigma_-^{\bar{e}e}$ for direct leptonic annihilation appear to be very small compared to the one describing rearrangement reactions or proton–antiproton annihilation in flight. The latter cross-section ($\sigma^{\bar{p}p} = (0.14/\sqrt{\epsilon_i})a_0^2$ [3]) is included in Fig. 3 and is seen to be practically proportional to the one for direct leptonic annihilation. However, direct hadronic annihilation is about three orders of magnitude more likely than leptonic annihilation in flight in the entire range of considered energies. Assuming the accuracy of the present result to be about 10%, a more precise calculation is not likely to change the basic conclusion of this work, namely that direct leptonic annihilation in flight is a negligible effect in hydrogen–antihydrogen scattering.

4. CONCLUSIONS

When an atom and its antiatom approach each other, the leptons might in principle annihilate before the hadrons do. This work finds that this is not the case. Although the annihilation reaction constant for *para*-positronium

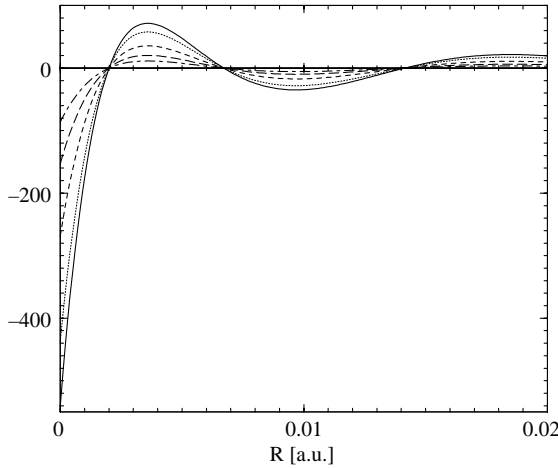


Fig. 4. Values of the hadronic wave function $f_0(\mathbf{k}_i, R)/R$ (in a.u.) at the coalescence point ($R = 0$) for various collision energies: $\varepsilon_i = 10^{-4}$ (solid), 10^{-5} (dotted), 10^{-6} (dashed), 10^{-7} (longly dashed), and 10^{-8} a.u. (dot-dashed).

is *larger* than that for protonium ($A_{+}^{\bar{e}e} = 4.9 \times 10^{-6}$ a.u. $> A^{\bar{p}p} = 1.69 \times 10^{-7}$ a.u.), the probability of direct $e^{+} - e^{-}$ annihilation is negligible.

The reason is that at any interhadronic distance R the leptonic coalescence density has to be weighted by the hadronic probability density at that distance. Because of that, $e^{+} - e^{-}$ annihilation occurs mainly within the interval $\Delta R \simeq 1a_0$ in the vicinity of $R \simeq 3a_0$ (see Fig. 2) with the probability proportional to $A^{\bar{e}e}P(R \simeq 3)|f_0(R \simeq 3)|^2\Delta R$ (see equation (19)) whereas the hadrons annihilate basically at $R = 0$ with the probability proportional to $A^{\bar{p}p}Y_{00}|\chi_{\mathbf{k}_i}(R = 0)|^2$ [5]. The relative probability of the two processes should be, therefore, roughly of the order of

$$\frac{\sigma^{\bar{p}p}}{\sigma^{\bar{e}e}} \frac{A^{\bar{p}p}}{A^{\bar{e}e}} \frac{|\chi_{\mathbf{k}_i}(0)|^2 Y_{00}^2}{|\chi_{\mathbf{k}_i}(3)|^2 P(3) \times 3^2 \times 1} \simeq 4.7 \times 10^3.$$

Since $\chi_{\mathbf{k}_i}(R)$ is considerably enhanced at $R = 0$ (see Fig. 4) the $p-\bar{p}$ annihilation dominates over $e^{+}-e^{-}$ annihilation.

More precisely, the cross-section for the in-flight annihilation of the $e-e^{+}$ pair according to



has been found to be three orders of magnitude smaller than the corresponding cross-section for proton-antiproton annihilation. Thus, the contribution to the total loss of antihydrogen due to the positron-electron

annihilation in flight is small and not important for the kinetics of a dilute hydrogen–antihydrogen gas at low temperatures.

ACKNOWLEDGEMENTS

The present contribution is dedicated to Osvaldo Goscinski on the occasion of his 65th birthday. One of us (PF) would like to gratefully acknowledge the many years of collaboration and interactions with Osvaldo within the Department of Quantum Chemistry at the Uppsala University and in life aside the academy. It is hard to imagine meeting the spring without the ritual lunch on the last of April at Osvaldo's and Gunilla's home. Fortunately, they seem to be inclined to keep up this tradition even after Osvaldo's retirement. Happy birthday Osvaldo!

This research has been supported by grants to PF and SJ from the Swedish Research Council; by grants to AS from the *Stifterverband für die Deutsche Wissenschaft* and the *Deutsche Forschungsgemeinschaft*; and by grants to AD from the Office of Basic Energy Sciences at the US Department of Energy. We also acknowledge the support from the National Science Foundation through grants to the Institute for Theoretical Atomic and Molecular Physics and to the Center for Ultracold Atoms.

REFERENCES

- [1] M. Amoretti *et al.*, *Nature*, 2002, **419**, 456.
- [2] G. Gabrielse *et al.*, *Phys. Rev. Lett.*, 2002, **89**, 213401.
- [3] P. Froelich, S. Jonsell, A. Saenz, B. Zygelman and A. Dalgarno, *Phys. Rev. Lett.*, 2000, **84**, 4577.
- [4] S. Jonsell, A. Saenz and P. Froelich, *Nucl. Phys. A*, 2000, **663**, 659c.
- [5] S. Jonsell, A. Saenz, P. Froelich, A. Dalgarno and B. Zygelman, *Phys. Rev. A*, 2001, **64**, 052712.
- [6] B. Zygelman, P. Froelich, A. Saenz, S. Jonsell and A. Dalgarno, *Phys. Rev. A*, 2001, **63**, 052722.
- [7] B. Zygelman, A. Saenz, P. Froelich and S. Jonsell, *Phys. Rev. A*, 2004, **69**, 042715.
- [8] S. Jonsell, A. Saenz, P. Froelich, B. Zygelman and A. Dalgarno, *J. Phys. B*, 2004, **37**, 1195.
- [9] P. Froelich and A. Voronin, *Preliminary result, to be presented at the ICAP-2004*.
- [10] P. A. Sinha and A. S. Ghosh, *Europhys. Lett.*, 2000, **49**, 558.
- [11] A. Voronin and J. Carbonell, *Nucl. Phys. A*, 2001, **689**, 529.
- [12] E. A. G. Armour and C. W. Chamberlain, *J. Phys. B*, 2002, **35**.
- [13] A. Czarnecki and S. G. Karshenboim, in *Proceedings of the 14th International Workshop on High Energy Physics and Quantum Field Theory (QFTHEP99, Moscow 1999)* (eds B. B. Levchenko and V. I. Savrin), MSU Press, East Lansing, WI, 2000, pp. 538–544.
- [14] A. Asai, A. Orito and N. Shinohara, *Phys. Lett. B*, 1995, **357**, 475.
- [15] C. Itzykson and J.-B. Zuber, *Quantum Field Theory*, McGraw-Hill, New York, 1985.

- [16] W. Kolos, D. L. Morgan, D. M. Schrader and L. Wolniewicz, *Phys. Rev. A*, 1975, **11**, 1792.
- [17] M. Abramowitz and I. A. Stegun (eds), *Handbook of Mathematical Functions*, 10th edn., Dover Publications, New York, 1972.
- [18] E. Armour, J. Carr and V. Zeman, *J. Phys. B*, 1998, **31**, L679.
- [19] K. Strasburger, *J. Phys. B*, 2002, **35**, L435.

Index

A

- Ab initio 26, 53, 58, 66, 69, 91, 194, 380, 426
- Activated complex 8, 9, 14, 20
- Adiabatic basis 336, 338
- Adiabatic electron affinity 429, 434, 439, 456
- AGP index set 114, 124
- Aharonov–Bohm effect 239
- Aharonov–Casher effect 241
- Alchemy 423
- Alcohol–water 51, 52, 61
- Alternant conjugated hydrocarbons 349
- Amphoteric 52
- Angular integral 138, 147
- Angular momentum eigenfunction 132, 133, 149
- Approximate CC variants 210
- Arbitrary-precision computation 145, 148
- Aromatic–alcohol interaction 89
- Aromatic–aliphatic interactions 65, 76
- Aromatic–amide(B) interactions 75, 81, 91
- Aromatic–amide(S) interactions 79
- Aromatic–amine interaction 86
- Aromatic–aromatic interactions 70, 78
- Aromatic–thiol interactions 85
- Asymptotic behaviour 352, 353, 355, 360, 364, 366
- Atomic polarizabilities 38
- Attractor 277, 284, 287, 289, 290
- Average path potential 298
- Average rotational energy transfer 343

B

- Band gap 351, 353, 358, 359, 361, 425
- Bargmann–Segal space 223, 234, 235
- Basis set 26, 37, 48, 56, 57, 61, 69, 157, 159–162, 165, 172, 188, 193, 198, 202, 205, 216, 217, 219, 220, 255, 261, 267, 270, 275, 277–281, 286, 288, 290, 293, 300, 301, 303, 312, 323, 324, 331, 336–338, 383, 471
- Basis sets, correlation-consistent 201
- Basis set superposition error 56, 69
- Berry phase 240, 242–244, 251, 372

Binding energy 28, 29, 33, 34, 51, 54,
56–59, 61, 304, 437, 469, 459
Boltzmann weights 57
Born approximation 254
Born–Oppenheimer regime 241, 242,
246, 249, 251
Born–Oppenheimer limit 242
Born–Oppenheimer state vector 243
Born–von Kármán zone 374, 375,
378, 380, 384–391
Branch-point singularities 197

C

Canonical coefficients 114, 116, 117,
124, 125
Carbon chain 388
Cartesian laboratory frame 255
CASSCF/CASPT2/SOC 38
Catalysis 16
CCSDT 210, 212, 220
CCSDT-3 209, 210, 214–216, 220,
221
 $\text{CH}_3\text{HO}\cdot\text{H}_2\text{O}$ 51, 52, 54–58
 $\text{CH}_3\text{OH}\cdot\text{OH}_2$ 51, 52, 54–56, 58
Charge-mass-permutation
invariance 146
Charge exchange differential
cross section 266
Charge transfer 34, 261, 266–268,
275, 279, 280, 282, 370
CHARMm force field 60, 65, 67, 68,
70, 73, 78, 81, 84, 85, 91
Chiral lithium amide 16
Circularly-polarized light 394
Clusters of gold 426
Coherent-dissipative system 98
Complex screening parameters 144
Configuration interaction
coefficients 123
Confining potential 290
Conjugated polyenes 348
Conjugated polymers 369, 370, 383

Convergence classes 197
Coordinate systems 118, 142, 183
Coordination number 54
Correlated Gaussians 131
Coset factorization 116
Coset generators for $\text{SU}(2)$
factors 117
Coset generators for $\text{USp}(\omega)$
factors 120
Coset generators for $\text{SU}(2\xi)$
factors 121
Cotton–Mouton constant 178
Cotton–Mouton effect 178
Coulomb gauge 373, 377, 378
Coulomb potential 53, 386
Counterpoise correction 56–58, 61
Coupled-cluster theory 194, 209
CPT invariance 94, 97
Cremer–He criteria 201

D

De Broglie–Bohm quantum
mechanics 333
Deflection function 255, 258–263
Delta-function properties 144
Density operator 100, 103, 125, 169,
293–299, 301, 309, 310–313, 410
Deprotonation 8, 14, 16, 20
DFT 316, 317, 326, 328
Diabatic basis 283, 284, 338
Diabatic potential energy 277, 288,
289
Dianion 434, 456, 459
DICE 53
Dipole approximation 373, 377, 404,
409, 410, 412
Dipole moment 37, 39, 41, 46, 48,
172, 173, 177, 180, 189, 249, 282,
370, 415
Direct differential cross section 253,
260, 263, 264, 266, 268
Dissipative dynamics 294, 309, 313

Dominant singularity 198, 199
 Dynamical symmetry 394

E

Effective nuclear Hamiltonian 241
 Effective potentials 293, 295, 298, 312
 Eikonal or sudden approximation 254
 Ehrenfest potential 298
 Electric dipole 179, 180, 183, 184, 250, 373, 377
 Electric field 41, 171–173, 177–180, 182, 184, 249–251, 282, 370, 371, 390, 410, 415
 Electric field gradient 178
 Electric field polarizabilities 178
 Electric quadrupole 179, 180, 182, 184
 Electron affinity 214, 429, 434, 439, 456
 Electronic Hamiltonian 240, 241, 244, 249, 251, 256, 276, 284, 286, 288, 289
 Electronic moment 179
 Electron-Nuclear dynamics (END) 254
 END trajectories 255, 257, 260
 Electronic rearrangement 294, 300, 302
 Electron transfer 254, 266, 280, 283, 303, 312, 332
 Enantiomer 3, 4, 8, 9, 12–14, 16, 17
 Energy bands 398
 Equation-of-motion methods 210
 Evolution operator 94, 279
 Excitation energy 214
 Excited state 37, 40, 42–44, 48, 109, 158, 159, 164–166, 174, 179, 194, 196, 198, 200, 201, 205, 212, 287, 303, 317, 321, 322, 324, 326–328
 Exponentially correlated integrals 145–146
 —, branch tracking 143, 144
 —, closed formula 143, 148, 225–228, 231

—, relations between 220, 225, 227
 —, singularity cancellation 143
 Exponentially correlated wavefunctions 129, 143, 145

F

Factorization procedure 212
 Fermi–Fock space 111
 Few-body problem 129, 130
 First-order density matrix 160, 168–170
 Floquet–Bloch Hamiltonian 398
 Floquet theorem 234, 235, 394, 396
 Floquet theory 224, 232
 Fock operator 194
 Four-body problem 131, 132, 145
 Franck–Condon factor 224, 279
 Full configuration interaction 195

G

Gauge translation 185, 188
 Gegenbauer expansion 147
 Generalized Sturmian 157, 159–162, 165, 166, 168, 170, 171, 174
 Generalized electronic diabatic (GED) approach 276
 Generalized time-reversal symmetry 395
 Generator coordinate method 131, 315–317
 Generator coordinate Hartree–Fock method 315
 Gold 423–426, 428, 430, 436, 437, 441, 442, 446, 447, 449, 450, 452, 453, 456–460, 463
 —, nobleness 424, 425
 —, cluster 26, 56, 57, 60, 61, 176, 194, 197, 200, 204, 209, 423–430, 432, 434–438, 440–443, 445, 446, 448–452, 455–460, 463, 464
 Goscinskian 163–165, 170–172

H

Hamiltonian 275–277, 279, 281, 283, 284, 286, 288, 289, 294–302, 309–313, 318, 326, 337, 338, 340, 344, 347–349, 351, 354, 359, 373, 394–400, 402, 403, 405, 406, 408, 409, 412, 413, 415, 420, 468, 470, 473, 474
 Hamiltonian–Jacobi equation 333
 Hartree–Fock approximation 174
 Hellmann–Feynman force 298, 305, 308
 Hermite–Padé approximants 200
 High-order harmonic generation 393, 394, 404, 409
 Hill–Wheeler equation 315, 317
 HOMO 353, 428, 432, 439, 440, 442, 447, 449
 HOMO–LUMO gap 456
 Hückel model 347, 348, 375, 381, 382
 Hydrodynamic formulation 331, 335
 Hydrogen bond 51–58, 60, 61, 69
 Hydrogen molecular ion 262, 266, 268
 Hydrogen Sturmian 159
 Hydrophobic interaction 52
 Hylleraas method 129, 133, 146, 148
 Hylleraas integrals 148
 Hyperpolarizability 371
 Hyperspherical harmonics 159, 174

I

Impact parameter model 280
 Infrared spectra 437
 Interparticle coordinates 129–131, 141, 145
 Ionization potential 209, 210, 214, 217–219, 316

J

Jahn–Teller systems 239–241, 249–251
 Jordan block 93–98, 100, 102, 106

K

Kaon 95, 97, 98, 102
 Kinetic energy operator 27, 129, 133, 134, 163, 249, 276, 282, 386

L

Lennard–Jones potential 71
 Levenberg–Marquardt method 65, 72
 Lie algebra 110–113, 117, 124, 126, 235, 236
 Lie algebra decomposition 124
 Limonene 3
 Liouville equation 103, 304
 Liouville–von Neumann equation 293
 Liouvillian 92, 98, 102
 Liquid phase 51
 LMTOs 383
 Lorentz–Berthelot combination rules 68
 LUMO 428, 432

M

Magnetic dipole 177, 179, 180, 189, 249
 Magnetic susceptibility 177, 180–182, 184, 187, 188
 Markov approximation 332
 Mesomolecules 144
 Metallic chain 358, 359
 Methanol 51–61, 426
 Metropolis Monte Carlo method 53
 Microwave rotation-tunneling spectroscopy 52
 Molecular mechanics 66
 Molecule-surface scattering 331, 340, 343
 Møller–Plesset partitioning 193

Møller–Plesset perturbation
theory 193
Monte Carlo calculations 148
Morse oscillator 227, 229, 230
Mulliken population analysis 266
Multiconfiguration time-dependent
Hartree method 332
Multireference perturbation
theory 206

N

Nanostructured materials 425
Natural orbitals 157, 160, 169, 170,
315, 325
NBO analysis 13
Neutrino mass problem 98
Nonlinear least squares fitting 71
Non-selfadjoint extension 94
N-representability problem 103
Numerical propagation 295, 300
NVT ensemble 53

O

ODLRO 99, 101, 104, 106
Open quantum system 98
Operator algebra 223, 224, 229, 230,
232, 237
OPLS-AA 53

P

Padé approximants 200
Parity 137, 138, 141, 281, 282, 284,
466, 468, 469
Partial Wigner transform 293–295
Particle-ghost pair 97
PbO 37, 39, 42–48
Peierls theorem 348
Peierls instability 347, 348
Peierls dimerization 348, 360

Perimetric coordinates 130, 141
Perturbation theory 37, 38, 41, 46, 57,
61, 180, 193–195, 206, 309, 316,
347, 348, 355, 359, 360, 361, 391,
394
Phase space 110, 124, 257, 293
Phase density 296, 297
Photoelectron spectroscopy 23, 25
Photoexcitation 294
Polarizability 37, 39, 41, 46–48, 67,
177, 178, 180–184, 186–188, 371,
374
Polyacetylene 347, 348, 350, 354,
359, 360, 364, 369, 371, 383
Polycarbonitrile 383, 384
Polymers 369–372, 380, 383, 391
Positive charge background 275, 276
Positronium molecule 144
Post-Born–Oppenheimer
approach 275
Potential energy surface
(PESs) 254, 423, 425
Protic liquid 61
Proton acceptor 51, 52
Proton donor 51, 52, 55
Proton insertion 23, 24, 28, 30, 33

Q

Quadratic approximants 200, 202–
204, 206
Quantum coherence 295, 306
Quantum diffraction 340
Quantum potential 333, 334, 336
Quantum ring 393, 394
Quantum trajectory 337
Quasienergy bands 397

R

Radial distribution function 54, 169,
170
Rayleigh depolarization 59, 60

Reduced density matrices 93, 106, 108, 127
 Reduced density operator 125, 294
 Relativistic effective core potentials 425
 Relax-and-drive procedure 90, 302, 305, 312
 Response function 108, 109, 114, 179, 182
 Rotamer 436, 437, 460
 Rotational energy transfer 340, 342, 343, 345
 Rotation matrices 150

S

Schiff approximation 255, 258, 259, 264, 266, 272
 Segré characteristic 93–95, 98, 102
 Segregation 52
 Self-organization structure 95
 Semiempirical calculations 311
 Short wavelengths 293, 297, 312
 Similarity transformed Hamiltonian 212
 Single-walled carbon nanotubes 394
 Singularity of the energy function 195
 Six-j symbol 141, 150
 Slater determinant 162, 169, 323
 Slater–Condon rule 160, 166–168
 Solvation 61
 Spin-orbit 27, 29, 37–39, 41–43, 45, 48, 162, 163, 166, 168, 169, 171, 288, 289
 Split-operator 305
 Squeezed states 223, 224, 230, 231, 237
 State to state total cross section 269, 271

Stereoselectivity 4, 5, 8, 9, 13, 14, 16, 17, 21
 Sternheimer nuclear shielding 178
 Summation approximant 193, 199
 Su–Schrieffer–Heger hamiltonian 348

T

Thouless coefficients 256, 261
 Three-body system 131, 142, 145, 146
 Three-j symbol 132, 141, 149
 Three-state model 275, 283
 Time-dependent Hartree-Fock theory 257
 Time-dependent amplitudes 255, 269
 Time-evolution operator 271
 Time-periodic (Floquet) Hamiltonian 394, 396, 420
 Time-reversal symmetry 395
 Total cross section 268–272
 Transition state 7, 276, 283, 432, 434, 446, 449, 459, 460
 Travelling Gaussians 255
 Tungsten oxide 23, 24

V

Vertical electron detachment energy 429
 Vibronic Hamiltonian 241, 246, 249, 251

W

Wannier functions 369, 385, 387–391
 Wigner transform 293–296